

DEVELOPMENTS IN CIVIL ENGINEERING, 8

MANUAL OF SURFACE DRAINAGE ENGINEERING

Volume II

Stream Flow Engineering
and
Flood Protection

B.Z. KINORI and J. MEVORACH

ELSEVIER



MANUAL OF SURFACE DRAINAGE ENGINEERING

Volume II Stream Flow Engineering and Flood Protection

Developments in Civil Engineering

- Vol. 1 The Dynamics of Explosion and its Use (Henrych)
- Vol. 2 The Dynamics of Arches and Frames (Henrych)
- Vol. 3 Concrete Strength and Strains (Avram et al.)
- Vol. 4 Structural Safety and Reliability (Moan and Shinozuka, Editors)
- Vol. 5 Plastics in Material and Structural Engineering (Bares, Editor)
- Vol. 6 Autoclaved Aerated Concrete, Moisture and Properties (Wittmann, Editor)
- Vol. 7 Fracture Mechanics of Concrete (Wittmann, Editor)
- Vol. 8 Manual of Surface Drainage Engineering, Volume II (Kinori and Mevorach)
- Vol. 9 Space Structures (Avram and Anastasescu)

MANUAL OF SURFACE DRAINAGE ENGINEERING

Volume II

Stream Flow Engineering
and Flood Protection

B.Z. KINORI (1908-1981) and J. MEVORACH
Technion, Israel Institute of Technology Haifa, Israel



ELSEVIER

AMSTERDAM – OXFORD – NEW YORK – TOKYO

1984

ELSEVIER SCIENCE PUBLISHERS B.V.
1, Molenwerf,
P.O. Box 211, 1000 AE Amsterdam, The Netherlands

Distributors for the United States and Canada:

Elsevier Science Publishing Company Inc.
52, Vanderbilt Avenue
New York, N.Y. 10017

ที่ 31 ส.ค. 2530

ทะเบียน 100655

สมุดหนังสือ

TC
470
K55
V.2

ISBN 0-444-42280-3 (Vol. 8)
ISBN 0-444-41715-X (Series)

© Elsevier Science Publishers B.V., 1984

All rights reserved. No part of this publication may be reproduced, stored in a retrieval system or transmitted in any form or by any means, electronic, mechanical, photocopying, recording or otherwise, without the prior written permission of the publisher, Elsevier Science Publishers B.V., P.O. Box 330, 1000 AH Amsterdam, The Netherlands

Printed in The Netherlands

CONTENTS

Preface	vii
PART 1	
Chapter 1 – The Watershed and Elements of Hydrography	3
Chapter 2 – Elements of Hydrometric Measurements	27
Chapter 3 – Morphology of Stream Channels	77
Chapter 4 – The Regime Concept of Canals and Stream Channels	133
PART 2	
Chapter 5 – Supplement to the Hydraulics of Alluvial Channels	169
Chapter 6 – Sediment Properties	191
Chapter 7 – Bed Forms and their Effect on the Roughness	215
Chapter 8 – Transportation of Suspended Load	239
Chapter 9 – The Bed-Material Load	269
PART 3	
Chapter 10 – Flood Protection	333
Chapter 11 – Stream Outlets	497
Index	515

ACKNOWLEDGEMENTS

Acknowledgements are due to

- The American Society of Civil Engineers, 345 East 47th Street, New York, N.Y.
- The American Geophysical Union, 1909 K Street, N.W., Washington, D.C.
- The California Institute of Technology, Pasadena, California.
- CIRIA, Construction Industry Research and Information Association, 6 Storey's Gate, London.
- The Colorado State University, Fort Collins, Colorado.
- The Hydrological Service (Israel), Ministry of Agriculture, Jerusalem.
- The Institute of Hydraulic Research, The University of Iowa, Iowa City, Iowa.
- The International Association for Hydraulic Research, Rotterdamseweg 185, Delft.
- Maccaferri, River and Sea Gabions (London) Ltd., 2 Swallow Place, Princess Street, London.
- Nedeco, Netherlands Engineering Consultants, The Hague.
- TAHAL, Water Planning Ltd., Tel Aviv.
- UNESCO, Place de Fontenoy, Paris.
- U.S. Corps of Engineers, Waterways Experiment Station, Vicksburg, Miss.
- U.S. Department of Interior, Geological Survey, Denver Federal Center, Denver, Colorado.
- U.S. Department of Interior, Bureau of Reclamation, Denver Federal Center, Denver, Colorado.

PREFACE

In Volume I of the Manual of Surface Engineering general aspects of open-channel hydraulics and related flow problems have been treated, with particular regard to the needs of practising engineers. The same line has been adopted in the present Volume II, but here the subject is surface drainage engineering proper in its most prominent aspects.

Although in recent years great progress has been achieved in understanding complex physical mechanisms governing many of the phenomena pertaining to the drainage engineering, notably sediment transport and erosion-deposition processes in natural streams, there still are baffling and confusing differences in approaches, and hence large discrepancies in numerical computations and predictions of morphological consequences. Unlike researchers, practising engineers in most cases have no possibility to undertake time-consuming preliminary studies and investigations, and are bound instead to produce tangible and clear-cut decisions within reasonably short time, as well as definite numerical quantities needed for the design work. It is, therefore, no wonder that many practising engineers still resort to simplified and straightforward, mainly empirical approaches, which scientifically have often somewhat shaky foundations, but are based on long-term experience and lead to direct engineering solutions.

It is for this reason that in the present text two main lines have been followed: on the one hand, where the plethora of conflicting theoretical approaches was confusing, only a reasonable sample of the most representative and seemingly valid theories has been selected; on the other hand, in many instances simplified empirical approaches and formulae have been given due consideration, since they often are the everyday staple of the engineering trade.

Natural watercourses treated in the present text are intended to be *not larger than small rivers*. The authors have been of the opinion that large rivers have their own specific mechanisms that cannot readily be applied to smaller streams, and vice versa. In order to be more explicit on this point, the term used throughout the text for all watercourses has consistently

been “stream” and not “river”, since large rivers are generally not called streams.

A great number of worked-out numerical examples have been included in the text, with a view to providing the practising engineer with ready reference to the material dealt with in the text. It is hoped that through these examples many otherwise perhaps not readily assimilated points will become clear.

As mentioned already, there is no place for detailed discussion of all the subjects treated in a text intended to give an overall review of the drainage engineering. Ample references and bibliography have therefore been included at the end of each chapter, directing the reader to the specialized literature, where detailed treatment of the subject is available.

A special part of the text has been dedicated to drainage problems and solutions to drainage engineering in semi-arid and arid regions, which practically include all of the Mediterranean basin. The importance of these regions has in recent years been greatly enhanced, due to the fact that many of the developing nations belong to this category, and above all many of the oil-rich countries.

The system of units used throughout the text, with one single exception, is International System of Units (SI).

B.Z. Kinori
J. Mevorach

PART 1

CHAPTER 1

THE WATERSHED AND ELEMENTS OF HYDROGRAPHY

Symbols

A	– total area of watershed, km^2 ; area, km^2
A_1, A_2, \dots, A_n	– areas enclosed between the isochrones, km^2
A_r	– reduced area, km^2
a	– partial area, km^2 ; designation of line
b	– designation of line
C	– empirical coefficient
c	– designation of line
D	– point on the watershed
D_d	– density of drainage system index
D_t	– density of tributaries index
H	– point on the watershed
\bar{H}	– mean elevation of the partial area, m
i	– intensity of rainfall, mm/hr; grade of a tributary
K	– empirical coefficient
L	– total length of all the tributaries, km
$l_1, l_2 \dots l_n$	– particular length of any tributary
N_i	– total number of tributaries of a given grade i
Q	– discharge, m^3/sec
t	– time
t_c	– time of concentration of a watershed
t_r	– effective duration of the rainfall
V	– volume of water, m^3
v	– mean velocity, m/sec
x_B	– distance to point B, m
x_D	– distance to point D, m

1.1 Classification of Natural Watercourses

Precipitation on a land surface – after deduction of surface storage, infiltration and evaporation – will eventually form a surface runoff. Such surface flow is actually a wide-open-channel flow, either laminar or turbulent, known in hydrology as *overland flow*, and its hydraulic properties are still poorly defined [1, 2]. At the beginning such runoff is likely to flow as a thin sheet of water over the surface, but it will soon start concentrating in small natural depressions, or cutting small gullies in the soil. From this moment on, the flow will become a *channel flow* (for comprehensive discussion of its engineering aspects see [11]). These smallest distinct channels could be graded as No. 1 in a natural watershed system, see Fig. 1.1. Two or more No. 1 watercourses will eventually join together to form a larger creek, marked No. 2. The collector channel carrying water from two or more No. 2 channels is marked No. 3, and then successively No. 4, No. 5, etc. The last

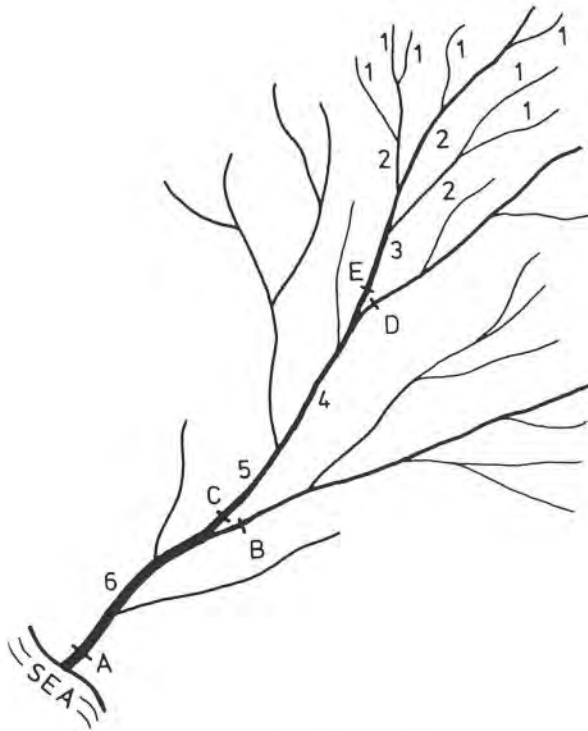


Fig. 1.1 Classification of watercourses

and the biggest stream channel – perhaps a large river – may be graded No. 10, or No. 20, and so on, depending on the branching of tributaries.

The point at which the waters from all the stream channels meet together (point A on Fig. 1.1) is generally known as the *point of concentration*.

Obviously, point of concentration should not be regarded as always necessarily located close to the outlet. There will be partial points of concentration collecting waters from one group of watercourses only (as points B and C) or other points which concentrate the water from even smaller groups (points D and E).

1.2 The Watershed

1.2.1 Definition

Total area from which surface runoff flows to a given point of concentration is called a *watershed* or a *catchment area*. Hence a watershed is always connected to a certain point of concentration, the lowest point of the respective basin. In Fig. 1.2, the point A denotes the final concentration point for the given watershed (beyond that point no runoff flow pertaining to the catchment area is possible), whereas at point H the runoff flow from the *partial* watershed area (hatched) is concentrated. Therefore, whenever specifying a watershed area of a given stream, it should always be clearly stated *upstream* of which point on the stream course is it related to ("the watershed of the river Po upstream of Cremona has an area of X km²"). By summarizing the partial watershed areas of all the tributaries, and by adding the areas draining directly into the stream, total area of the watershed above the concentration point is obtained.

The imaginary line delimiting various watersheds is known as *water-dividing line* or *water-divide*. Its configuration depends on the topography only, and it runs along the highest points of the surrounding area. Precipitations falling outside the area enclosed by this line will form a runoff flowing to another stream, over another catchment area (see Fig. 1.2).

The farther downstream along the stream the point of concentration, the more tributaries will join the stream and the larger the respective watershed. Growth of watershed area along the main watercourse can also be graphically represented, see Fig. 1.3. It is generally a good practice to plot separately watershed areas deriving from the right and left bank of the stream; by convention, the respective side of a stream is determined facing downstream the course of water.

Sudden increases of area indicate the inflow of a large tributary, the point at which the whole partial watershed of the tributary joins the watershed

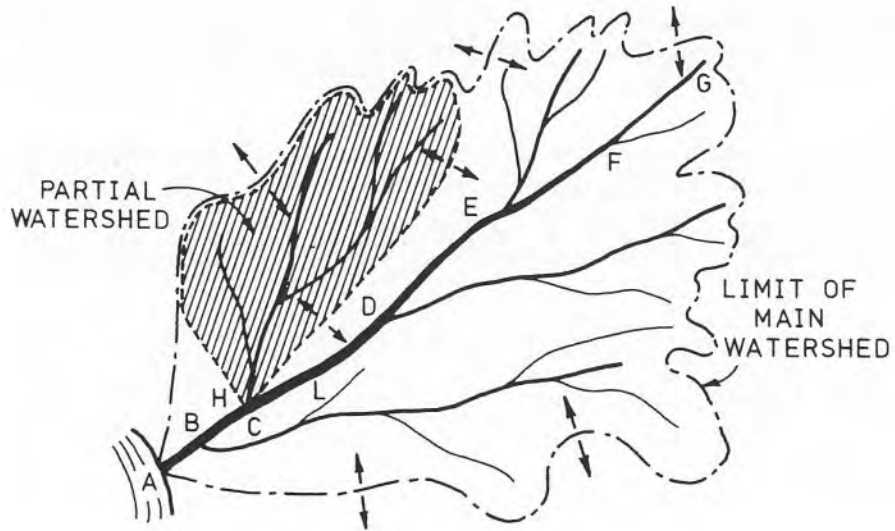


Fig. 1.2 Watershed boundaries.

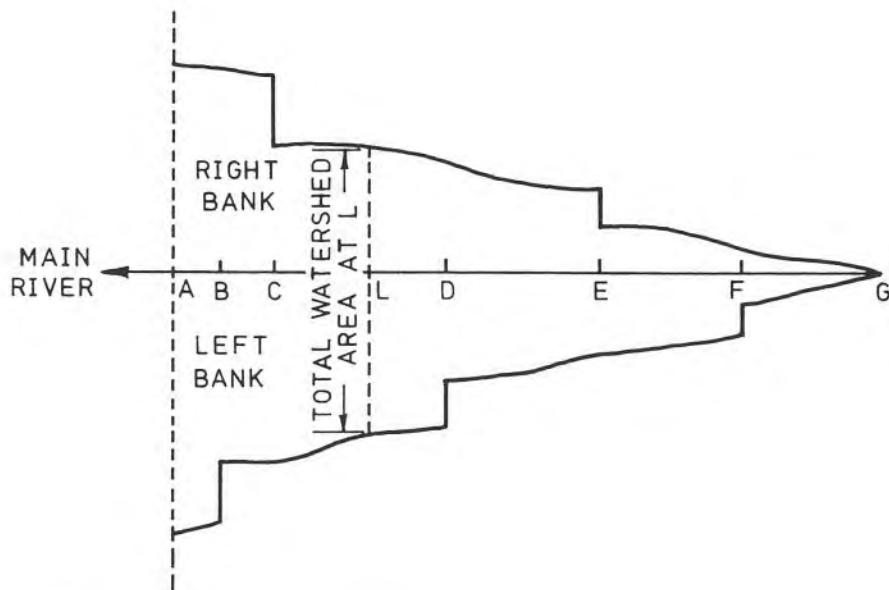


Fig. 1.3. Graphical representation of watershed area.

of the main watercourse. Gradual increases are derived mainly from over-land flow areas or small gullies.

1.2.2 *Effect of Watershed Shape on the Runoff Flow*

There are many factors which influence the hydraulic characteristics of a watershed as a part of an overall fluvial system. These factors may generally be summarized as follows:

1. Watershed geometry – which, among others, includes area, shape, location, length of streams, average main-stream slope, drainage density, etc.
2. Soil characteristics – type of soil, grain-size distribution, texture, erosivity, etc.
3. Vegetation cover – types and distribution, interception, transpiration, etc.
4. Hydrology – infiltration rate, groundwater, peak discharges, type of flow (perennial or ephemeral), yearly hydrographs, etc.
5. Geology – structure, bedrock and surface-soil types and distribution, etc.
6. Climate – temperature, precipitation type, seasonal occurrence and duration, frequency, etc.
7. Sediment yield – erosion and transport mechanism, sources of, etc.
8. Human influence – degree and type of development, construction activity, deforestation, etc.

While the characteristics under 2 to 8 have a preponderant influence on the volume of the runoff from a given watershed area, geometric characteristics affect the form of the hydrograph and the peak discharge. In the present paragraph effects of the watershed geometry will be briefly discussed, while the influence of some other characteristics are briefly reviewed in the next paragraph.

Watersheds can obviously have infinite variations of shape, according to the given topography. Analytical analysis of hydrograph forms and corresponding peak discharges have been carried out by many hydrologists [6, 7], and in Fig. 1.4 a very illustrative diagram of such an analysis is given [6].

Watersheds in Fig. 1.4 all have the same area and the same characteristics except the geometrical shape. Uniform rainfall intensity of duration $t_r = t_c$ is supposed to prevail. The symbol n_B denotes the ratio between the length of the watershed and its width.

In spite of the infinite number of possible watershed shapes, the majority may nevertheless be usually reduced to three main configuration groups:

(1) elongated watershed, (2) broad watershed, and (3) fan-shaped watershed, Fig. 1.5.

In order to illustrate more clearly the effect of watershed shape on the hydrograph and peak discharge, a simple numerical example will be analyzed.

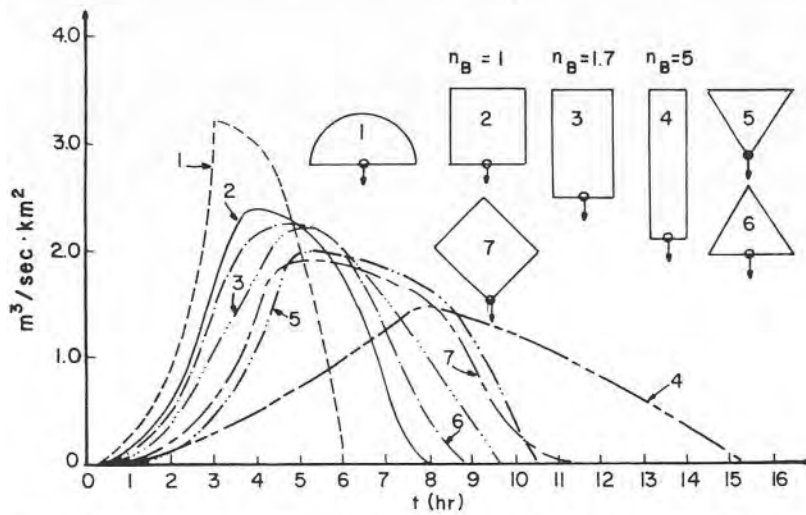


Fig. 1.4 Effect of geometrical shape of watershed on hydrograph form and peak discharge after [6].

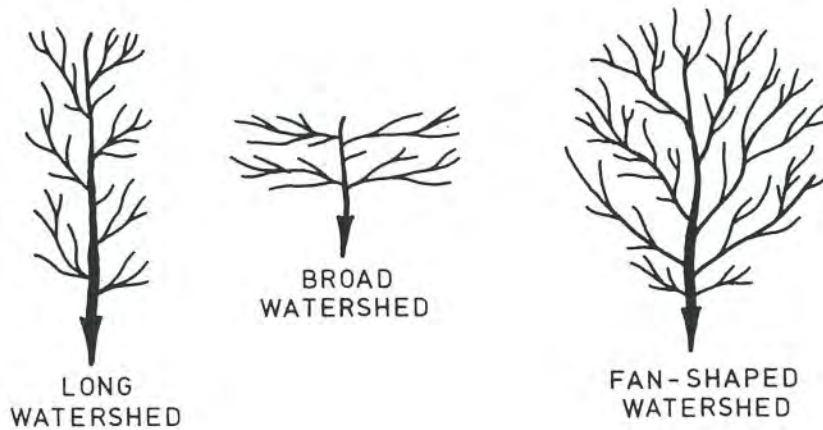


Fig. 1.5 Simplified watershed shapes.

Three highly imaginary watershed shapes are assumed, two rectangular and one semi-circular, with constant slope of the topography and without any tributaries. Although it is quite improbable for such types of watersheds to be found in nature, they may be encountered in urban areas, airports, etc. For reasons of simplicity, channel-storage and channel routing are neglected. The land-slope is supposed uniform towards the main stream channel.

Example 1.1

a. (see Fig. 1.6)

Data:

Width of the watershed:	2 km
Length of the watershed:	5 km
Area of the watershed:	$A = 10 \text{ km}^2$
Mean velocity of overland flow:	$v_1 = 0.1 \text{ m/sec}$
Mean velocity of channel flow:	$v_2 = 1.0 \text{ m/sec}$
Area of simultaneous rainfall:	the whole watershed
Uniform intensity of rainfall:	$i = 10 \text{ mm/hr}$
Runoff coefficient (indicating that part of the rainfall which turns into surface runoff):	$C = 0.4$

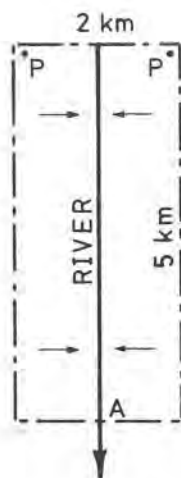


Fig. 1.6 (Ex. 1a).

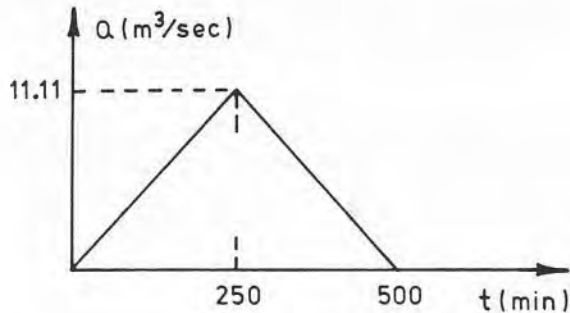


Fig. 1.7 (Ex. 1.1a).

Required: Draw the theoretical hydrograph for the given watershed at point A.

Solution:

Step 1 – Time of concentration (i.e. the time required for a water particle to arrive from the most remote point of the watershed to the point A):

$$t_c = \frac{1000}{0.1} + 5000 = 15,000 \text{ sec} = 250 \text{ min}$$

Step 2 – Assumption: duration of rain (t_r) equals the time of concentration (t_c): $t_r = t_c$

Step 3 – Until the end of the time of concentration, an ever increasing area will supply water to point A. At the time $t = t_c$, the whole of the watershed area supplies water, but because of the assumption that $t_r = t_c$, at the same moment the rain stops. At any time $t > t_r$, all parts of the watershed close to the point A cease supplying water, but it will continue to arrive from areas farther away. At the time $t = 2t_r$, the last drop of rain will reach the point A and the runoff will become zero.

Step 4 – At the time $t_r = t_c$, theoretical runoff discharge may be estimated by using the rational formula [2], [5],

$$Q_{\max} = ciA = 0.4 \times \frac{0.01}{3600} \times 2000 \times 5000 = 11.1 \text{ m}^3/\text{sec}$$

Step 5 – The theoretical hydrograph:

b) (see Fig. 1.8)

Data:

Width of watershed:	5 km
Length of watershed:	2 km
Duration of rainfall as in a:	$t_r = 250$ min
All other data as in case 1.1a.	

Required: Theoretical hydrograph for the watershed at point A.

Solution:

$$\text{Step 1} - t_c = \frac{2500}{0.1} + 2000 = 27,000 \text{ sec} = 450 \text{ min}$$

Hence, $t_c > t_r$

Step 2 – In order to compute the reduced watershed area which will be contributing runoff to the point A at the moment the rain stops, first the distances to points T and U should be determined.

$$\frac{X_T}{0.1} + 2000 = 15,000 \text{ sec}$$

$$\therefore X_T = 1300 \text{ m}$$

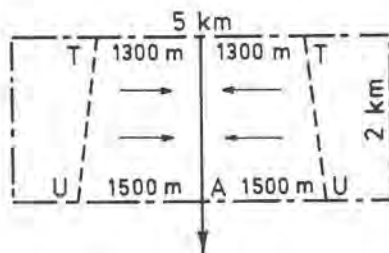


Fig. 1.8 (Ex. 1.1b).

$$\frac{X_U}{0.1} = 15,000 \text{ sec}$$

$$\therefore X_U = 1500 \text{ m}$$

Step 3 – Accordingly, the reduced area:

$$A_r = (1300 + 1500) \times 2000 = 5.6 \times 10^6 \text{ m}^2 = 5.6 \text{ km}^2$$

Step 4 – The estimated discharge (rat. form.),

$$Q_{\max} = ciA_r = 0.4 \times \frac{0.01}{3600} \times 5.6 \times 10^6 = 6.2 \text{ m}^3/\text{sec}$$

Step 5 – The theoretical hydrograph:

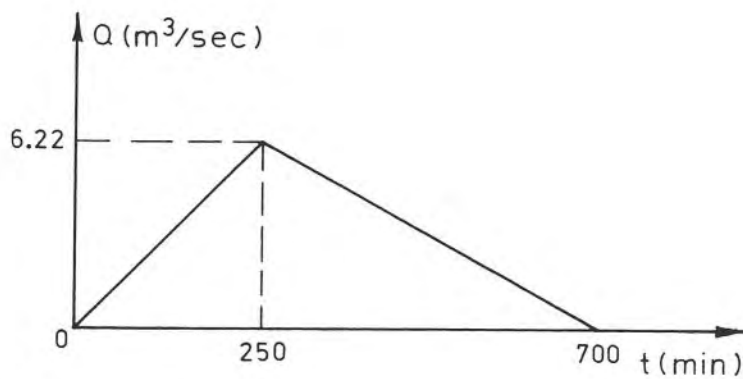


Fig. 1.9 (Ex. 1.1b).

By comparison of alternatives a and b, it can be seen that, for the same total area of the watershed, the same duration and intensity of rain and the same mean flow velocities, a broad and short watershed is likely to yield smaller maximum discharge than a narrow and longer one.

c) (see Fig. 1.10)

Data: Everything as in case 1.1a, but for the geometry of the watershed which now is assumed to be a semi-circle with a radius of $r = 2524$ m.

Solution:

Step 1 – Total area of the watershed:

$$A = \frac{2524^2 \times \pi}{2} \cong 10 \times 10^6 \text{ m}^2 \cong 10 \text{ km}^2$$

Step 2 – Using elementary mathematics, time of concentration is found to be $t_c \cong 25,370 \text{ sec} \cong 423 \text{ min}$

Hence, $t_r < t_c$.

Step 3 – Boundaries of the partial area supplying water to the point A when the rain stops, are found to be:

$$l \cong 2180 \text{ m}$$

$$X_B \cong 1275 \text{ m}$$

$$X_D \cong 1500 \text{ m}$$

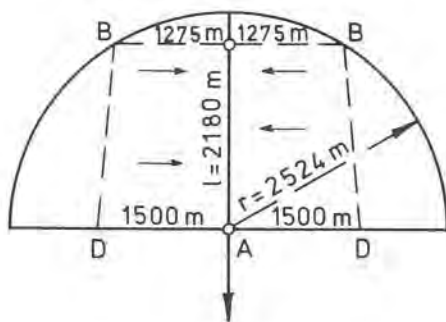


Fig. 1.10 (Ex. 1.1c).

Step 4 – Hence, the partial area supplying runoff to the point A at the moment the rain stops may be computed to be:

$$A_r \cong 6.5 \times 10^6 \text{ m}^2$$

Step 5 – The peak discharge estimated by the rational formula:

$$Q_{\max} = ciA_r = 0.4 \times \frac{0.01}{3600} \times 6.5 \times 10^6 = 7.2 \text{ m}^3/\text{sec}$$

Step 6 – The approximate theoretical hydrograph:

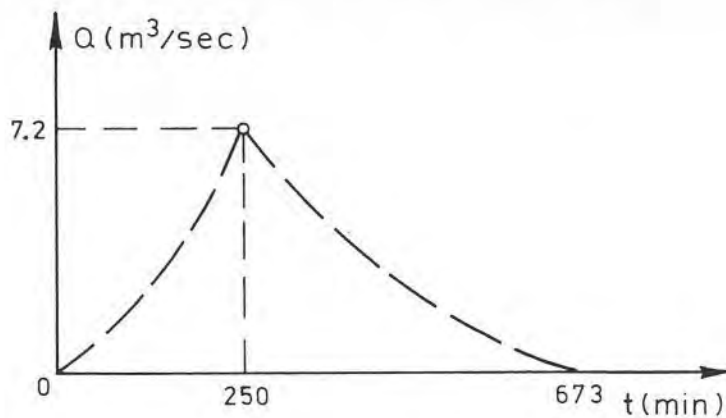


Fig. 1.11 (Ex. 1.1c).

As emphasized before, the assumed watersheds and their physical characteristics are rather hypothetical, not only on account of their simplified shape, but also because it very rarely occurs that on a long stretch of natural ground the flow remains overland flow. Normally, either there are low-grade natural channels, or the runoff water itself will cut gullies. In both cases, overland flow changes into channel-flow, with considerably higher velocities. Indeed, in some hilly areas, length of the overland flow very often is quite negligible.

In all the hypothetical watershed basins analyzed, the so-called “rational formula” had been used to estimate the discharge from the given rain intensity. The formula is generally acceptable for small watersheds, provided that the coefficient is judiciously chosen. In the case of larger and more complex

watersheds, appropriate hydrologic methods should be applied. Discussion of these methods is beyond the scope of the present text, and could be found in texts on engineering hydrology, such as [2] or [9].

1.2.3 Other Factors that Influence the Runoff Flow

Many additional factors are likely to complicate the flow pattern, but their discussion is rather in the field of surface hydrology than of drainage engineering. The most important of them will nevertheless be briefly reviewed, due to their primary importance.

In the first place there is the fact that shape, topography, slopes and runoff coefficients are never uniform, but in fact vary from place to place. Roughness of the flow channels and soil surface also change along a given watershed, not only in space, but in time as well (vegetation, seasonal changes, sediments, etc.).

Rainfall intensity also is unlikely to be uniform throughout the duration of the storm, and the precipitation generally does not necessarily cover simultaneously the whole watershed, with exception of very small catchment areas. As a general rule it is assumed that the larger the area covered by a storm rainfall, the lower will be its intensity. The relationship of watershed area to intensity cannot of course be expressed by some universal mathematical function, since it varies from location to location. However, well-organized meteorological services often do prepare area-intensity charts for important locations within their national borders.

An important factor influencing the peak discharge from a given watershed is the rain-progress direction. If the movement of rain clouds coincides with the direction of flow in the stream channel, the peak discharge is likely to be considerably higher than for a windless cloud cover; when the clouds move in the opposite direction, the peak discharge may be expected to be much lower [2].

As a consequence of the above mentioned factors, and indeed many more which have not been referred to, there obviously does not exist a general formula that could be applied, but rather every case should be studied according to its own characteristics. For all that, there are a few more or less common features typical to certain watercourses, and these will be briefly reviewed in the following.

Hydrograms of relatively small and mainly mountain streams (grades 1, 2 and sometimes even 3, see Fig. 1.1) react rapidly to the onset and to the cessation of the rainfall. Such streams may have no flow at all during dry seasons; on the other hand, discharge will reach the peak shortly after the end of the highest-intensity rainfall (a few minutes or hours, up to one day),

and the flow then will continue for a day or so before the discharge again falls off to zero, see Fig. 1.12a. The ratio Q_{\max}/Q_{\min} tends to infinity as the dry season approaches, but even during the rainy season it generally has high values. Large fluctuations of discharge induce fluctuations of the same order of magnitude in velocity and sediment transportation. It has often been observed in such streams that during the dry season the stream-bed is unobstructed and with adequate cross section, while after a few high-intensity rainfalls, the bed is found to be completely clogged by sand and gravel.

In medium-size streams – mainly in foothill regions – differences in the time of concentration of the tributaries bring about a certain balance and compensation of the varying rainfall intensities. The ratio Q_{\max}/Q_{\min} is generally smaller, and flood waves have a longer cycle, see Fig. 1.12b.

Coming to large rivers (mainly on flat land), even the tributaries – themselves also at least medium-size streams – have a partly balanced flow regime, and this balancing action becomes more pronounced in the main stream itself. The hydrogram is flat, and the flood waves have very long periods, often weeks and sometimes even months, see Fig. 1.12c.

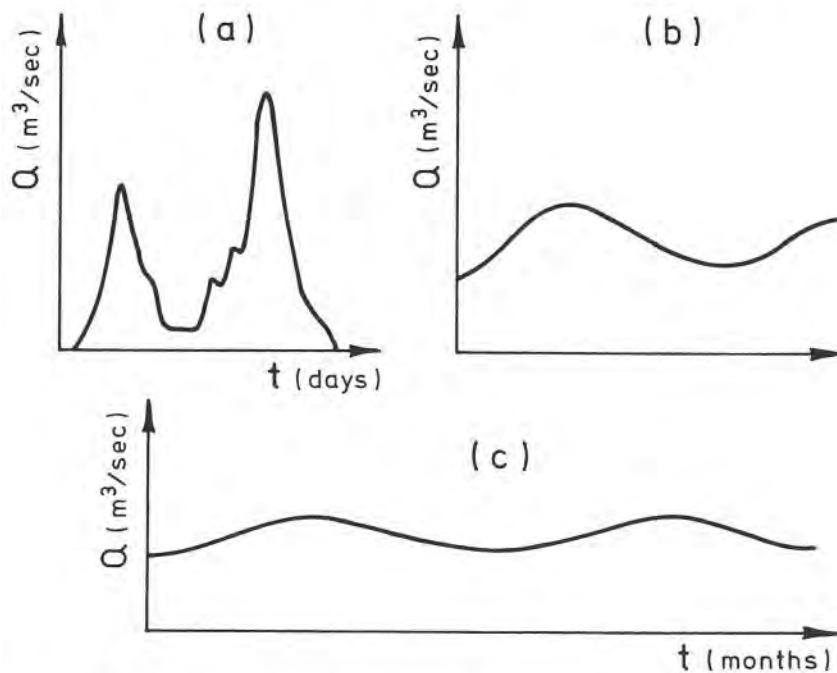


Fig. 1.12 Characteristic stream hydrograms.

1.3 Relative Size of the Watershed

Much has been said and written about *small watersheds*, and about the hydrology of small watersheds. The boundary between small and large watersheds has been arbitrarily set at about a few tens of square kilometers, but in fact there are as many recommended boundaries as there are researchers and authors.

However, all these more or less arbitrary figures probably have little justification. It would perhaps be more correct to state the following: a watershed that has a main watercourse which reacts quickly to precipitation (say, within 1–2 days), could be considered as small, while if its reaction lag is longer, it will behave as a large one. In mountain areas, where flow velocities are high, of both the overland flow and along the major streams, runoff waters will reach the main stream within a few days; in a hilly country of mild slopes, however, flow velocities will be much lower, and accordingly the same area may have the characteristics of a larger watershed.

It should be mentioned here that it is customary to designate as “small watersheds” catchment areas up to about roughly 30–40 sq. km. These small basins, particularly characteristic of Mediterranean and semi-arid regions, have in fact many distinctive features which set them apart from conventional and larger watersheds. In the following chapters these particular features will be briefly reviewed and discussed.

1.4 Some Characteristic Curves Describing Watersheds – Indices

There are many useful and helpful characteristic curves and indices used in the engineering hydrology to better describe and gain clearer understanding of the watershed under study. Some of these auxiliary tools will be discussed in the following.

1.4.1 Hypsometric Curve

In larger watersheds important information may be obtained from the hypsometric curve, which graphically describes the progressive change of the cumulative area with the change of elevation (above the mean sea level) throughout the basin, see Fig. 1.13. This information is an important factor as far as temperatures, precipitations and evaporation are concerned.

Hypsometric curve is obtained by plotting the areas enclosed between successive topographic contour lines on a graph having as abscissa areas (in km^2) and as ordinate absolute elevations (in m). Any point taken on the

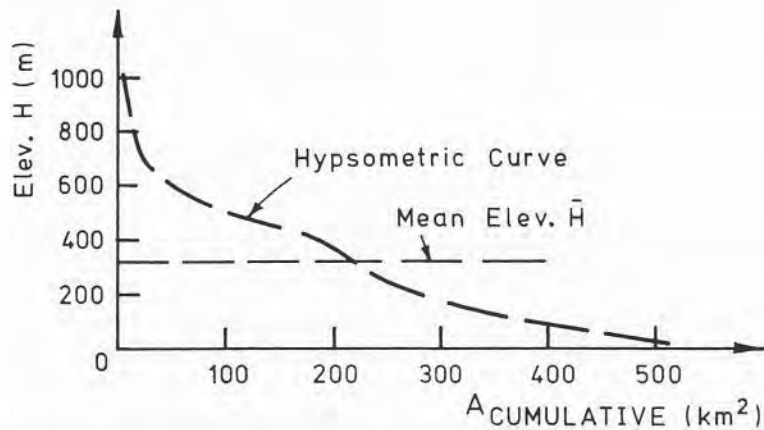


Fig. 1.13 Hypsometric curve.

curve gives the cumulative area for which the elevation is given on the ordinate. The *mean elevation* of the basin may be computed from the expression

$$\bar{H} = \frac{\sum a \times H}{A} \quad (1.1)$$

where a – partial area between two successive topographic contour lines, in m^2 , H – mean elevation of the partial area, in m , A – total area of the basin, in m^2

The very shape of the hypsometric curve for a given watershed may provide hints as to the formative stage of the stream [6].

1.4.2 Logitudinal Profile and Mean Slope of the Main Stream

Longitudinal profile along the main stream of the watershed will often provide valuable information about its properties and the extension of its various parts in respect of the elevation, see Fig. 1.14.

Upper course – Generally large longitudinal slopes, hence high velocities of flow, and continuous erosion of the bed. Typically erosive stream characteristics.

Middle course – Longitudinal slope of the stream gradually eases, tributaries join the main stream, and therefore often sudden changes of flow regime. Although stretches of erosion and deposition frequently exchange,

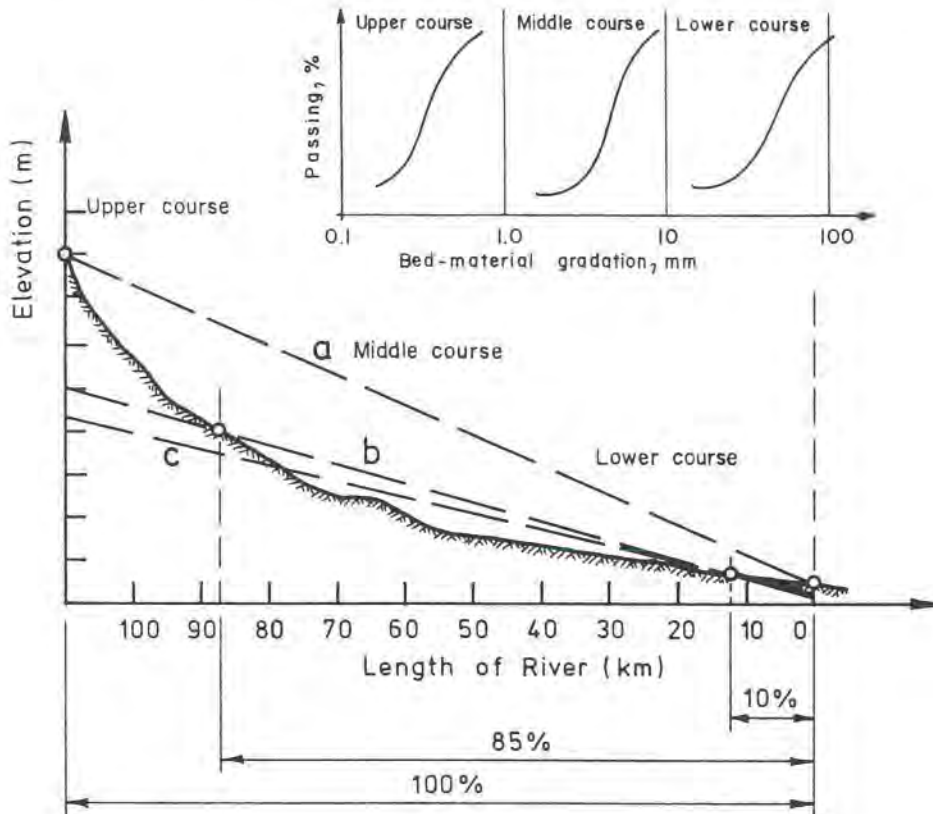


Fig. 1.14 Longitudinal profile and mean slope.

Line a – obtained by connecting the extreme points of the stream; Line b – connecting the points on the longitudinal profile corresponding to 10% and 85% of the total length; Line c – line of compensation, drawn in such a way that the triangular area it encloses between the coordinate axes is equal to the total area between the longitudinal profile and the coordinate axes.

both in space and time, this transitional reach of the stream is on the whole generally the most stable and balanced part. Stream characteristics obtained from the middle course are frequently used as basis for the design of stream training projects (see par. 10.3).

Lower course – Longitudinal slope flattens, discharge increases. Gradual deposition of sediment eroded upstream, hence relatively short-period shifting and changing of the main stream channel.

According to Shulits [14], the concave horizontal profile of a stream channel could be given in terms of distance along the stream as

$$I_x = I_0 e^{-\alpha x} \quad (1.1a)$$

in which I_x – the longitudinal slope at any station a distance x downstream from any reference point, I_0 – the slope at the reference point, α – an empirical coefficient of slope change.

Generally speaking, there are three methods to obtain the mean slope of a stream, and the choice between them for any given stream will depend on the judgement of the engineer (see Fig. 1.14a, b and c).

Catchment area itself is obviously a three dimensional plane crossed by many streams of secondary grades. In many cases the mean slope as defined above is also quite representative of this plane, and no further study is needed. In some other cases there may be the need for more detailed information. This may be obtained by dividing the watershed into smaller areas by means of a rectangular net and computing the slopes at the nodes. Thus it is easily possible to obtain a graph of the watershed slope vs. frequency, see Fig. 1.15.

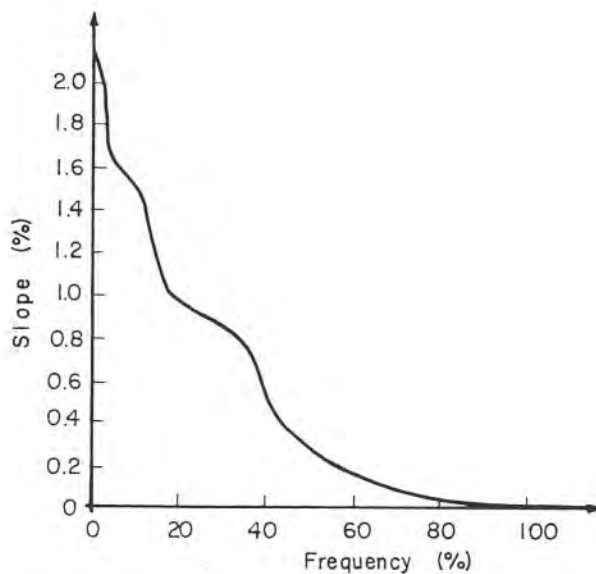


Fig. 1.15 Slope vs. frequency curve.

1.4.3 Cumulative Duration Curve

One more of the characteristic curves widely used in drainage engineering should be mentioned in this brief survey of stream hydrography. It is the *cumulative duration curve of stream discharge*, obtained by plotting the cumulative duration of observed discharges against time, see Fig. 1.16.

Any point on the curve indicates a discharge, Q , with the corresponding duration, t , related to a period of 365 days, meaning that during t days out of 365 days of the year, stream discharge was equal to or higher than Q .

Discharge duration curves obtained from measurements during many years (let us say 20 years or more) give the possibility for statistical elaboration. Of particular interest for the practicing engineer is the probability of occurrence of exceptionally high or low rates of flow. Family of curves thus obtained is similar to those shown in Fig. 1.16a, with the ordinate giving the discharge in m^3/sec and abscissa number of days.

Some of the particular values of Q , used in drainage engineering, are also shown on the graph:

Normal high flow – Discharge corresponding to the duration of $\frac{1}{4} \times 365$ days,

Normal low flow – Discharge corresponding to the duration of $\frac{3}{4} \times 365$ days,

Median discharge – Discharge corresponding to $\frac{1}{2} \times 365$ days,

Mean discharge – Discharge derived from the relation $\Sigma V/t$, in which ΣV – total volume of water which passed the outlet section during the observation time t ,

Modal discharge – Discharge corresponding to the highest frequency.

A similar diagram may be obtained if instead of discharge, water level (stage) is plotted on the ordinate, Fig. 1.16a. As an example, the water depth should be expected to be lower than 6.5 m during about 290 days, with a probability of 50%.

1.4.4 Indices

Several indices also are in general use, with the aim of gaining better characterization of a watershed under study, and enabling the engineer to make comparative analysis. Here two of them will be mentioned [3]:

1. *Density-of-tributaries index*, defined by the relation

$$D_t = \frac{N_i}{A} \quad (1.2)$$

in which N_i – total number of tributaries of a given grade i , A – total area of the watershed.

According to the American experience, a good correlation could generally be obtained between the density-of-tributaries index D_t and the grade of the tributaries, using the general expression

$$\log D_t = KN_i - C \quad (1.3)$$

where K and C denote empirical coefficients which have to be established for every specific natural stream.

2. *Density-of-drainage-system index*, given by the relation

$$D_d = \frac{L}{A} \quad (1.4)$$

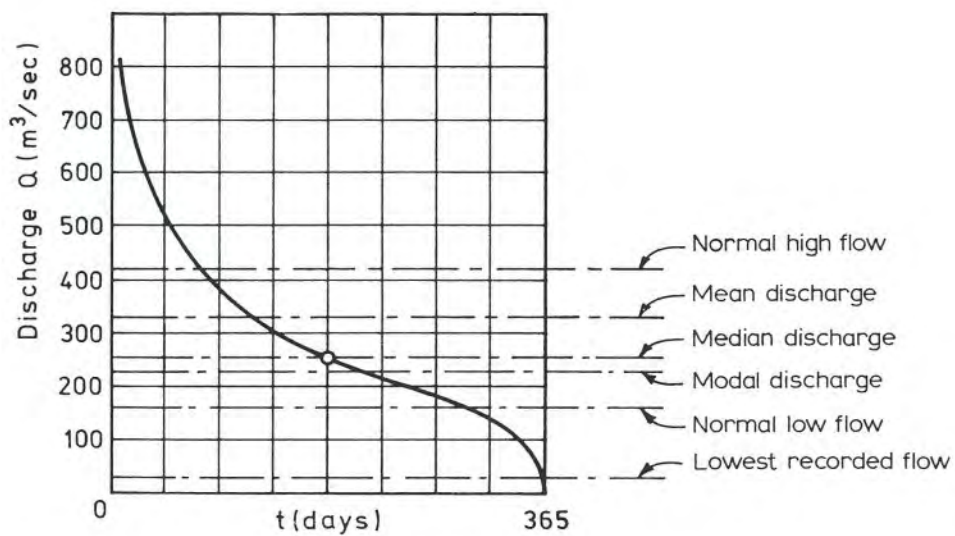


Fig. 1.16 Cumulative duration curve (discharge).

where $L = l_1 + l_2 + \dots + l_n$ – total length of all the tributaries, of any grade, within the system, A – total area of the watershed.

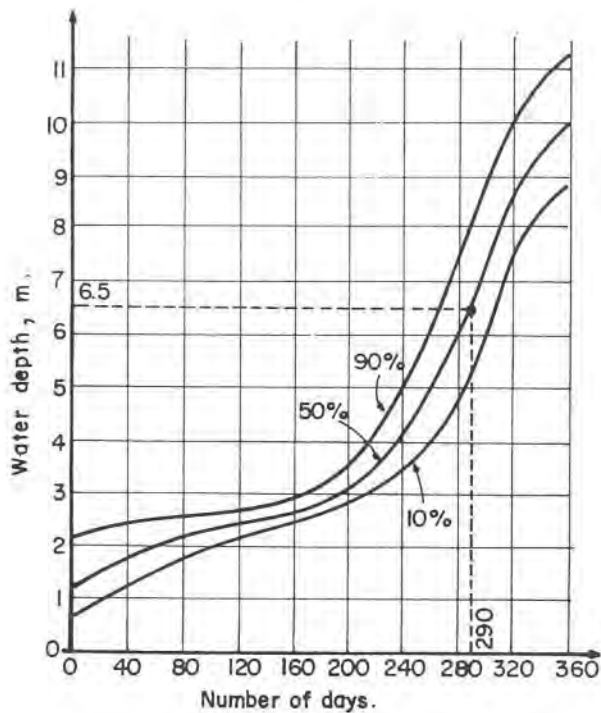


Fig. 1.16a Cumulative duration curve (stage), River Niger at Lohoja, after [12].

1.5 Method of Isochronal Lines

When the discharge of the main stream is directly influenced by the rainfall, a fairly reliable method for the estimate of peak discharges is the *method of isochronal lines* [4, 5]. Isochronal lines connect the points of equal runoff travel time to the gauging station. It is obvious that sound engineering judgment and a fairly good estimate of the channel flows – regarding discharge, cross section, slope, etc. – are essential.

It is assumed that the stream system of the given watershed is known and mapped out, see Fig. 1.17. It is further assumed that the peak discharge at the outlet A will occur when $t_r \geq t_c$. The engineer has to obtain from the

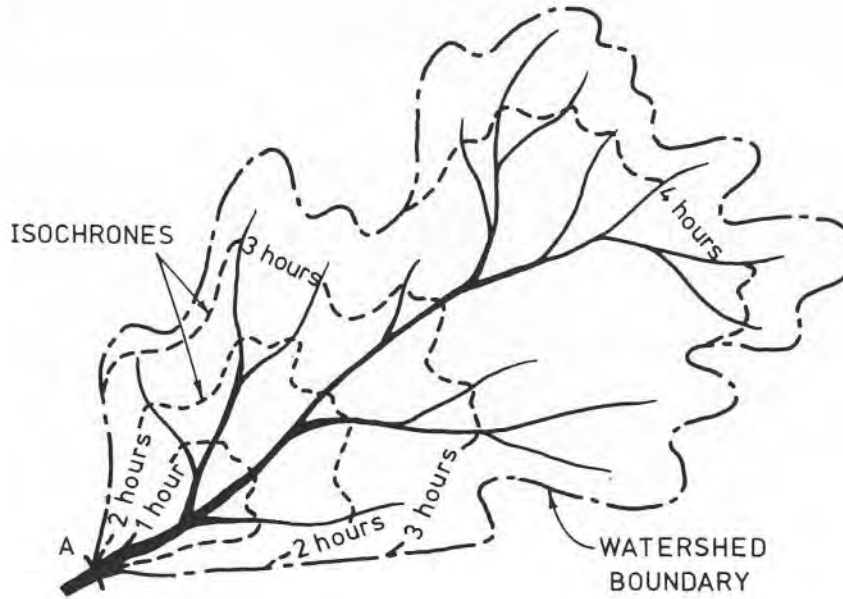


Fig. 1.17 Isochronal watershed map.

meteorological service rainfall intensities, i , at the given region for various hourly rain durations, referring to a specified *return period*. This return period (or cumulative frequency) to be used as a basis for the calculation will mainly depend on economic considerations (for instance, if the purpose of the project is flood protection of a purely agricultural area, a return period of about 50 years, or 2% cumulative frequency, is generally considered as adequate).

On the topographic map and in a scale adequate for the purpose, points of equal travel time to the gauging station must be located. After that, with due attention to topographical features of the watershed, isochronal lines are drawn, and the areas enclosed between them measured. Let these areas be denoted $A_1, A_2 \dots A_n$ respectively. Rain intensity is supposed to be constant in space, but not in time; hence the respective average rainfall intensities will be $i_1, i_2 \dots i_n$.

After time t_1 , the discharge reaching the gauging station will be

$$Q_1 = i_1 A_1 \quad (1.5)$$

After time t_2

$$Q_2 = i_2 A_1 + i_1 A_2 \tag{1.6}$$

Hence the general expression for the discharge Q at the gauging station after time t_n

$$Q_n = i_n A_1 + i_{n-1} A_2 + \dots + i_1 A_n \tag{1.7}$$

In order to take into account all the losses, each term on the right side of Eq. (1.7) should be multiplied by the appropriate flow coefficient. If the intensity of the rainfall is constant in time also, Eq. (1.7) becomes, of course, much simpler.

Maximum discharge at the gauging station for a given rainfall intensity will be obtained when the rain duration, t_r , is equal to the concentration time, t_c , for the whole of the watershed. On the other hand, the longer the duration of the rainfall, the lower generally will be its intensity. Hence it is

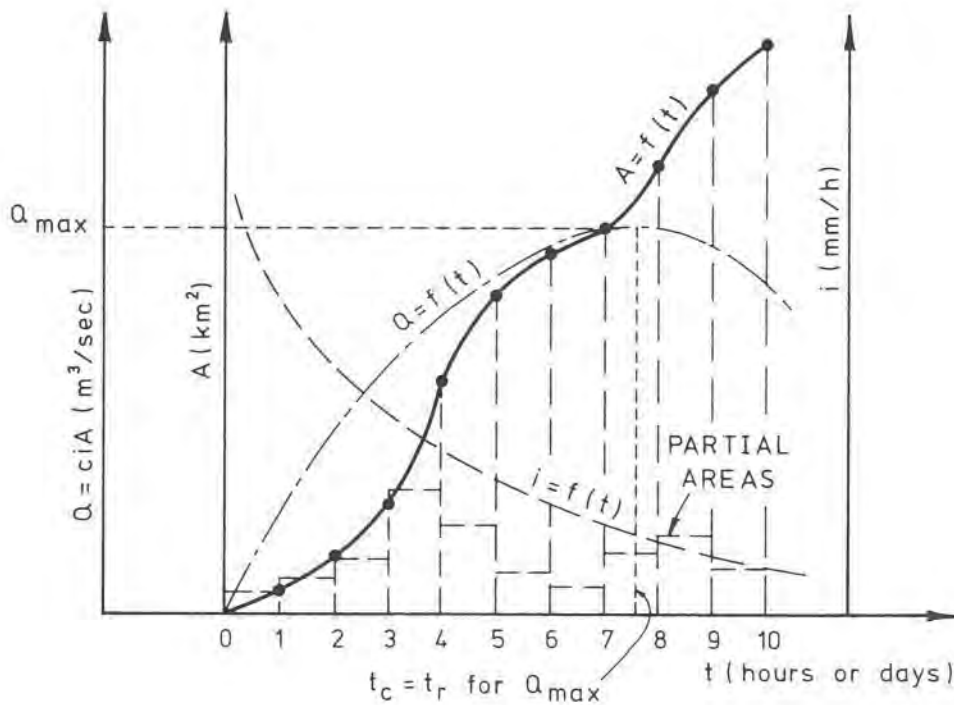


Fig. 1.18 Characteristic curves for the method of isochronal lines.

generally not clear in advance which rainfall duration is going to yield the highest discharge.

In Fig. 1.18 a qualitative diagram of the characteristic curves for the method of isochronal lines is shown. The function $A_i = f(t_i)$ depends on many parameters, as for instance on topography, soil conditions, vegetation etc., and can, therefore, rarely be expressed in form of a mathematical function. The relation $i_i = f(t_i)$ is generally of somewhat more constant nature, particularly if it is the result of statistical analysis.

The method as such is fairly reliable and, if properly applied, can be accurate. Its limitation, however, is the fact that it is difficult to determine the position of isochronal lines on the map of the watershed.

References

1. V.T. Chow, Open-Channel Hydraulics, McGraw-Hill, New York, N.Y., 1959.
2. R.K. Linsley et al., Applied Hydrology, McGraw-Hill, New York, N.Y., 1960.
3. D. Tonini, Elementi di idrografia ed idrologia, vol. II, Libreria Universitaria, Venezia, 1966.
4. D.M. Gray, editor, Handbook on the Principles of Hydrology, Water Information Center Inc., Huntington, N.Y., 1973.
5. J. Nemeč, Engineering Hydrology, McGraw-Hill, London, 1964.
6. B.D. Richards, Flood Estimation and Control, Chapman & Hall, London, 1950.
7. E.M. Wilson, Engineering Hydrology, Macmillan, London, 1969.
8. N.C. Grover and A.W. Harrington, Stream Flow, Dover, New York, N.Y., 1966.
9. V.T. Chow, Handbook of Applied Hydrology, McGraw-Hill, New York, N.Y. 1964.
10. N.P. Chebotarev, Theory of Stream Runoff, Isr. Progr. Sci. Transl., Jerusalem, 1966.
11. A.J. Raudkivi, Hydrology, Pergamon Press, Oxford, 1979.
12. Nedeco, River Studies, Niger and Benue, North Holland, Amsterdam, 1959.
13. C.O. Wisler and E.F. Brater, Hydrology, Wiley, New York, N.Y., 1949.
14. S. Shulits, Rational equation of river-bed profile, Trans. Am. Geophys. U., 22 (1941).

CHAPTER 2

ELEMENTS OF HYDROMETRIC MEASUREMENTS

Symbols

A	– area, m ²
A_L	– area of the diagram
b, b_1, \dots, b_i	– width or spacing, m
C	– drag coefficient
C_0, C_1	– concentration of the indicator, mg/l
C_{wl}	– wash-load concentration
c	– center of gravity; variable concentration
d	– water depth, m
d_1, d_2, \dots, d_i	– water depth at a given section, m
d_c	– critical depth, m
g	– acceleration of gravity, m/sec ²
H	– water stage, m
i, \dots, i_n	– number of section
J	– hydraulic gradient
K, K_1, K_2	– conveyance for open-channel flow
L, L_1, \dots, L_n	– length, m
n	– any number; Manning coefficient; number of items in a statistical population
Q	– total discharge, m ³ /sec
q, q_1, \dots, q_i	– partial discharge, m ³ /sec; rate of indicator injection
q_s	– partial sediment discharge, m ³ /sec/m
q_w	– partial water discharge, m ³ /sec/m
R	– hydraulic radius, m
s	– standard deviation
S, S_1, S_3, \dots	– signal emitters or reflectors; scale for distances

T	– cumulative duration
t	– time
U_0	– volume of the injected indicator
V	– local velocity, m/sec
\bar{V}	– average velocity, m/sec
V_b	– bottom velocity, m/sec
V_s	– surface velocity, m/sec
$V_1, V_{0.8}$	– local velocity at given depth, m/sec
v	– point velocity at any depth, m/sec
W	– submerged weight of the wing, N
w	– rising velocity of air bubbles
x	– coordinate
y, y_1, \dots, y_i	– coordinate; partial depth
z	– coordinate
α	– angle of inclination
ρ	– density, kg/m ³
σ	– standard deviation of population

2.1 Introduction

A major part of our knowledge and understanding of the morphology and behaviour of natural watercourses has been gained or derived from many long-term observations and measurements. This is necessarily the case with all engineering branches that rely heavily on empirical data in order to build some sort of coherent causal system into the bewildering and ever-changing variety of natural phenomena. These measurements, as far as alluvial channels are concerned (see par. 3.1), can generally be classified into the following groups:

1. Geodetic measurements,
2. Position fixing,
3. Water-level measurements,
4. Depth sounding,
5. Velocity measurements,
6. Discharge measurements, and
7. Sediment transport measurements.

Omitted from the list are measurements dealing with water quality, salinity, etc., because they are outside the scope of the present text. In the concise survey that follows, the first two measurement groups, which actually belong to surveying methods, will not be included; strictly speaking,

they do not make part of hydrometric measurements, but are auxiliary to them. Any textbook on surveying methods will do in this respect. Group 4, concerning water-depth measurements, being in many of its aspects a boundary group, will also be reviewed rather briefly.

2.2 Water-Level Measurements

2.2.1 Staff Gauges (Fig. 2.1a)

One of the simplest ways for detecting and measuring changes in water levels of a stream is by means of a graduated pole sunk vertically into the water and fastened to bed, banks or some stable structure, if available, Fig. 2.1a.

Often it may prove to be impractical for a single gauge to meet the full range of water levels, from the low mark to the peak-flow stage. In such a case, a series of gauges at different heights are placed at a given site, called a *sectional staff gauge*. In artificial channels use is sometimes made of *inclined staff gauges* (Fig. 2.1c) laid on side slopes, and graduated in such a way to give direct readings of the vertical depth.

Frequency of water-stage readings generally is determined by the type of the stream, by the scope of information intended to be obtained, but also by the available manpower and the accessibility of the measuring site.

Fixed bench-mark on the shore serves in the first place for regular checks on possible vertical displacements of the gauge; it can also serve to connect the site to the main geodetic system of position-fixing and levelling.

Some regular maintenance has to be provided, as gauges may have to be replaced if washed away by bank erosion, or repaired when damaged by

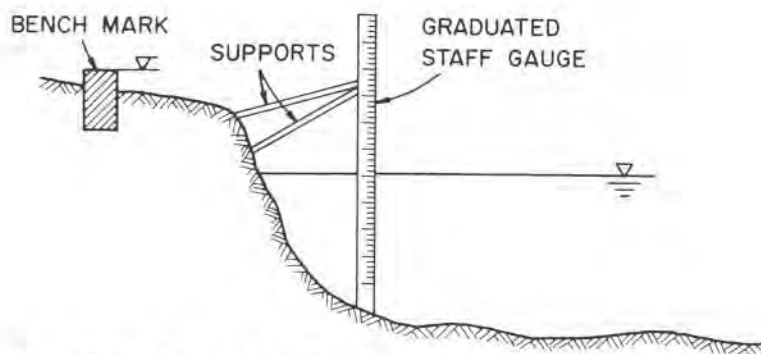


Fig. 2.1a. Staff gauge (sketch not to scale).

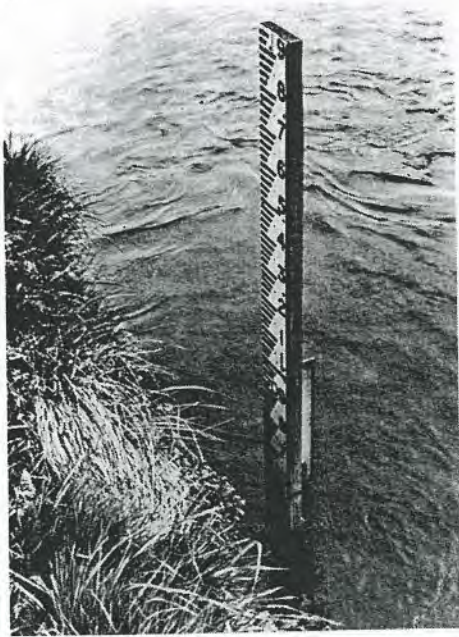


Fig. 2.1b. Staff gauge (by courtesy of CIRIA, London).



Fig. 2.1c. Inclined staff gauge (by courtesy of CIRIA, London).

floating debris or similar causes. Accuracy of staff-gauge readings is generally not very high, but they have advantages of being inexpensive, easy to erect, simple to use, and hence readings often can be entrusted to untrained local inhabitants.

2.2.2 *Suspended-Weight Gauge*

This is also a relatively simple device for measurement of water-level changes, but unlike staff gauge, it is a portable instrument used in connection with any suitable fixed structure, such as bridges or streamside constructions. Water levels are determined by means of a cord or steel tape held tight by a suspended weight, and lowered from a fixed point until it touches the water surface (Fig. 2.2). There are on the market various gadgets that facilitate the measurement of cord length.

It is often difficult to visually determine when the suspended weight touches the water surface, particularly in case of waves. A simple electrical circuit that lights up a small control lamp as soon as the weight touches the water can be of considerable help in this respect.

Such gauges are handy and cheap whenever no long-term measurements are needed, but only a limited number of readings.

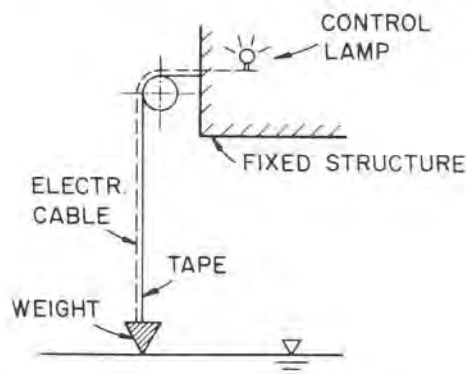


Fig. 2.2. Suspended-weight gauge.

2.2.3 *Portable Automatic Gauge*

There are often cases where no local manpower is available for daily readings of the gauge and recording it on especially prepared forms, or where large number of daily stage readings is required. Automatic stage recorders can then be used.

Light portable gauge generally requires no more than about a one-hour job to be placed in position. It consists of a steel tube sunk vertically into the stream; holes drilled in the tube allow water in it to rise or fall with changes of the stream level. A freely movable float at the end of a thin cable, held taut by means of a counterweight, is connected to a recorder pen housed in a protective cylinder placed on the top of the tube. The pen continuously records to a reduced scale the changing water stage upon a roll of paper wrapped around a drum kept slowly rotating by a clockwork. Self-recording capacity by a clockwork is generally of about 7–8 days.

2.2.4 Permanent Automatic Gauge

At those places along a watercourse where continuous water level recording is wanted, usually a permanent structure will have to be erected. Recording instrument is housed in a small shelter connected to a stilling-well beneath it, see Fig. 2.3.

Water from the stream reaches the well through a connecting pipe, and changes in level are transmitted to the recording instrument by means of a float and a counterweighted cord.

Water-level readings taken through a relatively large stilling-well are likely to be more accurate than by means of any previously mentioned device, because waves and uprush disturbances are eliminated inside the well. However, the ratio of the well area to the area of the connecting pipe should not be too large, particularly in streams with high velocities of flow or rapid level changes, in order to avoid possible level differences between the well and the watercourse.

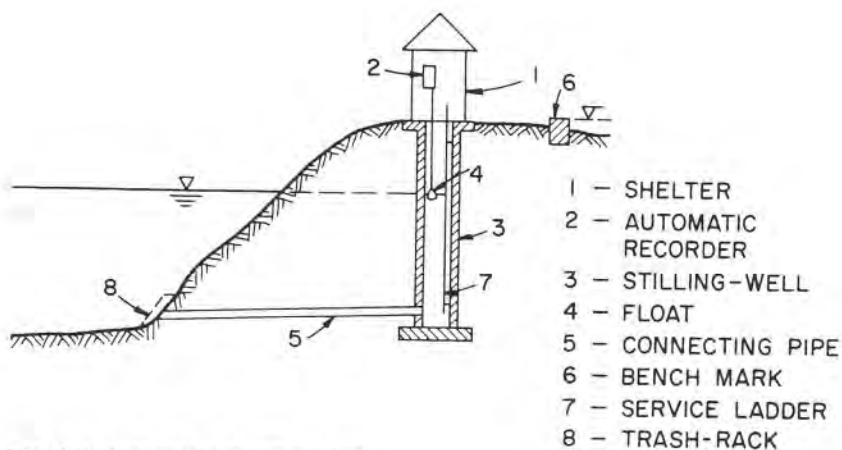


Fig. 2.3. Automatic-gauge station.

It is essential that both the connecting pipe and the stilling-well be thoroughly cleaned from time to time. This can easily be done with water pumped from the stream. In arid and semi-arid zones, where practically no base-flow is available between sudden flood-waves, and the stream-bed remains dry during long periods of time, it is desirable to have automatic recording instruments that can be left unattended during long intervals. In order to get round the inconvenience of frequent obstructions of the connecting pipe, and hence the need for inspections and costly cleanings, an electronic gauge is presently under development in many hydrometric laboratories [1]. It is based on a strain-gauge placed on the bed of the stream that detects changes in water-level (variations of pressure) and transmits them electronically to a potentiometer which drives the pen of the recorder, see Fig. 2.4. Converted pressure signal may also be directly conveyed by means of a long-distance wireless transmitter to a central recording station, which further simplifies the data-collecting process. Generally, the signal transmission enters into operation when triggered from the central station.

Other types of gauges less frequently used are *bubble-type pneumatic gauge*, which measures the air pressure needed to produce bubbles against the water pressure; *electromagnetic gauge*, which is based on a high-frequency oscillator placed in a stilling-well at a fixed position, and the measurement of the time interval in which the signal is reflected back by the water surface in the well, connected to the channel; or finally the so-called *Archimedes gauge*, consisting of a staff partly suspended in the water and

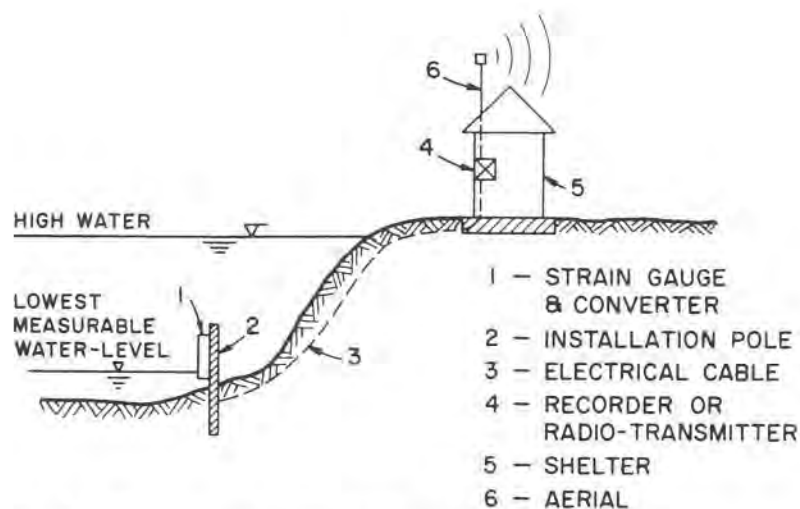


Fig. 2.4. Electronic water-level gauge.

attached to a sensitive spring which measures variations of uplift forces due to variations of the stream level.

2.2.5 Peak Stage Indicator

At locations where no permanent hydrometric recording station is available, a simple maximum-water-level-indicating gauge may be of great advantage. Information about the peak stage reached during the passage of the flood wave is often a valuable contribution to the analysis of flows in watercourses and flood protection studies in general. Occasional gauge readings by hydrometric personnel may easily miss the highest stage.

The simplest form of such an indicator is a staff gauge covered by some sort of special paper or dye which change hue upon wetting. Maximum water stage may thus be read many days after the event took place. There are, of course, other similar devices available, but the general idea is identical to all of them.

2.3 Depth Sounding

2.3.1 Sounding Rod

This is undoubtedly the simplest method for the depth sounding. The conveniently graduated rod, at whose lower end a square plate is fixed, is sunk into the water from an appropriate vessel until it reaches the bottom; the depth is then read on the scale, the zero being at the base of the rod. The rod must not necessarily be in the vertical position, provided the angle it makes with the water surface is duly taken into account.

The use of the sounding rod in shallow water is more advantageous than any other method, and if proper precautions are taken, the expected accuracy of readings is of 1–3 cm, which is adequate for routine $H=f(t)$ or cumulative duration curves (see Fig. 1.16a), but may not be accurate enough for the determination of water-surface slopes over relatively short reaches.

2.3.2 Sounding Lead Line

When water depth is large, the use of the rod becomes unwieldy, and then a cable-and-weight are more advantageous. The sounding operation is carried out, as in the previous case, either from a boat or a *cableway* (see par. 2.5.1.2 on discharge measurements). The weighted cable is lowered into the water, either by hand-line suspension or reel suspension, until the weight touches the bottom, and then the depth is read on the tightly held line.

The accuracy of the sounding is often not satisfactory for the following disadvantages:

a) it is difficult to keep the line vertical in flowing water or from a moving vessel; b) position of the weight is sometimes uncertain, hence also the zero mark; on very soft beds, penetration of the weight may be unavoidable, c) if the line is made of a hemp or flax rope, there may be shrinkage or stretching when wetted (wetting the line before the use goes a long way to eliminate this drawback); d) in deep watercourses, the line takes on a curved shape, and readings should therefore be corrected (correction tables are available).

Field experience has shown that in routine soundings with the lead-line, the overall accuracy is generally less than with the rod. In depths of 1–3 m, the expected error is 4–8 cm, whereas in greater depths it may reach as much as 10–20 cm, and even more.

A common drawback of both the sounding rod and the lead-line is that they do not give a continuous depth profile along the measuring route, and hence minimum or maximum points may be missed. However, for depths up to about 1.5 m, these two methods have a clear advantage over any other more sophisticated method, not only as to the cost, but also in regard to the accuracy.

In non-perennial watercourses of arid and semi-arid zones, bed cross-section measurements are carried out during dry periods according to the standard surveying methods.

In addition to the already mentioned requirements for a proper location of gauging stations, [37] may be consulted for the complete and detailed list. The same reference also deals extensively with questions regarding sources of errors and expected levels of accuracy.

2.3.3 *Echo Sounding*

This method has been borrowed from nautical depth sounding, and it is based on the use of the physical properties of the sound propagation in water. High-frequency sound impulses emitted from a base vessel are reflected from the bottom and received back as an echo. The time interval between the emission of the signal and its back-reception is proportional to the depth of the water. Thus practically a continuous depth profile can be obtained [2].

Today there are many types of echo-sounders on the market, and their specific electronic or mechanical properties cannot be discussed in the present text. In modern instruments there are automatic built-in adjustments for the water temperature and its density. Use of echo-sounders in shallow water often requires taking into account horizontal distances within

the set-up of the apparatus itself, as well as the position of the oscillator below the water surface.

It is generally believed that the overall accuracy of an echo-sounder is better than lead-line, but less accurate than a sounding-rod in shallow water. The actual figures are best taken from makers' handbooks. Echo-sounders should be frequently calibrated, let us say about once every day during the measuring campaign.

The main difficulty in continuous echo-sounding is the position-fixing needed for accurate mapping. There are several surveying methods to achieve this, and they should be selected with great care and experience for every specific case, as they will to a great extent determine the cost of the field work. Details of these surveying methods and geodetic measurements cannot be discussed here, and appropriate texts should be consulted on this subject.

2.4 Velocity Measurements

2.4.1 Floats

Measurement of flow velocities by means of floats is the simplest method, but also the least accurate one. By measuring the time interval it takes a light-weight float to cover a predetermined distance between two fixed cross-sections, surface velocity can be obtained. In order to deduce from this the average velocity needed for the determination of discharge, use is made of coefficients that are in the range of 0.6 to 0.9. It is obvious that guessing the right coefficient even by an experienced engineer cannot be very accurate, particularly so because it is dependent on the depth of water. More accurate measurements may be obtained by calibration, in which simultaneous to floating some more precise method is used to determine the ratio between the average velocity and the surface velocity for different depths of water. Thereafter only float measurements can be carried out. Some simple floats are shown in Fig. 2.5.

Floats should be used on straight reaches of watercourses, and the distance between the measuring sections should not be less than about 20–30 m [2]. On large streams measurements should be made along more than one line.

Special floats, consisting of a stick weighted at its lower end so that it remains vertical and protrudes above the water-line for only a small part of its overall length, are sometimes used. It is often claimed that such floats measure the average velocity, provided they cover as much as possible of the depth but never actually touch the bottom.

Another and better type of calibrated float, in the form of streamlined

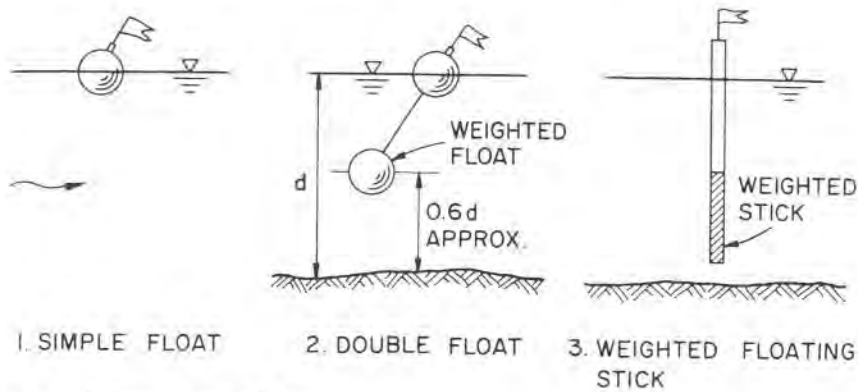


Fig. 2.5. Some types of floats.

wings (pendulum meters), has been developed by some laboratories [2]. The float is kept suspended in the stream by means of a steel wire. Under action of the hydrodynamic thrust exerted by the stream, the float moves downstream, and the wire makes an angle with the vertical that can easily be read on the appropriate dial, Fig. 2.6a. Local velocity at any depth is directly proportional to the angle α , according to the expression obtained from conditions of equilibrium,

$$V^2 = \frac{2W}{CA\rho} \tan \alpha \tag{2.1}$$

where V – local velocity, in m/sec, W – submerged weight of the wing, in N,

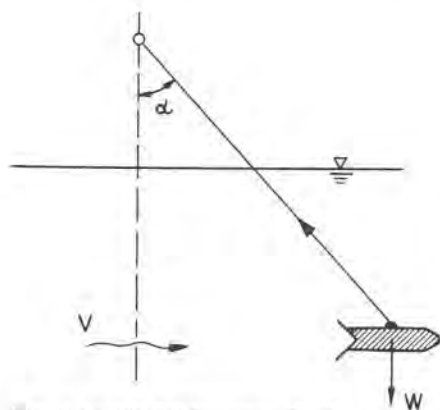


Fig. 2.6a. Hydrodynamic float.

C – drag coefficient for the wing, A – area of the wing perpendicular to the direction of flow, in m^2 , ρ – density of the water, in kg/m^3 .

Generally, different wings are used for low velocities of flow (small weight W and large area A) and for higher velocities (greater weight W and smaller area A). Together with all the pertinent data about the wing itself (weight, drag coefficient, etc.), manufacturers also provide correction tables to take into account the curving of the wire under hydrodynamic thrust. After a series of measurements with wings lowered to various depths in one vertical, a diagram of velocity distribution in the vertical can be obtained. Hydrodynamic floats are as a rule laboratory calibrated by the manufacturer (Fig. 2.6b).

Generally speaking, in recent times floats have been largely supplanted by more reliable current meters.

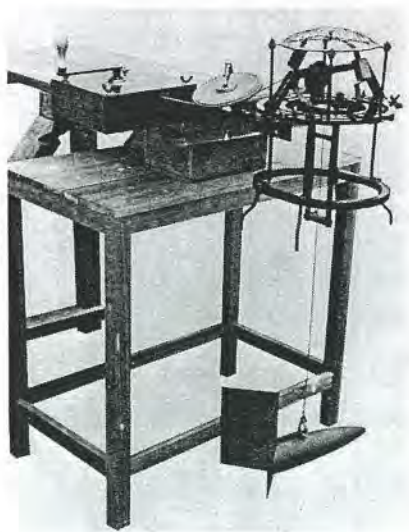


Fig. 2.6b. Pendulum meter (by courtesy of CIRIA, London).

2.4.2 Current Meters (Fig. 2.7b)

Current meters are still the most widely used measuring instrument in hydrometry. They convert the momentum of the liquid into torque that can be calibrated in terms of velocity. The conversion is achieved by means of propellers or cups rotating on a horizontal or vertical axis. Measurement of flow velocities serves as the basis for determination of discharges, whence the

widespread use of current meters in hydrometric works, see Figs. 2.7a and 2.7b.

By laboratory testing, the number of revolutions of the propeller or the cup-wheel is calibrated against the velocity of flow. Average number of revolutions at a given location in the flow section is determined during a certain time interval, and from this the time-average velocity is obtained from the calibration chart. Rotating element should ideally be sensitive to only the velocity component perpendicular to the flow section, but unfortunately this is extremely difficult to achieve fully. Hence caution should be used when applying current meters to streams with strong cross-currents. The instrument is generally built to be sturdy enough to withstand any stresses during immersion, and all the bearings are well protected from sediment-laden water.

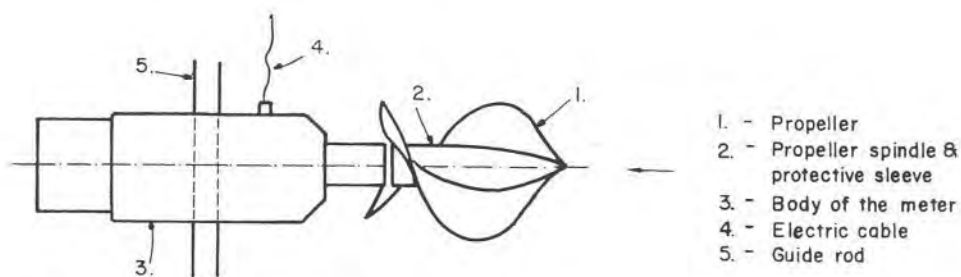


Fig. 2.7a. Typical current meter.

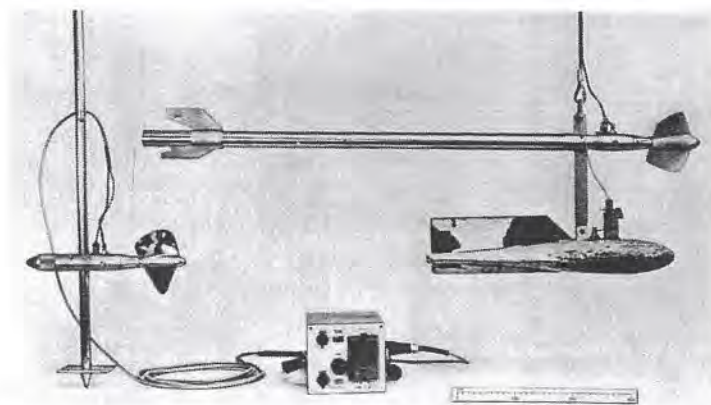


Fig. 2.7b. Current-meter measuring assembly parts (by courtesy of CIRIA, London).

No detailed description of different current meters currently available on the market can be made here, and interested readers should consult specialized texts [2–5]. Price current meter is a typical representative of vertical-axis cup-wheel; it is held in water by suspension from a steel cable, and the stability is achieved by means of a tail-fin and a streamlined sinker. Neyrpic meter, Ott meter, Tamam meter, are typical of the horizontal-axis propeller meters. They are either suspended in water on a cable and weighted by a streamlined sinker, Fig. 2.8, or the meter is traversed along a suspended cable. Every propeller current meter is generally provided with two or more exchangeable propellers, one for low velocities of flow (about 4–80 cm/sec) and one for higher velocities (say 40–350 cm/sec). Within each range, there is a linear relationship between the velocity V and the number of revolutions, n , per second of the propeller. A battery-operated electro-mechanical digital counter is connected by a cable to the instrument, and is generally equipped with a time selector for 30 seconds and 60 seconds settings.

Calibration accuracy of a current meter is $\pm 1\%$ to 2% , but in field work an accuracy of $\pm 5\%$ is much more realistic. Frequent laboratory calibrations are essential if an acceptable accuracy is to be kept up after longer periods of field service. Regular maintenance is also of utmost importance, and every instrument, when not in use, should be stored in a protective box. If not properly maintained, the mechanical resistance in the bearings is liable to increase with time, thus causing the meter to underestimate the velocities, especially in the lower range.

The influence of highly turbulent flows, as found in many natural water-courses, on the performance of current meters has been the subject of some controversy. As far as meters are concerned, the two main phenomena connected with the turbulent flow are: 1) cross-currents, 2) fluctuations of

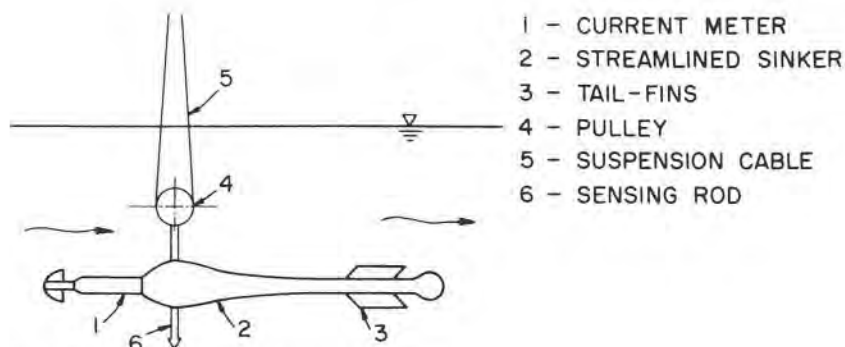


Fig. 2.8. Cable-suspended current meter.

velocity. It has been generally assumed that for horizontal-axis propellers, cross-currents tend to produce an underestimate of velocity, while fluctuations cause an overestimate; for vertical-axis cup-wheels the deviation is thought to be positive on both accounts. There would be, therefore, a compensating effect for horizontal-axis meters, and a cumulative effect for vertical-axis meters. It is for this reason that vertical-axis meters have not been recommended for highly turbulent streams. Some recent researches, however, have cast serious doubt on these conclusions, suggesting that the influence of the turbulence on both types of meters is almost identical [6]. As a general rule, for measurements with current meters, a straight reach of the channel should be selected, as far as possible from bends.

2.4.3 Chemical Methods

Application of chemical methods to the measurement of flow velocities, and hence also of discharges, of natural watercourses is only of recent development. In fact, most of these methods have been primarily developed for measurement either in closed conduits or in artificial channels of well-defined geometry and hydraulic properties. Although basically simple, the techniques and the specific knowledge required for their successful application are still being developed and refined. Ecological awareness in recent years, and the public involvement in the preservation of the natural habitat, have restricted the use of some methods, and virtually eliminated a few others. This applies to both the methods for measurement of flow velocity as well as of discharges (see par. 2.5.4).

In general, all chemical methods may be classified in one of the two categories:

- 1) Methods based on the propagation velocity of the indicator substance,
- 2) Methods based on the dilution of the indicator substance (Fig. 2.9a).

The first group of methods is used for measurement of velocities, while the second one serves for discharges.

2.4.3.1 Salt-Velocity Method

The so-called salt-velocity method is typical for the first category, and it is used for measurement of flow velocities. The method makes use of the fact that by introducing common salt into the stream, electrical conductivity of the water is increased [7]. Small doses of a saturated solution of common salt are injected at an upstream section of the stream and are carried along at a velocity nearly equal to the mean velocity of the water. At a detection station downstream, an ammeter coupled to a power supply is connected in series to electrodes placed in the stream. It registers the electric current



Fig. 2.9a. Discharge measuring by chemical dilution method (by courtesy of CIRIA, London).

flowing between the electrodes, which is directly proportional to the salt concentration in the water. Hence a graph is obtained showing the passage of salt-waves plotted against time (Fig. 2.9b). If the time elapsed between the passage of two successive salt-waves is T and the distance between the injection and detection stations L , the mean velocity of flow is obtained from the relationships $V = L/T$. Computation of discharge by this method can only be contemplated in the case of a fixed-boundary artificial channel between the stations.

The method, when properly applied, can be very accurate. Indeed, it is claimed that it should be possible at the 95% confidence level to achieve an accuracy of about ± 5.0 in natural streams under the best conditions [8]. The method is generally considered costly because of the long duration of measurement and long experience required if reliable results are to be secured. There are already international standards for the use of this method and similar others described in the next paragraph [9].

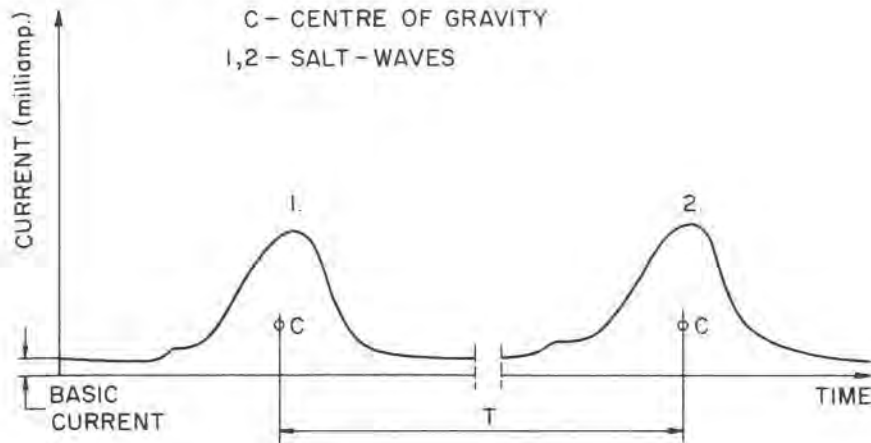


Fig. 2.9b. Salt-velocity method.

2.4.3.2 Color-Velocity Method

This method is essentially similar to the previous one, but is less expensive and also less accurate. As mentioned before, it is generally objectionable from the point of view of environmental protection.

The coloring substance is released into the stream by the first observer who marks the time of injection; the second observer, placed a distance L downstream, watches and marks the beginning of the color-wave and of its end. It is thus possible to determine the mean time T passed between the injection and the passage of the wave. The mean velocity again is obtained from the simple relationship $V = L/T$.

The two coloring indicators most frequently used are *fluorescein* and *rhodamine* (both fluorescent tracers), or *potassium iodide* and *lithium chloride* (both chemical tracers). All of these tracers are rather sensitive to the influence of the sun rays.

2.4.4 Experimental Methods

In this paragraph a short review is made of a few velocity-measurement methods that are still in various stages of experimental development. Some are promising, at least for special and specific applications, while others seem to be less suitable for practical engineering application.

2.4.4.1 Magnetic Induction Method

This is an attempt to adjust an accurate velocity-measuring method in closed conduits to open-channel flow. It is based on the measurement of

induction current generated when an electrical conductor moves across a magnetic field. This current is linearly related to the velocity of the conductor, in this case the flowing water [10, 11].

Two electrodes are placed perpendicular to both the flow direction and the magnetic field, in a straight reach of the channel. The electric current between electrodes is then proportional to the mean velocity of flow. The frame for the establishment of the magnetic field is placed on the banks and across the bottom of the channel, so that no floating objects can affect the results. By switching over to a horizontal magnetic field, a continuous measurement of the water stage is also possible. If the cross-section at the measuring site is fixed and known, the current recorder may be calibrated to directly indicate discharges.

The application of the method requires an adequate power supply, and the magnetic field can easily be affected by any steel structures or motors in the vicinity. So far it has been mainly applied to rectangular cross-sections, but attempts are under way to adapt it to other shapes as well. Absolute conductivity of the water is generally of minor importance, provided it remains constant during the measuring period. The cost of the erection and operation of a magnetic gauging-station should be comparable to that of a conventional current-meter cable station.

2.4.4.2 Ultrasonic Method

This method also is an attempt to apply the existing technique of measurement in closed conduits to flow in open channels. By sending a series of ultrasonic impulses from one side of the stream to the other, first against the current and then with the current, either the time difference or the frequency shift can be measured caused by the influence of the average stream velocity on the travel time of the signal (Fig. 2.10). Several tech-

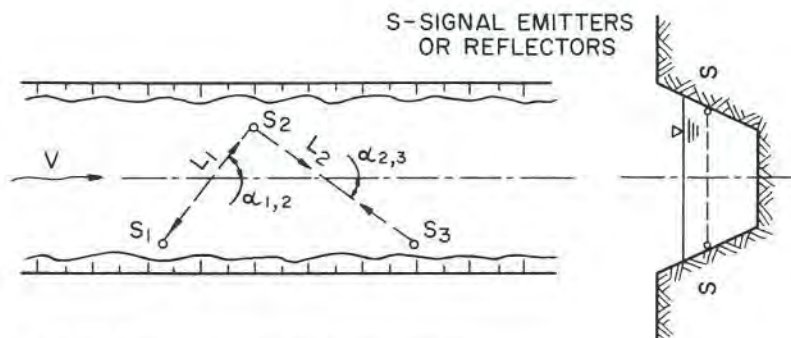


Fig. 2.10. Ultrasonic velocity measurement.

niques have been developed for the practical application of the basic principle, and their suitability for any specific case should be carefully examined [8, 12, 13].

Because of the fact that the ultrasonic celerity is dependent on several time-variable parameters (water temperature, density, etc), techniques are already available which ensure that wave celerity is cancelled out.

It should be pointed out that the method does not yield the average velocity in the vertical, but only in the width of the flow section at the given depth. The vertical average must be computed using the known correction coefficient relating the measured velocity at a given depth to the average velocity for the measuring section. Some serious problems remain yet to be solved: limitations as to the width of the channel and its cross-section, sediment and air content, low velocities and others. Among its main advantages: continuous and automatic measurement, no obstacles to flow, convenient telemetric and digital recording, etc. For the time being, it has not yet been standardized. In uncalibrated stations, the accuracy of measurement is not likely to be better than about $\pm 10\%$ or more [8].

2.5 Discharge Measurement

The final scope of all the hydrometric measuring methods discussed so far is generally to obtain a fairly accurate, economically and technically acceptable estimate of the discharge at a given flow section.

2.5.1 Average Velocity

There are several methods to obtain the average velocity in a vertical, which then serves for the computation of discharge.

2.5.1.1 One-Point Method

The velocity is measured at the depth of $0.5-0.7d$, depending on local conditions and depth; it is assumed to represent the average velocity in the vertical. This assumption is mainly derived from the theoretical considerations based on logarithmic velocity distribution. The method is used when discharge estimate is needed within short time, at low stages or in shallow streams.

2.5.1.2 Two-Point Method

Velocity is measured at two points in the vertical: at $0.2d$ and $0.8d$; the mean velocity in the vertical is assumed to be the arithmetical average

between the two measurements. The method is in extensive use, and it is thought to give good results for fairly uniform velocity distributions and in flow depths above about 0.7 m.

2.5.1.3 Three-Point Method

Measurement of local velocity is made at $0.15d$, $0.5d$ and $0.85d$; arithmetic average is assumed to be the average velocity in the vertical. This method is particularly used in weed-overgrown channels.

2.5.1.4 Five-Point Method

Local velocity is measured at $0.2d$, $0.6d$, $0.8d$, at the water surface and as close to the bottom as possible. The average is then computed from the expression

$$\bar{V} = 1/10 (V_s + 3V_{0.2} + 2V_{0.6} + 3V_{0.8} + V_b) \quad (2.2)$$

where $V_{0.2}$, $V_{0.6}$, $V_{0.8}$ – local velocities at respective depths, m/sec, V_s – surface velocity, m/sec, V_b – bottom velocity, m/sec.

This method is preferred to others when the vertical velocity distribution is of a non-uniform shape.

These are general methods, but local preferences and habits may, of course, slightly differ from the given values. In order to obtain an estimate of the discharge passing a given flow section, average velocity is calculated for a number of verticals across the stream, assuming that it is representative for a cross-sectional area extending half-way to the two adjacent verticals. Number of verticals for a specific watercourse, and hence the distance between them, will depend on local conditions and accuracy desired.

However, according to the recommendations of ISO [38], based on a large number of experimental measurements, number of verticals should be as large as possible, and preferably not less than about 20 for all natural streams (standard deviation of computed discharges appears to be very sensitive to the number of verticals); on the other hand, number of points in the vertical (as long as it is more than one), seems to be of minor importance. Time of measurement at any point must also not be exaggerated, even with large depths, and a measuring period of about 30 seconds should, as a general rule, always be quite sufficient.

Another possibility is to cover the entire flow section with as many point measurements as is practical, without computing average velocities; curves of equal velocity are then drawn, assuming again that every curve represents an area extending half-way between two adjacent curves (Fig. 2.11).

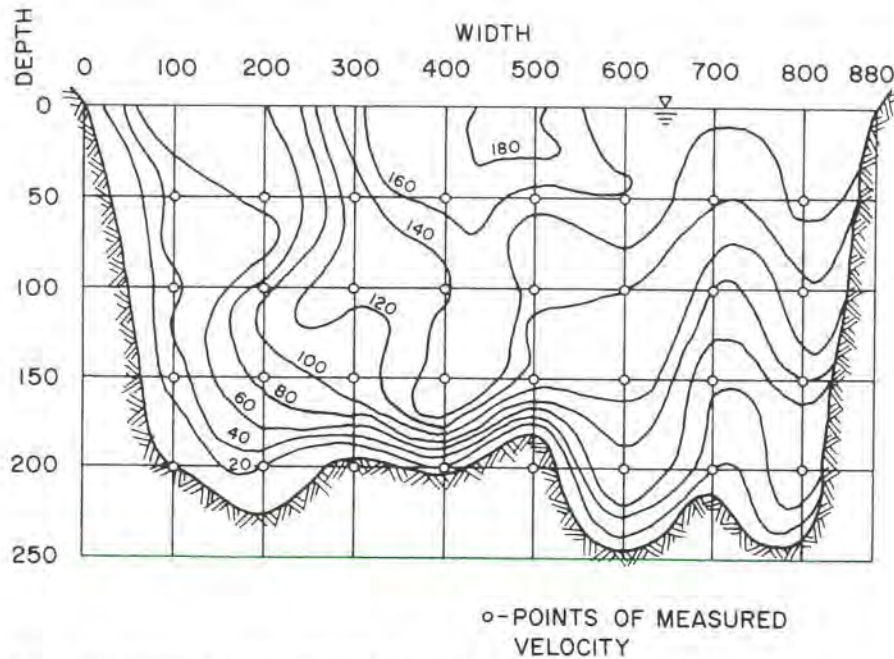


Fig. 2.11. Curves of equal velocity for a natural stream.

2.5.2 Discharge Measurement with Current Meters

In the following, some of the standard methods are briefly discussed.

2.5.2.1 Measurement by Wading (Fig. 2.11a)

In this type of measurement, the operator wades the stream on foot, wearing protective boots. Obviously, this is possible only in shallow streams and relatively low velocities. A straight and unobstructed stretch of the stream should be chosen, offering a secure wading section. Next a measuring tape is stretched across the stream to locate the verticals, which usually are spaced 0.5–1.0 m apart. Average velocity for each vertical is then determined either by one-point or two-point method, according to the depth of flow, bottom roughness, type of instrument, etc. The wading rod that carries the current meter must be held vertically, and the operator should stand somewhat downstream of the rod and to the side of it.

The method is simple and cheap, but seldom very accurate.



Fig. 2.11 a. Measurement by wading (by courtesy of CIRIA, London).

2.5.2.2 Cable Station (Fig. 2.12b)

It is generally a fixed structure consisting of a cableway that spans the stream and supports the weight of a traversing carriage with a suspended current meter and a finned streamlined sinker, as well as anchor supports on both banks, Fig. 2.12a. Being a permanent fixture, it has usually attached to it a small hut that serves as shelter and depot for use of the hydrometric staff.

The actual measurements can start as soon as the zero point for distance marking is fixed on one of the banks and the current meter lowered into the water. Point velocities are then taken according to one of the methods reviewed previously. Coupled with velocity measurements, water depth at various verticals is usually taken also.

Since the meter is not rigidly suspended in the water, it is essential for it to be equipped with an adequate sinker in order to prevent turbulence-induced vibrations and straying from the correct position (see par. 2.3.2).

Cable stations are obviously limited to relatively narrow streams, generally not exceeding about 100 m in width. Their main advantage is that they permit fairly easy and rapid measurements with good accuracy, and dispense altogether with the suitable location for discharge measurements.

On narrow streams, a light bridge is sometimes erected in place of a cable-way. If it does not interfere with the flow, it has all the advantages of a cable station, with possibly the exception at very high flood waves, when the water may reach the substructure of the bridge.

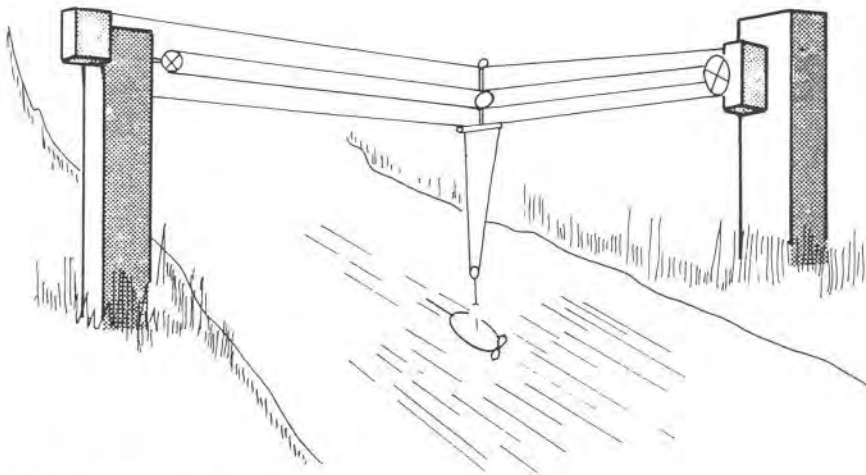


Fig. 2.12a. Cable station.



Fig. 2.12b. Permanent cable station (by courtesy of CIRIA, London).

2.5.2.3 Existing Bridges

There are many cases where the construction of a cable station is impractical, and hence it may become necessary to avail oneself of some existing bridge as a substitute. Such measurements, although of course better than nothing, are seldom very correct and often unreliable. Bridge piers cause considerable flow disturbances, eddies, and high degree of turbulence, particularly at higher stages. It is generally almost impossible to assess the effect of such disturbances, or to correct them by introduction of coefficients. It has been mentioned already that when bridges are low, high waters often reach the substructure, thus causing additional difficulties.

2.5.2.4 Measurements from Boats or Gauging Rafts

Current meter measurement on larger streams are usually carried out from boats or rafts, equipped with hand-operated winches and traversing cables. The measuring operation takes place almost from the water surface, as in wading, whereas the traversing is essentially similar to the cableway method. Verticals are marked either by a measuring tape stretched across the stream, or when impractical, by means of some standard surveying method. Keeping the vessel in a fixed position during the measuring operation may cause problems in high-velocity flows, but there are, however, many ways to overcome such a difficulty.

2.5.2.5 Methods for Computation of Discharge

All pertinent traverse-taking data are carefully entered on special hydro-metric forms, which subsequently serve as the basis for calculation of discharge in the technical office. In the following, some of the computational methods are briefly reviewed.

2.5.2.5.1 Arithmetical methods. a) The simplest and most frequently used method consists in computing average values of flow velocity and depth between two adjacent verticals (Fig. 2.13).

Partial discharge between two verticals is obtained from the expression

$$q_{i \rightarrow (i+1)} = \frac{(\bar{V}_i + \bar{V}_{i+1})}{2} \frac{(d_i + d_{i+1})}{2} b_{i \rightarrow (i+1)} \quad (2.3)$$

where $q_{i \rightarrow (i+1)}$ – partial discharge between verticals i and $(i + 1)$, m^3/sec , \bar{V}_i – average velocity in vertical i , m/sec , \bar{V}_{i+1} – average velocity in vertical $(i + 1)$, m/sec , d_i – water depth in vertical i , m , d_{i+1} – water depth in vertical $(i + 1)$, m , and, $b_{i \rightarrow (i+1)}$ – spacing between verticals i and $(i + 1)$, m .

When the spacing between verticals is equal, there are in use many addi-

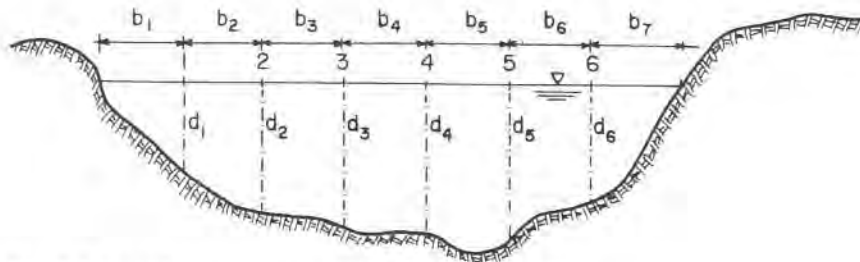


Fig. 2.13. Arithmetical computation of discharge (a).

tional formulae for partial discharge, but in general results obtained are almost identical to those from the basic expression, Eq. (2.3). Total discharge for the flow section is arrived at by summation,

$$Q = \sum_{i=1}^n q_i \tag{2.4}$$

b) Another similar arithmetical method is often applied, and is preferred by some hydrometrists. Partial discharges q_i are computed on basis of segments represented by the verticals, Fig. 2.14.

Formula used in this case is

$$q_i = d_i \bar{V}_i \left(\frac{b_i}{2} + \frac{b_{i+1}}{2} \right) \tag{2.5}$$

where q_i denotes the partial discharge for the vertical i , and the rest of the symbols according to Fig. 2.14.

Total discharge, Q , passing the flow section is again obtained by summation, Eq. (2.4).

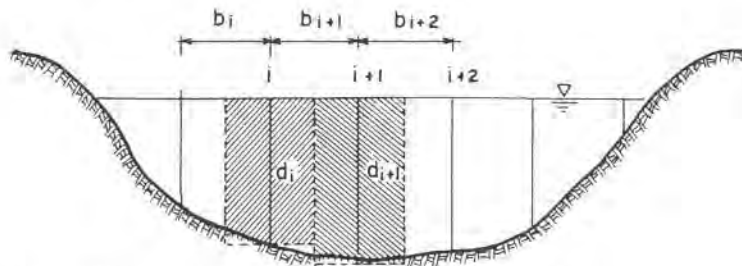


Fig. 2.14. Arithmetical computation of discharge (b).

2.5.2.5.2 *Graphical methods. a) Graphical integration:* Velocity distribution curves are drawn for all the verticals, and areas enclosed between the curves and the verticals determined by planimetric measurement; or average velocities are computed by one of the methods discussed under par. 2.4, and respective areas obtained using the equation

$$\int_0^d v(dy) = \bar{V}d \quad (2.6)$$

where v – local velocity at any depth, m/sec, \bar{V} – average velocity in the vertical, m/sec, y – partial depth, d – depth of flow, m.

Measured or computed partial areas are then marked out to scale on the transverse section of the stream and a smooth curve is traced connecting the obtained points, Fig. 2.15.

If the x-scale for distances is S_1 and the y-scale for velocity-distribution areas S_2 , total discharge for the flow section is given by

$$Q = A \times S_1 \times S_2 \quad (2.7)$$

where A denotes the hatched area on the diagram measured off by means of a planimeter.

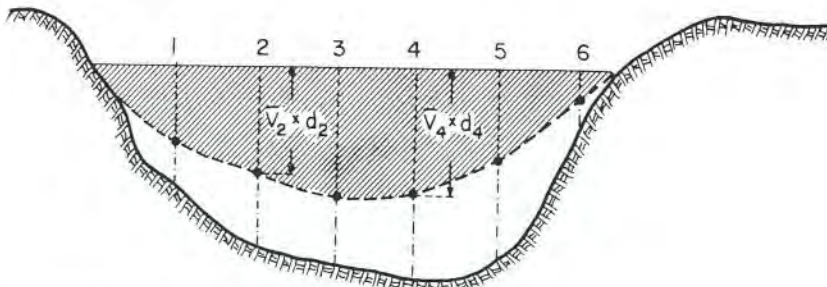


Fig. 2.15. Graphical computation of discharge (a).

b) Equal velocity diagram. This method has already been discussed in par. 2.4 and Fig. 2.11.

After the equal-velocity diagram is drawn from the measuring data, partial areas, extending halfway between the adjacent velocity curves, are taken off with a planimeter. A new diagram is then drawn, having velocities as abscissa and areas as ordinate.

Area enclosed between the curve obtained and the abscissa represents the total discharge for the flow section.

It is obvious that the same result can be arrived at without graphical integration, using the equation

$$Q = \sum_{i=1}^n V_i \times A_i \quad (2.8)$$

in which V_i – velocity represented by a given curve on the equal-velocity diagram, A_i – partial area belonging to the given curve.

2.5.3 Discharge Measurement by Means of Permanent Hydraulic Structures

These important methods, which include weirs, measuring flumes, sluice gates, overflow gates, etc., cannot be included in the present text, since they are part of open-channel hydraulics, and specialized texts should be consulted, as for instance [14, 15].

Brief mention should be made here, however, concerning the use of existing culverts for hydrometric purposes on small streams. When the flow through the culvert is not submerged (tail-water downstream does not submerge the critical depth in the culvert), there is a control section in the culvert, and hence a definite relationship between the discharge and the upstream depth. Accordingly, by measuring and recording the upstream depth, fair information about the discharges can be obtained. This information is likely to become less accurate at low discharges, when there is probably no control section, unless special devices are used to overcome this difficulty. At very high flows, culverts may become submerged; in that case, depth readings should be taken on both the upstream and the downstream side of the culvert. For flow regimes a and b in Fig. 2.16, when the control is either at the entrance or exit sections, depth measurement at section 1 will suffice;

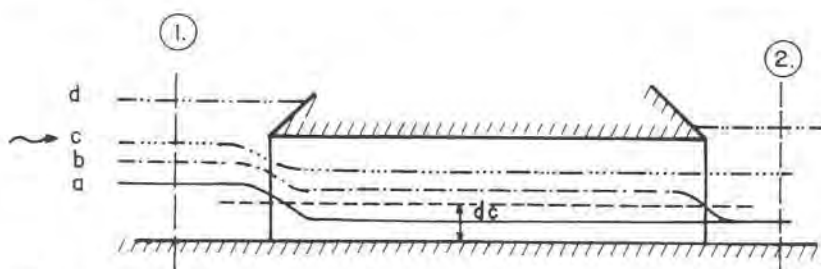


Fig. 2.16. Discharge measurements at a culvert.

for flows c and d, depth readings at two sections, 1 and 2, must be taken. In all cases, head-loss coefficients will have to be assumed.

The use of highway and railway culverts for flow measurements on small ephemeral streams of arid zones is in wide use. It is cheap, efficient, accurate enough and reliable. For submerged flows, the station is best calibrated by laboratory model investigation, if reliable results are required.

2.5.4 Chemical Methods for Discharge Measurement

All of these methods are based on the dilution process of the indicator substance in water, as has already been pointed out in par. 2.3.3. They are based on the fact that by injecting a known quantity of a soluble indicator into the stream, concentrations are obtained that are inversely proportional to the rate of flow.

2.5.4.1 Intermittent-Injection Method

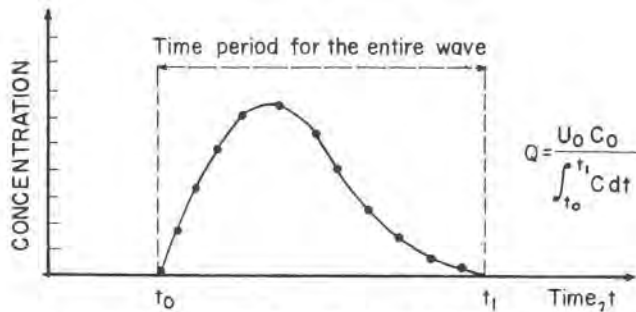
An impulse injection of the indicator, of known quantity and concentration, is made upstream, and concentration variation is monitored some distance downstream, sufficient for thorough mixing. Water samples are taken during the entire period of the wave passage (Fig. 2.17a). Assuming no loss of the injected indicator substance along the measuring reach, simple continuity balance equation gives:

$$Q = \frac{U_0 C_0}{\int_{t=t_0}^{t=t_1} c dt} \quad (2.9)$$

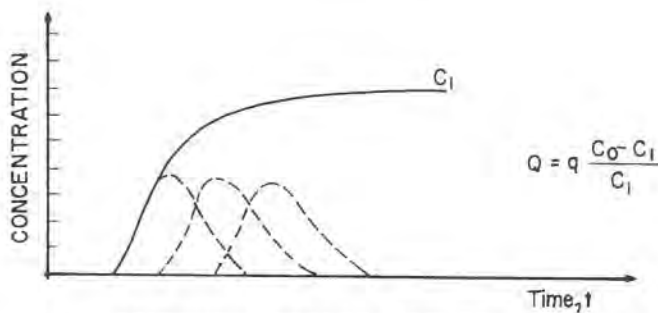
where U_0 – the volume of the injected indicator substance, C_0 – its concentration, c – variable concentration at the measuring section.

In the derivation of Eq. (2.9) it has further been assumed that there is zero-concentration of the indicator substance in the stream prior to the injection. Hence, the numerator represents the total mass of the injected stuff, while the denominator represents the area enclosed below the concentration-versus-time curve (Fig. 2.17a).

Concentration samples should always be taken at several points along the width of the measuring section. Although the injection technique itself is simple and inexpensive (small quantities of indicator substance), sampling and subsequent analyses are cumbersome.



a. INTERMITTENT INJECTION METHOD



b. CONTINUOUS-FEEDING METHOD

Fig. 2.17. Chemical dilution method.

2.5.4.2 Continuous-Feeding Method

According to this method, the indicator substance of concentration C_0 is fed in at a constant rate q until at some section downstream, sufficiently distant for good mixing, a fairly uniform and constant concentration C_1 is obtained along the entire width of the stream. If again no loss of indicator substance is assumed, and also zero concentrations prior to the starting of injections, continuity yields,

$$C_0 q = (Q + q) C_1$$

from which

$$Q = q \frac{C_0 - C_1}{C_1} \tag{2.10}$$

in which Q is the required rate of flow for the stream. In most cases C_0 is many orders of magnitude larger than C_1 , hence C_1 in the numerator of Eq. (2.10) can safely be omitted.

The method could in fact be described as a continuous succession of impulse-injections that yield a constant concentration, see Fig. 2.17b.

Example 2.1

In order to measure the discharge in a mountain torrent after the training works, continuous-feeding method of rhodamine dye was adopted. Measurement section was chosen at a distance of about 1500 m downstream from the injection point. Continuous dye injection was carried out during 8 minutes, and was repeated three times. Laboratory analysis of the dye-concentration in water samples was carried out a short time after the measurement. The final data were as follows:

Injection rate of the water-dye mixture, $q = 3.0$ ml/sec.

Dye concentration, $C_0 = 20,000$ mg/lit.

Steady dye concentration at the measuring station, $C_1 = 0.0042$ mg/lit.

Hence the computed discharge,

$$Q = \frac{3}{10^6} \frac{2 \times 10^4 \times 10^3}{4.2} = 14.3 \text{ m}^3/\text{sec}$$

The number of samples that have to be taken in order to determine the constant concentration C_1 is generally small, and the entire operation can usually be carried out by a single trained person. On the other hand, the feeding apparatus is more complicated and more expensive, and indicator quantities are much larger.

Both methods are recommended for application on streams that are not suited for current-meter measurements (shallow water, high turbulence, etc.). They both have the advantage of not requiring good knowledge of the stream geometry. Widely used indicator substances today are the non-toxic rhodamine dyes which can be detected in very low concentrations, but they usually require some preliminary calibration.

2.5.4.3 Air-Bubbling Method

In many aspects it is still an experimental method, but one of the promising ones. It is based on the extension of the float-integration method for the measurement of mean flow velocity in a vertical. According to this method, a float is released from the bed of the stream, and the average velocity is obtained by dividing the horizontal distance to the point where the float emerges from the water by the time elapsed [16, 17].

A simplified theory of air-bubbling method, in which the float is replaced by a stream of air bubbles, is schematically outlined in Fig. 2.18. Slope of the air-bubble rising curve, diagram 3, is given by

$$\frac{dx}{dz} = \frac{v}{w} \tag{2.11}$$

where v – point velocity at any depth, variable with depth, w – rising velocity of the air bubble, assumed constant.

Solution of Eq. (2.11) gives the total length L measured from the vertical to the point where the bubble reaches the water surface,

$$L = \frac{1}{w} \int_0^d v dz = \frac{1}{w} q \tag{2.12}$$

Here q denotes specific discharge, having dimensions $L^2 T^{-1}$.

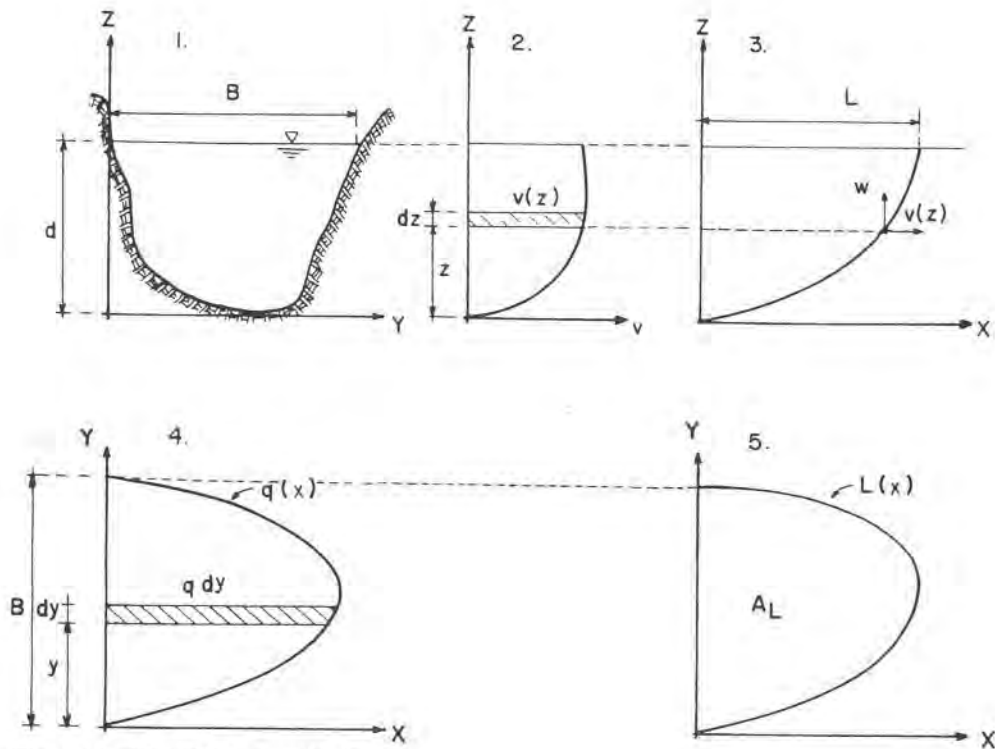


Fig. 2.18. Air-bubbling method.

In order to obtain the total discharge, an additional integration is necessary,

$$Q = \int_0^B q \, dy = w \int_0^B L \, dy \quad (2.13)$$

The term $\int_0^B L \, dy$ represents the area A_L , diagram 5, enclosed by the curve $L(x)$. Hence finally,

$$Q = w A_L \quad (2.14)$$

The weak link of the method is the bubble-rising velocity w . Its absolute velocity depends on many parameters (temperature, Reynolds Number, sediment content, etc.), and the simplifying assumption that it is constant along all of the path is certainly not correct.

Good photographic equipment for the recording of $L(x)$ curve formed on the surface of the flowing water is essential. In wide and shallow streams, where the ratio L/B is small, photographic distortion can be considerable. Air feeder pipe should closely follow the contour of the measuring section.

2.5.4.4 Conveyance-Slope Method

This method is mainly used where an approximate estimate of flood discharge is necessary, and there are no hydrometric stations available. Use is made of Manning's uniform flow equation $Q = KJ^{1/2}$ in which K denotes the conveyance, $K = 1/n AR^{2/3}$, and J the hydraulic gradient between two stations. Roughness coefficient n must be estimated, and is assumed to be constant over the measuring stretch; area A for a given water level, and hydraulic radius R , have to be measured and computed. The longitudinal slope of the water surface, assumed constant between two stations relatively close to each other, is obtained either from staff gauge records, if available, or from high-water marks.

Expression for the computation of discharge can be easily derived applying energy equation, continuity and the Manning formula for uniform flow. For a two-station system it is given by

$$Q = \left[\frac{\Delta d_{1-2}}{\frac{L}{K_1 \times K_2} - \frac{1}{2g A_1^2} \left[1 - \frac{A_1^2}{A_2^2} \right]} \right]^{1/2} \quad (2.15)$$

and for a three-station system

$$Q = \left[\frac{\Delta d_{1-3}}{\frac{L_{12}}{K_1 \times K_2} + \frac{L_{23}}{K_2 \times K_3} - \frac{1}{2gA_1^2} \left[1 - \frac{A_1^2}{A_3^2} \right]} \right]^{\frac{1}{2}} \quad (2.16)$$

In the above equations K_1, K_2, K_3 – conveyance factors for each station, Δd – difference in water elevation between stations as denoted in the subscript, m, L – distance between stations denoted in the subscript, m, g – acceleration of gravity, m/sec², A – calculated cross-sectional area at the given station for the measured high-water mark, m², Q – discharge, m³/sec.

If the cross-sections at the stations that serve for discharge estimates are measured before the passage of the flood wave, they should be checked after the event; small changes may be neglected, but for larger ones, average values are preferable. For checking purposes, longitudinal water slopes derived from observations should be compared to longitudinal slopes of the stream bed.

Measuring site and sections should be chosen with great care. The chosen stretch of the stream must be as straight as possible and relatively stable. The distance between the sections should be at least about 20 m for gradient slopes of 10‰, about 200 m for slopes of 1‰, and about 2000 m for slopes of 0.1‰ [8].

According to Benson [39], the length of the measuring reach should be at least 75 times the mean depth, or 5 times the mean width, or at least about 300 m, whichever is the largest. He also recommends that the water surface descent over the reach should be about 15 cm at least, if reliable results are wanted. If during the passage of high waters flood plain is partially covered, possible variation of the roughness coefficient along the width of the flow section should also be taken into account.

Accuracy of such measurements is generally low, but it is often of great help, particularly in arid and semi-arid zones, serving for estimates of flash-floods in mountain streams, where regular hydrometric methods are of little use.

Example 2.2

High water marks have been measured after the passage of a flash-flood wave in a certain ephemeral Mediterranean stream having no hydrometric station along its course, with a view to estimating the maximum flow rate. According to these marks, wetted areas have been measured by surveying at sections, A, B and C, considered fairly stable and more or less uniform; wetted perimeters were also measured, from which subsequently hydraulic

radius has been calculated. Manning roughness coefficient has been estimated as $n = 0.035$. Pertinent measures and calculated data are summarized in Tables 2.1 and 2.2.

TABLE 2.1

Measured value (m)	A - B	B - C
L	163	90
Δd	0.37	0.28

in which L - distance between sections, m, Δd - vertical distance between high-water marks, m.

TABLE 2.2

Section	n	$1/n$	A (m ²)	R (m)	$R^{2/3}$	K
A	0.035	28.57	234	3.85	2.45	16,408
B	0.035	28.57	240	3.70	2.39	16,389
C	0.035	28.57	250	4.00	2.52	16,982

Using Eq. (2.16),

$$Q = \left[\frac{0.65}{\frac{163}{16,408 \times 16,389} + \frac{90}{16,389 \times 17,989} - \frac{1}{19.6 \times 234^2} \left[1 - \frac{234^2}{250^2} \right]} \right]^{\frac{1}{2}}$$

$$Q = \left[\frac{0.65}{(6.06 + 3.05 - 1.15) 10^{-7}} \right]^{\frac{1}{2}} = 904 \text{ m}^3/\text{sec}$$

This is the estimated peak discharge. Its accuracy is probably low, but it nevertheless gives a reliable order of magnitude.

2.5.4.5 Other Methods

Any of the previously mentioned methods for velocity measurements, in conjunction with stage recording and cross-sectional geometry surveying, can also be applied to discharge gauging. In fact, in most cases velocity measurements are carried out with a view to deriving from them a discharge estimate. As the final result of such measurements, a so-called $Q-H$ curve (or rating curve) can be drawn, giving the discharge of the stream, Q , in dependence of the water stage, H . Such measurements should best be made during prevalently steady-flow conditions at different stages. Because of the unavoidable scattering of the plotted points, a best-fit regression curve has to be drawn. This can be done either by visual estimation, or using any appropriate analytical method. An indication of the reliability of such a curve is the standard deviation, which is supposed to represent the population; standard error of estimate, equal to $\sigma/n^{1/2}$ (in which σ – standard deviation of the population, and n – number of individual plotting points), may next be calculated. The rating curve, with 95% confidence belts, is the final result of the procedure, Fig. 2.19.

It is obvious that the number of the plotting points (measurements) should be as large as possible, and the obtained rating curve be frequently checked, since the water stage for a given discharge is dependent on parameters (wetted area, roughness coefficient, longitudinal slope, etc.) generally variable in alluvial streams.

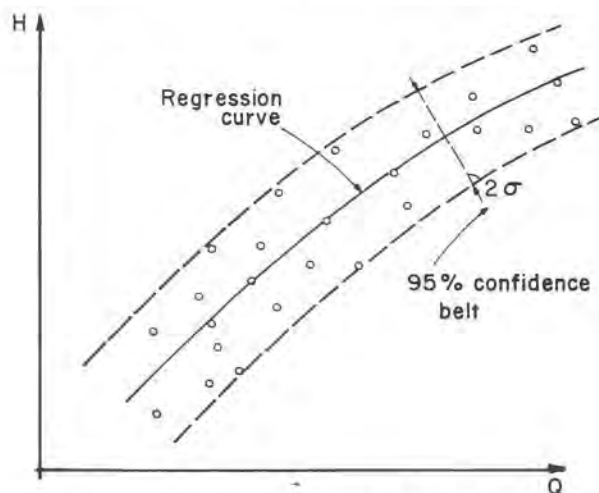


Fig. 2.19. $Q-H$ curve (rating curve) with 95% confidence belt.

The present short review does not pretend to cover, even to a limited extent, all the methods in use, and particularly those of a highly experimental character, with little practical application for the foreseeable future. No mention has been made of methods for discharge measurements by means of radioactive tracers; the reason is that the environmental pollution they entail is generally inadmissible in the modern society. Laboratory calibrations by hydraulic models have only been given a cursory mention, because they also are outside the scope of the present text.

2.6 Sediment Transport Measurements

There can be no doubt about the engineering importance of obtaining fairly reliable information in respect of the sediment transporting capacity of a watercourse under study. In fact, for good understanding of an alluvial stream and its characteristics, such information is essential. Sediment transport and its properties, as well as its decisive influence upon the morphology of alluvial streams and their general behavior, will be extensively discussed in the next chapters. In the present paragraph it is intended to briefly review some of the general techniques for quantitative measurement of sediment transport in alluvial channels.

It is customary for measuring purposes to assume that the total sediment load of a stream consists of two parts:

1. *Suspended load (discharge)*, carried by the water across a stream section above the bed layer. It consists of particles that stay suspended for an appreciable length of time, and may contain sand and finer fractions, such as silt and clay.

2. *Bed load (discharge)*, sediment that is carried across a stream section inside the bed layer or close to it. Particles move by means of small jumps (saltation), rolling or sliding.

It may be seen that the above terminology is based entirely on sediment transportation models, and not necessarily on grain-size distribution. There is in fact no sharp demarcation line between these two components, since some particles may part of the time move as bed load and then be entrained by the stream-turbulence forces and move as suspended load. The distinction, by no means precise and even qualitatively vague and approximate, is used in the present context mainly for the sake of convenience. A detailed review of sediment transport phenomena is given in Chapters 8 and 9.

Total sediment load across a stream section is obtained as the sum of the suspended load and the bed load.

2.6.1 Suspended Load

This part of the total sediment load is generally measured by means of some sort of *integrating samplers*, which are either *point-integrating* or *depth-integrating*. The latter collects a sample while it is being vertically moved through a given distance, whereas the former gathers a sample at a given point. Use of *instantaneous samplers* is restricted almost exclusively to marine measurements; they are lowered to the desired depth, at which an instantaneous sample of water-sediment mixture is trapped into a container of a given capacity.

2.6.1.1 Point-Integrating Samplers

The simplest form of such a sampler is a series of bottles fastened to a measuring rod at desired vertical distances. Each bottle has an entrance nozzle-tube pointing upstream and an air-exhaust tube. The rod with the attached bottles is lowered into the water, an operation which generally can be done quickly, so that no control valves are needed (Fig. 2.20).

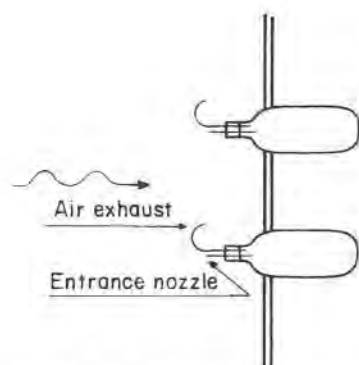


Fig. 2.20. Bottles for suspended-sediment sampling.

Bottles slowly fill up with sediment-laden water, so that time-integrated mean sediment concentrations for different flow depths can easily be obtained.

More elaborate samplers have been developed by many laboratories and water resources agencies (such as the Hydraulic Laboratory at Delft, Neyrpic-Grenoble, U.S. Interagency Committee on Water Resources, etc.). These devices generally consist of a streamlined outside metal body with tail vanes, and a removable inside collector bottle. Water-sediment mixture enters through an upstream directed nozzle-tube, and the entrapped air

leaves through an exhaust tube, both controlled by special solenoid-activated valves. In some types of such samplers, inside pressure within the body can also be regulated, in order to avoid possible initial surge at the start of the sampling operation. Such samplers generally can contain a quantity of about 30–100 kg, and are lowered into the water fastened to a hanger-bar or cable and reel. The volume of the internal collector bottle is about 0.5–1.0 liter.

There is often need for automatic suspended-load measurements, without direct intervention of field personnel. This is particularly important in arid and semi-arid regions, where most of the flows occur during flash-flood of relatively short duration. In addition, there may be considerable differences in sediment content between the ascending and descending legs of the flood hydrogram. Simple automatic devices for separate sampling during rising and falling water stages have been developed by several hydrometric agencies. Here a brief description is given of an automatic sampler developed by the Israel Hydrometric Service [18].

Rising water stage, Fig. 2.21. Sediment-laden water starts entering the bottle as soon as the level reaches tube (2), while the displaced air escapes through tube (3). When the sampler is almost full, the float (4) begins rising with the water, until it closes the air vent and thus prevents any more water from entering the bottle. A battery of such samplers placed at different heights above the bed will adequately sample the rising stage of the flood wave.

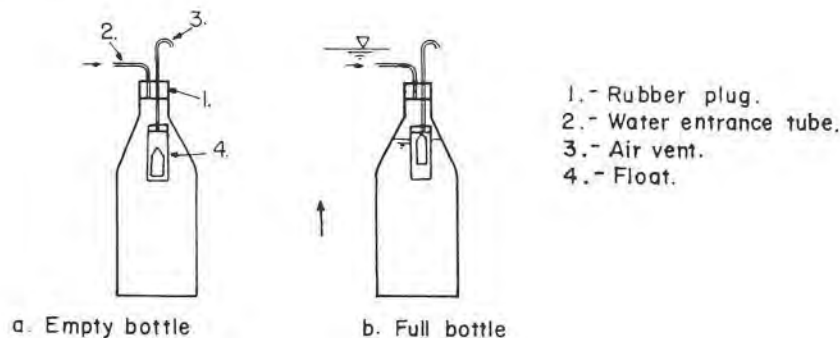


Fig. 2.21. Automatic sampler for the rising stage.

Falling water stage, Fig. 2.22. In this device the water enters the sampler also through the tube (2), as before, but air escape through the vent (3) is controlled by the valve (4) attached to the float (5). This valve is kept closed by a spacer (6), made of a substance rapidly soluble in water, held in place

by the disk (7). When the rising water reaches the upper float chamber, it starts entering into it through the opening (8) while the air escapes through the opening (9). Rising water finally reaches the spacer and dissolves it, but no water can enter the sampler as yet, because the upper float keeps the air vent closed. When the water begins falling past the upper chamber, the float valve frees the air passage, and the bottle starts filling up. As soon as the sampler is filled up, float (10) prevents any more water from entering by closing the air vent.

By placing several such samplers at different heights, sediment concentrations for falling flood water can be obtained.

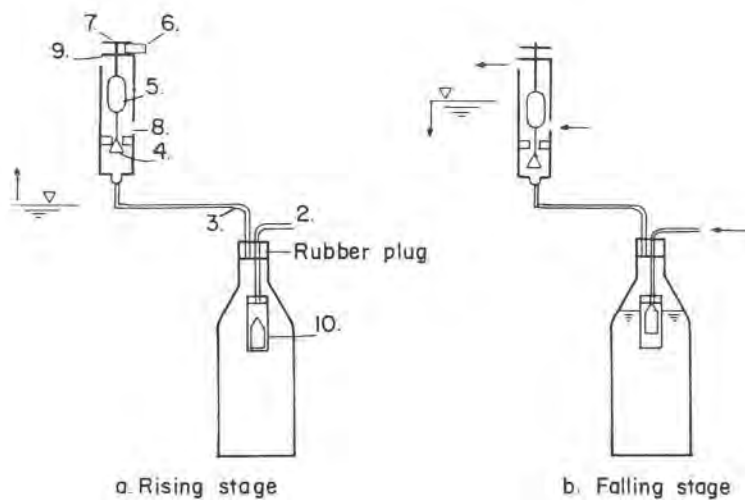


Fig. 2.22. Automatic sampler for the falling stage.

Collected sediment samples are left to settle and subsequently are dried in an electric oven. Volumetric concentrations are then computed, and if required a sieving analysis is done. Velocity and discharge measurements or estimates are made for the particular flood wave. Suspended load can then be estimated by applying any of the formulae for the suspended sediment load (see Chapter 8), or using any simpler evaluation method.

Wash load, consisting of minute silt particles, is generally collected in large containers and left to settle sufficiently during longer periods of time (ten or more days) before drying in the oven [2]. In the upper layers of the flow it is generally assumed that the velocity of wash-load particles is equal to the velocity of water, and hence partial sediment discharge may be estimated using the simple relationship

$$q_s = C_{wl} q_w \quad (2.16)$$

in which q_s – partial sediment discharge, $\text{m}^3/\text{sec}/\text{m}$, q_w – partial water discharge, $\text{m}^3/\text{sec}/\text{m}$, C_{wl} – wash-load sediment concentration by volume.

2.6.1.2 Depth-Integrating Samplers

This type of sampler is somewhat simpler than the previous one, because in all but very deep watercourses (say, over about 10 m depth), they do not require any control valves. *Average suspended-sediment density* in a vertical is obtained by traversing it in a single trip from the surface to just above the bed. It consists essentially of a streamlined metal body protecting a sampling bottle, with an intake nozzle-tube and an air vent. It is therefore obvious that any point-integrating sampler can also be used as a depth-integrating sampler.

The sampler is lowered into the water in the open position and at a steady rate, until it touches the bottom, at which a simple trigger mechanism closes the air vent, and the sampler is raised in the closed position.

Estimate of the sediment discharge is obtained essentially in the same way as mentioned in the previous paragraph.

Depth-integrating sampler developed by the Delft Hydraulic Laboratory departs basically from the conventional types. It is schematically shown in Fig. 2.23.

Water with suspended sediment enters the sampler through a long narrow nozzle-tube 1, where its velocity is greatly reduced. It is claimed that owing

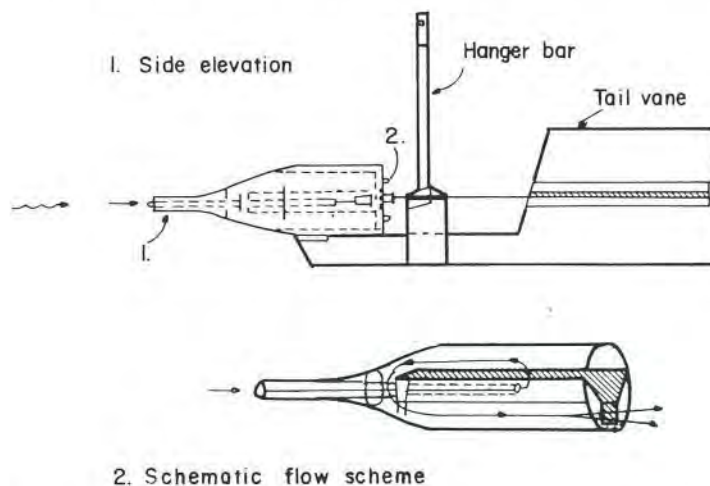


Fig. 2.23. Delft sampler DF1, after Delft Laboratory brochure.

to this, most of the solid particles settle out during the passage through the sampler, while the water leaves through the rear cover plate with holes, 2. Each instrument is laboratory-calibrated, and hence the total sediment discharge can be easily calculated. Because the entrapped water, it is further argued, continuously gets out from the sampler leaving behind solid particles, larger quantities of sediment can be collected than with any of the conventional samplers.

2.6.1.3 Sampling Across the Stream

In all but very small streams, the concentration of the suspended load across the stream is not uniform, and hence a single vertical, say in the middle of the stream or at the thalweg, will not do. If simultaneous velocity and water-discharge measurements are made or the information is available beforehand, it will be a good practice to locate the verticals for suspended-load sampling following the relative distribution of the stream discharge. The number of verticals across the stream for any given case, however, will depend not only on discharge distribution, but also on the intended accuracy of measurement. When no or little hydrometric information is available, a visual survey and experienced engineering judgement are the best guide.

Apart from the mentioned possibility of a single vertical in midstream or at the thalweg, a widely used practice is to locate the verticals at about $\frac{1}{4}$, $\frac{1}{2}$ and $\frac{3}{4}$ of the width. More elaborate schemes are generally used only for important investigations, and they consist essentially in either dividing the overall width of a larger number of equally spaced increments, or locating the verticals as close as feasible at centroids of equal-discharge increments.

If measurements of suspended load are made by point-integrating samplers, a proper selection of sampling points in each vertical is also of importance. There are several commonly applied methods, similar to those discussed in paragraph 2.4 for velocity measurements, based on either equally or differently weighted samples. More extensive discussion of this often very important point can be found in specialized treatises on hydrometry, and notably in the Report of the Interagency Committee on Water Resources [19, 20].

2.6.2 Bed Load Measurements

Estimation of the bed load carried by an alluvial stream is more difficult and uncertain than estimation of the suspended load. Any relatively large sampler immersed into the flowing water is bound to cause disturbance, and hence affect the sediment transport mechanism itself to a certain degree. In the comparatively narrow layer along the bottom where the bed load moves,

this disturbance becomes more strongly marked and more troublesome. Variations of flow parameters that govern the sediment transport is much more pronounced close to the bed, both in respect of time and space. It is, therefore, of little surprise that all of the many types of bed load samplers currently in use call for caution, and quantitative results obtained require careful analysis. Combined methods based partly on *in situ* observations of bed-forms movement and partly on theoretical calculations, or use of sonic samplers, also require utmost care and sound engineering judgement for any reliable bed load evaluation. There is, however, also another side to the coin, which compensates for the inherent inaccuracy of measurement: the main importance of the bed load from the engineering point of view is its being responsible for most of the morphological features of the stream-bed, and not so much its quantitative evaluation.

2.6.2.1 Mechanical Bed-Load Samplers

Common feature to all types of bed load samplers is the need for laboratory calibration, in order to determine the *efficiency coefficient* under various conditions of flow and duration of sampling. This coefficient gives the approximate ratio between the quantity indicated by the sampler and the true bed load discharge.

2.6.2.1.1 Box-type and basket-type samplers. These types of samplers, widely used in many slightly different forms, generally consist of a pervious container for the collecting of the sample, some sort of a rigid frame to which supporting cables are fastened, and a steering fin for directional stability. A typical sampler is shown schematically in Fig. 2.24, the so-called "Arnhem" B.T.M.A. meter, developed by the Netherland Rijkswaterstaat and calibrated by the Delft Hydraulic Laboratory [2].

The sampler is lowered onto the stream bottom and is left there for a certain period of time (about two minutes) and then is lifted out of the water. During the lowering and lifting operations the sampler remains closed, but is opened as soon as it touches the bottom. The amount of bed load particles trapped in the pervious basket (300μ –48-mesh sieve), after the water has slowly drained away, is then emptied and measured. The operation should be repeated several times for the same periods of sample-collecting time, and the results averaged. The true bed load discharge per meter width of the stream is subsequently determined making use of laboratory calibration coefficients.

Saltation load, generally sand particles transported up to about 50 cm above the stream bottom, will not be caught by bed load samplers, and may be left unaccounted for by suspended-load samplers. Special streamlined

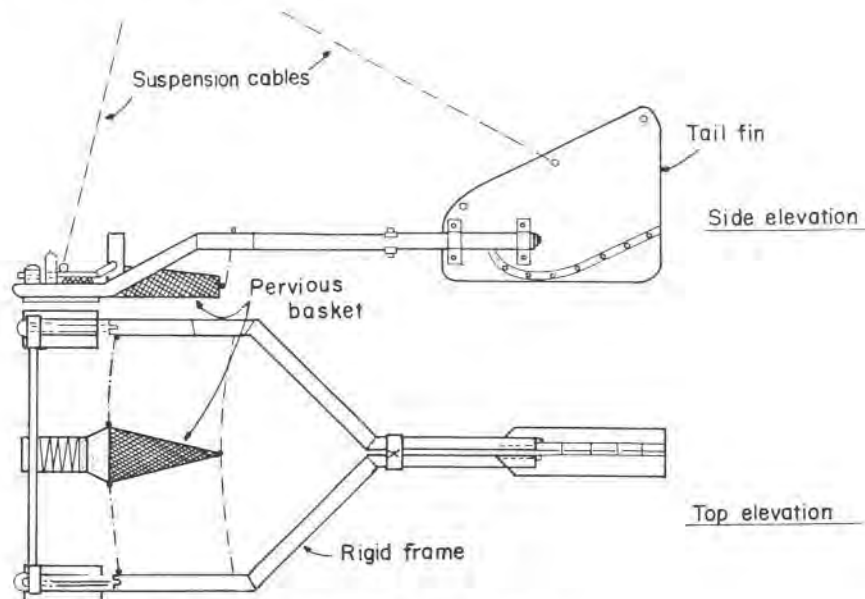


Fig. 2.24. B.T.M.A. bed load sampler, after [2].

bottle samplers have been developed, similar to those discussed in the previous paragraph, but mounted on some sort of metal sleigh, on which they can easily be held fixed or moved along the bottom at variable heights, say from 15 to 40 cm. Collection time usually is 10 to 20 minutes. The amount of the saltation load is generally added to the bed load sample for the evaluation of the total bed load discharge.

Modern bed load samplers are all of the pressure-difference type, which ensure the elimination of many drawbacks characteristic of older types (deposition of particles in front of the sampler, increased resistance, etc.). Sampler walls slightly diverge in the downstream direction, thus making the intake velocity almost equal to the stream velocity.

2.6.2.1.2 Tray-type samplers (Fig. 2.25). It seems that these samplers are extensively used only in the USSR, in streams with low flow velocities and relatively small bed load discharges. They consist of a metal tray with two side walls. The tray usually has a system of baffles to retard the flow of sediment-laden water and entrap the solid particles.

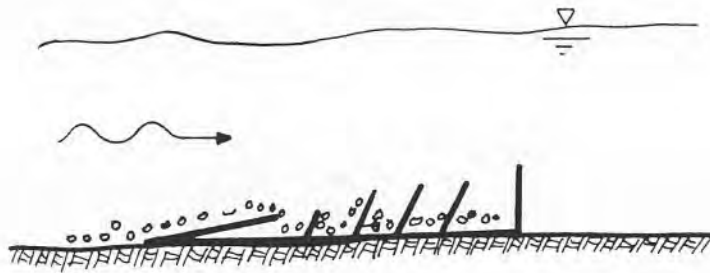


Fig. 2.25. Tray-type sampler.

2.6.2.1.3 *Pit-type samplers (Fig. 2.26).* These comprise a fixed or moveable pit (depression) installed on the stream bottom, and a mechanical device (pump) which can remove the accumulated sediment to a weighing tank. Use of such samplers is still rather restricted because of the difficulty to operate them in field measurements.

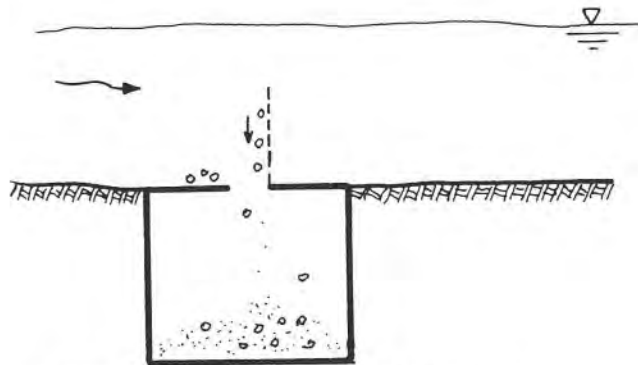


Fig. 2.26. Pit-type sampler with by-flow screen.

2.6.2.2 *Automatic Samplers for Arid Zones*

It has already been mentioned that in arid zones automatic sampling devices are almost indispensable, if any significant sediment-transport information is to be gathered. Such devices, cheap, simple to operate and fairly reliable, have been developed as far as suspended sediment is concerned. Automatic bed load measurement is a much more arduous task, and no satisfactory mechanical contrivance has so far been developed.

One of the automatic devices put forward during a four-year research and development project at the Technion, Israel Institute of Technology, is

shown schematically in Fig. 2.27 [21]. It is a tipping-bucket automatic sampler that is meant to give an electric pulse each time it tips. Recording of these pulses will indicate the rate at which bed load material entered the trap.

Bed load particles are intercepted by an opening flush with the bottom, and then collected in one of a pair of smaller compartments that form the tipping bucket. As the compartment fills up to a preset weight, the bucket tips and pours its contents into a large container beneath the stream bed, exposing the second compartment to the incoming material. After the passage of the flood wave, sediment collected in the large container is emptied and measured, and the apparatus is ready for the next wave. Extensive laboratory and field investigations were carried out to test the instrument, establish its definitive dimensions and calibrate it under various conditions.

Other automatic devices studied in the same project also included a *rotating-drum sampler* and a *drop structure* for measurement and disposal of bed load sediment. However, the authors are not aware that any of these automatic samplers have been introduced into ordinary hydrometric practice.

As part of the said research project, simple pit traps were also tested in a few of the typical ephemeral streams in the coastal plain of Israel. It has been found that they could be useful tools for collecting data on a single-storm basis, in reaches with prevalently sandy beds and relatively small

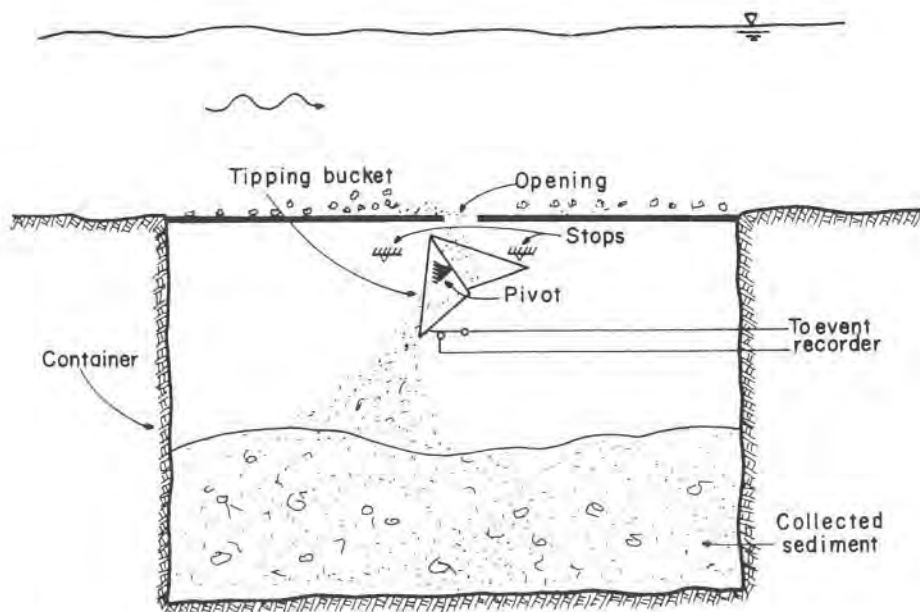


Fig. 2.27. Tipping-bucket automatic sampler, after [21].

drainage areas; trap containers should have adequate anchorage to protect them from being swept away by the flood water, and have sufficient capacity to collect all the sediment.

2.6.3 Acoustic Method

This method utilizes audible sound waves produced when bed load particles scrape along the bottom. A relatively simple acoustic system can pick up these waves and transmit them to a monitor or recorder, after being amplified and their frequency analyzed. A schematic diagram of an acoustic measuring system is shown in Fig. 2.28.

No reliable quantitative measurements have so far been achieved, but qualitative information obtained can often be of considerable interest, particularly if the acoustic pick-up is directly attached to a conventional bed load sampler. Laboratory and field calibration of acoustic systems is very difficult and laborious. An additional difficulty is the background noise produced by the turbulence which must be filtered out.

Another type of acoustic system is based on ultrasonic sound waves, and absorption of signals with different energy levels according to the water-sediment mixture. It seems that good quantitative results could be obtained if the sediment contains mainly fine sand particles [22].

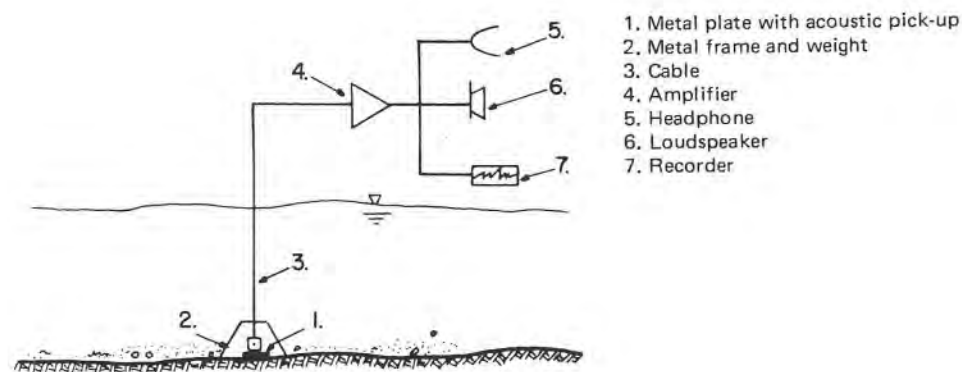


Fig. 2.28. Schematic diagram of an acoustic system.

2.6.4 Observation of Bed Forms Movement

Theoretical calculation of the bed load is thought to be possible, if there is information concerning the porosity of the bed, the average velocity and the average height of the bed forms (see Chapter 9.6.2).

In clear and shallow water direct observations can be made by experienced

hydrometric staff, but even then the porosity of the bed must be estimated by a competent engineer. In turbid and deeper water, which is the most common case, continuous mapping of bottom contours is necessary in order to derive average values of the above parameters. This can be achieved by ultrasonic sounding of bed profiles [23, 24].

2.6.5 Sampling of Bed Load Composition

Another method of applying basic bed load discharge formulae is by providing information about the bed load composition, and this can only be done experimentally. Whatever the accuracy of the sampling job in the field, the final result obviously cannot be more correct than the formula and the analytic procedure adopted. Analytical methods for the calculation of the bed load will be discussed in Chapter 9.

Although in fact bed material composition at different stages should be known, usually a single representative water stage for sampling is chosen. Bed load samples are generally retrieved by means of some sort of bed-material sampler, which is usually a streamlined grabbing device in the form of a scoop bucket that springs open upon contact with the bottom. An alternative method is a boring sampler, which is simply a pipe forced into the bed material and then hauled out of the water. Several samples are taken across the stream bed and subsequently analyzed in a laboratory for grain-size distribution curves.

2.6.6 Other Methods

So far it has been assumed that separate measurements are made for the two parts of the total sediment load, subject to different transport mechanism, i.e. suspended load and bed load. In many streams carrying only small-fraction particles (sands or smaller) and reaches of high turbulence, suspended sediment may very nearly represent the total sediment load. Such high turbulence, if not available naturally, can often be artificially induced by means of turbulence-producing obstructions placed over a short reach of channel. There is ample discussion on the subject in [19], while information on experimental turbulence-flumes can be found in [25, 26].

Another highly promising method for measuring sediment discharge has until recently been the *tracer method*, which is presently either completely banned, or practised only on an experimental and very restricted basis because of pollution problems. A suitable and stable tracer material, having very nearly the same properties as the natural sediment, is applied and introduced into the stream. Labelled particles are subsequently tracked, sampled

and analyzed in the usual way. Tracer material used in stream hydrometry is of radioactive-tracer type or paint and fluorescent type. Extensive information about the former can be found, among others, in [27, 28], and the latter in [29].

It should finally be mentioned that in recent years there have been a few attempts to set normative guidelines for sediment measurements. Notably, such efforts made by the International Organization for Standardization (ISO) are of particular interest [34, 35]. Norms in the field of sediment transportation, however, should always be applied judiciously and with caution, with due regard to the general characteristics of sediment load, and particular load conditions. No norms should be expected to free the design engineer from the need for routine sampling on rise, fall and peak in flood waves, which generally carry the bulk of the sediment load.

References

1. R. Zayc, Wasserstandsermittlung durch Druckmessung, Symposium Hydrometrie, Koblenz, 1970.
2. Nedeco, River Studies, North Holland, Amsterdam, 1959.
3. A.T. Troskolanski, Hydrometry, Pergamon Press, Oxford, 1960.
4. F.C. Hayes, Guidance for hydrographic and hydrometric surveys, Delft Hydrological Lab., publication no. 200, 1978.
5. ASME, Fluid meters, ASME, New York, N.Y., 1971.
6. R.W. Carter, Genauigkeit von Fluegelmessungen, Symposium Hydrometrie, Koblenz, 1973.
7. H. Dumas, Méthode chimique pour la mesure d'écoulement dans le cours d'eau, La Houille Blanche, no. 8, 1953 and no. 7, 1962.
8. F.G. Charlton, Measuring Flow in Open Channels: A Review of Methods, CIRIA, London, 1978.
9. International Organization for Standardization (ISO), Liquid flow measurement in open channels – Dilution methods for measurement of steady flow, ISO 555/I and 555/II, 1973.
10. Centre de Recherches et d'Essais de Chatou, Mesure de vitesse dans les eaux naturelles: méthode electromagnétique, Chatou, 1964.
11. H. Gils, Das Messen der Abflusse offener Gewaesser mit Magnet-Induktion, Symposium Hydrometrie, Koblenz, 1970.
12. Proceedings, Symposium on River Gauging by Ultrasonic and Electromagnetic Methods, Water Research Centre, Medmenham, Reading, 1974.
13. T. Kinoshita, Ultrasonische Abflussmessung an Fluessen, Symposium Hydrometrie, Koblenz, 1970.

14. M.G. Bos, editor, Discharge measurement structures, Lab. of Hydr. and Catchment Hydr., Rapport 4, Wageningen, 1976.
15. V.T. Chow, Open-Channel Hydraulics, McGraw-Hill, New York, N.Y., 1959.
16. V.E. Vid and V.I. Semjonov, Opit izmerenia rashodov vodi v kanalach integralno-fotografitseskim metodom, Meterologia i Hidrologia, no. 3, 1964.
17. L. David, Die Geschwindigkeitsmessung mit Luftblasen und ihre Anwendung, Symposium Hydrometrie, Koblenz, 1970.
18. D. Kornitz, Hydrometrische Stationen in Trockengebieten, Symposium Hydrometrie, Koblenz, 1970.
19. Interagency Committee on Water Resources, A study of methods used in measurements and analysis of sediment loads in streams, report no. 14, Minneapolis, Minn., 1963.
20. Task Force Committee on Preparation of Sedimentation Manual, Sediment measurement techniques, A. fluvial sediment, proceedings, ASCE, 95 (HY5);(1969).
21. I. Seginer et al., Development of a device for automatic measurement of bed load in streams, third annual report, Water Resources Laboratory, I.I.T., Haifa, 1970.
22. K. Debski, Continental Hydrology, Hydrometry, vol. I, translated from Polish, U.S. Dept. of Interior, 1965.
23. D.W. Hubbel, Apparatus and techniques for measuring bedload, U.S. Geol. Survey, Water-supply paper no. 1748, 1964.
24. S. Karaki, Modern Measuring Techniques, in: River Mechanics, H.W. Shen (ed.), Fort Collins, 1971.
25. P.C. Benedict et al., Total sediment load measured in turbulence flume, proceedings, ASCE, 79 (1953).
26. D.D. Gonzales et al., Stage-discharge characteristics of a weir in a sand-channel stream, U.S. Geological Survey, Water-supply paper no. 1898-A, 1969.
27. D.W. Hubbel and W.W. Sayre, Sand transport studies with radioactive tracers, proceedings, ASCE, 90 (HY3) (1964).
28. U.J. Crickmore and G.H. Lean, The measurement of sand transport by means of radioactive tracers, Proc. Roy. Soc., London, 266 (1962).
29. C.F. Nordin and R.E. Rathburn, Field studies of sediment movement using fluorescent tracers, World Meteorol. Org., Symposium, Koblenz, 1970.
30. R.W. Herschy, Hydrometry, Wiley, Chichester, 1978.
31. G.V. Zheleznyakov, Theoretical Principles of Hydrometry, Sidro-Meteoizdat, Leningrad, 1968.
32. G.V. Zheleznyakov, Hydrometry, Izdatelstvo, Kolos, Moscow, 1972.
33. M.J. Moroney, Facts From Figures, Penguin Books, London, 1958.
34. International Organization for Standardization (ISO), Liquid flow measurements in open channels – methods for measurement of suspended sediment, ISO 4363, 1977.
35. International Organization for Standardization (ISO), Liquid flow measurements in open channels – methods for bed material sampling, ISO 4364, 1977.
36. J. van den Berg and M. de Vries et al., Principles of River Engineering, Pitman, London, 1979.

37. International Organization for Standardization (ISO), Establishment and operation of a gauging station and determination of the stage-discharge relations, ISO Recommendation R-1100, 1969.
38. International Organization for Standardization (ISO), Investigation of the total error measurement of flow by velocity-area methods, TC113/WG1, nos. 177–179, 1971.
39. M.A. Benson, Measurement of peak discharge by indirect methods, World Meteorol. Org., publication no. 225, TP 119, Geneva, 1968.

CHAPTER 3

MORPHOLOGY OF STREAM CHANNELS

Symbols

A	– area, m^2 ; given point
a	– area for unit width of channel, m^2 ; meander amplitude, m ; section
B	– water surface width, m ; given point
b	– width of channel, m ; section
D	– ratio of longitudinal slopes
d	– water depth, m
d_s	– particle diameter, mm
\bar{d}	– hydraulic depth, m
E	– energy per unit mass, m
F	– a function
F_R	– Froude number
G	– a function
g	– acceleration of gravity, m/sec^2
I	– longitudinal slope
i	– water surface slope
i_y	– water surface slope in y -direction
J	– hydraulic gradient
L	– length of valley line, m
l	– actual stream channel length, m
M	– meandering index
m	– ratio of shear stresses
n	– Manning roughness coefficient
Q	– discharge, m^3/sec
Q_s	– sediment discharge, kg/m^3
q	– specific discharge, $m^3/sec/m$

R	– hydraulic radius, m
r	– cross-sectional index; radius of curvature, m
u_*	– shear velocity, m/sec
V	– velocity, m/sec; mean velocity, m/sec
V_b	– increased velocity along the bend, m/sec
V_x	– velocity in x -direction, m/sec
V_y	– velocity in y -direction, m/sec
V_0	– velocity in the straight reach, m/sec
v	– point velocity, m/sec
v_x, v_y	– point velocity in x - and y -direction respectively
x	– coordinate
y	– coordinate
z	– coordinate
α	– angle of confluence, angle
γ	– specific weight (force), N/m ³
ρ	– density, kg/m ³
τ	– shear stress, N/m ²
Δ	– parameter

3.1 Definition of an Alluvial Stream

Alluvial stream may be defined as an open conduit, with geometric dimensions – cross section, longitudinal profile and slope – changing with time, in dependence of discharge, material of the stream bed and banks, and quantity and quality of the solid sediment carried by the water.

The discharge in natural watercourses is governed by meteorological events, which are stochastic processes, likely to be subject to large fluctuations, and only to a minor extent amenable to human control. The flow in artificial channels, on the other hand, may also be non-uniform and unsteady, but it always remains more or less under the control of men.

Alluvial channels are virtually free to adjust their dimensions and shape in response to changing hydraulic conditions of flow and discharge in the first place; it is evident, therefore, that most parts of the stream bed and its banks are composed of the material transported by the stream under recent flow conditions (discharges), or at least during the latest geological age. This material, mainly the product of rock-weathering processes during long periods of time (see Chapter 6), is transported by the stream and slowly deposited upon the original geological formations. It is called *alluvium* (from the Latin “luere” – to wash), hence the name alluvial stream.

3.2 Erosion, Deposition and Sediment Transport Capacity

It can be shown by elementary hydraulics that, by equating the friction force along the wetted walls of an elementary channel stretch to the component of the gravitational force in the direction of flow, the shear stress (often also called *tractive force*), τ , is approximately a function of the hydraulic radius, R , and the hydraulic gradient, J , according to the equation:

$$\tau = \gamma R J = \rho g R J \quad (3.1)$$

where γ denotes specific weight, ρ – density, and g – acceleration of gravity. For further discussion of the subject, see Vol. I of the Manual.

Shear stress is related to the so-called shear or friction velocity, extensively used in fluid mechanics, by the expression

$$u_* = (\tau/\rho)^{1/2} = (gRJ)^{1/2} \quad (3.2)$$

in which u_* – shear velocity, ρ – density of water.

Use of shear velocity in basic equations of turbulent flow will be further discussed in Part 2 of the present text.

It should be borne in mind, however, that the approximate expression for the shear stress as given by Eq. (3.1) represents only the part caused by the flowing water. Additional forces are likely to act particularly upon stream banks, and their effect on the overall shear stress should be added to the value derived from Eq. (3.1). These additional forces are due to such factors, among others, as – flood variation, wind waves, piping, stage variations, seepage forces, freeze-thaw, etc., and may often increase the shear stress due to the flowing water by as much as 50%. If the maximum shear stress acting on the stream banks is estimated to be about 75% of τ as given by Eq. (3.1) – see par. 7.1 of Vol. I – the total shear stress may reach as much as about 1.25 τ . If this shear stress results higher than the critical shear stress as obtained from Shields diagram (see Fig. 9.2), erosion of banks is to be expected unless protected.

In order to gain an idea about the relative weight of different factors, some approximate values as indicated by Simons et al. [16] for noncohesive soils are given in Table 3.1.

Dynamic equation of flow in open channels in the form given by Manning, reads

$$Q = \frac{A}{n} R^{2/3} J^{1/2} \quad (3.3)$$

in which n is the Manning coefficient of roughness. It is also a function of the same parameters R and J , hence one may write: $\tau = f_1 (R, J)$; $Q = f_2 (R, J)$, and consequently $\tau = f_3 (Q)$.

TABLE 3.1. ADDITIONAL FORCES CAUSING SHEAR STRESSES [16]

Factors causing erosion	Relative value
Shear stress or velocity	1.0
Flood variation	0.03
Wind waves, surface erosion and piping	0.04
Stage variations	0.08
Seepage forces	0.08
Gravitational forces	0.09
Freeze-thaw	0.02

Example 3.1

Data: A broad stream, nearly rectangular, with width $b = 100$ m. $J = 0.5\%$; $n = 0.025$; permissible shear stress (for discussion of the permissible shear stress see Vol. 1, p. 74), $\tau_0 = 10 \text{ N/m}^2$.

Required: (1) For $J = \text{const.}$, determine the functions: $Q = f_1 (R, J)$; $\tau = f_2 (R, J)$; $\tau = f_3 (Q)$. (2) Find the discharge for which $\tau = \tau_0$.

Solution:

Step 1 – Approximate cross-sectional area is given by $A = bd$, in which b – width of the channel, m; d – water depth, m.

Step 2 – Using Eq. (3.3), the discharge can be computed:

$$Q = \frac{100d}{0.025} R^{2/3} \left[\frac{0.5}{1000} \right]^{1/2}$$

For wide and nearly rectangular channels $R \sim d$, hence it may be written $Q \cong 89.4d^{5/3}$, from which

$$d \cong R \cong \left[\frac{Q}{89.4} \right]^{3/5}$$

Step 3 – The shear stress

$$\tau = \gamma R J = 9.8 \times 10^3 \times \left[\frac{Q}{89.4} \right]^{3/5} \left[\frac{0.5}{1000} \right] \cong 5.0 \left[\frac{Q}{89.4} \right]^{3/5} \cong 0.337 Q^{3/5}$$

Step 4 – The calculated values of Q and τ are tabulated in Table 3.2.

Step 5 – In Fig. 3.1a, b and c, graphs are drawn of functions $Q = f_1(R)$, $\tau = f_2(R)$ and $\tau = f_3(Q)$, respectively.

TABLE 3.2. COMPUTED VALUES (Ex. 3.1)

$d \approx R$ (m)	Q m^3/sec	τ (N/m^2)
0.5	28.2	2.5
1.0	89.4	5.0
2.0	283.8	10.0
3.0	557.6	15.0
4.0	900.5	20.0

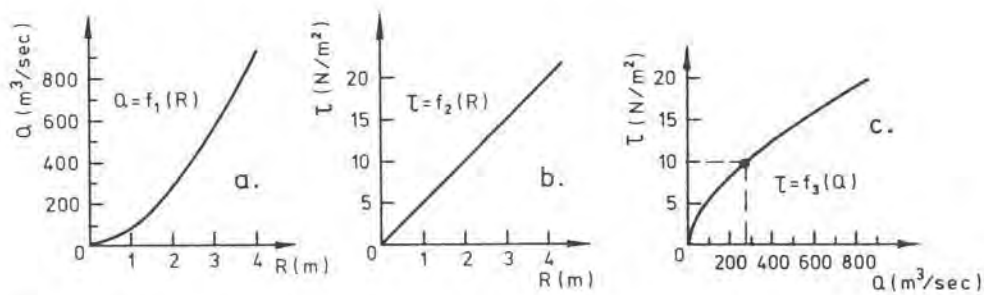


Fig. 3.1. Functions $Q = f_1(R)$, $\tau = f_2(R)$ and $\tau = f_3(Q)$.

Step 6 – As seen from Table 3.2 and from Fig. 3.1c, for the permissible shear stress of $\tau = 10 \text{ N/m}^2 = \tau_0$, the computed discharge is $Q \cong 284 \text{ m}^3/\text{sec}$.

Although the shear stress along the channel bed and banks is believed to be one of the main factors causing erosion, one should be well aware of the fact that shear stress alone is not the only factor responsible for the incipient erosion in a stream channel. Indeed, the phenomenon is far too complex for any simplistic approach to the full interpretation of its mechanism, besides the fact that the process is not fully understood to this very day. On the other hand, when dealing with the process on a macroscopic scale, as is done in the present chapter, the shear stress is likely to be the dominant factor in the majority of erodible stream channels. Hence the emphasis given to the shear stress in the discussion which follows.

Full discussion of all other factors likely to affect the incipient motion of sediment particles, and consequently the whole process of sediment transportation, will be given in Part 2 of the present text.

Main characteristics of alluvial stream channels – erosion, transportation and deposition – generally are directly linked to changes of the mean shear stress, which in its turn is governed by the flow rate in the stream. With increasing discharge, shear stress, τ , will eventually become larger than the permissible shear stress for the given channel, τ_0 , and then erosion is likely to begin. Water starts scouring at the stream bed, soil particles are picked up by the flowing water and transported downstream; this process will be intensified with increasing discharge, until the entire cross-section of the channel is affected.

As soon as the rate of flow starts falling off, a stage is reached when sediment particles, previously eroded and carried by the flowing water, start settling on the stream bottom. This deposition process obviously will take place at some location farther downstream from the region of the original scour.

Longitudinal slope of the channel bed is also affected by the continuous process of erosion and deposition, and in its turn it causes changes in mean velocities, and ultimately in the hydraulic gradient along the channel. The overall working cycle of an alluvial stream is thus a self-perpetuating and self-compensating process, since the shear stress itself depends both on the hydraulic radius and the hydraulic gradient.

Until eventually regime-type equilibrium conditions in a natural stream are established, there will be a continuous interplay between erosion and deposition separated by brief periods of temporarily stable conditions. At the start of the erosion cycle, local drawdown effects are gradually propagated upstream, causing increase in the sediment load and progressive coarsening of the bed material. This situation, however, is not likely to go

on for a long time, because the increased sediment load will soon start the deposition cycle, which will slowly move upstream due to local backwater effects. Eventually another period of short-lived equilibrium state will be reached, but aggradation upstream will in its turn reduce the sediment load, and a new erosion cycle will thus be initiated. Given enough time without external intervention, however, the magnitude and temporal extension of the oscillating cycles is bound to decline, leading in the end to a more or less permanent equilibrium condition.

During cycles of instability, channel dimensions tend to adapt to flows causing most of erosion or deposition. The erosion cycle will produce a channel of increased capacity, and hence the return period of the channel-shaping discharge will be extended. When depositing, capacity is diminished and the return period shortened.

It may, therefore, be said that an alluvial stream has no permanent geometry, since both its cross-section and slope are subject to continuous changes, and hence are in temporary equilibrium only. On the other hand, the erosion process generally has its own natural limits, determined by the finite carrying capacity of the water. In other words, the stream can increase its total sediment load by erosion until a certain limit is reached. Sediment load carried at this condition is an important characteristic of alluvial streams, and in the present text it will be called *sediment transport capacity* (STC). Being a mass per unit volume and unit time, STC is expressed in the units of g/lit/sec or equivalent. It depends on many flow parameters, among others discharge, shape of the channel bed, grain size, grain form, cohesion, specific gravity, etc. It is assumed that the water cannot transport more sediment than its STC. This means that if from any source whatsoever there already is a certain quantity of solids in the water, the stream will carry on its erosive activity only until its STC eventually is reached. It follows that clear water will erode more than sediment-laden water, and if STC is reduced following a decrease of the mean velocity, a part of the sediment will have to be settled and aggradation takes place.

Aggradation in alluvial streams, originally in equilibrium, due to increase in sediment supply has recently been studied analytically [2, 3], and some limited results have been obtained. It has further been reported from laboratory studies that the rate of sediment transport under non-uniform flow during the aggradation process appears to be generally smaller than that for uniform flow at the same mean velocity [4].

A great number of researches and field works have been directed towards the quantitative determination of the functional relationship between STC and the various flow parameters, but unfortunately up to the present it has remained a rather elusive goal.

In the following paragraphs the analysis will, therefore, be mainly confined to qualitative aspects only.

Although in the present text the shear stress approach to the channel scour and erosion is preferred, many engineers still find it handy to use the old concept of the *permissible mean velocity*. Tables listing these velocities for both non-cohesive and cohesive soils, and for various conditions of flow, are extensively given in Vol. I of the Manual, Part I, Chapter 4. It has been questioned, however, whether these mean values, prevalently obtained for perennial streams, may be also applied to ephemeral streams of arid and semi-arid regions. Recently, analysis of data collected from many such streams in southern USA, with only intermittent flow, appears to suggest [36] that permissible velocity values as given by Fortier and Scobey more than 50 years ago for non-cohesive soils, and Russian values for cohesive soils as reported by V.T. Chow [37], are fairly appropriate not only for constant flow conditions, but also for intermittent flows of ephemeral streams.

3.3 Evolution and Formation of Alluvial Streams

3.3.1 Symbols and Terminology

- Q – water discharge of the stream, m^3/sec .
 Q_{s0} – sediment discharge of the stream; quantity of sediment passing a cross-section during unit time, kg/sec
 d_s – a characteristic dimension of sediment particles, mm
 r – cross-section index,
 M – meandering index.
- Sediment – all solid material carried by the water in any way,
 Bed load – part of the sediment moving along the channel bottom, or close to it, by rolling, sliding or saltating,
 Suspended load – part of the sediment carried in suspension,
 Wash load – part of the sediment brought into the stream from the watershed, either by the overland flow or by the action of wind. It consists mainly of clay and silt particles, settling only in nearly stagnant water.
 Bed-material load – that part of the sediment which originates from the stream bed; hence it includes both the bed load and the suspended load.

3.3.2 Cross-Section Index and Meandering Index

It has already been pointed out that alluvial stream channels, due to the continuous process of erosion and deposition, have ever-changing cross-sections, now being aggraded (deposition), now being degraded (erosion). In order to express these changes, a characteristic ratio, called *cross-section index*, is often used

$$r = \frac{\bar{d}}{B} = \frac{A}{B^2} \quad (3.4)$$

in which $\bar{d} = A/B$ – hydraulic depth; B – water-surface width, see Fig. 3.2.

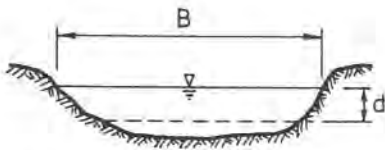


Fig. 3.2. Definition of the cross-section index.

Flow in natural stream channels is unsteady for most of the time. Generally speaking, fluctuations of depth in alluvial channels for a given change in discharge are less than for fixed-boundary channels, because alluvial channels continuously adapt the flow section and roughness. In the final analysis, however, all of its main geometric characteristics are likely to be affected to some degree by each separate group of discharges, by the duration of single flow rates, their intensity and sequence.

Alluvial streams rarely flow for any appreciable length along a straight line, but rather in a series of curves, called *meanders*. Even those streams which at first sight appear not to meander for longer stretches, will unvariably prove to be also subject to natural oscillations. Because meandering is an essential aspect of alluvial channel mechanism, it will be discussed in more detail in par. 3.7. At this point only the geometric aspect of a meandering stream is expressed by a characteristic index which denotes to what extent a given alluvial stream deviates from following the center-line of the valley, see Fig. 3.3.

The ratio of the actual stream channel alignment to the corresponding length of the valley line is called the *meandering index*, denoted M ,

$$M = \frac{\sum l_i}{\sum L_i} \geq 1 \quad (3.5)$$

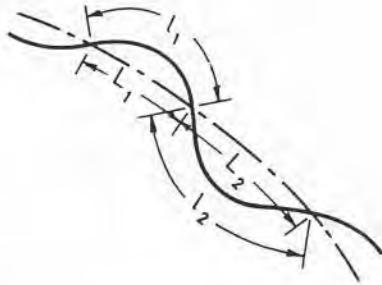


Fig. 3.3. Meandering stream.

According to the very nature of alluvial streams, meandering index is never a constant for a given alluvial channel, but is rather continuously varying around a characteristic value. Lack of constancy for both the cross-section index and the meandering index is another expression of the fact that alluvial streams are generally in temporary and precarious equilibrium only.

3.3.3 Development Process of the Stream

The complexity of morphological processes which determine the continuous formation and deformation of an alluvial stream has already been repeatedly emphasised. These processes deal with the behavior of materials forming and flowing through the alluvial bed; hence the temporary nature of any given state of equilibrium. It is, therefore, reasonable to ask whether there is a possibility at all to make at least a qualitative engineering evaluation or prediction about the mutual influence of the various parameters on which interplay these processes largely depend.

Morphological processes in any natural stream are ultimately the product of many varying rates of flow, each one adding to the chain of events that give shape to the alluvial channel. In spite of this fact, it has been argued for a long time that the steady discharge which would grossly produce the same shapes and dimensions as the natural sequence of events, is to be considered as the *formative discharge*. According to laboratory experiments and field-data correlation [30, 38], it appears that approximately the bankful discharge of the channel, or the discharge transporting most sediment and having a recurrence period of about one year, is to be considered as the formative discharge. The latter part of this rule, however, obviously cannot be applied to ephemeral streams of semi-arid and arid regions (see par. 10.6).

If it is again assumed, as it has been so far, that the two dominant physical

parameters are the shear stress and the STC of the stream, some simple conclusions, fairly well supported by the evidence from observations in nature, can be arrived at. It is believed that the accumulated data and experience about many streams in different parts of the world do justice to such an approach, without understanding the influence of many other parameters concurring in the overall process to a greater or lesser degree.

A similar approach has been adopted by Kuiper [1] who has tried to explain various flow cases by means of a hypothetical hydraulic model. In the present text the model has been replaced by a natural stream system, in keeping with the authors' view that the conclusions of the analysis generally hold good for any alluvial stream under normal conditions. The system has been greatly simplified in order to make sure that the main features of the stream mechanism do not become obscured by too many complicating factors. The simplified flow system is shown in Fig. 3.4.

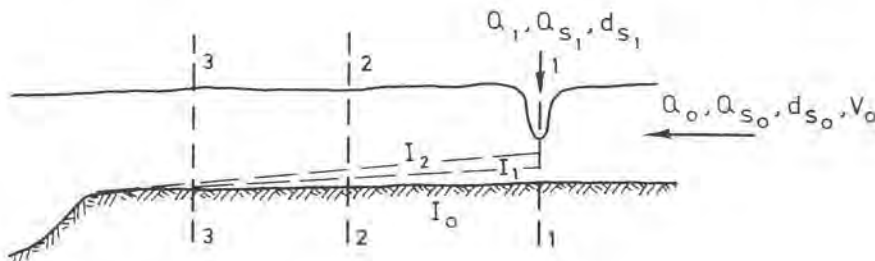


Fig. 3.4. Natural river system.

Let us assume first that in the main stream channel the rate of flow, Q_0 , the sediment discharge, Q_{s0} , and the mean diameter of sediment particles, d_{s0} , remain constant during all the time of observations. It is further assumed that the longitudinal slope of the stream, I_0 , is very mild, and that it has not yet reached its sediment transport capacity. Local sedimentation phenomena due to stream confluences are not considered in the present context, but are analysed in par. 3.7.

Case 1

A small tributary joins the main stream at section 1. It has the discharge, sediment load and mean diameter given by Q_1 , Q_{s1} and d_{s1} respectively. As long as Q_1 and Q_{s1} stay relatively small, they probably will not cause the main watercourse to reach its STC and will be carried along with the water. If the sediment load from the tributary increases, the main stream may

eventually reach its STC, and then a part of the combined sediment load, Q_{si} , will be deposited somewhere downstream of section 1. Because of this, when coming to section 2, the water will contain less sediment, and at section 3 it will be further reduced in quantity. Given sufficient time, a new bottom line will be developed, having a steeper slope, $I_1 > I_0$. Following the increased combined discharge and the steeper slope, the average velocity in the main stream also will increase, $V_1 > V_0$. Should the stream at this stage still not attain its STC, this process will go on until a new and steeper longitudinal slope is developed, $I_2 > I_1$, and the velocity is further increased to $V_2 > V_1$. At this or at some other stage, the mainstream is likely to eventually reach its STC, and then the sediment deposition will start. By that time the stream will have arrived at a temporary equilibrium.

If the sediment concentration (sediment discharge relative to water discharge) in the tributary does not stay constant, but actually increases with increasing discharge, as is generally the case in natural streams, the above analysis remains essentially unchanged, but for the time-table of the events.

Case 2

The initial state is the end of Case 1, by which time a new, steeper, longitudinal slope in the main stream, I_i , is supposed to have been developed.

Both the liquid and the solid discharge from the tributary, Q_1 and Q_{s1} respectively, start now decreasing. Reduced combined discharge, Q_i , will lower STC in the main stream, but on the other hand the combined sediment discharge, Q_{si} , will also be lower, hence the temporary equilibrium arrived at by the end of Case 1 is likely to be maintained for some time. If both discharges from the tributary go on falling off, the STC of the main stream will eventually become too small to cope with the combined solid discharge, and then deposition is likely to start again, until a new slope I_i is formed, steeper than the initial-state slope, bringing the system closer to a new temporary equilibrium.

In the alternative case of the diminishing liquid discharge, Q_1 , from the tributary, but constant solid discharge, Q_{s1} , the overall picture remains unchanged, but the deposition process and the formation of a steeper slope I_i are likely to be somewhat accelerated.

Case 3

The initial state is assumed to be the end of Case 1, with the longitudinal slope in the main channel being I_i .

If now the liquid discharge from the tributary, Q_1 , starts increasing while the solid discharge, Q_{s1} , remains constant, after a certain period of time the main stream will be below its STC. Hence, erosion will start until a new state

of temporary equilibrium is reached by adjusting the STC of the main stream to some new and reduced characteristic sediment concentration. When that stage is reached, a new longitudinal slope will be established, milder than the initial one at the end of Case 1 period.

In very general terms, it could be said that if the solid discharge and the characteristic grain size, Q_s and d_s , remain essentially constant, while the liquid discharge keeps growing, the trend will be toward erosion and milder slope. With a decreasing discharge under similar conditions, the trend is likely to be reversed, i.e., toward deposition and steeper slope. During periods of increasing or decreasing flow rates without comparable variation in solid discharge, there is generally a short transitional interval during which all the main morphological parameters are in some state of unstable equilibrium. In small mountain streams, where there are large variations of discharge ($Q_{\max} \gg Q_{\min}$), changes of longitudinal slope also are extreme ($I_{\min} \ll I_{\max}$), while the duration of the temporary equilibrium may be no more than a matter of hours. In larger streams, discharge variations and corresponding slope changes are likely to be much less pronounced, with temporary equilibrium periods generally longer (days, weeks or even months).

Case 4

Again the initial state is assumed to be the end of Case 1.

The case is now considered in which the liquid discharge stays more or less constant, while the solid discharge undergoes changes. This situation is mostly brought about through human activity, such as construction of a dam, soil conservation, urbanisation of the watershed, deforestation, afforestation, and similar.

When the solid discharge, Q_s , starts falling off, the stream will soon be below its STC, and consequently the erosion process will be initiated and will go on until a new milder longitudinal slope is formed. If there is an increase of the solid discharge, the sediment content in the stream is bound to eventually exceed its STC, and this will cause the deposition process to be started. The initial longitudinal slope, I_i , will slowly be changed into a new, steeper one.

It should once more be stressed that the simple criterion adopted for the above analysis is no doubt incomplete, and that many additional parameters, other than STC, should also be taken into account if a full picture is to be obtained. However, it is nevertheless believed that the general conclusions about the morphological trends reached by the simple analyses are essentially valid in the qualitative sense for all alluvial streams. Additional parameters are likely mainly to affect the quantitative analysis and the timetable of the events.

In the following, three typical cases are considered, frequently met with in the engineering practice. They are brought about through human interference, hence are not included in the context of the previous analysis, although obviously can easily be deduced from it.

Case a: Liquid discharge, Q , solid discharge, Q_s , and mean grain diameter, d_s , remain constant, while the longitudinal slope I is artificially decreased. This frequently is the case in irrigation or drainage earth channels, or in small natural streams, when drops are built in order to prevent scouring due to steep longitudinal slope. Direct result of such a stream training is the lowering of the STC, and subsequent diminishing of the erosion. This effect is generally attained for the design discharge and higher rates of flow, but on the other hand, deposition is likely to be increased at lower discharges.

Case b: The opposite situation, in which Q , Q_s and d_s remain essentially constant but the longitudinal slope is made artificially steeper, is also sometimes encountered in engineering practice. It generally occurs when for whatever purpose the stream channel is transferred from a natural location of mild slope to another one of steeper slope. Such operations will be discussed in the chapter on flood-protection.

At the beginning, for periods that may range from a few years to tens of years, there will be an increased erosion due to higher values of the STC. Slow flattening of the longitudinal slope will take place during long periods of time, until a milder bottom slope is established.

Case c: This is in fact an extension of the Case b, but is here briefly reviewed under a separate heading, because in engineering practice it is known as a stream cut-off (see Fig. 3.5).

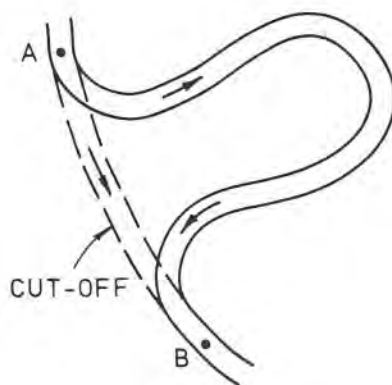


Fig. 3.5. The cut-off.

The use of cut-offs and their application in drainage engineering will be discussed in later chapters. In the present context it is only pointed out that if the elevations at points A and B remain unaltered, the longitudinal slope between the two points along the cut-off is considerably increased. There are two transitions: (a) from the mild slope upstream of point A to the steeper slope of the cut-off; (b) from the steeper slope of the cut-off to the mild slope downstream of point B.

The erosion generally starts not far from point A, and the eroded material is first carried by the water along the cut-off and then deposited in the vicinity of point B. With time, the erosion moves upstream from point A, and the sedimentation advances downstream from point B (see Fig. 3.6).

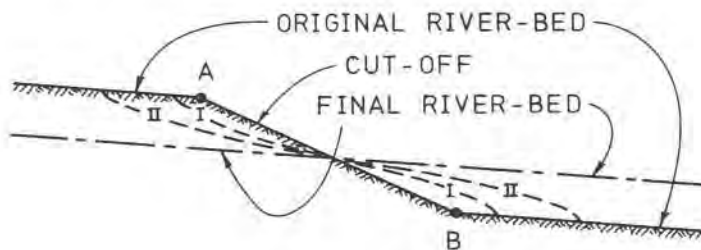


Fig. 3.6. Erosion and deposition at cut-off.

This so-called “back erosion” and the progressing deposition are carried on by the stream until eventually a new longitudinal slope is established, more or less similar to the original slope. It is worth noticing that the stream bed upstream from point A will be lowered with time, while downstream from point B it will be raised above the original stream-bed before the construction of the cut-off. Such reduction of the channel capacity in the downstream part may often cause flooding at higher discharges, since the water can no longer be contained within the stream channel.

3.3.4 Self-adjustment of the Cross-section

In keeping with the general tendency of natural phenomena to approach a state of temporary equilibrium, alluvial streams tend to adjust themselves to the changing conditions of flow and the many parameters that are connected with it, and which determine their dynamic balance. This generally does not only imply the adjustment of the longitudinal slope, as discussed in the

preceding paragraph, but of the flow section as well, which means the depth and the width of the channel.

If again we adopt the greatly simplified but acceptable view that the average shear stress, τ , is the decisive factor determining the general trend of morphological processes in alluvial streams, one could say that at all stages the stream tends to a state of constant shear stress, $\tau = \text{constant}$. And again: this obviously is not meant to say that the influence of other important factors always remains negligible, but rather that in most cases the qualitative analysis based on the simplified assumption is very likely to be acceptable.

Let us look at a broad stream channel with constant liquid and solid discharges, Q and Q_s respectively. At some station its longitudinal slope changes from I_1 to I_2 (see Fig. 3.7). The new depth of flow, d_2 , obviously is determined by the slope I_2 , but it is assumed that the width b of the channel remains constant; the parameters d_s , M and the Manning roughness coefficient, n , also stay constant. Only straight stretches of uniform flow are considered.

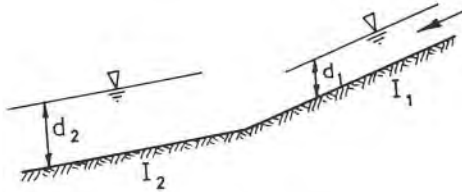


Fig. 3.7. Change of longitudinal slope.

According to the above assumptions:

$$Q_1 = Q_2 = Q = \text{const.}$$

$$B_1 = B_2 = B = \text{const.}$$

$$q_1 = q_2 = q = Q/B = \text{const.}$$

Area for unit width of the channel, $a_1 = d_1$, $a_2 = d_2$.

For broad channels it can be assumed that hydraulic radius is equal to the depth of flow, hence $R_1 \cong d_1$, $R_2 \cong d_2$.

Using the Manning equation for uniform flow, and by continuity,

$$q = \frac{d_1}{n} d_1^{2/3} I_1^{1/2} = \frac{d_2}{n} d_2^{2/3} I_2^{1/2} \therefore \left[\frac{d_1}{d_2} \right]^{5/3} = \left[\frac{I_2}{I_1} \right]^{1/2}$$

and from here

$$d_2 = d_1 \left[\frac{I_1}{I_2} \right]^{3/10}$$

Now, the average shear stress from Eq. (3.1) and using the above relationships, $\tau_1 = \gamma d_1 I_1$; $\tau_2 = \gamma d_2 I_2 = \gamma d_1 I_1^{3/10} I_2^{7/10}$.

From the above expression for τ it is evident that the shear stress is not constant, although the depth of flow has changed from d_1 to d_2 according to the dynamic equation for uniform flow, Eq. (3.3); indeed, if $I_1 > I_2$, the factor $(I_1^{3/10} I_2^{7/10}) < I_1$, meaning that $\tau_2 < \tau_1$, and vice versa. Hence under these conditions the stream will not be able to attain its goal of keeping constant shear stress along its course.

In fact, change of slope, as a general rule, is accompanied by a corresponding change not only in the depth of flow but also in the channel width. Let us consider again an alluvial channel having a more or less rectangular section. Longitudinal slope changes from I_1 to I_2 as before. The requirement this time is constant shear stress, i.e. $\tau_1 = \tau_2$.

From consideration of continuity and the Manning equation for uniform flow, roughness coefficient, n , assumed constant for both stretches of the channel,

$$A_1 R_1^{2/3} I_1^{1/2} = A_2 R_2^{2/3} I_2^{1/2} \quad (3.6)$$

On the other hand, from the requirement $\tau_1 = \tau_2$, and using Eq. (3.1), $R_1 I_1 = R_2 I_2$ from which

$$R_2 = R_1 \frac{I_1}{I_2} \quad (3.7)$$

Introducing this expression into Eq. (3.6), the following relation is obtained,

$$A_2 = A_1 \left[\frac{I_2}{I_1} \right]^{1/6} \quad (3.8)$$

Rewriting Eqs. (3.7) and (3.8),

$$\frac{B_2 d_2}{B_2 + 2d_2} = \frac{B_1 d_1}{B_1 + 2d_1} \frac{I_1}{I_2}$$

$$B_2 d_2 = B_1 d_1 \left[\frac{I_2}{I_1} \right]^{1/6}$$

Simultaneous solution of the above two equations yields a quadratic equation:

$$2d_2^2 - (B_1 + 2d_1) \left[\frac{I_2}{I_1} \right]^{7/6} d_2 + B_1 d_1 \left[\frac{I_2}{I_1} \right]^{1/6} = 0 \quad (3.9)$$

Denoting: $I_2/I_1 = D$; $B_1 D^{1/6} = G$; $(B_1 + 2d_1) D^{7/6} = F$, Eq. (3.9) can be written $-2d_2^2 - Fd_2 + Gd_1 = 0$, having the solutions

$$d_2 = \frac{F \pm (F^2 - 8Gd_1)^{1/2}}{4} \quad (3.10)$$

and the new channel width that satisfies the requirement $\tau_2 = \tau_1$,

$$B_2 = B_1 \frac{d_1}{d_2} D^{1/6} \quad (3.11)$$

The solution for d_2 has a real value only when $F^2 \geq 8Gd_1$, or writing in the expanded form,

$$\left[\frac{8B_1 d_1}{(B_1 + 2d_1)^2} \right]^{6/13} \leq \frac{I_2}{I_1} \quad (3.12)$$

Similar expressions, algebraically much more complicated, could easily be developed for any other prismatic channel section. For any arbitrary relationship between the shear stresses, $\tau_2/\tau_1 = m$, Eqs. (3.10)–(3.12) become

$$d_2 = \frac{\frac{1}{m^{5/3}} F \pm \left[\frac{1}{m^{10/3}} F^2 - 8 \frac{1}{m^{2/3}} Gd_1 \right]^{1/2}}{4} \quad (3.13)$$

$$B_2 = \frac{1}{m^{2/3}} B_1 d_1 \left[\frac{I_2}{I_1} \right]^{1/6} \quad (3.14)$$

$$\left[\frac{8 m^{8/3} B_1 d_1}{(B_1 + 2d_1)^2} \right]^{6/13} \leq \frac{I_2}{I_1} \quad (3.15)$$

Now let the foregoing be applied to two simple numerical examples.

Example 3.2

Given: $B_1 = 5.0$ m	$I_2 = 1.0\%$
$d_1 = 2.0$ m	$\tau_1 = 5.5$ N/m ²
$I_1 = 0.5\%$	

Required: find B_2 and d_2 , so as to fulfil the requirement $\tau_2 = \tau_1$.

Solution:

1. First check for real roots of the quadratic equation,

$$I_2/I_1 = D = 2$$

Hence, applying Eq. (3.12),

$$\left[\frac{8 \times 5.0 \times 2.0}{(5.0 + 2 \times 2.0)^2} \right]^{6/13} = 0.994 < 2$$

Accordingly, real solution is possible.

$$2. \quad G = B_1 D^{1/6} = 5.0 \times 2.0^{1/6} = 5.6$$

$$F = (B_1 + 2d_1) D^{7/6} = 20.2$$

Hence, the quadratic equation has two roots, $d_2' = 9.5$ m; $d_2'' = 0.6$ m.

From the physical point of view, the second root is relevant. The new width of the channel downstream,

$$B_2 = B_1 \frac{d_1}{d_2} D^{1/6} = 18.7 \text{ m}$$

Self-adjustment of such a magnitude, enlargement of the stream channel by almost 400%, obviously would require many years or decades to take place. During this long period of time the dominant discharge, and accordingly d_1 and B_1 , will probably have changed several times, so that the final adjustment will have to reflect these fluctuations. The adjustment process may be shortened by stream training in which the channel is artificially made wider.

In the next example it is assumed that the permissible shear stress in the steeper channel is higher.

Example 3.3

Data: As in Example 3.2.

Required: B_2 and d_2 , so that $\tau_2 = 1.4 \tau_1$.

Solution:

Using Eq. (3.12), $1.5 < 2$, real solution possible. By Eq. (3.10), $d_2 = 0.92 \sim 0.9$ m, and finally Eq. (3.11) gives $B_2 = 8.96$ m ~ 9 m.

Morphological formation patterns of alluvial streams considered so far may occur either under action of natural dynamic conditions induced by the masses of flowing water, or by human interference into natural equilibrium conditions. In the latter case the time span for changes to occur may be relatively short, months or years; in the former one, the formative period is likely to be measured in decades or hundreds of years. Major changes of whole stream systems due to slow shifting of earth-crust layers, or to cyclic climatic alterations, generally take place during much longer periods of time, hence are of minor concern from the engineering point of view.

Recent reanalysis of Schumm's data for Great Plain perennial streams using multiple regression techniques suggests that channel-perimeter sediment characteristics play only a minor role in the development of channel shape. Discharge (i.e. velocity, or finally the shear stress) appears to be the dominant factor controlling the ratio of width to depth [25].

3.4 Grain-Size Gradation of the Sediment

In the present paragraph a brief discussion is given about some of the purely qualitative aspects of the sediment gradation and its influence on the

morphological behavior of stream channels.

So far mainly the relations between the liquid discharge, Q , solid discharge, Q_s , and alluvial-stream geometry have been studied in some detail. Very little has been said about the influence of the grain size and other parameters characterising the agglomerate of sediment grains.

With the growing rate of flow and higher velocities, the shear stress is bound to increase, and consequently larger forces are exerted on discrete sediment grains. Larger and heavier grain particles will be lifted, removed and finally transported by the flowing water. In other words, the mean grain size of the sediment transported by the stream is largely dependent on the dominant liquid discharge.

Considering a stretch of the channel in which for a given time period the longitudinal slope is assumed to remain constant, one can say that the mean grain size is dependent on the discharge, or $d_s = f(Q)$. Here the discharge, Q , is the independent variable, whereas the mean grain size, d_s , is largely determined by the functional relationship. Schematic graphical presentation of the various functional relationships is given in Fig. 3.8.

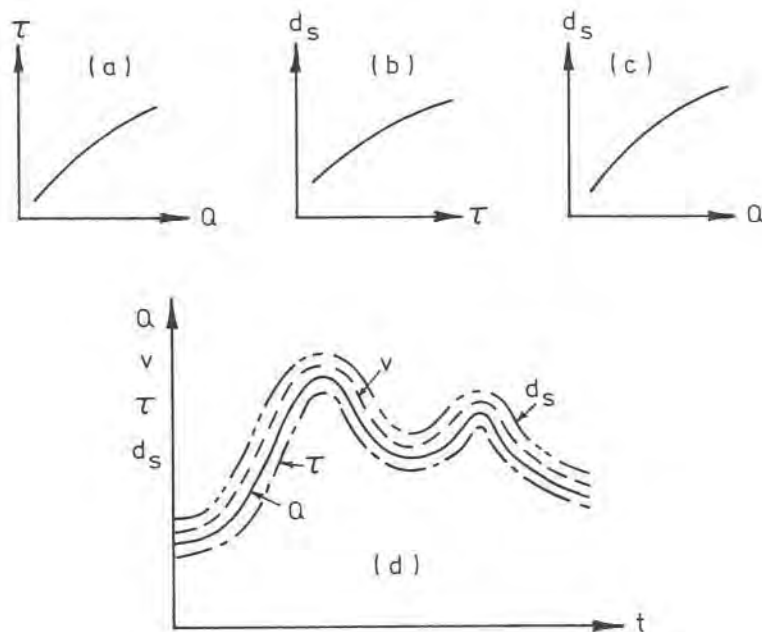


Fig. 3.8. Dependence of mean grain size on liquid discharge.

On diagram (d) all the parameters are qualitatively presented as functions of time, with the purpose of stressing the fact that all of them vary in time more or less as does the discharge, Q .

The agglomerate forming the stream-bed is generally composed of a wide spectrum of grain-size fractions, such as silt, fine and coarse sand, gravel, pebbles, etc., and all or most of them could be found in the bed material at any time. However, not all the sediment fractions are necessarily being transported at any given time.

As long as there is a low rate of flow in the stream, the water will generally be able to pick up and remove only fine sediment particles, leaving behind the coarser material. If the flow goes on decreasing, or eventually ceases altogether, the hitherto transported fines will start settling down on top of the coarser particles. As a result of this process, there will finally be stretches of the channel-bed covered mainly with coarser particles, and other stretches covered mainly with fine sand and silt.

At higher discharges probably all fractions are removed and transported, except perhaps heavy and large stones. When the flow starts falling off, first larger and heavier particles begin settling; with further decrease of discharge, fines also start settling. Both processes are schematically shown in Fig. 3.9.

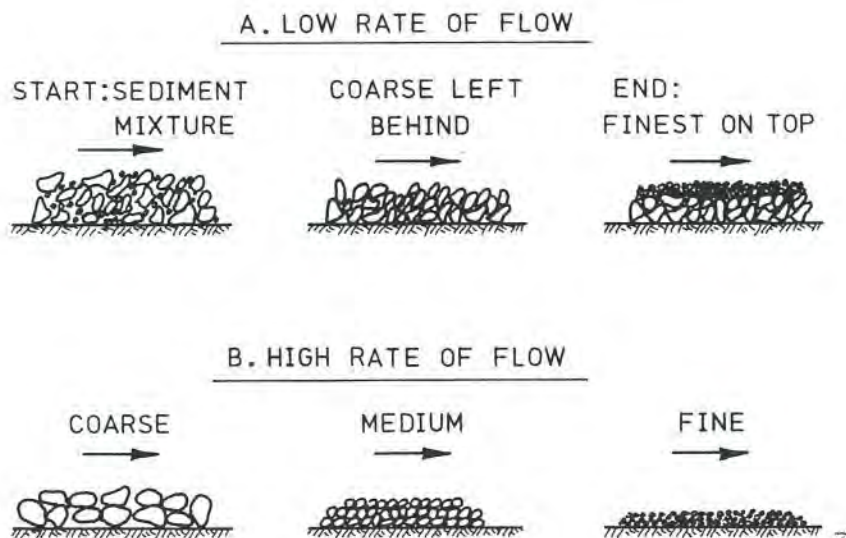


Fig. 3.9. Stream-bed composition in dependence of discharge.

After a cloud-burst which covers practically the whole of a small watershed area – a frequent occurrence in semi-arid climates – there may be a sudden and steep flood-wave accompanied by very high discharge during a relatively short time period; high flow often ceases as suddenly as it began. In such cases it is quite possible to find coarse material on top of the fines along short stream stretches, see the schematic drawing in Fig. 3.10.a.

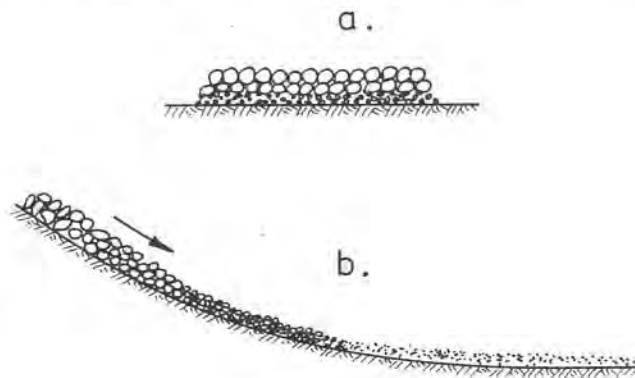


Fig. 3.10. Schematic grain-size gradation along a stream.

Varying slopes along a stream channel, and accompanying variations of the average flow velocity, generally have a distinct effect upon the grain-size gradation. In the upper mountain reaches, where the longitudinal slope is steep, sediment particles of almost all fractions are entrained by the water flowing at high velocities, with possible exception of large stones and boulders. Eventually all finer fractions are carried away by the stream, leaving behind only larger ones and boulders, which with the help of armouring effect are able to withstand the entrainment forces. As soon as plain-hills are reached, the slope becomes less steep and flow velocity correspondingly drops; as a result, bigger stones stop being rolled along the bed by the flowing water and stay motionless, while larger fractions of sediment start settling on the bed. When finally the stream enters the alluvial plain, the slope flattens further, and the stream channel becomes wider and deeper, with additional reduction of flow velocities. At this stage the stream can carry only the fines, which also are deposited in the end-reaches of the watercourse, where the slope becomes almost horizontal. The above process, very schematically outlined, is the cause of the typical grain-size

gradation profile along a stream course, schematically shown in Fig. 3.10b. Varying discharges and flood waves, as well as engineering structures obstructing the water passage to some degree, are likely to make the overall picture much more complex than the one obtained from a simplified analysis, but the general trends nevertheless remain valid.

In the preceding short analysis of the highly complex natural phenomenon of grain-size gradation in a typical stream channel, only broad trends have been emphasised, rather than a detailed and complicated picture, which probably would only obscure these features of general validity.

Summing up, it could be said that the grain-size gradation is mainly determined by parameters such as: longitudinal slope changes due either to topography or the erosion-deposition processes previously discussed; variations in discharge, nature and size of sediments brought to the stream from the watershed, obstructions to flow, etc. Some of these parameters, and many others of lesser importance, are mutually dependent, and others are independent. Causal relationships between these parameters and the sedimentation process itself generally are not amenable to mathematical analysis, although lately attempts have been made to build mathematical models adapted to specific rivers, which can then be numerically solved by the simplifications and neglect of many less important parameters, so that their forecast of sediment movement should always be corroborated by field observations and measurements.

3.5 Alluvial Cones and Fans

At locations in which an alluvial stream suddenly changes its slope from relatively steep to mild, as for instance when leaving mountainous area and entering alluvial plain, or where a steep tributary meets a flat stream, an alluvial fan may develop, calling for the strict attention of the design engineer. These alluvial formations in fact are similar to stream-deltas, which will be discussed in the following paragraph, but instead of water, they are deposited on land, and are particularly characteristic of arid and semi-arid zones (see par. 10.6).

Several chronological stages of the alluvial-fan development are schematically shown on Fig. 3.11.

Stage (a) – A relatively unobstructed or recently regulated stream channel carries the water safely within its banks;

Stage (b) – Beginning of sediment deposition, part of the available cross-section is blocked;

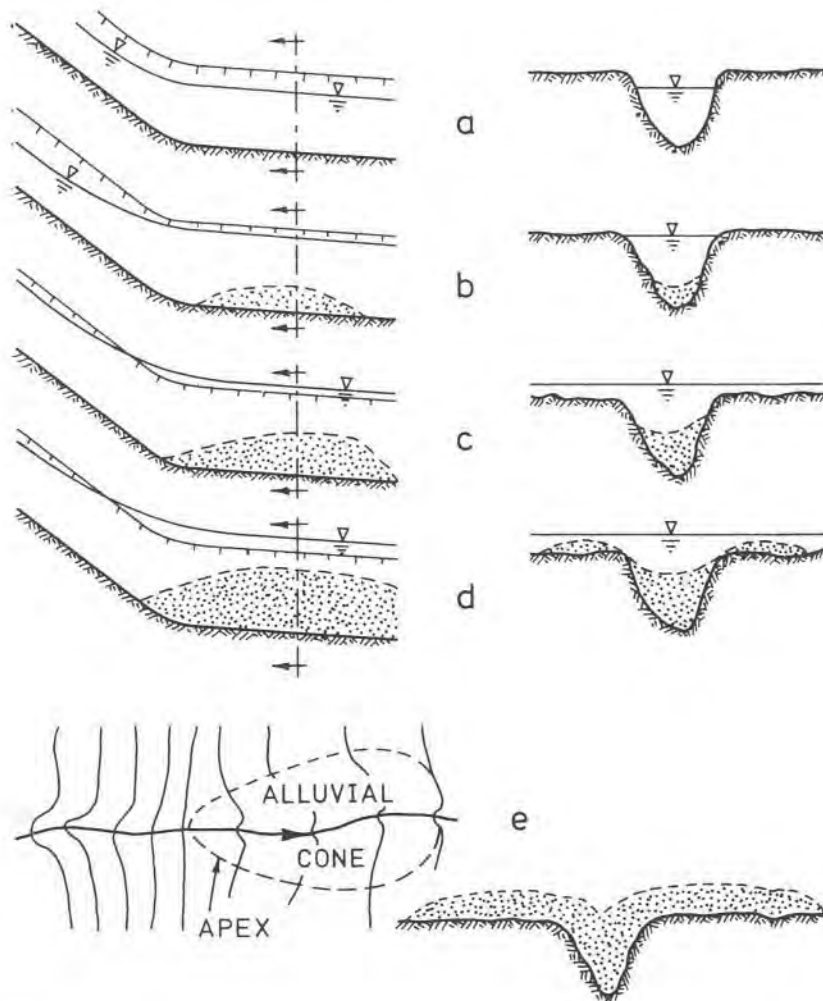


Fig. 3.11. Alluvial cone and fan formation stages.

Stage (c) – Sediment deposition continues, stream channel fills up and the water starts to overflow the banks, flooding part of the adjacent area, the flood-plain;

Stage (d) – The water which has overflowed the banks moves with a very low velocity over the flood plain, and fine sediment settles down on both sides of the stream-bed. This is already a highly undesirable situation, since the flood-waters cannot be drained back into the main stream channel;

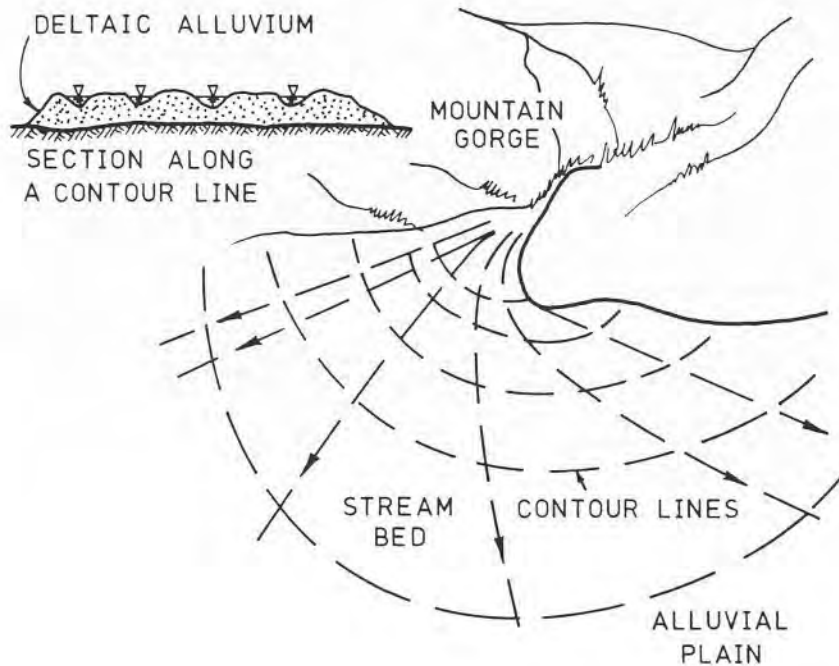


Fig. 3.12. Alluvial fan.

Stage (e) – At this stage the channel bed is higher than the surrounding area, and this situation is justly known as an “elevated stream-bed”. It consists mainly of recently deposited fine sediment. The area of sediment deposition outside the stream channel proper grows continuously from this stage on.

This elevated area is called the *alluvial cone*. When the water flowing over the cone fans out in the form of branching gullies, it is known by the name of *alluvial fan* (see Fig. 3.12).

As mentioned before, the main cause for the formation of an alluvial cone is probably the abrupt changes of the channel slope, but recent studies [5] and field observations seem to indicate that the deposition is also the result of change in channel width and the corresponding reduction of flow volume as the water fans out over an ever larger area.

The apex of the cone is located at the head of the mountain front, and from this point deposits spread out fan-like into the plain and finally merge with it. At the apex the sediment is generally a mixture of gravel and sand, becoming progressively finer toward the margins. Slope of the cone is the

steepest at the apex, diminishing toward the periphery, but it appears that near-critical slope is probably the natural condition for the majority of alluvial fans [6].

Recent field observations and measurements also seem to indicate that the slope of the fan surface varies directly as the steepness of the stream grade and indirectly with watershed size upstream of the cone apex. Erodibility of drainage basins, climatic regional characteristics and tectonic environment are additional parameters influencing the shape, extension and composition of alluvial fans [7].

Long-term observations point to erratic and unpredictable behavior of flows over alluvial fans. During flood waves, temporary channels are formed that are rather prone to lateral migration and sudden relocation, often during the one and the same hydrological event [6]. Because of this, practically all parts of the fan are exposed to potential flooding hazards (see Chap. 10).

3.6 Stream Delta

When a stream finally reaches the sea, or any other expanse of water, it loses most of its tractive power and deposits all of its sediments, including the finest silt and clay fractions. The deposited sediment generally takes the form similar to an alluvial fan, but its formation is much more complex, because of additional parameters that are of considerable influence, such as sea waves and breakers, offshore currents and tidal motion. Tectonic and geological properties of the coastal plain are also of great importance to the formation of natural stream mouths, particularly the soil subsidence under the sediment load, and the uplift forces. From the engineering point of view, stream mouths may generally be of three main types: 1) *estuaries*, 2) *lagoons*, and 3) *deltas*. In the following only delta-type stream mouths will be reviewed, not only because they are by large the most widespread, but also because they have many features in common with all the other forms. The name given to deltaic stream-mouth depositions refers to the Greek letter delta, and historically was first attributed to the mouth of the river Nile by the Greek historian Herodotus about the year 450 B.C.

Delta is a highly dynamic natural phenomenon, since it is actually the result of a continuous contest and interaction between the stream and the sea or other water expanse. The stream manages to deposit its sediments more quickly and efficiently than the dispersive action of sea waves and currents to carry them off into the sea.

Climatic conditions of the drainage basin determine to a great extent the shape of the delta. In temperate climates, where the flow and the sediment

load generally are more or less evenly distributed throughout the year, stream channels of the delta tend to be stable and well adapted to the whole range of discharges conveyed by the stream. In arid climates, on the other hand, flood conditions tend to be erratic, and large quantities of water and sediment are carried by the stream during relatively short periods of time. As a consequence, distributary channels never fully adjust themselves to such large influx of water and sediment. Many new channels are rapidly formed during the flood wave, to be filled up and abandoned as floodwaters recede. This process, often repeated, causes instability and migratory tendency of the whole deltaic system.

Within the delta proper, sediment transportation is in form of bed load and suspended load, but mainly in the latter form. Stability of distributary channels depends to some degree on the form of sediment transportation: channels carrying larger volumes of bed load generally tend to be wide and shallow, and are subject to rapid lateral migration; high concentrations of suspended load, on the other hand, tend to cause narrow and deep channels that are relatively much more stable.

Absolute quantity of the sediment load also exerts an additional control on the shape and extent of the delta. In fact, the greater the difference in density between the stream water and sea water, the narrower the sediment plume that moves offshore from a stream mouth. Thus the lateral spreading of the sediment load is controlled to some degree by the density of flood waters. A typical small-stream delta is shown in Fig. 3.12a.



Fig. 3.12a. Delta of a small stream (Jordan River at the Dead Sea). High difference in density between the stream water and sea water [Hebrew University].

Formation of sand islands in the delta region is also sometimes a characteristic of the deposition process, particularly in regions of larger tidal movements of the sea.

A typical cross-section through a stream delta generally shows several sets of bed layers superimposed one on top of the other. In the subaerial part (see Fig. 3.13) mostly channel sands and natural silts are found. Deposits at the delta front are laid down in a subaqueous environment immediately seaward of the delta coastline, and are of much finer gradation. In general, it can be said that all deposits tend to grade from coarser to finer in the offshore direction, and from finer to coarser in a vertical section, starting upward from the bottom. Organic debris from stagnant waters and lagoons, characteristic of all delta formations, can often be found intermingled in most of the strata. It is interesting to note that in recent years geological surveys have shown that much of the world's natural oil resources are increasingly found in ancient deltaic rocks [34].

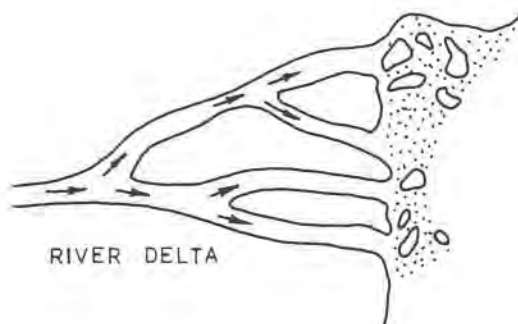
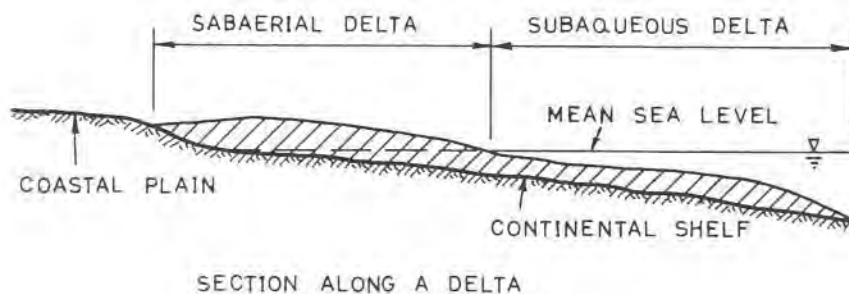


Fig. 3.13. Formative stages of a river delta.

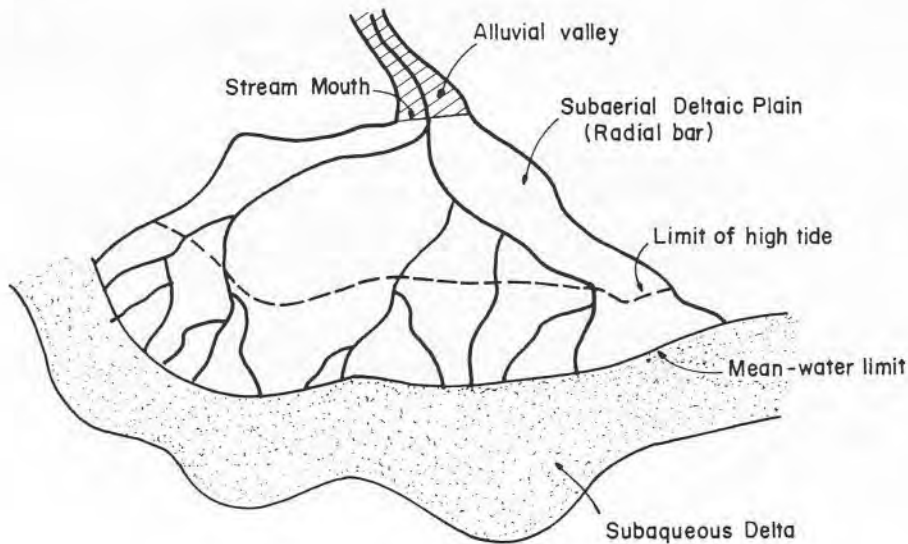


Fig. 3.13a. Schematic drawing of a river delta.

The formative process of a stream delta is schematically shown in Figs. 3.13 and 3.13a.

Deltas sometimes develop in estuaries, at the mouth of rivers entering the sea along a coastline subject to large tidal motion. Sediment load generally is deposited in the narrow channel leading to the sea.

In the case of a radical reduction of sediment discharge, due to large-scale engineering interference in the upstream course of the stream channel (such as the erection of a large dam), the existing temporary equilibrium between the sediment transport and the sea currents may be grossly disturbed. As a consequence, sea currents are likely to attack and erode existing sediment deposits, thus actually shortening the delta. A situation of this kind has been evolving at the Nile river delta after the construction of the High Aswan Dam.

3.7 Stream Confluence

At the meeting point of two watercourses, and especially in the case of a large tributary entering the main stream, particular sedimentological conditions are likely to develop. It is here understood that the tributary may also be any larger artificial earth channel. Small tributaries generally have negligible influence upon the main stream. A few typical cases will be qualitatively

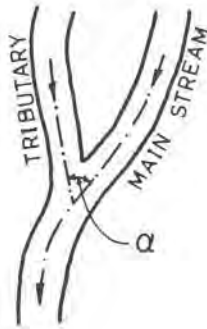


Fig. 3.14. Stream confluence.

analysed in the following. A stream confluence is schematically shown in Fig. 3.14.

Let it be assumed first that the bottom elevation of the tributary at the confluence is roughly the same as that of the main stream. Liquid discharge, sediment discharge, mean grain size and the hydraulic gradient in the main stream are Q_1 , Q_{s1} , d_{s1} and J_1 respectively; in the tributary they are Q_2 , Q_{s2} , d_{s2} and J_2 . Both streams carry the maximum sediment discharge according to their respective sediment transport capacity under the given flow conditions.

The situation is considered first in which the flood wave in both streams occurs roughly at the same time. Water stage in the main stream during the passage of the flood wave is usually higher than in the tributary, and hence back-water curve will develop in the tributary (Fig. 3.15a). As a result of this, hydraulic gradient in the tributary, in the reach upstream of the confluence,

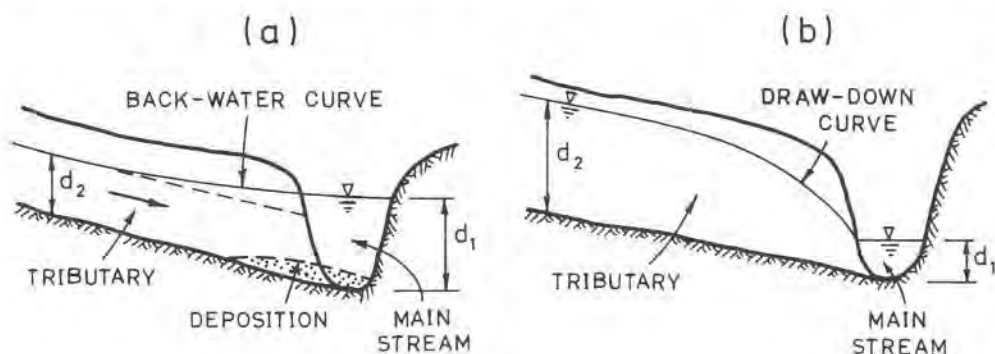


Fig. 3.15. Flow situation at confluence.



Fig. 3.15a. Stream confluence.

will decrease, causing a part of the sediment to be deposited close to the stream-mouth. Downstream of the confluence liquid discharge in the main stream will increase from Q_1 to $(Q_1 + Q_2)$, and the sediment discharge from Q_{s1} to somewhat less than $(Q_{s1} + Q_{s2})$, because a relatively small part of Q_{s2} will already have been deposited. The sedimentological situation in the main channel downstream of the confluence has been previously analysed (see par. 3.3.3); it can be assumed that there will be deposition, because STC will not be sufficiently high. Sand bars downstream of the confluence will mainly consist of coarser sediment fractions from the tributary, since the finer ones will probably be carried by the increased water volume in the main stream.

Next let us consider the case in which during the flood wave in the tributary, there is low water in the main stream (Fig. 3.15b). The situation now will be the reverse: water level in the tributary will be higher than in the main stream, and hence a drawdown curve will have to form in the tributary upstream of the confluence. Due to flow velocities higher than for normal flow, STC of the tributary will be high enough in the vicinity of the meeting

point to carry all of the sediment load, Q_{s2} . So the tributary is likely to stay clean.

On the other hand, the main channel downstream of the confluence most probably will be in a worse situation. The combined discharge ($Q_1 + Q_2$) may well be too low to carry the aggregate sediment load ($Q_{s1} + Q_{s2}$), and hence a considerable part of it is likely to be deposited downstream of the confluence, causing large sand bars.

In the case of low water in the tributary during the passage of a flood wave in the main stream, flow situation is essentially similar to that schematically shown in Fig. 3.15a, with back-water curve extending much farther upstream into the tributary. In spite of the reduced flow velocities caused by the backed-up water, sediment load in the tributary will be relatively low, and the tributary is likely to be capable of handling it. Hence little deposition is expected to take place in the tributary.

To high volume of sediment load, deriving from higher concentrations of sediment during flood waves, there is relatively modest addition from the tributary. High flow velocities in the main stream are likely to raise its STC just enough to carry the additional load without much difficulty, and hence probably little or no deposition in the main channel either. A typical confluence of a small stream is shown in Fig. 3.15a.

It seems also that some importance should be attached to the relative position of river bottoms at the point of confluence. So far it has been assumed that their elevation is more or less equal. As long as water levels in both streams are nearly equal – a situation that is generally not a frequent occurrence – there is little importance to the relative elevation of river bottoms. However, the situation may be quite different if water level in the tributary is higher than in the main stream and the bed elevation of the tributary at the confluence is higher than in the main stream (see Fig. 3.16). There will be a drawdown curve in the tributary upstream of the confluence, accompanied by high velocities, and severe erosion is to be expected along the bed of the tributary. After some time, a part of channel bed may collapse, shifting the drop from 1 to 2; this process, generally known as *back-erosion*, may repeat itself several times (points 3, 4, etc.), and thus endanger the stability of the channel. The eroded material will ultimately be carried into the main stream, settling downstream of the confluence until entrained by high water during flood waves (see also the discussion on stream outlets in Chap. 11). See Fig. 3.16.

Angle of confluence, α , is also an important factor influencing the sedimentological processes which take place at the meeting point or close to it. Curvature of the stream reaching the main watercourse from the tributary obviously depends on the angle formed by the axes of the channels,

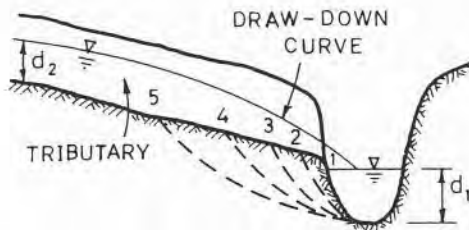


Fig. 3.16. Back-erosion at confluence.

and the rate of deposition to a large extent depends on the streamline curvature. A tributary entering almost perpendicular to the axis of the main stream will have greater effect upon it than a tributary with a sharp angle of confluence. In fact, at larger angles of intersection, onrushing water from the tributary virtually pushes aside the flow in the main channel, concentration of high velocities at its outer banks may cause erosion there, and local deposition is likely to form, interfering with the normal process of the channel meandering.

At very small angles of confluence the two streams often have the tendency not to mix for a considerable distance downstream of the confluence, and hence to flow as though side by side with little mutual interference. As a result of such a flow configuration, a slender and elongated sand spit may form in the main channel roughly along the division line between the two almost parallel streams. This narrow sand bar of fairly limited length is not stable; it is eventually shortcut by water currents at high discharges from the tributary and made into a sand island which is subsequently eroded and carried away. The formative cycle then begins again.

Further discussion concerning the angle of confluence and its influence downstream will be given in the chapter dealing with outlets (see Chap. 11).

A *bifurcation* occurs when the main watercourse divides into two branches, which is the opposite of a confluence (Fig. 3.17). This is generally

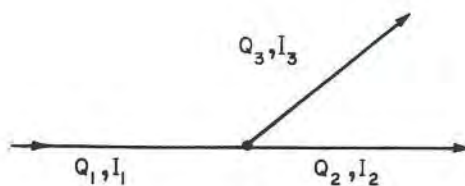


Fig. 3.17. Schematic bifurcation.

the case when an artificial earth channel branches off from the main stream.

Although in both cases of confluence and bifurcation the main watercourse meets two streams, there are some important differences. The geometry of the branching channels at the bifurcation and the available head determine the magnitude of discharges Q_2 and Q_3 . The sorting of the sediment at the bifurcation also depends mainly on the geometry. There is generally no backwater effect at the bifurcation.

3.8 Flow in Channel Curves

Natural streams seldom flow in straight channels, and when they do, then mostly for short reaches only. Before taking a look in the next paragraph at such natural phenomena as meandering and braided streams, it is necessary for better understanding to make a short review of the main features that are characteristic of channel flow in curves.

Although there is still no full agreement as to all the aspects of dynamic and sedimentological processes connected with channel bends, it is nevertheless generally accepted that the main features are determined by the *centrifugal force* acting upon water particles moving along curved trajectories. In the present text the expression centrifugal force has been adopted for the reaction to the centripetal force acting upon those particles when in curved motion. It can also be viewed as the normal component of the inertia vector, representing the tendency of water particles to break away from the axis of rotation. The particular reference to this reactive force has been chosen in order to keep in line with current engineering practice. For the following analysis, the flow is assumed to be steady and subcritical. Upon reaching the curved portion of the channel, each water particle is acted upon by the centripetal force and its reaction the centrifugal force, which tends to deviate it from the movement along a generally straight line path. This force is directed at right angles to the main flow, and acts to cause a lack of dynamic equilibrium in y -direction (see Fig. 3.18).

In order to restore the equilibrium, a transversal gradient, i_y , is impressed on the water surface, giving rise to a force in the direction opposite to the centrifugal force. This compensating force also acts upon every water particle; it is equal for all particles in the vertical, and is proportional to the average of the velocities squared in a given vertical. Now, due to asymmetrical velocity distribution in the x -direction, diagram (d) on Fig. 3.18, water particles near the surface move with a higher velocity than the average velocity in the x -direction, \bar{V}_x , and near the bottom they move with a lower

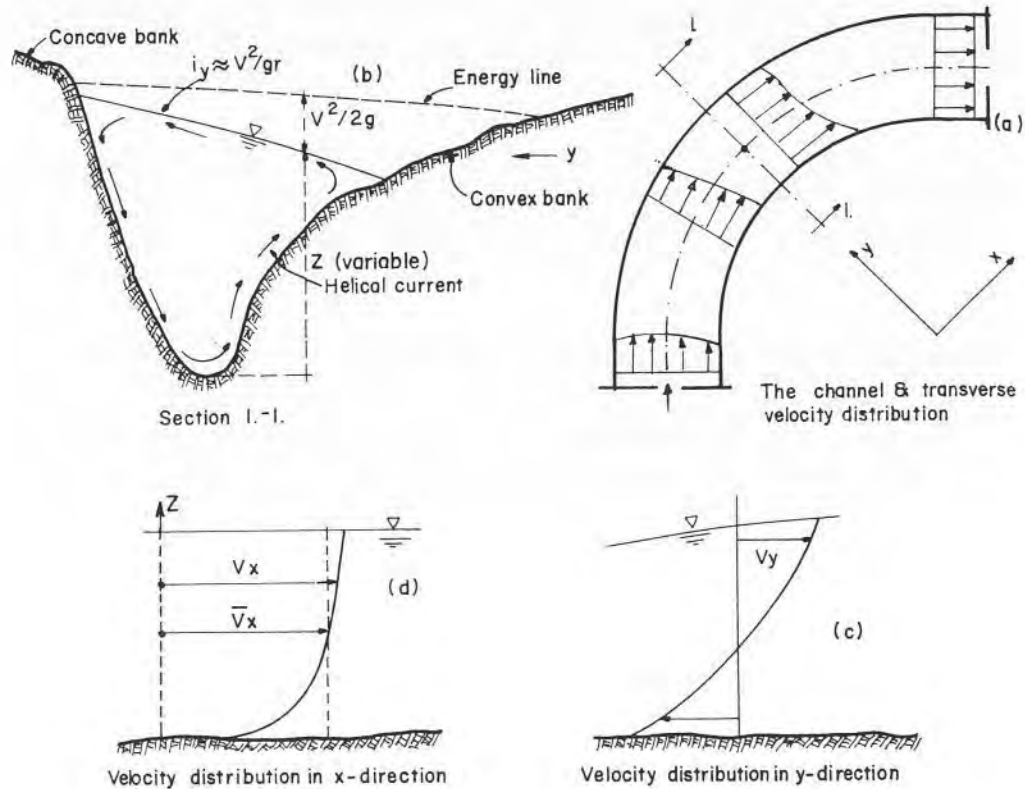


Fig. 3.18. Flow in bend.

velocity than the average. Centrifugal force is proportional to the velocity of flow in the x -direction, while the opposite force caused by the gradient i_y remains constant for all particles; hence as a result, particles near the surface are deviated in the direction of the centrifugal force, i.e. toward the concave bank; particles near the bottom, on the other hand, are deflected toward the convex bank, i.e. direction opposite to the centrifugal force. Hence a secondary velocity distribution in the y -direction is induced, as shown in diagram (c), so that a helical transverse current is added to the normal movement in the x -direction. Because of the continuity, the net result is a closed-loop, three-dimensional spiral flow; particles near the water surface, which move outward, dip to the bottom along the relatively steep concave bank, move inward along the bottom, and rise to the surface along the flat convex bank (see Fig. 3.18b).

From the conditions of transverse equilibrium, and neglecting the flow resistance along the bottom of the channel, it can easily be shown that the transverse water-surface gradient is given by

$$i_y = \frac{dz}{dy} \approx \frac{V^2}{gr}, \quad (3.10)$$

where y is the direction as indicated on Fig. 3.18(a), and V is the average velocity in the vertical under consideration.

Hence, the so-called *superelevation* in the radial direction across the stream channels is given by

$$\Delta z = i_y \cdot B = \frac{V^2 B}{gr} \quad (3.10a)$$

Here B denotes the top width of the stream at the bend.

Referring to Fig. 3.19, total energy at any section across the flow is assumed to be constant, hence

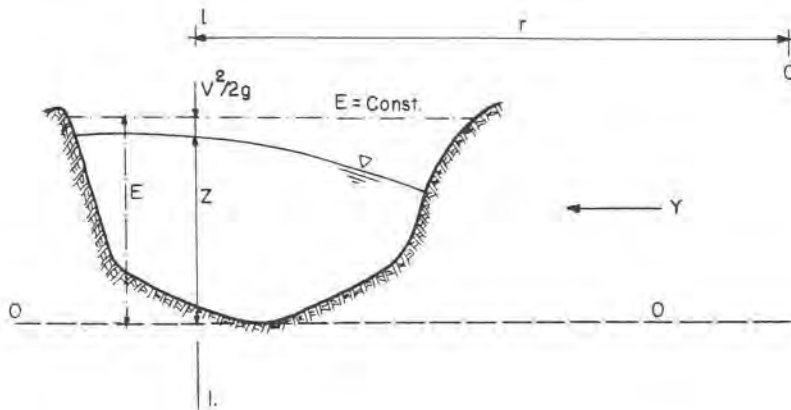


Fig. 3.19. Cross-section at bend.

$$z + \frac{V^2}{2g} = E = \text{const.} \quad (3.11)$$

Assuming hydrostatic pressure distribution and writing for the normal

component of the angular acceleration (centrifugal acceleration) $a_y = V^2/r$, application of Euler equation of motion gives

$$\frac{dz}{dy} = \frac{V^2}{gr} \quad (3.12)$$

On the other hand, by differentiation in the y -direction of Eq. (3.11) we obtain

$$\frac{dz}{dy} + \frac{V}{g} \frac{dV}{dy} = 0 \quad (3.13)$$

From Eqs. (3.12) and (3.13) the following expression can be obtained:

$$\frac{dV}{dy} + \frac{V}{r} = 0 \quad (3.14)$$

By analysing Eqs. (3.12) and (3.14), it is seen that since both V/r and V^2/gr are always positive, theoretically velocity V decreases and depth z increases in the positive y -direction, i.e. from the inner convex, to the outer concave bank. Measurements of transverse water profiles in small- and medium-size streams however, have shown the profile in many cases to be actually concave, often with a central trough. It is believed that this is due to the influence of the transverse spiral currents, not taken into account when computing equilibrium conditions across the stream.

It has generally been observed that the velocities of the secondary currents are typically about one order of magnitude lower than the average primary velocities [8]. The main parameters on which the strength of circulation depends are: Reynolds number of the flow, position along the bend, ratio of the radius of curvature to width, and the ratio of width of the stream to its depth.

Field measurements appear to show that the secondary circulation at bends is the strongest at medium discharges, and weaker at low and high flows [8]. This is probably due to the fact that the centrifugal force, which causes it and which depends on the ratio of the square of the main velocity to radius of curvature, is not constant. At low flows, point bars on the inside of bends remain exposed, and hence the flow tends to follow the channel thalweg, which is sharply curved at bends. Primary velocity, however, is low, so that the centrifugal force and the secondary circulation stay low

also. At medium flows, point bars are partly submerged, and hence the main current less curved; on the other hand, primary velocity is higher. Although the curvature of the current is less, it nevertheless remains sharp enough in order to produce, in combination with higher flow velocity, relatively strong centrifugal force. Finally, at high flows, point bars are completely submerged, and the main current no longer follows the line of the thalweg. Primary velocity is high but the radius of curvature also is large, hence centrifugal force tends to be actually weaker than at medium flows.

Existence of transverse secondary currents and of water-surface gradient leads to important modifications in the velocity distribution along the bend, and these also affect the sediment transport by the stream. Exchange of momentum between different layers of water is intensified by the cross-currents, and thus a further redistribution of velocities both in the main direction of flow and across the stream, will take place [8]. Starting from the entrance to the bend, where the transverse slope across the stream begins forming, the line of maximum velocity moves gradually to the inner, convex bank; increased exchange of momentum and the gradual disappearance of the transverse slope, however, cause the line of maximum velocity to be

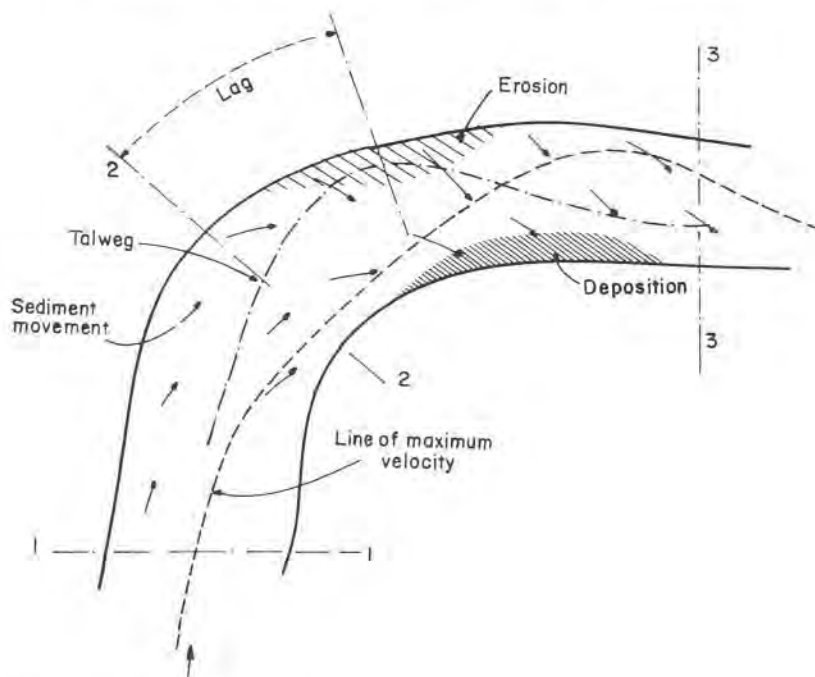


Fig. 3.20. Flow in a bend.

shifted toward the concave bank at the exit from the bend, or somewhat further downstream (see Figs. 3.18a and Fig. 3.20).

Sediment transportation along the bend and its vicinity is affected to a great extent by cross currents. Transverse current directed outward dips along the concave bank and causes erosion there; inward-directed spiral current along the bed carries the sediment toward the convex bank, where it is eventually partly deposited, causing local accretion of the channel bed (Fig. 3.20).

As a direct result of the above scouring and deposition processes, a transverse bed slope is formed, which is one of the major characteristics of flow in alluvial curved channels. Theoretical prediction of this transverse slope is generally based on the dynamic equilibrium equation between the fluid drag and submerged weight of the particle acting on the radial plane [11, 12], but the calculation of the secondary current differs widely. Flow situation in an alluvial curved channel is schematically shown in Fig. 3.21.

According to many field observations all over the world, maximum erosion at the concave bank generally does not occur at the section of maximum curvature, but rather downstream of it [9]. According to field observations made on river Rhine and river Seine, the distance from the center of curvature to the center of eroded pool is about a quarter of the

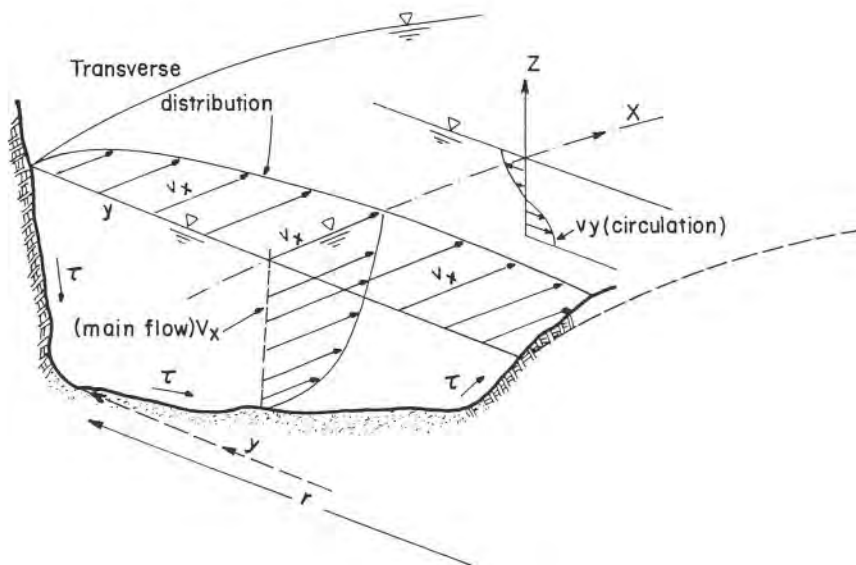


Fig. 3.21. Flow pattern in curved alluvial channel.

total length of the bend, or about 1.5 times the width of the channel. There is actually a "lag", or a shift of the erosive action of the stream (see Fig. 3.20).

A possible physical explanation of the phenomenon could be as follows. Due to the formation of the transverse water-surface gradient along the bend, the longitudinal gradient along the outer bank diminishes, and hence also the shear stress of the stream $\tau = \gamma R J$. This reduction of the tractive force, however, is compensated by the spiral motion of the sediment, carried toward the convex bank (Fig. 3.17c). As a result, there is no sediment deposition in the stretch between sections 1–2. On the inner side, tractive force increases, but there is an additional supply of sediment from the outer bank; accordingly, there is no deposition here either.

In the second part of the bend, between sections 2–3, the situation is reversed. Along the outer bank there is an increase in the tractive force of the stream, but there is no compensating supply of sediment, because its movement continues to be toward the inner bank along the bottom. This causes severe erosion along the outer bank. On the other hand, along the inner bank sediment transport capacity of the stream must diminish, while the additional supply of sediment carried by the spiral motion is still present; hence, there is sediment deposition along the inner bank between sections 2–3.

In the above analysis it has been assumed that the friction resistance along the bed was negligible in comparison with the kinetic strength of the spiral motion. In many natural streams, however, this may not always be the case. When the ratio of depth to width is small, forces responsible for producing spiral flow in a bend may be of the same order of magnitude as friction forces from bed and bank, so that any spiral motion across the stream is practically non-existent.

Flow along a bend is accompanied by a loss of head requiring some rise in water surface at the entrance to the curved section. This clearly indicates that for a stream channel of subcritical flow, a bend has a backwater effect upstream from the flow obstruction.

As far as shear-stress distribution in curved channels is concerned, there is experimental evidence [8, 13] that it generally can be compared to straight reaches, at least for low and high discharges. At medium rates of flow, when the secondary circulation appears to be the strongest, the distribution appears to be less uniform than in straight reaches.

Reliable method for prediction of bed-shape changes in alluvial stream bends is for the time being not available, in spite of its importance in drainage engineering. In fact, both the deterministic and more recent stochastic approaches fail to give satisfactory results.

A relatively simple method for evaluating the increased velocity, and

hence also the corresponding shear stress, along the concave bank *at the exit from the bend*, has been proposed by Karaki et al. [39]. The computation has been facilitated by the use of two graphs, given in Fig. 3.21a. The method will be explained by means of a numerical example.

Example 3.4

Given a stream bend having the following properties:

- Radius of curvature to the center line of the curve, $r_c = 450$ m
- Angle of the bend, $\alpha = 65^\circ$
- Channel width, $B = 100$ m
- Mean depth of flow, $d = 4.5$ m
- Maximum depth of flow, $d_{\max} = 5.5$ m
- Longitudinal slope, $I = 1.7 \times 10^{-4}$
- Manning roughness coefficient, $n = 0.027$.

Compute the maximum velocity in the bend, and the ratio between the shear stress in the bend to that in the straight reach.

Solution:

Step 1 – First an auxiliary parameter Δ is evaluated,

$$\Delta = 0.42 \alpha \frac{d_{\max}}{B} \frac{(g)^{1/2}}{C} \quad (3.15)$$

in which C denotes Chezy factor of flow resistance. For a large stream it can be assumed that the hydraulic radius is approximately equal to the mean depth of flow, hence $R \approx 4.5$ m. Chezy factor can then be evaluated (see Vol. 1, Chapter 2) from the expression

$$C = \frac{R^{1/6}}{n} = \frac{4.5^{1/6}}{0.027} = 47$$

The parameter Δ can now be computed using Eq. (3.15) –

$$\Delta = 0.42 \cdot 65 \frac{5.5}{100} \frac{(9.8)^{1/2}}{47} = 0.1$$

Step 2 – For the use of graphs in Fig. 3.21a – $\Delta \times 10^2 = 10$, and then from the graph b. in Fig. 3.21a – $\Delta V_{\max} \times 10^2 = 3.9$; $2x/B = 0.43$, from which distance x from the centerline of the channel can be evaluated:

$$x = \frac{0.43 \times 100}{2} = \sim 21.5 \text{ m}$$

Step 3 – Next the mean velocity in the channel is determined using Manning equation (see Vol. 1, Chapter 2):

$$V_0 = \frac{1}{n} R^{2/3} I^{1/2} = \frac{1}{0.027} \cdot 4.5^{2/3} \cdot (0.00017)^{1/2}; \quad V_0 = 1.3 \text{ m/sec}$$

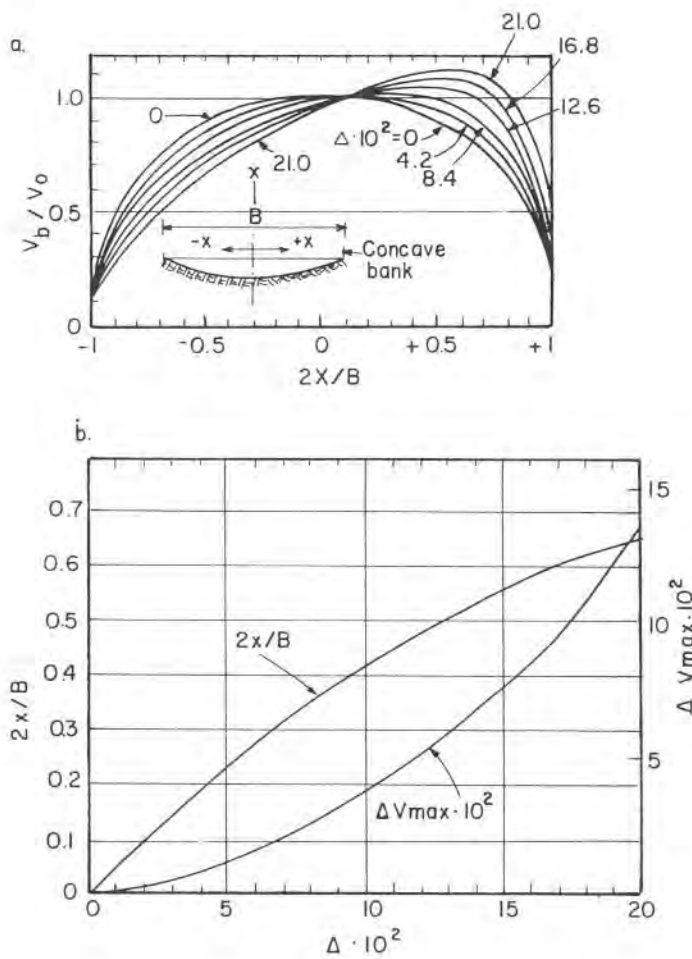


Fig. 3.21a. Distribution of velocity at the exit of a bend, after [39].

Step 4 – Using now graph a. of Fig. 3.21a for $2x/B = 0.43$ and $\Delta \times 10^2 = 10$:

$$V_b/V_0 \cong 1.03$$

where V_b – Maximum velocity on the concave bank at the exit from the bend. Hence,

$$V_b = 1.03 \times V_0 = 1.03 \times 1.3 = 1.34 \text{ m/sec}$$

Step 5 – Since the shear stress is roughly proportional to the square of velocity –

$$\frac{\tau_{\text{bend}}}{\tau_{\text{straight}}} = \left[\frac{1.34}{1.3} \right]^2 = 1.06$$

For the given case, the velocity is likely to be increased by about 3%, and the shear stress by about 6%.

3.9 Meandering and Braided Stream Channels

As mentioned in the previous paragraph, alluvial streams generally flow in a succession of clockwise and anti-clockwise bends, interconnected by relatively short straight reaches called crossings. Such geometrical alignment is generally known as a “meandering river”, allegedly from the name of a river in ancient Phrygia noted for its windings. Even such watercourses which apparently show little meandering pattern, like for instance some of the braided river channels, can be shown by long-term investigations to be subject to meander-like oscillating alignment. Moreover, some straightened and regulated streams with well-protected banks also start to build gravel or sand shoals and take up meandering pattern. A typical meandering stream is shown in Fig. 3.22.

There seems to exist a natural tendency for oscillating, sinuous flow in alluvial channels which for the time being eludes any comprehensive theoretical analysis, although in recent years many attempts at a mathematical formulation have been made, such as [14] and others. It seems possible that one of the main causes of this complex natural phenomenon is to be found in many slight departures from symmetry of flow and bank



Fig. 3.22. Meandering river.

erosion which tend to deviate the bulk of the flow to one side or the other of the channel. There also appears to be some connection between the longitudinal slope of the stream and the intensity of its meandering; indeed, field measurements have shown that slopes of meandering streams generally are very mild, and in recent years a few attempts have been made to quantitatively determine the “threshold slope” for specific groups of natural streams. On the other hand, meander-like patterns have been observed in the oceanic Gulf Stream and in some jet streams of the upper atmosphere. It is therefore possible that stream meandering is a part of the general wave phenomena in nature. Schematic layout of a typical meandering stream is shown in Fig. 3.23.

A watercourse is generally called a “meandering stream” when the ratio between its actual length and the length of the valley is 1.5 or more (the ratio is rarely more than about 2.5). A meander usually is thought to comprise two consecutive bends and the straight stretch between them, if there is one.

The actual shape of bends in a meandering stream is rarely symmetrical and geometrically well-defined. Radius of curvature varies over a wide range, depending upon the type of bend. Free bends in plain alluvial material, easily erodible and mobile, generally have the ratio of the radii of curvature to the width of the stream in the range of 4–5, while in case of more consolidated bank materials, the ratio may be as high as 7–8. On the other hand, in forced bends, formed by a stream being deflected by a practically non-eroding bank, the ratio may be as low as 2–3. Field observations show that in bends

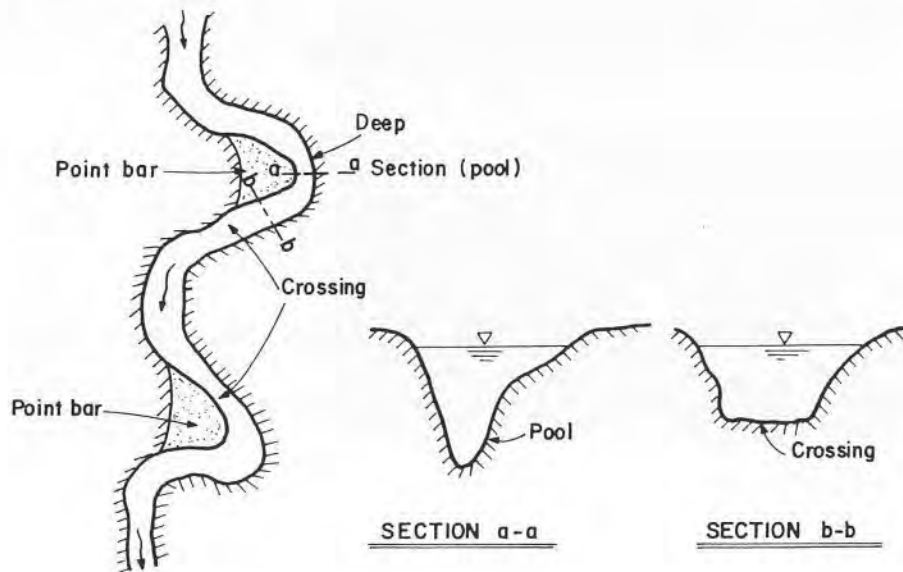


Fig. 3.23. Schematic lay-out of a meandering stream.

of larger ratios, maximum depth of water is generally found some distance downstream of the apex of the concave bank, while in small-ratio bends the depth sharply increases at the entrance to the bend and thereafter gradually turns back to normal.

A general characteristic of all meandering watercourses is the migration of the bends downstream, and under certain circumstances even laterally. The migration velocity changes from stream to stream, and there are slow-moving and fast-moving streams; movements as large as about 800 m per year have been observed in some alluvial streams.

As mentioned before, short straight reaches connecting consecutive bends are known under the name of "crossings", and they generally are relatively shallow compared to deep parts of the bends that precede and follow them. A considerable part of the bed material eroded from the concave bank of the bend is deposited in the crossings by the spiral cross currents which do not decay as soon as they leave the bend, but extend downstream. At lower discharges, sand bars also may be formed in the crossings. Fig. 3.24 shows a qualitative picture of a meander bend followed by a straight reach before the next bend.

As has been already explained in par. 3.8, the main erosion process is to be expected at the concave side of the flow channel. The form and extent

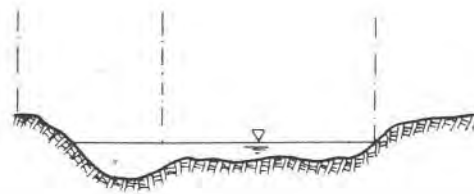
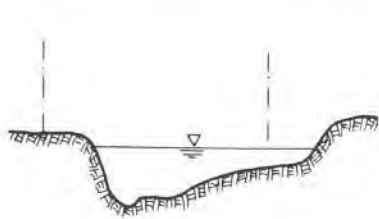
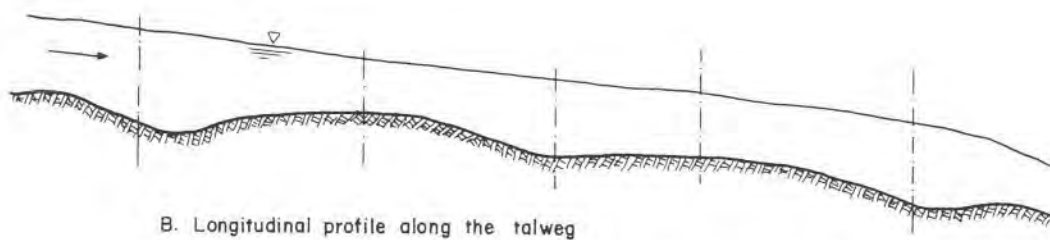
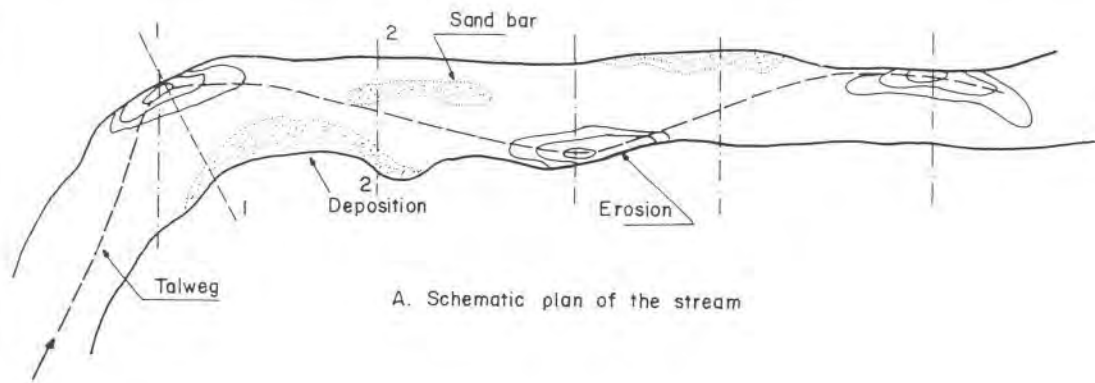


Fig. 3.24. A bend followed by a crossing.

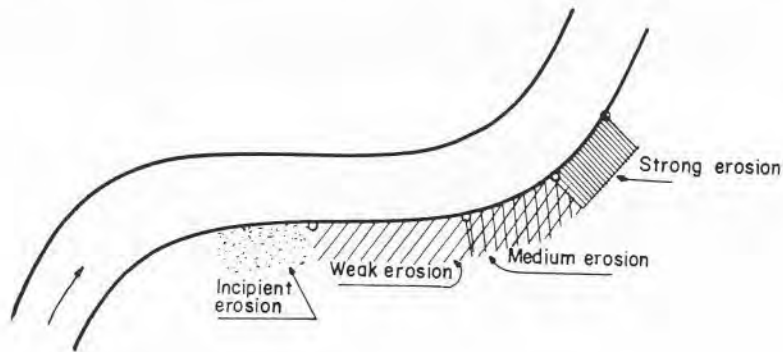


Fig. 3.25. Generalized erosion gradation at a bend.

such erosion assumes for any specific case will vary from stream to stream. Nevertheless, there seems to be discernible a general pattern, which on a statistical average can be regarded as most likely to be followed. A general qualitative erosion pattern for a meandering stream is schematically shown in Fig. 3.25.

An alternative alignment of an oscillating alluvial watercourse is known as a *braided stream*. The characteristic features of such a configuration are a wide channel, unstable and poorly defined banks and shallow water. The watercourse consists of a number of entwined channels divided by islands, which meet, cross and separate again. Observed from the air, they form a braided pattern. The channels are highly unstable and change position unpredictably. At high stages, during flood waters, the whole of the channel is inundated, most of the sand bars are washed away, and the stream appears to be a wide straight channel. A typical braided form of an alluvial channel is shown in Fig. 3.26.

The main causes which bring about the braiding of a stream seem to be [15]: 1) supply of more sediment than warranted by its STC, hence part of the load is deposited, 2) steep longitudinal slopes that tend to produce a wide and shallow channel in which bars readily form, become stabilised by armouring and vegetation and form islands, and 3) easily erodible banks, allowing the widening of the stream channel at high flows.

It is generally assumed that a braided channel has a steep slope, a large bed load in comparison with the suspended load, and usually small amounts of silt and clay particles in both bed and banks [16].

A decrease in longitudinal slope may often change a channel from braided into meandering. Important changes of the dominant discharge of a stream

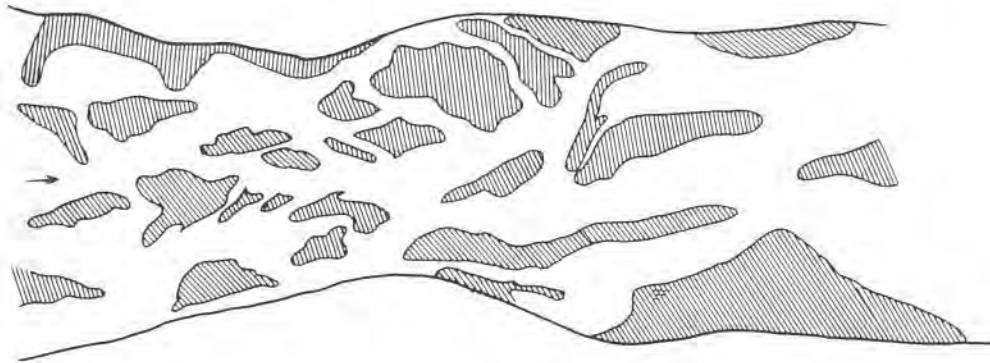


Fig. 3.26. A braided stream.

(as for instance reduction of discharges brought about as a result of flood routing through a reservoir) may also cause considerable alteration of the basic river alignment. Often a single meandering channel may turn into a braided pattern when one or several bars are formed, as may be the case downstream of a tight bend where coarse material from the pool bottom in the bend is brought up. New subdivided channels, being generally smaller than the single one, are less efficient, and therefore they have to be compensated by increased longitudinal slope achieved through erosion of the bed.

The three basic alluvial-channel patterns, namely straight, braided and meandering, in spite of striking differences between them, are actually closely interrelated. One and the same stream may in fact exhibit any one of the three patterns, depending on the mutual relationship between the many variables which determine the morphological behavior of the stream. Increased longitudinal slope, for instance, caused by any natural or man-made agent, is likely to convert a relatively stable meandering stream into a much less stable braided pattern. Many researchers and engineers have tried to quantitate this alluvial-stream tendency, or at least to classify it. Lane [15] has proposed a simple relationship, mainly based on laboratory investigations and some U.S. streams.

$$\begin{aligned}
 IQ^{0.25} &\leq \sim 0.0007 && \text{— meandering stream} \\
 IQ^{0.25} &\geq \sim 0.004 && \text{— braided stream}
 \end{aligned}
 \tag{3.15}$$

in which I denotes the longitudinal slope, and Q the liquid discharge in m^3/sec . In between the above values, the stream is in an intermediate state.

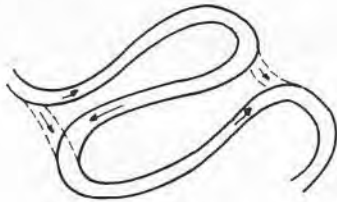


Fig. 3.27. Formation of cut-offs.

Erosion of outer channel banks and the general tendency of meander trains to move down the valley may cause progressive sharpening and tightening of the bends. This process favors the short-circuiting of individual loops by forming cut-offs between them, as schematically shown in Fig. 3.27. If the downstream motion of the meander train is suddenly obstructed by rocks or non-erodible banks, piling-up of meanders upstream of obstacles may ensue, resulting in formation of cut-offs between the tight loops. As mentioned before, slope reduction generally is accompanied by increased sinuosity of the channel alignment, hence this condition also favors formation of cut-offs.

There is substantial evidence that secondary circulation exists in all channels, without distinction of their alignment. The cause of the circulation is still an object of scientific speculation. It is further not at all clear whether the uneven distribution of sediment carried by a stream is in some way instrumental to the generation of currents, or whether the lack of uniformity in sediment distribution is in fact a result of secondary currents. Recent investigations, however, seem to indicate that the secondary circulation is independent of sediment or of temperature. How far the channel stability is affected by it is also open to debate, but according to the prevalent engineering evaluation it is probably of minor importance.

Thalweg of an alluvial stream, as introduced in the present section, is the line which connects the deepest point in successive channel cross sections at a given stage of water-level. For purposes of river navigation, this simple definition may not be sufficiently accurate, particularly if there are more than one channel, or there are several maxima. However, since the present text does not include river navigation, for the sake of clarity the simpler definition has been adopted.

Many attempts have been made by practising drainage engineers and laboratory investigators to establish generalised causal relationships concerning the geometry and related features of meandering streams. Unfortunately, in most cases both the number of observations and their

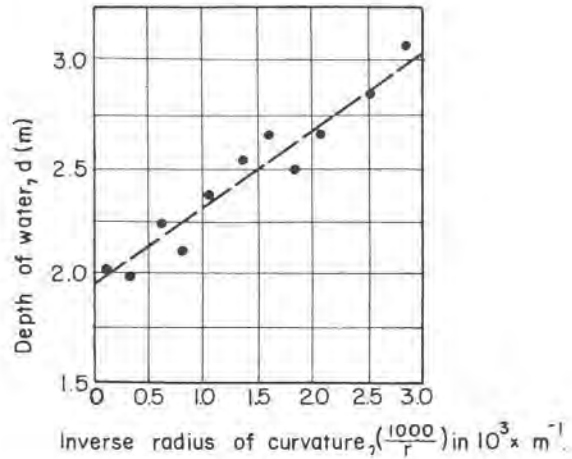


Fig. 3.28. Depth vs. radius of curvature for the river Elbe.

scope hardly warrant a generalisation. Quantitative predictions, therefore, should always be taken with due caution, bearing in mind that sound engineering judgment and detailed study of local conditions are the best guide to their application in drainage engineering. A few types of such generalised relationships are given in the present chapter, while another one will be found in par. 4.5.

Attempts have also been made [17] to plot the relationship between the water depth and the radius of curvature, based on observations made on the Elbe river, Fig. 3.28.

The *quantitative* correlation obtained is certainly a characteristic of the Elbe river; on the other hand, it could be argued that it *qualitatively* represents a general tendency of meandering rivers.

Some general qualitative relationships, based mainly on model investigations, are given by Ackers and Charlton [18], among others. Briefly recapitulated, they seem to indicate that

$$I_{\text{meander}} > I_{\text{straight}}$$

$$A_{\text{meander}} > A_{\text{straight}}$$

$$V_{\text{meander}} < V_{\text{straight}}$$

where I – mean value of longitudinal slope along the thalweg, A – average flow section, V – mean velocity.

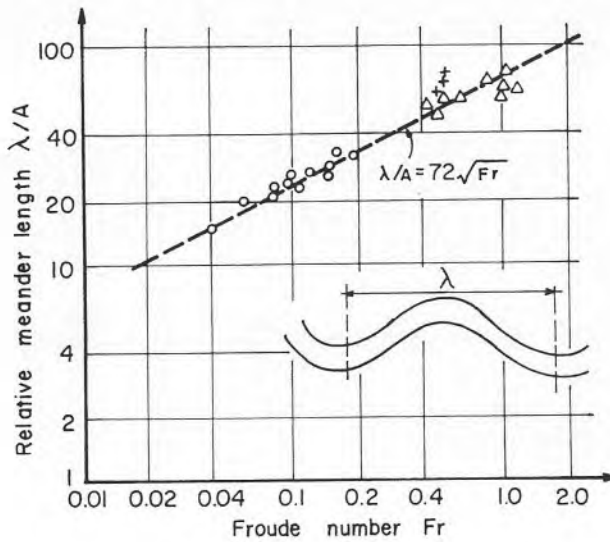


Fig. 3.29. Experimental relationship between relative meander length and flow Froude number (A – stream cross-sectional area), after [26].

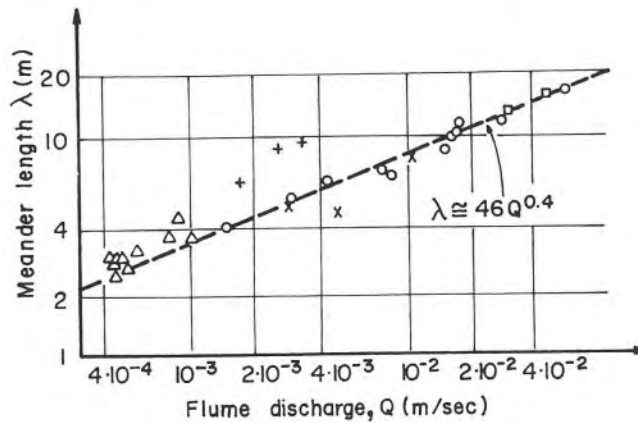


Fig. 3.30. Experimental relation between meander length and flume discharge after [26].

Basing his deduction on laboratory flume experiments of different researchers, Anderson [26] tried to establish a quantitative relationship between the relative meander length and the flow Froude number, and between meander length and discharge (Figs. 3.29 and 3.30).

Other researchers have also tried to deduce similar relationships. Inglis [27] proposed the empirical relation $\lambda \propto (Q)^{1/2}$, while Charlton and Benson [28] suggested $\lambda \propto Q^{0.515} d_s^{-0.285}$ (d_s = mean particle diameter); Hansen [29] obtained a semi-empirical relation between λ , discharge and sediment mean diameter as $\lambda \propto Q^{0.525} d_s^{-0.316}$, whereas Ackers and Charlton [30] found the relation $\lambda \propto Q^{0.467 \pm 0.24}$ to hold for many streams. Leopold et al. [31] suggested for streams and flumes the relation $\lambda \cong 10 B$, in which B denotes the channel width, and Zeller [32] arrived at an almost identical relationship. Relations proposed for meander amplitude (see Fig. 3.31), a , differ widely, from $a = 4.5B$ by Zeller [32] to $a = 18.4B$ by Inglis [33]. Leopold and Wolman [35] also suggested two additional relationships: $r/B \cong 2.3$ and $L \cong 4.7 r$, in which L denotes the length of the valley line. Q indicates bankful discharge.

3.10 Summary

In the present chapter we attempted to give a brief survey of the main physical processes that govern the morphological behavior of a stream system. It certainly does not pretend to be exhaustive or to reflect in any way the full extent of the present-day available information, knowledge or

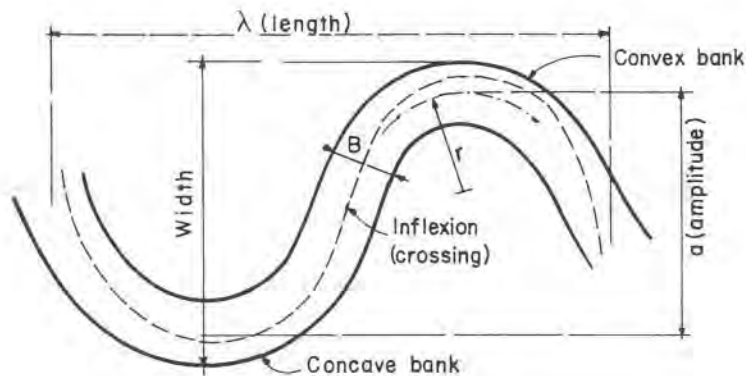


Fig. 3.31. Main parameters in a meander,

general state-of-the-art. Engineering aspects of the natural phenomena discussed have been the guiding thread for the presentation, and above all for the selection of topics and their necessarily very limited treatment.

A fluvial system should not be regarded as an isolated unit. In fact, it comprises the watershed, channels and a great number of elements, mutually interdependent, which together continuously seek an elusive state of equilibrium, and practically forever adjust themselves to changing conditions. Hence a highly dynamic system, and from the mathematical point of view extremely non-linear. The forces involved in the process are generally of two types: gravity forces and inertia forces, which comprise friction and cohesion. Their interplay is generally so pervasive and complicated that often one is baffled and frustrated when trying to draw a balance sheet.

Although far from being fully understood, and still loaded with conflicting information, nevertheless current knowledge allows the engineer to master the governing physical processes and to make fairly correct predictions, or to design works in order to change or influence the natural course of events. Only if the complex processes are well recognised and comprehended is there a good chance that a fluvial system will be correctly analysed and the future response sufficiently well estimated.

References

1. E. Kuiper, *Water Resources Development*, Butterworths, London, 1965.
2. M. De Vries, *River-bed variations – aggradation and degradation*, Delft Hydrological Lab., publication no. 107, 1973.
3. J.P. Sony et al., *Aggradation in streams due to overloading*, proceedings, ASCE, 106 (HY1) (1980).
4. J.P. Sony et al., *Non-uniform flow in aggrading channels*, proceedings, ASCE, 103 (WW3) (1977).
5. W.B. Bull, *Geomorphology of segment alluvial fans in Western Fresno County, California*, U.S. Geol. Survey, Prof. paper 352E, 1963.
6. D.R. Dowdy, *Flood estimates on alluvial fans*, proceedings, ASCE, 105 (HY11) (1979).
7. M. Morisowa, *Streams*, McGraw-Hill, New York, N.Y., 1968.
8. J.C. Bathurst, *Secondary flow and shear stress at river bends*, proceedings, ASCE, 105 (HY10) (1979).
9. J.L. Rozovski, *Flow of water in bends of open channels*, *Isr. Progr. Sci. Transl.*, Jerusalem, 1963.
10. Nedeco, *River Studies*, North Holland, Amsterdam, 1959.
11. L. Gottlieb, *Three-dimensional flow pattern and bed topography in meandering*

- channels, Inst. of Hydr. Eng., Techn. Univ. of Denmark, Series Paper 11, 1976.
12. H. Kikkawa et al., Flow and bed topography in curved open channels, proceedings, ASCE, 102 (HY9) (1976).
 13. A.N. Mamdouh and R.D. Townsend, Shear stress distribution in stable channel bends, proceedings, ASCE, 105 (HY10) (1979).
 14. F. Engelund and O. Skovgaard, On the origin of meandering and braiding in alluvial streams, *Journal of Fluid Mechanics*, vol. 57 (1973).
 15. E.W. Lane, A study of the shape of channels formed by natural streams flowing in erodible material, U.S. Army Eng. Div., Corps of Eng., Sediment Series no. 9, 1957.
 16. Analysis of Watershed and River Systems, Research Institute of Colorado, 1979.
 17. S. Leliavski, An introduction to fluvial hydraulics, Constable, London, 1954.
 18. P. Ackers and F.G. Charlton, Meandering of small streams in alluvium, Hydr. Res. Station, report no. INT 77, Wallingford, 1969.
 19. H.W. Shen, editor, *River Mechanics*, Fort Collins, Colorado, 1971.
 20. J. Larras, *Embouchures, estuaires, lagunes et deltas*, Eyrolles, Paris, 1964.
 21. R.J. Garde and K.G. Ranga Raju, *Mechanics of sediment transportation and alluvial stream problems*, Wiley Eastern, New Delhi, 1978.
 22. K.J. Gregory, Editor, *River Channel Changes*, Wiley, Chichester, 1977.
 23. J.S. Smart, Determinism and randomness in fluid geomorphology, *Trans. Am. Geophys. U.*, 60/36, 1979.
 24. H.W. Shen et al., *Modeling of Rivers*, Wiley, New York, N.Y., 1979.
 25. T.K. Miller and L.J. Onesti, The relationship between channel shape and sediment characteristics in the channel parameter, *Geol. Soc. Am. Bull.*, 90 (3) (1979).
 26. A.G. Anderson, On the development of stream meanders, proceedings, 12th Congress IAHR, Fort Collins, Colorado, 1967.
 27. C.C. Inglis, Meanders and their bearing on river training, *Inst. Civ. Eng., Maritime & Waterways*, paper no. 7, 1947.
 28. F.G. Charlton and R.W. Benson, Effect of discharge and sediment charge on meandering of small streams in alluvium, *Symp. Central Water & Power Research Station, Poona*, 2 (1966).
 29. E. Hansen, On the formation of meanders as a stability problem, *Inst. of Hydr. Eng., Techn. Univ. of Denmark*, progress report 13, 1967.
 30. P. Ackers and F.G. Charlton, Meander geometry arising from varying flows, *Journal of Hydrology*, 11 (3) (1970).
 31. L.B. Leopold et al., *Fluvial Processes in Geomorphology*, W.H. Freeman, London, 1964.
 32. J. Zeller, *Flussmorphologische Studie zum Mäanderproblem*, *Geographica Helvetica*, 22 (2) (1967).
 33. C.C. Inglis, The effect of variations in charge and grade on the slopes and shapes of channels, proceedings, 3rd Congr. IAHR, Grenoble, 1 (11) (1949).
 34. R. Davis, *Coastal Sedimentary Environments*, Springer Verlag, New York, N.Y., 1978.
 35. L.P. Leopold and M.G. Wolman, River meanders, *Bull. Geol. Soc. Am.*, 71 (1960).
 36. W.C. Huges, Scour velocities in ephemeral channels, proceedings, ASCE, 106 (HY9) (1980).

37. V.T. Chow, *Open-Channel Hydraulics*, McGraw-Hill, New York, N.Y., 1959.
38. M.G. Wolman and J.P. Miller, Magnitude and frequency of forces in geomorphic processes, *Journal of Geology*, 68 (1960).
39. S. Karaki et al., *Highways in the river environment: hydraulic and environmental design considerations*, Colorado State University, Fort Collins, Colorado, 1974.

CHAPTER 4

THE REGIME CONCEPT OF CANALS AND STREAM CHANNELS

Symbols

A	– cross-sectional area, m^2
a	– coefficient
B	– average width, m
B'	– incorrectly estimated value of B , m
\bar{B}	– top width, m
C	– sediment concentration, ppm; Chezy coefficient
C_B	– meandering coefficient
C_L	– meandering coefficient
c	– coefficient
D	– mean depth, m
D'	– incorrectly estimated value of D , m
d_m	– mean grain diameter, mm or m
F_b	– bed factor
F_{b0}	– bed factor for sand
F_R	– Froude number
F_s	– side factor
f	– exponent
g	– acceleration of gravity, m/sec^2
I	– longitudinal slope
J	– hydraulic gradient
j	– exponent
K	– coefficient
K_1, K_2, \dots	– coefficients
k	– coefficient
M_B	– amplitude of a meander, m

M_L	– length of a meander, m
n	– Manning coefficient; exponent
P	– wetted perimeter, m
p	– coefficient
Q	– discharge, m ³ /sec
Q_s	– sediment discharge, m ³ /sec
Q_w	– water discharge, m ³ /sec
q	– specific discharge, m ³ /sec/m
R	– hydraulic radius, m
r	– radius of curvature, m
S	– suspended sediment load (including wash load), m ³ /sec
s_b	– error in evaluation of F_b
s_s	– error in evaluation of F_s
V	– average velocity, m/sec
x	– empirical coefficient
α	– $(F_b/F_s)^{1/2}$
β	– $(F_s/F_b^2)^{1/3}$
γ	– $F_b^{5/6} \cdot F_s^{1/12} \cdot \nu^{1/4} / 3.63 \text{ g}$
δ	– $(F_b \cdot F_s)^{1/6}$
ν	– kinematic viscosity, m ² /sec
τ	– shear stress, N/m ²

4.1 Introduction

In the foregoing chapter the highly complex and often unpredictable character of alluvial stream morphology, dependent on a great number of continuously changing and stochastic parameters, has been sketched. It is only natural that engineers, particularly those active in the field of stream training, have always tried hard to introduce some element of deterministic and predictable causal relationship between the main parameters and the morphological processes expected to take place in alluvial streams. The obvious way toward this goal has been to pare down the number of parameters to the minimum essential, on the one hand, and to introduce many simplifying assumptions, on the other hand. An attempt of this kind has been briefly discussed in par. 3.3.4. Although one should be extremely wary when applying this or similar methods to actual natural streams, they nevertheless have the advantage of indicating, at least in qualitative terms, the basic trends of dynamic equilibrium responsible for physical responses to be expected.

A further step in this direction, on a scale and purpose of achievement incomparably larger and more methodical than any other endeavor of this kind, has been the introduction of the so-called Regime Theory, first enunciated in a paper by E.S. Lindley [1] at the beginning of the present century. It was originally intended to cover only the design of man-made earth channels, but was later extended by G. Lacey [2, 3], C. Inglis [4], T. Blench [5, 10, 24] and others to natural alluvial streams as well. Based mainly on an impressive number of field observations and measurements in the vast irrigation systems of the Punjab area situated in present-day Pakistan and Northern India, it was originally a purely empirical set of formulae for practical engineers supported by physical reasoning derived from the careful analysis of the accumulated data. Born as it was during a period in which civil engineering in general was much more practically oriented than today, it has increasingly come under attack for its lack of theoretical background as civil-engineering disciplines also started applying a basic scientific approach to the analysis of their problems. Only recently, however, have attempts been made to analyze and justify the validity of regime equations in the light of up-to-date theories of turbulence and sediment-transport mechanics. Similarity criteria, minimum-energy degradation and Einstein's bed load function, among other approaches, have been used to show that the hydraulic geometry of regime channels reflects the equilibrium conditions between the sediment transport and the cross-sectional stability. On the other hand, however, these works have also shown that the coefficients of the regime equations could not be considered numerical constants, as generally postulated by the concept, but are rather dependent on discharge and sediment properties.

According to the long-term observations by the authors, there is fairly good agreement between the actual behavior of small-stream alluvial channels or earth canals, and the predictions obtained by the regime concept, at least as long as the climatic and soil conditions are similar to those in Pakistan, India or Egypt. It is furthermore practically the only available set of criteria for the design of stable earth-channels with sediment transport, giving fairly dependable average values for the engineering applications. Judicious use of regime equations under proper circumstances, combined with due respect for the basic concepts of alluvial channel mechanics, can be a very useful tool indeed in the hands of a practising engineer. Their inherent limitations, however, should always be borne in mind by those using them, if miscalculations and often erroneous conclusions are to be avoided.

Basic notions of the regime concept were first stated by Lindley in 1919 [1]: "When an artificial channel is used to convey silty water, both bed and banks scour or fill . . . until a state of balance is attained at which *the channel is said to be in regime*. These regime dimensions depend on discharge,

quantity and nature of bed and berm silt, and roughness of the silted section. . .” (authors’ italics).

In other words, hydraulic characteristics of flow, sedimentological properties, and stability of the channel bed, are considered as one integral unit by the proponents of the regime theory. About forty years later, when he extended the regime concept to include the case of variable soil conditions over the river bed, T. Blench [5], stated that a stream is “in regime” when “. . . the average values of the quantities we appreciate as constituting regime (discharge, width, depth, average velocity, sediments, slope and meanders) do not show a definite trend over some interval – usually of the order of a score of two years. . .”

He further tried to explain his general concept by analogy, saying that the regime of a watercourse is something like the climate of a territory. The weather, of course, is changing from day to day, and its prediction is not amenable to exact analysis, but for all that a general regime of weather, or climate, is definitely recognizable, and some distinct laws governing it may be established.

Another nagging question, which for years has been worrying engineers making use of regime equations, has been the choice of discharge to be applied. Ideally, these equations are valid for a constant discharge only, a condition which obviously cannot be met, either in artificial or natural channels. The concept of the “dominant discharge”, already mentioned and used in the present text, still remains rather vague and indefinite. Such expressions as “bank-full discharge” or “channel-forming discharge” (*Bettbildende Wassermenge*) frequently met with in the literature on the regime theory, are generally ill-defined and subject to different interpretations. Some researchers, particularly Wolman and Leopold [6], Nixon [7], have tried to introduce the concept of frequency of discharges into regime equations, but so far their efforts have unfortunately not been followed up by other researchers, so the experimental evidence remains very scant. For further discussion of “dominant discharge”, see par. 9.7 in Part 2.

4.2 Principles of the Regime Theory

According to Blench [4], the three basic regime equations are as follows:

$$F_b = V^2/D \quad (4.1)$$

$$F_s = V^3/B \quad (4.2)$$

$$V^2/gDJ = 3.63 (VB/\nu)^{1/4} \quad (4.3)$$

In the above equations, F_b is the bed factor and F_s the side factor. Both factors are dimensional, hence they depend on the system of units used; on the other hand, numerical coefficient 3.63 is dimensionless. Eqs. (4.1)–(4.3) are subject to several constraints, among others: steady discharge, erodible cohesive banks hydraulically smooth, steady bed load discharge, uniform slope, straight alignment, etc. Eq. (4.1), moreover, indirectly suggests that channels with similar hydraulic and sediment characteristics tend to adjust the depth of flow to reach similar Froude numbers.

After some algebraic transformations, Eqs. (4.1)–(4.3) can be written in a more suitable form:

$$B = \left[\frac{F_b}{F_s} Q \right]^{1/2} = \alpha Q^{1/2} \quad (4.4)$$

$$D = \left[\frac{F_s}{F_b^2} Q \right]^{1/3} = \beta Q^{1/3} \quad (4.5)$$

$$J = \frac{F_b^{5/6} F_s^{1/12} \nu^{1/4}}{3.63 g Q^{1/6}} = \gamma Q^{-1/6} \quad (4.6)$$

$$V = (F_b F_s Q)^{1/6} = \delta Q^{1/6} \quad (4.7)$$

In the above equations, D is the average depth of flow and $B = A/D$ is the average width of flow. The question of what discharge, Q , is to be used in Eqs. (4.4)–(4.7) has already been discussed in the previous paragraph. Extreme care and experience will be required from the practising engineer, because the regime theory is not explicit in this respect. Not all the values are equally affected by an incorrect choice of the “dominant discharge”; hydraulic gradient $J = f_1(Q^{-1/6})$, Eq. (4.6), would be only slightly influenced, the depth $D = f_2(Q^{1/3})$, Eq. (4.5), to a much larger extent, but still maybe tolerable, whereas the width $B = f_3(Q^{1/2})$, Eq. (4.4), is considerably more sensitive. Insight and keen observation of stream behavior are probably the best guide to find the right answer; in the absence of these, one will have to adopt one of the more or less arbitrary criteria as given by various regime-theory researchers.

The original dimensionless constant of Eqs. (4.3) and (4.6), having the numerical value of 3.63, was later amended to read [9]: $3.63(1 + aC)$. In

this expression, C is the bed load sediment concentration in ppm, and a is an empirically determined numerical coefficient (for streams with sandy beds, Blench suggests $a \approx 1/2330$). As long as the sediment discharge is small, the expression $(1 + aC)$ tends to unity and Eq. (4.3) may be applied in its original form; when the sediment discharge becomes larger, $(1 + aC)$ is greater than unity, and therefore should be properly computed. This aspect of the regime equations will be studied in more detail in par. 4.4.

In the computed example 4.1, it has been assumed that the regime factors F_b and F_s can be estimated for a given watercourse by an experienced drainage engineer. In such a case, all the regime values are a function of the "dominant discharge", Q , and their dependence on this important parameter will be illustrated.

Example 4.1

For a given watercourse the following data are available, or are estimated:

Dominant discharge	$Q = 100 \text{ m}^3/\text{sec}$
Bed factor	$F_b \cong 0.02 \text{ m}/\text{sec}^3$
Side factor	$F_s \cong 0.02 \text{ m}^2/\text{sec}^3$
Kinematic viscosity	$\nu = 10^{-6} \text{ m}^2/\text{sec}$
Sediment discharge	very small

Required: B , D , J and V for the given discharge and for other discharges

Solution:

$$\text{Step 1 - } \alpha = \left[\frac{F_b}{F_s} \right]^{1/2} = \left[\frac{0.3}{0.02} \right]^{1/2} = 3.87$$

$$\beta = \left[\frac{F_s}{F_b^2} \right]^{1/3} = \left[\frac{0.02}{0.3^2} \right]^{1/3} = 0.61$$

$$\gamma = \frac{F_b^{5/6} F_s^{1/12} \nu^{1/4}}{3.63 \times g} = \frac{0.3^{5/6} 0.02^{1/12} (10^{-6})^{1/4}}{3.63 \times g} = 0.00023$$

$$\delta = (0.3 \times 0.02)^{1/6} = 0.43$$

$$\text{Step 2 - } B = \alpha Q^{1/2} = 3.87 \times (100)^{1/2} = 38.7 \text{ m}$$

$$D = \beta Q^{1/3} = 0.61 \times (100)^{1/3} = 2.8 \text{ m}$$

$$J = \gamma Q^{-1/6} = 0.00023 \times (100)^{-1/6} = 0.00011 = 0.11\%$$

$$V = \delta Q^{1/6} = 0.43 \times (100)^{1/6} = 0.93 \text{ m/sec}$$

Step 3 – Variation of the computed values for discharges other than the one given is summarized in Table 4.1.

TABLE 4.1. COMPUTED VALUES (Ex. 4.1)

Q (m ³ /sec)	B (m)	D (m)	J (%)	V (m/sec)	B/D
100	38.7	2.8	0.11	0.93	13.8
10	12.2	1.3	0.16	0.63	9.4
1	3.9	0.6	0.23	0.43	6.5
0.1	1.2	0.3	0.34	0.29	4.0

While the discharge changed in the range of 1:1000, width B varied only in the range of 1:31.6, the depth in about 1:10, hydraulic gradient J and the average velocity V in about 1:3.2 (the latter directly proportional, the other inversely proportional to the discharge), and the ratio B/D in the range of about 1:3.2. All these results, of course, are obvious from the form of Eqs. (4.4)–(4.7) themselves, and they are brought here only to underline their physical implications. In fact, generally speaking, large watercourses have flatter cross-sections than smaller ones (higher B/D ratios), and their longitudinal slopes (roughly equal to the hydraulic gradient) also are flatter.

It may further be of some interest to check the calculated values obtained for the Manning roughness coefficient, assuming uniform-flow conditions, from the expression $n = (R^{2/3} J^{1/2})/V$, using the values as listed in Table 4.1. Results of this calculation are summarized in Table 4.2.

It is remarkable that the values of n thus obtained are almost constant. Incidentally, Manning roughness coefficient of about 0.02 corresponds to channels with sandy or silty bed. On the other hand, it has already been pointed out in respect to Eq. (4.1) that for similar flow characteristics,

TABLE 4.2. COMPUTED VALUES (Ex. 4.1)

Q (m ³ /sec)	n
100	0.0205
10	0.0210
1	0.0211
0.1	0.0212

regime theory assumes similar Froude number; for the present example, $F_R = V/(gD)^{1/2}$ for all discharges is about 0.175.

4.3 Evaluation of F_b and F_s – Factors for Small Sediment Discharges

For practical application of regime theory equations, a good estimate of the two basic factors is of primary importance. Yet the available information on this subject is neither plentiful nor accurate.

First, distinction should be made between small and large sediment discharges. The actual boundary between the two is not clearly defined, but it is generally recommended as $C \cong 20$ ppm. Hence, sediment discharges for which $C \leq 20$ are considered as being small.

For sediment particles falling into the range of sands, i.e. $0.06 \text{ mm} \leq d_m \leq 2 \text{ mm}$, the bed factor can be estimated from

$$F_{b_0} \cong 0.58 (d_m)^{1/2} \quad (4.8)$$

Here d_m denotes the median-by-weight grain size diameter in millimeters. F_b -values accordingly are in the range of about 0.14–0.82 m/sec².

The available information as to the side factor F_s is even sketchier and less reliable. According to Blench, the factor depends on the cohesion of sandy-loam particles making the bank material. As a rough guide, he gives the following values:

For sandy loams with little cohesion – $F_s \approx 0.009 \text{ m}^2/\text{sec}^3$

For sandy loams with medium cohesion – $F_s \approx 0.019 \text{ m}^2/\text{sec}^3$

For sandy loams with high cohesion – $F_s \approx 0.028 \text{ m}^2/\text{sec}^3$

The definition of both the "sandy loam" and the degree of cohesion remain vague and unreliable. On the other hand, regime equations are not unduly sensitive to errors in the evaluation of the factors, as illustrated in Example 4.2.

Example 4.2

Given a wide channel. Specific discharge: $q = Q/B = \text{const. } q = V \times D$.
From Eq. (4.1),

$$F_b = \frac{V^2}{D} = \frac{q^2}{D^3}$$

and therefore,

$$D = \left[\frac{q^2}{F_b} \right]^{1/3}$$

If the error in evaluation of F_b is denoted as s_b , and the depth obtained from the incorrect estimate of F_b as D' , then the ratio between the two depths is

$$\frac{D'}{D} = \left[\frac{1}{1 \pm s_b} \right]^{1/3}$$

Hence a $\pm 30\%$ error in F_b will cause only about -9% or $+13\%$ deviation of the estimated depth. Similarly, if F_b is assumed to be correct, but there is an error s_s in the evaluation of F_s , then from Eq. (4.4)

$$\frac{B'}{B} = \left[\frac{1}{1 \pm s_s} \right]^{1/2}$$

From here, a $\pm 30\%$ error in F_s will produce a deviation of about -12% or $+19\%$ of the estimated width of channel.

Since from Eqs. (4.4) and (4.5) the following ratios can be obtained:

$$\frac{B'}{B} = \frac{(1 \pm s_b)^{1/2}}{(1 \pm s_s)^{1/2}}, \quad \frac{D'}{D} = \frac{(1 \pm s_s)^{1/3}}{(1 \pm s_b^2)^{1/3}}$$

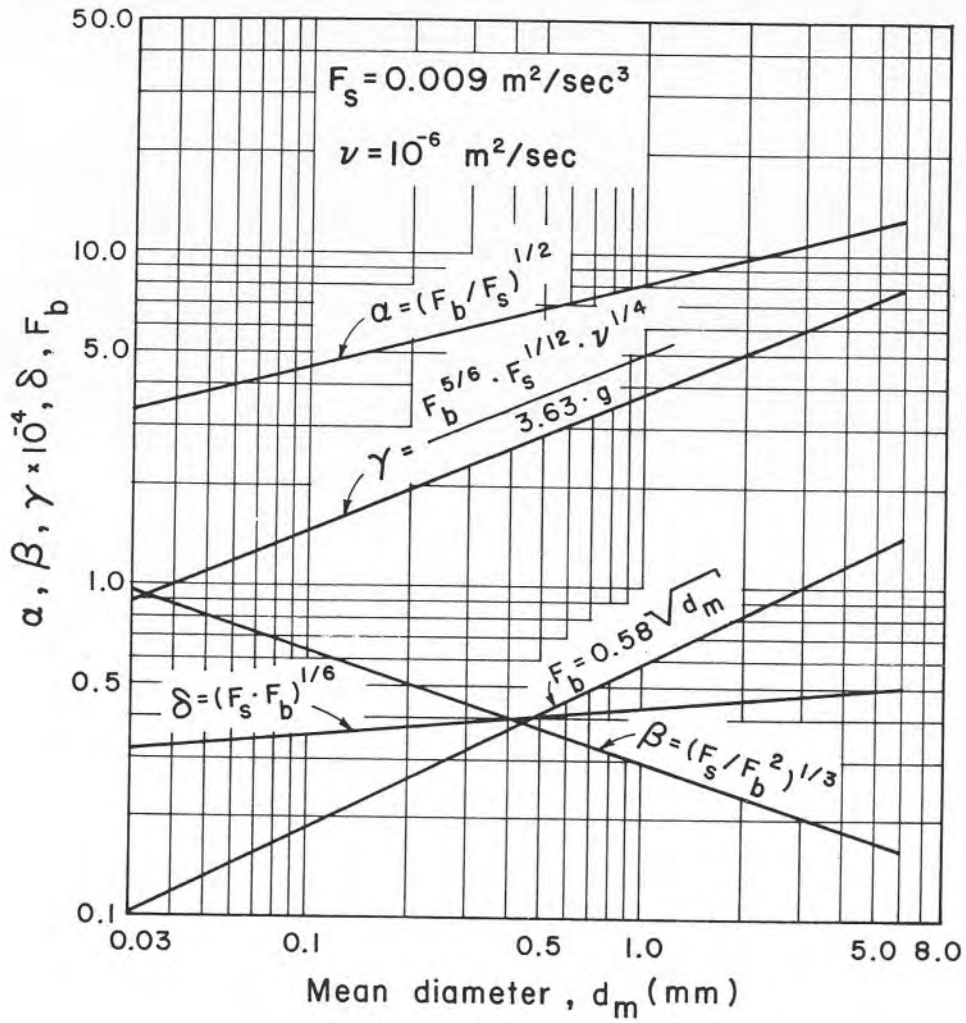


Fig. 4.1. Regime functions for small sediment discharges.

it is evident that a simultaneous error of the same sign in both F_b and F_s will reduce the deviation, while errors of opposite signs will increase it.

In Fig. 4.1 functions (4.4)–(4.7) are shown graphically on logarithmic paper. F_b -values are derived from Eq. (4.8) for mean sediment diameters in the range of sands, whereas the side factor is assumed constant, $F_s = 0.009 \text{ m}^2/\text{sec}^3$ (sandy loam with small cohesion). Corresponding numerical values of functions α , β , γ and δ for side factors F_s other than the assumed one, can easily be obtained by multiplying or dividing according to functional relationships.

Example 4.3

Given: $d_m = 1 \text{ mm}$; $Q = 15 \text{ m}^3/\text{sec}$; $F_s = 0.02 \text{ m}^2/\text{sec}^3$; $\nu = 10^{-6} \text{ m}^2/\text{sec}$.

Required: D, B, J, V

Solution:

Step 1 – From Fig. 4.1:

$$\alpha = 8.0; \beta = 0.3; \gamma = 3.8 \times 10^{-4}; \delta = 0.4$$

Step 2 – Values of the functions after correction for $F_s = 0.02$,

$$\alpha' = 8.0 \left[\frac{0.009}{0.02} \right]^{1/2} = 5.4$$

$$\beta' = 0.3 \left[\frac{0.02}{0.009} \right]^{1/3} = 0.4$$

$$\gamma' = 3.8 \times 10^{-4} \left[\frac{0.02}{0.009} \right]^{1/12} = 4.1 \times 10^{-4}$$

$$\delta' = 0.4 \left[\frac{0.02}{0.009} \right]^{1/6} = 0.5$$

Step 3 – The required values,

$$B = 5.4 \times (15.0)^{1/2} = 20.9 \text{ m}$$

$$D = 0.4 \times (15.0)^{1/3} \cong 1.0 \text{ m}$$

$$J = 4.1 \times 10^{-4} \frac{1}{(15.0)^{1/6}} = 2.6 \times 10^{-4} = 0.26\text{‰}$$

$$V = 0.5 \times (15.0)^{1/6} \cong 0.8 \text{ m/sec}$$

Step 4 – For checking purposes, Manning's roughness coefficient can be computed, if $R \sim D$

$$n = \frac{R^{2/3} J^{1/2}}{V} = \frac{1.0^{2/3} (2.6 \times 10^{-4})^{1/2}}{0.8} \cong 0.021$$

The above value seems reasonable for a sandy channel bed.

4.4 Evaluation of Factors for Large Sediment Discharge

It has already been mentioned in par. 4.2 that later regime-theory investigators had amended the constant in Eq. (4.6) to read $3.63 (1 + \alpha C)$, instead of only 3.63. When sediment concentration is expressed in parts per million, coefficient α , according to Blench, can be taken as $\sim 1/2330$. Sediment concentrations less than about $C \cong 20$ ppm (or equal to) generally are considered to be "small" in regime-theory application, simply because the expression between brackets remains practically equal to unity (for $C = 20$, the deviation from unity is less than 1%).

Bed factor F_b for bed load discharge concentrations greater than about $C = 20$ ppm should be obtained from the expression [9],

$$F_b = F_{b0} (1 + 0.012C) \quad (4.9)$$

where F_{b0} denotes the factor computed by Eq. (4.8). According to Blench, this equation should be used for subcritical flow only, and he gives another expression for supercritical flow. Different values of F_b for the two flow

regimes are probably due to Blench's assumption that dunes are formed only in subcritical flow, while in supercritical flow bed stays flat. Later investigations, however, have shown that this view was not correct (see Chapter 7).

Eq. (4.6) for large sediment-discharge concentrations, therefore, can be written as:

$$J = \frac{[F_{b0} (1 + 0.012C)]^{5/6} F_s^{1/12} v^{1/4}}{3.63 (1 + C/2330) g Q^{1/6}} \quad (4.10)$$

Side factor F_s is considered unaffected by the sediment load, and depends only on the cohesion of bank material.

In addition to the often useful expression for the depth D derived in Example 4.2, other similar expressions can easily be obtained by elementary algebra. Some of these expressions are given in Table 4.3.

TABLE 4.3. ALTERNATIVE FORMULAE FOR REGIME THEORY

Symbol	Basic form	Alternative form
B	$(F_b/F_s Q)^{1/2}$	$F_b/F_s q$
D	$(F_s/F_b^2 Q)^{1/3}$	$(q^2/F_b)^{1/3}$
Q	$(D^3 B^2 F_b)^{1/2}$	$(D^3 B^4 F_s)^{1/3}$

Three additional expressions, given by Blench and arrived at by simple algebraic transformations and substitutions, concern hydraulic gradient J (Eq. 4.6), and are given below,

$$1. \quad J = \frac{F_{b0}^{5/6} F_s^{1/12} f_1(C)}{K Q^{1/6}} \quad (4.11)$$

$$2. \quad J = \frac{F_{b0}^{7/8} f_2(C)}{K B^{1/4} D^{1/8}} \quad (4.12)$$

and

$$3. \quad J = \frac{F_{b0}^{11/12} f_3(C)}{K B^{1/6} Q^{1/12}} \quad (4.13)$$

where

$$K = \frac{3.63g}{\nu^{1/4}} \quad (4.14)$$

$$f_1(C) = \frac{(1 + 0.012C)^{5/6}}{1 + C/2330} \quad (4.15)$$

$$f_2(C) = \frac{(1 + 0.012C)^{7/8}}{1 + C/2330} \quad (4.16)$$

$$f_3(C) = \frac{(1 + 0.012C)^{11/12}}{1 + C/2330} \quad (4.17)$$

Sediment discharge concentration C is in ppm.

Example 4.4

In a small alluvial stream, a fairly representative reach seems to be in a state of temporary equilibrium during a period of several years. For the design of a stream-training scheme in some other parts along the channel, characteristic regime-theory parameters have to be derived from the mean data gathered in the given reach.

Data appertaining to the stable reach: Dominant discharge, $Q = 85 \text{ m}^3/\text{sec}$. (Let us say, the discharge which can maintain the channel in relative equilibrium, and is not exceeded frequently enough to cause appreciable flood-plain formation). $D = 3.0 \text{ m}$; $B = 35.0 \text{ m}$; $J = 0.2\text{‰}$; $d_m = 0.01 \text{ mm}$; $\nu = 10^{-6} \text{ m}^2/\text{sec}$.

Required: F_b , F_s , F_{b0} , V .

Solution:

Step 1 – Using Eq. (4.4)

$$B = \left[\frac{F_b}{F_s} \right]^{1/2} Q^{1/2}$$

$$35.0 = \left[\frac{F_b}{F_s} \right]^{1/2} 85^{1/2}$$

whence

$$\frac{F_b}{F_s} = 14.4$$

Step 2 – From Eq. (4.5)

$$D = \left[\frac{F_s}{F_b^2} \right]^{1/3} Q^{1/3} \quad (a)$$

after solving for the given data,

$$\frac{F_s}{F_b^2} = 0.094 \quad (b)$$

Step 3 – Simultaneous solution of Eqs. (a) and (b) yields

$$F_b = 0.74 \text{ and } F_s = 0.05$$

Step 4 – Using Eq. (4.6)

$$\left[1 + \frac{C}{2330} \right] = \frac{F_b^{5/6} F_s^{1/12} \nu^{1/4}}{3.63 g Q^{1/6} J}$$

and introducing the numerical values, sediment discharge concentration is obtained, $C \cong 666 \text{ ppm} > 20$, hence it is a large concentration.

Step 5 – From Eq. (4.9)

$$F_{b0} = \frac{F_b}{1 + 0.012C} = 0.082 \text{ m/sec}^2$$

If $F_{b0} = f(d_m)^{1/2}$, $f = 0.82$

Step 6 – Eq. (4.7) yields

$$V = (F_b F_s Q)^{1/6} = (0.74 \times 0.05 \times 85)^{1/6} = 1.2 \text{ m/sec.}$$

Step 7 – If 35 m³/sec are pumped out of the stream, but the sediment discharge remains almost unaltered, find how this is likely to affect channel characteristics under regime conditions.

(a) Remaining discharge in the channel, $Q_1 = 50 \text{ m}^3/\text{sec}$. New approximate sediment discharge concentration

$$C_1 = 666 \frac{85}{50} = 1132 \text{ ppm.}$$

$$(b) F_{b1} = F_{b0} (1 + 0.012C) = 0.082 (1 + 0.012 \times 1132) = 1.2 \text{ m/sec}^2$$

$$(c) B_1 = \left[\frac{F_{b1}}{F_s} Q_1 \right]^{1/2} = \left[\frac{1.2}{0.05} 50 \right]^{1/2} = 34.6 \text{ m}$$

$$D_1 = \left[\frac{F_s}{F_{b1}^2} Q_1 \right]^{1/3} = 1.2 \text{ m}$$

$$J_1 = \frac{F_{b1}^{5/6} \times F_s^{1/12} \times (10^{-6})^{1/4}}{3.63 (1 + C_1/2330) g Q_1^{1/6}} = 0.000283 = 0.283\text{‰}$$

$$V_1 = (F_{b1} F_s Q)^{1/6} = 1.2 \text{ m/sec}$$

(To check arithmetical computations, discharge may be computed from $Q = A \cdot V = 34.6 \times 1.2 \times 1.2 = 49.8 \text{ m}^3/\text{sec}$). Increase of about 70% in sediment discharge concentration will cause a decrease in depth D of about 40%, the width of the channel will remain almost unaltered, longitudinal slope will increase by about 41%, and velocity V will stay unchanged.

(d) Manning roughness coefficient for the given stream at the two flow conditions results

First case: $D = 2.0 \text{ m}$, $J = 0.2\text{‰}$, $V = 1.2 \text{ m/sec}$

$$n = \frac{D^{2/3} J^{1/2}}{V} = \frac{2.0^{2/3} 0.0002^{1/2}}{1.2} \cong 0.019$$

Second case: $D_1 = 1.2$ m, $J = 0.28\%$, $V_1 = 1.2$ m/sec

$$n_1 = \frac{D_1^{2/3} J_1^{1/2}}{V_1} \cong 0.016,$$

giving a difference of about 16%.

Example 4.5

A low weir has been built across the original stream of Example 4.4, causing most of the sediment load to settle upstream of the weir, leaving the discharge unchanged. Let us assume that the sediment discharge concentration downstream of the weir is $C_2 = 300$ ppm. Find the characteristics of the channel, if it is to adapt itself to more or less stable regime conditions.

Given data: $Q = 85$ m³/sec; $C_2 = 300$ ppm; $\nu = 10^{-6}$ m²/sec; $F_s = 0.05$; $d_m = 0.01$ mm.

Required: F_b ; B , D and J .

Solution

Step 1 — F_{b_0} and F_s remain unchanged, hence $F_{b_0} = 0.082$; $F_s = 0.05$.
 $F_{b_2} = F_{b_0} (1 + 0.012C) = 0.082 (1 + 0.012 \cdot 300) = 0.38$ m/sec²

Step 2 —

$$B_2 = \left[\frac{F_{b_2}}{F_s} Q \right]^{1/2} = 25.4 \text{ m}$$

$$D_2 = \left[\frac{F_s}{F_{b_2}^2} Q \right]^{1/3} = 3.1 \text{ m}$$

$$V_2 = (F_{b_2} \times F_s \times Q)^{1/6} = 1.1 \text{ m/sec}$$

$$J_2 = \frac{F_{b_2}^{5/6} \times F_s^{1/12} \times (\nu^{-6})^{1/4}}{3.63 (1 + C_2/2330) \times g Q^{1/6}} = 0.00013 = 0.13\%$$

As a result of the reduced sediment load (about 45% of the original load), one should expect a heavy bed erosion (mean depth D_2 increased by about 70%), a reduction in width B_2 (by about 28%), and finally a reduced

hydraulic gradient J_2 (by about 35%).

If the stream of Examples 4.4 and 4.5 is analyzed following the simplified procedure outlined in par. 3.3.4, in which change in sediment discharge was disregarded, and the basic assumption has been that at all stages the stream tends to a state of constant shear stress $\tau = \text{const.}$, the following results are obtained:

1. Given: $Q = 85 \text{ m}^3/\text{sec}$; $D = 2.0 \text{ m}$; $B = 35.0 \text{ m}$; $J = 0.2\text{‰}$

Computed: $A = 70 \text{ m}^2$; $P = 39 \text{ m}$; $R = 70/39 = 1.8 \text{ m}$, whence $\tau = \gamma R J \cong 3.5 \text{ N/m}^2$

2. Given: $Q = 85 \text{ m}^3/\text{sec}$; $D_2 = 3.1 \text{ m}$; $B_2 = 25.4 \text{ m}$; $J = 0.13\text{‰}$

Computed: $A = 78.7 \text{ m}^2$; $P = 31.6 \text{ m}$; $R = 78.7/31.6 = 2.5 \text{ m}$; $\tau = 3.2 \text{ N/m}^2$

Difference in the computed shear stress is about 8%.

4.5 Stream Meandering According to the Regime Theory

The question of stream meandering and its engineering aspects have already been discussed in par. 3.9. Here a very short review is given of regime-theory's contribution in this field, based on observations of natural water-courses over many years. The approach again is wholly empirical, founded on the often observed correlation between the channel width and the curvature of meanders.

Mean width of the channel according to Eq. (4.4) is a function of discharge, $B = \alpha Q^{1/2}$.

The two main meander-curvature characteristics (see Fig. 4.2) are related to the mean width

$$M_B = f_1(B) = C_B (Q_{\max}^{1/2}) \quad (4.18)$$

and

$$M_L = f_2(B) = C_L (Q_{\max}^{1/2}) \quad (4.19)$$

Here Q_{\max} according to Blench [10] is the discharge having return period of about 100 years. Coefficients C_B and C_L have dimensions $L^{-1/2} T^{1/2}$, and therefore depend on the system of units used. Observations show that the average range of the coefficient C_L in metric units is $34 \leq C_L \leq 76 \text{ m}^{-1/2} \text{ sec}^{1/2}$.

For average medium-size streams Blench recommends using a mean value of $C_L \cong 50 \text{ m}^{-1/2} \text{ sec}^{1/2}$. Based on the analysis of many streams in India and the USA, he further proposes to use the following empirical relationships,

$$M_B/M_L \cong 0.5 \text{ for slightly meandering channels}$$

$$M_B/M_L \cong 1.5 \text{ for strongly meandering channels}$$

or any intermediate value according to the degree of meandering.

All the above empirical coefficients and ratios should be applied only with the utmost care and sound engineering judgement. It should also be noted that in the evaluation of coefficients no weight has apparently been given to the type of soil or sediment characteristics, which certainly have some influence upon the shape of meanders for a given watercourse.

Values of meander distinguishing features M_B and M_L according to Eqs. (4.18) and (4.19), and on evidence from field observations, depend on the stream discharge, and hence are likely to vary with changing discharge. Higher values of the ratio M_B/M_L mean sharper curvature. All other parameters assumed equal, a small stream (low discharge) will generally have sharper meander bends than larger streams.

In some recent works on the subject [11], "wave-length" of a typical meander in metric units was found to be $M_L \cong 61.2 Q^{0.467}$ (where Q is a "representative" discharge in m^3/sec), which is within the range suggested by T. Blench. They have also found that the ratio M_L/M_B could be expressed as a function of discharge,

$$\frac{M_L}{M_B} = \frac{2.06}{Q^{0.038}} \quad (4.20)$$

For the range of discharges from $1 \text{ m}^3/\text{sec}$ to $1000 \text{ m}^3/\text{sec}$, the ratio calculated from the above expression lies in the range of 2.06 to 1.58 respectively. This is somewhat higher than the range as given by the regime-theory, namely 1.5–0.5.

From a laboratory investigation on hydraulic models, Friedkin [12] obtained a correlation between meander dimensions and discharge, shown in Fig. 4.2. It is, however, highly questionable whether the curves could be applied to natural streams, with vastly higher discharges; some doubts could also be raised in connection with the scaling of the models used in the above investigation.

Although the quantitative prediction of meander shape is probably beyond the reach of the present state-of-the-art, the available empirical

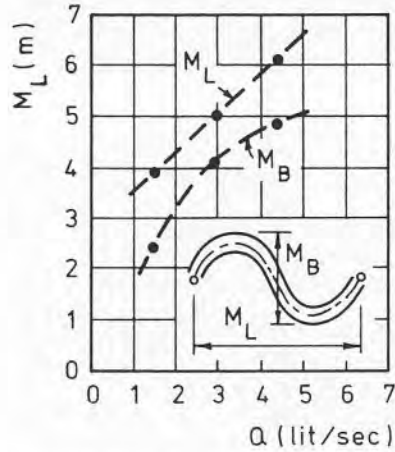


Fig. 4.2. Meander dimensions from model investigation, after [12].

relationships mentioned, and many others not reviewed, nevertheless it may often be of help to the practising engineer in order to find his “bearings” in this intricate field. They further seem to clearly indicate that *qualitatively* both dimensions depend on the discharge, i.e. $M_L, M_B = f(Q)$. There also appears to be good evidence that the shape of the meander adapts itself fairly rapidly to the requirements of higher discharges, gradually changing with decreasing rates of flow.

During investigations on hydraulic models, Bordes [13] found that the length of the meander, M_L , seems to augment with the increase of the difference $\Delta Q = Q_{\max} - Q_{\min}$, and with the frequency of large-discharge occurrence.

A different approach was adopted by Shahjahan [14] who tried to establish a functional relationship between the length of the meander, M_L , and the median grain size, d_{50} . He finally proposed a relatively complicated dimensionless expression,

$$\frac{M_L}{d_{s50}} = K \left[\frac{Q^{2/5}}{g^{1/5}} d_{s50}^{-1} \right]^x \quad (4.21)$$

where Q – a characteristic discharge, m/sec; d_{s50} – median grain size, m; g – acceleration of gravity, m/sec²; K – empirical coefficient; x – empirical exponent.

He has not indicated any specific values for K and x , but has given instead a series of non-dimensional graphs in which he analyzed the data

from his own laboratory experiments and from other researchers as well. On log-log paper, a family of straight lines is obtained for different values of the dimensionless parameter $d_{s50} g^{1/3} / \nu^{2/3}$ (ν – kinematic viscosity) ranging from 2 to about 520. Exponent x for all lines is virtually identical, $x \cong 1.14$; coefficient K varies from about 15 for high values of the dimensionless parameter, to about 45 for low values.

From the above study, and from many others in recent years, [15–17] and others, it has become evident that no simple relationship for meander length, M_L , could possibly be established. Besides the already mentioned parameters, it probably depends also on the longitudinal slope, I , and the relative sediment discharge, $Q_{\text{sediment}}/Q_{\text{water}}$.

It seems that meander amplitude, M_B , is even less amenable to any consistent empirical relationship, and indeed very few have so far been proposed. Correlation between meander length, M_L , and its amplitude, in the form of

$$M_B = K M_L \quad (4.22)$$

has been sought by many researchers. Unfortunately, values of the coefficient K vary widely between 0.25 to about 1.7, which incidentally lies roughly within the range indicated by the regime theory.

Some additional conclusions reached by the previously mentioned study [14] can be summarized as follows:

- The values of M_L , M_B , r (radius of curvature) and B (width of the channel) increase with the increase of the valley slope, I . The stream becomes deeper with the decrease of I , provided discharge, sediment load, bank and bed materials are not changed.
- Increase of relative sediment discharge, Q_s/Q_w , reduces the values of M_L and B , whereas values of M_B , r and water depth D are increased.

4.6 Some Further Developments of the Regime-Theory Concept

4.6.1 Leopold and Maddock Equations for Hydraulic Geometry of the Channel

From experimental data referring to about 120 gauging stations in about ten different watershed basins across the United States, and discharges in the wide range of about 0.5 m³/sec to 15,000 m³/sec, Leopold and Maddox [18] applied the regime-theory concept to alluvial streams in the U.S.

Considering the water and sediment discharges as independent variables determined by watershed characteristics, and channel dimensions as dependent variables, they introduced the concept of the “hydraulic geometry of the channel” as an exponential function of the discharge. In order to take into account the variability of the stream flow in natural watercourses, they used discharges of equal frequency at different gauging stations along the channel. Thus they tried to link the ill-defined “dominant” discharge to be used in regime-theory equations to the selected stochastic frequency. As a result of these investigations, they established a general set of relations, all functions of discharge Q :

$$B = a Q^b \quad (4.23)$$

$$D = c Q^f \quad (4.24)$$

$$V = k Q^m \quad (4.25)$$

$$S = p Q^j \quad (4.26)$$

From continuity considerations, Leopold and Maddock concluded that:

$$a c k = 1 \quad (4.27)$$

$$b + f + m = 1$$

and gave a set of characteristic values for the various exponents, which proved to be fairly constant for all the streams studied. Coefficients a , c and k showed larger variations for different streams. No final values have been given for the coefficient p and exponent j .

For each station along a given stream, the above set of equations gives a family of characteristic curves as function of discharge frequency. These curves they designated as the “hydraulic geometry of the stream.” Some interesting conclusions reached by Leopold and Maddock from the study of such curves and other pertinent experimental data are as follows:

1. Since the exponent m is always a positive quantity, and the discharge Q increases in the downstream direction, mean velocity of a stream should increase in the downstream direction.

2. Increase of the suspended load in the downstream direction is generally less than the increase in discharge, and hence the sediment discharge concentration of suspended sediment decreases in the downstream direction.

3. A narrow stream with a given velocity carries a larger suspended load

than a wider stream with a similar velocity and discharge.

4. A natural channel of a given width and discharge generally will increase the mean velocity and decrease its depth, if its suspended sediment load is increased.

5. For discharges of the same frequency along the stream, the roughness coefficient is nearly constant.

6. Changes of roughness coefficient, due to extreme discharge variations in channels with sandy beds, are of much greater significance than changes in longitudinal slope from the same cause.

4.6.2. *Extension of the Regime-Theory by Simons and Albertson*

In order to correct some of the shortcomings of the regime-theory, Simons and Albertson [19] extended their investigations and analysis to many additional field data from Indian and North American sources. Although the system proposed by them actually relates to the design of equilibrium earth channels, it is nevertheless included in the present chapter, because it is based on field observations of natural streams and directly reflects their behavior.

They distinguished between five main types of earth channels:

1. Sand bed and sand banks.
2. Sand bed and cohesive banks.
3. Cohesive bed and cohesive banks.
4. Coarse non-cohesive material.
5. Similar to type 2, but with sediment discharge concentration of 2,000–8,000 ppm.

A set of equations in general form is given, but the empirical coefficients and exponents they contain can be fitted to any of the five channel types listed above. Both the coefficients and the exponents have been slightly rounded off in respect to their original values, since excessive accuracy does not seem to be warranted.

$$P = K_1 Q^{0.5} \quad (4.28)$$

$$B = 0.9 P \quad (4.29)$$

$$B = 0.92 \bar{B} - 0.6 \quad (4.30)$$

$$R = K_2 Q^{0.36} \quad (4.31)$$

$$D = 1.21R \quad (R \leq 2 \text{ m}) \quad (4.32)$$

$$D = 0.6 + 0.93R \quad (R \geq 2 \text{ m}) \quad (4.33)$$

$$V = K_3 (R^2)^n (J)^n \quad (4.34)$$

$$\frac{C^2}{g} = \frac{V^2}{gDI} = K_4 \left[\frac{VB}{\nu} \right]^{0.37} \quad (4.35)$$

In the above equations \bar{B} is the surface width of the wetted cross-section, C is the Chézy coefficient, and the rest of the symbols as given before in the present chapter. The coefficients in metric units and the values for the exponent n are given in Table 4.4.

TABLE 4.4. COEFFICIENTS AND EXPONENT n FOR EQS. (4.28)–(4.35)

Coefficient and exponent	Channel type				
	1	2	3	4	5
K_1	6.33	4.7	4.0	3.17	3.1
K_2	0.57	0.48	0.41	0.27	0.36
K_3	9.3	10.7	—	10.9	9.7
K_4	0.33	0.54	0.87	—	—
n	0.33	0.33	—	0.29	0.29

The same set of equations can also be solved with the aid of diagrams given in Figs. 4.3 to 4.10 in metric units. These diagrams are based on the original ones supplied by Simons & Albertson in English units, but all the experimental points leading to the proposed curves have been omitted for the sake of simplicity. The following steps of the design procedure are suggested:

Step 1 – From Fig. 4.3 find the appropriate wetted perimeter P for the given design discharge Q .

Step 2 – Estimated side slopes of the channel are determined by using Figs. 4.4 and 4.5, from which widths B and \bar{B} can be obtained.

Step 3 – Fig. 4.6 gives the estimated hydraulic radius R for the design dis-

charge Q and the type of the earth channel. At this stage the cross-sectional area can be computed from $A = PR$, and the mean velocity from $V = Q/A$.

Step 4 – In the next step the mean depth D can be determined from Fig. 4.7, and now the detailed shape of the trapezoidal channel can be fixed. While the values for the hydraulic radius and wetted perimeter should be retained, values for the mean depth, widths B and \bar{B} can be adjusted if needed. Side slopes of the channel should be determined to suit the type of soil available.

Step 5 – Fig. 4.8 is next used to obtain the estimated value of the parameter R^2I for the computed average velocity V . From the known value of R , the longitudinal slope I can be computed.

Step 6 – Values of average velocity V and width B can now be used to obtain from Fig. 4.9 the estimated value of the parameter V^2/gDI , from which again the longitudinal slope I can be computed.

Step 7 – Additional estimate of the longitudinal slope I can be gained from the permissible shear stress τ obtained from Fig. 4.10. (This diagram is based on the work published by Lane [20], in which shear stresses acting in canals were correlated with the material through which the canals had been constructed).

So at this stage the design engineer will have three possible values of longitudinal slope I to choose from. Engineering skill and experience, as always, will be needed to select the final design slope.

Some geometrical discrepancies are likely to be unavoidable when using values obtained from the method just outlined, but they probably will remain of minor importance. One should never forget that the proposed system of equations is mainly empirical, and therefore some minor inconsistencies are almost inevitable. Inherent limitations of the regime-theory approach have been already discussed in the introduction to the present chapter, and should always be borne in mind.

Example 4.6

In order to illustrate the use of the diagrams in Figs. 4.3–4.10, let us determine design assumptions for a stable alluvial channel concerning an arbitrary stream.

a) Design discharge: $Q = 100 \text{ m}^3/\text{sec}$; b) Sand bed and cohesive banks;
c) Mean sand diameter $d_{50} \cong 0.3 \text{ mm}$; d) Kinematic viscosity of water: $\nu = 1 \times 10^{-6} \text{ m}^2/\text{sec}$.

All point fixings are shown on respective diagrams by dashed lines, and coordinate values are numerically annotated.

Step 1 – Introducing the given discharge, and observing that the channel

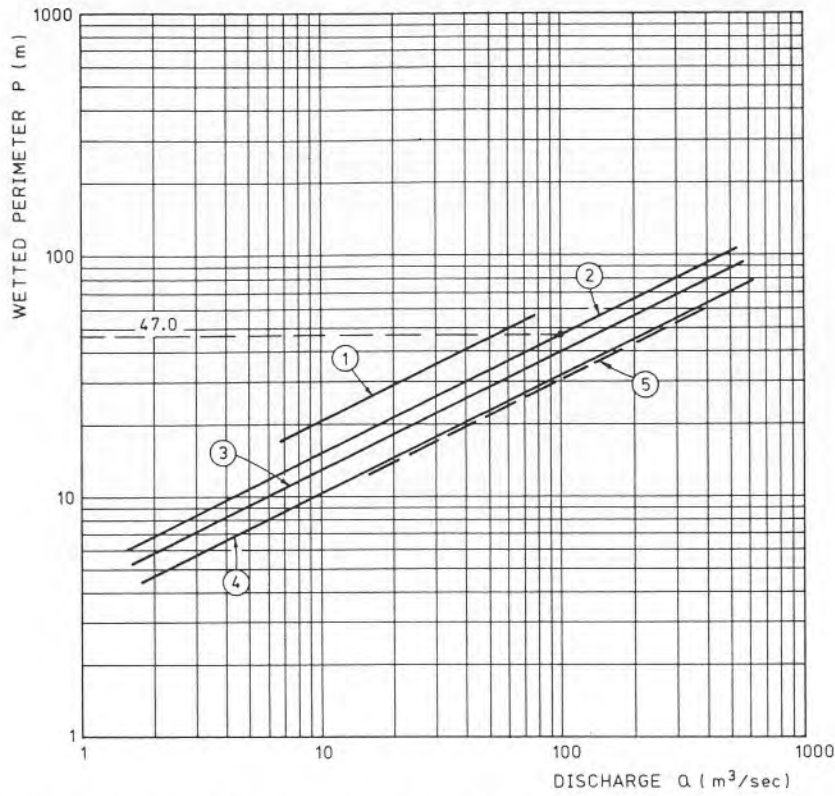


Fig. 4.3. Variation of wetted perimeter with discharge for regime channels, after [19]. (All experimental points have been omitted.)

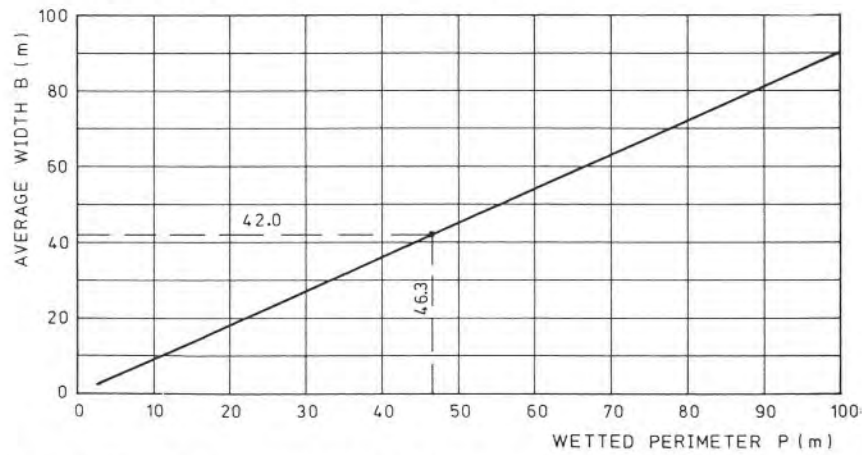


Fig. 4.4. Variation of average width with wetted perimeter for regime channels, after [19]. (All experimental points have been omitted.)

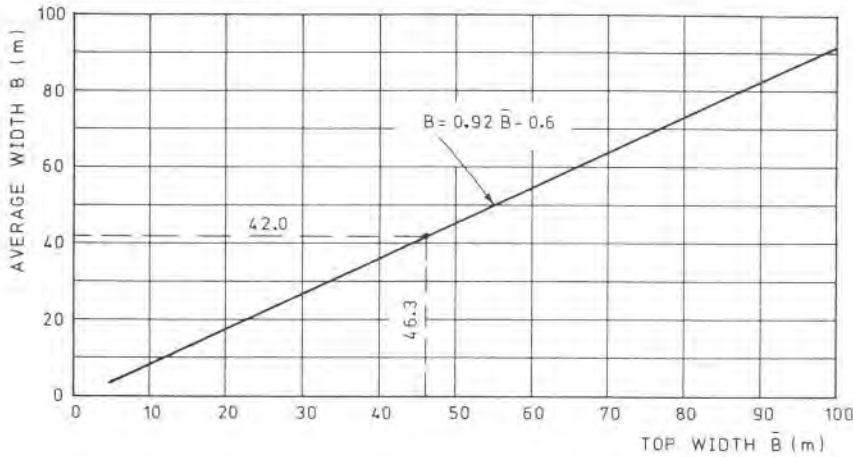


Fig. 4.5. Variation of top width \bar{B} with average width for regime channels, after [19]. (All experimental points have been omitted.)

is of type 2, from Fig. 4.3 the recommended wetted perimeter is obtained as $P = 47.0$ m.

Step 2 – From Figs. 4.4 and 4.5 the average width is obtained, $B = 42.0$ m, and the top width, $\bar{B} = 46.3$ m.

Step 3 – Using the diagram on Fig. 4.6, hydraulic radius can now be determined to be $R = 2.5$ m. The cross-sectional area and the mean velocity are computed next:

$$A = P \cdot R = 47.0 \times 2.5 = 117.5 \text{ m}^2, \quad \bar{V} = Q/A = 100/117.5 = 0.85 \text{ m/sec.}$$

Step 4 – In this step the mean depth is obtained from the diagram in Fig. 4.7, $D = 2.9$ m. From the data obtained so far, side slopes of the channel can now easily be estimated to be about $m = 1.5$. The general cross-section of the channel is by now fixed; small adjustments of the obtained values, particularly of B and \bar{B} , are possible at this stage, in order to secure suitable side slopes according to the available soil.

Step 5 – Average velocity \bar{V} , computed in Step 3 above, is now used in order to obtain from the diagram in Fig. 4.8 the value of the parameter $R^2 I = 5.4 \times 10^{-4}$. Inserting the known value of the hydraulic radius R , the longitudinal slope can be derived as $I_1 \cong 8.5 \times 10^{-5}$.

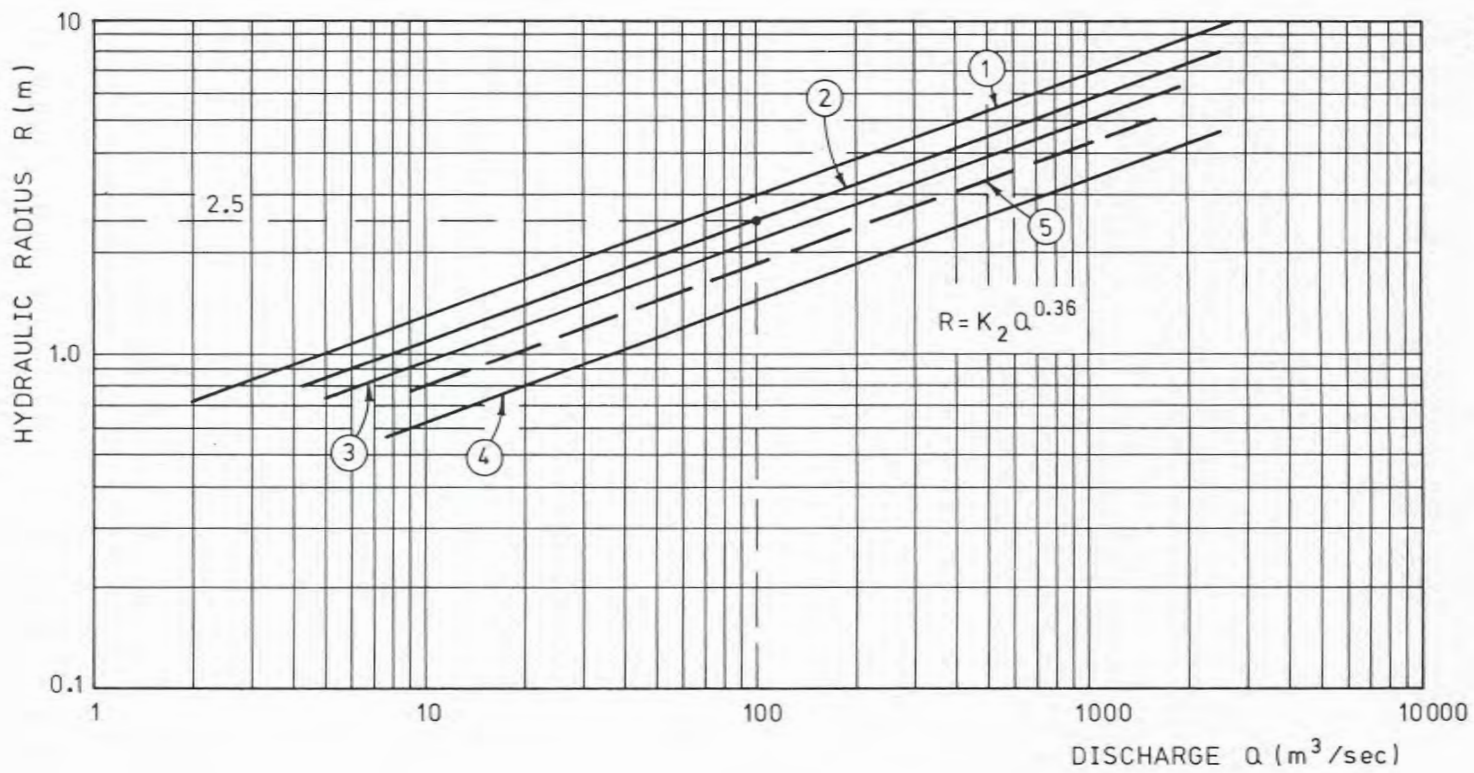


Fig. 4.6. Variation of hydraulic radius R with discharge for regime channels, after [19]. (All experimental points have been omitted.)

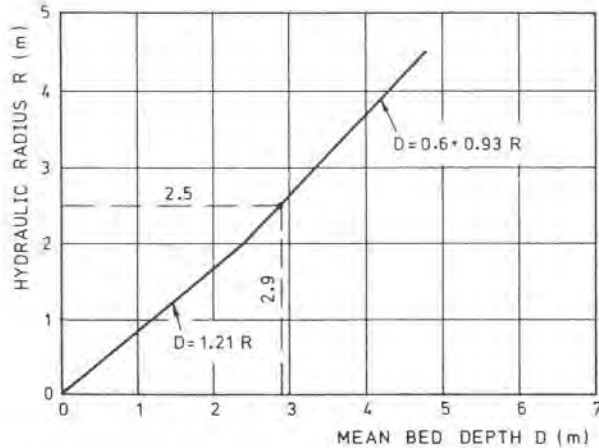


Fig. 4.7. Variation of mean bed depth with hydraulic radius for regime channels, after [19]. (All experimental points have been omitted.)

Step 6 – Using again the computed average velocity \bar{V} and the average width B , the parameter $VB/\nu = 35.7 \times 10^6$ can now be plotted on the diagram of Fig. 4.9, and the ordinate gives the value of $\bar{V}^2/gDI \cong 320$; from here an additional value for the longitudinal slope is obtained, $I_2 \cong 7.7 \times 10^{-5}$.

Step 7 – In order to obtain yet another estimate of the longitudinal slope, the mean grain size of the bed material must be either known or estimated. Making use of this information, the diagram on Fig. 4.10 yields the estimated value of the shear stress τ for the given type of channel.

If it is assumed that $d_{50} = 0.3$ mm, corresponding shear stress is found to be about $\tau = 1.8$ N/m². From this, the longitudinal slope can be computed, $I_3 = 7.2 \times 10^{-5}$. Because of relatively small angles that the characteristic curves on the graph make with the base line, values of I_3 are very susceptible to estimated values of d_{50} , unless the average line only is used. Hence for small changes in d_{50} , considerable differences of I_3 will necessarily follow. It is, therefore, obvious that the estimated d_{50} should be based on a careful and realistic field survey, if any significant I_3 value is to be gained from the present step. The use of the average line for extreme values of d_{50} is likely to give unrealistic values for I_3 .

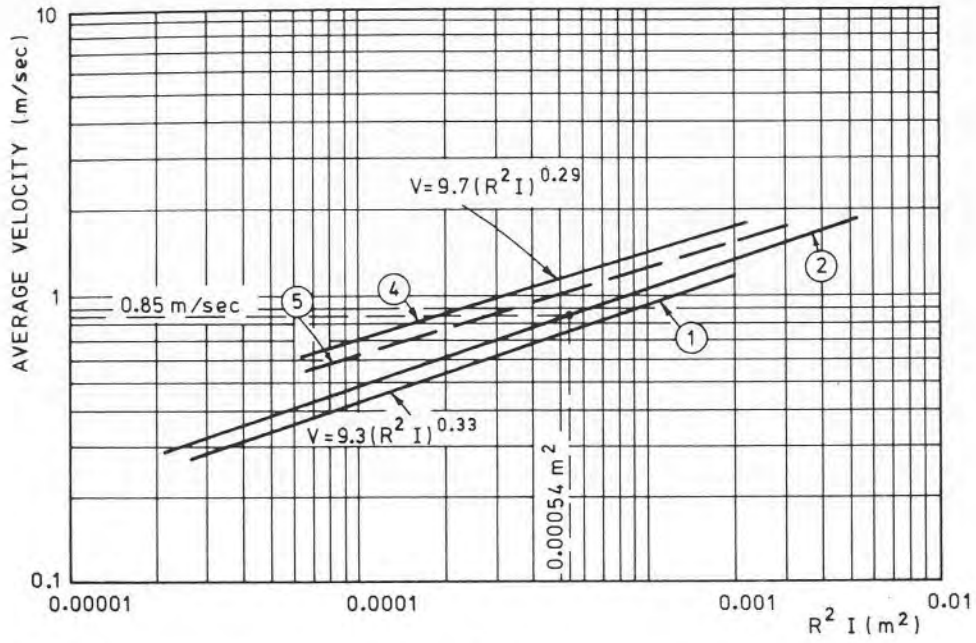


Fig. 4.8. Variation of average velocity with $R^2 I$ for regime channels, after [19].
(All experimental points have been omitted.)

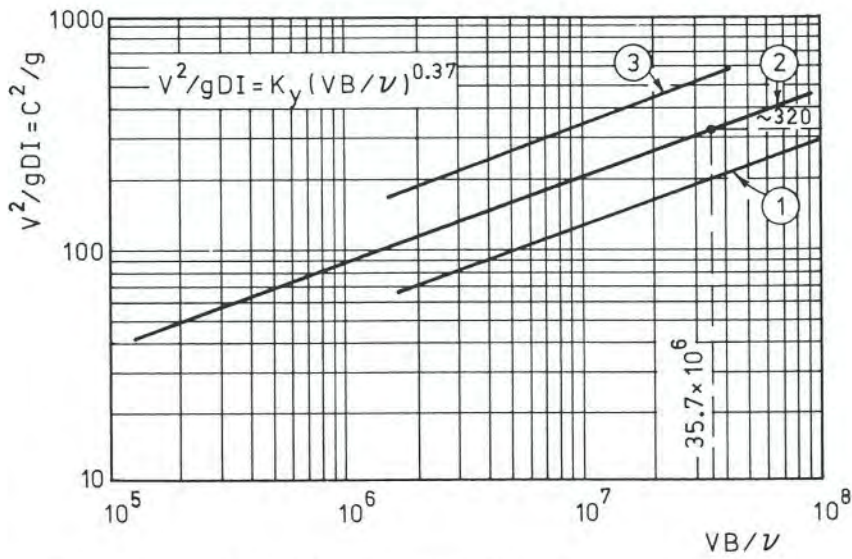


Fig. 4.9. Variation of (V^2/gDI) with (VB/v) for regime channels, after [19].
(All experimental points have been omitted.)

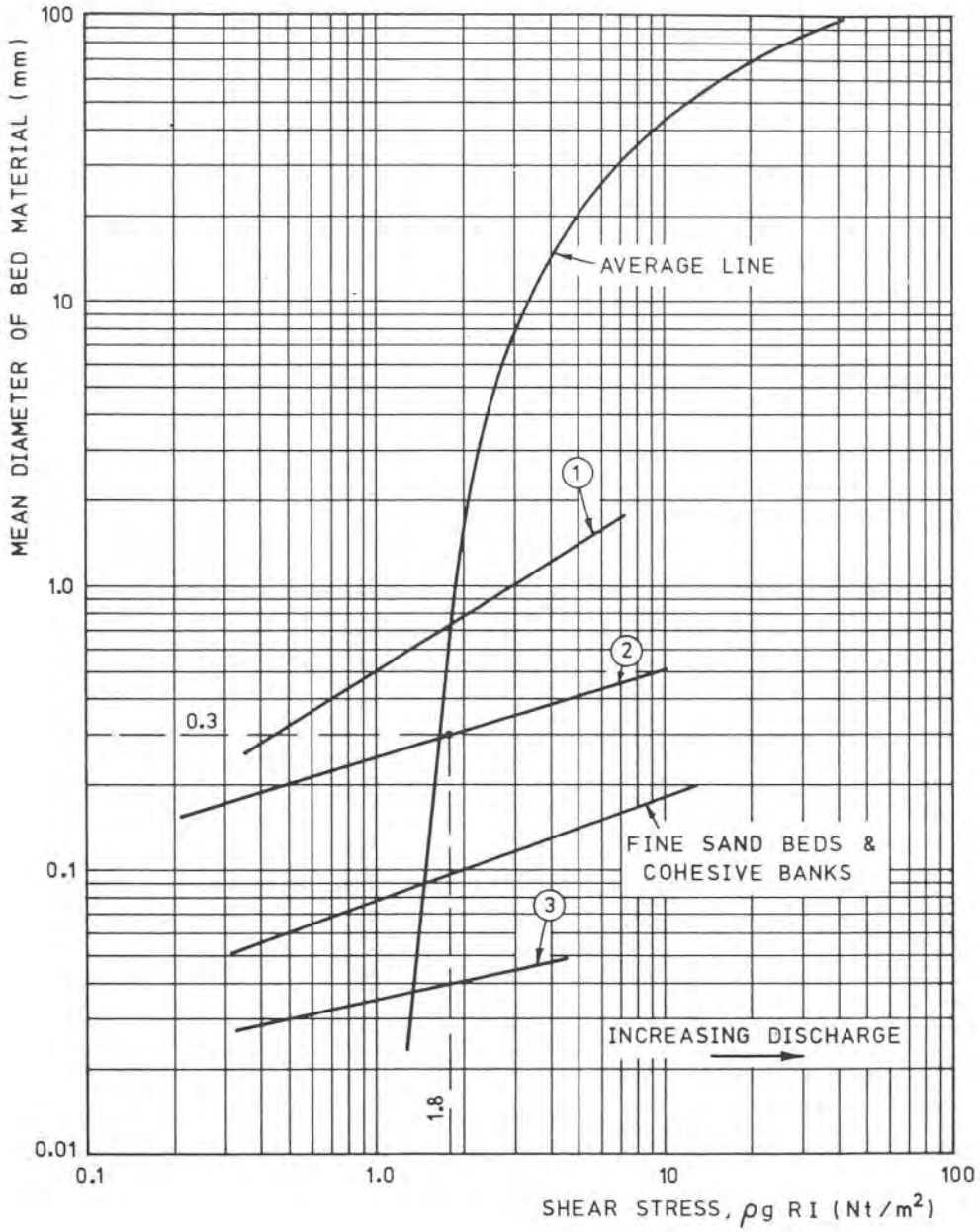


Fig. 4.10. Variation of shear stress with mean size of bed material for regime channels, after [19]. (All experimental points have been omitted.)

There are at this stage three estimated values of the longitudinal slope:

$$I_1 \cong 8.5 \times 10^{-5}$$

$$I_2 \cong 7.7 \times 10^{-5}$$

$$I_3 \cong 7.2 \times 10^{-5}$$

All the three estimates obtained give very small longitudinal slopes, and the differences between them also are small, not more than about 10–15%. The final choice of the slope will have to be based on the experience and judgement of the engineer.

Discussion of the Results

The three alternative longitudinal slopes obtained, all less than 0.1‰, seem to be rather small for the given discharge and the type of soil.

Using the data derived from the diagrams, and an average value for the longitudinal slope, Manning's roughness coefficient can be evaluated as

$$n = \frac{R^{2/3} J^{1/2}}{V} = \frac{2.5^{2/3} \cdot (8 \cdot 10^{-5})^{1/2}}{0.85} = 0.019$$

As could be expected, it is also rather small for a natural channel with sand bed and cohesive banks. A more acceptable value would be about, say, $n \cong 0.025$, for which the corresponding longitudinal slope from the Manning's formula would be about $I \cong 0.13\text{‰}$.

No indication bearing upon the longitudinal slope could be gained from the cross-sectional channel dimensions, since these are quite reasonable and acceptable for the given circumstances.

The shear stress as obtained from the diagram of Fig. 4.10 for $d_{50} = 0.3$ mm, $\tau \cong 1.8$ N/m², seems also to be below the commonly used values for sandy soils (see Vol. I, Chapter 3). A value as high as about $\tau = \sim 3$ N/m² would still be acceptable, and this again would give a larger longitudinal slope.

Finally, we can try to compare the results obtained to those which would be obtained from the general regime-theory by Blench, i.e. applying the given data to Eqs. (4.4)–(4.7).

$$Q = 100 \text{ m}^3/\text{sec}; F_b = 0.25 \text{ m}/\text{sec}^2; F_s = 0.02 \text{ m}^2/\text{sec}^3; \nu = 10^{-6} \text{ m}^2/\text{sec};$$

Small sediment concentration. Calculations give the following results:

$$B = 40 \text{ m}$$

$$D = 2.8 \text{ m}$$

$$V = 0.9 \text{ m/sec}$$

$$I \cong 1.0 \times 10^{-4} \cong 0.1\text{‰}$$

These results are very close to those obtained from the Simons and Albertson method, but for the longitudinal slope that is somewhat larger. In practice, most probably such a slope would be adopted, while generally retaining the rest of the results derived from the method.

References

1. E.S. Lindley, Regime channels, proceedings, Punjab Eng. Congr., 7 (1919).
2. G. Lacey, Stable channels in alluvium, Proc. Inst. of Civ. Eng., 229 (1929–30).
3. G. Lacey, A general theory of flow in alluvium, Proc. Inst. of Civ. Eng., 237 (1933–34).
4. C. Inglis, Divergence from regime in stable channels in alluvium, Central Irrigation & Hydrodyn. Res. Station, Poona, India, Annual Report, 1941–42.
5. T. Blench, Regime Behaviour of Canals and Rivers, Butterworths, London, 1957.
6. M.G. Wolman and L.B. Leopold, River flood plains: some observations on their formation, U.S. Geol. Survey, Prof. Paper no. 282-C, 1957.
7. M. Nixon, A study of the bank-full discharges of rivers in England and Wales, Proc. Inst. of Civ. Eng., 12 (1959).
8. F.M. Henderson, Open Channel Flow, Mcmillan, New York, N.Y., 1969.
9. T. Blench, Regime formulas for bed load transport, Proc., 6th Congr. IAHR, The Hague, 1955.
10. T. Blench, Mobile-bed fluviology, Dept. of Techn. Services, University of Alberta, Edmonton, 1965.
11. P. Ackers and F.G. Charlton, Dimensional analysis of alluvial channels with special references to meander length. AIRH Jour. of Hydr. Res., 8 (3) (1970).
12. J.F. Friedkin, A laboratory study of the meandering of alluvial rivers, U.S. Waterways Exp. Station, Vicksburg, Va., 1945.
13. M. Bordas, Contribution à l'étude des relations entre le débit generateur et les méandres d'une rivière. Thèse présentée à la Faculté des Sciences, Université de Toulouse, 1963.
14. M. Shahjahan, Factors controlling the geometry of fluvial meanders, Bull. Intern. Assoc. Scient. Hydrology, 1970.

15. S.A. Schumm, Meander wavelength of alluvial rivers, *Science*, 157 (1967).
16. J. Zeller, Meandering channels in Switzerland, Symposium on River Morphology, Bern, 1967.
17. L.B. Leopold and M.G. Wolman, River meanders, *Bull. Geol. Soc. of America*, 71 (1960).
18. L.P. Leopold and T. Maddock, The hydraulic geometry of stream channels and some physiographic implications, U.S. Geol. Survey, Prof. Paper 252, 1953.
19. D.B. Simons and M.L. Albertson, Uniform water conveyance channels in alluvial material, proceedings, ASCE, vol. 86 (HY5) (1960).
20. E.W. Lane, Progress report on studies on the design of stable channels, proceedings, ASCE, 79 (280) (1953).
21. H.W. Shen, *River Mechanics*, Fort Collins, Colorado, 1971.
22. R.J. Garde and K.G. Ranga Raju, *Mechanics of Sediment Transportation and Alluvial Stream Problems*, Wiley Eastern, New Delhi, 1977.
23. V.A. Vanoni et al., Lecture notes on sediment transportation and channel stability, California Inst. of Technol., report no. KH-R-1, 1961.
24. A.W. Peterson and T. Blench, Graphed equilibrium parameters of channels formed in sediment, *Canadian J. Civ. Eng.*, 7 (1) (1980).
25. G. Lacey and W. Pemberton, A general formula for uniform flow in self-formed alluvial channels, *Proc. Inst. Civ. Eng.*, 53 (2) (1972).

PART 2

CHAPTER 5

SUPPLEMENT TO THE HYDRAULICS OF ALLUVIAL CHANNELS

Symbols

A	– area, m^2 ; $1/\kappa$
B	– $-1/\kappa \ln m$
B'	– $-1/\kappa \ln \beta$
b	– width of the channel, m
C	– Chezy factor of flow resistance; constant of integration
C'	– Chezy factor for sediment-laden water
C_m	– average concentration of sediment by weight, N/m^3
g	– acceleration of gravity, m/sec^2
I	– longitudinal slope
J	– hydraulic gradient
K_s	– roughness height, m
l	– mixing length, m
m	– a dimensionless constant; side slope of trapezoidal channel
n	– Manning roughness coefficient
P	– wetted perimeter, m
Q	– flow discharge, m^3/sec
q	– specific discharge, $m^3/sec/m$
R	– hydraulic radius, m
u	– point velocity, m/sec
u_0	– velocity at the boundary between the laminar and turbulent layers, m/sec
u_*	– shear velocity, m/sec
\bar{V}	– mean velocity in a cross-section, m/sec
W	– settling velocity, m/sec
W_{35}	– settling velocity for d_{35} -size of sediment, m/sec

x	– Einstein correction factor; coordinate axis
y	– distance from the bed, m; coordinate axis
y_0	– distance within the sublayer for which $u = 0$
α	– a dimensionless factor
β	– a function
γ	– specific weight of water, N/m ³
δ	– thickness of the laminar sublayer, m
κ	– v. Karman constant
ν	– kinematic viscosity of water, m ² /sec
ρ	– density of water, kg/m ³
τ	– shear stress, N/m ²

5.1 Introduction

Although the hydraulic behavior of alluvial channels is known to be in many respects different from the behavior of rigid-boundary channels, there is to this day no theoretical set of equations applying specifically to the flow in movable-bed channels. In general, the accepted procedure is to use the kinematic and dynamic equations as developed for rigid-boundary channels, and to introduce empirical coefficients or relationships supposed to suitably modify them in order to better fit movable-bed conditions. This is certainly not a satisfactory solution, particularly from the point of view of drainage engineers, but it is the only feasible one with the present state of the art.

General principles of the open-channel hydraulics have been extensively treated in Volume I of the present manual, and will, therefore, not be discussed here. However, in order to gain a better theoretical background for the sediment transport mechanism in alluvial watercourses, to be discussed in the following pages, some additional aspects of the open-channel flow, with special bearing upon alluvial channels, will be briefly introduced first.

It can hardly be sufficiently stressed that the limitations and constraints of theoretical considerations, when applied to alluvial streams, should always be borne in mind by practising engineers, if a correct understanding of actual physical processes is to be reached. It has already been pointed out in the opening sentences of the present chapter that substantial differences exist between the rigid-boundary and movable-bed hydraulics, and at this point it may be of interest to mention some of them.

As soon as the flow has started, an alluvial channel begins to continuously adapt and change its deformable boundaries. Indeed, its characteristic roughness is determined not only by some mean grain size protruding into

the water, but usually by bed forms as well, or often even more by the latter factor than by the former. In the latter case of *form roughness*, the ratio between the roughness height (the effective height of the roughness elements, a measure of linear dimension designating their effect upon the flow) and depth of flow is generally several orders of magnitude larger than for fixed-bed channels.

Moving sediment elements and their continuous shifting of position are likely to induce additional shear stresses; progressive movement of bed forms, on the other hand, may cause disturbances in flow pattern due to changing water depth. Moreover, suspended sediment carried by the water, especially when in higher concentrations, often has also an influence upon the turbulence level of the flow.

Although the quantitative analysis and the extent of the mentioned and other influences due to the movable-bed conditions of alluvial channels largely elude our present knowledge, they should be carefully kept in mind whenever applying flow concepts developed for rigid-boundary conditions to flows in deformable conduits.

5.2 Velocity Distribution for Rigid-Boundary Channels

In the following, only velocity-distribution concepts for turbulent uniform flow will be briefly reviewed. Experimental evidence from which the constants used in the velocity-distribution equations have been obtained relates mainly to data on the flow in pipes. However, it is generally accepted that in spite of this fact, universal velocity-distribution equations thus arrived at may also be applied to turbulent flow in open channels.

In analogy with the kinematic theory of gases, Prandtl [1] assumed that a particle of fluid in turbulent flow is displaced at distance l , called mixing length, before its momentum is changed by the new environment. Hence, turbulent velocity fluctuation in both x - and y -directions is proportional to $l \cdot du/dy$. For further discussion of the theory, see [1, 2, 3], or any other text on Fluid Mechanics. From the above mixing-length theory, a useful expression can be derived for the turbulent shear stress. If furthermore it is assumed that near the boundary the mixing length, l , is proportional to the distance from the boundary, y , then

$$l = \kappa y \quad (5.1)$$

where κ denotes a dimensionless constant to be deduced from experiments; and if the shear velocity, u_* (see par. 3.2 of Part I), is introduced, Prandtl's differential equation for the turbulent shear stress can be integrated. The integration yields

$$u = \frac{u_*}{\kappa} \ln y + C \quad (5.2)$$

in which u denotes average point velocity at a distance y from the boundary (the averaging is related to turbulent fluctuations in time). C is a constant of integration which must be determined from the boundary conditions, requiring that close to the boundary the turbulent and the laminar velocity distributions must join each other. On the other hand, since within the laminar sublayer turbulent-flow conditions are no longer valid, the constant of integration may be adjusted to give a zero velocity at some distance y_0 within the sublayer (see Fig. 5.1). The distance y_0 is presumed chosen in such a way as to ensure a smooth blending of the profiles somewhere in the transition zone.

Hence, when $y = y_0$, $u = 0$, and the constant of integration is obtained $C = -(u_*/\kappa \ln y_0)$. Eq. (5.2) can, therefore, be written in the form

$$u = \frac{u_*}{\kappa} (\ln y - \ln y_0) \quad (5.3)$$

Order of magnitude of the laminar sublayer is about ν/u_* , ν denoting kinematic viscosity. Accordingly, $y_0 = m \nu/u_*$, in which m is a dimensionless constant. Eq. (5.3) can now be written in the dimensionless form

$$\frac{u}{u_*} = \frac{1}{\kappa} \left(\ln \frac{yu_*}{\nu} - \ln m \right) \quad (5.4)$$

Finally, denoting $A = 1/\kappa$ and $B = -1/\kappa \ln m$, the resulting logarithmic equation is

$$\frac{u}{u_*} = A \ln \frac{yu_*}{\nu} + B \quad (5.5)$$

Eq. (5.5) is generally known as the *Prandtl – von Karman universal velocity distribution law*, valid for all types of conduits.

Laboratory studies have shown that velocity distribution is to a great

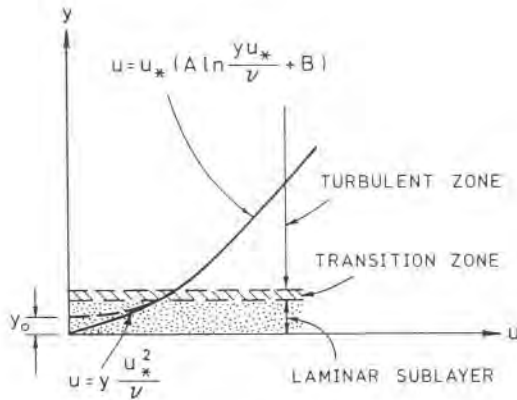


Fig. 5.1. Turbulent velocity distribution.

extent influenced by the roughness of the boundary. Consequently, distinct expressions are obtained for different ranges of roughness conditions.

For *hydraulically smooth boundaries*, Nikuradse's experiments [4] indicate the constants in Eq. (5.5) to be $A = 2.5$ and $B = 5.5$. This means that the constant κ in Eq. (5.1) is equal to 0.4. The numerical value of κ for a long time was thought to be universally constant for the turbulent flow, regardless of the boundary configuration or value of Reynolds number. It has later been argued, however, that the constant is not independent of the boundary configuration, and probably not of the Reynolds number either (see par. 5.4). Introducing the above constants leads to the expression

$$\frac{u}{u_*} = 2.5 \ln \frac{yu_*}{\nu} + 5.5 = 5.75 \log \frac{yu_*}{\nu} + 5.5 \cong 5.75 \log 9 \frac{yu_*}{\nu} \quad (5.6)$$

In order to derive a suitable expression of Eq. (5.3) for *hydraulically rough boundaries*, we have to introduce the *roughness height*, K_s , having the dimension of length, Fig. 5.2.

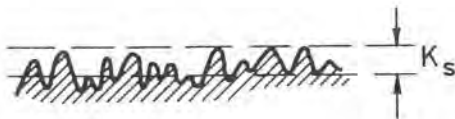


Fig. 5.2. Definition of the "roughness height" K_s .

Starting from Eq. (5.3) again and applying dimensional analysis, a similar reasoning as adopted for the smooth-boundary conditions leads to the conclusion that $y_0 = \beta \nu / u_*$, in which $\beta = f(K_s u_* / \nu)$. Introducing as previously the constants $A = 1/\kappa$ and $B' = -1/\kappa \ln \beta$, Eq. (5.5) is obtained.

From Nikuradse's experiments it can be deduced that as long as $K_s u_* / \nu \leq 3.6 \sim 5$, B' is independent of the function f above, i.e. $\beta = m$, and it has a constant value of 5.5. This conclusion means that as long as the thickness of the laminar sublayer is sufficient to completely cover the roughness height K_s , Eq. (5.6) will be valid also for rough boundaries.

When, on the other hand, $K_s u_* / \nu \geq \sim 70$, Nikuradse's experiments indicate that

$$B' = 8.5 - 2.5 \ln \frac{K_s u_*}{\nu} \quad (5.7)$$

Hence, using again Eq. (5.5),

$$\frac{u}{u_*} = 2.5 \ln \frac{y u_*}{\nu} + 8.5 - 2.5 \ln \frac{K_s u_*}{\nu} \quad (5.8)$$

or finally

$$\frac{u}{u_*} = 5.75 \log \frac{y}{K_s} + 8.5 \cong 5.75 \log 30 \frac{y}{K_s} \quad (5.9)$$

This is the velocity-distribution equation for flow over rough boundaries.

For the *transition zone* between the smooth and completely rough rigid boundaries ($\sim 5 < K_s u_* / \nu \leq \sim 70$), velocity-distribution equation is found also to be of the general form

$$\frac{u}{u_*} = 5.75 \log \frac{y}{K_s} + B' \quad (5.10)$$

Here B' has not a constant value, but is according to Nikuradse a function of the dimensionless parameter $K_s u_* / \nu$. Subsequent investigations have shown, however, that the transition curve obtained by Nikuradse for uniform-grain distribution does not hold for non-uniform roughness conditions generally encountered in engineering practice. Indeed, transition curve giving B' values for non-uniform roughness seems to be much more gradual.

A more simplified approach regarding velocity distribution for flow over

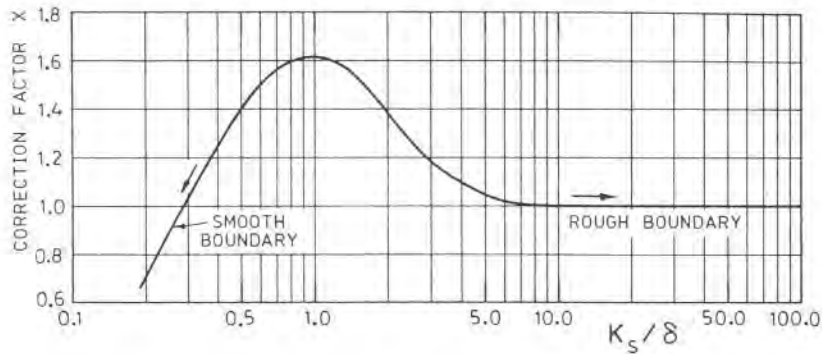


Fig. 5.3. Correction factor x in the logarithmic velocity-distribution Eq. (5.11).

rigid boundaries was later proposed by H.A. Einstein [5]. It is supposedly valid for all three boundary conditions (hydraulically smooth, rough or in transition region), and is given by

$$\frac{u}{u_*} = 5.75 \log \left(30.2 \frac{y}{K_s} x \right) \quad (5.11)$$

Roughness height K_s denotes here $d_{s_{65}}$, i.e. grain diameter determined so that 65% are equal to it or smaller, and x is a correction factor which depends on the ratio K_s/δ , where δ stands for the thickness of the laminar sublayer, Fig. 5.3.

By integrating Eq. (5.11) over the vertical section, Einstein [5], following previous Keulegan's [6] deductions, has proposed expressions for the average velocity in turbulent flow,

Smooth boundary:

$$\frac{\bar{V}}{u_*} = 5.75 \log \left[3.67 \frac{Ru_*}{\nu} \right]$$

Rough boundary and transition

$$\frac{\bar{V}}{u_*} = 5.75 \log \left[12.27 \frac{R}{K_s} x \right] \quad (5.12)$$

where R denotes the hydraulic radius.

Example 5.1

Given a trapezoidal channel with non-deformable bed, bottom width $b = 40$ m, side slopes $m = 2$, mean depth $d = 2.0$ m and longitudinal slope $I = 0.2\%$. The flow is supposed to be uniform, or very nearly so, and fully turbulent ($Re > 10^6$). Ratio $b/d = 20$, hence in the middle of the stream the effect of the side walls may be neglected.

Required: a) find the theoretical velocity distributions for the following boundary-roughness conditions: 1) Smooth boundary; 2) Rough boundary; 3) Transition zone, and b) average velocities for the three roughness conditions.

Solution:

Area of the flow section – $A = 2.0 (40 + 2 \times 2.0) = 88 \text{ m}^2$.

Wetted perimeter – $P = 40 + 2 \times 2.0 (5)^{1/2} = 49 \text{ m}$.

Hydraulic radius – $R = A/P = 1.8 \text{ m}$.

Shear stress at the bottom – $\tau = \gamma R I \cong 10^3 \cdot 9.8 \cdot 1.8 \cdot 0.0002 = 3.5 \text{ N/m}^2$.

(the flow is assumed to be uniform)

Shear velocity according to Eq. (3.2) –

$$u_* = (gRI)^{1/2} = (9.8 \cdot 1.8 \times 0.0002)^{1/2} \cong 0.059 \text{ m/sec}$$

Estimated thickness of the laminar sublayer δ (see Eq. (5.15)),

$$\delta \cong 11.6 \nu / u_* = 11.6 (10^{-6} / 0.06) \cong 0.0002 \text{ m}$$

Here ν denotes the kinematic viscosity of the water, taken as $10^{-6} \text{ m}^2/\text{sec}$.

Smooth boundary, Eq. (5.6)

$$\frac{u}{u_*} = 5.75 \log \frac{yu_*}{\nu} + 5.5$$

or

$$u = 0.059 \left[5.75 \log \frac{0.059y}{10^{-6}} + 5.5 \right]$$

Results of the computations are summarized in Table 5.1.

Rough boundary, Eq. (5.9)

$$\frac{u}{u_*} = 5.75 \log \frac{y}{K_s} + 8.5$$

or

$$u = 0.059 \left[5.75 \log \frac{y}{K_s} + 8.5 \right]$$

If the roughness height is assumed to be $K_s = 3$ mm, then

$$\frac{K_s u_*}{\nu} = \frac{0.003 \times 0.059}{10^{-6}} \cong 177 > \sim 70$$

Being much larger than about 70, the boundary conditions are definitely rough. Results of the computations are given in Table 5.1.

TABLE 5.1. COMPUTED VALUES (Ex. 5.1)

y (m)	Smooth bound u (m/sec)	Rough bound u (m/sec)	Transition u (m/sec)
2.0	2.04	1.46	1.75
1.5	2.00	1.42	1.71
1.0	1.94	1.36	1.65
0.5	1.84	1.25	1.55
0.2	1.70	1.12	1.41
0.1	1.60	1.02	1.31
0.05	1.50	0.92	1.21

Transition, Eq. (5.11)

Roughness height is assumed to be $K_s = 0.5$ mm, hence

$$\frac{K_s u_*}{\nu} = \frac{0.0005 \times 0.059}{10^{-6}} \cong 29 > \sim 5,$$

the roughness is in the transition state. Velocity-distribution equation is given by

$$\frac{u}{u_*} = 5.75 \log \left[30.2 \frac{y}{K_s} x \right]$$

or

$$u = 0.059 \left[5.75 \log \left[30.2 \frac{y}{0.0005} x \right] \right]$$

$$\text{Parameter } \frac{K_s}{\delta} = \frac{0.0005}{0.0002} = 2.5$$

Here the thickness of the laminar sublayer δ for the transition was assumed to be approximately equal to that previously obtained for the smooth boundary. This is certainly not entirely correct, but is a fairly good approximation for comparison purposes (see par. 5.3). From Fig. 5.3, the correction factor is found to be $x = 1.22$. Results of the computations are shown in Table 5.1.

The three calculated velocity-distribution curves are graphically represented in Fig. 5.4.

Average velocity, Eq. (5.12)

$$\frac{\bar{V}}{u_*} = 5.75 \log \left[12.27 \frac{R}{K_s} x \right]$$

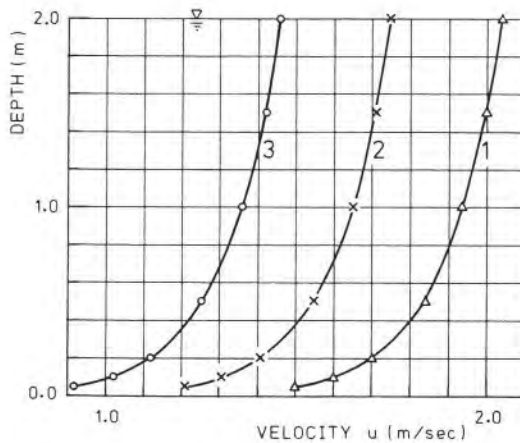


Fig. 5.4. Velocity-distribution curves for Example 5.1. 1 – smooth boundary; 2 – transition boundary; 3 – rough boundary.

or

$$\bar{V} = 0.059 \times \left[5.75 \log \left[12.27 \frac{1.8}{K_s} x \right] \right]$$

Smooth boundary

$$\bar{V} = u_* \times 5.75 \log \left[3.67 \frac{Ru_*}{\nu} \right]$$

$$\bar{V} = 0.059 \times 5.75 \log \left[3.67 \frac{1.8 \times 0.059}{10^{-6}} \right]$$

which gives $\bar{V} \cong 1.89$ m/sec.

Rough boundary

$$\frac{K_s}{\delta} = \frac{0.003}{0.0002} = 15; \quad x = 1.0$$

hence,

$$\bar{V} = 0.059 \times 5.75 \log \left[12.27 \frac{1.8}{0.003} \times 1.0 \right]; \quad \bar{V} \cong 1.31 \text{ m/sec}$$

Approximate evaluation of the average velocity from the velocity-distribution curve, Fig. 5.4, assuming straight lines between the calculated point velocities given in Table 5.1, yields the results as shown in Table 5.2.

$$\bar{V} \cong \frac{2.6}{2.0} = 1.3 \text{ m/sec}$$

It is practically identical to the average velocity computed from Eq. (5.12).

Transition

From previous computations, $x = 1.22$, and hence $\bar{V} = 0.059 \times 5.75 \log (12.27 \times 1.8/0.0005 \times 1.22)$ which yields $\bar{V} \cong 1.61$ m/sec.

TABLE 5.2. COMPUTED VALUES (Ex. 5.1)

y (m)	Δy (m)	u (m/sec)	\bar{u} (m/sec)	$\Delta y \times \bar{u}$
2.0		1.46		
1.5	0.5	1.42	1.44	0.72
1.0	0.5	1.36	1.39	0.70
0.5	0.5	1.25	1.30	0.65
0.2	0.3	1.12	1.19	0.36
0.1	0.1	1.02	1.07	0.11
0.05	0.05	0.92	0.97	0.05
0	0.03	0	0.46	0.01
				Σ 2.60

Example 5.2

Using Eq. (5.12), giving average velocity for rough boundaries, try to find an approximate correlation between the Manning's roughness coefficient n and roughness height K_s , for large channels (negligible effect of side boundaries) and completely rough boundary.

Eq. (5.12) can also be written in the following form:

$$\bar{V} = 18 (RJ)^{1/2} \log \left[12.27 \frac{R}{K_s} \right]$$

Setting it equal to the Manning's equation, $\bar{V} = 18 (RJ)^{1/2} \log (12.27 R/K_s) = 1/n R^{2/3} J^{1/2}$, and from here,

$$n = \frac{R^{1/6}}{18 \log (12.27 R/K_s)} \quad (5.12a)$$

The results of the calculations are summarized in Table 5.3 and Fig. 5.5.

Roughness coefficients n obtained from this very approximate method should be applied only to broad channels with non-cohesive bed material. However, it may sometime be of aid to practising engineers in the choice of the roughness coefficient.

TABLE 5.3. COMPUTED VALUES (Ex. 5.2)

$R(m)$ $K_s(mm)$	0.5	1.0	2.0	3.0	4.0	5.0	6.0	7.0	7.0	9.0	10.0
0.05	0.0098	0.0104	0.0111	0.0114	0.0118	0.0121	0.0123	0.0125	0.0126	0.0128	0.0129
0.1	0.0105	0.0110	0.0117	0.0121	0.0124	0.0127	0.0129	0.0131	0.0133	0.0134	0.0135
0.5	0.0123	0.0128	0.0134	0.0138	0.0142	0.0144	0.0146	0.0149	0.0150	0.0151	0.0153
1.0	0.0132	0.0137	0.0143	0.0148	0.0151	0.0153	0.0155	0.0158	0.0159	0.0161	0.0162
5.0	0.0162	0.0166	0.0170	0.0174	0.0177	0.0179	0.0181	0.0184	0.0185	0.0187	0.0188
10.0	0.0180	0.0182	0.0186	0.0189	0.0192	0.0194	0.0196	0.0197	0.0199	0.0200	0.0202
50.0	0.0240	0.0234	0.0234	0.0235	0.0236	0.0238	0.0240	0.0240	0.0241	0.0242	0.0243
100.0	0.0280	0.0269	0.0264	0.0263	0.0263	0.0263	0.0264	0.0265	0.0265	0.0266	0.0267

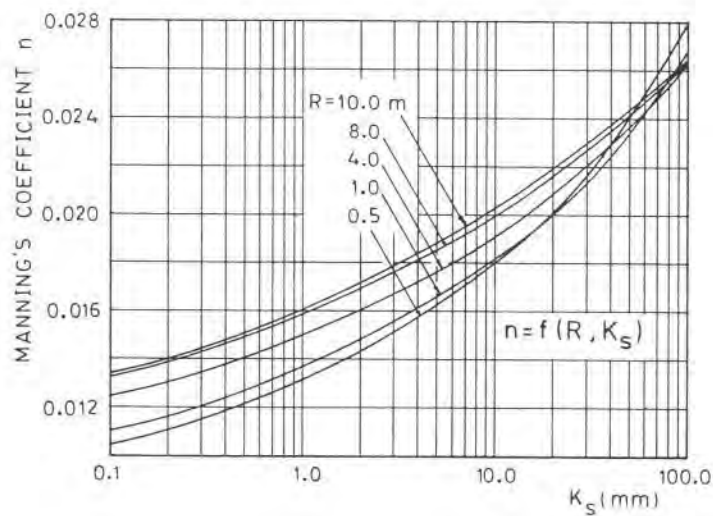


Fig. 5.5. Manning's n as approximate $f(R, K_s)$.

5.3 Thickness of the Laminar Sublayer

Theoretical classification of boundary roughness is largely dependent on the relation between roughness protrusions and the thickness of the laminar sublayer.

As already mentioned, large volume of experimental study has shown that the three roughness regimes can best be distinguished in relation to a dimensionless parameter $K_s u_* / \nu$, also called Reynolds number related to grain size. Summarizing,

$$\text{Smooth boundary} - \frac{K_s u_*}{\nu} \leq 3.6 \sim 5$$

$$\text{Rough boundary} - \frac{K_s u_*}{\nu} > \sim 70$$

$$\text{Transition} - 3.6 \sim 5 < \frac{K_s u_*}{\nu} \leq \sim 70$$

In order to obtain the thickness of the laminar sublayer, it is assumed that at the boundary between the laminar and turbulent layer, the shear stress of the laminar flow, $\tau = \mu (du/dy)$, is equal to that of the turbulent flow. Hence

$$\mu \frac{du}{dy} = \rho u_*^2 \quad (5.13)$$

Let us next denote the velocity at the boundary between the two layers as u_0 ; then du/dy may be approximately written as u_0/δ , where δ is the thickness of the sublayer. If the velocity-distribution curve within the thin laminar sublayer is represented by a straight line, then it is possible to write

$$\frac{u}{u_0} = \frac{y}{\delta} \quad (5.14)$$

Experiments have shown that the thickness δ is related to a constant value of the dimensionless parameter $u_0 \delta / \nu = \text{const.}$, and the numerical value of the constant has been found to be about 135 [7]. Since within the sublayer $\tau = \mu (du/dy) \cong \mu (u_0/\delta)$, it follows that $u_0 = \tau (\delta/\mu)$; substituting this into the former expression for the constant parameter, it can be deduced that $\tau \cdot \delta^2 / \rho \cdot \nu^2 = 135$, whence $(u_* \cdot \delta / \nu) = (135)^{1/2} = 11.6$. Finally from this:

$$\delta = 11.6 \frac{\nu}{u_*} \quad (5.15)$$

In order to compare the thickness of the sublayer with the height of a roughness element, let us write Eq. (5.15) in a different form,

$$\frac{K_s}{\delta} = \frac{1}{11.6} \frac{K_s u_*}{\nu} \quad (5.16)$$

If now for smooth boundary $K_s u_* / \nu \leq 3.6 \sim 5$, it follows that

$$\frac{K_s}{\delta} = \frac{1}{11.6} (3.6 \sim 5) = \frac{1}{3.2} \sim \frac{1}{2.3} \quad (5.17)$$

For completely rough boundary, the parameter $K_s u_* / \nu \geq \sim 70$. Hence similarly,

$$\frac{K_s}{\delta} = \frac{1}{11.6} 70 \cong 6 \quad (5.18)$$

In the transition region the ratio K_s / δ must be between the limits given by Eqs. (5.17) and (5.18).

From the above approximate comparisons it can be concluded that for smooth boundaries the thickness of the laminar sublayer is not less than about three times the roughness height K_s . For rough boundaries, the thickness is not more than about one sixth of the roughness height.

5.4 Effect on Velocity-Distribution of the Movable Boundary in Alluvial Channels

All the theoretical velocity-distribution equations discussed in the preceding paragraphs presuppose clear water and rigid boundaries. These conditions can but very exceptionally be met with in sediment-laden alluvial watercourses. Not only are sediment particles carried along in suspension, thus changing probably some of the basic parameters of the turbulent flow; the situation is further complicated by the fact that movable and ever-changing bed forms are also likely to have influence upon the velocity-distribution structure of the stream.

A logical analysis of the dynamic equilibrium conditions in the turbulent flow leads to the conclusion that the energy spent on the entrainment of sediment particles by the water should somehow damp the turbulent momentum-transfer mechanism, and hence the random velocity fluctuations, as compared to the clear water. Following this reasoning, one is likely to conclude that sediment particles should lag behind the water particles, and that their turbulent *mixing length* should be shorter on the average. It implies as well that the von Karman universal constant for turbulent flow κ , so far assumed to be 0.4, would be reduced.

Laboratory experiments reported by the ASCE Task Committee [8] show a reduction of the constant κ as large as about 50% for a suspended sediment concentration of 15,800 ppm, see Fig. 5.6. The diagram clearly shows that for the same depth, slope and bed surface, velocity for sediment-laden stream is greater than for the clear water. Taking into account Eq. (5.2), this implies that the constant κ must be smaller.

However, these and more recent experiments have not been conclusive, since they also have shown that this reduction of flow resistance can be more than offset by the increase in resistance caused by bed formations. This fact may well explain many field observations which tend to indicate that sediment-laden water brings about more resistance to flow, and not less as suggested by carefully executed experiments.

While experiments by Vanoni et al. [9, 10], suggest that for clear water the value of the constant κ always tends to be close to 0.4, whatever the bed

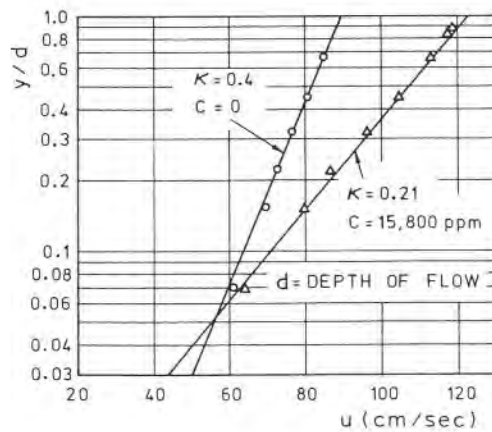


Fig. 5.6. Comparison of the velocity profiles for clear water and suspended sediment, after ASCE Task Committee [8]; $d = 9$ cm, $d_s = 0.1$ mm, $I = 0.0025$.

formation, some later experiments, cited by the Task Committee, seem to indicate that the bed formations may reduce κ -values even for clear water flows. Some field observations have also hinted that the sediment-transfer coefficient may in some cases be greater than the momentum-transfer coefficient for water particles.

Einstein et al. have tried several times to experimentally determine the variation of the von Karman coefficient κ in dependence of characteristic sediment parameters [11, 12], and subsequently to derive an equation for the velocity distribution in alluvial streams. These equations have been unduly complicated for engineering applications. Adopting the view that there should exist an average value of κ for both the velocity and the suspended-load distributions down to a point close to the bed, Einstein and Abdel-Aal [13] finally proposed an experimental correlation curve between the coefficient κ and sediment parameters, see Fig. 5.7. Here W_{35} denotes the settling velocity for d_{s35} – size of sediment (35% by mass smaller than the given size); d_{s65} – grain size for which 65% by mass of all grains are smaller; q – specific discharge (discharge per unit of width); J – hydraulic gradient.

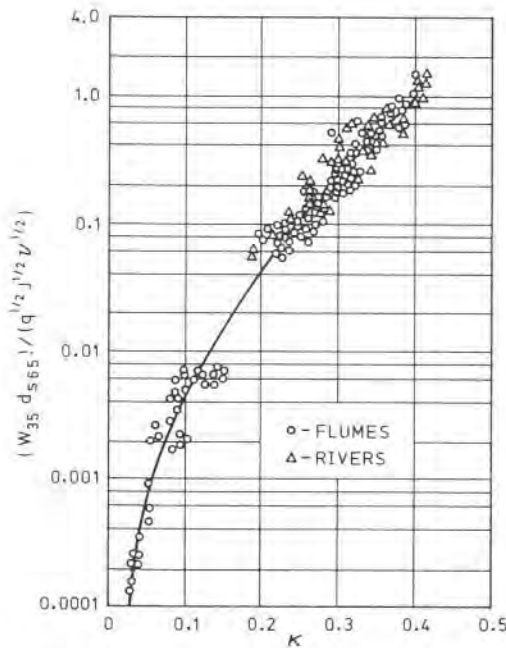


Fig. 5.7. Coefficient κ as function of dimensionless sediment parameter $(W_{35} d_{s65}) / (q^{1/2} J^{1/2} \nu^{1/2})$, after [13].

They further put forward a set of relatively simple equations for the vertical velocity distribution and for the average velocity. It was claimed that good agreement had been found between experimental values from both laboratory and field measurements, and values predicted by the equations.

Equation proposed for the vertical velocity distribution is similar to Eq. (5.11), and it reads:

$$\frac{u}{u_*} = \frac{2.3}{\kappa} \log \left[30.2 \frac{y}{K_s} \cdot x \right] \quad (5.19)$$

Here x denotes the correction factor to be taken from the diagram on Fig. 5.3. Average velocity is expressed in a similar manner,

$$\frac{\bar{V}}{u_*} = \frac{2.3}{\kappa} \log \left[30.2 \frac{d}{K_s} \cdot x \right] \quad (5.20)$$

where d denotes the depth of water.

However, it should again be emphasized that the question whether the coefficient κ is indeed lower for sediment-carrying water than for clear water is far from being settled. Recently it has again been argued [19] that κ is essentially constant over a range of conditions for flows of clear water as well as flows with full load of suspended sediment. The claim is based on the reevaluation of the early data together with some new data in the light of the currently accepted forms of the velocity-defect law that contain so-called wake-flow terms, in addition to the original Prandtl-Karman terms. The analysis would show that the existence of these additional terms clearly points to the need for evaluating κ from straight-line fits to experimental velocity profiles in the lower 15% of the flow, i.e. in the region where the wake-flow terms are negligible, and not out in the more central regions of the flow as done previously.

Recently experiments have been carried out to determine the influence of sediment concentration on the "roughness coefficient" for use in the open-channel flow equations. Zagustin [14] has summarized the results of his laboratory experiments in a diagram giving Chezy coefficient for sediment-laden water C' vs. the coefficient for clear water under the same flow conditions (for definition of the Chezy coefficient see Vol. I of this Manual, Chap. 2). Since the movable bed in the channel was kept flat during all the experiments, it is claimed that the results reflect only the effect of the sediment concentration (Fig. 5.8)

A family of curves is given as function of a dimensionless factor $\alpha =$

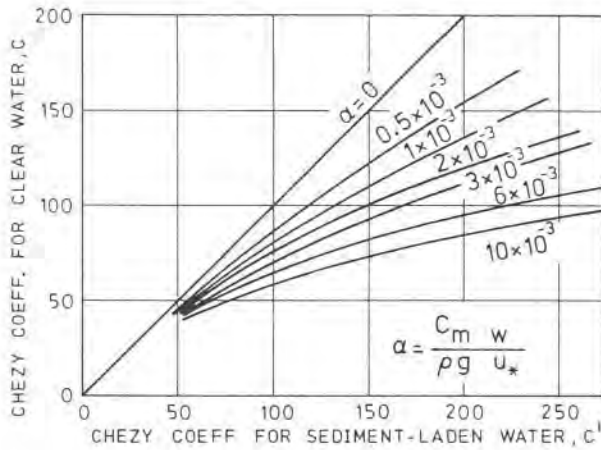


Fig. 5.8. Chezy coefficient for sediment-laden water vs. Chezy coefficient for clear water, after [14].

$(C_m \cdot W/\gamma u_*)$, in which C_m is the average concentration by weight, W is the settling velocity of sediment particles (see par. 6.2.4), γ is the specific weight of water, and u_* is shear velocity. Manning roughness coefficient n is related to Chezy coefficient by $n = R^{1/6}/C$, where R denotes the hydraulic radius.

Example 5.3

The data as in Example 5.1. In addition it is assumed that $K_s = 0.3 \text{ mm} \approx d_{s35}$; $d_{s65} \approx 1 \text{ mm}$.

Required: To find how the vertical velocity distribution for the given alluvial channel is likely to be affected because of suspended sediment transport.

Solution:

For $d_{s35} = 0.3 \text{ mm}$, the settling velocity in still water is estimated to be $W_{35} \approx 0.05 \text{ m/sec}$ (see Chap. 6).

Using Manning formula, discharge can be estimated, $Q = KI^{1/2}$; $K = A/n R^{2/3}$. Roughness coefficient n can be estimated from Table 5.3 for $K_s = 0.3 \text{ mm}$; the corresponding value for hydraulic radius $R = 1.8 \text{ m}$ is $n \approx 0.0126$. Hence,

$$Q = \frac{88}{0.0126} 1.8^{2/3} 0.0002^{1/2} = \sim 146 \text{ m}^3/\text{sec}$$

Specific discharge,

$$q = \frac{Q}{b} = \frac{146}{40} = \sim 3.6 \text{ m}^2/\text{sec}$$

The dimensionless sediment parameter for obtaining the coefficient κ from the diagram on Fig. 5.7 is computed next,

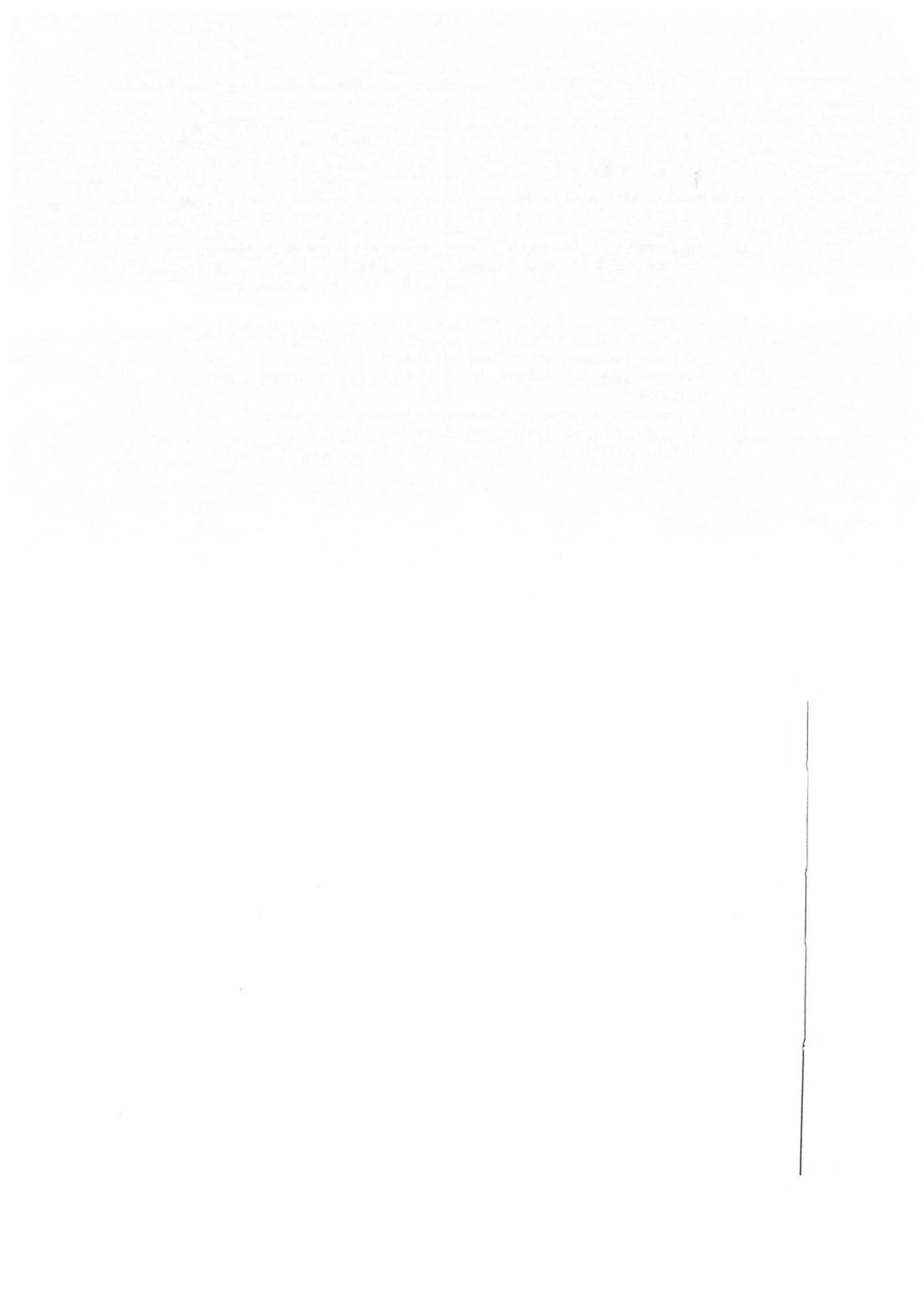
$$\frac{W_{35} d_{s65}}{q^{1/2} I^{1/2} \nu^{1/2}} = \frac{0.05 \times 0.001}{3.6^{1/2} \times 0.0002^{1/2} \times (10^{-6})^{1/2}} = \sim 1.9$$

Coefficient κ should, therefore, remain unaffected under the given conditions, and the velocity distribution as given by curve 3 in Fig. 5.4 can be accepted as valid.

References

1. L. Prandtl, *Fuehrer durch die Stroemungslehre*, Vielweg, Braunschweig, 1965.
2. H. Schlichting, *Grenzschicht-Theorie*, Verlag G. Braun, Karlsruhe, 1965.
3. V.L. Streeter, *Handbook of Fluid Dynamics*, McGraw-Hill, New York, N.Y., 1961.
4. J. Nikuradse, *Stroemungsgesetze in rauhen Rohren*, VDI-Forschungsheft, No. 361, 1933.
5. H.A. Einstein, *The bed-load function for sediment transportation in open channels*, U.S. Dept. of Agriculture, Soil Consv. Service, Technical bulletin no. 1026, 1950.
6. G.H. Keulegan, *Laws of turbulent flow in open channels*, Nat. Bureau of Standards, Jour. of Res., 21 (1938).
7. H. Rouse, *Engineering Hydraulics*, Wiley, New York, N.Y., 1960.
8. ASCE Task Committee, *Sediment transportation mechanics: suspension of sediment*, proceedings, ASCE, 89 (HY5) (1963).
9. V.A. Vanoni, *Some effects of suspended sediment on flow characteristics*, proceedings, 5th Hydr. Conf., State University of Iowa, Studies in Eng., Bulletin no. 34, 1953.
10. V.A. Vanoni and N.H. Brooks, *Laboratory studies on the roughness and suspended load of alluvial streams*, Sed. Lab., California Inst. of Technol., Report no. E-68, 1957.
11. H.A. Einstein et al., *Second approximation to the solution of suspended-load theory*, University of California, Inst. of Res., report no. 3, 1954.

12. H.A. Einstein et al., Transport of sediment mixtures with long range of grain size, University of Missouri, Div. of Sediment Sizes, no. 2, 1955.
13. H.A. Einstein and Abdel-Aal, Einstein bed load function at high sediment rates, proceedings, ASCE, 98 (HY1) (1972).
14. K. Zagustin, Variación del coeficiente de rugosidad en canales con el grado de suspensión de sedimento, IV Congr. Latinoamericano de Hidr., 1970.
15. Y.O. Hinze, Turbulence, McGraw-Hill, New York, N.Y., 1975.
16. S. Yalin, On the average velocity of flow over a movable bed, La Houille Blanche, no. 1, 1964.
17. A.J. Raudkivi, Loose Boundary Hydraulics, Pergamon Press, London, 1967.
18. I.H. Shames, Mechanics of Fluids, McGraw-Hill, New York, N.Y., 1962.
19. N.L. Coleman, Velocity profiles with suspended sediment, Jour. Hydr. Res., 19 (3) (1981).



CHAPTER 6

SEDIMENT PROPERTIES

Symbols

A	– area, m^2
a	– longest axis of the particle, m
b	– intermediate axis of the particle, m
C	– Chezy factor of flow resistance; sediment concentration, ppm or kg/m^3
C'	– increased Chezy factor due to sediment
C_m	– average sediment concentration in water, ppm or kg/m^3
C_D	– drag coefficient
c	– shortest of the three mutually perpendicular axes
d	– flow depth, m
d_s	– particle diameter, m or mm
d_{s90}	– particle diameter for which 90% is finer
d_{s75}	– particle diameter for which 75% is finer
d_{s65}	– particle diameter for which 65% is finer
d_{sa}	– mean diameter computed from extreme values of the interval Δp_i , (m)
d_{sm}	– mean particle diameter, m
F_D	– drag force, N
F_d	– drag acting on a particle, N
g	– acceleration of gravity, m/sec^2
J	– hydraulic gradient
K	– constant
K_1	– constant
K_2	– numerical coefficient
n	– Manning roughness coefficient; porosity of the particle material
n'	– corrected Manning roughness coefficient

Δp_i	– interval in percentage
R	– hydraulic radius, m
R_w	– particle Reynolds number
S	– specific gravity
S_f	– specific gravity of fluid
S_s	– specific gravity of solids
SF	– shape factor
u_*	– shear velocity, m/sec
V	– approach velocity, m/sec
V_a	– apparent volume of particle, m ³
V_m	– volume of a mixture, m ³
V_s	– volume of solids, m ³ ; volume of material without pores, m ³
V_v	– volume of pores, m ³
V_w	– volume of the liquid fraction, m ³
W_s	– weight of material without pores, N
w	– settling velocity, m/sec
α	– a dimensionless factor
γ	– specific weight, N/m ³
γ_0	– mean specific weight, N/m ³
γ_s	– specific weight of solids, N/m ³
μ	– dynamic viscosity, kg/m.sec
ν	– kinematic viscosity, m ² /sec
ρ	– density, kg/m ³
ρ_m	– density of the mixture, kg/m ³
ρ_w	– density of water, kg/m ³
ρ_s	– density of solids, kg/m ³

6.1 Introduction

Engineering aspects of alluvial-stream mechanics, such as transportation of sediment, aggradation, degradation and erosion, spatial distribution, etc., depend to a great extent on the physical properties of individual sediment particles and their aggregates; and also on the mutual relation between them and the carrier medium – the water. Main properties of the solid phase – the sediment – will, therefore, be briefly reviewed in the following paragraphs of the present chapter.

The treatment must necessarily be spare and deal with only those properties thought to have direct bearing upon the transportation phenomena.

The geological origin of sediment particles is mainly due to the process

called *rock weathering* (see Chapter 3), by which solid rocks are broken down and decayed during long periods of time. In general there are three types of weathering processes: chemical, mechanical and organic.

Atmospheric agents responsible for the chemical weathering are mainly oxygen, carbon dioxide and water vapor, which either loosen the rocks or increase their volume and thereby cause their cracking. Most common mechanical agents include expansion brought about by chemical changes and freezing water, or scaling from abrupt changes of temperature. Water easily penetrates into cracks and fissures of rocks, where upon freezing it considerably increases in volume, causing large forces capable of splitting them apart.

Primary organic agents (living organisms) are roots of trees and plants, and often burrowing animals.

Like soils, sediments are broadly classified as *non-cohesive* and *cohesive*. Non-cohesive are those consisting of discrete particles, the kinetic and dynamic properties of which depend mainly on external forces acting upon them, and on physical qualities of individual particles, or their position in respect to other particles. In cohesive sediments, on the other hand, erosion depends primarily on chemical and electrical bonds between the particles, and these forces generally outweigh all other physical parameters of individual particles.

Only non-cohesive sediment systems will be considered, because they represent the bulk of engineering concern, and because even cohesive particles, once entrained by the water, essentially behave like non-cohesive in respect to the transport mechanism.

Definition of the technical terms generally used in the technology of sediment properties will be given as they come along.

6.2 Physical Properties

6.2.1 Size

Physical size of particles carried by an alluvial stream is generally a property that can be measured with relative ease. It is also an important property, with definite bearing upon the transportation mechanism; being one of the basic parameters of alluvial streams, it has a great significance for hydraulic engineers.

Sediment load carried by a natural watercourse is never of an uniform size, hence the *size distribution*, or gradation curve, of the material forming the bed and banks is of great importance. Characteristic sediment-size parameters used in most kinematic or dynamic equations are actually statistical values, and generally do not refer to any individual particle.

TABLE 6.1. CLASSIFICATION OF SEDIMENT ACCORDING TO SIZE

Denomination of the fraction	Size of the grain	Aggregation
Clay	$< 2 \mu$	Always found
Fine silt	$2 - 6 \mu$	Sometimes found
Medium silt	$6 - 20 \mu$	No aggregates
Coarse silt	$20 - 60 \mu$	No aggregates
Fine sand	$60 - 200 \mu$	No aggregates
Medium sand	$200 - 600 \mu$	No aggregates
Coarse sand	$600 \mu - 2 \text{ mm}$	No aggregates
Fine gravel	$2 - 6 \text{ mm}$	No aggregates
Medium gravel	$6 - 20 \text{ mm}$	No aggregates
Coarse gravel	$20 - 60 \text{ mm}$	No aggregates
Cobbles	$60 - 200 \text{ mm}$	No aggregates

As previously mentioned, grain-size distribution changes along the course of a stream due to weathering, which acts upon all particles. Changes in the mean diameter, however, may also be due to the fact that smaller particles move faster than larger ones.

Classification of sediment according to size, as generally adopted in hydraulic engineering, is given in Table 6.1. The range limits designated in the table are rather a generally accepted standard, and should not be viewed as sharp physical classification boundaries.

Grain size or "diameter" is actually an artificial parameter, since only rarely are natural sediment particles spherical in shape. Common terminology referring to the definition of the diameter is as follows:

1) *Sedimentation diameter* – diameter of an equivalent sphere of the same settling velocity and the same density, in the same fluid. It should, however, be mentioned that according to some researchers [1], the terminal settling velocity (see par. 6.2.4) of irregularly-shaped particles is affected by the temperature of the water, and hence they specify that the determination of the sedimentation diameter be done at 24°C ; they propose to call such a diameter "standard sedimentation diameter."

2) *Nominal diameter* – diameter of a sphere with the same volume as the particle.

3) *Sieve diameter* – size of opening of a square mesh sieve that will just

pass the particle. As a first approximation, sieve diameter is often taken equal to the nominal diameter.

For sand and small gravel, sieve analysis is generally used for grain-size determination; for clay, silt and very fine sand, settling analysis is convenient; larger gravel and cobbles can be measured by calipers or by volumetric displacement.

6.2.2 *Shape*

It has already been stressed that rarely are natural sediment particles of spherical shape, and the question is rather how much they deviate from this ideal shape. There can be no doubt that statistical shape properties of sediment particles affect the transport mechanism to some degree, but there is presently no direct way of reliably assessing this influence. The only effect which has been quantitatively evaluated, at least to some degree, is upon the settling velocity of a single particle in water at rest. It is furthermore of interest to note that greatest irregularities of shape are to be found in fine fractions, whereas larger particles tend to some approximate spherical shape. Sharp edges of larger particles, carried along the bottom or close to it, are constantly blunted by collision with other particles; finer particles, carried in suspension, hardly touch each other and thus are more likely to keep their irregular shape.

The U.S. Interagency Committee on Water Resources [1] has adopted as a measure of irregularity of shape the so-called Shape Factor (SF) defined as $SF = c/(ab)^{1/2}$, in which a , b and c are the triaxial dimensions of the particle, such that a = longest axis; b = intermediate axis; and c = shortest of the three mutually perpendicular axes of the particle. The definition of the factor, however, is obviously not precise and given to different interpretations; on the other hand, since all axes must be perpendicular, the absolute values of a , b and c for a given particle depend on which axis is chosen first. Application of SF on settling (fall) velocity will be discussed in par. 6.2.4.4.

6.2.3 *Density, Specific Weight (Force), Specific Density (Gravity) and Concentration*

Density of a substance, ρ , is its mass per unit volume. In the SI system of units, mass is expressed in kilograms, and hence the units of density are kg/m^3 or $\text{N} \cdot \text{sec}^2/\text{m}^4$. Whenever only a quantity of matter is to be indicated, it may directly be given in kilograms of mass, and its density be stated in kg/m^3 . In fluid mechanics it is often advantageous to use a derived quantity called *specific weight*, which expresses the gravitational *force* exerted upon a

mass of unit volume. This quantity is generally denoted by the Greek letter γ , and it is related to the density by the relationship $\gamma = \rho \cdot g$, in which g stands for the acceleration of gravity. It is obviously a quantity that changes with location. In the SI system, its units are N/m^3 .

Water-borne sediment particles are mainly quartz and feldspathic minerals with a specific density or gravity (for definition see farther ahead) of about 2.65, but whenever some different mineral composition is thought likely, appropriate laboratory measurements should be commissioned.

Particular attention should be paid to porous solid particles, in which some of the pores may be communicating with the atmosphere, while others may be without such contact. These latter ones may be either empty or full of some other substance. When such particles are submerged, some of the pores fill with water and become saturated. One should particularly distinguish between the specific weight of the particle material, given by

$$\gamma_s = \frac{W_s}{V_s} \quad (6.1)$$

where W_s – weight of the material without pores, N; V_s – volume of the material without pores, m^3 , and other kinds of specific weight, in which water accumulated in the pores, and possible swelling of the particle, are taken into consideration. This distinction is especially appropriate for light-weight porous material often used in movable-bed models of alluvial streams. When all the pores are communicating with the atmosphere, *mean specific weight* can be expressed by

$$\gamma_0 = \gamma_s (1 - n) + \gamma n \quad (6.2)$$

where n – porosity of the particle material, given by

$$n = \frac{V_v}{V_a} \quad (6.3)$$

in which V_v – volume of pores, V_a – apparent volume of the particle, and γ – specific weight of the water, N/m^3 .

The *specific density* of a substance is the ratio of its density to that of water at the temperature of its maximum density. In other words, if ρ is the density of the substance and ρ_w the density of the water, the specific density of the substance is $S = (\rho/\rho_w)$.

Specific density being the quotient of two densities having the same units, it has no units and is a pure number. By equivalence, the same reasoning

could obviously be extended to the quotient of two specific weights, γ , and then it is known as *specific gravity*. Numerical value of both ratios is equal, provided that the weight of both substances be referred to equal gravitational acceleration.

Example 6.1

For a research into local scouring processes, sediment grains having a mean specific weight of about 13.5 kN/m^3 are sought. A tender has been received from a pumice-stone supplier offering particles of the desired size having material specific gravity of $S \cong 1.5$ and porosity $n \cong 25\%$.

It is required to examine whether the material is suitable. Using Eq. (6.2): $\gamma_0 = \gamma_s (1 - n) + \gamma n \cong 15 \times 10^3 (1 - 0.25) + 9.8 \times 10^3 \cdot 0.25 \cong 13,700 \text{ N/m}^3 = 13.7 \text{ kN/m}^3$.

It is within less than 2% of the desired mean specific weight, and consequently would certainly be acceptable.

In order to determine the density of water with suspended sediment (fine silt or clay), the mass equilibrium equation can easily be written as:

$$V_m \rho_m = \rho V_w + \rho_s V_s \quad (6.4)$$

in which V_m – volume of the mixture, ρ_m – density of the mixture, ρ – density of the water, V_w – volume of the liquid fraction, ρ_s – density of the solid material, V_s – volume of the solid material.

Writing instead of V_m : $V_m = V_w + V_s$ and introducing it into Eq. (6.4), then

$$\rho_m = \frac{\rho V_w + \rho_s V_s}{V_w + V_s} \quad (6.5)$$

If the concentration by volume of the suspended material is given, the density of the mixture can be evaluated. Instead of density, specific weight could be obtained in the same manner.

Example 6.2

The following data were obtained during the work on a river sediment-investigation project:

$$\begin{aligned}\rho_s &= 2550 \text{ kg/m}^3 \\ \mathcal{V}_w &= 0.86 \text{ lit} \\ \mathcal{V}_s &= 0.14 \text{ lit}\end{aligned}$$

Evaluate the density of the mixture.

Solution

Using Eq. (6.5),

$$\rho_m = \frac{\rho \mathcal{V}_w + \rho_s \mathcal{V}_s}{\mathcal{V}_w + \mathcal{V}_s} = \frac{1000 \times 0.86 + 2550 \times 0.14}{1.0}$$

$$\rho_m \cong 1217 \text{ kg/m}^3$$

The given volumetric sediment concentration of about 30×10^4 ppm is, of course, very high and generally not encountered in river engineering. At lower concentrations, the additional mass is often relatively quite small, and therefore neglected by practising engineers; however, it may often be of importance in laboratory investigations.

Sediment concentration is usually expressed either as the ratio of dry weight to total weight of the water-sediment mixture or as the volumetric ratio, and is given in parts per million (ppm) or the equivalent (mg/lit).

6.2.4 Settling Velocity

The terminal velocity, w , at which a single solid particle falls in a still and unconfined liquid under the influence of gravity, is called its settling (fall) velocity. This terminal and constant velocity is reached as soon as there is equilibrium between the gravitational force acting on the particle, expressed by its submerged weight, and the resisting force caused by the fluid drag. Settling velocity for spheres and some other regular geometrical shapes have been theoretically and experimentally evaluated.

Although in drainage engineering the liquid is almost never at rest, and solid particles are seldom of a regular shape and are never single, the settling velocity as previously defined is nevertheless a primary factor in sediment-transport mechanics. It is of particular importance in respect of the suspended load, where the interplay between the settling movement and the turbulent diffusion, which tends to oppose it, plays a major role. The effect of particle shape and sediment concentration on the settling velocity will be

briefly discussed in the following paragraphs.

6.2.4.1 Definition of the Drag

A force is exerted on a solid body when there is motion of a fluid relative to it. This force, called *drag*, is defined as the force component parallel to the vector of the approach velocity but opposite in direction, and is caused either by tangential shear stresses acting on the body (skin drag), or by pressure difference (form drag). The general equation for the drag is given by

$$F_D = C_D A \frac{\rho V^2}{2} \quad (6.6)$$

in which C_D is the drag coefficient, ρ is the density of the fluid, A is the projected area of the body in a plane normal to the flow, and V is the approach velocity. In the particular case of settling sediment particles, terminal settling velocity w will be written instead of V . By means of the dimensional analysis, it can be shown that the drag coefficient, C_D , depends on two main parameters,

$$C_D = f(R_w, SF) \quad (6.7)$$

where $R_w = (w d_s / \nu)$ – Reynolds number of the particle; SF – shape factor of the particle (see par. 6.2.2). Diagram on Fig. 6.1 gives kinematic viscosity ν of water vs. temperature.

6.2.4.2 Stokes Range

When the particle Reynolds number is very small, inertial forces may be neglected and the drag is predominantly due to viscous forces. The strict limit from the theoretical point of view has been set at $R_w = 0.1$. In this range the drag coefficient is also virtually independent of the shape factor.

The first to formulate the dynamic equation for the drag at low particle Reynolds number was Stokes [2]. He used several basic assumptions for his analysis: inertial forces completely omitted from the Navier-Stokes equations; particles are spherical in shape; no slip of the fluid at the boundary; infinite expanse of fluid. Theoretically derived expression for the drag is then given by

$$F_d = 3\pi d_s \mu w \quad (6.8)$$

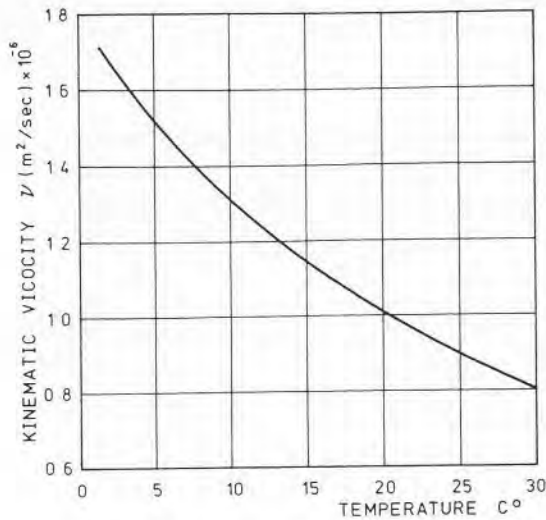


Fig. 6.1. Kinematic viscosity of water.

Here μ – dynamic viscosity (kg/m.sec). If this expression for the drag at low Reynolds numbers is set equal to Eq. (6.6), drag coefficient C_D can be arrived at,

$$C_D = \frac{24}{(d_s \rho_w)/\mu} = \frac{24}{R_w} \quad (6.9)$$

Stokes Law, as expressed by Eqs. (6.8) and (6.9) has been fully confirmed by experimental evidence. It is widely accepted that Stokes Law may be applied in practice up to $R_w \cong 1.0$, with negligible deviations from the experimentally measured values. For sediment grains of specific density of about 2.65, the upper limit for $R_w \cong 1.0$ is about $d_s = 0.2$ mm.

Now, in order to find the terminal settling velocity of a sphere falling through a fluid at rest, drag force acting on the particle must be equal to its submerged weight. Accordingly, the terminal settling velocity is found to be

$$w = \frac{1}{18} \left[\frac{S_s}{S_f} - 1 \right] \frac{g d_s^2}{\nu} \quad (6.10)$$

where S_s – specific gravity of the particle, S_f – specific gravity of the fluid.

An easily remembered formula for Stokes range is given by

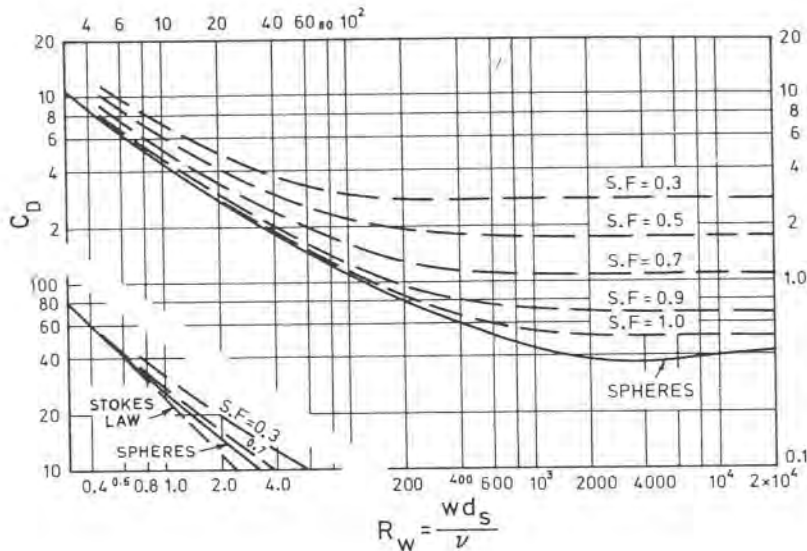


Fig. 6.2. Drag coefficient vs. particle Reynolds number. (Adapted from Rept. No. 12, Subcommittee on Sedimentation, Inter-Agency Committee on Water Resources, 1968; experimental points have been omitted).

$$w \cong 9,000 d_s^2 \tag{6.11}$$

in which w is in centimeters per second, d_s is in centimeters, and the constant is valid for water at 20°C and $S_s \cong 2.65$. The graph for some C_D -values in the Stokes range is shown in Fig. 6.2.

Example 6.3

The terminal settling velocity for a sediment particle, measured in a small test tube, was $w = 0.8$ cm/sec. Specific gravity of the particle material had been previously determined as $S_s \cong 2.6$; the test was carried out in water at 20°C . Estimate the diameter of the particle.

Solution

1. Using Eq. (6.10), we can write,

$$d_s = \left[\frac{18 w \nu}{((S_s/S_f) - 1) g} \right]^{1/2} = \left[\frac{18 \times 0.008 \times 10^{-6}}{((2.6/1.0) - 1) 9.8} \right]^{1/2}$$

$$d_s \cong 0.96 \times 10^{-4} \text{ m} = 0.096 \text{ mm}$$

2. Particle Reynolds number,

$$R_w = \frac{w \cdot d_s}{\nu} = \frac{0.008 \cdot 0.96 \cdot 10^{-4}}{10^{-6}} \cong 0.77$$

3. Using Eq. (6.11) instead of Eq. (6.10),

$$d_s \cong \left[\frac{w}{9,000} \right]^{1/2} = 9.4 \times 10^{-3} \text{ cm} = 0.094 \text{ mm}$$

Deviation of about 2% as compared to the result obtained using Eq. (6.10).

6.2.4.3 Settling Velocity for Particles of R_w Greater than Unity

As soon as the particle Reynolds number, R_w , is greater than about 1.0, inertial forces cannot be neglected anymore, and the incipient turbulence introduces many new and complicating factors. In fact, there is no simple and generalized law of drag for higher R_w -numbers. An approximate experimental law (having notable exceptions) states that

$$F_D \approx K_1 d_s^2 w^2 \rho \quad (6.12)$$

where K_1 denotes a constant which can be determined experimentally only for spherical particles.

If again use is made of Eq. (6.6) and of the notion that at the terminal settling velocity the drag must be equal to the submerged weight of the particle, it ensues

$$C_D \frac{\pi d_s^2}{4} \rho \frac{w^2}{2} = K_2 \rho g \left[\frac{S_s}{S_f} - 1 \right] d_s^3 \quad (6.13)$$

Here K_2 is a numerical coefficient, which also can be determined only for spherical particles, for which it is $K_2 = (\pi/6)$. From Eq. (6.13), settling velocity for spheres can be derived as

$$w^2 = \frac{4}{3} \frac{g}{C_D} \left[\frac{S_s}{S_f} - 1 \right] d_s \quad (6.14)$$

Experimental C_D -values must be taken from the diagram on Fig. 6.2. It is

obvious that the numerical evaluation of Eq. (6.14) necessitates a cumbersome trial and error procedure. If in Eq. (6.14), on the other hand, $C_D = (24/R_w)$ is substituted, Eq. (6.10) results for the Stokes range.

Another more convenient expression for the computation of settling velocity in the range $R_w > 1$ was proposed long ago by Rubey [24]. Although the theoretical premises on which it is based are not generally accepted, it is still widely used

$$w = \left[\frac{2}{3} g (S_s - 1) d_s + \frac{36 \nu^2}{d_s^2} \right]^{1/2} - \frac{6 \nu}{d_s} \tag{6.14a}$$

The equation is dimensionally homogeneous, hence can be used in any system of units.

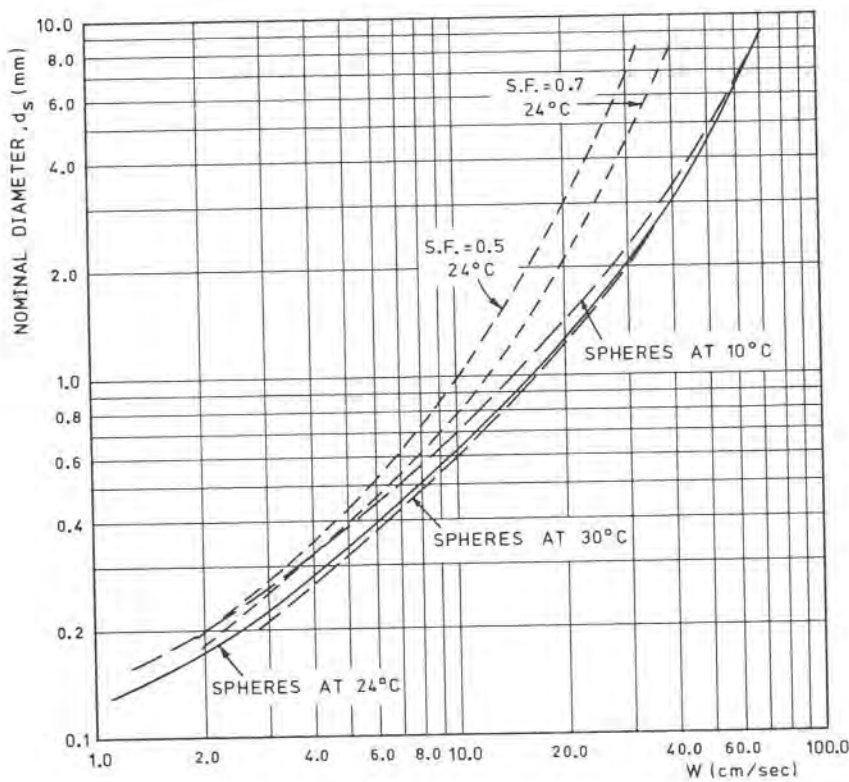


Fig. 6.3. Settling velocity of quartz particles ($S_s = 2.65$); influence of temperature and Shape Factor. (Adapted from Rept. No. 12, Subcommittee on Sedimentation, Inter-Agency).

Direct determination of settling velocity is also possible using specially prepared diagrams, one of which is given in Fig. 6.3. By interpolation, the effect of a wide range of practical temperatures can be estimated. The diagram is for quartz particles ($S_s = 2.65$) only, since these are the most commonly found in nature.

Example 6.4

Find the settling velocity for a spherical sediment quartz particle ($S_s = 2.65$) having nominal diameter $d_s = 2$ mm. Water temperature is 20°C .

1. Let us use Eq. (6.14). Assuming in the first trial that $w = 20$ cm/sec, particle Reynolds number can be computed as

$$R_w = \frac{w d_s}{\nu} = \frac{0.2 \times 0.002}{10^{-6}} = 400$$

From the diagram of Fig. 6.2, drag coefficient can now be found to be $C_D \cong 0.6$. Hence the settling velocity can now be obtained from Eq. (6.14).

$$w^2 = \frac{4}{3} \frac{g}{C_D} \left[\frac{S_s}{S_f} - 1 \right] d_s = \frac{4}{3} \cdot \frac{9.8}{0.6} \times 1.65 \times 0.002 = 0.0697$$

from here $w \cong 0.26$ m/sec > 0.2 m/sec as assumed.

For the second trial let us assume $w = 27$ cm/sec:

$$R_w = \frac{0.27 \times 0.002}{10^{-6}} = 540$$

From Fig. 6.2, $C_D \cong 0.56$. Then Eq. (6.14) yields,

$$w^2 = \frac{4}{3} \frac{9.8}{0.56} \cdot 1.65 \times 0.002 = 0.0756$$

and finally $w = 0.275$ m/sec.

This result is less than 2% off from the assumed settling velocity, and generally will be sufficiently accurate; however, if desired, a third trial can be made.

2. From the diagram on Fig. 6.3, settling velocity for $d_s = 2$ mm can be read off directly, $w \cong 29.5$ cm/sec. The slight discrepancy between the two

results (about 7%) is probably due to the inaccuracy in C_D -readings, rounding off of the numerical values, approximation of the kinematic viscosity, etc.

Application of the Rubey's equation to the given data results in a much lower settling velocity, $w = \sim 14.5$ cm/sec.

In Table 6.2 are tabulated the quartz grain sizes ($S_s = 2.65$) for which $R_w \cong 1$ and $R_w \cong 2000$ at different temperatures, and the respective settling velocities. All grain sizes less than those tabulated for $R_w \cong 1$ will be in the Stokes range; for all grain sizes larger than those for which $R_w \cong 2000$, drag coefficient C_D can be assumed constant at 0.4.

Example 6.5

The following data are available for a wide alluvial stream ($b > 10d$):

Average sediment load: 3000 ppm

Average sediment size: $d_s = 0.5$ mm

Average depth of flow: $d = 5$ m

Average hydraulic gradient: $J = 0.0003$

Water temperature: 24°C

Estimated Manning coefficient for clear water: $n = \sim 0.025$

Required: Estimate the Manning roughness coefficient for the sediment-laden water.

Solution

1. From Fig. 6.3 (Sphere's at 24°C), the settling velocity is found to be $w = \sim 8$ cm/sec.

TABLE 6.2. VARIATION OF d_s AND w AS FUNCTION OF R_w AND $^\circ\text{C}$

$^\circ\text{C}$	$R_w \cong 1$		$R_w \cong 2,000$	
	d_s (cm)	w (cm/sec)	d_s (cm)	w (cm/sec)
10	1.24×10^{-2}	1.06	0.51	52.2
15	1.14×10^{-2}	1.01	0.46	49.5
20	1.04×10^{-2}	0.97	0.42	47.3
25	9.6×10^{-3}	0.94	0.39	45.6
30	8.9×10^{-3}	0.90	0.36	43.8

2. Particle Reynolds number

$$R_w = \frac{d_s \cdot w}{\nu} \cong \frac{0.0005 \times 0.08}{0.95 \times 10^{-6}} \cong 38$$

3. Transformation of Manning n into Chezy C (see Vol. 1, par. 2.1):

$$C = \frac{R^{1/6}}{n} \cong \frac{d^{1/6}}{n} \cong \frac{5.0^{1/6}}{0.025} \cong 52$$

4. Shear velocity,

$$u_* = (gRJ)^{1/2} \cong (gdJ)^{1/2} \cong (9.8 \cdot 5.0 \cdot 0.0003)^{1/2}$$

$$u_* \cong 0.12 \text{ m/sec}$$

5. In order to use the diagram on Fig. 5.8, factor α has to be evaluated,

$$\alpha = \frac{C_m \cdot w}{\rho \cdot u_*} = \frac{3.0 \cdot 0.08}{10^3 \cdot 0.12} = 0.002$$

$$(3000 \text{ ppm} = 3 \text{ kg/m}^3)$$

6. For the above α -value, and $C \cong 52$, it is found that $C' \cong 62$, which is an increase of about 15%.

7. The estimated corrected Manning coefficient,

$$n' = \frac{R^{1/6}}{C} = \frac{5.0^{1/6}}{62} = 0.021$$

8. If the sediment load were 10,000 ppm, the corresponding Manning coefficient would be $n' \cong 0.018$, i.e. a reduction of about 28%.

6.2.4.4 Effect of Particle Shape on Settling Velocity

As pointed out in par. 6.2.2, efforts have been made to evaluate, at least approximately, the influence of particle shape upon its settling velocity. Shape Factor, first introduced by Schulz et al. [3], and defined as SF =

$c/(ab)^{1/2}$, has been chosen as most suitably expressing the shape of a natural particle, however vague the definition remains. At best, it can convey only roughly the actual shape of a nonspherical particle, without indicating whether it is rounded or angular, rough or smooth.

On Fig. 6.2 and Fig. 6.3, a few curves were drawn showing the likely effect of SF upon the settling velocity of quartz sediment particles. In the Stokes range, where the drag is wholly of viscous nature, there is no or negligible influence of the shape factor.

An extensive discussion of the influence of shape upon the settling velocity may be found, among others, in [1].

Example 6.6

Particle data are the same as in Example 6.4, but the shape now is supposed to be irregular, with SF = 0.5.

From the diagram on Fig. 6.3, the settling velocity is found to be about $w = 15.5$ cm/sec, which would be about 47% less than the corresponding velocity obtained for spheres under the same conditions.

6.2.4.5 Effect of Sediment Concentration on Settling Velocity

As mentioned previously, all the available information on settling velocity has been related to a single sediment particle falling freely in an infinite expanse of still water. In nature, on the other hand, each particle is surrounded by many others, depending on the sediment concentration. It is generally recognized that this is liable to have a definite influence on the settling velocity because of the interaction between the particles forming the sedimentation system. Unfortunately, there is to date no reliable information in this respect. The available experimental evidence is definitely too limited, both in quantity and scope, to justify any attempt at generalization, or even some more limited extrapolation to different sedimentation systems.

It appears, however, that the influence of sediment concentration upon the settling velocity is very small for all concentrations usually found in alluvial streams away from the bed. *Hindered settling* due to the increased sediment concentrations is of importance only near the bed, where concentrations are very high [4, 5].

6.2.5 Frequency Distribution of Grain Sizes

Natural sediment particles carried by a stream are never of uniform size, but have some characteristic distribution of differing sizes. The method generally used for the determination of grain-size gradation is by sieve

analysis, and results are in the form of *grain-size distribution curves*. Such curves are obtained when on ordinate fractions by weight of a sediment sample are plotted that are smaller or larger than the particle size indicated on the abscissa. Fig. 6.4 shows a typical distribution curve for an alluvial stream, plotted from the sieving results given in Table 6.3.

There is unfortunately no conclusive physical evidence as to the question which frequency best represents a given sediment mixture, and the choice is still rather a matter of opinion or convenience. Some of the most frequently met typical grain sizes are (see Fig. 6.4):

- d_{s50} – the median diameter, widely used in sedimentation engineering;
- d_{s35} – particle size for which 35% of the sediment mixture is finer; used by Einstein, among others;
- d_{s65} – size for which 65% is finer; also used by Einstein as representing sediment roughness;
- d_{s90} – size for which 90% is finer; used by Meyer-Peter (see Chap. 9).

TABLE 6.3. SIEVE ANALYSIS

Sieve opening (mm)	Remaining on sieve (gm)	Remaining on sieve (%)	Passing through sieve (%)
11.2	0	0	100
5.6	1.5	1.2	98.8
2.8	6.1	4.7	95.3
1.6	20.3	15.8	84.2
0.6	45.7	35.6	64.4
0.3	98.2	76.5	23.5
0.15	127.0	98.8	1.2
0.105	128.2	99.8	0.2
0.09	128.3	99.9	0.1
0.075	128.4	99.9	0.1
0.06	128.5	100	0
less	128.5	100	0
Total	128.5	100	

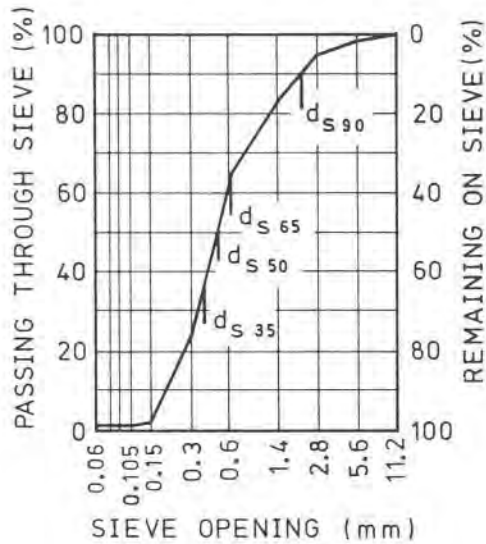


Fig. 6.4. Typical grain-size distribution curve.

It is generally assumed by drainage engineers that only rarely can a sediment mixture be represented by a single grain size. The median diameter d_{s50} is also often misleading, since it is not sensitive to the range of the distribution curve or its shape. In cases of very skewed distribution curves, therefore, statistical values may be tried, such as the so-called “mean diameter” which can be calculated from the distribution curve by

$$\frac{1}{d_{sm}} = \frac{1}{100} \sum \frac{\Delta p_i}{d_{sa}} \tag{6.15}$$

in which Δp_i – interval in percentage, d_{sa} – mean value of the size computed from the extreme values of the interval Δp_i (arithmetic mean).

Computation of the mean diameter is certainly time-consuming, hence it is generally carried out only when there is reason to believe that it might be substantially different from either d_{s50} or d_{s60} . More advanced statistical values, such as quartile and moment measures, are rarely used except in laboratory investigations.

Example 6.7

For the sediment distribution curve shown in Fig. 6.4, compute the mean

diameter d_{sm} , and compare it with d_{s50} and d_{s60} .

1. Table 6.4 summarizes the computation of the area $\Sigma(\Delta p_i/d_{sa})$ for the distribution curve given in Fig. 6.4 and in Table 6.3, while in Fig. 6.5 this area is graphically shown. Values of d_{sa} have been computed from Fig. 6.4. Hence, using Eq. (6.15),

$$\frac{1}{d_{sm}} = \frac{1}{100} \sum \frac{\Delta p_i}{d_{sa}} = \frac{1}{100} \times 242.8$$

from which, $d_{sm} = 0.42$ mm.

2. From the distribution curve given in Fig. 6.4: $d_{s50} \cong 0.45$ mm; $d_{s60} \cong 0.55$ mm. Hence, d_{s50} is only about 7% off from the mean diameter, which in most cases would be considered a negligible difference. On the other hand, d_{s60} would probably be unsuitable. For more skewed distributions, however, differences might be much greater.

TABLE 6.4. COMPUTED VALUES (Ex. 6.7)

Percentage limit (%)	d_{sa} (mm)	$\frac{1}{d_{sa}}$	Mean $\frac{1}{d_{sa}}$	Interval Δp_i (%)	$\frac{\Delta p_i}{d_{sa}}$
100	11.2	0.09			
90	2.0	0.50	0.29	10	2.9
80	1.0	1.00	0.50	10	5.0
70	0.8	1.25	1.12	10	11.2
60	0.55	1.80	1.52	10	15.2
50	0.45	2.20	2.00	10	20.0
40	0.40	2.50	2.35	10	23.5
30	0.32	3.10	2.80	10	28.0
20	0.26	3.80	3.45	10	34.5
10	0.20	5.00	4.40	10	44.0
0	0.15	6.70	5.85	10	58.5

Σ 242.8

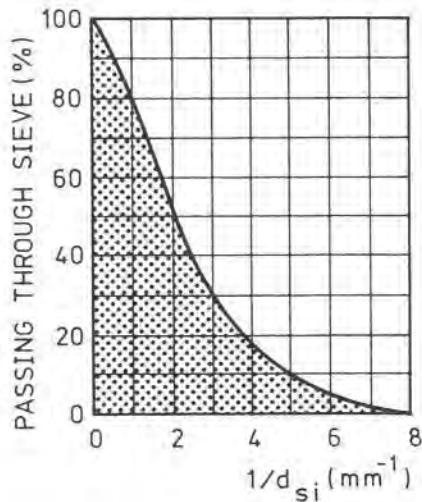


Fig. 6.5. Area $\Sigma (1/d_{si} \Delta p_i)$ (Ex. 6.7).

6.2.6 Aggregation of Sediment Particles

Fine silt and clay particles in general tend to form aggregates, particularly if the water is polluted and contains flocculating agents. This phenomenon may considerably affect the physical properties of the suspended sediment load.

Small clay or colloidal particles collide with other similar particles during their motion in the water, they adhere to them, and start forming aggregates, also called *floccules*. These aggregates, which may consist of only a few particles or many of them, will eventually acquire a higher settling velocity. Individual floccules may again combine to form aggregates of higher order, held together by chemical and electrostatic forces. Physical bonds of higher-order aggregates may be weaker than those of lower-order aggregates. Also the volume of higher-order aggregates is generally greater than the sum of lower-order aggregates they are composed of.

There is no reliable way for analytically determining the settling velocity of an aggregate. However, as long as it is in the Stokes range, Krone [6] has suggested that Eq. (6.10) may still be used, provided that instead of the specific gravity of the particle, the specific gravity of the aggregate is used.

6.2.7 Evaluation of Manning Roughness Coefficient from Grain-Size Distribution

It is a generally accepted approach to consider the total roughness resistance in alluvial channels as made up of two separate components – resistance due to grain roughness, and resistance caused by alluvial bed forms (to be discussed in the next chapter). Many semi-empirical formulae have been proposed by different researchers, and there is practically no possibility to say which one is the best for a given specific case. A few of the best-known of these expressions are listed below:

1. Meyer-Peter and Müller [21]

$$n = (d_{s90})^{1/6} / 26 \quad (6.16)$$

in which d_{s90} (in meters) is the grain size for which 90% of the sediment mixture is finer.

2. Transformed Strickler formula

$$n = (d_{s65})^{1/6} / 75.7 \quad (6.17)$$

here d_{s65} (in millimeters) is the grain size for which 65% of the sediment mixture is finer.

3. Keulegan [22]

$$n = (d_{s90})^{1/6} / 86.7 \quad (6.18)$$

in which d_{s90} is in millimeters.

4. For gravel-paved mountain streams, Lane and Carlson [23] proposed the formula

$$n = (d_{s75})^{1/6} / 67 \quad (6.19)$$

where d_{s75} is given in millimeters.

If any of the above formulae is substituted for n in Manning equation for uniform flow, and the ensuing expression divided by shear velocity $u_* = (gRI)^{1/2}$, a general equation is obtained having the form

$$\frac{V}{u_*} = K \left[\frac{R}{d_s} \right]^{1/6} \quad (6.20)$$

in which K denotes a numerical coefficient dependent on the formula used, R – hydraulic radius and d_s – characteristic grain size. This form of expression is suitable to be used for the analysis of measured data for a given stream.

Eqs. (6.16) to (6.19) have been applied to the sediment distribution given in Fig. 6.4, $d_{s90} = \sim 2$ mm, $d_{s65} = \sim 0.6$ mm, $d_{s75} = \sim 1$ mm, and the results are summarized in Table 6.5.

Since Eq. (6.19) is valid mainly for gravel-paved beds, the average value of $n = 0.013$ would be a reasonable assumption.

TABLE 6.5. COMPARISON OF FORMULAE (6.16) TO (6.19)

Eq. no.	n
6.16	0.014
6.17	0.012
6.18	0.013
6.19	0.015

References

1. U.S. Interagency Committee on Water Resources, Measurement and analysis of sediment load in streams, report no. 12, Some fundamentals of particle size analysis, 1968.
2. G. Stokes, Trans. Cambridge Phil. Soc., 9 (1951).
3. E.F. Schulz et al., Influence of shape on the fall velocity of sedimentary particles, Missouri River Div., Sed. Series, report no. 5, Corps of Eng., U.S. Army, 1954.

4. H.A. Einstein and N. Chien, Effects of heavy sediment concentration near the bed on the velocity and sediment distribution, University of California, Inst. Eng. Res., MRD Sediment series, no. 8, 1955.
5. J.W. Lavell and W.C. Thacker, Effects of hindered settling on sediment concentration profiles, Jour. Hydr. Res., 16 (4) (1978).
6. R.R. Krone, A study of rheological properties of estuarial sediment, Hydr. Eng. Lab., University of California, 1963.
7. H. Rouse, Engineering Hydraulics, Wiley, New York, N.Y., 1950.
8. A.J. Raudkivi, Loose Boundary Hydraulics, Pergamon, London, 1967.
9. W. Jarocki, A Study of Sediment (translated from Polish), N.S.F. and Center Inst. Inf., Warszawa, Poland, 1963.
10. J. Larras, Embouchures, Estuaires, Lagunes et Deltas, Eyrolles, Paris, 1965.
11. J. Larras, Hydraulique et Granulats, Eyrolles, Paris, 1972.
12. W.H. Graf, Hydraulics of Sediment Transport, McGraw-Hill, New York, N.Y., 1971.
13. H.W. Shen, River Mechanics, vol. I, Fort Collins, Colorado, 1971.
14. F. Sentürk, Les masses spécifiques des matériaux poreux, Acad. Sci., Paris, Comptes Rend, vol. 261, 1965.
15. D.W. Taylor, Soil Mechanics, Wiley, New York, N.Y., 1950.
16. H. Varlet, Usines de Dérivation, Tome I, Eyrolles, Paris, 1958.
17. Nedeco, River Studies, North Holland, Amsterdam, 1959.
18. G. Supino, Le Reti Idrauliche, Patron Ed., Bologna, 1965.
19. V.A. Vanoni et al., Lecture notes on sediment transportation and channel stability, California Inst. of Technol., report no. KH-R-1, 1961.
20. D. Simons and F. Sentürk, Sediment transport technology, Fort Collins, Water Resources Publication, 1976.
21. E. Meyer-Peter and R. Müller, Formulas for bed load transport, proceedings, 3rd Meeting of IAHR, Stockholm, 1948.
22. G.H. Keulegan, Laws of turbulent flow in open channels, Jour. Nat. Bur. Stand., Research Paper 1151, vol. 21, 1938.
23. E.W. Lane and E.J. Carlson, Some factors affecting the stability of canals constructed on coarse granular materials, proceedings Minnesota Int. Hydr. Conven., 1953.
24. W.W. Rubey, Settling velocity of gravels, sands and silt particles, Am. Jour. Sci., 25, (148) (1933).

CHAPTER 7

BED FORMS AND THEIR EFFECT ON ROUGHNESS

Symbols

d	– depth of flow, m
d_s	– particle diameter, m
F_R	– Froude number
g	– acceleration of gravity, m/sec ²
I	– longitudinal slope
J	– hydraulic gradient
K_s	– roughness height, m
n	– Manning roughness coefficient
n'	– Manning coefficient due to grain roughness
n''	– Manning coefficient due to form drag
Q	– flow discharge, m ³ /sec
R	– hydraulic radius, m
R'	– hydraulic radius with respect to the grain, m
R''	– hydraulic radius for bed forms, m
R_b	– hydraulic radius with respect to the bed, m
R_w	– particle Reynolds number
s	– geometric standard deviation
S	– specific gravity
u_*	– shear velocity, m/sec
u'_*	– shear velocity with respect to the grain, m/sec
u''_*	– shear velocity for bed forms, m/sec
\bar{V}	– mean velocity in a cross section, m/sec
w	– settling velocity, m/sec
x	– correction factor
γ	– specific weight, N/m ³
δ	– thickness of the laminar sublayer, m

δ'	– estimated value of δ
ν	– kinematic viscosity, m^2/sec
ρ	– density of water, kg/m^3
ρ_s	– density of solids, kg/m^3
$\Delta\rho_s$	– $(\rho_s - \rho)/\rho$
τ	– shear stress, N/m^2
τ'	– shear stress resulting from grain resistance, N/m^2
τ''	– shear stress due to form drag, N/m^2
ψ'	– dimensionless parameter

7.1 Introduction

In contrast to rigid-bed channels, in which the bed configuration is known and constant for all flow regimes, in alluvial channels the movable bed will take on different and changing forms, depending on the interaction between the sediment and the flow of water. At the present state of the art, there is no way for the exact analysis of these forms, and their dynamic equilibrium still escapes our full understanding. One of the main reasons for this lack of theoretical background is the large number of variables involved and their prevalently random nature. However, a general picture of bed forms and their relationship with flow regimes is essential for engineering purposes, as the resistance to flow in alluvial channels is largely determined by bed configuration.

Flowing over an alluvial bed, water exerts a shear stress on individual sediment particles, given as $\tau = \gamma R J$ (see Chap. 3). If Manning equation for uniform flow is used, this shear stress can be expressed as

$$\tau = \gamma n^2 R^{-1/3} V^2 \quad (7.1)$$

in which n is the Manning roughness coefficient, R the hydraulic radius and V the mean velocity. Assuming further that n and R are constant, this is a simple quadratic relation between τ and V . If, on the other hand, roughness coefficient n changes as a result of the shear stresses on the loose bed, the above simple relationship generally assumes a form similar to the one shown in Fig. 7.1.

7.2 Bed Forms

Within the framework of the present text there is no possibility to follow

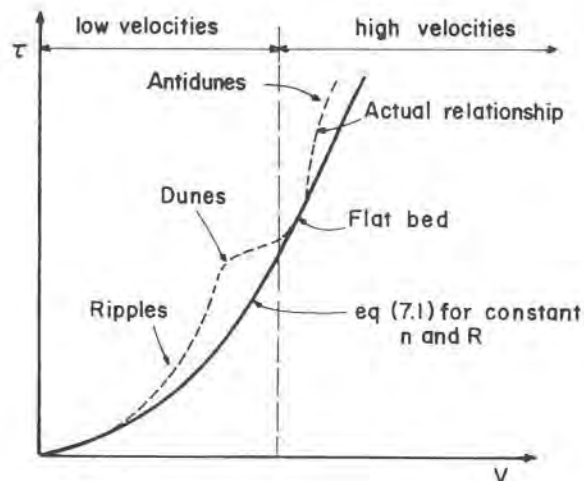


Fig. 7.1 Schematic relationship $\tau = f(V)$ in alluvial channels.

a rigorous classification of bed forms, and therefore only a general review will be given under the present heading. For more detailed discussion of the topic, Refs. [1] or [2] may be consulted, among many others. Bed forms to be described in the following should not be considered as a fixed set of different geometrical shapes, but rather as a system of constantly moving and changing patterns, always adapting to the flow and interacting with it. In fact, because of this mutual influence between the bed and flow, and vice versa, it is often difficult in alluvial channels to consider them separately, but rather as a combined system, mutually interdependent.

7.2.1 Ripples and Dunes

Let us consider an alluvial stream of a given depth, and a bed consisting mainly of sand particles of different sizes. As long as the velocity of flow is very low, individual particles cannot be removed by the water, and hence the configuration of the bed will remain unchanged, whatever its form. At this stage, the boundary of the channel may be considered as rigid for all practical purposes.

As the velocity gradually increases, the shear stress also becomes higher, until a certain critical velocity is reached, at which individual particles start being removed and entrained by the water. As a result of this action, small relatively regular sand waves will start forming along the bed, called *ripples*

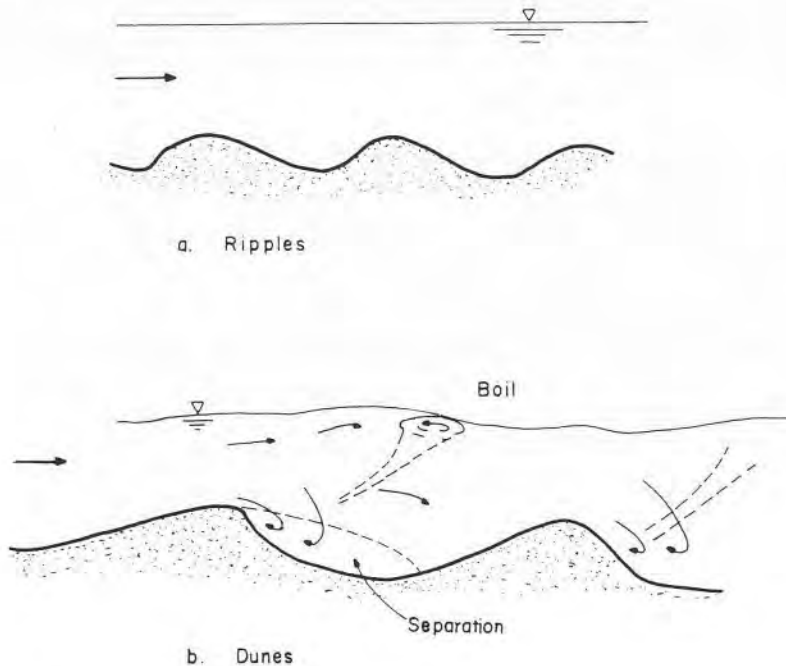


Fig. 7.2. Ripples and dunes.

(see Fig. 7.2a). Their height generally does not exceed about 5 cm, and the wave length about 30 cm. At the beginning, they tend to appear as more or less regular rows of parallel crests, not necessarily in straight lines, but if the velocity increases still further, they tend to assume a more haphazard configuration.

With an additional increase of velocity, sharp-crested, roughly triangular shapes will start forming, moving downstream with the flow. The generally accepted denomination for these continuously changing and downstream-moving features is *dunes*. They are much larger than ripples, reaching in bigger rivers lengths of tens of meters and corresponding heights. It is obvious that such a bed must be considered a deformable boundary.

The upstream slope of a typical dune formation is rather gentle, while downstream it is much sharper (40° – 45°), see Fig. 7.2b.

Water profile above the dunes is relatively smooth at lower velocities, becoming wavy at higher flows. Water-surface waves are generally out of phase with the sand waves; “boils” of high turbulence just downstream of dune crests often accompany these water waves.

Although in most cases a rippled bed will precede the dunes, recent in-

vestigations seem to indicate that if $d_{s50} > \sim 0.6$ mm, dunes may form directly, without any preliminary ripples. Water surface generally remains plane and undisturbed with a ripple bed, and there is practically no suspended load. Dunes, on the other hand, seem to be common up to $d_{s50} \approx 15$ mm; for Froude numbers of flow not too low (say, $F_R > \sim 0.3$), water surface above a dune-covered bed shows undulatory pattern, and bed material can be found in suspension.

The exact mechanism of ripple and dune formation is still unknown, although in recent years attempts have been made at its mathematical and physical analysis, such as [3, 4, 5], among many others. Most of the offered explanations are based on the assumption of some inherent instability between the liquid and granular material, but all of them fail to account reliably for every aspect of this interesting natural phenomenon.

On the lee-side of the dunes, there is a flow-separation zone, Fig. 7.2b, which not only affects their formation mechanism, but also the movement along the channel bed. According to the recent laboratory investigations concerning this separation zone [22], two interesting characteristics, among many others, seem to have a general validity:

1. The length of the flow separation behind dunes is independent of the Froude number, and virtually independent of the flow depth, as long as the F_R -number is less than about 0.5, and the ratio between the depth of water and dune height is greater than about 5.
2. The length of the flow separation behind dunes is dependent on the sand-grain roughness on the dunes when they are flat. When dunes are steep (height of the dune to its length greater than about 0.05), the effect of the sand-grain roughness is virtually negligible. In fact, the separation length for steep dunes is approximately equal to four times the height.

7.2.2 *Transition and Flat Bed*

As the velocity of flow is further increased, dunes start to be washed out, and patches of flattened bed appear intermittently with still discernible dune stretches. Velocity at which the transition regime sets in depends mainly on the grain size of the bed material; it is lower with fine sands, and higher with coarser fractions. Roughness differences caused by this rather erratic bed configuration are likely to produce rough water surface, in addition to standing waves which usually accompany tranquil flows at higher Froude numbers. During the transition, dunes gradually change shape, they become lower and more elongated.

If the velocity keeps increasing, dunes will eventually be completely washed out, and the bed will become flat. It should be noted that this occurs

for Froude numbers below unity, but may extend well beyond $F_R = 1$, depending on the characteristics of the bed material. The bed shows great mobility, and there is considerable transport of sediment, both in suspension (2,000–3,000 ppm) and as bed load.

7.2.3 Antidunes

When the Froude number approaches unity, the flow becomes unstable (see specific energy diagram, Vol. I of the Manual, par. 2.4) and standing cross-waves appear on the water surface. Trains of dunes start forming again along the bed, they grow in height until eventually the dynamic equilibrium is disturbed and they break to be reformed again. After the flow changes to super-critical, $F_R > 1$, both the bed and water surface become wavy, but now the water and bed are in phase, as should be expected in supercritical flow (Fig. 7.3). These new bed waves are generally called *antidunes*. According to the classification adopted by the ASCE Task Committee [2], which has included in the antidune regime all bed configurations that form wave trains, they may be stationary, move downstream with the flow, or upstream against the flow. In the more conservative classification schemes, however, antidunes generally refer only to those bed forms that move upstream against the flow.

Formation of antidunes has been experimentally studied by many researchers, but probably the most thorough investigation was made by Kennedy [3, 6]. He tried to show theoretically why dunes or antidunes should form and develop at all in alluvial channels in the first place. If it is assumed that variations in sediment discharge lag behind the corresponding variations of flow velocities near the bed, by theoretical argumentations it can be shown that at low Froude-number values, an initially small disturbance will eventually develop into dunes of finite amplitude. According to his conclusions, the minimum wave length (distance between adjacent crests or troughs) of antidunes is given by $L = 2\pi \bar{V}^2 / g$, where \bar{V} is the mean

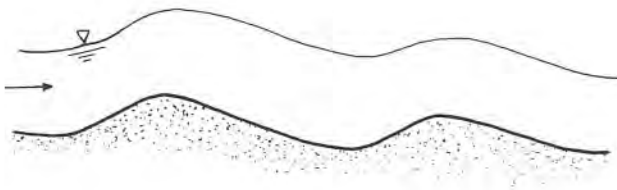


Fig. 7.3. Antidunes.

velocity of flow, but the actual length for any specific case depends on velocity and depth. For a conservative estimate of antidunes height, the value of $h \approx 0.14 \cdot 2\pi V^2/g$ is recommended [6].

The Froude number of flow required for the formation of antidunes varies with changes in depth and grain size; it is directly proportional to the size of sand grains, and inversely proportional to the depth. Similarly to the theoretical relationship derived from the theory of deep-water waves, antidune waves will collapse when $h \cong L/7$, where h denotes the wave height (vertical distance from the bottom of trough to top of crest) and L wave length as previously defined. A generally accepted schematized classification of different bed forms has been given by Simons et al. [1] and is represented in Fig. 7.4.

7.2.4 Bars

Bed forms generally called bars are as a rule much larger, both in area and height, than all the previously discussed shapes, and in fact the basic mechanism of their formation is quite different. They are mentioned here,

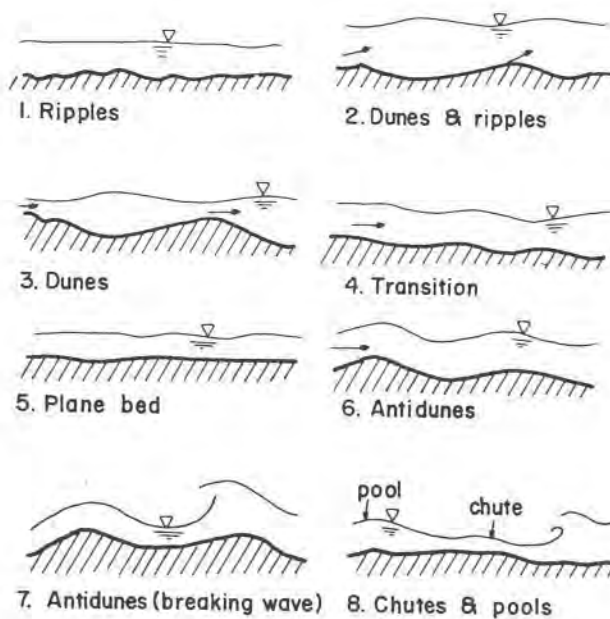


Fig. 7.4. Schematized bed forms, after [1].

because they also represent an important element of the alluvial-channel roughness, and may be of crucial significance for navigable waterways.

Bars often reach heights comparable to the water depth, and at low stages often stick out of the water; they have generally elongated shapes, usually reaching lengths equal to channel width or more. Different types of bars have already been discussed in previous paragraphs, and they are here summarized for the sake of convenience.

1. *Point bars* are formed on the convex side of channel bends or meandering alluvial streams. The mechanism of their formation and their morphological properties have been discussed in par. 3.8.

2. *Alternate bars* are generally a characteristic feature of crossings, i.e. straight stretches between successive meanders. They appear alternately along both banks of the stream, and as a rule occupy much less than the width of the channel. Alternate bars have been discussed in par. 3.9.

3. *Tributary bars* are formed at confluence of tributaries with the main stream, and they extend downstream. Tributary bars developed during high flows may appear as detached small islands during low water. Confluences have been discussed in par. 3.7. For easy reference, main types of bars are schematically summarized in Fig. 7.5

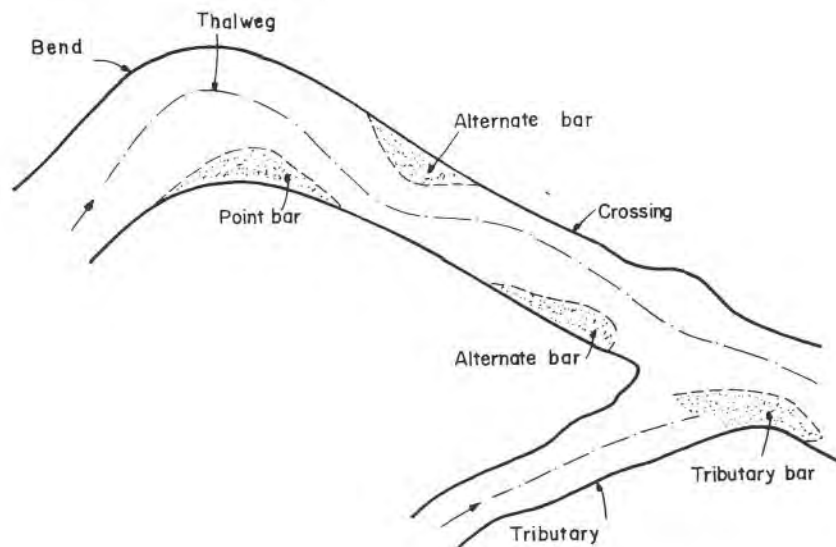


Fig. 7.5. Types of bars.

7.5 Effect of Bed Configuration on Roughness

As interesting and instructive as the knowledge of different bed forms may be for hydraulic engineers, their main concern is no doubt to learn how and to what extent these configurations affect the flow – and above all the resistance to it. This resistance to flow is generally expressed by some *friction factor*, relating the rate of energy dissipation of the flow to the roughness, liquid properties, mean velocity, etc. As long as the flow is confined to pipes, or rigid-boundary open conduits, the relationship is relatively simple and straightforward, and there is plenty of detailed information about it. However, in alluvial, deformable channels, where the parameters affecting the resistance to flow are interrelated and not amenable to separate and independent analysis (relationship essentially nonlinear from the mathematical point of view), the experimental information so far remains inconclusive, with large scatter and inconsistencies, and the proposed analytical methods are unreliable and often excessively laborious. In the following a brief review of the present concepts on this difficult and controversial subject will be given; this will certainly not enable hydraulic engineers to obtain a clear-cut answer to their problems, but may contribute to the right direction of their judgement, and be of some guidance to their final decision.

Results of many researches and field observations seem to indicate that the two-phase flow of water and sediment has by itself some quite distinctive effects upon flow phenomena, such as

- Friction coefficient tends to decrease with increasing suspended sediment concentration.
- v . Karman universal constant κ is often found to be smaller than with flow of water without sediment load.
- Velocity gradient, du/dy , generally becomes larger with increasing quantity of suspended sediment.
- Scale of turbulence and mixing length seem to be reduced.
- Experimentally measured velocities near the channel bed appear to be larger than predicted by theoretical considerations.

A graph showing qualitative influence of stream-bed configuration on the resistance to flow is given in Fig. 7.5a. A similar quantitative graph is given in Fig. 7.8.

A reasonable approach to the problem of flow resistance in alluvial channels has been proposed by Einstein and Barbarossa [7]. They reasoned that the total resistance to flow could be seen as composed of two elements: resistance due to the roughness of the sediment itself (skin friction), and resistance arising from deformable bed forms (form drag). They also assumed that the shear stress, τ , may be divided into two parts,

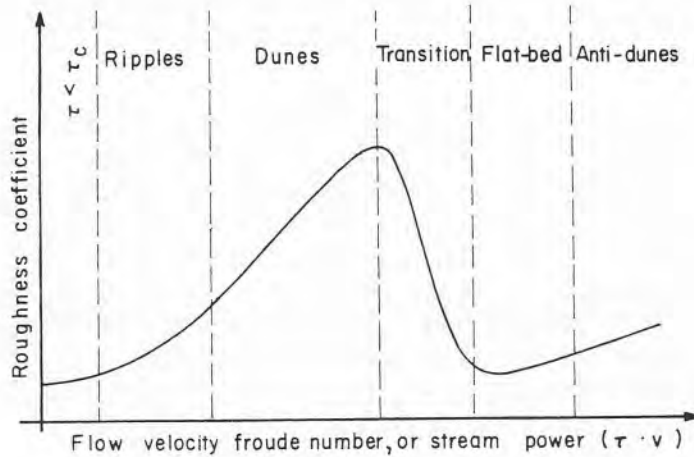


Fig. 7.5a. Qualitative influence of stream-bed configuration on roughness, after [16].

$$\tau = \tau' + \tau'' \quad (7.2)$$

in which τ' – is the shear stress resulting from the grain resistance only, τ'' – is the additional shear stress due to the form drag arising from bed forms (such as dunes or bars).

Although the two forms of the “shear” are of quite different origin, they have been lumped together for the sake of convenience. Hydraulic radius R is also divided into two parts, such that

$$\tau' = \gamma J R' \quad (7.3)$$

and

$$\tau'' = \gamma J R'' \quad (7.4)$$

Here, according to this approach, R' denotes the hydraulic radius “with respect to the grains”, while R'' is the hydraulic radius the stream must have in order to carry the flow with the same velocity and gradient without additional dune resistance. Relative shear velocities are further defined as

$$u'_* = (g R' J)^{1/2} \quad (7.5)$$

and

$$u_*'' = (gR''J)^{1/2} \quad (7.6)$$

Also

$$u_* = u_*' + u_*'' \quad (7.7)$$

In order to establish the relation between the mean velocity \bar{V} and R' , use is made of Eq. (5.12), written in the form

$$\frac{\bar{V}}{u_*} = 5.75 \log \left(12.27 \frac{R'}{K_s} x \right) \quad (7.8)$$

in which $K_s = d_{s_{65}}$ and x is the correction factor given in Fig. 5.3.

From the above equations, by a laborious trial and error method, R' and u_*' can be obtained for any specific case. Then the shear velocity for bed form resistance u_*'' may be found applying Eq. (7.7).

Using data collected from a large number of natural watercourses, they prepared a characteristic graph of \bar{V}/u_*'' vs. a dimensionless parameter $\psi' = \Delta\rho_s (d_{s_{35}}/R'J)$, where $\Delta\rho_s$ stands for $(\rho_s - \rho)/\rho$ (ρ_s - density of the sediment and ρ - density of water), called the bar-resistance curve (see Example 7.2). Vanoni and Brooks [8] have later simplified the computational method by adding an auxiliary graph which eliminates the lengthy trial and error procedure.

Unfortunately, the scatter of measured points around the bar-resistance curve is considerable. Although the method has the definite advantage of giving a ready quantitative answer, its reliability seems to be limited, and it may lead to large errors.

In the discussion of Einstein's paper, Bajorunas [9] has proposed a graph, claimed to be based on actual stream measurement, which gives the influence of bed forms on Manning coefficient n , Fig. 7.6. In a similar way to the previously described method, he assumed that $n = n' + n''$, i.e. n' - due to the grain roughness, and n'' - due to the form drag. On the abscissa of the graph is the reciprocal value of the Einstein's nondimensional parameter ψ' . Here the specific gravity of sediment particles has been taken as $S_s = 2.68$ (hence, $(S_s - S_w)/S_w = 1.68$), and in wide channels, according to Einstein, it can usually be assumed that $R' \cong R \cong d$.

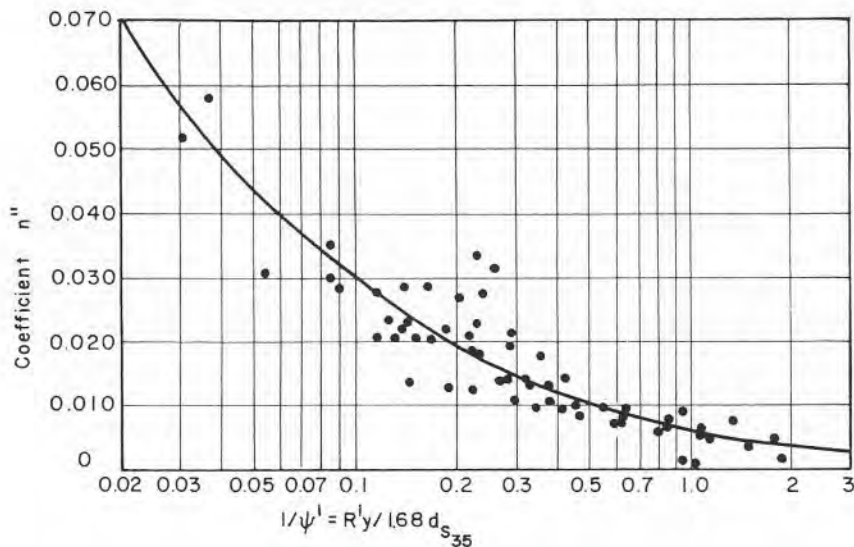


Fig. 7.6. Manning coefficient n due to bed forms (after Bajorunas [9]).

Example 7.1

In Series II of flume measurements carried out by Vanoni and Brooks [8] in order to investigate the effect of bed forms on roughness coefficient, some results were obtained as given in Table 7.1. The sand bed had a median grain size of $d_{sm} = (d_{s84} \times d_{s16})^{1/2} = 0.152$ mm, with a geometric standard deviation of $s = (d_{s84}/d_{s16})^{1/2} = 1.76$; relatively high value of the standard deviation indicates that the sand was not uniform. Values for the hydraulic radius have been corrected to apply only to the bed, and not to the walls.

Required:

1. Compute Manning coefficient n'' for all experimental runs, due to bed-form resistance,
2. Draw graphs of slope I vs. mean velocity \bar{V} , and of n'' vs. mean velocity.

Solution

1. In Table 7.1 find summarized the experimental data of the 11 runs in which the depth of flow was kept constant at $d \cong 0.075$ m, while the discharge and longitudinal slope gradually increased. In the final column are listed the computed n'' -values (rounded up).

TABLE 7.1. DATA FOR SERIES II (Ex. 7.1)

No.	Slope I	Mean vel. \bar{V} (m/sec)	Hydr. rad. R_b (m)	$I^{1/2}$	$R_b^{2/3}$	n''
1.	0.0020	0.244	0.0671	0.0447	0.165	0.030
2	0.0024	0.277	0.0671	0.0490	0.165	0.029
3	0.0026	0.299	0.0668	0.0510	0.165	0.028
4	0.00275	0.317	0.0671	0.0524	0.165	0.027
5	0.0027	0.366	0.0653	0.0520	0.162	0.023
6	0.0024	0.421	0.0619	0.0490	0.157	0.018
7	0.00225	0.472	0.0595	0.0474	0.153	0.015
8	0.0021	0.515	0.0564	0.0458	0.147	0.013
9	0.0020	0.558	0.0537	0.0447	0.142	0.011
10	0.00225	0.628	0.0521	0.0474	0.140	0.011
11	0.0039	0.811	0.0540	0.0624	0.143	0.011

2. Let us take for instance run No. 3. Using Manning equation for uniform flow, $\bar{V} = (1/n'') R_b^{2/3} I^{1/2}$, n'' can be easily derived from $n'' = R_b^{2/3} I^{1/2} / \bar{V}$. Hence,

$$n''_3 = \frac{0.165 \times 0.051}{0.299} = 0.0281$$

In the same manner, all other n'' -values can be computed.

2. Fig. 7.7 shows the graph of I vs. mean velocity \bar{V} , and Fig. 7.8 coefficient n'' vs. mean velocity. Description of bed configuration on Fig. 7.8 was given by the researchers.

Example 7.2

In continuation of Example 7.1, additional data for the Series II, corrected to apply only to the bed without the influence of walls, are given in Table 7.2. For the given grain-size distribution, $d_{s35} = 0.123$ mm, $d_{s65} = 0.191$ mm, and water temperature 25°C .

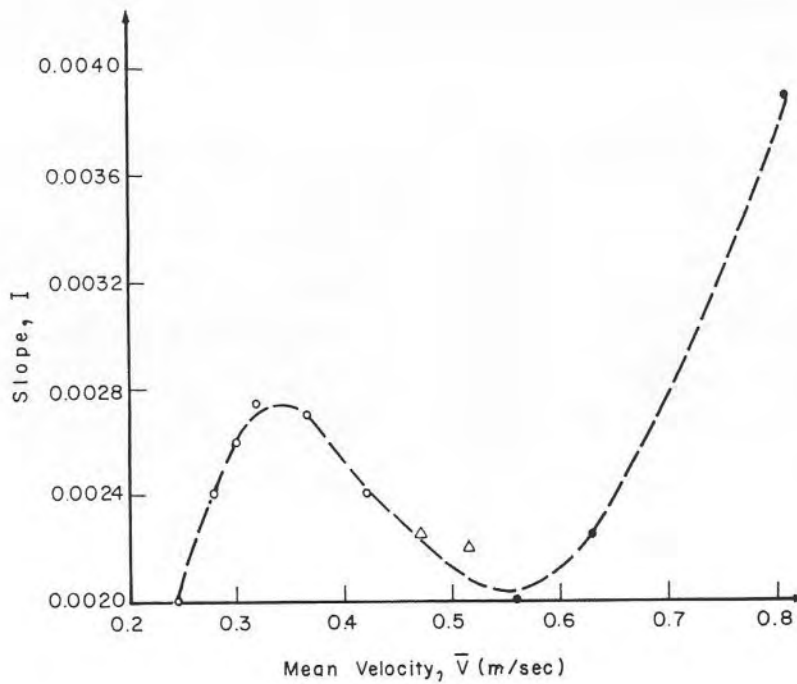
Fig. 7.7. Slope I vs. mean velocity \bar{V} (Ex. 7.1).

TABLE 7.2. DATA FOR SERIES II (Ex. 7.2)

No.	Bed hydr. rad. R_b (m)	Bed shear velocity u_{*b} (m/sec)	Froude number F_R	\bar{V}/u_*''	ψ'
1	0.067	0.036	0.29	7.4	8.7
2	0.067	0.040	0.33	7.7	7.0
3	0.067	0.041	0.35	8.0	6.3
4	0.067	0.043	0.37	8.3	5.7
5	0.065	0.041	0.43	10.2	4.6
6	0.062	0.038	0.50	13.7	3.8
7	0.060	0.036	0.55	17.7	3.3
8	0.056	0.034	0.61	23.7	2.9
9	0.054	0.032	0.66	32.7	2.6
10	0.052	0.034	0.74	43.3	2.1
11	0.054	0.045	0.95	34.8	1.3

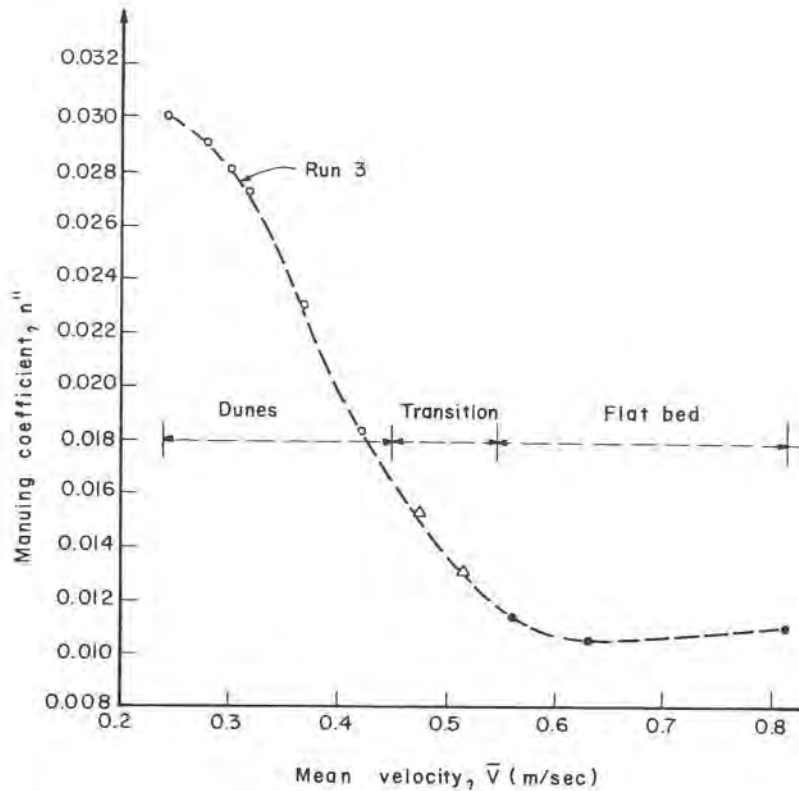


Fig. 7.8. Manning coefficient n'' vs. mean velocity \bar{V} (Ex. 7.1).

Required: Compare the experimental data with Einstein's bar-resistance curve.

Solution

In order to make the required comparison, parameters \bar{V}/u_*'' and ψ' have to be computed for each one of the experimental runs. The computational procedure by trial and error will be shown here for the run No. 3. All the pertinent data are given in Tables 7.1 and 7.2.

First trial – Let us assume: $u_*' = 0.02$ m/sec. Then the first estimate of the laminar sublayer, using Eq. (5.15) –

$$\delta' = 11.6 \frac{\nu}{u_*'} = 11.6 \frac{0.955}{10^6 \cdot 0.02} = 0.00055 \text{ m}$$

In order to apply Eq. (5.12), first the correction factor x has to be found. Therefore,

$$\frac{K_s}{\delta'} = \frac{d_{s65}}{\delta'} = \frac{1.9 \times 10^{-4}}{5.5 \times 10^{-4}} = 0.345$$

From the graph on Fig. 5.3 it is found that $x = 1.12$. Eq. (5.12) can now be solved for R' ,

$$\frac{\bar{V}}{u_*'} = 5.75 \log \left(12.27 \frac{R'}{K_s} x \right)$$

Introducing the numerical values,

$$\frac{0.299}{0.02} = 14.95 = 5.75 \log \left(12.27 \frac{R'}{0.000191} \cdot 1.12 \right),$$

and from here: $R' = 0.0055 \text{ m}$.

Now, in order to check our first trial value, let us use Eq. (7.5),

$$u_*' = (gR'I)^{1/2} = (9.81 \times 0.0055 \times 0.0026)^{1/2} \quad u_*' = 0.012 \text{ m/sec}$$

This is less than the assumed value of 0.02 m/sec, hence a second trial has to be made.

Second trial – $u_*' = 0.018 \text{ m/sec}$;

Thickness of the laminar sublayer:

$$\delta' = 11.6 \frac{0.955}{10^6 \times 0.018} = 0.00062 \text{ m}$$

$$\frac{K_s}{\delta'} = \frac{1.91 \times 10^{-4}}{6.2 \times 10^{-4}} = 0.309$$

From Fig. 5.3: $x \cong 1.0$. Applying Eq. (5.12),

$$\frac{0.299}{0.018} = 16.7 = 5.75 \log \left(12.27 \frac{R'}{0.000191} \times 1.0 \right)$$

from which: $R' = 0.0124$ m. Checking the assumption by Eq. (7.5)
 $u'_* = (9.8 \times 0.0124 \times 0.0026)^{1/2} = 0.0178$ m/sec. The result is almost identical with the assumed value of u'_* , hence no further trials are necessary.

Finally, parameters (\bar{V}/u''_*) and ψ' must be determined.

$$R'' = R - R' = 0.067 - 0.0124 = 0.0546 \text{ m}$$

From Eq. (7.6),

$$u''_* = (gR''I)^{1/2} = (9.8 \times 0.0546 \times 0.0026)^{1/2}$$

$$u''_* = 0.037 \text{ m/sec}$$

$$\frac{\bar{V}}{u''_*} = \frac{0.299}{0.037} = 8.08$$

$$\psi' = \Delta\rho_s \frac{d_{s35}}{R'I} = 1.65 \frac{0.000123}{0.0124 \times 0.0026} = 6.3$$

(ρ for water – 1000 kg/m^3 ; ρ for quartz particles – 2650 kg/m^3).

In the same manner all the rest of \bar{V}/u''_* and ψ' values listed in Table 7.2 have been computed. The comparison with Einstein's bar-resistance curve [7] is shown in Fig. 7.9.

The scatter of the experimental points relative to the bar-resistance curve is rather extensive, but no explanation has been suggested by the researchers. Maximum scatter for natural streams, as given by Einstein and Barbarossa [7], was indicated as about $\pm 30\%$. It should, however, be borne in mind that the experimental data refer to a narrow flume (width about 0.27 m); and though these data have been corrected in order to relate only to the influence of the bed, they nevertheless may well be affected by the walls and other distortions due to small-scale laboratory experiments (for instance, more pronounced sand uniformity).

Looking at Fig. 7.7, it is interesting to note that at the beginning, the hydraulic gradient I increases with the rise in mean velocity, corresponding to developed dunes; at a certain state, the slope begins diminishing with increasing velocity, which indicates that the process of obliterating of the

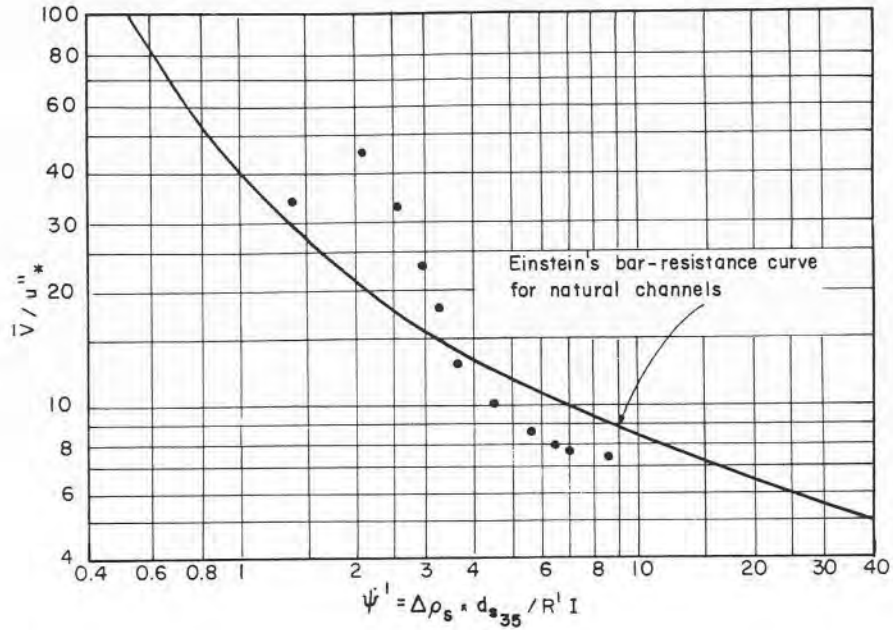


Fig. 7.9. Comparison with Einstein's bar-resistance curve (Ex. 7.2).

dunes has started; in the final stage, flat bed is reached, and the curve again begins to go up. Even more astonishing is the fact that for a given slope and depth, there may be as many as three possible velocities which would sustain the flow for different bed formations. This is apparently due to the fact that the reduction of the friction factor due to the disappearance of dunes is much greater than the additional turbulence arising from the increased velocity.

Influence of bed configuration may also be at least partly responsible for the often encountered phenomenon of the so-called *loop-rating-curve* for natural watercourses, as schematically shown in Fig. 7.10. For the same depth, the discharge may be lower on the falling stage than on the rising stage. Main part of the difference can be explained by the kinematics of the flood-wave propagation (a topic which is outside the scope of the present text, but could be found in many advanced textbooks on flow in open channels, as for instance [10]), which shows that the deviation from the rating curve for uniform flow is positive in the rising stage and negative in the subsiding stage. The deviation, however, is often much too large to be accounted for by this factor alone. It seems plausible to assume that on the

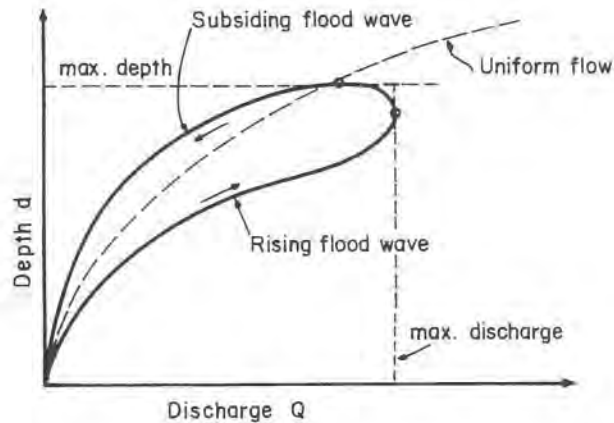


Fig. 7.10. Loop rating curve.

rising stage, dunes have not enough time to fully develop, particularly in streams with rapidly rising flood waves (matter of hours or a few days rather than weeks). Hence, much higher resistance to flow on the falling leg of the hydrogram, and consequently lower flow rate for the same depth. For similar phenomena concerning sediment discharge in ephemeral streams of arid zones, see par. 8.4.

As already mentioned, it is generally thought that suspended sediment tends to reduce the friction factor, and also the von Karman constant κ . In laboratory experiments [8] this reduction (in relation to clear water) was observed to be about 5% for suspended sediment load of 3640 ppm, and about 28% for 8100 ppm. However, reduction due to bed configuration (at constant depth) may be as high as a few hundred percents between dune-forming velocities and flat-bed velocities. It may be, therefore, generally assumed that the reduction of friction factor due to suspended sediment is of practical engineering importance only in streams with very high load over flat beds, and may safely be neglected when there are dune formations on the bed.

According to Simons and Richardson [16] if antidunes do not break, resistance to flow is about the same as for a plane bed with sediment movement, i.e. slightly more than that due to the grain roughness, with Chezy roughness coefficient in the range of 44 to 72, depending mainly on the frequency of their formation and breaking. On the other hand, if the frequency of antidune breaking is high, roughness coefficient due to bed form may be in the low range of about 31 to 62.

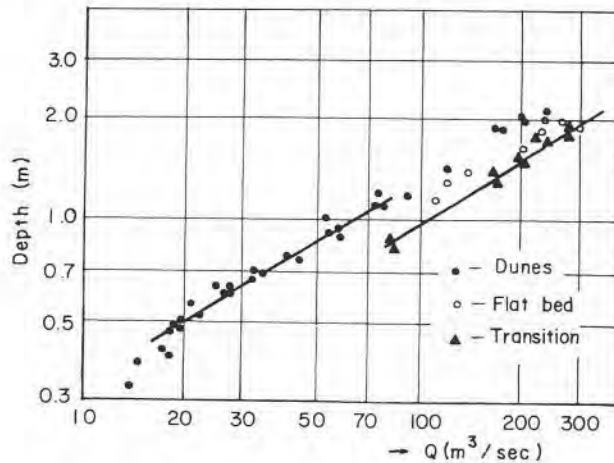


Fig. 7.11. Discharge rating curve for Elkhorn River, Nebraska, after [11].

So far influence of bed configuration on the roughness has been considered for a constant depth. It has been shown, however, both in laboratory studies [1] and field observations [11], that with slope and bed-material essentially constant, an increase in depth may cause the bed to change from dunes to antidunes or flat bed, and that a fall in depth may reverse the process. Accordingly, it is possible to obtain a considerable increase in discharge with no or very little change in depth (see for instance, Fig. 7.11). This is one of the reasons, among others, for the difficulty in deriving a reliable rating curve for alluvial streams.

Settling velocity of sediment particles and longitudinal slope also affect the friction factor due to bed configuration. For a given depth of flow and slope, settling velocity may be responsible to a great extent for the actual bed forms which are likely to develop. According to Sentürk [12], if the settling velocity increases, with all other parameters constant, the following effects may be expected:

1. For a dune bed, there will be an increase in resistance,
2. For a ripple bed, a decrease in resistance should be expected,
3. Ripple bed will tend to transform into dunes.

For dune beds prevalently composed of grains having settling velocity of more than about 6 cm/sec, an increase in slope is likely to increase the friction factor. If the settling velocity is less than about 6 cm/sec, at shallow depths a reduction of resistance should be expected, while at greater depths the influence is negligible.

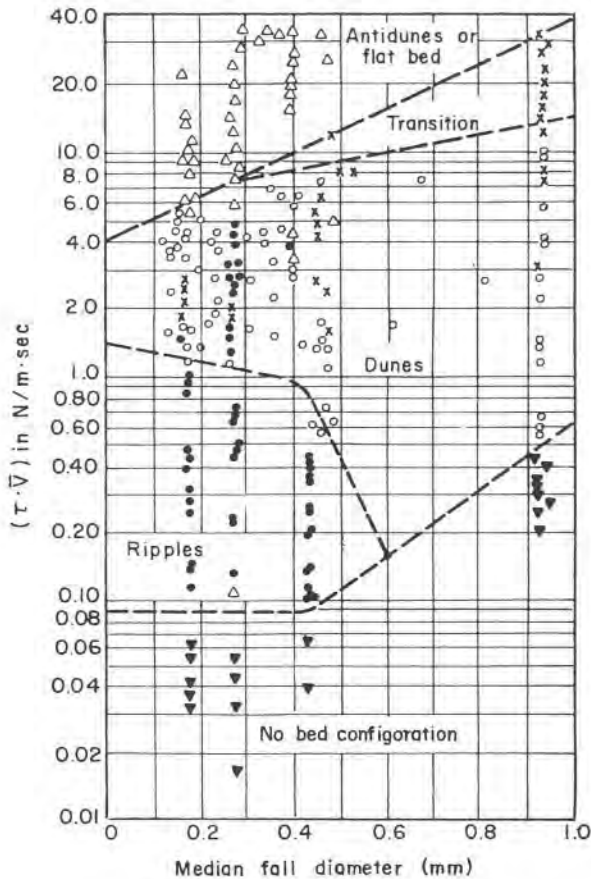


Fig. 7.12, Bed form in relation to stream and sediment properties, adapted from [16].
 Δ – no bed configuration; \bullet – ripples; \circ – dunes; Δ – antidunes or flat bed; \times – transition.

Prediction of bed configuration likely to be developed for a given set of data has been the object of many theoretical and experimental investigations. Purely theoretical approaches, [3, 13, 14, 15] among others, have up to now not yielded results in good agreement with laboratory experiments or field observations. Experimental approaches have given better results, [16, 17] among many others, although even these have considerable limitations and are not of general validity. As a representative sample of these empirical methods, Fig. 7.12 shows a graph proposed by Simons and Richardson

[16], based on data from laboratory flumes and field observations. The coordinates are the so-called *stream power* ($\tau\bar{V}$) – in which τ is the shear stress, defined by Eq. (3.1) – and \bar{V} is the mean velocity; and the *median fall diameter* – which is the equivalent diameter of a sphere having a specific gravity of 2.65, and the same terminal settling velocity as the median particle, in clear water at 24°C. It is claimed that the graph gives fairly good predictions for natural streams. Latest investigations, unfortunately, appear to indicate large deviations from predictions based on this graph.

In stream beds composed mainly of coarser grain fractions, as is often the case in mountain streams, it is generally assumed that no bed forms will occur if the particle Reynolds number $R_w = (w d_s / \nu) > 100$. For lower Reynolds numbers, bed configuration generally follows the concepts discussed so far. However, when R_w exceeds ~ 100 , friction factor cannot be determined from the Manning formula, but must be related to grain size and also to bed load transport [18]. Computation methods proposed by Shen [19] and Veiga de Cunha [20], though giving fairly good indication, have still not been experimentally confirmed.

It should finally be mentioned that in recent years the application of spectral or time-series analysis to the examination of sedimentary dunes (both in nature and in laboratory) has made considerable progress. Indeed, there seems to be a fairly good probability that through detailed and methodical analysis of the dune profiles and movement, better or improved parameters could eventually be developed for the prediction of the total sediment load in alluvial streams [21].

References

1. D.B. Simons and E.V. Richardson, Form of bed roughness in alluvial channels, Trans., ASCE, 87 (1961).
2. Task Committee, Nomenclature for bed forms in alluvial channels, Jour. Hydr. Div., ASCE, 92 (HY3) (1966).
3. J.F. Kennedy, The mechanics of dunes and antidunes in erodible-bed channels, Jour. of Fluid Mech., 16, part 4 (1963).
4. A.J. Raudkivi, Loose Boundary Hydraulics, chap. 12, Pergamon Press, London, 1966.
5. D.B. Simons and E.V. Richardson, Flow in alluvial channels, River Mechanics, Shen (ed.), vol. 1, Fort Collins, Colorado, 1971.
6. J.F. Kennedy, Stationary waves and antidunes in alluvial channels, Report no. KH-R-2, California Inst. of Technol., Pasadena, California, 1961.
7. H.A. Einstein and Barbarossa, River channel roughness, Trans. ASCE, 117 (1952).

8. V.A. Vanoni and N.H. Brooks, Laboratory studies of the roughness and suspended load of alluvial streams. California Inst. of Technol., Sed. Lab., Pasadena, Calif., 1957.
9. L. Bajorunas, Discussion of river channel roughness, by Einstein and Barbarossa, Trans. ASCE, 117 (1952).
10. F.M. Henderson, Open Channel Flow, Macmillan, New York, N.Y., 1966.
11. J.K. Culbertson and D.R. Dawdy, A study of fluvial characteristics and hydraulic variables, Middle Rio Grande, New Mexico, U.S. Geol. Survey Water Supply paper 1498-F, 1964.
12. F. Sentürk, Mechanics of Bed Formation, La Houille Blanche, 1967.
13. D.B. Simons, E.V. Richardson and C.F. Nordin, Unsteady movement of ripples and dunes related to bed load transport, IAHR Congress, Leningrad, 1965.
14. F. Engelund, Hydraulic resistance of alluvial channels, Jour. of Hydr. Div., ASCE, 92 (HY2) (1966).
15. A.G. Mercer, Analytically determined bed-form shape, technical note, Jour. of Eng. Mech. Div., ASCE, 97 (EM1) (1971).
16. D.B. Simons and E.V. Richardson, Resistance to flow in alluvial channels, U.S. Geol. Survey, Prof. paper 422-J, 1966.
17. J.L. Bogardi, Some recent advances in the theory of sediment movement, Hydr. Journal, 38 (1958).
18. H. Gladki, Resistance to flow in alluvial channels with coarse bed materials, Jour. Hydr. Res., IAHR 17 (2) (1979).
19. H.W. Shen, Development of roughness in alluvial channels, Jour. Hydr. Div., ASCE, 88 (HY3) (1962).
20. Veiga de Cunha, About the roughness in alluvial channels with comparatively coarse bed material, IAHR Congress, Colorado, vol. 1, 1967.
21. J.C. Willis and J.F. Kennedy, Sediment transport in migrating bed forms, proceedings, 26th Ann. Hydr. Div. Spec. Conference, University of Maryland, College Park, N.Y., ASCE, August 1978.
22. P. Engel, Length of flow separation over dunes, ASCE, Hydr. Div., 107 (HY10) (1981).

CHAPTER 8

TRANSPORTATION OF SUSPENDED SEDIMENT

Symbols

A_E	– dimensionless ratio, a/d
a	– distance of reference plane from the bed, m
b	– width of the channel, m
C	– suspended sediment concentration, ppm or kg/m^3
C_a	– suspended sediment concentration at reference level $y = a$ from the bed, ppm or kg/m^3
C_a^t	– partial suspended sediment concentration at reference level $y = a$ from the bed, ppm or kg/m^3
C_y	– suspended sediment concentration at distance y from the bed, ppm or kg/m^3
\bar{C}	– average volumetric concentration, ppm or kg/m^3
c	– local sediment concentration
d	– water depth, m
d_s	– grain diameter, m
\bar{d}_s	– mean grain diameter, m
g	– acceleration of gravity, m/sec^2
I	– longitudinal slope
I_1, I_2	– Einstein integral functions
J	– hydraulic gradient
K_s	– roughness height, m
M_{sed}	– rate of downward movement caused by gravity
M_{turb}	– rate of diffusion transport
n	– Manning roughness coefficient
Q_s	– total suspended sediment discharge, kg/sec
q	– specific water discharge, $\text{m}^3/\text{sec.m}$
q_s	– suspended load discharge, kg/sec.m
R	– hydraulic radius, m

R_b	– hydraulic radius with respect to the bed, m
R_w	– particle Reynolds number
S_s	– specific gravity of the sediment
S_f	– specific gravity of the fluid
u	– mean point velocity at distance y from the bed, m/sec
u_y	– instantaneous value of vertical component of turbulent fluctuation, m/sec
u_1, u_2	– point velocities at levels y_1 , and y_2 , m/sec
u_*	– shear velocity, m/sec
u'_*	– shear velocity due to grain roughness, m/sec
v	– point velocity, m/sec
\bar{V}	– average velocity in the vertical, m/sec
$V_{1.0}$	– sediment volume carried by unit volume of water, m ³ /sec
w	– settling velocity, m/sec
z	– exponent; coordinate
x	– coordinate; correction factor
y	– coordinate; unspecified depth
y'	– dimensionless ratio y/d
β	– coefficient of proportionality
δ	– thickness of laminar sublayer, m
ϵ	– kinematic eddy viscosity
κ	– von Karman universal constant
ν	– kinematic viscosity of water, m ² /sec
ρ	– density of water, kg/m ³
ρ_s	– density of solids, kg/m ³
τ	– bed shear stress, N/m ²
ϕ	– coefficient

8.1 Introduction

In the last two chapters in Part 2 of the present text, some of the analytical or semi-analytical methods will be discussed which try to quantitatively predict sediment discharge for a specific set of measurable data. These predictions, as many hydraulic engineers have with sorrow experienced, are far from being accurate, and sometimes far off the target. It has already been repeatedly shown that natural phenomena connected with sediment transport are a continuously changing process of mutual interaction and adaptation, of immense complexity. All analytical methods are conceptual models which necessarily try to reduce the bewildering array of variables to some practically acceptable number. Empirical coefficients they often include

cannot embrace all possible combinations of physical factors met with in nature, and hence they lack the general validity to cover all engineering cases. The final test of any equation, or set of equations, is the agreement with field measurements or laboratory experiments. At the design stage, before the change in channel alignment or flow conditions have been carried out, no direct measurement of results is possible, and therefore some understanding of the transportation mechanism is indispensable. Here analytical methods, with all their shortcomings, are nevertheless of invaluable help to the design engineer. To quote Einstein [1] : “the analytical method may not be very accurate, but it has the great advantage that it allows us to predict a result which must be expected under conditions that are not yet realized.”

8.2 Some Preliminary Definitions

The division of the *total sediment load* carried by a stream into distinctive constituent parts has already been briefly mentioned in par. 2.5 of Part 1, in which sampling methods were discussed. Setting-up of physical models for sediment transport mechanisms has inevitably required a suitable division of sediment load to match these models.

The division as given in this text is the one generally followed in the literature on sediment engineering, and though its definition leaves many aspects rather vague and unsatisfactory, it has at least the advantage of being relatively simple compared to any other more complicated subdivisions. A part of sediment particles carried by a stream move along the bed or close to it, by rolling, jumping or sliding; this material is called the *bed load*. The rest of the particles are carried away from the bed, and are kept in suspension by the upward component of turbulent velocities, while being swept along by the current; this part is called the *suspended load*. In the region near the bed this division fails to give clear-cut distinction, since a particle that at one moment moves along the bed may a short while later be entrained into suspension, and vice versa. Vanoni et al. [2] state: “The two terms (bed load and suspended load) are used for convenience in discussing transportation, but actually have no other use.” U.S. Inter-Agency Committee on Water Resources [3] has defined the suspended sediment as the part “that is supported by the upward components of turbulence currents and that stays in suspension for appreciable lengths of time”; this definition is no less vague than the previous one, although it tries to exclude from the suspended load particles near the bed, entrained into suspension only for short periods of time, Fig. 8.1.

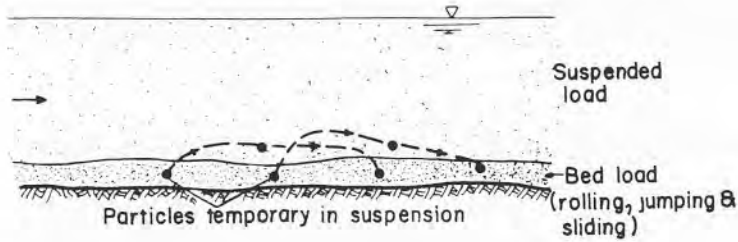


Fig. 8.1. Sediment load according to mode of transport.

When particle size is taken as the characteristic parameter, sediment load of a stream can be divided into the *wash load*, which comprises finer fractions found only in negligible quantities on the bed; and *bed-material load*, which consists of larger particles, found prevalently on the bed. The wash load is carried almost entirely in suspension, and it is generally accepted that it is mainly related to watershed and rainfall characteristics, and only marginally to water depth or velocity.

The sum of either the suspended load and bed load, or of the wash load and bed-material load, constitutes the *total load* of the stream. A schematic sketch of the above division is outlined in Fig. 8.1a.

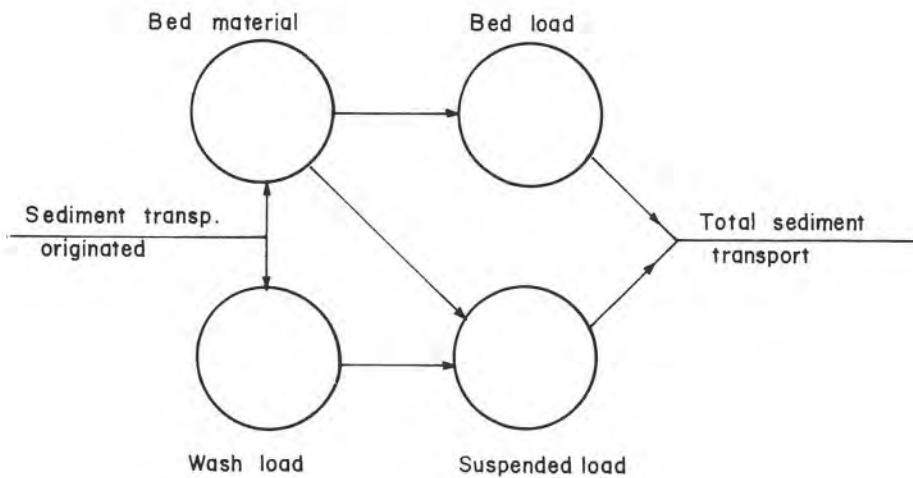


Fig. 8.1a. Schematic division of total sediment transport.

According to [3], bed load should be further subdivided into *saltation load* and *contact load*, but the definitions of these two subdivisions are not generally accepted.

As mentioned before, the origin of the wash load is mainly in the watershed area; its quality depends on the physical properties of the watershed soil particles, such as size, specific gravity, settling velocity, resistance to wear, cohesion etc. Most of the organic matter found in a stream normally also is carried as wash load. Einstein writes in respect of the wash load that in "most streams the finer part of the load, i.e. the part which the flow can easily carry in large quantities, is limited by its availability in the watershed; this part of the load is designated as wash load."

Rate of movement of the coarser part of the load, on the other hand, is essentially controlled by the STC (Sediment Transport Capacity) of the watercourse, and this is determined by the geometric properties of the stream channel on the one hand, and by hydraulic properties of the flow, such as discharge, velocity distribution, tractive force, longitudinal slope, roughness, etc., on the other hand.

As a matter of fact, there is no definite separation line between the wash load and bed-material load, since this depends on the characteristics of a specific channel and its contributing watershed. Nevertheless, some engineers have a rough criterion, by which particles larger than about 0.06 mm belong to the bed-material load (roughly the separation point between sand silt). There are, however, notable exceptions to such a simplified rule-of-thumb, as for instance in many desert streams where the bed is mainly composed of loess particles, generally much finer than 0.06 mm. Generally, only a very small part of the wash load is deposited along the channel, hence its part in the bed-material load is only fractional.

8.3 Suspended Load Mechanism

One part of the total load of a stream is carried in suspension. Gravitational field causes the suspended particles to constantly fall towards the channel bottom, but this is being continuously balanced by the upward turbulence velocity components. Hence, no suspension of sediment is possible without the turbulence of the flow.

No historical review of the many theories concerning sediment suspension will be attempted here. Most of the earlier theories anyway do not conform to our present understanding of fluid dynamics. The two most representative theoretical approaches to suspended sediment movement under equilibrium conditions are the *diffusion theory* and *energy theory*. Only the former will

be more extensively treated in the present text, because its predictions generally agree much better with the observed results, both in natural water-courses and laboratory flumes.

Let us consider an elementary area in a two-dimensional turbulent flow parallel to the bed (x -axis), see Fig. 8.2. The mean velocity at a distance y above the bed is u , while u_y is the instantaneous value of the vertical component of the turbulent fluctuation. This vertical velocity fluctuation changes continuously, both in magnitude and direction. If there is no net flow in any direction, the mean value of u_y over a given interval of time must be zero, or in other words, the net volume of flow across the elementary area in plus and minus directions must be equal. On the other hand, sediment concentration C above the elementary area is less than below it (see Fig. 8.2b). Hence, though there is no net liquid flow across the area ($dx \cdot dz$), there will be a net sediment flow in the upward direction, due to the difference in sediment concentration.

The rate of this upward turbulent diffusion transport per unit area is given by

$$M_{\text{turb}} = \beta \epsilon \frac{dc}{dy} \quad (8.1)$$

in which M_{turb} – rate of diffusion transport, β – coefficient of proportionality, ϵ – *kinematic eddy viscosity* (comparable to the kinematic molecular viscosity ν , and dependent upon the density, velocity and size of the turbulent eddies), c – local sediment concentration.

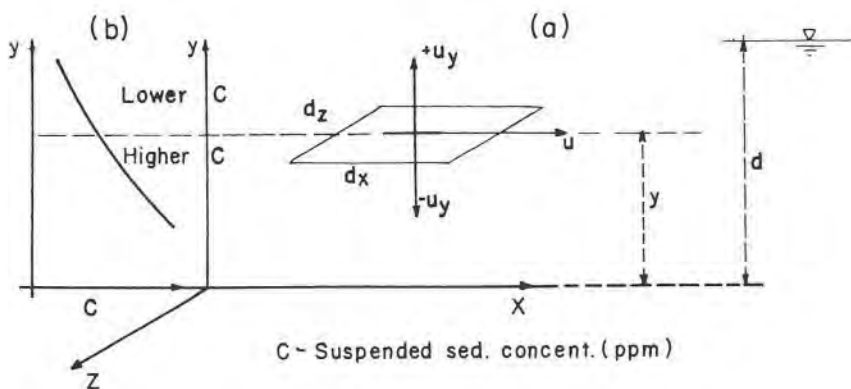


Fig. 8.2. Turbulent fluctuation of sediment-laden stream.

Under equilibrium conditions, this net upward movement of sediment due to the turbulent diffusion process must be balanced by the downward movement per unit area caused by the force of gravity, equal to

$$M_{\text{sed}} = -c w \quad (8.2)$$

where w stands for the settling velocity of sediment grains.

Hence, setting the two sediment rates of flow equal,

$$c w + \beta \epsilon \frac{dc}{dy} = 0 \quad (8.3)$$

If it is further assumed that Prandtl-von Karman relationship for velocity distribution (see Ch. 5 of Part 2) is valid for sediment-bearing flows also, the kinematic eddy viscosity can be expressed in terms of the shear velocity u_* and the relative depth y/d (see for instance [5]):

$$\epsilon = \kappa u_* y \left[1 - \frac{y}{d} \right] \quad (8.4)$$

in which κ is the von Karman universal constant.

Substituting Eq. (8.4) into Eq. (8.3) and integrating, an expression for the relative distribution of sediment concentration in a two-dimensional steady uniform flow can be obtained,

$$\frac{C}{C_a} = \left[\frac{d-y}{y} \frac{a}{d-a} \right]^z \quad (8.5)$$

in which C_a – sediment concentration at some reference level $y = a$ from the bed and

$$z = \frac{w}{\beta \kappa u_*} \quad (8.6)$$

Eq. (8.5) was first presented by Rouse [6]. The equation is applicable to the sediment fraction having the mean settling velocity w . Several Russian researchers, as for instance, Makkaveev, Karaushev and others, have later derived similar expressions for the relative suspended-sediment concentrations, but their basic assumptions for the vertical velocity distribution are not in agreement with our present-day notions. In Fig. 8.3 a graph is pre-

sented showing a family of curves obtained solving Eq. (8.5) for various values of z , and with the reference level at $a = 0.03 d$. The assumption of a reference plane at distance a from the bottom is necessary, because otherwise the concentration at the bottom would result infinite. Each curve gives the relative concentration of suspended sediment for a different value of z , as function of the ratio $(y-a)/(d-a)$. It can easily be inferred from the graph that for large values of z , the suspended sediment tends to be concentrated near the bed, while at lower z -values the suspension tends to be uniformly distributed. For a given flow, the denominator in Eq. (8.6) is constant, and hence the quantitative value of z depends on the numerator, i.e. settling velocity w . Accordingly, coarser particles will mainly be found near the bed, whereas finer fractions will be more or less evenly distributed. On the other hand, taking a sediment fraction with a given mean settling velocity w , the value of z , and hence the pattern of suspension distribution, depends on the shear velocity u_* , i.e. bed shear stress τ ; higher shear stress yields lower z -values, meaning uniform distribution, and lower shear stress gives higher values of z , hence distribution less uniform. Vanoni [2] appropriately suggests that in fact the term u_* in the denominator of Eq. (8.6) is a measure of

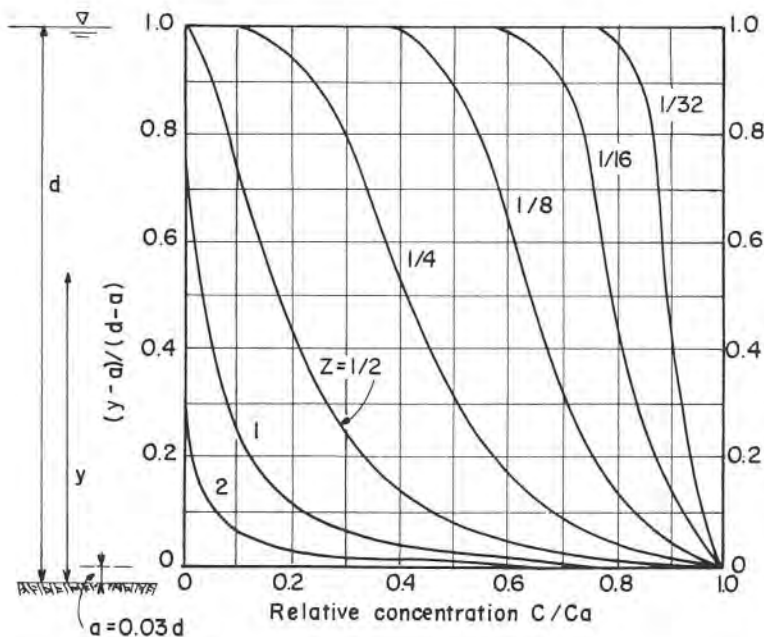


Fig. 8.3. Suspended-sediment distribution according to Eq. (8.5).

the transporting capacity of the stream, since large shear stresses ($\tau \cong \gamma dJ$) are associated with deep and steep streams, of high STC. On the other hand, $z \propto (w/u_*)$ may be seen as a measure of the relative energy a stream must employ in order to transport in suspension sediment having settling velocity w .

Since the wash load consists mainly of small particles, it generally is associated with low z -values, and hence is uniformly distributed over the whole cross section of the flow.

Some comment is due on the two coefficients β and κ in the denominator of Eq. (8.6). In many preliminary calculations it is customary to assume $\kappa = 0.4$, the value for clear water. However, it has been shown in Chap. 5 that for sediment-bearing streams this coefficient apparently tends to be lower. As to the coefficient β , which expresses the relationship between the diffusion coefficient and kinematic eddy viscosity, it is generally assumed to be unity. There is sufficient experimental evidence, for instance [7–9] among others, that for finer particles, $\beta \cong 1$ is a good approximation, while for coarser particles, β tends to be less than unity. Einstein and Chien [7] have tried to give a graph for determination of β -values for coarse sediment, but the scatter of measured values (mainly flume studies) is very large.

As to the general agreement of Eq. (8.5) with observed suspended-sediment distributions in both laboratory flumes and natural streams, Vanoni et al. [2] have reported that it was fairly good. z -values were checked by plotting measured concentration C -values against $d^{-\gamma}/y$; on logarithmic paper, Eq. (8.5) plots as a straight line, with slope proportional to z . For a given size fraction, the actual sediment concentrations are measured at several depths and plotted on the logarithmic paper.

Determination of z -values for streams where no concentration measurements are available is rather difficult and often not very reliable. In order to obtain more realistic values, the influence of sediment concentration on w and κ must be estimated. Ways evaluating this influence have been discussed in the foregoing chapters, but the reference concentration has to be assumed beforehand in any case. It is appropriate to again quote Vanoni et al. [2]: “. . . In view of the imperfect state of theories of sediment suspension, the prediction of the distribution of sediment in a flow must continue to involve the exercise of judgement and the result can only be considered an estimate”; although written about twenty years ago, it still rings true today.

On the other hand, knowledge of the z -value for a stream may give the engineer an insight into its sediment-carrying character; indeed, it can easily be inferred from Fig. 8.3 that a stream with higher z -value (say, about 2 or more) will carry its suspended load mainly in the lower layers. If there are no appreciable amounts of wash load, the water will appear clear. In the

opposite case of lower z -values, the water should be expected to appear dirty.

Kalinske et al. [13] have derived an expression similar to Eq. (8.5), also based on the diffusion theory, but assuming that the diffusion coefficient is a constant. Recent experimental and theoretical evidence seems to indicate, furthermore, that the exponent of the term $(d-\gamma)/\gamma$ in Eq. (8.5) should not always be unity, but generally $(1 + \phi)$, in which $\phi \geq 0$ [22]. Hence, Eq. (8.5) should be a particular case for which $\phi = 0$. Some experimental values for the coefficient ϕ are given, but for the time being the interesting fact is that the Eq. (8.5) should probably be more complicated than it actually is.

8.4 Suspended Sediment Discharge

It has already been emphasized that the suspended sediment load, i.e. that part of the total stream load that is carried in suspension, is actually composed of two distinct parts: 1) particles kept in suspension by the stream, and which in fact are part of the bed-material, and 2) fine silt particles, originating from the watershed, which form the wash load. The transport rate of the wash load is in fact determined only by the available upstream supply rate, and its fine silt particles can be found in the bed-material in negligible quantities only. An additional reason for the scarcity of fine particles (silt and clay) in the bed is the fact that for these particles the settling velocity w is proportional to the square of the diameter d_s (see Eq. 6.10), whereas for larger particles it is proportional to the square root of d_s (see Eq. 6.14). Hence, velocities of flow required to remove silt and clay particles are much smaller than those needed for sand particles. Because of the different origins of the suspended load, the total transporting capacity of a stream is often much larger than the actual transport. It should, however, be pointed out that the relationships developed for the suspended-sediment concentration, and for the rate of transport, to be discussed in the following, refer only to the bed-material and not to the wash load.

Due to the decreasing longitudinal slope of a stream entering into the coastal lowlands, and hence diminishing velocity and turbulence, the main part of the suspended load is eventually carried off to the sea, or deposited on the flood plains. There is, however, a general tendency for deposition of larger suspended particles while going downstream. Thus a part of the suspended load is being transferred to the bed-material, and this contributes to the decrease, in the downstream direction, of the mean grain size found in the bed load.

The amount of suspended sediment transported by natural streams is

generally high; it is usually larger than that of the bed load, and in some cases even much larger.

In order to compute the suspended load discharge of a stream, partial volumes of water and sediment passing unit areas 1.0 m wide and dy high, Fig. 8.4, per unit time, have to be summed up. In other words, the unit suspended-sediment discharge is given by

$$q_s = \int_a^d c v dy \quad (8.7)$$

If logarithmic velocity distribution is assumed, local velocity v at any depth y can be obtained from Eq. (5.9); suspended-sediment concentration can be found using Eq. (8.5). After substituting these two equations into Eq. (8.7), the integration can be carried out. Unfortunately, even then the integral cannot be evaluated unless there is either quantitative information about the reference concentration C_a , or some estimate is made about it. Unlike flume experiments, natural stream sediment is graded over many size fractions, and hence the integration has to be carried out for each fraction separately, and subsequently summed up.

Several methods have been proposed in order to overcome the difficulties arising from the evaluation of the integral given by Eq. (8.7), as for instance those given in [10–12], among others. In the following only Einstein's approach [10] will be dealt with in some detail, since it is today the most widely used method to estimate suspended sediment load when no reliable measurement data are available.

The integration of Eq. (8.7) is carried out using several simplifying assumptions. Coefficient β has been assumed to be $\beta = 1$ and Prandtl's con-

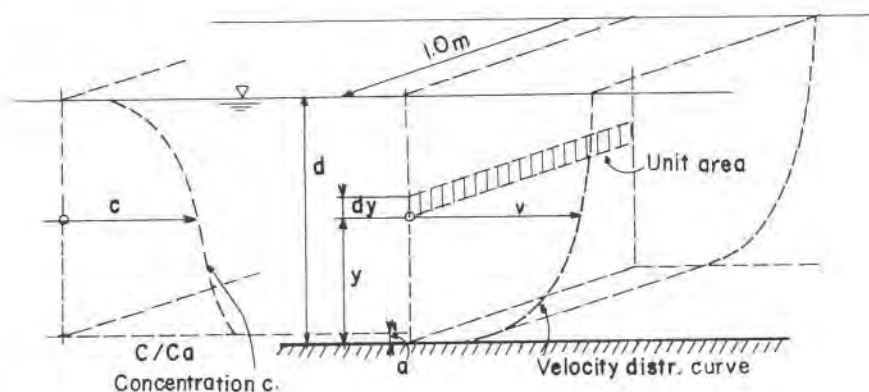


Fig. 8.4. Suspended-sediment discharge computation.

stant $\kappa = 0.4$, as for clear water. Shear velocity u_* has further been replaced by the shear velocity due to the grain roughness $u_*' = (gR_b J)^{1/2}$, in which R_b denotes the bed hydraulic radius (see Chap. 7). With these assumptions, Eq. (8.6) reduces to

$$z = \frac{w}{0.4 u_*'} \quad (8.8)$$

Substituting now Eq. (8.5) for sediment concentration, and Eq. (5.11) for logarithmic velocity distribution, Eq. (8.7) can be written,

$$q_s = \int_a^d C_a \left[\frac{d-y}{y} \frac{a}{d-a} \right]^z 5.75 u_*' \log \left[30.2 \frac{y}{K_s} x \right] dy \quad (8.9)$$

Here q_s denotes the suspended-load transport rate in weight per unit time and unit width. Further, C_a denotes suspended sediment concentration at the reference-level distance a from the bed, K_s the roughness diameter, and x the logarithmic velocity-distribution correction factor. Introducing also dimensionless ratios $A_E = a/d$ and $y' = y/d$, Eq. (8.7) becomes:

$$q_s = \int_{A_E}^1 v \cdot C \cdot dy' \quad (8.10)$$

and finally,

$$q_s = 5.75 C_a u_*' d \left[\frac{A_E}{1-A_E} \right]^z \left[\log \left[\frac{30.2 d}{K_s} x \right] \int_{A_E}^1 \left[\frac{1-y'}{y'} \right]^z dy' + 0.434 \int_{A_E}^1 \left[\frac{1-y'}{y'} \right]^z \ln y' dy' \right] \quad (8.11)$$

Integration of the above equation in the closed form proved to be impossible, hence Einstein's transformed Eq. (8.11) into a form more amenable to numerical integration,

$$q_s = 11.6 u_*' C_a a \left[2.303 \log \left[\frac{30.2 d}{K_s} x \right] I_1 + I_2 \right] \quad (8.12)$$

in which

$$I_1 = 0.216 \frac{A_E^{(z-1)}}{(1-A_E)^z} \int_{A_E}^1 \left[\frac{1-y}{y} \right]^z dy \quad (8.13)$$

$$I_2 = 0.216 \frac{A_E^{(z-1)}}{(1-A_E)^z} \int_{A_E}^1 \left[\frac{1-y}{y} \right]^z \ln y dy \quad (8.14)$$

Results of the numerical integration of functions I_1 and I_2 according to Einstein for various values of A_E and z are given in Fig. 8.11 and Fig. 8.12.

Einstein further assumed that the thickness of the bed layer, which supplies all the material carried in suspension, is $a = 2d_s$, where d_s is the representative grain size of the bed material. Within this layer, no suspension of material is possible.

In continuation of his bed-load theory, which will be discussed in the next chapter, Einstein also developed a relationship between bed-load transport and suspended-load transport for all grain-size fractions for which a bed-load function exists. This relationship will also be given in the next chapter.

Example 8.1 (taken from [2])

Table 8.1 below gives velocity distribution and suspended sand distribution for the fraction of the material passing the 0.105 mm sieve and retained on the 0.074 mm sieve at the measuring vertical C-3 on the Missouri River at Omaha on 4.11.1952. On this day the slope of the stream was 0.00012, depth was 2.4 m, width was 245 m, water temperature 7°C, and the flow was approximately uniform. Specific gravity of the sediment = 2.65.

Required:

a) Plot the velocity profile on semilogarithmic graph paper (v vs. $\log y$) and concentration profile on log-log paper (c vs. $(d-y)/y$). Draw straight lines giving the best fit to the plotted points.

b) Estimate from the data given and your graphs the following values:

u_* — shear velocity

\bar{V} — mean velocity (at vertical C-3)

κ — von Karman constant

n — Manning friction factor

z — exponent of suspended-load equation from the graph

z — $w/\kappa u_*$

c) Estimate the rate of transport of this particular size fraction of sand in Newtons per second per meter.

TABLE 8.1. DATA FOR EXAMPLE 8.1

Distance up from bottom y (m)	Velocity v (m/sec)	Concentration (in size fraction 0.074 – 0.105 mm) (ppm)
0.21	1.31	411
0.27	1.37	380
0.37	1.41	305
0.43	1.45	299
0.52	1.47	277
0.67	1.56	238
0.80	1.62	217
0.88	1.65	—
0.98	1.65	196
1.04	1.65	—
1.13	1.68	184
1.28	1.71	—
1.46	1.71	148
1.77	1.74	130
2.07	1.81	—
2.40	—	—

Solution

Step 1 – The graph of the velocity profile is drawn in Fig. 8.5, and the graph of C vs. $(d-y)/y$ in Fig. 8.6.

Step 2 – Shear velocity is given by

$$u_* = (gRJ)^{1/2} \cong (gdJ)^{1/2} = (9.8 \times 2.4 \times 0.00012)^{1/2}; \quad u_* = 0.053 \text{ m/sec}$$

Step 3 – Next the mean velocity is computed. The data were taken from the graph on Fig. 8.5, but they could also be directly calculated from the data given in Table 8.1. Results are summarized in Table 8.2. From here the mean velocity – $\bar{V} = (3.077/1.87) = 1.64 \text{ m/sec}$.

Step 4 – Von Karman constant. For the determination of the constant κ , it is convenient to use the equation for velocity distribution developed by Brooks [18] from Eq. (5.3),

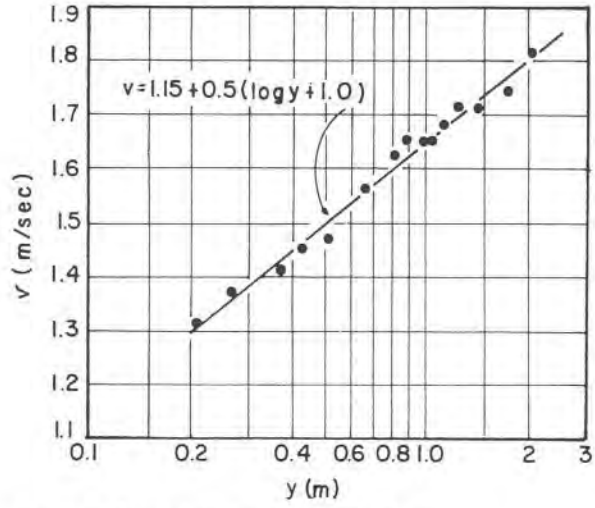


Fig. 8.5. Graph of v vs. $\log y$ (Ex. 8.1).

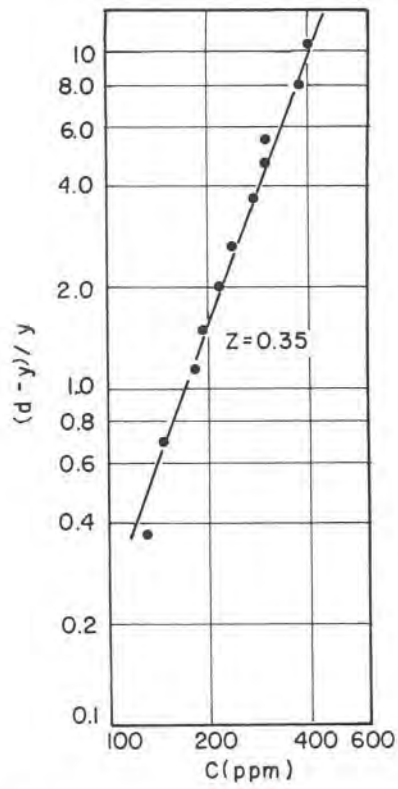


Fig. 8.6. Concentration C vs. $(d-y)/y$.

TABLE 8.2. SUMMARY OF RESULTS (Ex. 8.1).

Partial range (m)	Δy (m)	\bar{v} (m/sec)	$\bar{v} \cdot \Delta y$
0.2–0.4	0.2	1.39	0.278
0.4–0.6	0.2	1.50	0.300
0.6–0.8	0.2	1.57	0.314
0.8–1.0	0.2	1.62	0.324
1.0–1.2	0.2	1.67	0.334
1.2–1.4	0.2	1.71	0.342
1.4–1.6	0.2	1.74	0.348
1.6–1.8	0.2	1.76	0.352
1.8–2.07	0.27	1.79	0.485
Σ	1.87		3.077

$$u = \bar{V} + \frac{1}{\kappa} u_* (1 + 2.3 \log (y/d)) \quad (8.15)$$

in which \bar{V} denotes the average velocity in the vertical. From Eq. (8.15) it is possible to write

$$u_2 - u_1 = \frac{2.3}{\kappa} u_* \log \frac{y_2}{y_1} \quad (8.16)$$

Here u_1 and u_2 are velocities at levels y_1 and y_2 above the bottom. Hence, κ can easily be calculated from a pair of points taken from the velocity profile, Fig. 8.5.

The two points chosen are:

$$y_1 = 2.0 \text{ m} - u_1 = 1.8 \text{ m/sec}$$

$$y_2 = 0.3 \text{ m} - u_2 = 1.5 \text{ m/sec}$$

Accordingly, by applying Eq. (8.16),

$$1.8 - 1.5 = \frac{2.3}{\kappa} 0.053 \log \frac{2.0}{0.3}$$

and from here, $\kappa \cong 0.33$.

Step 5 – Manning coefficient. Making use of Eq. (5.12a),

$$n \cong \frac{R^{1/6}}{18 \log(12.27(R/K_s))}$$

in which for large channels depth d may be substituted for R . For K_s let us use the geometric mean grain size,

$$K_s \cong (0.074 \times 0.105)^{1/2} = 0.088 \text{ mm}$$

Hence,

$$n = \frac{2.4^{1/6}}{18 \log(12.27(2.4/0.00088))} \cong 0.0116$$

Step 6 – Exponent z . The slope of the best-fit line on the graph in Fig. 8.6 has been measured to be about $z \cong 0.35$.

In order to evaluate z analytically, settling velocity has to be determined first. Kinematic viscosity of water for 7°C is about $1.45 \times 10^{-6} \text{ m}^2/\text{sec}$. Settling velocity is in the Stokes range, hence applying Eq. (6.10),

$$w = \frac{1}{18} \left[\frac{S_s}{S_f} - 1 \right] \frac{g d_s^2}{\nu} = \frac{1}{18} \cdot 1.65 \cdot \frac{9.8 (8.8 \cdot 10^{-5})^2}{1.45 \cdot 10^{-6}} ; w = 0.0048 \text{ m/sec}$$

$$R_w = \frac{w \cdot d_s}{\nu} = \frac{0.0048 \times (8.8 \times 10^{-5})}{1.45 \cdot 10^{-6}} = 0.29$$

Finally,

$$z = \frac{w}{\kappa u_*} = \frac{0.0048}{0.33 \times 0.053} = 0.27$$

This value for z is about 25% lower than the value derived from the slope of the line on the graph of Fig. 8.6. Full agreement could hardly be expected, but in the present case a considerable part of the discrepancy should probably be attributed to the inaccuracy of the graphical method on a small-scale drawing.

Step 7 – Estimate of the rate of transport. Rate of transport in kilograms per second per meter has been calculated by approximate integration of the product ($c \cdot v$) across the effective depth of the stream per unit width. Numerical integration has been carried out in both tabular and graphical way.

Table 8.3 summarizes the data for the numerical integration. In this table: 1 – partial range of water depth in meters; 2 – average sediment concentration \bar{C} in kg/m^3 (taken from Table 8.1); 3 – average velocity \bar{v} for the chosen range, in m/sec (from Table 8.1); 4 – product ($\bar{C} \cdot \bar{v}$) in $\text{kg}/\text{sec} \cdot \text{m}^2$; 5 – extension of the range, Δy , in meters; 6 – partial sediment discharge for the range, $\Delta Q = (\bar{C} \cdot \bar{v}) \cdot \Delta y$ in $\text{kg}/\text{sec} \cdot \text{m}$.

Suspended sediment discharge for the given fraction and unity of width (1.0 m) results as $Q = \Sigma \Delta Q = 0.511 \text{ kg}/\text{sec} \cdot \text{m}$. Graphical integration is shown in Fig. 8.7, which is self-explanatory. All the data for the graph are taken from Table 8.3. Total discharge, equal to the area under the graph of ($\bar{C} \cdot \bar{v}$) vs. y , has been measured as $A = 0.516 \text{ kg}/\text{sec} \cdot \text{m}$. It is almost identical with the tabular integration.

Example 8.2

The following data are available for a natural watercourse:

1. Width of the channel, $b = 100 \text{ m}$,
2. Water stage, $d = 3.0 \text{ m}$,
3. Longitudinal slope, $I = 0.001$,

TABLE 8.3. DATA FOR NUMERICAL INTEGRATION (Ex. 8.1)

1	2	3	4	5	6
0.21–0.37	0.351	1.36	0.477	0.16	0.076
0.37–0.52	0.285	1.44	0.410	0.15	0.062
0.52–0.80	0.242	1.54	0.373	0.28	0.104
0.80–0.98	0.202	1.63	0.329	0.18	0.059
0.98–1.13	0.186	1.66	0.309	0.15	0.046
1.13–1.46	0.162	1.70	0.275	0.33	0.091
1.46–1.77	0.136	1.73	0.235	0.31	0.073
			Σ	1.56	0.511

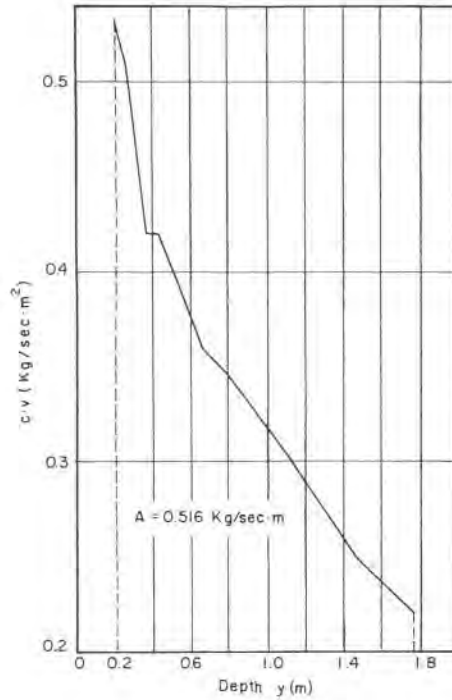


Fig. 8.7. Graphical integration of suspended-sediment discharge (Ex. 8.1)

4. Water temperature: 20°C ,
5. Sediment concentration measured at height of $a = 10$ cm above the bottom, $C_a = 40$ kg/m^3 , this concentration is assumed to be the maximum for the suspended load,
6. Grain size distribution of the sediment material is given in Fig. 8.8.
7. Specific gravity of the sediment, $S = 2.65$.

Required:

1. Estimate the suspended-sediment distribution in the vertical for the fraction 0.3 $\text{mm} < d_s < 0.5$ mm .
2. Estimate the suspended-sediment discharge for the same fraction and for unit width of the stream.
3. Estimate the total suspended-sediment discharge for unit width.
4. Estimate the average suspended-sediment concentration in relation to the water discharge.

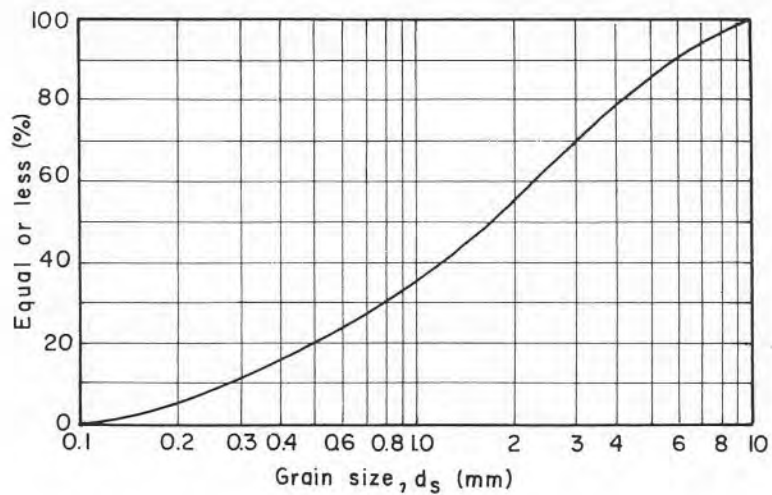


Fig. 8.8. Grain-size distribution for Example 8.1.

Solution

Step 1 – Geometric mean sieve diameter for the fraction $0.3 < d_s < 0.5$

$$\bar{d}_s = (0.3 \times 0.5)^{1/2} = 0.39 \text{ mm}$$

Step 2 – Neglecting the effect of the sediment concentration upon the motion of particles, settling velocity can be directly found from the graph on Fig. 6.3. $w \cong 6 \text{ cm/sec}$.

Step 3 – Grain shear velocity – $u'_* = (gR_bJ)^{1/2}$.

Since the given watercourse is large, effect of channel banks is small, and may be neglected; hence, $R_b \cong R \cong d = 3.0 \text{ m}$.

$$u'_* \cong (gRJ)^{1/2} = (9.8 \times 3.0 \times 0.001)^{1/2} = 0.17 \text{ m/sec}$$

Step 4 – Exponent z –

$$z = \frac{w}{0.4 u'_*} = \frac{0.06}{0.4 \times 0.17} = 0.88$$

Step 5 – Total suspended-sediment concentration as measured $C_a = 40$ kg/m^3 . The given fraction constitutes about 9% of the total (from 11% to 20%, see Fig. 8.8). Hence, the partial concentration referring to the given fraction, $C'_a \cong 0.09 \times 40 = 3.6$ kg/m^3 .

Step 6 – In order to illustrate the procedure of calculation for the vertical sediment distribution, let us compute the estimated concentration at $y = 2.0$ m, using Eq. (8.5).

$$C_y = C_a \left[\frac{d-y}{y} \cdot \frac{a}{d-a} \right]^2$$

$$C_{2.0} = 3.6 \left[\frac{3-2}{2} \cdot \frac{0.1}{3-0.1} \right]^{0.88} = 0.1 \text{ kg/m}^3$$

Step 7 – In Table 8.4 are given concentration values as computed in a similar manner for other values of y , and in Fig. 8.9 a graphical profile of the concentration distribution for the given fraction is shown.

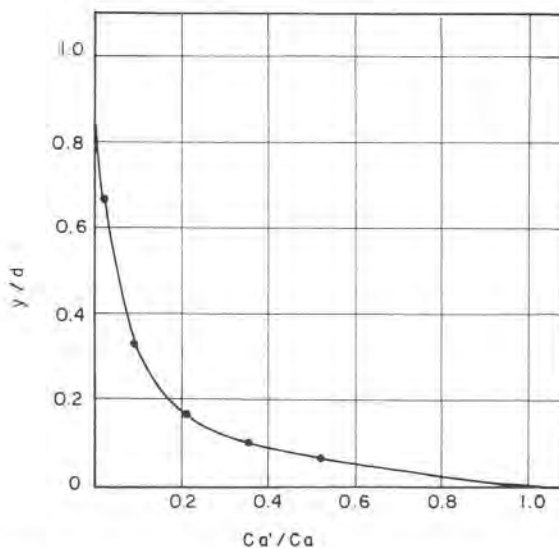


Fig. 8.9. Vertical suspended-sediment distribution for the fraction $0.3 < d_s < 0.5$ (Ex. 8.2).

TABLE 8.4. CONCENTRATION VALUES (Ex. 8.2)

y (m)	y/d	C_y	C_y/C_a
0.2	0.067	1.89	0.525
0.3	0.100	1.28	0.355
0.5	0.167	0.77	0.214
1.0	0.333	0.34	0.094
2.0	0.670	0.1	0.028
3.0	1.0	0	0

In order to compute the estimated suspended-sediment discharge for the given fraction, some additional values have first to be found.

Step 8 – Kinematic viscosity for clear water at the temperature of 20°C, from Table 6.1, is $\nu \cong 1.0 \times 10^{-6}$ m²/sec.

Step 9 – Thickness of the laminar sublayer can be estimated using Eq. (5.15),

$$\delta \cong 11.6 \frac{\nu}{u_*'} = 11.6 \frac{10^{-6}}{0.17} \cong 7 \times 10^{-5} \text{ m}$$

Step 10 – Roughness height $K_s \cong d_{s_{65}} \cong 2.8$ mm. Parameter $K_s/\delta = (2.8 \times 10^{-3})/(7 \times 10^{-5}) \cong 40$.

From Fig. 5.3, the correction factor for the above value of the parameter K_s/δ is found to be $x \cong 1.0$.

Step 11 – Now the suspended-sediment discharge for the given fraction can be computed using Eq. (8.12).

$$q_s = 11.6 u_*' C_a \cdot a \left[2.303 \left[\log \frac{30.2 \cdot d}{K_s} \cdot x \right] I_1 + I_2 \right]$$

$$\text{Parameter } A_E = \frac{a}{d} = \frac{0.1}{3.0} = 0.033$$

From the graphs on Figs. 11 and 12, functions I_1 and I_2 for $z = 0.88$ are found to be $I_1 = 0.68$, $I_2 = -1.50$. Hence, from Eq. (8.12)

$$q_s = 11.6 \times 0.17 \times 3.6 \times 0.1 \left[2.303 \log \left[\frac{30.2 \cdot 3.0}{0.0028} \cdot 1.0 \right] 0.68 - 1.50 \right]$$

$$q_s = 0.71 (7.06 - 1.50) = 3.95 \text{ kg/sec.m}$$

Step 12 – Similar computations have been carried out for all the other fractions composing the sample shown on Fig. 8.5. Results of these computations are summarized in Table 8.5.

Values of functions I_1 and I_2 marked with asterisk have been estimated by extrapolation, since the highest z -value for which these functions have been numerically evaluated is 5.0. Contribution of fractions with z -values higher than 5.0 to the overall suspended-sediment discharge is negligible, but here the computation had been intentionally carried further in order to emphasize this point. Indeed, the contribution in the present case of the last two large fractions, transported mainly as bed load, is in fact negligible: about 2% of the total discharge.

The total estimated suspended-sediment discharge per unit width of the stream is $\Sigma q_s = 32.4 \text{ kg/sec.m}$. The total estimated discharge for the whole stream is $Q_s = \Sigma q_s \cdot b = 32.4 \times 100 = 3240 \text{ kg/sec}$.

TABLE 8.5. SUMMARY OF COMPUTATIONS (Ex. 8.2)

Fraction	\bar{d}_s (mm)	w cm/sec	z	C'_a (%)	C'_a (kg/m ³)	I_1	I_2	q_s (kg/sec.m)
0.1–0.3	0.17	1.54	0.23	11	4.4	3.000	–3.500	24.0
0.3–0.5	0.39	6.0	0.88	9	3.6	0.680	–1.500	4.0
0.5–1.0	0.71	11.0	1.62	15	6.0	0.255	–0.630	2.4
1.0–2.0	1.40	23.0	3.38	20	8.0	0.093	–0.250	1.1
2.0–3.0	2.50	34.0	5.00	15	6.0	0.051	–0.160	0.4
3.0–5.0	3.90	46.0	6.76	15	6.0	0.037*	–0.110*	0.3
5.0–10.0	7.10	63.0	9.26	15	6.0	0.028*	–0.076*	0.2
			Σ	100	40.0			32.4

Step 13 – Specific discharge carried by the stream (discharge per unit width) can be estimated assuming uniform flow. Manning roughness coefficient can be estimated from Fig. 5.5 for $K_s = 2.8$ mm and $R \cong 3.0$ m as $n \cong 0.016$. Hence, the specific discharge, applying Manning equation for uniform flow,

$$q = \frac{1}{n} \cdot d \cdot R^{2/3} I^{1/2} = \frac{1}{0.016} \cdot 3.0^{5/3} (0.001)^{1/2}$$

(since the ratio b/d is about 33 for the given stream, $R \cong d$). Hence, $q = 12.2$ m³/sec.m.

Step 14 – The volume of the total suspended-sediment discharge for bed material of specific gravity $S - 2.65$ can be obtained from

$$V = \frac{q_s}{\rho_s} \cong \frac{32.4}{2650} \cong 0.0122 \text{ m}^3/\text{sec.m}$$

Step 15 – Unit volume of water discharge carries a unit sediment volume

$$V_{1.0} = \frac{V}{q} \cong \frac{0.0122}{12.2} \cong 0.001 \text{ m}^3/\text{sec}$$

Hence, the average volumetric concentration of the suspended sediment is $\bar{C} = 1000$ ppm.

Step 16 – Finally, this average concentration makes up in relation to the water discharge – $(0.001/1.0) \times 100 \cong 0.1\%$

The above computations relate to one water stage only. A typical flood-wave hydrograph, however, is composed of many more stages for different durations of time. In order to obtain an estimate of the quantity of the suspended-sediment carried by a stream during the passage of a flood wave, similar computations have to be made for different water-stage intervals. Total quantity of sediment is then computed by multiplying each unit stage discharge by the corresponding time duration taken from the hydrograph.

It is once again emphasized that the total quantity of suspended load thus computed does not include the wash load, which must be added to it.

Reference height “a” from the bottom, which should represent the demarcation line between the suspended load and bed load, cannot be deter-

mined with any certainty, since there is in fact a transition zone rather than a clear-cut separation plane. In its vast field-measurement works on the rivers Niger and Benue, Nedeco [14] adopted, based on their experience on the Rhine, a constant height of 0.40 m above the bottom as the boundary between the suspended load and bed load (including the saltation load).

In arid and semi-arid zones, with long dry seasons followed by heavy rains, a typical hysteresis curve is often obtained when total suspended-sediment load (including the wash load) is plotted on a graph against the water discharge, see Fig. 8.10 (for similar phenomena concerning flood rating curves, see par. 7.3). In such streams, the wash load often accounts for 80% or more of the total sediment transport, including the bed load. The hysteresis may be explained by the fact that the first heavy rains, after the long dry spell, erode large amounts of hardened and weathered soil; however, after the initial high erosion, more stable soil is reached, and the erosion is then reduced to normal levels (see par. 10.4).

The suspended load, without the wash load, generally equals the bed load, or exceeds it in various amounts, sometimes by as much as about 100% or more.

Einstein and Abdel-Aal [15] at a later stage have tried to refine the expression for suspended-sediment discharge by using the corrected value of the Prandtl's factor κ , instead of assuming it constant. This correction has already been discussed in Chapter 5, and is given in Fig. 5.7.

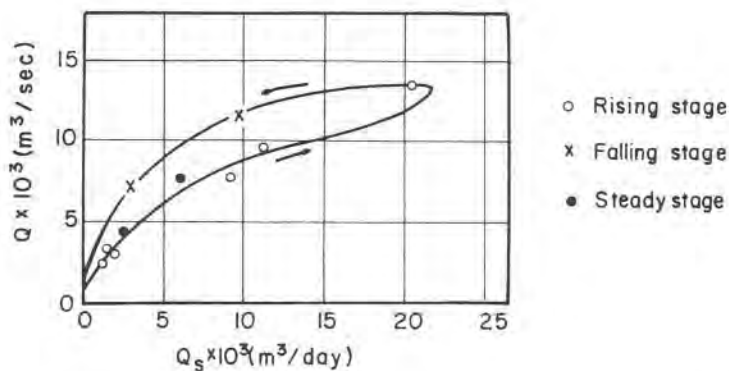


Fig. 8.10. Measured total suspended load in relation to discharge for river Benue at Makurdi (after Nedeco [14]).

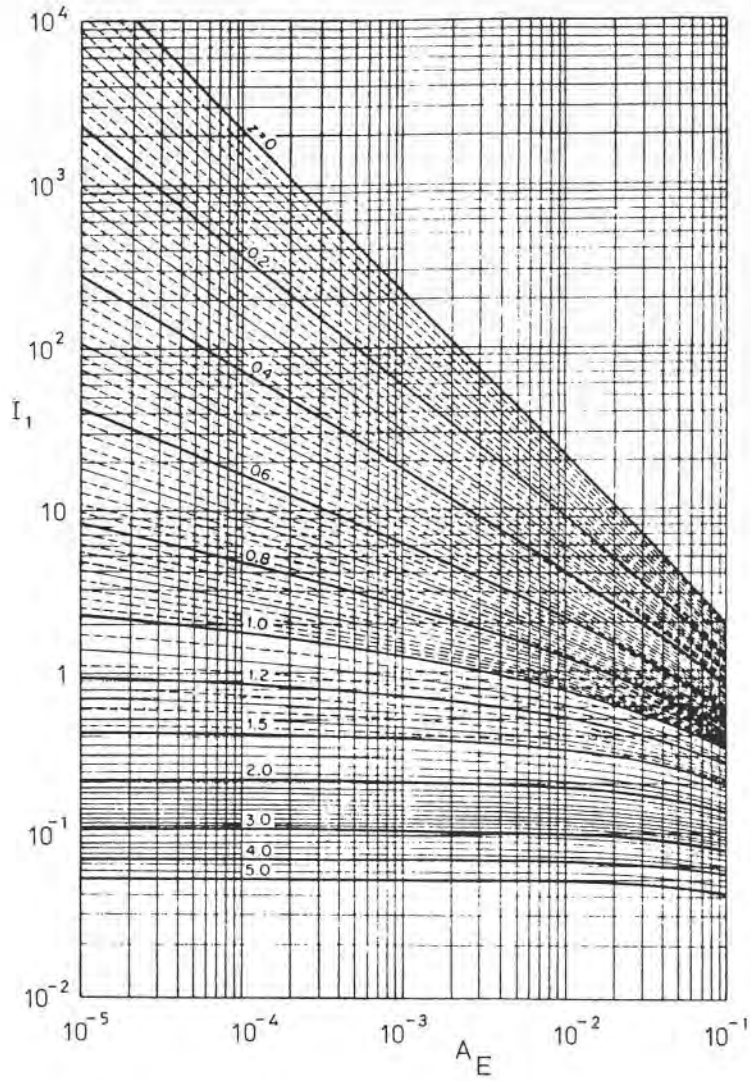


Fig. 8.11. Function I_1 in terms of A_E for different values of z (after Einstein [10]).

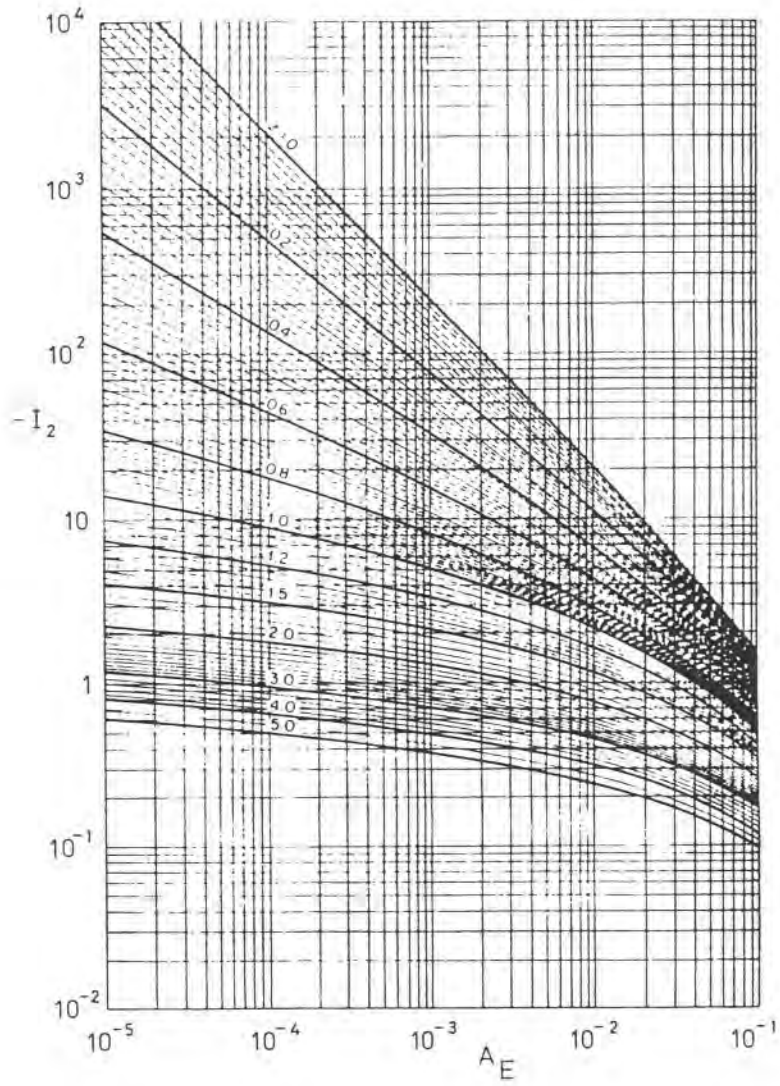


Fig. 8.12. Function I_2 in terms of A_E for different values of z (after Einstein [10]).

8.5 Other Approaches to the Determination of Suspended-Sediment Discharge

In addition to the diffusion (exchange) theory, on which the equations developed so far are based, there is also a different approach that tries to solve the problem attacking it from the point of view of the energy balance. Chief representative of this approach is Bagnold [16]. He tried to equate the available net power for transporting the suspended sediment load to the work rate required for its transport. From this an expression for the discharge has been developed.

Another approach has been proposed by Velikanov [17], known as the gravitational theory, which in fact is a modified energy-balance procedure. The final expression obtained for the suspended-sediment discharge is similar to the one developed by Bagnold.

Finally, mention should be made of recent works which try to apply the general diffusion theory to describe the mass transfer of suspended sediment. Quantities represented in dynamic equations are averaged either over time, local volume or probability. It is argued that this direct analysis of the mass transfer, unlike other approaches which study the laws governing the motion of a single particle and subsequently extend them to apply to a group of particles, is likely to become a basic tool of applied sediment-suspension problems. Engineering application of the method, however, for the time being has not been known. More detailed discussion could be found in [19–21], among others.

8.6 Conclusions

From the purely engineering point of view, the state-of-art concerning the transport in suspension of bed material is not satisfactory, in spite of the great progress made in relatively recent time. As mentioned before, even the most advanced procedure so far proposed requires the knowledge of an unknown factor, the value of which can be obtained only by extensive field measurement. This indispensable information does not belong to the basic stream data that can routinely be reached by the design engineer. Hence it appears that for all but preliminary designs, field measurements are still by far the most reliable method. However, if the reference suspended-load density can be more or less reliably evaluated, Einstein's method offers a sound tool for the estimate of the suspended load.

Wash load, in many streams the major part of the suspended load, is not covered by any of the proposed methods, and can be estimated by measurements only.

References

1. H.A. Einstein, Determination of rates of bed-load movement, proceedings, Federal Sed. Conf., Denver, Colorado, 1948.
2. V.A. Vanoni, N.H. Brooks and J.F. Kennedy, Lecture notes on sediment transportation and channel stability, California Inst. of Technol., Pasadena, report no. KH-R-1, 1961.
3. U.S. Inter-agency Comm. on Water Resources, A study of methods used in measurement and analysis of sediment load in streams, report no. 14 – Determination of fluvial sedimentation discharge, 1963.
4. H.A. Einstein, Sedimentation, part II: River sedimentation. Handbook of Applied Hydrology, V.T. Chow (ed.), McGraw-Hill, New York, N.Y., 1964.
5. L. Prandtl, Fuehrer durch die Stroemungslehre, 6 Auflage, F. Vieweg & Sohn, Braunschweig, 1965.
6. H. Rouse, Modern conceptions of the mechanics of turbulence, Trans. ASCE, 102 (1937).
7. H.A. Einstein and N. Chien, Second approximation to the solution of the suspended-load-theory, University of California, Inst. Res., no. 3, 1954.
8. V.Y. Matyukhin and O.N. Prokofyev, Experimentalnoe opredyelenie koeficientov vertikalnoi turbulentnoi difuziyi v vode dlya assajdayushtcichsya chiastitc, Sov. Gidrologiya, no. 3, 1966.
9. H. Majumdar and M.R. Carstens, Diffusion of particles by turbulence: effect of particle size, Water Res. Center, WRC-0967, Georgia Inst. of Technol., Atlanta, GA, 1967.
10. H.A. Einstein, The bed-load function for sediment transportation in open channel flows, U.S. Dept. Agric., Soil Conserv. Serv., T.B. no. 1026, 1950.
11. N.H. Brooks, Calculation of suspended load discharge from velocity concentration parameters, proceedings, FED. Ag. Sed. Conf., U.S. Dept. Agr., publication no. 970, 1963.
12. C.L. Chang et al., Total bed-material discharge in alluvial channels, proceedings, XIIth Congr. IAHR, Fort Collins, Colorado, 1967.
13. A.A. Kalinske et al., Engineering calculations of suspended sediment, Trans. Am. Geophys. Union, vol. 22, 1941.
14. Nedeco, Netherlands Eng. Consultants, River Studies, Niger and Benue, North Holland, Amsterdam, 1959.

15. H.A. Einstein and F.M. Abdel-Aal, Einstein bed-load function at high sediment rates, *Jour. of Hydr. Div., ASCE*, 98 (HY1) (1972).
16. R.A. Bagnold, An approach to the sediment transport problem from general physics, U.S. Geol. Survey, Prof. paper 422-J, 1966.
17. M.A. Velikanov, Principi gravitacionoj teorii dvizenya sedimentov, *Akad. Nauk, USSR, Geof. Series*, no. 4, 1954.
18. N.H. Brooks, Boundary shear stress in curved canals, a discussion, proceedings, *ASCE*, 89 (HY3) (1963).
19. S.M. Antsyferov et al., Sediments suspended in stream flow, proceedings, *ASCE*, 106 (HY2) (1980).
20. R.D. Kos'yan et al., O Primenimosti difuzionoi teorii k raschotam raspredelenia nanosov v otkritom patoke, *Metorologijia i Hidrologya*, no. 1, 1976.
21. N.A. Mikhailova, Pjerenos tvjerdich chastitz turbulentnim patokom vadi *Gidrometeoizdat, Leningrad*, 1966.
22. T. Itakura and T. Kishi, Open-channel flow with suspended sediments, proceedings, *ASCE*, 106 (HY8) (1980).

CHAPTER 9

THE BED MATERIAL LOAD

Symbols

A	– cross-sectional area, m^2
a	– percentage quantity
b	– width of channel, m; percentage quantity
C	– a coefficient
c	– percentage quantity
d	– depth of flow, m
d_s	– diameter of grain, mm or m
f	– Darcy-Weissbach friction factor
G_s	– bed load discharge, kg/sec.m, N/sec.m
g	– acceleration of gravity, m/sec^2
g_h	– <i>average amplitude</i> of dunes or ripples, m
I	– longitudinal slope of stream bed
J	– hydraulic gradient
K	– a coefficient, ψ/γ^2
n	– Manning coefficient
n_B	– Manning coefficient for bed roughness
n_g	– Manning coefficient for grain roughness
n_w	– Manning coefficient for wall roughness
P	– hydraulic perimeter, m
$p, \Delta p$	– percent of total for a given fraction
Q	– water discharge, m^3/sec , lit/sec
Q_B	– part of water discharge apportioned to bed, lit/sec
q, q_1	– specific water discharge, $m^3/sec.m$
q_c	– critical specific water discharge, $m^3/sec.m$
R	– hydraulic radius, m
R_B	– hydraulic radius relative to bed, m

Re	– Reynolds number
R_w	– particle Reynolds number
u_*	– shear velocity, m/sec
V_c	– critical velocity of the incipient sediment motion, m/sec
V_s	– average velocity of dunes or ripples, m/sec
V	– total volume of the sample, cm^3
V_s	– volume of voids in the sample, cm^3
γ	– specific weight of water, N/m^3
γ_s	– specific weight of solids, N/m^3
λ	– porosity of the sand bed
ν	– kinematic viscosity of water, m^2/sec
$\bar{\xi}$	– mean height of sand dunes, m
ρ_s	– density of sediment, kg/m^3
ρ	– density of water, kg/m^3
τ	– shear stress, N/m^2
τ_c	– critical shear stress, N/m^2
ψ	– Straub dimensional coefficient, $N/m^3 \cdot sec$

Special symbols used for Einstein bed load function

A_b	– cross-sectional area pertaining to bed, m^2
A_T	– total area of cross-section, m^2
i_B	– fraction of bed load in a given grain size
i_b	– fraction of bed material in a given grain size
k_s	– roughness height, m
q_B	– bed load discharge, $N/sec \cdot m$
R_b	– hydraulic radius for bed, m
R'_b	– hydraulic radius for individual grains, m
R''_b	– hydraulic radius for bed forms, m
S_s	– specific gravity of solids
\bar{u}	– average flow velocity, m/sec
u'_*	– shear velocity with respect to the grain, m/sec
u''_*	– shear velocity for channel irregularities, m/sec
x	– logarithmic velocity distribution correction factor
X	– characteristic grain size of mixture, m
Y	– pressure correction in transition smooth-rough
β	– a logarithmic function
β_x	– a logarithmic function
δ	– thickness of the laminar sublayer, m
Δ	– apparent roughness, k_s/x
ξ	– “hiding factor” of grains in a mixture

τ_p	– bed shear stress, N/m ²
τ_b	– shear stress acting on individual sediment grains, N/m ²
τ'_b	– shear stress acting on bed forms, N/m ²
ϕ_*	– dimensionless parameter for intensity of transport on individual grains
ψ	– dimensionless parameter for intensity of shear on particle
ψ_*	– dimensionless parameter for intensity of shear on individual grain size
ψ'	– dimensionless parameter for intensity of shear on representative particle

9.1 Introduction

Movement of sediment particles in the relatively thin layer (less than about 5% of the depth of water) forming the deformable alluvial bed proper is considered to be due to a mechanism different from the one as previously described for the suspended sediment. Indeed, it has already been emphasized in par. 8.2 that this very difference in the physical models is at the root of the somewhat artificial division of the *total bed-material load* into two distinct parts, in order to conveniently account for the different transport mechanisms. It should, however, always be kept in mind that in both cases, for the bed load as well as for suspended load, the source of the sediment is movable alluvial bed. Hence, the sum of the bed load and suspended load gives the *total bed-material load*. As repeatedly stated, it does not include the wash load, consisting of small-size particles, practically unsetting in the moving water, and almost wholly dependent on the solid supply from the watershed.

According to the modern concepts of the sediment-transport mechanism, as soon as some critical value of the bed shear stress is exceeded, solid alluvial particles are set into motion. They move by rolling along the bed, sliding or saltating (jumping) close to the bed surface. Some of these smaller particles are caught by the stream (see Fig. 8.1) and carried into suspension while others again settle on the bed. There is actually a continuous exchange of particles across some sort of imaginary demarcation line between the bed load and suspended load. The location of this line, however, cannot be indicated with any precision, much less measured for any specific case. In fact, such vague expressions as “near the bed” or “away from the bed”, lacking any quantitative meaning, are commonly used to distinguish between

the two modes of transport. It is customary, therefore, to arbitrarily set this line some relative distance from the bottom (see Fig. 8.3). Recently, however, attempts are being made to quantitatively set the limit between saltation and suspension, by defining, for instance, a particle in suspension if and when it is carried beyond the saltation limit corresponding to the supportive turbulent velocity fluctuations [53] as obtained by mathematical models of saltation phenomena. Although interesting and probably in the right direction, such and similar approaches so far have little engineering application.

In most of the alluvial streams, the total combined suspended load, comprising the bed-material suspended load and the wash load, is much larger than the bed load; the suspended-sediment movement, moreover, generally starts at lower rates of flow than the bed load movement. According to Zeller [1], this is apparently true even for mountain streams of Switzerland, which should be rich in relatively large-size bed load particles, as can be seen from the graphs on Fig. 9.1. It is indeed generally accepted that the ratio of bed load to total load is much lower in lowland streams than in mountain streams.

According to the studies made by Lane and Borland [2], there are three main parameters which are likely to affect the amount of bed load a stream may carry: 1) size of bed material or the settling velocity of the particles it is made of, 2) longitudinal slope of the stream or the average stream velocity, and 3) nature of the channel, including the depth, size, shape and roughness. Taking into account the above parameters, they have tried to set forth some practical criteria for the aid of hydraulic engineers.

1) The smaller the actual concentration of suspended sediment, the higher usually will be the percentage of the bed load to the total load,

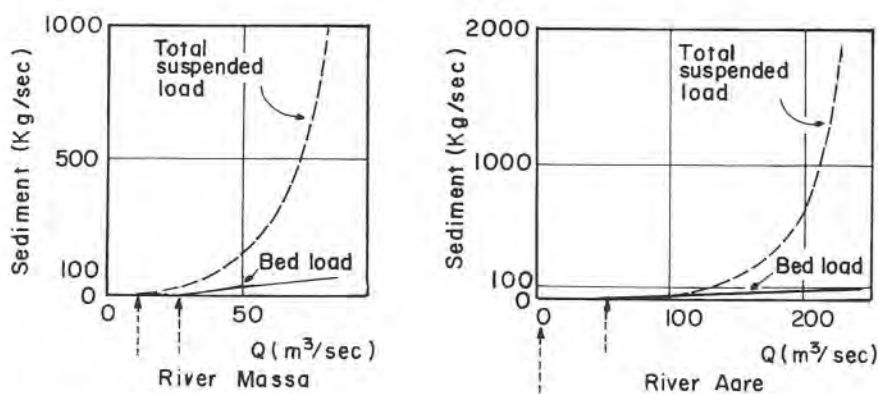


Fig. 9.1. Bed load and suspended load for some streams in Switzerland, according to Zeller [1].

2) The smaller the difference in particle sizes of the bed load and suspended-load material, the higher will be the percentage of the bed load to total load,

3) The ratio of bed load to suspended load is likely to be larger for low or medium stages than for high stages (thus a stream in which the flow does not fluctuate widely is apt to carry a larger percentage of bed load; in steep mountain streams, however, bed load may become higher with increasing discharge),

4) Streams with wide shallow channels usually carry a higher proportion of sediment as bed load than streams with deep narrow channels, and

5) Streams with higher degrees of turbulence tend to have smaller amounts of bed load.

It is further emphasized that whenever the average bed load over a period of time is sought, the flow variability must be taken into consideration. The bulk of the sediment load of a stream is carried during high-flow periods, when both discharge and sediment concentration are high. Because of greater depths of flow and higher turbulence levels, the bed load content of the stream tends to be lower, at least as far as the sand sizes are concerned. It can, therefore, be expected that at higher flow stages, bed load will be of smaller percentage relative to suspended load than at low stages. For this reason, streams with more variable flows are likely to have smaller bed loads, when expressed as a percentage of the total quantity of measured suspended load for the period under observation.

If the above cited criteria are applied, for instance, to ephemeral streams in the semi-arid regions, they would indicate relatively low bed load. Measurements carried out by Poreh et al. [3] in some of the ephemeral streams of Israel have indeed shown the bed load to be no more than about 3–5% of the total sediment load; in some streams the storm and the ensuing flood wave must be very strong before any appreciable bed movement of sediment could be detected at all.

Table 9.1, given by Lane and Borland [2], summarizes some recommended predictions of the bed load movement for different typical conditions met with in alluvial streams, and intended as a first-estimation aid for hydraulic engineers.

Bed load in the strict sense, i.e. as one part of the total bed-material load, is often quantitatively small and hence does not represent a severe problem of sedimentation. On the other hand, as the main factor of the bed-formation process, it is always of major importance. Roughness of alluvial channels is to a great extent determined by the movement of the bed load.

Bed load formulae which will be mentioned or treated in the present chapter, have been the cause of the some debate for many years. It is indeed

TABLE 9.1. BED-LOAD TRANSPORT IN ALLUVIAL STREAMS

Concentration of suspended load (ppm)	Type of material forming the channel of the stream	Texture of the suspended material	Bed load in terms of measured suspended load (%)
Less than 1000	Sand	Similar to bed material	25–150
Less than 1000	Gravel, rock or consolidated clay	Small amount of sand	5–12
1000–7500	Sand	Similar to bed material	10–35
1000–7500	Gravel, rock or consolidated clay	25% sand or less	5–12
Over 7500	Sand	Similar to bed material	5–15
Over 7500	Gravel, rock or consolidated clay	25% sand or less	2–8

argued by many researchers and engineers that any truly correct bed load equation should in fact be capable of being extended to include the suspended load also, since in fact the suspension is nothing else but an advanced stage of the bed-material movement. The same should apply, of course, to all suspended-load equations as well. Such a view in that respect is held, among others, by Vanoni et al. [4], who consider that actually all of the transport formulae are total bed-material load formulae, “but each one applies to a limited set of conditions, depending on the data upon which it is based.” Einstein [5] and Scheidegger [6], however, and a few other researchers, see some objective justification in having two separate sets of equations for the total bed-material load. It is further generally recognized that in any case no precise and scientifically reliable method is available to separate quantitatively the two mutually closely linked modes of transportation.

From the engineering point of view, where a rough estimate of the total bed-material discharge is needed, sediment transport formulae discussed or

mentioned in the present chapter may be considered to give a quantitative approximation of both the suspended and bed load transported by a given stream. At low and medium flow rates, when the major part of the sediment moves along the bed or near to it, sediment transport formulae probably approximate well enough the total bed-material load. At high discharges, when the part of the suspended load is much larger, there is no conclusive evidence that this is also the case. Hence in every given case the practising engineer will have to decide on the face of the known stream characteristics whether to evaluate the total bed-material load from one of the formulae or methods as given in the present paragraph, or to add to it additional quantities obtained using one of the methods as outlined in Chapter 8.

9.2 Incipient Motion

The question of some critical state at which sediment particles forming the bed of the channel just start moving, or of the *incipient motion*, may seem quite academic at first glance. Yet in the engineering practice it is of a definite interest, when the problem is to design a non-scouring earth channel for the design discharge. It is furthermore an important parameter in a few of the bed load equations.

Some of the researchers in the field, notably Einstein [7] among others, have been of the opinion that no definite and generally valid criterion for the incipient motion of sediment particles could be established and that only statistical laws should be applied. It seems reasonable also that some distinct lower limit of *frequency* should be set at which sediment particles are entrained into motion, since obviously a number of sporadic or very infrequent bursts of motion would be of little interest from the engineering point of view. In fact, in turbulent flows it is likely that the initiation of transport is caused by some instantaneous fluctuation of a dominant parameter (velocity, shear stress, etc.) that is much larger than the time-average value used for the evaluation of the critical state.

At low rates of flow, before the critical stage is reached, there is practically no movement of sediment particles (see Fig. 9.3b). Three main lines of approach have been used so far in order to set criteria for the incipient motion when the discharge increases. Two of these lines of attack will be mentioned only briefly, because they either do not reflect the modern thinking on fluid mechanics, or are based on concepts still poorly understood.

Critical velocity, just able to move grains of a given size and weight, as a measure of incipient motion no doubt has been the simplest and first-used

approach, and indeed is still used by many hydraulic engineers, at least as a very rough estimate. It has often been based on purely empirical data and related to the mean velocity of flow. Such a table of *permissible mean velocities* for different types of soil was given in Volume 1 of the present manual, Chapter 4, Table 12.

Attempts at a theoretical link between the critical velocity and the grain size have been tried by many researchers and engineers. According to Forchheimer [8], as early as 1753 A. Brahms (who allegedly also established the dynamic equation of the uniform flow in open channels, independently from A. Chezy) equated the dynamic force on the particle to the resisting force, and arrived at the conclusion that the square of the critical velocity is proportional to the diameter of the sediment particle. This is equivalent to saying that the critical velocity is proportional to the one-sixth power of the immersed weight of the bed material. The above proportionality is valid only relative to the so-called “bed-velocity”, which should probably be measured at the top of the grain. More recent analyses, made among others by Goncharov [9], Neill [10] and Garde [11], have tried to correlate critical velocity not only to the grain size but to the depth of flow also, i.e. to the parameter d/d_s (d – depth of flow, d_s – diameter of grain). Here also, critical velocity is measured at the grain level approximately, see par. 9.2.2.

Sediment particles resting on the bed are subjected to a lift force, caused by the pressure difference between the bottom (velocity zero) and the top (velocity greater than zero). *Lift approach* to the incipient motion is based on the reasoning that when the lift exceeds the submerged weight of the particle, it will be raised from the bottom and entrained by the flow. As the particle reaches higher level, the lift is reduced, and it falls back to the bottom. The present state-of-the-art concerning the sediment transport, however, leaves too many gaps in our understanding of the lift forces acting on sediment particles; consequently, this approach is of limited engineering applicability for the time being.

9.2.1 Shear Stress Approach

The analysis based on the *critical shear stress* (tractive force) is today widely accepted as the one which is in the best agreement with the modern concepts of fluid mechanics, although it also has many weak points.

Here again one should first mention the attempts to list purely empirical values of the critical shear stress. Such a table, based on the work of Fortier and Scobey [12], can be found in Volume 1 of the present Manual, Chapter 3, under the name of “permissible tractive force”. As a matter of fact, both the “permissible” velocity, mentioned before, and the “permissible” shear

stress, should necessarily be somewhat lower than the critical values for the incipient motion, in order to avoid scouring. The method is by its very nature very approximate, but it is undoubtedly extremely handy for practising engineers when trying to design stable earth channels, and hence is still widely used.

Many semi-empirical formulae have been proposed during the first half of the present century, endeavoring to correlate the critical shear stress and sediment characteristics. Some of them are dimensionally not homogeneous; this was probably considered a minor fault at the time of their birth, but renders them almost unacceptable to our modern concepts of scientific exactness. Among the best known of these formulae, one should mention those proposed by Schoklitsch [13], U.S. Waterways Experiment Station [14], or Indri [15].

Shields [16] tried to theoretically analyse the incipient motion. After lengthy physical reasoning, into which he introduced many far-reaching simplifications, he arrived at relatively simple functional relationships between the two main parameters governing the beginning of the sediment motion. This correlation could not be evaluated analytically, and hence Shields obtained it through his own laboratory experiments, and using available data from other sources.

There is no great interest in going through Shield's theoretical analysis. The two main parameters can easily be derived by way of dimensional analysis.

Neglecting some parameters of marginal importance, the main quantities which influence the initial motion of bed particles are,

- τ_c — critical shear stress
- $(\rho_s - \rho)$ — difference in density between the sediment and the water
- d_s — diameter of the particles
- ν — kinematic viscosity, and
- g — acceleration of gravity.

The above quantities yield two dimensionless parameters,

$$\frac{(\tau_c/\rho)^{1/2} d_s}{\nu} = \frac{u_* d_s}{\nu} \quad (9.1)$$

$$\frac{\tau_c}{(\rho_s - \rho) g d_s} = \frac{\rho u_*^2}{d_s (\rho_s - \rho) g} \quad (9.2)$$

The first of the parameters is a Reynolds number related to shear velocity

u_* , and the second a Froude number also in terms of shear velocity. The following equation

$$\frac{\tau_c}{(\rho_s - \rho) g d_s} = f \left[\frac{u_* d_s}{\nu} \right] \quad (9.3)$$

defines the conditions for the incipient motion in a general way. The functional relationship has been graphically presented by Shields, see Fig. 9.2, and although the diagram is by now more than forty years old, it is still accepted as fairly reliable. It has been developed for flat bed, for small longitudinal slopes, which is generally the case with alluvial channels, and for uniform grains. At all points below the line, sediment particles will stay at rest, while above the line, they will be moved by the flow. It should be noted from the diagram that beyond the point of parameter $u_* d_s / \nu = \sim 500$, the parameter

$$\tau_c / (\rho_s - \rho) g d_s = 0.06 = \text{const.}, \quad (9.4)$$

which means that beyond that point, the critical shear stress is directly proportional to the diameter of the particle. Taking the density of quartz particles as $\rho_s = 2650 \text{ kg/m}^3$ and of water as $\rho = 1000 \text{ kg/m}^3$, one can write $\tau_c \text{ (N/m}^2\text{)} = 0.06 \times 1650 \times 9.8 \times d_s \text{ (m)} = 970 d_s \text{ (m)}$; if d_s is inserted in

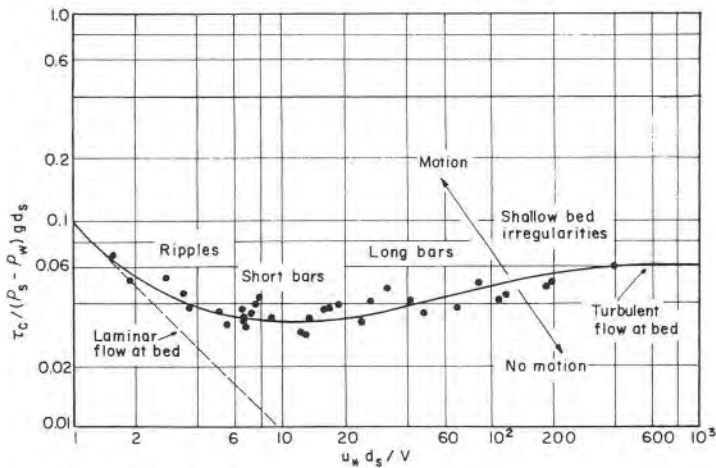


Fig. 9.2. Shields diagram for incipient motion [16].

millimeters and 970 is rounded up to 1000, a simple and handy expression is obtained for particles having $R_w \geq 500$: $\tau_c \text{ (N/m}^2\text{)} \cong d_s \text{ (mm)}$.

It should be emphasized, however, that recent experimental evidence seems to indicate two main deviations from the Shield's diagram: 1) for values of $R_w < 1$ (laminar flow at bed), the slope of the characteristic straight line should be much less than 45° ($\tau_c / (\rho_s - \rho_w) g d_s \cong 0.1 R_w^{-0.3}$ instead of $0.1 R_w^{-1}$); 2) for turbulent flows, Shields curve should be replaced by a band, giving more freedom to the possible values of τ_c as function of R_w [47, 48].

In hydraulic engineering practice there is frequent use of the so-called "threshold" discharge at which the incipient motion of bed material is started. If the hydraulic rating curve of the stream is known, or can be computed by a synthetic procedure, and information about the sediment gradation is available, such threshold discharge for a specific stream may be easily obtained making use of the Shields diagram. Values arrived at in this way are generally quite reliable for sand-bed channels, but caution should be used for gravel-bed channels, where packing of the gravel and imbrication may significantly affect the threshold values.

Example 9.1

An earth channel passing through prevalently sandy soil has to convey the design discharge of $Q = 9.0 \text{ m}^3/\text{sec}$. Manning roughness coefficient has been estimated as $n = 0.02$, and the most convenient longitudinal slope set at $I = 0.3\text{‰}$. The geometry of the proposed channel is given as: bottom width $b = 4.0 \text{ m}$, depth of water for uniform flow $d = 1.5 \text{ m}$, and side slopes $m = 2$. It was furthermore requested to avoid scouring along the channel, in order to get the water as free as possible from sand particles in the downstream pumping plant.

Step 1 – Computation of geometric data for the proposed channel:

$$A = 10.5 \text{ m}^2 \text{ – wetted area}$$

$$P = 10.7 \text{ m – wetted perimeter}$$

$$R = A/P = 0.98 \text{ m – hydraulic radius}$$

Step 2 – Using Manning equation for uniform flow:

$$Q = \frac{A}{n} R^{2/3} I^{1/2} = \frac{10.5}{0.02} \cdot 0.98^{2/3} \cdot (0.0003)^{1/2} = 9.0 \text{ m}^3/\text{sec}$$

and the shear stress

$$\tau = \rho \cdot gRI = 1000 \cdot 9.8 \cdot 0.98 \cdot 0.0003 = 2.9 \text{ N/m}^2$$

where ρ is the density of water and g the acceleration of gravity. The design of the channel seems to be adequate, but it has to be checked whether it is below the limit of incipient scouring.

Step 3 – Field tests have shown a median diameter of quartz sand particles ($\rho_s = \sim 2650 \text{ kg/m}^3$) to be $d_s = \sim 1.4 \text{ mm}$, and the analysis has to be done for water temperature of 16°C . Shear velocity has first to be computed,

$$u_* = (\tau/\rho)^{1/2} = (2.9/1000)^{1/2} = 0.054 \text{ m/sec}$$

Here ρ denotes the density of water. The parameter on the horizontal scale of Fig. 9.1,

$$\frac{u_* d_s}{\nu} = \frac{0.054 \cdot 0.0014}{1.11 \times 10^{-6}} = 58.4$$

Here ν is the kinematic viscosity of water. Now, the parameter on the ordinate,

$$\frac{\tau_c}{(\rho_s - \rho)g d_s} = \frac{2.9}{1650 \cdot 9.8 \cdot 0.0014} = 0.13$$

Locating the corresponding point on the Shields diagram (Fig. 9.1) shows that the proposed channel, though hydraulically acceptable, will be scouring (the characteristic point falls *above* the line). Hence an alternative channel has to be proposed. This could be achieved only by decreasing the longitudinal slope, i.e. by inserting water drops along the lay-out of the channel.

Step 4 – An alternative design was, therefore, put forward. The longitudinal slope was reduced to $I = 0.1\%$, and the bottom width increased to $b = 5.0 \text{ m}$; the corresponding depth of uniform flow $d = 1.83 \text{ m}$. Hence,

$$A = 15.8 \text{ m}^2; \quad P = 13.2 \text{ m}; \quad R = A/P = 1.2 \text{ m}; \quad R^{2/3} = 1.13$$

$$Q = \frac{15.8}{0.02} \cdot 1.13 \cdot (0.0001)^{1/2} = 8.93 \text{ m}^3/\text{sec}$$

Checking for scouring,

$$\tau = \rho g R I = 1000 \times 9.8 \cdot 1.2 \cdot 0.0001 = 1.18 \text{ N/m}^2$$

$$u_* = (\tau/\rho)^{1/2} = (1.18/1000)^{1/2} = 0.034 \text{ m/sec}$$

$$\frac{u_* d_s}{\nu} = \frac{0.034 \times 0.0014}{1.11 \times 10^{-6}} = 42.9$$

$$\frac{\tau}{(\rho_s - \rho)g d_s} = \frac{1.18}{1650 \cdot 9.8 \cdot 0.0014} = 0.052$$

The characteristic point is still somewhat above the line on the diagram of Fig. 9.1, but it nevertheless may be taken as satisfactory.

Although longitudinal slopes of alluvial streams are generally mild enough to be considered practically "flat", they mostly are covered with dunes which have locally steep slopes. It is questionable whether the diagram also adequately covers these conditions, since the shear stress may hardly be assumed to be uniformly distributed, and the weight component parallel to the bed should be taken into account. On the other hand, however, it may well be that the above-mentioned forces to a certain degree compensate for each other, making the diagram valid on the whole, which would also explain its wide acceptance and application by hydraulic engineers.

White [17] later tried to solve the problem of incipient motion analytically by considering the dynamic equilibrium of grains resting on a flat bed. He finally derived a simple expression for the critical shear stress causing incipient motion,

$$\tau_c = C (\rho_s - \rho)g d_s \quad (9.5)$$

in which τ_c is in N/m^2 , ρ_s and ρ are in kg/m^3 , g is in m/sec^2 , and d_s in mm. C is a coefficient which depends on the particle Re-number $u_* d_s/\nu$, its shape, density, and the position on the bed. It has already been shown that according to the Shields diagram, such a simple relationship is valid only when the parameter $u_* d_s/\nu$ is larger than about 500.

Since the publication of Shields diagram, many attempts have been made to modify it or to improve on it, as for instance, Bogardi [18] or Task Committee on Preparation of Sedimentation Manual [19]. These and other corrections, however, have not taken root in engineering practice.

Of particular interest is a working diagram prepared by Lane [20] more

than 25 years ago, but still widely used for the design of stable earth channels. The diagram, Fig. 9.3, is based on many field data collected and analysed by the author, and is supposed in fact to give the “permissible” shear stress for various conditions. The different curves are as follows:

1. USSR canals with clear water,
2. Straub’s values for critical shear stress,
3. Recommended values for canals with clear water,
4. Recommended values for canals with low content of fine sediment in the water,
5. Recommended values for canals with high content of fine sediment in the water,
6. USSR canals with 2.5% colloids in water,
7. USSR canals with 0.1% colloids in water,
8. Recommended values for canals in coarse noncohesive material, and
9. All hatched areas: Nuerenberg Kulturamt.

More recently efforts have been made to derive the relationship between the critical shear stress causing incipient motion and particle Re number by theoretical analysis, such as, among others, Egiazaroff (1965) or Jwagaki

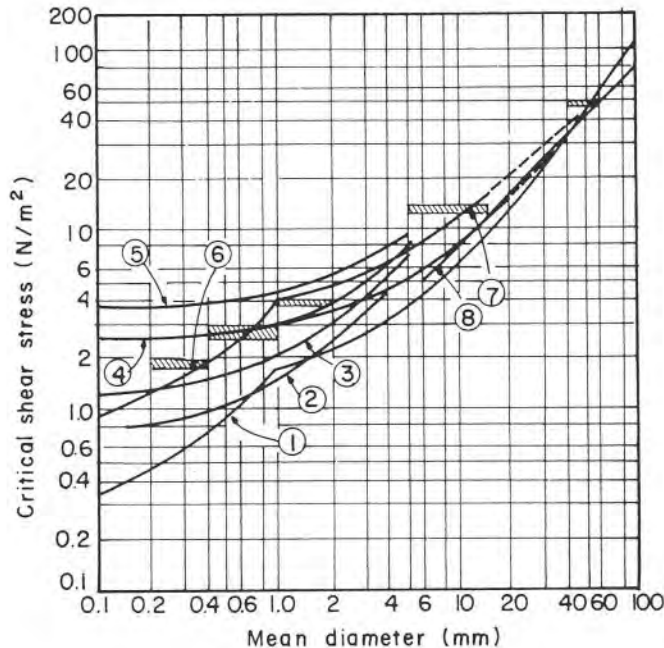


Fig. 9.3. Critical shear stress vs. grain diameter (after Lane [20]).

(1956). All these attempts so far, however, have failed to give a satisfactory solution to the problem which by the very nature of its complexity, will probably defy any purely theoretical analysis for still many years to come.

Finally, it should be pointed out that extremely scarce information is available concerning the effect of non-uniformity of sediment upon the critical shear stress, or how a representative grain size should best be selected. In fact, the available information is conflicting, since according to some researchers, critical shear stress is smaller for non-uniform grain distributions than for uniform ones; while others predict the opposite effect. However, the experimental evidence appears to indicate that higher values of critical shear stress apply to non-uniform grain distributions.

Presence of cohesive materials in the alluvium inhibits the initiation of motion. Since here electrochemical forces play a major role, little is reliably known at present that would warrant any quantitative prediction.

9.2.2 *Some Additional Remarks About the Critical-Velocity Approach*

Although the shear-stress approach, as discussed in the previous paragraph, is today considered to be the most rational method for the analysis of the incipient motion in alluvial streams, the critical-velocity approach is still widely used by practising engineers. It is particularly handy for the preliminary design stages, when the available information about the stream may still be scarce, and approximate values of the design parameters are sufficient. All the formulae for the critical velocity (the lowest mean velocity of the stream at which the bed-material sediment starts being entrained) are empirical expressions that best agree with the data which they had been derived from, but by a sound selection and often a judicious adaptation, more or less reliable preliminary-design values can be obtained.

In the following, a few of such critical-velocity formulae will be reviewed. The order of presentation reflects only the date of their first publication, and not any particular merit.

1. *Levi formula* [59]

Critical velocity is given by two formulae:

$$V_c = 1.4 (gd_s)^{1/2} \ln \frac{d}{7d_s}, \text{ for } \frac{d}{d_s} > 60 \quad (9.7)$$

$$V_c = 1.4 (gd_s)^{1/2} \left[1 + \ln \frac{d}{7d_s} \right] \text{ for } 10 < \frac{d}{d_s} < 60 \quad (9.8)$$

In the case of highly non-homogeneous bed material, the above expressions should be multiplied by the factor $(d_{s\max}/d_s)^{1.7}$. The formulae have been derived from measured data on streams in USSR. Characteristic grain size, d_s – mean diameter of the bed material.

2. *Goncharov formula* [9]

The proposed formula reads

$$V_c = \left[\frac{2g(\gamma_s - \gamma)d_s}{3.5\gamma} \right]^{1/2} \log \frac{8.8d}{d_s} \quad (9.9)$$

The formula, according to its author, is conditioned only by the existence of turbulent flow in the stream. It is also based on streams in USSR. Grain diameter d_s is the mean diameter of the bed material. However, if the bed material is highly non-homogeneous, the denominator of the fraction under the log sign should be d_{s95} instead of d_s (d_{s95} – grain size for which 95% of the mixture is smaller).

3. *Neill formula* [10]

It is given by,

$$V_c = 1.414 \left[\frac{d}{d_s} \right]^{1/6} [(\gamma_s - \gamma) d_s / \rho]^{1/2} \quad (9.9a)$$

According to the author, the formula corresponds to the Shield's parameter constant value of 0.03, instead of the usual 0.06, since according to his investigations, at the value of 0.06 there is already a small, but definite movement of the bed material. The formula is based on Canadian streams and laboratory tests, and should be particularly suitable for coarse sediment. Characteristic grain size – mean diameter.

4. *Garde formula* [11]

For hydrodynamically rough beds, it is given by:

$$V_c = \left[0.50 \log \left[\frac{d}{d_s} \right] + 1.63 \right] [(\gamma_s - \gamma) d_s / \rho]^{1/2} \quad (9.10)$$

d_s – mean diameter

A comparative graph of the reviewed equations is given in Fig. 9.3a.

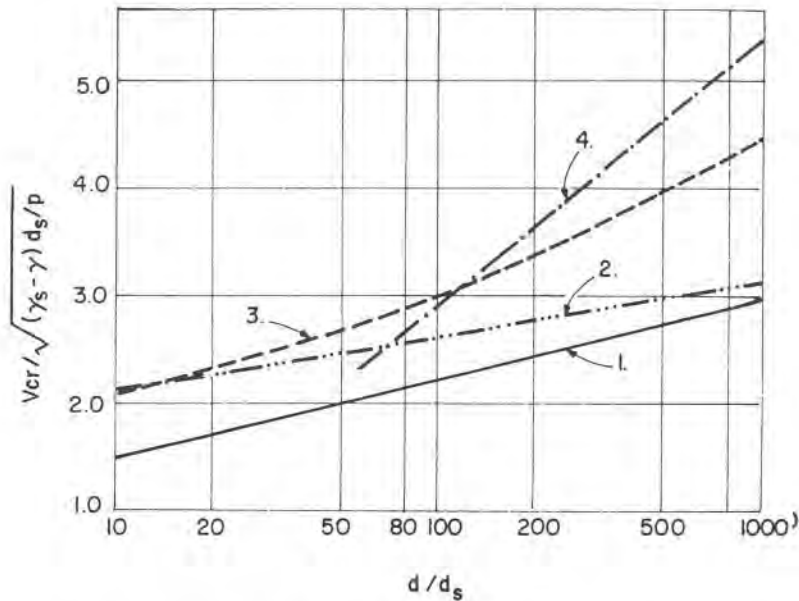


Fig. 9.3a. Comparative graph of some critical velocity formulae, 1 – Goncharov, 2 – Garde, 3 – Neill, 4 – Levi.

Values from the Levi's formula have been computed assuming the submerged weight of sand particles as $\gamma_s - \gamma = 1.65 \times 10^4 \text{ N/m}^3$.

Finally, as far back as 1935 a graph was proposed by Hjulström [60] for the critical velocity causing incipient motion as function of the grain size. It is still often used by practising engineers as first indication of order of magnitude. Critical velocity is given as a band of possible values, rather than a single curve. An additional merit of the graph is that it clearly illustrates two physical facts: 1) critical velocity of incipient motion is the lowest for the sand fraction, and it increases at both ends – both for silts and other small fractions with cohesive properties, and for larger fractions, coarse sand and gravel, 2) once set in motion by the current, the particle will probably remain transported at velocities much lower than the critical velocity. The curve for the settling velocity should be considered as giving some average values, since grain characteristics other than the size and fluid properties have not been specified. The graph is reproduced in Fig. 9.3b.

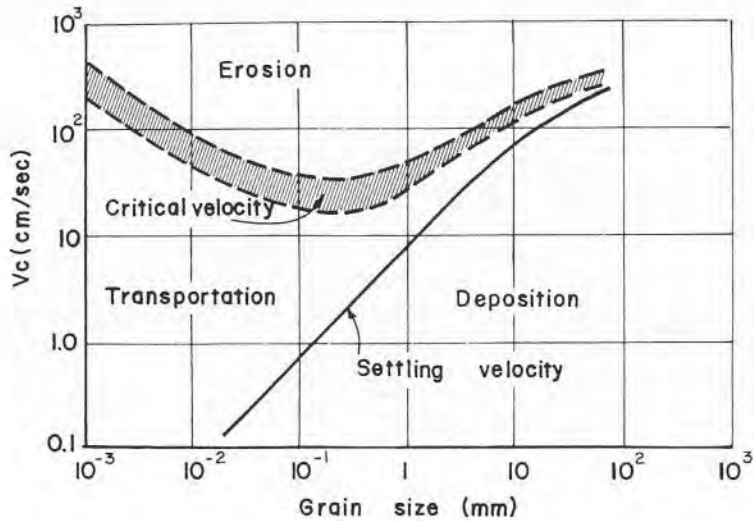


Fig. 9.3b. Critical velocity of incipient motion, after [61].

9.3 Bed Load Transport

When it comes to the estimate of the bed load transport, perhaps the most surprising aspect is the plethora of the proposed methods and formulae. For a practicing engineer, if he has no definite preferences or personal habits, this is a confusing situation; the more so, since using different formulae for the same set of given data may yield widely differing results. In a text that strives to remain a manual and to cover a wide range of topics, not all of these formulae can be reviewed. Omitted are all those mainly empirical approaches reflecting specific local conditions, rather than more general aspects. The selection of the representative formulae for the main methods of approach is based largely on the extensive work and analysis made by Shulits [21], whose main criterion has been the needs of practicing engineers for the design purposes.

Since the publication of his analysis and recommendations in 1968, however, new formulae have been proposed and tested (for instance, [54, 55]). Two of these newer methods seem to give good agreement with measured results for *sandy beds*: 1) Engelund-Hansen formula, and 2) Toffaleti formula. Hence, a brief review of these two formulae is added in Appendix 1 to the present chapter.

9.3.1 First Approach: Bed Load Expressed in Terms of the Discharge

Relating the quantity of transported sediment to water discharge had been one of the main approaches adopted before the notion of shear stress gained prominence in later years. Main formulae of this kind are those proposed by Schoklitsch (1934) [22], Meyer-Peter (1934) [23], Casey (1935) [24], Haywood (1940) [25] and Schoklitsch (1943) [26]. In the following, Schoklitsch (1934) formula will be discussed, because according to Shulits's analysis, it happens to agree better with other formulae than any of the others mentioned, and not because it is thought to be more accurate or better attuned to the laws of sediment-transport mechanics.

9.3.1.1 Schoklitsch Formula (1934)

The stream is supposed to be wide, hence the sediment discharge relates to unit width of the bed. The mainly empirical expression reads:

$$G_s = 7000 \frac{J^{3/2}}{d_s^{1/2}} (q_1 - q_c) \quad (9.11)$$

Here, G_s – bed load in kg/sec/m, d_s – grain diameter in mm, J – hydraulic gradient (slope), q_1 – specific water discharge in m²/sec, and q_c – critical discharge in m²/sec.

For quartz particles of specific density 2.65, the critical discharge, i.e. the discharge which causes incipient motion, is given by Schoklitsch as:

$$q_c = 1.94 \times 10^{-5} \frac{d_s}{J^{4/3}} \quad (9.12)$$

He obtained the values of critical discharge for given grain diameters by plotting bed load as ordinate and longitudinal slope I as abscissa, and then extrapolating to zero bed load to obtain the intercept on the abscissa.

Eqs. (9.11) and (9.12) have been developed for uniform grain distribution. It is, however, generally applied to non-uniform distributions also, taking d_{s50} as the characteristic diameter for the mixture, which is based on Schoklitsch's own recommendation that it should be somewhere between d_{s40} and d_{s60} . This simple procedure may not always be a good one, and d_{s50} could be considerably off the target. Schoklitsch indeed suggested a more accurate method, which is as follows: sediment mixture is arbitrarily divided into several size subranges having mean diameters d_{sa} , d_{sb} , d_{sc} , etc., and the partial quantity of each subrange is then determined and expressed as percentage of the total quantity. Subsequently, partial bed loads, G_a , G_b , G_c , etc.,

are computed for each mean diameter d_{sa} , d_{sb} , d_{sc} , etc., using Eqs. (9.11) and (9.12) for the given discharge q_1 and the given slope I . The total bed load for the sediment mixture is then obtained,

$$G = a G_a + b G_b + c G_c + \dots \quad (9.13)$$

Here a , b , c . . . indicate the percentage quantities that each partial sub-range is of the total.

If for any of the coarser fractions the critical discharge q_c is obtained larger than the given discharge q_1 , the result will obviously be a negative bed load for that particular subrange, and should, therefore, be introduced into Eq. (9.13) with its negative sign. Although Schoklitsch tries to explain such a physically improbable result as caused by the finer grains which cover the bed and hinder the movement of coarser fractions, thus reducing the total bed load, it still remains a questionable aspect of the proposed procedure.

No direct indication has been given as to the range of grain sizes to which Eqs. (9.11) and (9.12) are applicable. It is, however, generally presumed that the formula is largely based on the experimental data supplied by Gilbert [27], which were related to grain sizes in the range of 0.3–7.0 mm approximately.

Those interested in other formulae of the same type, as partially listed in par. 9.3.1, should consult the original papers indicated in the References at the end of the chapter, or any exhaustive textbook on sediment transport. The given formula is only an illustration of Q -type bed load formulae, which “. . . merely happens to agree better with other formulae in use within arbitrary limit of $\pm 30\%$ [21]”.

9.3.2 Second Approach: Bed Load Expressed in Terms of the Shear Stress

This approach is no doubt much more favored today, because of the importance accorded to the shear stress in all aspects of the sediment movement in alluvial channels. It is however, not claimed that transport formulae based on this concept are necessarily any more accurate than other formulae, since anyway they are largely empirical, and hence the determining factor remains probably the extent of the experimental background and its patient and methodical analysis. Samples of formulae of this type are those by Straub-Du Boys (1935) [28, 29], Waterways Experiment Station (1935) [30], Shields (1936) [16], Kalinske (1947) [31], Meyer-Peter and Mueller (1948) [32], Elzerman and Frijlink (1951) [33] and Pezzoli (1980) [34]. The best known of these, and probably the most widely used, is the Meyer-Peter and Mueller formula; it also gives the best agreement with other for-

mulae, according to Shulits's analysis.

9.3.2.1 Meyer-Peter and Mueller Formula

The original Meyer-Peter formula was first published in 1934, and it was of the discharge type as described in the previous paragraph. Fourteen years of meticulous and patient research were needed to arrive at a new type of formula (1948) in collaboration with R. Mueller at the E.T.H. in Zuerich [32].

The formula as given by the authors is as follows:

$$0.25 \left[\frac{\gamma}{g} \right]^{1/3} \left[1 - \frac{\gamma}{\gamma_s} \right]^{2/3} G_s^{2/3} = \frac{Q_B}{Q} \left[\frac{n_G}{n_B} \right]^{3/2} \gamma d J - 0.047 (\gamma_s - \gamma) d_s \quad (9.14)$$

In which, G_s – dry weight of the transported sediment, in N/sec per meter width of the channel, γ – specific weight of the water, in N/m^3 , g – acceleration of gravity, in m/sec^2 , Q – total discharge, in m^3/sec , Q_B – part of the discharge apportioned to the bed, in m^3/sec , n_G – Manning grain-roughness coefficient, n_B – Manning bed roughness coefficient, d – depth of flow, in m, J – hydraulic gradient (slope), γ_s – specific weight of the sediment, in Nt/m^3 , d_s – representative diameter of bed material, in m.

The correction factor Q_B/Q has been introduced into the formula mainly in order to account for laboratory flumes and small channels, where the side wall effect may be of importance. It is given by

$$\frac{Q_B}{Q} = \frac{b n_B^{3/2}}{b n_B^{3/2} + 2 d n_w^{3/2}} \quad (9.15)$$

where b – width of the channel in m, n_w – wall roughness coefficient.

The derivation of Eq. (9.15) is based on rather arbitrary assumptions and its physical basis is somewhat unrealistic. However, in most cases of natural streams, where hydraulic radius may be safely replaced by the depth of flow, this factor tends to unity, hence can altogether be omitted.

The bed roughness coefficient n_B , which comprises the bottom roughness due to the sediment and to form resistance (dunes, ripples, bars, etc), should be estimated. The grain roughness coefficient, n_G is defined by

$$n_G = \frac{d_{s90}^{1/6}}{26} \quad (9.16)$$

Here d_{s90} signifies the grain diameter of the bed material at which 90% of the mixture by weight is finer. Eq. (9.14) is valid only for fully developed turbulence; in all other cases, Moody diagram should be used, by first obtaining the Reynolds numbers as $Re = V(4R_B)/\nu$, and the relative roughness using $d_{s90}/4R_B$. The bed hydraulic radius can be obtained from Eq. (9.17),

$$R_B = \frac{Q_B}{Q} \cdot d \quad (9.17)$$

Then the roughness coefficient could be estimated from

$$n_G = (f/8g)^{1/2} R_B^{1/6} \quad (9.18)$$

Here f denotes the Darcy-Weissbach friction factor. Again, in most engineering cases it can be assumed, at least for preliminary estimates, that $n_G \cong n_B$, and thus the factor $(n_G/n_B)^{3/2}$ may also be eliminated. There are presently no reliable data for the values of n_G/n_B in alluvial streams.

The representative grain diameter d_s should best be determined, according to the authors, by dividing the grain-size distribution curve into several fractions, and then computing the grain size by

$$d_s = \frac{\sum \bar{d}_s \Delta p}{100} \quad (9.19)$$

in which \bar{d}_s – average size of grains in a size fraction, Δp – percentage of a given fraction in respect to the total.

Simple analysis of Eq. (9.14) shows that all the three terms composing it are shear stresses (tractive force). The first term on the right-hand side is the total shear stress (γdJ), diminished to account for the possible reduction of discharge and for the form resistance; the second term on the right-hand side has the form of a critical shear stress, i.e. a stress at which individual grains just start to move, as function of bed material. The term on the left-hand side, consequently, is the net shear stress available for the transport of bed load.

As stated before, this is one of the most popular formulae for the estimate of bed load in natural streams, and particularly so on the European continent. The two numerical coefficients included in the formula are often adjusted by practicing engineers to render the formula more suitable to specific conditions of a given alluvial stream. Such an insight into the stream

behavior can often be gained by choosing a characteristic stream length and measuring and observing hydraulic and sedimentological data, until a more or less reliable correlation between them is possible.

Meyer-Peter and Mueller formulae (Eq. (9.14)) may be used with any system of units. There is no conclusive evidence about the accuracy of its predictions for sandy streams, since serious researchers have reported contradictory results. It seems, however, to give fair agreement with measured quantities for coarser sediment, i.e. for gravel or cobble-bed streams. In such cases, obviously, the method will yield bed load only, and suspended load has to be computed separately in order to obtain total load.

9.3.2.2 Straub-Du Boys Formula (1935)

About the time Meyer-Peter and Mueller started carrying out their extensive laboratory experiments, which eventually enabled them to publish their shear-stress formula for bed load transport, Straub [29] extended the existing Du Boys [28] expression for bed load by providing for the numerical values left missing by Du Boys. The equation as given by Straub has the form

$$G_s = \frac{\psi}{\gamma^2} \tau (\tau - \tau_c) \quad (9.20)$$

wherein G_s – bed load (dry weight), in N/sec/m, ψ – a coefficient expressing sediment characteristics, in N/m³/sec, γ – specific weight of the water, in N/m³, τ – shear stress, in N/m², τ_c – critical shear stress, in N/m²

Shear stress τ can be computed by Eq. (3.1), or its equivalent for relatively wide streams in which $R \cong d$,

$$\tau = \gamma dJ \quad (9.21)$$

Eq. (9.20) is often encountered also in the form

$$G = K \tau (\tau - \tau_c) \quad (9.22)$$

in which $K = \psi/\gamma^2$. Straub has also given values for the critical shear stress τ_c . Values of the coefficient K and of τ_c as function of grain size d_s (mm) are given in Fig. 9.4. In the original publication, d_s is vaguely defined as “the mean diameter”, without further explanation; however, in his later publication [35], Straub indicates that what he had in mind was in fact d_{s50} to represent the mixture.

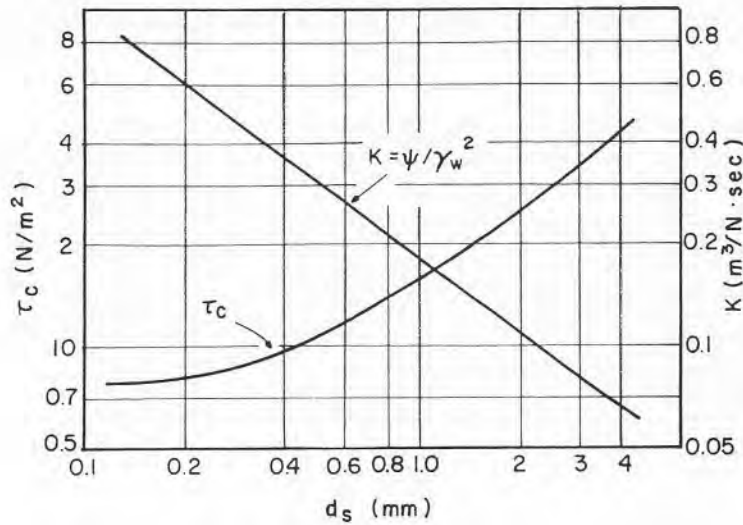


Fig. 9.4. Values of the critical shear stress τ_c and of coefficient K ($\rho = 1000 \text{ kg/m}^3$) vs. mean grain size d_s after Straub [35].

Du Boys' mathematical model of sliding sediment layers, on which his original expression for sediment transport is based, has been abandoned many years ago. Straub's own experimental evidence, which he used for the determination of the characteristic values of ψ and τ_c , has been criticized by many researchers as insufficient and mainly based on laboratory experiments. That may well be true, although Straub was never very explicit on this point. Eqs. (9.20) or (9.22) have the advantage, however, of being extremely simple for use and straightforward, and, strangely enough, giving quite acceptable engineering results. Indeed, according to Shulits' analysis, on which the selection in the present text is based, it qualifies as being within 30% of other shear-stress formulae.

If Eq. (9.24) is used in English units, coefficient K and the critical shear stress τ_c should be taken from the graph on Fig. 9.5.

9.4 Selection of Bed Load Formulae

The three bed load formulae presented so far, out of a bewildering and confusing array of similar expressions, are by no means thought to be the

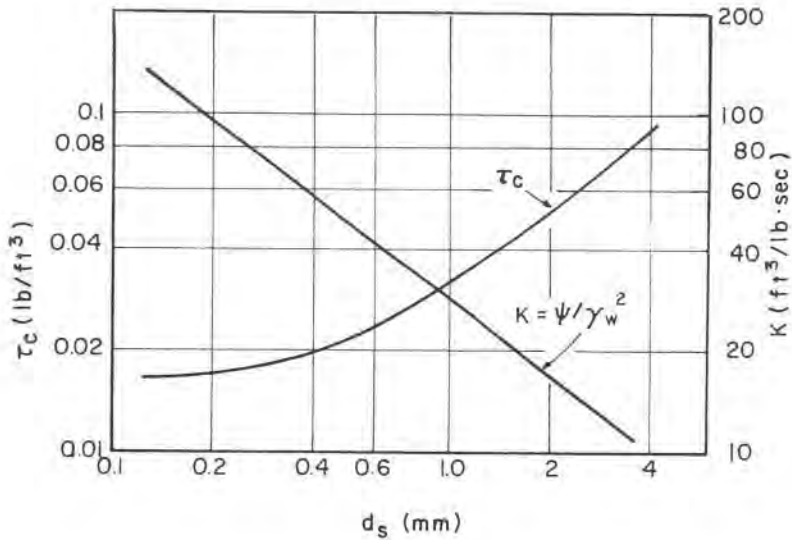


Fig. 9.5. Values of the critical shear stress τ_c and of coefficient K , vs. mean grain size d_s in English units, after Straub [35].

most accurate ones, or theoretically best suited to define the complicated physical process of sediment transport. As stated before, according to Shulits' analysis they merely happen to agree better with the other formulae in use. The adopted comparison procedure and limits of agreement between the different formulae seem quite reasonable from the engineering point of view. Only wide channels have been treated, for which hydraulic radius may be substituted by the depth of flow, thus making $Q_B \cong Q$.

Some results of the extensive examination concerning the best-known discharge formulae are graphically represented in Fig. 9.6. The Schoklitsch (1934) formula has been taken as the base line, and the differences have been computed relative to it. Good agreement of the Schoklitsch (1934) formula with most other formula, along at least a significant range of grain diameters, is evident from the graph.

It is generally assumed that the Schoklitsch (1934) formula adequately covers the range of grain sizes between 0.3 mm to 7 mm approximately.

Selection of a shear stress formula was more difficult and certainly more laborious, because the mutual relationship between different expressions changes with varying shear stress. For this reason it has finally been decided to adopt two formulae instead of one, i.e. Meyer-Peter and Mueller and Straub, which together cover most of the range within the deviation of $\pm 30\%$.

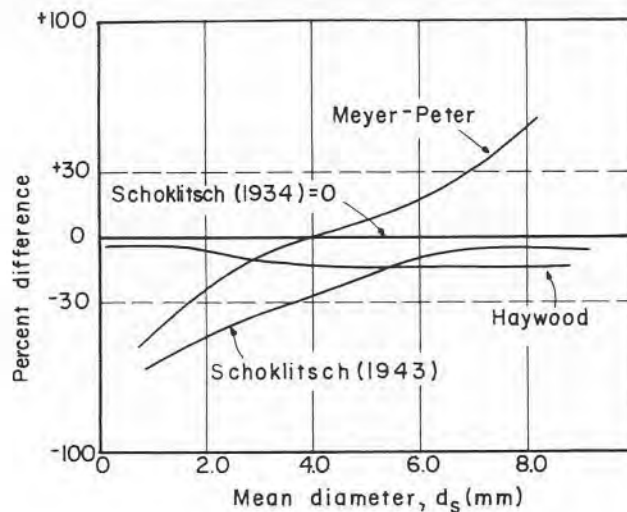


Fig. 9.6. Approximate deviation of discharge formulae from Schoklitsch (1934) formula, after Shulits [21].

Graphs on Figs. 9.7 and 9.8 show the relationship for two grain sizes, $d_s = 1$ mm and $d_s = 3$ mm. The curve for the values computed by the Shields formula has been obtained for Manning coefficient of $n = 0.04$ and hydraulic gradient of 0.01. Both formulae are valid for beds of uniform grains and for mixtures, provided the mean or effective diameter is computed as indicated before. The comparative study has been carried out for grain sizes in the range of 0.3–7 mm, common to all the formulae (only Meyer-Peter tested uniform-grain beds up to about 29 mm diameter). It is generally thought that the range of bed shear-stress for natural streams is in the range of about 2.5–29 N/m^2 . Agreement between different shear-stress formulae depends on τ , and is less satisfactory with increasing shear-stress (see Figs. 9.7 and 9.8); for τ -values beyond the above range, large differences between the formulae may be obtained.

It should once more be stressed that in the three formulae presented in the text, as well as in others only mentioned, there are empirical coefficients and factors, often obtained mainly from laboratory studies. These empirical values should be adapted, whenever possible, to fit local or regional conditions by follow-up measurements and observations, rather than be blindly taken as immutable and all-embracing.

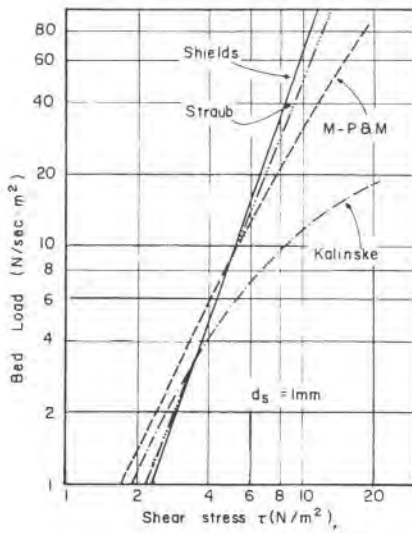


Fig. 9.7. Comparison of shear stress formulae for $d_s = 1\text{ mm}$, after Shulits [21].

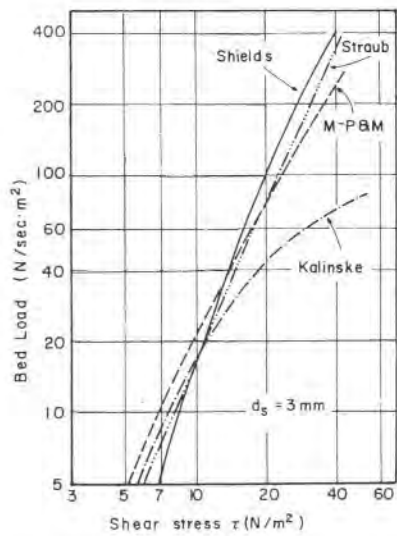


Fig. 9.8. Comparison of shear-stress formulae for $d_s = 3\text{ mm}$, after Shulits [21].

Example 9.2

Grain-size distribution curve as measured in a natural stream is given in Fig. 9.9. Hydraulic gradient in the stretch under observation has been estimated as $J = 0.75\%$, and the flow may be considered as uniform. Width of the channel is large in relation to the depth of the stream.

Estimate the bed-material discharge per meter width of the stream, for the specific discharge of $q = 4.0 \text{ m}^3/\text{sec.m}$ using Schoklitsch bed load formula.

Step 1 – Grain-size distribution curve is arbitrarily divided into 4 sections, and mean grain diameter for each section is determined, as well as the percentage of each section in relation to the total. These data are summarized in Table 9.2.

Step 2 – Next critical discharge q_c is computed for each partial mean grain-size \bar{d}_s , applying Eq. (9.12).

$$q_{c1} = 1.94 \times 10^{-5} \frac{4.9}{(0.00075)^{4/3}} = 1.4 \text{ m}^3/\text{sec.m}$$

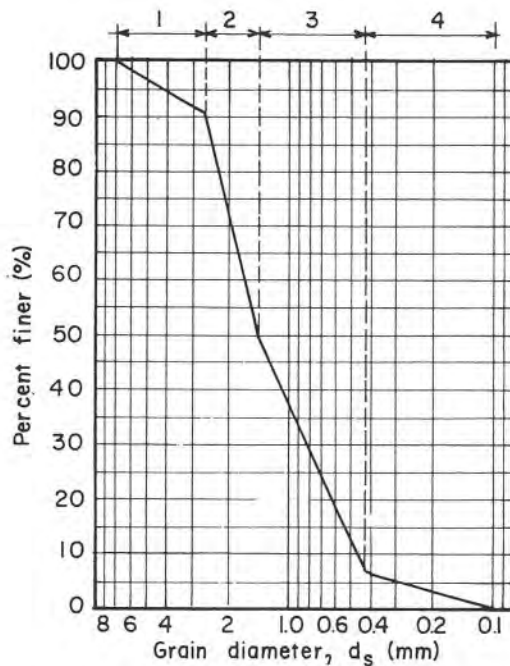


Fig. 9.9. Grain-size distribution curve for Example 9.2.

TABLE 9.2. GRAIN-SIZE DISTRIBUTION DATA (Ex. 9.2)

Section No.	\bar{d}_s (mm)	Percent (%)
1	4.9	9.0
2	2.15	41.0
3	0.96	43.0
4	0.26	7.0
		100%

Similarly, critical discharges for other values of \bar{d}_s may easily be obtained,
 $q_{c_2} = 0.6 \text{ m}^3/\text{sec.m}$; $q_{c_3} = 0.27 \text{ m}^3/\text{sec.m}$; $q_{c_4} = 0.074 \text{ m}^3/\text{sec.m}$

Step 3 – Now partial sediment discharges can be computed, using Eq. (9.11)

$$G_1 = 7000 \frac{(0.00075)^{3/2}}{(4.9)^{1/2}} (4.0 - 1.4) = 0.17 \text{ kg/sec.m}$$

$$G_2 = 7000 \frac{(0.00075)^{3/2}}{(2.15)^{1/2}} (4.0 - 0.6) = 0.34 \text{ kg/sec.m}$$

Similarly, $G_3 = 0.54 \text{ kg/sec.m}$; $G_4 = 1.1 \text{ kg/sec.m}$.

Step 4 – Total estimated bed load discharge for one meter width of the channel, according to Eq. (9.13).

$$G_s = 0.09 \times 0.17 + 0.41 \times 0.34 + 0.43 \times 0.54 + 0.07 \times 1.1$$

$$G_s = 0.46 \cong 0.5 \text{ kg/sec.m}$$

Had the sediment discharge been computed using d_{s50} instead of the recommended procedure, the result would have been $G_s \cong 0.42 \text{ kg/sec.m}$, i.e. about 9% less.

Example 9.3

It is required to make an estimate of the bed load discharge in a given stream, using Meyer-Peter and Mueller formula. Bed load analysis has given the data as reported on the grain-size distribution curve, Fig. 9.10. Mean value of the hydraulic gradient has been set at $J \cong 1\%$. The estimate is to be made for the stream depth of $d = 3.0$ m. Specific gravity of the sediment is $S_s = 2.65$. After a preliminary study, it has been decided that the value of the factor $(Q_B/Q) (n_G/n_B)^{3/2}$ be taken as 0.9.

Step 1 – In order to determine the mean bed load diameter, the distribution curve is divided into 4 sections (see Fig. 9.10), and for each one partial mean diameter and relative quantity of the total are determined. This is summarized in Table 9.3. Hence the mean bed load diameter,

$$\bar{d}_s = \frac{1}{100} (7.0 \times 5 + 2.5 \times 50 + 0.81 \times 37 + 0.35 \times 8)$$

$$\bar{d}_s \cong 1.93 \text{ mm}$$

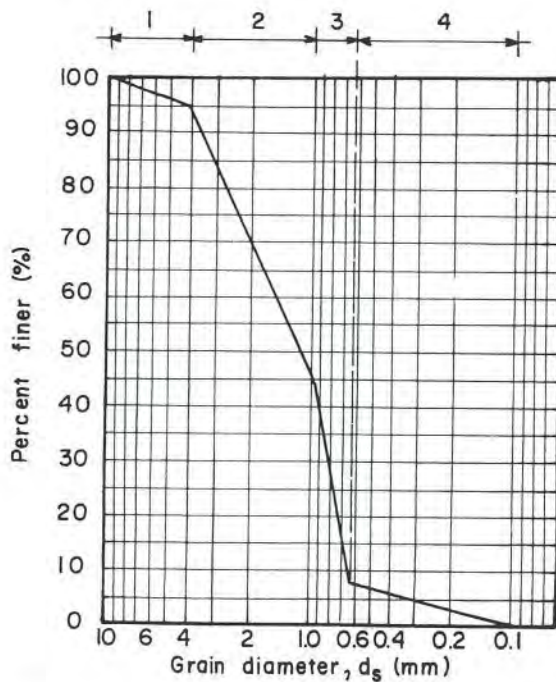


Fig. 9.10. Grain-size distribution curve for Example 9.3.

TABLE 9.3. GRAIN-SIZE DISTRIBUTION (Ex. 9.3)

Section No.	\bar{d}_s (mm)	Percent (%)
1	7.0	5
2	2.5	50
3	0.81	37
4	0.35	8
Total		100%

Step 2 – For the estimate of the bed load discharge, Eq. (9.14) is used,

$$0.25 \left[\frac{\gamma}{g} \right]^{1/3} \left[1 - \frac{\gamma}{\gamma_s} \right]^{2/3} G_s^{2/3} = \frac{Q_B}{Q} \left[\frac{n_G}{n_B} \right]^{3/2} \gamma d J - 0.047 (\gamma_s - \gamma) d_s$$

Introducing the numerical values

$$0.25 (1000)^{1/3} \left[1 - \frac{1}{2.65} \right]^{2/3} G_s^{2/3} = 0.9 \times 1000 \times 9.8 \times 3.0 \times 0.001 - 0.047 (2650 - 1000) 9.8 \times 0.00193$$

$$2.49 \times 0.73 \cdot G_s^{2/3} = 26.5 - 1.47 \cong 25$$

$$G_s = \left[\frac{25}{1.82} \right]^{3/2} = 50.7 \cong 51 \text{ N/sec.m}$$

Example 9.4

Using Meyer-Peter and Mueller formula, estimate the bed load discharge in a rectangular laboratory flume, for the grain-size distribution as shown in Fig. 9.11. Flume data are as follows:

Width of the flume: $b = 1.5$ m

Water depth: $d = 0.4$ m

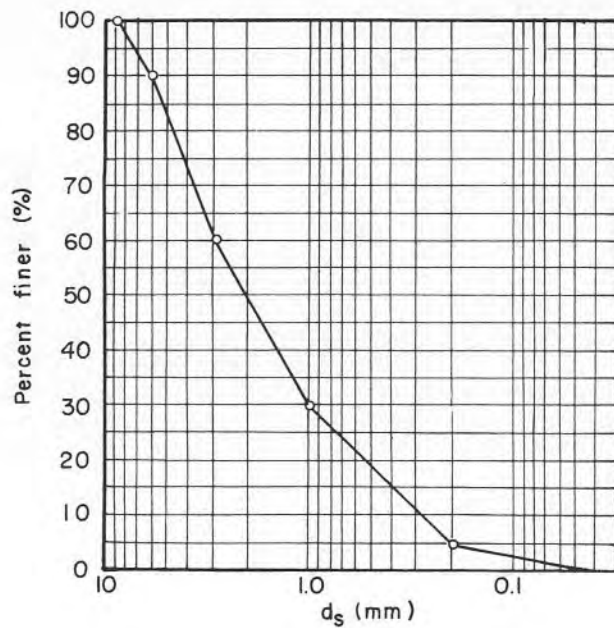


Fig. 9.11. Grain-size distribution for example 9.4.

Longitudinal slope: $I = 0.001$

Measured water discharge: $Q = 0.39 \text{ m}^3/\text{sec}$

Step 1 – Computation of the mean bed load diameter,

$$\bar{d}_s = (10 \times 7.3 + 30 \times 4.25 + 30 \times 1.75 + 25 \times 0.46 + 5 \times 0.1) \times 10^{-3} \times \frac{1}{100}$$

$$\bar{d}_s = 0.00264 \text{ m}; d_{s_{90}} = 6 \text{ mm} = 0.006 \text{ m}$$

Step 2 –

$$A = 1.5 \times 0.4 = 0.6 \text{ m}^2$$

$$P = 1.5 + 2 \times 0.4 = 2.3 \text{ m}$$

$$R = 0.6/2.3 = 0.26 \text{ m}$$

Step 3 – Manning grain-roughness coefficient can be estimated from Eq. (9.16),

$$n_G \cong \frac{d_{s90}^{1/6}}{26} = \frac{0.006^{1/6}}{26} = 0.0164$$

Step 4 – Assuming uniform flow in the flume, n_B can be estimated from the Manning equation for uniform flow,

$$n_B = (AR^{2/3} I^{1/2}) \frac{1}{Q} = (0.6 \times 0.26^{2/3} \times 0.001^{1/2}) \frac{1}{0.39}$$

$$n_B \cong 0.00774 \frac{1}{0.35} = 0.02$$

$$\left[\frac{n_G}{n_B} \right]^{3/2} = \left[\frac{0.0164}{0.020} \right]^{3/2} = 0.74$$

For glass walls, $n_w \cong 0.01$.

Step 5 – The ratio Q_B/Q can be estimated using Eq. (9.15),

$$\frac{Q_B}{Q} \cong \frac{b \times n_B^{3/2}}{b \times n_B^{3/2} + 2d n_w^{3/2}} \cong \frac{1.5 \times 0.02^{3/2}}{1.5 \times 0.020^{3/2} + 2.04 \times 0.01^{3/2}}$$

$$\frac{Q_B}{Q} \cong 0.84$$

Step 6 – Finally, applying Eq. (9.14),

$$0.25 \left[\frac{\gamma}{g} \right]^{1/3} \left[1 - \frac{\gamma_w}{\gamma_s} \right]^{2/3} G_s^{2/3} = \frac{Q_B}{Q} \left[\frac{n_G}{n_B} \right]^{3/2} \gamma d I - 0.047 (\gamma_s - \gamma) \bar{d}_s$$

$$0.25 \times (1000)^{1/3} \left[1 - \frac{1}{2.65} \right]^{2/3} G_s^{2/3} = 0.84 \times 0.74 \times 1000 \times 9.8 \times 0.4 \times$$

$$\times 0.001 - 0.047 (2650 - 1000) \times 9.8 \times 0.00265$$

$$1.82 G_s^{2/3} = 2.44 - 2.1 = 0.34$$

$$G_s = \left[\frac{0.34}{1.82} \right]^{3/2} \cong 0.081 \text{ N/sec.m}$$

This is a small sediment discharge, although not negligible for a laboratory flume. If the result were negative, the meaning would be that no sediment discharge under the given circumstances is to be expected.

Example 9.5

For the same stream data as given in Example 9.3, bed load discharge is to be estimated using the Straub-Du Boys formula, Eq. (9.22)

$$G = K\tau(\tau - \tau_c)$$

Step 1 – From the grain-size distribution curve, Fig. 9.10, $d_{s_{50}} = 1.2$ mm.

For this mean grain diameter, factor K and the critical shear stress τ_c can be obtained from the graph on Fig. 9.4, $K = \sim 0.6$; $\tau_c = \sim 1.8 \text{ N/m}^2$.

Step 2 – Bed shear stress τ can now be computed, $\tau \cong \gamma dJ = 1000 \times 9.8 \times 3.0 \times 0.001 = 29.4 \text{ N/m}^2$.

Step 3 – Bed load discharge accordingly, $G = 0.6 \times 1.8 (29.4 - 1.8) = 29.8 \text{ N/sec.m}$.

This result is about 41% lower than the bed load computed using Meyer-Peter and Mueller formula, Example 9.3. As far as bed load formulae go, this is not exceptional, though it is higher than the expected 30% difference. However, it should be borne in mind that the given bed shear stress $\tau = 29.4 \text{ N/m}^2$ is relatively high. From the diagram of Fig. 9.7 it can indeed be seen that for such high values of τ , the difference between the Meyer-Peter and Mueller formula and Straub formula cannot be expected to be within the limits of $\pm 30\%$ (for the given mean diameter of $d_{s_{50}} = 1.2$ mm).

9.5 Einstein Formula (1950)

In the present text, which is intended to be a manual for the practicing engineer, the number of the selected formulae has been deliberately reduced

to three, in order to avoid confusion which is likely to be felt by any engineer when confronted with a large number of formulae. It has nevertheless been decided to include, at least partially, the Einstein formula, for the main reason that up to the present date this formula, more than any other, is based on the general concepts of the modern fluid mechanics, and it is often in good agreement with measured quantities.

Einstein bed load function and the method itself are highly complicated and unwieldy. There is, indeed, no possibility to present the theoretical basis of the method within the framework of a manual, and the interested engineer is advised to consult and study the original publication [36]. Even after mastering the main theoretical tenets of the method, its actual engineering application still offers formidable difficulties. A numerical example is, therefore, worked out, following the steps as indicated by the author himself (see [36], pp. 42–60), and using a set of his own data. It is hoped that this might be of some help for whoever decides to try his hand at the actual application of the method.

The method is not based on any concept of some critical parameter (shear stress or discharge) for the incipient sediment transportation, because such a parameter, according to Einstein, is always difficult to define. The initiation and end of sediment motion is related instead to the concept of probability inherent in the mutual relationship between hydrodynamic lift forces and the submerged weight of the particles. The average distance travelled by any bed load particle between consecutive points of deposition in the bed is assumed to be constant (about 100 grain diameters). There is also the concept of linearity of friction, which allows shape resistance and surface drag to be added arithmetically. Thus the bed shear stress may be divided into two components: the one acting on individual sediment grains of the bed, τ_b' , and the other, τ_b'' , on bed forms, such as dunes, bars, etc. For wide channels, in which banks may be neglected, this means

$$\tau_b = \tau_b' + \tau_b'' \quad (9.23)$$

from which, since ρ and J are assumed constant, it is easily deduced that

$$R_b = R_b' + R_b'' \quad (9.24)$$

The stream discharge for the purpose of computing the sediment rate, is obtained using the bed hydraulic radius R_b , which is not necessarily equal to the discharge computed by the Manning (or Strickler) equation.

The *numerical application* of the method is shown in Example 9.6 for one segment of the original calculation for the Big Sand Creek.

Example 9.6

Carry out partial numerical computation of bed load discharge for the Big Sand Creek as given on pp. 46–59 of the original publication [36].

Steps 1–4 deal with the selection of the representative reach and the determination of the representative cross section and its geometric elements. The average slope was found to be $J = 0.00105$, and the geometric elements have been summarized in the graphs of Fig. 9.12. Next the grain-size composition of the bed sediment was carried out, (Step 5). The average grain-size analysis of the bed is given in Fig. 9.13.

From the graph: $d_{s_{35}} = 0.29$ mm; $d_{s_{65}} = 0.37$ mm.

Step 6 – Sediment discharge will be calculated for the fraction having the average grain diameter $d_s = 0.35$ mm. Bank friction will be neglected.

A. Hydraulic calculations

Step 7 (p. 51). R_b should be assumed as the first step in the calculation; hence $R'_b = 0.91$ m. (see Table 6 of [36], p. 52.)

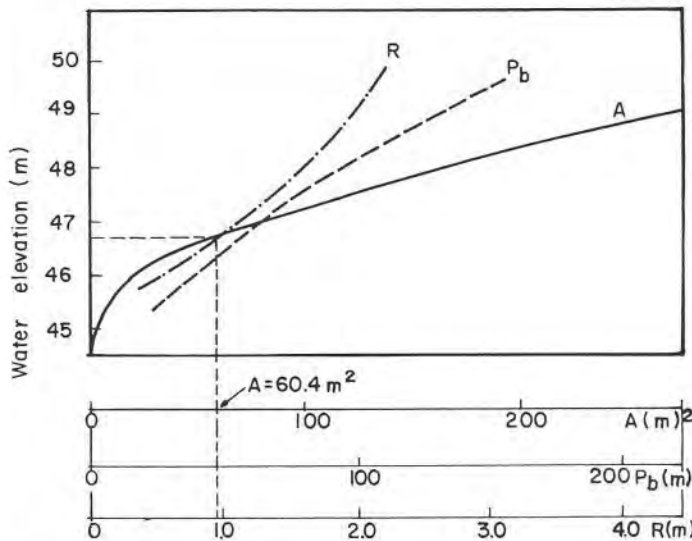


Fig. 9.12. Description of the average cross-section, Big Sand Creek, after [36].

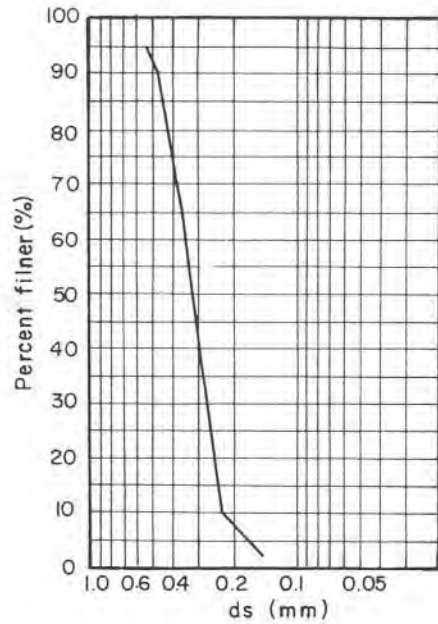


Fig. 9.13. Average grain-size analysis of the bed, Big Sand Creek, after [36].

Step 8 – Corresponding shear stress velocity,

$$u_*' = (R_b' Jg)^{1/2} = (0.91 \times 0.00105 \times 9.81)^{1/2} = 0.097 \text{ m/sec}$$

Step 9 – Thickness of the laminar sublayer, Eq. (5.15),

$$\delta = \frac{11.6 \nu}{u_*'} = \frac{11.6}{0.097 \times 10^6} = 0.000119 \text{ m}$$

Here the kinematic viscosity of water was assumed to be $\nu = 10^{-6} \text{ m}^2/\text{sec}$.

Step 10 – $k_s = d_{s_{65}} = 0.37 \text{ mm}$, hence

$$\frac{k_s}{\delta} = \frac{0.37 \times 10^{-3}}{0.000119} = 3.09$$

Step 11 (p. 53). For the value of $k_s/\delta = 3.09$, read the correction factor x from Fig. 5.3. $x = 1.17$.

Step 12 – Apparent roughness

$$\Delta = \frac{k_s}{x} = \frac{0.37 \times 10^{-3}}{1.17} = 0.000316 \text{ m}$$

Step 13 – Next the average flow velocity is computed,

$$\bar{u} = u_*' 5.75 \log \left[12.27 \frac{R_b'}{\Delta} \right] = 0.097 \times 5.75 \times \log \left[12.27 \frac{0.91}{0.000316} \right]$$

$$\bar{u} = 2.536 \text{ m/sec}$$

Step 14 – Dimensionless parameter ψ' ,

$$\psi' = \frac{\rho_s - \rho}{\rho_s} \frac{d_{s35}}{R_b' J} = (S_s - 1) \frac{d_{s35}}{R_b' J}$$

$$\psi' = (2.65 - 1) \frac{0.29 \times 10^{-3}}{0.91 \times 0.00105} = 0.5$$

Specific gravity for sand grains, S_s , has been assumed 2.65.

Step 15 – Now, from Fig. 5 [36], reproduced on Fig. 9.14, for $\psi' = 0.5$, we read directly $\bar{u}/u_*'' \cong 95$.

Although the graph on Fig. 9.14 was originally intended to be used for ψ' -values in the range of 0.5–40, Einstein himself made linear extrapolations beyond the 0.5-limit.

Step 16 – From the previous step, shear velocity for channel irregularities:

$$u_*'' = \frac{\bar{u}}{95} = \frac{2.536}{95} = 0.0267 \text{ m/sec}$$

Step 17 – Now hydraulic radius apportioned to channel irregularities:

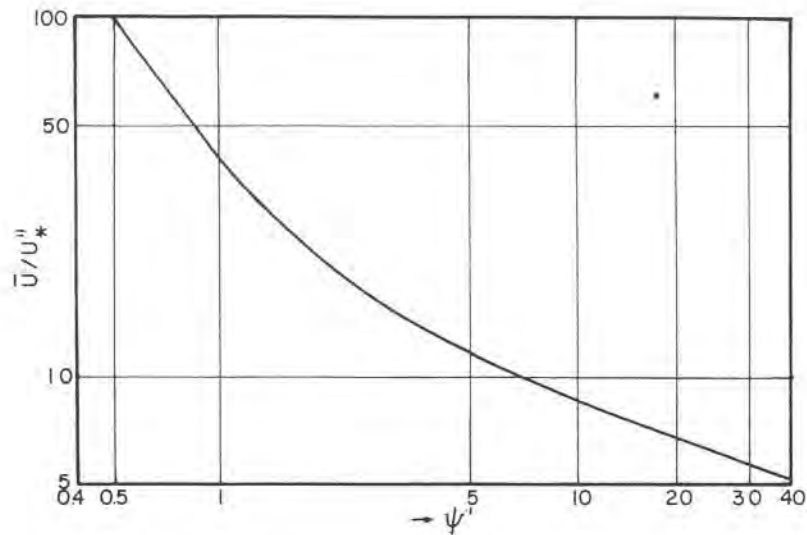


Fig. 9.14. \bar{u}/u_*'' vs. ψ' , after [36].

$$R_b'' = \frac{(u_*'')^2}{gJ} = \frac{(0.0267)^2}{9.8 \times 0.00105} = 0.0692 \text{ m}$$

Step 18 – Hydraulic radius R_b

$$R_b = R_b' + R_b'' = 0.91 + 0.0692 = 0.979 \text{ m}$$

It can be seen that R_b'' is only about 7% of the combined hydraulic radius R_b .

Step 19 – From the graph of geometric elements, Fig. 9.12, and for $R_b = 0.979 \text{ m}$ (R_b is the total hydraulic radius of the section when bank friction is neglected, see Step 6), it can be found, $A_b = A_T \cong 60 \text{ m}^2$.

Step 20 – The flow discharge is calculated as

$$Q = A_T \bar{u} = 60 \times 2.536 \cong 153 \text{ m}^3/\text{sec}$$

B. Bed-load calculations

Step 25 (p. 59). Intensity of shear, ψ , is calculated,

$$\psi = (S_s - 1) \frac{d_s}{R'_b J} = (2.65 - 1) \frac{0.35 \times 10^{-3}}{0.91 \times 0.00105}$$

For R'_b the value of 0.91 m is retained. $\psi = 0.604$. Here d_s is the average grain diameter for the chosen fraction, see Step 6.

Step 26

From Step 12 – $\Delta = 0.000316$ m.

From Step 9 – $\delta = 0.000119$ m.

Hence,

$$\frac{\Delta}{\delta} = \frac{0.000316}{0.000119} = 2.655 > 1.8$$

Since the ratio $\Delta/\delta > 1.8$, according to Einstein [36, p. 35] the characteristic grain size of mixture

$$X = 0.77 \Delta = 0.77 \times 0.000316 = 0.000243 \text{ m}$$

Step 27 – Calculate the ratio

$$\frac{d_s}{X} = \frac{0.35 \times 10^{-3}}{0.000243} = 1.44$$

Step 28 – For the d_s/X ratio just obtained, find the corresponding “hiding factor” of grains in a mixture, ξ , from Einstein graph No. 7, reproduced on Fig. 9.15.

From the graph on Fig. 9.15, $\xi = 1.0$. This means that, since $d_s = 0.35$ mm $> X$, there is no “hiding” of the fraction represented by this average grain size.

Step 29 – From Step 10, the value of the ratio $k_s/\delta = 3.09$.

Corresponding value of pressure-correction factor for the average particle of the fraction, Y , is found from Einstein Fig. 8, reproduced on Fig. 9.16, $Y \cong 0.55$.

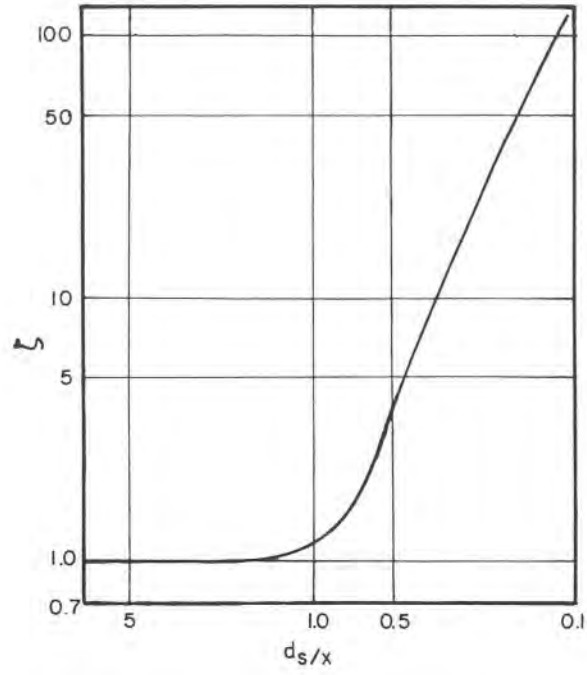


Fig. 9.15. ξ vs. d_s/X , after [36].

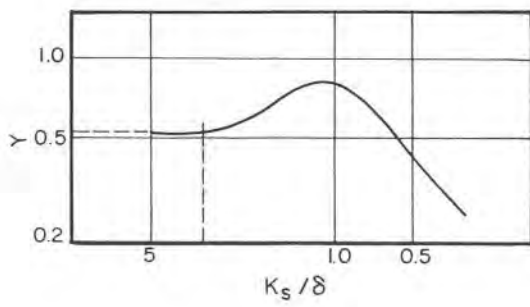


Fig. 9.16. Y vs. k_s/δ , after [36].

Step 30 – Compute function β_x ,

$$\beta_x = \log \left[10.6 \frac{X}{\Delta} \right] = \log \left[10.6 \frac{2.43 \times 10^{-4}}{3.16 \times 10^{-4}} \right] \quad \beta_x = 0.911$$

Step 31 – $\beta = \log(10.6) = 1.025$, then

$$\left[\frac{\beta}{\beta_x} \right]^2 = \left[\frac{1.025}{0.911} \right]^2 = 1.265$$

Step 32 – Now compute intensity of shear for individual grain size

$$\psi_* = \xi Y (\beta/\beta_x)^2 \psi = 1 \times 0.55 \times 1.265 \times 0.604 = 0.42$$

(ψ was found in Step 25 to be 0.604)

Step 33 – From Fig. 9.17, on which Einstein graph No. 10 is reproduced, we read for $\psi_* = 0.42$: $\phi_* \cong 19.0$.

Step 34 – Finally, the bed load discharge for the given fraction can now be calculated.

$$i_B q_B = \phi_* i_b \frac{\gamma_s}{g} g^{3/2} d_s^{3/2} (S_s - 1)^{1/2}$$

where i_b – fraction of bed load for a given average grain size; from Table 5 [36, p.51] that for the fraction having the average grain diameter $d_s = 0.35$ mm, $i_b = 40.2\%$.

$$i_B q_B = 19.0 \times 0.402 \times 2650 \times 9.81^{3/2} \times (0.00035)^{3/2} (2.65 - 1)^{1/2}$$

$$i_B q_B = 5.2 \text{ N/sec.m}$$

In order to compute the total bed load discharge, similar calculations would have to be carried out for each one of the fractions, and then all particle discharges added up.

It should be emphasized once more that the above numerical example is

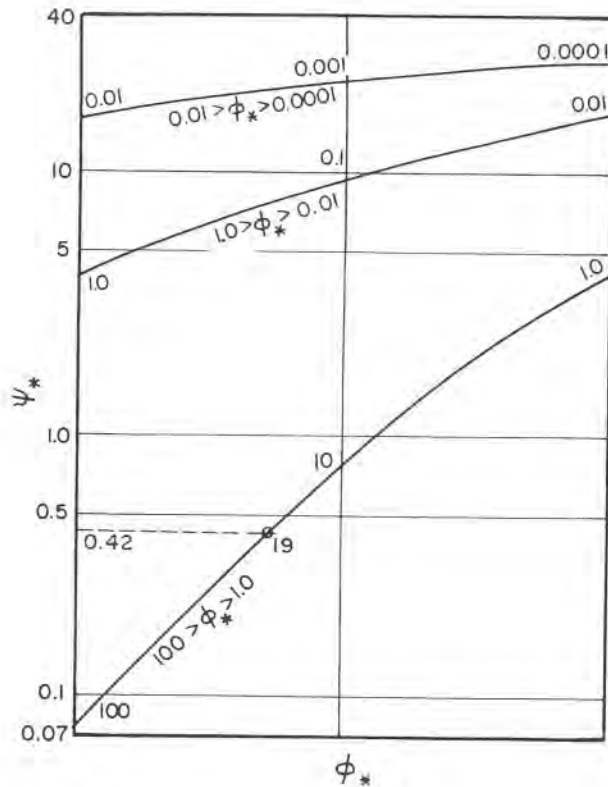


Fig. 9.17. ϕ_* vs. ψ_* , after [36].

by no means intended to substitute the serious study of the method. Such a study is indeed indispensable for any engineer wishing to apply the method to a concrete case.

On Fig. 9.18 a graph is given of computed bed load discharges according to the method discussed in the present text as compared with observed points, for the river Colorado according to V.A. Vanoni et al. [4].

9.6 Other Approaches

9.6.1 Particular Formulae for Specific Streams or Watersheds

As already mentioned in par. 9.3, within the restricted limits of the present text there is no practical possibility to discuss the merits and short-

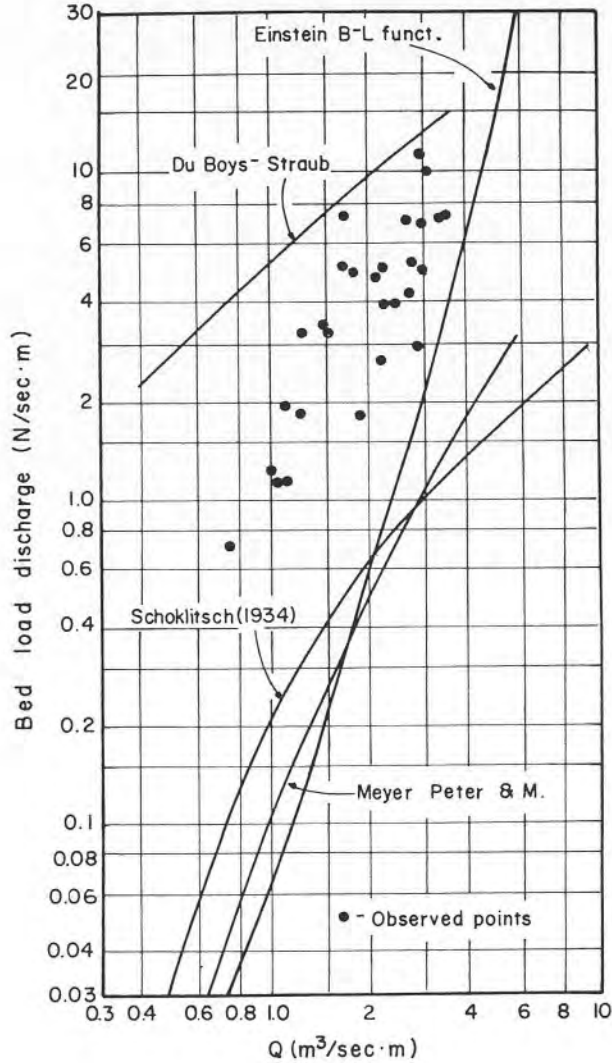


Fig. 9.18. Comparison between computed bed load rating curves and observed points, Colorado River, after [4].

comings of the great number of formulae that abound in the engineering literature. They are generally empirical expressions based on observed data of a single stream, or a system of streams. Many such formulae can be found in the civil engineering literature written in Russian and Polish (such as formulae from Jarocki, Goncharov, Levi, Shamov, Lopatin and others).

A good survey of them can be found in the work by W. Jarocki, which has been translated into English [37].

If for a given stream a number of measured or computed data is available, it is often convenient to express the relationships between the bed-material sediment discharge per unit width of channel, q_s (kg/hr/m), as an exponential function of the mean velocity (or sometimes a linear relation):

$$q_s = K V^n \quad (9.24a)$$

in which K is a coefficient and n an exponent, obtained either from a best-fit curve or linear regression for the logarithmic form of the equation. Scatter of the plotting points or standard deviation are good indications about the reliability of the relationship.

In the present text a definite effort has been made to reduce the number of bed load formulae to a minimum, in order to avoid as much as possible the confusion likely to be experienced by any engineer forced to choose between a bewildering number of proposed expressions. It is believed, therefore, that the use of particular empirical formulae certainly cannot add clarity, and is basically unnecessary. Local characteristics can always be taken account of by judiciously adjusting the empirical coefficients to better suit any set of measured values.

9.6.2 Bed Load Equation Based on Movement of Bed Forms

The possibility of using the movement of bed forms (dunes, ripples, bars, etc) for the calculation of sediment discharge has already been briefly mentioned in par. 2.5.4. The idea as such is not a new development. It has only become less academic since the relatively recent development of electronic equipment, generally reliable and easily portable, for rapid and accurate determination of bed configuration and the velocity of sand waves.

As developed by Richardson et al. [38], and later given by Simons et al. [39], the formula, derived from the general differential equation for bed load transport, reads as follows,

$$G_s = \gamma_s (1 - \lambda) V_s \frac{h}{2} \quad (9.25)$$

where G_s – bed load discharge, in N/sec.m, γ_s – specific weight of sediment, in N/m³, λ – porosity of the sand bed, V_s – average velocity of ripples or dunes in the direction of flow, in m/sec, h – average amplitude of the ripples or dunes, in m.

The above expression has been developed on the assumption of “almost continuous contact” of bed material with the bed, and that the dunes have triangular shapes.

Porosity of the bed material, equal to

$$\lambda = \frac{V_v}{V} \quad (9.26)$$

in which V_v – volume of voids in the sample, V – total volume of the sample, is generally in the range of 0.4 – 0.7.

Eq. (9.25) seems to be more suited for a dune-bed than for ripples, and for coarser material (about 1 mm grain diameter) than for fine fractions. The accuracy of the equation was found to “improve” when the dunes cover the entire width of the channel (straight, uniform channels of small width-to-depth ratios).

A similar method has recently been proposed by Engel and Lau [44, 61], who arrived at the expression,

$$G_s = 1.32 \gamma_s (1 - \lambda) \bar{\xi} V_s \quad (9.27)$$

in which the symbols used are identical to those of Eq. (9.25); $\bar{\xi}$ denotes the “mean departure of bed elevation from the mean level” (see Fig. 9.19). It is less than $h/2$ of Eq. (9.25), hence the fixed numerical coefficient of 1.32. The assumption of average shape values for the bed forms seems to be admissible, since from the research by Cheong and Shen [45] it could be concluded that although the shape of individual bed forms may change as they

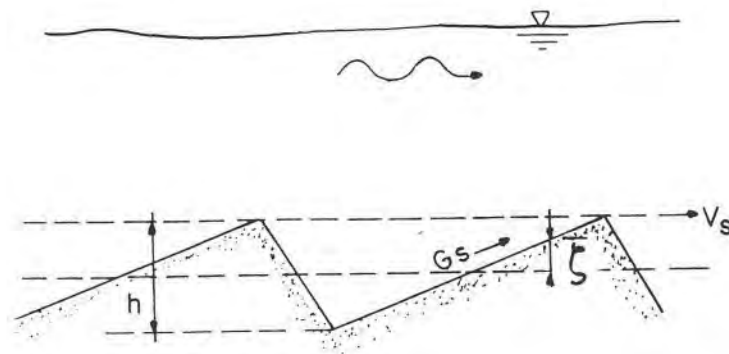


Fig. 9.19. Definition sketch of bed-form movement, after [39, 44].

move downstream, there nevertheless is a statistical constancy of form. The second assumption of triangular shape is probably also sufficiently accurate as far as computations of transport rates are concerned [46]. Although interesting methods for the estimate of bed load discharge in sandy streams, they have so far found limited practical application.

A special bed load formula has been proposed by M. Pica [40] for small ephemeral streams of torrential character, with extremely variable water discharges and dry beds during long summer months. Although derived only from data for fiumare in the Calabria region of Italy, for which there are almost no reliable hydrological records, and laboratory experiments, it nevertheless may be of interest in many other semi-arid regions with similar conditions, particularly in the Mediterranean Basin.

9.7 Conclusion

Reviewing analytically the many bed load formulae put forward during the last 50 years, one is led to the inevitable conclusion that the physical mechanism governing the transportation of the bed-material load has not yet been fully understood. Even methods claiming to be based on general principles of fluid mechanics, such as, among others, those of Einstein [36], Kalinske [31], Bagnold [41] or Yalin [42], have recently been challenged and many of the basic postulates on which they are based put under the question mark (see for instance [43]). Stochastic methods applied to bed load transport have also failed so far to bring any more reliable or consistent results even in laboratory flumes, let alone in natural streams. However, one should not be unduly discouraged by this state of the art, because it probably points more than any other thing to the fact that here we are confronted with an extremely complex natural phenomenon, not reducible to a "workable" physical or mathematical model. This would mean that introducing simplifying assumptions in order to avoid unwieldy mathematical procedures, simply does not work, as it does in many other instances.

If no more accurate results may be expected from complicated and tedious methods, it is reasonable to prefer simpler approaches, where relevant engineering results can be quickly obtained. Actual field measurements should be made whenever possible and the accuracy of the used formula checked out against them. Empirical coefficients can then be adjusted until an acceptable agreement with the measured results is obtained.

Finally, a few words should be said concerning the choice of the "representative" or "dominant" discharge, replacing the essentially stochastic and

time-dependent variable of any given stream (see par. 4.1 of Part I). The question has been frequently raised by many researchers and engineers, for instance [50]. No simple determination is likely to adequately reproduce the actual stream-flow regime. Since the advent of high-speed computers, however, in many cases where the flow probability distribution is known, there is often actually no need to determine a “representative” design discharge at all.

Whenever such a single design discharge is required, a frequently applied method of determination has been suggested as follows [49]: if the statistical probability distribution of discharges is known, $f(Q)$, then using any adequate sediment transport formula, the actual stream sediment capacity, $S(Q)$, can be computed. Hence, the sediment probability distribution will be given by $F[S(Q)] = f(Q) \cdot S(Q)$, from which the representative design discharge may be taken as the one corresponding to the mode or mean of the distribution.

Before closing the present chapter, it should once more be emphasized that after sufficient characteristic data for a specific stream are at hand, the engineer should try to select the most suitable transport formula for the given case, out of the large number of the existing equations. The relevant and detailed information about most of the proposed formulae and computational methods can easily be found in specialized textbooks, as for instance [21, 51, 52], and many others. Judicious adjustment of empirical coefficients, which generally are the stock-in-trade of sediment transport formulae, has proved also to be of help in many cases.

Appendix 1

1. *Engelund-Hansen Method* [56]

The basic expression for this method is given by:

$$f\phi = 0.1 \theta^{5/2} \quad (9.28)$$

in which f – total friction factor, computed from Darcy-Weissbach equation for friction losses, ϕ – dimensionless sediment discharge, given by

$$\phi = \frac{q_T}{[(S-1)gd_{s50}^3]^{1/2}} \quad (9.29)$$

where q_T – bed material discharge per unit width and time, S – specific weight of sediment grains, γ_s/γ , g – acceleration of gravity, d_{s50} – mean diameter of grains (characteristic grain size).

$$\theta = \frac{\tau_0}{\gamma(S-1)d_{s50}} = \frac{dJ}{(S-1)d_{s50}} \quad (9.30)$$

where θ – a dimensionless form of the bed shear τ_0 , d – mean depth of flow, J – hydraulic gradient.

It is generally assumed that the flow belongs to the dune regime. If ripples occur, it is stated that viscous effects should be taken into account.

By analogy with Darcy-Weissbach equation for friction losses, the total friction factor can be expressed as

$$f = \frac{2J}{F_R^2} \quad (9.31)$$

where F_R – Froude number of the stream flow.

Example 9.7

Given: $J = 0.5\%$; $S = \gamma_s/\gamma = 2.6$; $d_{s50} = 0.55$ mm; $d = 1.5$ m; $\bar{V} = 0.8$ m/sec, mean velocity of flow.

Compute the bed-material discharge per unit width and time.

Step 1 – From Eq. (9.30),

$$\theta = \frac{d \cdot J}{(S-1)d_{s50}} = \frac{1.5 \cdot 0.0005}{1.6 \cdot 0.55 \cdot 10^{-3}};$$

$$\theta = 0.852$$

Step 2 – $q = \bar{V} \cdot d = 0.8 \cdot 1.5 = 1.2$ m²/sec – specific discharge of the stream.

Step 3 – Using Eq. (9.31), the total friction factor can now be evaluated,

$$f = \frac{2J}{F_R^2} = \frac{2gdJ}{\bar{V}^2} = \frac{2 \cdot 9.8 \cdot 1.5 \cdot 0.0005}{0.8^2};$$

$$f = 0.023$$

Step 4 – From Eq. (9.28),

$$\phi = \frac{0.1}{f} \cdot \theta^{5/2} = \frac{0.1}{0.023} \cdot 0.852^{5/2} = 2.91$$

Step 5 – The bed-material discharge can now be computed using Eq. (9.29),

$$q_T = \phi [(S - 1) \cdot g \cdot d_{s50}^3]^{1/2} = 2.91 (1.6 \cdot 9.8 \cdot 0.00055^3)^{1/2} =$$

$$= 2.91 \cdot 5.11 \times 10^{-5} = 1.49 \times 10^{-4} \text{ m}^3/\text{sec/m}$$

The method is dimensionally homogeneous, hence any system of units can be applied. It is simple and convenient for use, and yet it seems to give fairly good estimates, particularly for sandy streams with high proportion of suspended bed-material sediment. Best agreement, however, may probably be obtained when the total friction factor is deduced from actual observations of the stream.

2. Toffaleti Method [57]

This method has been proposed as an extension and modification of the previously discussed Einstein approach [36], but surprisingly the agreement of its predictions with the measured quantities of sediment in many instances of sandy streams has proved to be remarkably good. This in spite of the fact that some of its basic concepts have been criticized by several researchers on sedimentation (see, for instance, [58]). Although it is mainly an extension of Einstein's method, there are differences in three basic points: 1) velocity distribution in the vertical, 2) reduction of several parameters into a single one, and 3) dependence of Einstein's stream parameters on sediment transport in all zones along the vertical. The method is laborious, but it is well suited for computer programming.

The method, as originally proposed, is valid only when a consistent system of American units is used (feet, pounds, tons, degrees Fahrenheit). Because of the lack of sufficient background information in the original paper of the author, it is unfortunately not possible to adapt the method to the metric SI system of units. Hence a deviation from the adopted line in the present text will have to be made in this case.

Toffaletti divides the water depth into a thin bed zone and three additional zones of varying thickness. For the velocity profile, a power expression is used, given by

$$U = (1 + Z_v) \bar{U} \left[\frac{y}{R} \right]^{Z_v} \quad (9.32)$$

All the symbols are listed at the end of the appendix. Z_v is an empirical coefficient obtained from the expression

$$Z_v = 0.1198 + 0.00048 T_F \quad (9.33)$$

where T_F denotes water temperature in degrees Fahrenheit.

Further, according to Toffaletti, Einstein's ψ versus ϕ curves (Fig. 9.17) may be replaced by an analytical expression

$$\psi = \frac{TA}{\bar{U}^2} \cdot 10^4 \cdot D_i \quad (9.34)$$

in which T is a dimensional parameter (ft/sec²) and A a dimensionless correction factor.

The "nucleus load" (tons per day) assuming the bed is composed entirely of one type of sand, can be evaluated by

$$G_F = 1.905 / (T \cdot A / \bar{U}^2)^{5/3} \quad (9.35)$$

From the nucleus load, total bed load for the given sand fraction can be computed. In order to compute the suspended sediment in the remaining three zones above the bed, it is assumed that the sediment concentration distribution is given by

$$C_y = C_L (R/y)^2 \quad (9.36)$$

in which C_y is the sediment concentration, and C_L concentration at some level L .

Finally, the middle-zone exponent Z is given by the expression

$$Z = \frac{\bar{U} \cdot H}{C_Z \cdot S \cdot R} \quad (9.37)$$

Here C_Z is a correction factor, given by

$$C_Z = 260.67 - 0.667 T_F \quad (9.38)$$

Exponents Z for the lower and upper zones are given as $0.756Z$ and $1.5Z$ of the value obtained for the middle-zone respectively.

In the following a step procedure of the total sediment discharge computation is given. The notation follows, with some slight variations, the one used by the author for computer programming.

Data input: \bar{U} , R , T_F , W , D , S , and bed-material gradation analysis. For notation – see list at the end of the appendix.

Step 1 – (Common to all sand fractions). Compute:

$$YA = R/11.24$$

$$YB = R/2.5$$

$$(SI) = S \cdot R \cdot C_Z$$

$$C_Z = 260.67 - 0.667 T_F$$

$$U_2 = \bar{U}/(g \cdot D \cdot S)^{1/2}$$

$$U_3 = \bar{U}/g \cdot \nu \cdot S$$

From Fig. 9.20 find the value of $U_1 = \bar{U}/u'_*$

From that value:

$$u'_* = \bar{U}/U_1$$

$$\overline{AM} = 10 u'_*$$

$$\overline{PAM} = P^{1/3} / \overline{AM}$$

From Fig. 9.21 evaluate factor A .

Check point:

In no case should $A < 16.0$; if $A < 16$, consider its value 16.0. (Steps 2–10 require a separate computation for each sand fraction).

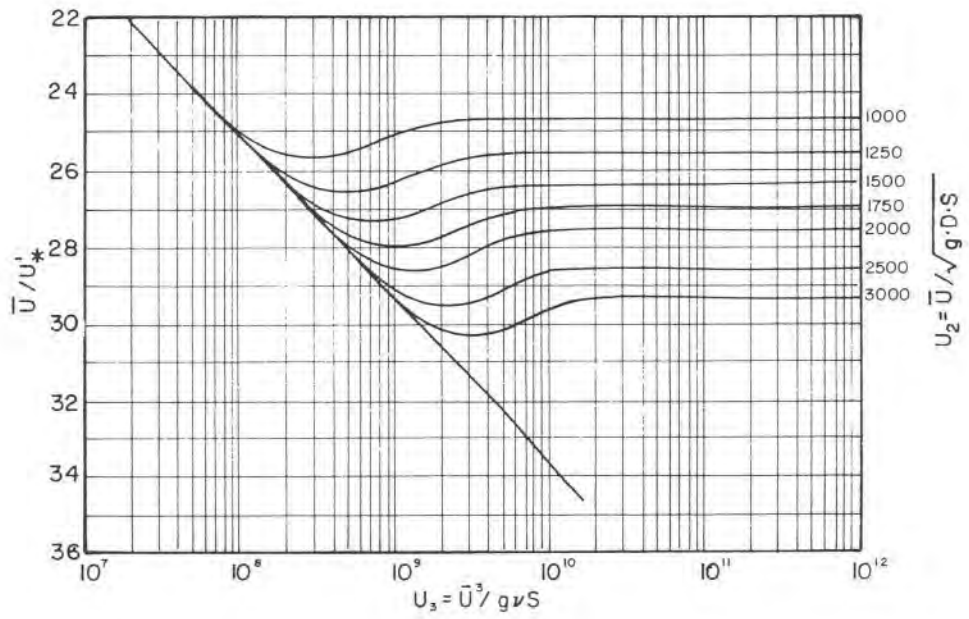
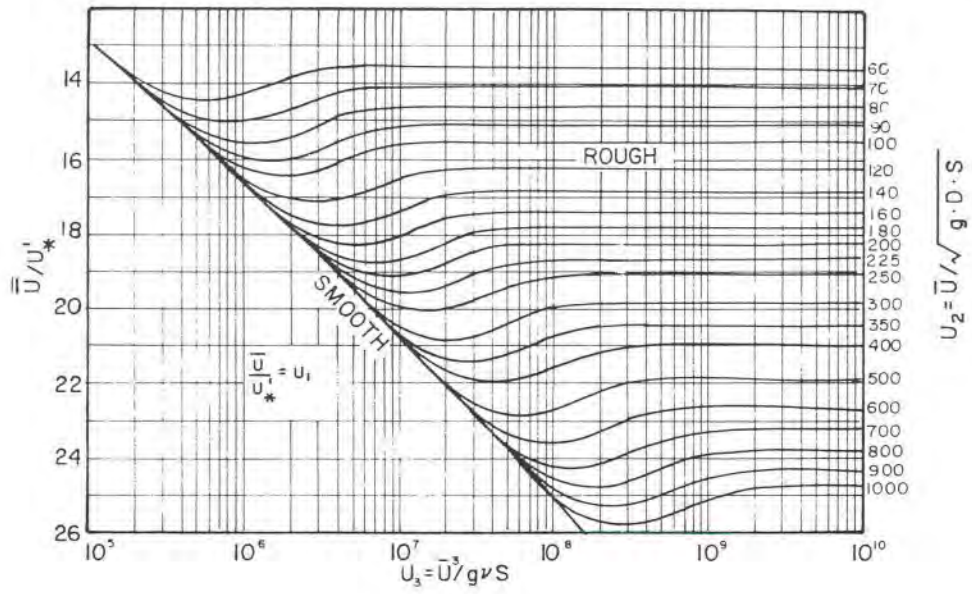
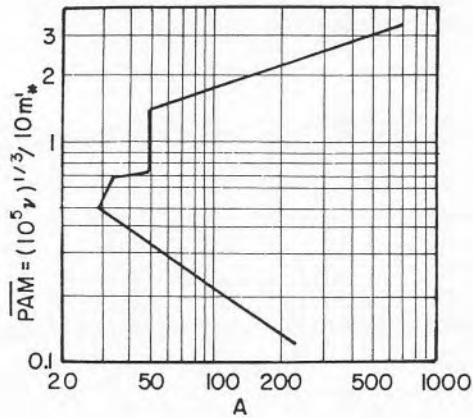


Fig. 9.20. Graph for solution of u_*' .

Fig. 9.21. Factor A .

Step 2 – For very fine sand fraction

$$D = 0.00029 \text{ ft}; \quad 2D = 0.00058 \text{ ft}$$

$$ZOM = H\bar{U}/(SI)$$

H to be taken from Fig. 9.22.

Check point:

$$\text{If } ZOM < 1.5 Z_v, \text{ use } ZOM = 1.5 Z_v, \quad Z_v = 0.1198 + 0.00048T_F$$

$$ZOL = 0.756 ZOM$$

$$ZOU = 1.5 ZOM$$

$$ZOL - Z_v = F_1$$

$$ZOM - Z_v = F_2$$

$$ZOU - Z_v = F_3$$

$$1 - F_1 = F_4$$

$$1 - F_2 = F_5$$

$$1 - F_3 = F_6$$

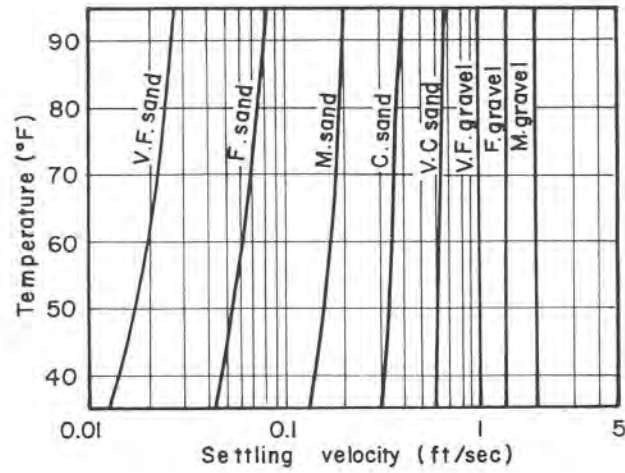


Fig. 9.22. Grain settling velocity for specific gravity 2.65 and shape factor 0.9.

Step 3

$$GF_1 = 1.905 / (T \cdot A / \bar{U}^2)^{5/3}$$

$$T = 1.10 T'$$

$$T' = g (0.00158 + 0.0000028 T_F)$$

Step 4

$$X = F_4 GF_1 / YA^{F_4} - (2D)^{F_4}$$

Step 5

$$C = Z_i \cdot W \cdot X$$

Step 6

$$\text{Bed load} = C \cdot (2D)^{F_4} \text{ (tons per day)}$$

Check point:

The concentration of sand moving as bed load (lb/ft³), considering that it is composed entirely of the sand fraction under consideration, is computed as follows:

$$1. U_D = C_v \bar{U} (2D/R)^{Z_v}$$

$$Z_v = 0.1198 + 0.00048 T_F; C_v = 1 + Z_v$$

2. Evaluate *UBL*

$$UBL = X/43.2 \cdot U_D \cdot 2D^{F_1} \text{ (lb/ft}^3\text{)}$$

If $UBL > 100 \text{ lb/ft}^3$, compute bed load as:

$$\text{Bed load} = 100/UBL \times \text{bed load (step 6)}$$

Step 7 – (for $y = 0$ to $y = YA$)

$$G_A = \frac{C}{F} [YA^{F_4} - (2D)^{F_4}] + \text{bed load (tons per day)}$$

Step 8 – (for $y = YA$ to $y = YB$)

$$G_B = \frac{C}{F_5} \cdot YA^{(F_2-F_1)} (YB^{F_5} - YA^{F_5}) \text{ (tons per day)}$$

Step 9 – (for $y = YB$ to $y = R$)

$$G_c = \frac{C}{F_6} YA^{(F_2-F_1)} \cdot YB^{(F_3-F_1)} (R^{F_6} - YB^{F_6}) \text{ (tons per day)}$$

Step 10 – (for $y_0 = 0$ to $y = R$)

$$G_T = G_A + G_B + G_C \quad (\text{tons per day})$$

For the next sand fraction, fine sand ($D = 2 \cdot 0.00029 = 0.00058$ ft)

$$GF_2 = GF_1/3.175$$

Repeat steps 4 through 10 for the fine sand fraction.

For the medium sand fraction ($D = 2 \cdot 0.00058 = 0.00116$ ft).

$$GF_3 = GF_2/3.175$$

Repeat steps 4 through 10 for the medium sand fraction. For all other fractions, repeat as previously outlined.

Total sand load = $G_{T_1} + G_{T_2} + G_{T_3} + \dots$

Method to be used with American units only.

Notation

A	– correction factor
\overline{AM}	– $10 u'_*$
C	– WZ_iX , evaluated separately for each sand fraction
C_v	– $(1 + Z_v)$, velocity distribution parameter
C_z	– temperature related parameter
C_L	– lift coefficient
D	– grain diameter (ft)
F_1, F_2, F_3	– exponents in point load equations for lower, middle and upper zones respectively
F_4, F_5, F_6	– exponents in integrated load equations for lower, middle and upper zones respectively
G_A	– sand fraction load, tons per day, in lower zone (0 to YA)
G_B	– sand fraction load (YA to YB), tons/day
G_C	– sand fraction load (YB to R), tons/day
G_T	– total load for each sand fraction
G_F	– nucleus load (tons/day) for the lower zone ($2D$ to YA)
g	– acceleration of gravity
H	– settling velocity of grain
P	– $\nu \cdot 10^5$

\overline{PAM}	– parameter
R	– mean depth (ft)
S	– energy gradient
(SI)	– $S \cdot R \cdot C_z$, for evaluation of ZOM
T'	– parameter
T	– parameter, expansion of T'
T_F	– temperature of water ($^{\circ}$ Fahrenheit)
U	– point velocity (ft/sec)
\bar{U}	– average velocity (ft/sec)
U_D	– point velocity at $y = 2D$, ft/sec
u'_*	– shear velocity related to the grain
U_2, U_3	– parameters
U_1	– correlation of \bar{U} and u'_*
UBL	– concentration of bed load (lb/ft ³)
W	– width of the stream (ft)
X	– product of factors for computation of point loads
y	– distance measured from bed (ft)
YA	– y -distance to upper limit of lower zone, $y = R/11.24$
YB	– y -distance to upper limit of middle zone, $y = R/2.5$
Z_i	– proportion of bed material of a given size fraction
Z_v	– exponent of velocity distribution
ZOL	– exponent in equation for sand concentration distribution in lower zone
ZOM	– as above, for middle zone
ZOU	– as above, for upper zone
ν	– kinematic viscosity (ft ² /sec)

References

1. Y. Zeller, Einführung in den Sedimenttransport offener Gerinne, Mitteil. der VAWE, ETH, Zuerich, Hefte 34, 35, 36, August and September, 1963.
2. E.L. Lane and W.M. Borland, Estimating bed load, Trans. Am. Geophys. Union, 32 (1) 1951.
3. M. Poreh and I. Seginer, Development of a device for automatic measurement of bed load in streams, project no. A 10-SWC-43, Water Res. Lab., Technion, Israel Institute of Technology, Haifa, 1968.
4. V.A. Vanoni, N.H. Brooks and J.F. Kennedy, Lecture notes on sediment transportation and channel stability, California Inst. of Technol., Report no. KH-R-1, January 1961.

5. H.A. Einstein, Determination of rates of bed-load movement, Proc. Fed. Inter-agency Sed. Conf., Denver, Colorado, 1947.
6. A.E. Scheidegger, Theoretical Geomorphology, Springer Verlag, Berlin, 1961.
7. H.A. Einstein, Formulas for the transportation of bed load, Trans. ASCE, 107 (1942).
8. P. Forchheimer, Hydraulik, 3rd ed., Teubner, Berlin, 1930.
9. V.N. Goncharov, Dynamics of Channel Flow, Isr. Progr. Sci. Transl., Jerusalem, 1964.
10. C.R. Neill, Note on initial movement of coarse uniform material, Jour. of Hydr. Res., IAHR, 6 (2) (1968).
11. R.J. Garde, Initiation of motion on a hydrodynamically rough surface – critical velocity approach, Jour. of Irrig. and Power, India, 27 (3) (1970).
12. S. Fortier and F.C. Scobey, Permissible canal velocities, Trans. ASCE, 89 (1926).
13. A. Schoklitsch, Handbuch des Wasserbaues, Springer Verlag, Wien, 1950.
14. U.S. Waterways Experimental Station, Studies of river-bed materials, publication no. 17, Vicksburg, 1935.
15. G. Supino, Le reti idrauliche, Casa Edit. Patron, Bologna, 1965.
16. A. Shields, Anwendung der Aehnlichkeitsmechanik und Turbulenzforschung auf die Geschiebebewegung, Mitt. Preuss. Versuchsanstalt fuer Wasser, Erd und Schiffbau, no. 26, Berlin, 1936.
17. C.M. White, Equilibrium of grains on bed of a stream, Proc. Roy. Soc. London, vol. 174A, 1940.
18. J.L. Bogardi, European concepts of sediment transportation, Jour. of Hydr. Div., proceedings, ASCE, 89 (HY3) (1965).
19. Task Committee on Sedimentation Manual, Sediment transportation mechanics: initiation of motion, proceedings, ASCE (HY2) (1966).
20. E.W. Lane, Progress report on studies on the design of stable channels of the USBR, proceedings, ASCE, 79 (1953).
21. S. Shulits, Bedload formulas, part A: A selection of bedload formulas, Penn. State University, U.S. Dept. Comm., 1968.
22. A. Schoklitsch, Der Geschiebetrieb und die Geschiebefracht, Wasserkraft und Wasserwirtschaft, 29 (4) (1934).
23. E. Meyer-Peter et al., Neuere Versuchsergebnisse ueber den Geschiebetrieb, Schweiz. Bauzeitung, 103 (13) (1934).
24. H.J. Casey, Ueber Geschiebebewegung, Translation no. 35-1, U.S. Army W. Exper. Stat., Vicksburg, 1935.
25. O.G. Haywood, Flume experiments on the transportation by water of sands and light-weight materials, Sc. thesis, Michigan Institute of Technology, 1940.
26. A. Schoklitsch, Berechnung der Geschiebefracht, Wasser und Energiewirtschaft, no. 1, 1949.
27. G.K. Gilbert, Transportation of debris by running water, U.S. Geol. Surv. Prof. paper no. 86, 1914.
28. P. Du Boys, Le Rhone et les rivières a lits affouillable, Annales P. et Ch., 5 ser., vol. 18, 1879.

29. L.G. Straub, Missouri river report, App. XV, U.S. series no. 9829, House document no. 238, 1935.
30. Waterways Experiment Station, U.S. studies of river bed materials and their movement, with special reference to the lower Mississippi River, paper 17 (1935).
31. A.A. Kalinske, Movement of sediment as bedload in rivers, *Trans. Am. Geophys. Union*, 28 (4) (1947).
32. E. Meyer-Peter and R. Mueller, Formulas for bed-load transport, *Int. Assoc. for Hydr. Res.*, 2nd meeting, Stockholm, 1948.
33. J.J. Elzerman and H.C. Frijlink, Present state of the investigations on bedload movement in Holland, IX Assem. *Int. Un. Geodesy and Geophys.*, Bruxelles, 1951.
34. G. Pezzoli, Considerazioni sul trasporto solido al fondo negli alvei a pelo libero, *Energia Elettrica*, no. 11–12, 1979.
35. L.G. Straub, Terminal report on transportation characteristics – Missouri river sediment, University of Minnesota, St. Anthony Falls, Hydr. Lab., Minneapolis, Sed. Series no. 4, 1954.
36. H.A. Einstein, The bed-load function for sediment transportation in open channel flows, U.S. Dept. of Agr., Soil Cons. Service, technical bulletin no. 1026, 1950.
37. W. Jarocki, A study of sediment, *Nat. Science Found. & Dept. of Int.*, OTS 60-21273, 1063 (translated from Polish).
38. E.V. Richardson et al., Sonic depth sounder for laboratory and field use, U.S. Geol. Survey, circular 450, 1961.
39. D.B. Simons et al., Bedload equation for ripples and dunes, U.S. Geol. Survey, Prof. paper 462-H, 1965.
40. M. Pica, Bed-load transport in mountain streams, *IAHR proceedings*, vol. 1, paper A50-1, Istanbul, 1973.
41. R.A. Bagnold, The flow of cohesionless grains in fluids, *Proc. Roy. Soc. London, Phil. Trans. Series A*. 249, no. 964, 1956.
42. M.S. Yalin, An expression for bed-load transportation, *proceedings, ASCE*, 90 (HY3), 221 (1963).
43. F.R. Luque and R. van Beck, Erosion and transport of bed-load sediment, *Jour. IAHR*, 14 (2) (1976).
44. P. Engel and L.Y. Lau, Computation of bed load using bathymetric data, *proceedings, ASCE*, 106 (HY3) (1980).
45. H.F. Cheong and H.W. Shen, On the propagation velocity of sand waves, *proceedings, 11th Congress IAHR, Sao Paulo*, 2 (1975).
46. J.C. Willis and J.F. Kennedy, Sediment discharge of alluvial streams calculated from bed form statistics, *IIHR report no. 202*, Iowa Inst. of Hydr. Res., 1975.
47. P.A. Mantz, Incipient transport of fine grains and flakes by fluids – extended Shields diagram, *proceedings, ASCE*, 103 (HY6) (1977).
48. S.M. Yalin and E. Karahan, Inception of sediment transport, *proceedings, ASCE*, 105 (HY11) (1979).
49. J. van den Berg, M. de Vries et al., *Principles of river engineering*, Pitman, London, 1979.

50. J.E. Prins and M. de Vries, On dominant discharge concepts for rivers, DHL publication no. 92, 1971.
51. W.H. Graf, *Hydraulics of Sediment Transport*, McGraw-Hill, New York, N.Y., 1971.
52. D.B. Simons and F. Sentürk, *Sediment transport technology*, Water Res. Publ., Fort Collins, Colorado, 1977.
53. P.J. Murphy, A definition of bed load, IAHR-workshop, Rapperswil (ed.), ETH, 1981.
54. Task Committee for Preparation of Sedimentation Manual, *Sediment transportation mechanics: sediment discharge formulas*, Jour. Hydr. Div., ASCE, 97 (HY4) (1971).
55. M.J. Amin and P.J. Murphy, Two bed-load formulas: an evaluation, Jour. Hydr. Div., ASCE, 107 (HY8) (1981).
56. F. Engelund and E. Hansen, *A monograph on sediment transport in alluvial streams*, Teknisk Forlag, Copenhagen, 1967.
57. F.B. Boffaleti, Definitive computations of sand discharge in rivers, proceedings, ASCE, 95 (HY1) (1969).
58. H.W. Shen, editor, *River Mechanics*, vol. 1, Fort Collins, Colorado, 1971.
59. J.J. Levi, *Dinamika ruslovi kh potokov* Gosenergoizdat, Leningrad, 1957.
60. F. Hjulström, *Studies of the morphological activity of rivers as illustrated by the river Fyris*, Bulletin, Geol. Inst. of Uppsala, vol. 25, Uppsala, Sweden, 1935.
61. P. Engel and Y. Lam Lau, Bed load discharge coefficient, Jour. Hydr. Div., ASCE, 107 (HY11) (1981).
62. K. Stelczer, *Bed-load transport*, Water Resources Publ., Washington, D.C., 1981.

PART 3



CHAPTER 10

FLOOD PROTECTION

Symbols

A	– point; location; area; flooded area
a	– parameter; part of lemniscate
B	– width of channel; point; width of spillway crest; location
b	– parameter; width of channel after contraction
C	– point; coefficient
C_q	– discharge coefficient
D	– point; diameter; duration of flood wave; riprap stone size; maximum depth of scour measured below water level
$D_1, D_2 \dots D_n$	– duration of flood wave
d	– depth of flow; depth of water on flood plain
d_n	– normal depth
d_{s50}	– median grain size
E	– point
e	– part of lemniscate
F	– point
F_R	– Froude number, $v/(gd)^{1/2}$
f	– part of lemniscate
$f_1, f_2 \dots$	– functions
H	– head over crest; height of revetment
HW	– high water
h	– head
$I, I_0, I_1 \dots$	– longitudinal slope
i	– interest rate
J	– energy gradient
$K, K_1, K_2 \dots$	– coefficient

L	– length of parabolic transition; length of channel; length of conduit; length between groynes
l	– length of chord
$l_1, l_2, l_3 \dots$	– length of arc
M	– meandering index
M_T	– total mass of the transported sediment
m	– exponent
NW	– normal water
n	– exponent; Manning roughness coefficient
$n_1, n_2 \dots$	– Manning roughness coefficient
P	– present value; point
Q	– discharge
Q_0	– uniform-flow discharge
\bar{Q}	– average discharge
$q, q_1, q_2 \dots$	– discharge
R	– circular-curve radius; hydraulic radius; annuity
R_0	– given radius
$R_1, R_2, R_3 \dots$	– circular radii
RVE	– reservoir volume – elevation
r	– cross-section index; radius of curvature
r_0	– part of lemniscate
S	– specific mass; stream stage above safety threshold; capital increased by compound interest; depth of scour below the bed level
s	– part of lemniscate
T	– length of tangent; time of direct observation
t	– time; duration of flooding
u_*	– shear velocity
\bar{V}	– mean velocity
V_0	– total storage
V_s	– storage below spillway crest
V_t	– temporary storage
v	– velocity
\bar{v}	– mean velocity
x	– part of lemniscate; coordinate
x_0	– part of lemniscate
y	– coordinate
y_0	– part of lemniscate
α	– angle; contraction ratio
β	– angle
γ	– angle

δ	– angle
$\eta_1, \eta_2, \eta_3, \eta_4$	– coefficients for evaluation of scour depth
ν	– kinematic viscosity
φ	– angle

10.1 Introduction

Flood protection of riverain areas, either as an end in its own right or as part of a multi-purpose scheme, is certainly one of the main staples of hydraulic engineering, for which a good knowledge and understanding of stream-flow mechanics, dynamics and morphology are essential. Many other related branches also are indispensable, such as hydrology, flood-wave propagation, water storage etc, not to mention social and economic aspects which will determine the scope and extension of any proposed flood-protection project. As a matter of fact, from the very dawn of civilization, with its agriculture, urban settlements and work distribution, until our own days, it has been an important building block of Civil Engineering. *Passive protection*, such as building on high grounds or on stilts above high-water marks, may be even today resorted to as a temporary or isolated protection measure; engineering science and technology, in contrast, are concerned with the *active protection*, which allows the continuation of normal human activities in the flood plain during a great part of flood events.

Complete elimination of flood hazards and ensuing damage for any given region of a flood plain is practically not feasible, due to the stochastic nature of flood events. It is very seldom, if ever, envisaged from the engineering and economic points of view, since it would lead to unacceptable financial outlays, far outweighing expected damages to property or crops. It follows, therefore, that what characterizes any proposed flood-control project is the extent to which flood damages are expected to be *reduced*, and not by any means their complete disappearance.

Although huge sums of public funds are being continuously spent on flood-protection works all over the world, inevitable flood damages on the whole not only do not diminish, but are, it appears, rather on the increase. Flat flood plains, with abundant water supply and high soil fertility, are often much cheaper for many economic activities. Valuable property enhanced by human activity is bound to grow rapidly in value from year to year. For this very reason, the modern approach to the problem, at least

as far as industrialized or intense-agriculture covered flood plains are concerned, stresses the point that for any flood-protection project to be really successful, it should be accompanied by a scheme for the management of the flood plain, enforced through political and legal means. Proponents of such a wide-ranging management organization actually consider the engineering flood-control works as an integral part of the overall scheme. Public ignorance of the true nature of any flood-protection project, which necessarily only reduces the frequency of flood damages, but never entirely eliminates their inevitable recurrence, has to be overcome if the consequences are to be minimized and loss of life avoided.

It seems inevitable, therefore, that the problem of damages caused by exceptional flood events will stay with us as long as flood plains remain an important area of human activity.

The present text, it should again be emphasized, only deals with small and medium-size streams, because large rivers, though in many respects similar to smaller watercourses, have nevertheless many important characteristics and various mechanical properties of their own. The following review of flood-protection works and methods also mainly covers small and medium-size streams.

Engineering methods for flood control and protection that will be discussed in the following pages are as listed below.

- 1) Stream training and regulation. Works concerning cross-section, alignment, longitudinal slope and roughness of a stream, with the scope of increasing its conveying capacity.
- 2) Reduction of peak discharges by means of flood routing through retention reservoirs for temporary storage of flood waters.
- 3) Flood protection by dikes or levees.
- 4) Attenuation of flood waves through diversion to other channels, or to less critical areas.

10.2 Design Discharge

As flood-protection works are actually designed to only reduce the frequency and extent of expected inundation damages, the first question which must be answered when considering any stream-training project is the determination of the *design discharge*. This is a problem which is well-known to hydraulic engineers, because it has to be solved for almost any engineering activity connected with natural streams, in which flow rates are a stochastic process, not amenable to deterministic methods.

It is assumed that for a given natural watercourse under consideration, discharge and possibly sediment-transport measurements over a representative time period (let us say, over a period of 15–25 years or more) are available, so that a suitable analytical method of statistical hydrology could be meaningfully selected and applied, in order to obtain by extrapolation probable discharge values for time periods greater than the actual year-series of measurements, and also with sufficient degree of confidence. When no such basic information is at hand, or when it is scarce or unreliable, special hydrologic methods must be applied, coupled with engineering insight and keen understanding, in order to develop a synthetic series from which to derive the design discharge.

In a general way, determination of design discharge for flood-protection works is founded on similar basic considerations as for many other hydraulic projects. Economic benefits from a proposed protection project over the expected useful life-span of the works should be equal to or greater than the compound cost of the project. In evaluation of the former, it is generally an accepted practice that only tangible and direct benefits should be drawn into consideration, i.e. those measurable in money-equivalent on the one hand, and those accrued directly as the result of the project, on the other. Overall cost of the proposed project should include all expenditures required for its completion, operation and maintenance, interest and depreciation. A simple optimization procedure for a flood-control project is schematically shown in Fig. 10.1. Curve 1 represents the annual cost of the project, curve

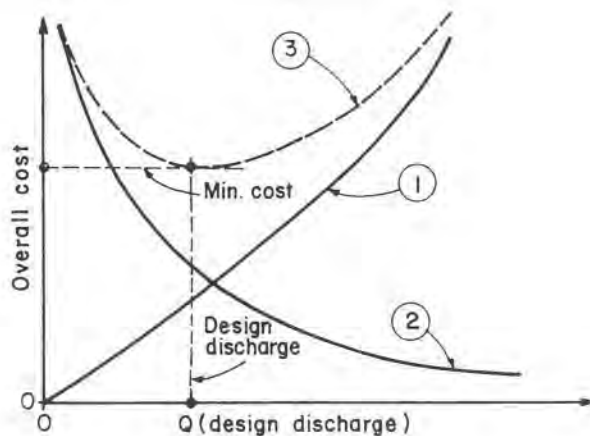


Fig. 10.1. Simple optimization procedure.

2 the remaining average annual flood damages, and curve 3 the sum of 1 + 2. The lowest point on curve 3 indicates the minimum annual cost of the project and the corresponding design discharge.

A complicating factor with many flood-protection projects is the possibility of loss of human life, an occurrence which obviously eludes evaluation in terms of material cost. While human life should be protected at the highest acceptable margin of safety, it is nevertheless reasonable to assume that no community could afford to finance a project of whatever benefit-cost ratio. It has already been stressed, moreover, that unwarranted public faith in protection works may often cause an increase in danger to human life *after* the completion of the project. As already mentioned, one possible answer to the dilemma is a comprehensive flood-plain management scheme which, among many other public tasks, should also keep the population informed and fully aware of risks that still do exist.

Fig. 10.2 shows a statistical analysis of maximum annual discharges during a period of 24 years for an ephemeral Mediterranean stream. Log-normal distribution has been found to give the best fit for the plotting points (measured values), and thus to allow a more or less reliable extrapolation for return periods longer than the measuring span, if needed. Although return periods for the design discharge are as a rule chosen to correspond to the specific circumstances of a given project, there are, nevertheless, some general *orientation rules* in this regard. Recommended return periods (equivalent to design peak discharges) for different flood-plain characteristics are shown in Table 10.1.

Return periods of 10,000 years and more are known to have been chosen in many cases of important population centers and industrial parks. Figures in Table 10.1 are obviously intended to give only a preliminary order of magnitude from which to start the economic and social analysis.

10.3 Stream-Training Works

10.3.1 Definition

The main purpose of a training scheme is to increase the carrying capacity of the alluvial stream, and thus to lower its water stages and finally to reduce the flood hazards. There are several ways to achieve this object, and they are used either singly or in combination with each other, as the case may be. In any of the cases, however, under the specific term of a "stream-training project", all of the methods undertaken with a view to increasing the capacity of the stream are comprised.

Any change introduced in the existing natural conditions of a stream with the aim of improving its performance or mitigating its destructive behavior, will necessarily affect the general pattern of the morphological aggradation-degradation processes. It has already been shown in previous chapters that the number of interdependent parameters which enter into play is very large, and that in any given case there is practically no way of isolating the influence of any single one of them. In fact, simultaneous action of many parameters may in some cases be cumulative, in others compensating, and channel reach under study cannot be seen as independent of its downstream

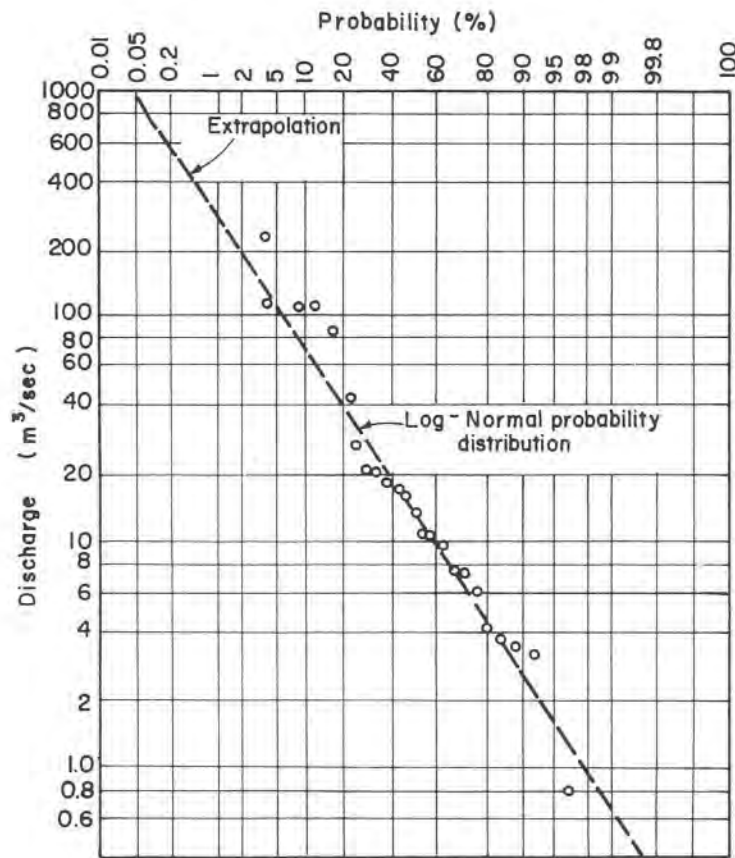


Fig. 10.2. Statistical analysis of annual peak flows.

TABLE 10.1. RECOMMENDED FLOOD RETURN PERIODS

Flood-plain characteristic	Recommended flood return period (years)
1. Extensive agriculture (grain farming)	6–7
2. Intensive agriculture	15–20
3. Thinly or medium populated living areas	100–200
4. Densely populated living areas and industrial centers	200–1000
5. Important urban centers	> 1000

or upstream continuations. Putting it simply, the process is extremely complicated, and perhaps with the exception of the simplest localized solutions, no simplistic approaches are worth trying.

Nevertheless, in the following some of the main parameters and their isolated effects upon the dynamic aggradation-degradation processes will be briefly recapitulated for better understanding of the stream-training methods to be reviewed in the next pages. More detailed discussion of these items is to be found in Chapters 3 and 4.

1) Increasing the depth without changing the width of the channel, is likely to decrease its STC (sediment transport capacity), and hence result in deposition.

2) If the longitudinal slope is increased or decreased, discharge remaining constant, STC of the stream will be affected in the same manner, with erosion in the first case and deposition in the second.

3) STC of an earth channel with constant longitudinal slope roughly varies directly proportional to the flow discharge. Any temporary deviation from this proportionality is likely to result in general erosion or deposition, as the case may be.

4) Narrowing the channel (say, by dikes or groynes), without changing the discharge or longitudinal slope, will generally increase its STC, and hence cause erosion.

5) Bed-material load diminishes with increasing median grain size. Accordingly, washing out of fine fractions is likely to eventually lead to some sort of stabilization. On the other hand, this reduction in sediment load may cause increased erosion downstream.

The stage which should precede any more important stream-training design is the investigation of the proper design parameters on which to base the regulation strategy and to predict the channel response to it. Among other information, these should include:

1) Identification of unstable channel sections. This may be obtained by direct observation of erosional and depositional activity of the stream over a number of years, which clearly is the best way. If such evidence is not available, conclusions may be reached by the observation of the channel shape, its longitudinal slope, average flow velocities and bed-sediment gradation curves. During erosion cycle, the stream tends to produce relatively deep and narrow channel, steeper slopes, higher average velocities, and sediment-gradation curves that are shifted towards coarser fractions. When active deposition occurs, a relatively wide and shallow channel is produced, with smaller slope, lower average flow velocity and sediment gradation curve moved towards finer fractions.

2) Bed-material transport discharge. Here also direct observation is the best method, but unfortunately this is often not available and there is not enough time to carry out a field campaign. In sand-bed channels the incipient discharge could be obtained using the Shields diagram (see par. 9.2.1), provided that hydraulic data for several flows are available, as well as the information concerning the sediment gradation.

3) Bank-erosion threshold discharge. This is valuable information obtainable only through field observations during several years.

Based on pertinent information, a regulation strategy can be defined that will best maintain the natural stability of the stream channel downstream of the regulated section.

In the following a review of the main stream-regulation methods will be given.

10.3.2 Improvement of Cross-Section

After the design discharge has been determined by a suitable method of statistical hydrology as mentioned in par. 10.2, the existing channel of the alluvial stream should be either improved or a new artificial channel designed, in order to safely convey the flood wave. Cross-section of the channel is usually computed assuming uniform flow at the peak discharge and adding adequate freeboard. One should bear in mind, however, that in many

instances the assumption of uniform flow for the flood propagation along the channel, which is essentially gradually varied and unsteady, may result in depths lower than the actual ones, at least in the upstream reaches, where little wave-attenuation can take place. It has already been stressed in par. 7.3 that for a given discharge, depth of flow is likely to be greater on the subsiding phase than on the rising phase, with a typical loop-like rating curve (see Fig. 7.10). This is due to the fact that in tracing the movement of a flood wave along the channel, not only the longitudinal slope of the bed must be taken into account (assumed equal to energy gradient for uniform flow), but also the actual energy gradient [1].

If the maximum discharge for a given station along the stream is taken from the rating curve derived by the uniform-flow equation, it may be significantly smaller than the actual discharge, as is readily seen from Fig. 7.10. Theoretically, the relation between the discharge Q_0 , resulting from the uniform-flow equation, and the actual discharge Q , for the same depth of flow is given by

$$Q/Q_0 = (1 + K)^{1/2} \quad (10.1)$$

Coefficient K , which is mainly dependent on the rate of the temporal change of the water stage, $\partial y/\partial t$, is positive on the rising phase, and negative on the subsiding phase. If, at a given station along the stream, information is available about the variation of stage and approximate celerity of the flood-wave propagation, coefficient K can be roughly evaluated, and hence also the actual discharge.

Channel cross-section is then computed and designed to convey the design discharge at uniform flow. For earth channels, both lined or unlined, the wetted cross-sectional area is obtained from hydraulic computations and from the condition that critical shear stress at the stream bed is not exceeded; the dimensions of the final cross-section should also be adapted to the available earth-moving or lining equipment. Methods of computation have been reviewed in Volume I of the present Manual.

If channel cross-section improvement is considered as the only means of stream training, it is generally thought a reasonable practice to increase the width of the channel, when the natural bed predominantly suffers erosion. In cases where deposition of sediment is the main characteristic (lower course), deepening of the cross-section is generally to be preferred. A combination of both may be the right solution, when no clear-cut tendency is evident. These simple thumb-rules, however, are not always as easy of implementation as it may seem. Often field observations may indicate heavy erosion during high water, and light deposition during low water. Hence, it is

to be expected that any change of cross-section intended to reduce erosion, might well cause much stronger deposition at low stages. The opposite might occur at high stages, if the cross-section is improved with a view to preventing deposition and clogging during low stages.

10.3.3 Alignment of the Channel

10.3.3.1 General

An alluvial stream seldom flows in a straight channel for long stretches, even when the alluvial bed is very compact or rocky. Meandering, therefore, is one of the main characteristics of any alluvial stream (see par. 3.8 and 3.9), which means that it is a sequence of more or less similar curves separated by relatively short straight reaches (crossings), forming some sort of an undulating line. The exact mechanism of this baffling phenomenon is not yet fully understood. Although such a system at first glance seems to be quite inefficient, it is in fact the result of a delicate interplay of many forces tending to find a state of dynamic equilibrium. This is best shown by morphological changes that generally follow when meanders are cut off (see par. 3.3.3). The excess potential energy thus made available causes erosion of bed and banks upstream, and deposition of the eroded material in the downstream channel (see Fig. 3.6). After this process has taken place for a considerable distance, the stream will start to form a new set of meanders, similar to those that previously existed.

Laboratory experiments and field observations seem to suggest that a water stream in non-cohesive granular material first forms a succession of more or less sinusoidal curves, which are relatively unstable. These simple curves, however, are gradually replaced by more complex curves, in which stronger cross-currents are developed, [2–5]. It appears that these modified curves show more stability, and are less subject to longitudinal or lateral shifting. A reach of stream that has developed to such a more stable state may be used for learning the meandering characteristics of the watercourse. It is understood that within such a reach stream banks generally remain stable during longer periods of time (let us say, more than about ten years), there is relatively little deposition, and no or little overflowing for discharges that correspond to shorter or unexceptional return periods.

Distinctive traits which should be studied are the *meandering index* M (see par. 3.3.2) of the representative reach, and the *cross-section index* r . The geometric meaning of the index M is schematically shown in Fig. 3.3. It is

implicitly assumed that the best way to improve the carrying capacity of an alluvial stream is by keeping it as close as possible to its natural characteristics. This implies that its relatively stable meandering pattern should be taken account of when deciding on the longitudinal alignment of the stream.

It is generally assumed that relative equilibrium characteristics of a stream are best found along its middle course (see par. 1.4.2), where *on the average* the natural channel and its longitudinal alignment show little permanent change.

Training works are often needed in the upper part of the middle course, in which the slope may still be high, and in order to counteract it, the stream forms meanders and ramifies in side-channels. After the training channel is substituted for the natural system, flow velocities and bed shear stress will usually be increased. This may call for an appropriate protection of the new channel.

When the meandering index has been derived from adjacent representative reaches, i.e. the information is available about the average length of the natural bend and average number of meanders – detailed design of the typical bend can be undertaken. If no adequately stable reach can be found, information has to be obtained from the available natural configuration, taking into account its relatively unstable character, or adjusting it according to the engineering intuition.

Sometimes expropriation costs of lands needed for the proposed training alignment may prove to be excessively high. This in turn may require adopting arcs shorter than originally planned, which means higher longitudinal slope. Here again adequate protection of the channel must be brought into consideration.

10.3.3.2 *Layout and Curve Fitting*

After the general meandering characteristics of a given stream have been studied and relevant conclusions drawn, detailed design of the curves has to be made. It is practically not feasible to reproduce the natural curves as they are, but besides the average meandering index, some general rules should be respected as far as possible.

1) The proposed layout should be mathematically simple, dependent on minimum number of parameters, and be relatively easy to set out in the field.

2) It should form a line of successive curves, with sufficient straight reaches between the single curves (crossings), see par. 3.9.

3) Change of curvature along each single curve should be continuous, reaching the minimum radius at the center.

Some of the most frequently used geometric curves in the stream-training practice are as follows.

a) *Circular Arc*

This is obviously the simplest of all possible curves, but it certainly does not conform to rule 3 as given above. Indeed, its radius of curvature is constant along the bend, and there is an abrupt change of the radius at both ends of the curve, where it jumps from $r = \infty$ to a finite value, or vice versa. This is likely to cause instability of flow inside the bend. In spite of its evident shortcomings, it is nevertheless widely used in stream-training practice, mainly because of its simplicity, both in office and in field work. One additional advantage of the circular arc is that, for a given radius of curvature, it requires the minimum space (see Fig. 10.9) – an important feature in many stream-regulation projects.

Values for simple circular-curve radii are customarily taken within the following ranges,

For large and medium streams: $\frac{R}{B} \approx 7 - 8$

For small streams: $\frac{R}{B} \approx 10 - 12$

where B denotes the width of the improved channel at water surface for the design discharge.

Two of the main values for a circular arc can easily be derived from simple geometric relations, see Fig. 10.3.

$$\text{Length of the chord: } l = 2R_0 \sin \frac{\pi - \beta}{2} \quad (10.2)$$

$$\text{Length of the tangent: } T = \frac{R_0}{\tan \beta/2} \quad (10.3)$$

Circular arc, in spite of its practical advantages, should only be used for small streams, and even then the concave bank of the bend should be protected against strong erosion.

An improvement of the simple circular curve, sometimes used in stream-training practice, is the *compound circular curve*, composed of several

circular arcs with different radii, Fig. 10.4.

If the curve is composed of three different radii, it is generally the accepted practice to take the radii approximately in the following range (see Fig. 10.4):

$$R_1 \approx (10 - 12) B$$

$$R_2 \approx (8 - 10) B$$

$$R_3 \approx (5 - 8) B,$$

where B denotes the width of the improved channel at water surface for the design discharge. The main geometric relationships obtained for the assumption that $l_1 = l_2 = l_3$ (usually the case) are as follows:

$$\beta = \frac{\alpha}{2 + 2R_1/R_2 + R_1/R_3}$$

$$\gamma = (R_1/R_2) \beta \tag{10.4}$$

$$\delta = (R_1/R_3) \beta$$

$$2(\beta + \gamma) + \delta = \alpha$$

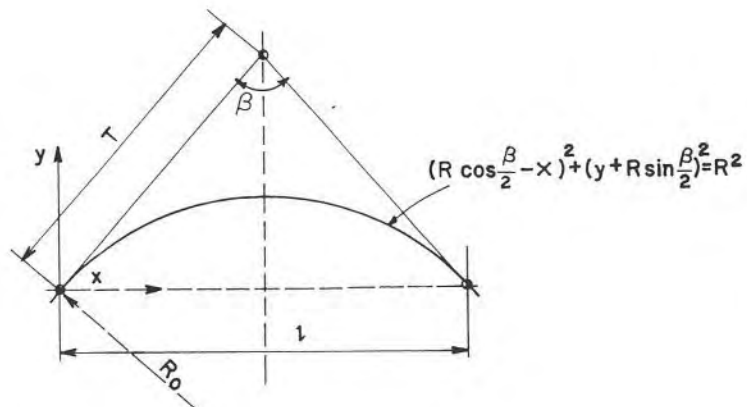


Fig. 10.3. Circular arc.

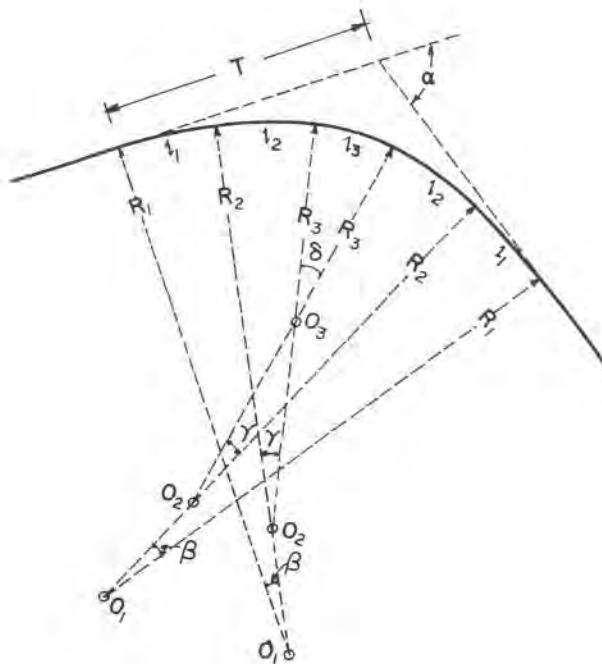


Fig. 10.4. Compound circular curve.

Although the compound circular curve does not altogether eliminate abrupt changes of curvature, it does provide at least for partial adjustment along the arc. It is obvious that the compound curve is longer than a simple circular curve of radius R_3 .

Example 10.1

In the preliminary design of curves in a stream-training project, a compound circular arc consisting of three different radii is to be tried. Width of the improved channel upstream and downstream of the bend for the design discharge is given as $B = 24.0$ m. Partial arcs l_1 , l_2 and l_3 are to be of equal length. Angle formed by the tangents at both ends of the bend is $\alpha = 70^\circ$.

According to the usual practice and considering local conditions, radii R_1 and R_2 have been set as follows: $R_1 = 240$ m, $R_2 = 200$ m. Convenient length of the tangent has been taken as $T = 140$ m.

Angles β , γ and δ , as well as radius R_3 have to be determined.

Solution

Keeping again within the recommended practice, a first trial value of the missing radius is taken as $R_3 = 120$ m. Then,

$$\frac{R_1}{R_2} = 1.2 \quad ; \quad \frac{R_1}{R_3} = 2.0$$

Using Eq. (10.2), angles can be computed,

$$\beta = \frac{\alpha}{2 + 2R_1/R_2 + R_1/R_3} = \frac{70}{2 + 2 \cdot 1.2 + 2.0} = 10.94^\circ$$

$$\gamma = \left[\frac{R_1}{R_2} \right] \beta = 1.2 \cdot 10.94 = 13.13^\circ$$

$$\delta = \left[\frac{R_1}{R_3} \right] \beta = 2.0 \cdot 10.94 = 21.88^\circ$$

Checking the results,

$$2(\beta + \gamma) + \delta = 2(10.94 + 13.12) + 21.88 = 70^\circ$$

Tangent T is given by the expression,

$$\begin{aligned} T = R_1 \tan \frac{\beta}{2} (1 + \cos \beta + \tan \frac{\alpha}{2} \sin \beta) + R_2 \tan \frac{\gamma}{2} \left\{ \cos \beta + \cos (\beta + \gamma) + \right. \\ \left. + \tan \frac{\alpha}{2} [\sin \beta + \cos (\beta + \gamma) \sin (\beta + \gamma)] \right\} + R_3 \tan \frac{\delta}{2} \left[\cos (\beta + \gamma) + \right. \\ \left. + \tan \frac{\alpha}{2} \cos (\beta + \gamma) \sin \frac{\delta}{2} \right] \end{aligned} \quad (10.5)$$

$$T = 240 \cdot 0.096 \cdot 2.115 + 200 \cdot 0.115 \cdot 2.843 + 120 \cdot 0.193 \cdot 1.034$$

$$\therefore T \cong 138 \text{ m}$$

The result is somewhat short of the assumed length of the tangent. If necessary, a slight adjustment of the radius R_3 can easily be made.

A further improvement can be achieved by fitting parabolic transition curves to the circular arc, similar to the road-building practice. The passage from the inflexion point, at which $R = \infty$, to the circular-arc radius is gradual and smooth, and there is further no need in shifting the point in the case of lateral dykes (see discussion later on). Such a bend is schematically shown in Fig. 10.5, where for the sake of clarity transitions have been much exaggerated in relation to the central circular arc.

From simple trigonometric considerations, angles β and γ are given by

$$\beta = \arctan \frac{L}{2R_0} \tag{10.6}$$

and

$$\gamma = \alpha - 2\beta \tag{10.7}$$

Length of the parabolic transition, measured projected on x -coordinate, is generally taken as $L = 0.2 R_0$, giving a 1% deviation in the computation

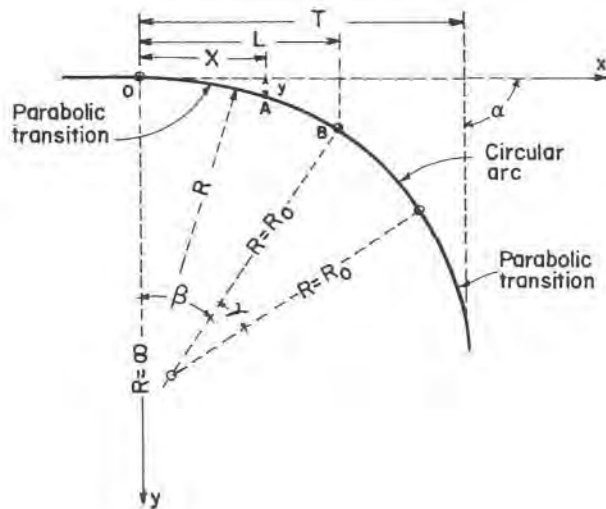


Fig. 10.5. Circular arc with parabolic transitions.

of the curvature. It is obvious that when $\alpha \rightarrow 2\beta$, $\gamma \rightarrow 0$, which means very flat central angle α , for which probably no transition curves are needed in the first place. Length of the tangent is given by

$$T = L + \frac{L^2}{6R_0} \tan \beta + \left[R_0 + \frac{L^2}{6R_0 \cos \beta} \right] \left[\frac{\sin \gamma/2}{\cos (\beta + \gamma/2)} \right] \quad (10.8)$$

Example 10.2

Width of the channel at water surface upstream of the bend is $B = 50$ m. Central angle $\alpha = 72^\circ$.

It is required to prepare a first proposal for a circular bend with parabolic transition curves.

Solution

Radius of the central circular arc is taken as

$$R_0 = 8B = 400 \text{ m}$$

Further, $L = 0.2 R_0 = 80$ m. It is now possible to compute all the missing parameters using Eqs. (10.6) and (10.7),

$$\beta = \arctan \frac{L}{2R} = \arctan 0.1 = 5.71^\circ$$

$$\gamma = \alpha - 2\beta = 72^\circ - 2 \cdot 5.71 = 60.58^\circ$$

Using further Eq. (10.8), length of the tangent is obtained as

$$T = 80 + 0.27 + 402.7 \cdot 0.62 = 331.15 \text{ m}$$

Plotting the parabola can be done by using the expression

$$y = \frac{X^3}{6LR_0} \quad (10.9)$$

which for the given case gives,

$$y = \frac{X^3}{6 \cdot 80 \cdot 400} = \frac{X^3}{1.92 \cdot 10^5}$$

Finally, plotting points are given in Table 10.2.

TABLE 10.2. PLOTTING POINTS (Ex. 10.2)

x (m)	y (m)
10	0.005
20	0.042
30	0.141
40	0.333
50	0.651
70	1.786
80	2.667

b) *Sinoidal Curve*

The general shape and main characteristics of this curve are shown in Fig. 10.6. General equation of the sinoidal curve is given by

$$y = a \sin bx \tag{10.10}$$

Parameters a and b are defined as follows:

If the central angle β and distance l are given, then it can easily be shown that

$$a = \frac{l}{\pi} \cot \frac{\beta}{2} \tag{10.11}$$

$$b = \frac{\pi}{l} \tag{10.12}$$

If, on the other hand, β and the length of the tangent T are given,

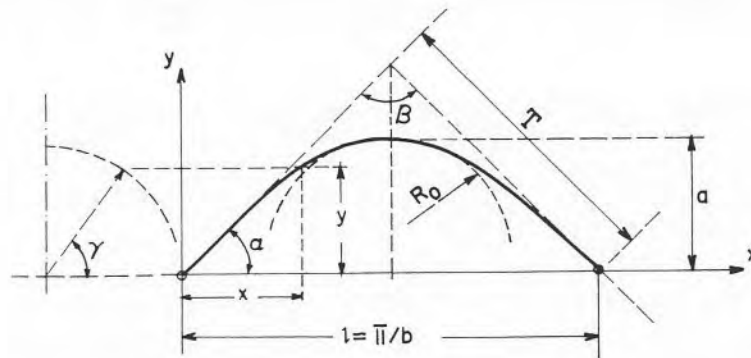


Fig. 10.6. Sinoidal arc.

$$a = \frac{2T \cos \beta/2}{\pi} \quad (10.13)$$

$$b = \frac{\pi}{2T \sin \beta/2} \quad (10.14)$$

Finally, if the radius of the circle tangent to the sinoidal arc at the apex is given, R_0 , and the central angle between the tangents β , the following relations can be written,

$$a = R_0 (\cot \beta/2)^2 \quad (10.15)$$

$$b = \frac{1}{R_0 \cot \beta/2} \quad (10.16)$$

and further, applying Eq. (10.11)

$$l = \pi R_0 \cot \beta/2 \quad (10.17)$$

Example 10.3

Given: Distance between inflexion points, $l = 600$ m; central angle, $\beta = 150^\circ$.

Required:

Compute the plotting points and length of the tangent for the sinoidal curve.

Solution

$$1. \quad b = \frac{\pi}{l} = \frac{\pi}{600} = 0.00524 \text{ m}^{-1}$$

$$a = \frac{l}{\pi} \cot \frac{\beta}{2} = \frac{600}{\pi} \cot 75^\circ = 51.17 \text{ m}$$

2. Length of the tangent, using Eq. (10.13),

$$T = \frac{a \cdot \pi}{2 \cos \beta/2} = \frac{51.17 \pi}{2 \cos 75^\circ} = 310.55 \text{ m}$$

3. General equation for plotting the curve is given by,

$$y = 51.17 \sin (0.00524 x)$$

Some of the values for the plotting points are summarized in Table 10.3.

Although sinoidal curve provides for a gradual transition from the inflexion point ($R = \infty$) to the minimum radius at the apex of the curve, it is nevertheless generally recommended for use only when central angle $\beta \geq 120^\circ$.

TABLE 10.3. PLOTTING POINTS (Ex. 10.3)

x (m)	bx	Corresponding γ°	$\sin (bx)$	y (m)
50	0.262	15	0.259	13.2
100	0.524	30	0.500	25.6
150	0.786	45	0.707	36.2
200	1.048	60	0.866	44.3
300	1.572	90	1.000	51.2

c. *Lemniscate*

General equation of the lemniscate is given in rectangular coordinates as

$$x^2 + y^2 = a^n (n \times y)^{1/2} \quad (10.18)$$

or in polar coordinates,

$$r = a^n [\sin(n\phi)]^{1/2} \quad (10.19)$$

However, in engineering practice only the lowest-degree lemniscate is used, for which the exponent $n = 2$. The form and main parameters of the curve are shown in Fig. 10.7. The whole of the lemniscate is a closed curve, but only a part of it is used, according to local conditions.

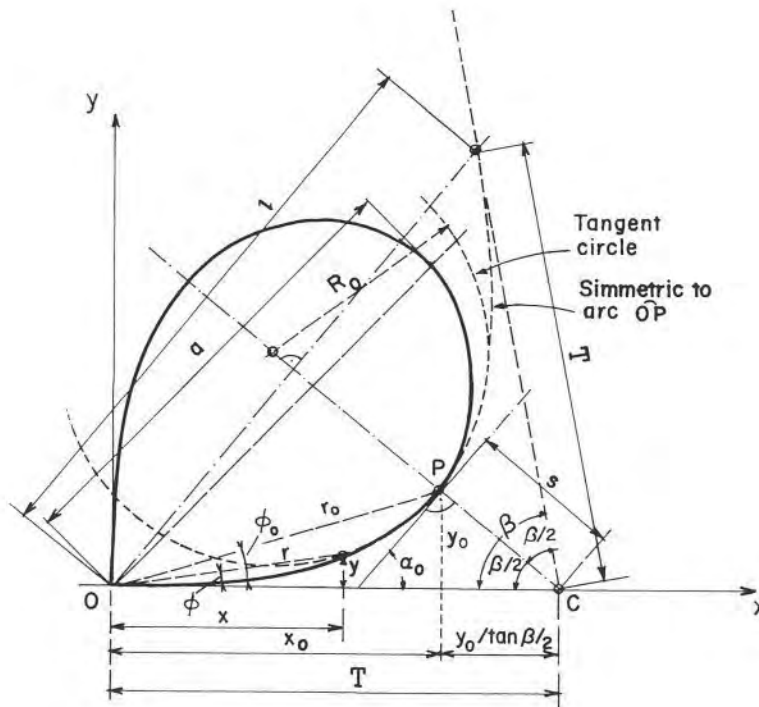


Fig. 10.7. Lemniscate curve.

This curve is generally considered to best approach the requirements set forth at the beginning of the paragraph for artificial stream bends. Some of the general relations for the lemniscate curve are as follows (see Fig. 10.7):

$$\text{Length of the tangent: } T = x_0 + y_0 \cot \beta/2 \quad (10.20)$$

Radius of the tangent circle (curvature) at point P :

$$R_0 = \frac{a}{3 [\sin (2\varphi_0)]^{1/2}} \quad (10.21)$$

Distance between the meeting point, C , of the tangents and the apex of the curve, P :

$$s = \frac{y_0}{\sin \beta/2} \quad (10.22)$$

Basic relationship of the lemniscate:

$$\alpha_0 = 3 \varphi_0 \quad (10.23)$$

and from this,

$$\varphi_0 = \frac{1}{6} (\pi - \beta) \quad (10.24)$$

Hence, Eq. (10.21) can be written in the form

$$R_0 = \frac{a}{3 [\sin (\pi - \beta)/3]^{1/2}} \quad (10.25)$$

Further,

$$x_0 = \frac{y_0}{\tan \varphi_0} = \frac{y_0}{\tan [1/6 (\pi - \beta)]} \quad (10.26)$$

Whence, using Eq. (10.20) and (10.26) and from Fig. 10.7,

$$T = y_0 (\cot \varphi_0 + \cot \beta/2) \quad (10.27)$$

Finally, constant a in Eqs. (10.13) and (10.19), which is the extension of the lemniscate loop along its axis of symmetry, can be evaluated from Eq. (10.18),

$$a = \frac{x_0^2 + y_0^2}{(2x_0y_0)^{1/2}} \quad (10.28)$$

In tables for the engineering use of lemniscate curves, meandering index M is introduced as one of the variables. It is given by

$$M = \frac{\text{arc } OP}{r_0} \quad (10.29)$$

Length of the arc corresponding to the given angle φ can be numerically computed by expanding the integral $\text{arc } OP = a (2)^{1/2} \int_0^{\varphi_0} f(\varphi) d\varphi$ into series. When the meandering index for a stream is given, the corresponding curves can easily be obtained.

As can be seen from Fig. 10.7, both Eq. (10.18) and (10.19) are based on the tangent to the curve. For the purpose of easier setting-out work in the field, it may often be more convenient to do it from the chord perpendicular to the bisector, along which length l is measured. The necessary transformation is shown in Fig. 10.8.

When Eq. (10.19) is used, new coordinates can be obtained thus

$$e = r \cos \gamma = r \cdot \cos (\pi - \beta/2 - \varphi) = r \sin (\beta/2 + \varphi) \quad (10.30)$$

and

$$f = r \sin \gamma = r \cdot \sin (\pi - \beta/2 - \varphi) = r \cos (\beta/2 + \varphi) \quad (10.31)$$

If Eq. (10.18) is preferred, transformation coordinates are given as follows,

$$e = (x + y \cot \beta/2) \sin \beta/2 \quad (10.32)$$

and

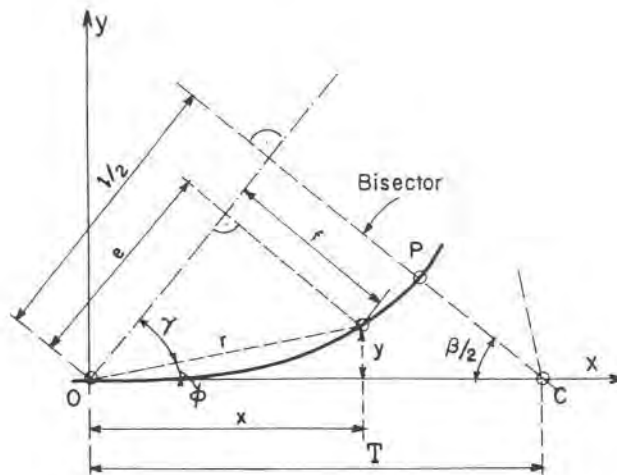


Fig. 10.8. Coordinate transformation for the lemniscate.

$$f = (x^2 + y^2 - e^2)^{1/2} \quad (10.33)$$

Example 10.4

Data are the same as in example 10.3. Length of the chord – $l = 600$ m; central angle between the tangents – $\beta = 150^\circ$.

This time the arc has to be designed as part of a lemniscate.

1. Length of the tangent, from Fig. 10.8:

$$T = \frac{l}{2 \sin \beta/2} = \frac{600}{2 \cdot \sin 75^\circ} = 310.6 \text{ m}$$

2. Applying Eqs. (10.19), (10.20) and (10.21):

$$\varphi_0 = \frac{1}{6} (\pi - \beta) = \frac{1}{6} (\pi - 150) = 5^\circ$$

$$y_0 = \frac{T}{\cot \varphi_0 + \cot \beta/2} = \frac{310.6}{\cot 5^\circ + \cot 75^\circ} = 26.5 \text{ m}$$

$$x_0 = \frac{y_0}{\tan \varphi_0} = \frac{26.5}{\tan 5^\circ} = 302.9 \text{ m}$$

and finally, using Eq. (10.28),

$$a = \frac{x_0^2 + y_0^2}{(2x_0y_0)^{1/2}} = \frac{302.9^2 + 26.5^2}{(2 \cdot 302.9 \cdot 26.5)^{1/2}} = 729.7 \text{ m}$$

3. Equation of the lemniscate can, therefore, be written in either of the two forms,

$$x^2 + y^2 = 729.7 (2xy)^{1/2}$$

or

$$r = 729.7 [\sin (2\varphi)]^{1/2}$$

4. For the setting-out work in the field, several values of r , e and f will be computed and tabulated using the hitherto obtained results (Table 10.4).

If the comparison is made with the sinoidal arc of example 103, it is found that the maximum ordinate is slightly larger for the lemniscate — 52.8 m instead of 51.2 m for the sinoidal arc.

It is claimed that the lemniscate arc gives satisfactory results for all central angles β practically encountered in stream training works (bends as sharp as

TABLE 10.4. SETTING-OUT COMPUTED VALUES (Ex. 10.4)

φ°	r (m)	e (m)	f (m)
1	136.3	132.2	33.0
2	192.7	187.8	43.3
3	235.9	230.7	49.0
4	272.2	267.2	51.9
5	304.1	299.5	52.8

about $\beta \cong 60^\circ$). In all cases, the arc is not excessively long, but nevertheless provides for a smooth and adequate transition. To facilitate the design of lemniscate arcs, there are ready-made computation tables to be found for standard central angles and unit chord, [6] among others.

In particular cases, where a symmetric lemniscate arc is not well suited because of local conditions, it is possible to design an asymmetric lemniscate bend, composed of two arcs for which central angle β between the tangents is divided into two unequal angles, β_1 and β_2 , so that $\beta_1 + \beta_2 = \beta$. Geometric requirements for the two arcs are that at the point of contact they should have common tangent and radius of curvature.

For the sake of comparison, in Fig. 10.9 are shown different arcs obtained for central angles $\beta = 60^\circ$ and 120° , and radius of the tangent circle at the apex of $R_0 = 100$ m. All values of T and l have been calculated by the equations as given before. For the central angle of $\beta = 110^\circ$, values of T and l are identical for both sinoidal and lemniscate arcs.

10.3.4 Channel Rectification

Although the meandering pattern of a stream is the result of the natural interplay between the many forces acting on the water and on the bed, rectification of a tortuous natural channel is nevertheless often undertaken as part of a flood-protection project. This may be done on a single stream loop, or several loops in series. Such an artificial short-cutting of natural stream alignment is achieved by means of *cut-offs*, Fig. 10.10.

Main morphological consequences to be expected from such a short-cutting of the stream channel have already been discussed in par. 3.3.3. These effects can be briefly resumed as follows:

a) Energy gradient of the stream along the cut-off channel and upstream of it is increased, hence also its sediment transport capacity. As a consequence, there will be erosion in the cut-off channel (unless protected), and in the natural channel upstream of it, while deposition will start in the downstream channel, see Fig. 3.6, since there the transport capacity has remained unchanged.

b) Because of reduced stream storage, peak discharge downstream of the cut-off is likely to be higher than before.

If most of the sharp bends of a natural stream are short-cut, it is estimated that the mean flow velocity may be increased by as much as about 40% [7]. In most cases, however, meander short-cutting alone is not sufficient to prevent the stream from overflowing its banks during the flood-protection design discharge, hence additional means are necessary, such as channel improvement or dikes.

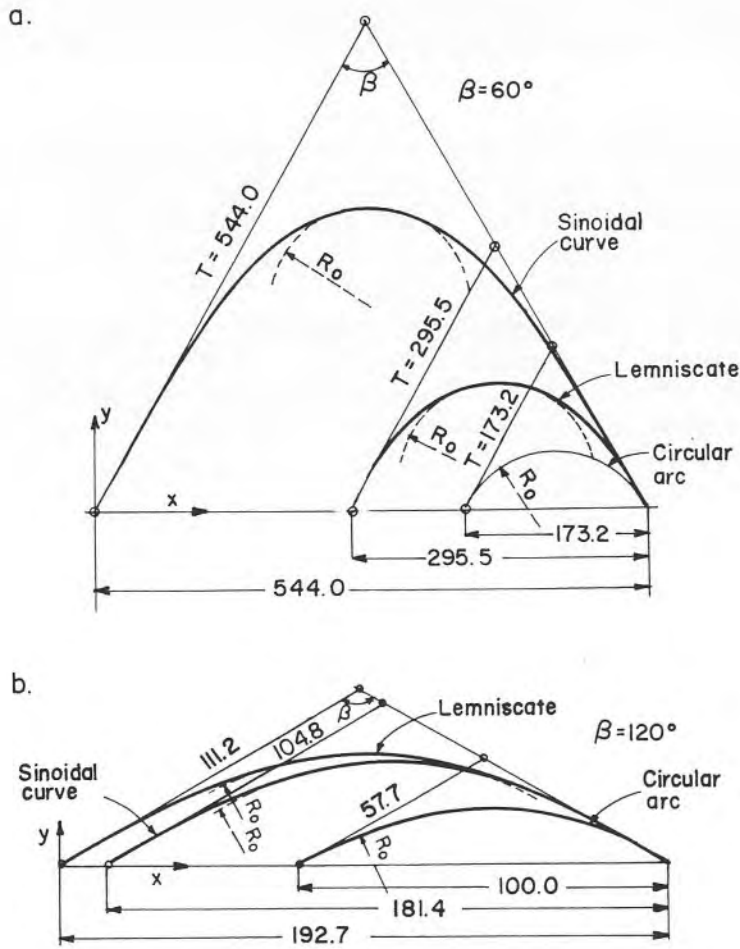


Fig. 10.9. Comparison of different arcs for $R_0 = 100$ m. All dimensions in meters.

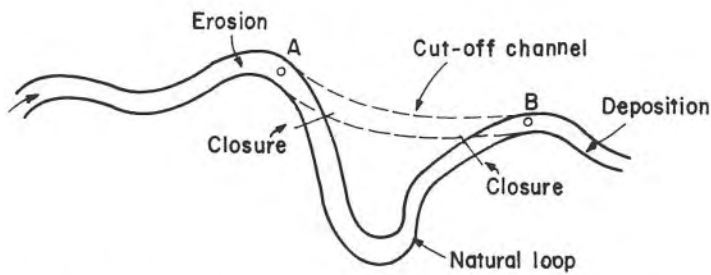


Fig. 10.10. Cut-off of a single loop.

In engineering practice there are several methods for the construction of cut-off channels. By one method, the designed channel is dredged in full between the points A and B, Fig. 3.6, after which the old channel is dammed off by means of dikes, allowed to be overtopped during exceptional floods.

According to the second method, developed mainly in connection with the flood-protection works in the U.S.A. [8], first a pilot channel is dredged to carry only about 10% of the flood discharge, while the natural loop is left open. It is then practically left to itself to develop into some sort of a natural channel, although often this lengthy process is accelerated by additional dredging at a later stage. In all cases, the process is expected to take two to four years until the cut-off channel can take over, and the loop be closed at both ends. Sometimes a low earth sill is built at the entrance to the pilot channel to prevent entrance of water at low rates of flow, at which deposition of sediment could take place. At higher discharges the sill is washed out by the water.

It is a good practice to make the cut-off channel tangent to the natural stream channel at both ends, hence it is generally made slightly curved.

10.3.5 Reduction of Longitudinal Slope by Means of Drop Structures

In the upper reaches of some streams, longitudinal slope is often excessively steep, and hence causes strong erosion. Large quantities of eroded material, often coarse gravel or even boulders, are then deposited in the lower reaches of the stream, where the slope flattens, and clog the channel, causing flooding and damages. This situation is often encountered in the upper reaches of Mediterranean streams, in semi-arid and arid zones in general. By means of a series of drops along the reach, the slope may be considerably reduced and the erosion-deposition cycle effectively improved, Fig. 10.11.

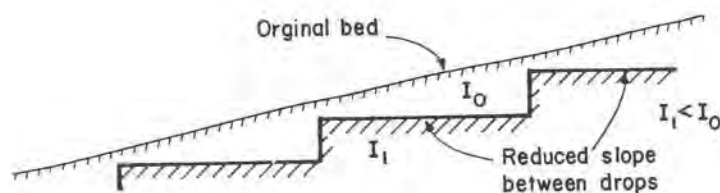


Fig. 10.11. Reduction of slope by means of drops-schematic drawing (not to scale).

Reduced slope between the drops is fixed in such a manner that the average shear stress at the design discharge remains below its critical value for the given soil conditions (see Vol. I of the Manual, Part 1, par. 3 and 4). Mean height of the drops, and hence their number along the regulated reach, should be decided upon only after careful study of all the hydraulic and economic aspects of the alternatives. It is evident that the same effect can be achieved either by a small number of higher drops, or a large number of low drops.

When the regulated slope must be very mild because of soil conditions, and the design discharge is rather high, it is often advantageous to choose a combined solution in which lateral dikes are added. Let us suppose that for a prevalently agricultural area a return period of 10 years had been chosen, giving an expected maximum discharge of $12 \text{ m}^3/\text{sec}$. Hydraulic calculations have shown that the required depth of flow was about 2 meters. It means that the depth of the regulated channel between the drops should be at least 2 m *at the drop*, and consequently more than that at all other places.

If now a smaller discharge is contemplated, say $6 \text{ m}^3/\text{sec}$ corresponding to a return period of 4 years, it may require a depth of only 1.3 m. If this solution which entails much less excavation works, is finally adopted, protection dikes will obviously be needed at some places to prevent flooding at the design discharge, Fig. 10.12.

Low and relatively close drops in such a case may require dikes all along the regulated channel, because the available depth at all sections, and not only near the drop, might not be sufficient to accommodate the design discharge. This may also require special provisions for the drainage of the flood plain after the subsidence of high waters. On the other hand, higher drops may only call for partial diking, and space enough for the drainage, see Fig. 10.13.

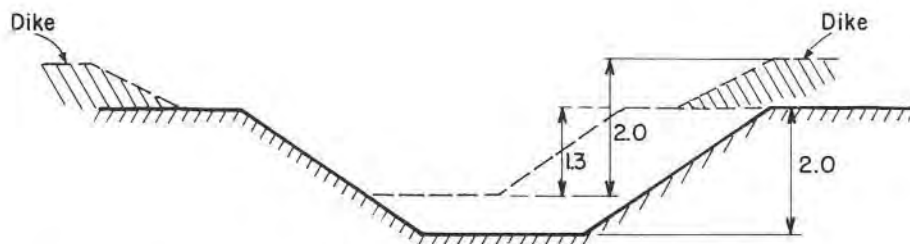


Fig. 10.12. Alternative design of the regulated channel (freeboard omitted).

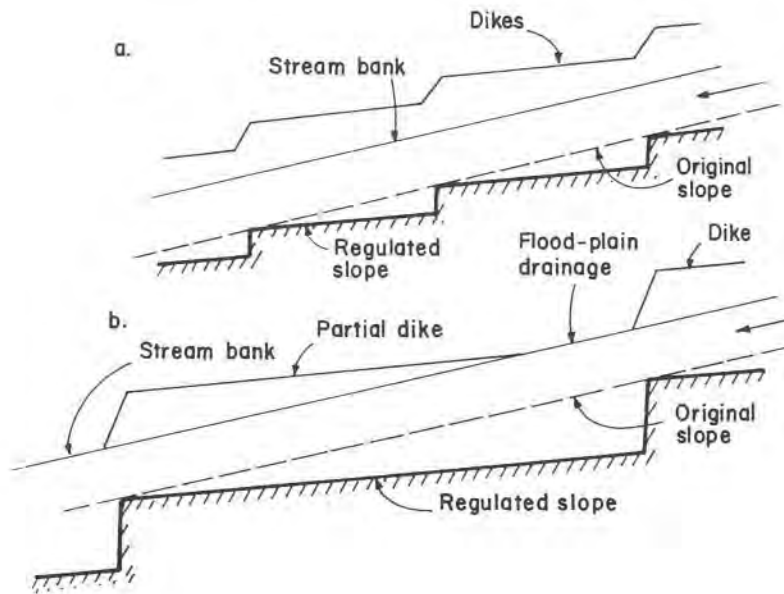


Fig. 10.13. Slope reduction by drops: a) small drops, b) large drops (not to scale).

Small drops, however, should not be made too close to each other, unless care is taken to prevent steep energy gradients at higher discharges. At lower rates of flow, energy gradient, which alone regulates the velocity, will indeed be parallel to the improved bed slope; at higher discharges, mainly responsible for the erosion and damage to the channel, this may not be the case, and the gradient remains more or less parallel to the original bed slope, thus completely cancelling the training works, see Fig. 10.14. Such a

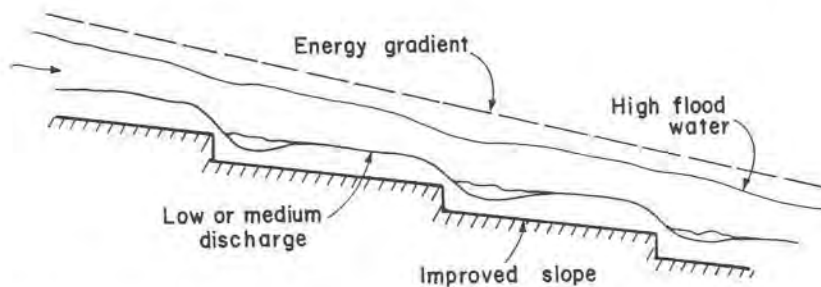


Fig. 10.14. Small drops at low and high discharges, (not to scale).

situation can be partially or completely avoided by providing adequate end sills at the brink of each drop, or similar measures [9]. If this proves to be too expensive for a large number of small and closely spaced drops, other solutions should be tried to stop the erosion, such as channel lining. An effective and relatively cheap method of channel protection in upper reaches of small ephemeral streams, successfully used in Israel, is by means of loosely strewn coarse gravel or cobbles.

From the hydraulic point of view, in any training scheme by drops three main parts can be distinguished, Fig. 10.15. Part 1 comprises the drop itself and the hydraulic jump which follows (for hydraulics of water drops and dissipation of energy – see Vol. I of the Manual, Part 1, Chap. 8); part 2, the reach between the drops, where uniform flow (or close to it) is established corresponding to the reduced longitudinal slope, and finally part 3 that includes the drawdown curve, leading toward the critical depth at the brink of the drop.

The drawdown curve, although relatively short and mainly concentrated at its downstream end (about 50–60% of the entire water-level drop in about 10–15% of the overall length), may cause erosion immediately upstream of the drop structure, because flow velocities increase due to the falling depth. If the earth channel upstream of the drop was designed for the maximum shear stress at the normal depth, it is likely to be eroded, and the drop structure itself endangered. End sills, or adequate contraction of channel section for a short length upstream of the drop, go far to improve the situation, and are frequently used, Fig. 10.16 (hydraulic design of such devices is reviewed in Chap. 11). Channel protection for a short length downstream of the stilling basin is also essential if back-erosion is to be avoided at flow rates higher than the design discharge. This protection should be extended to both the bed and banks of the channel, Fig. 10.17.

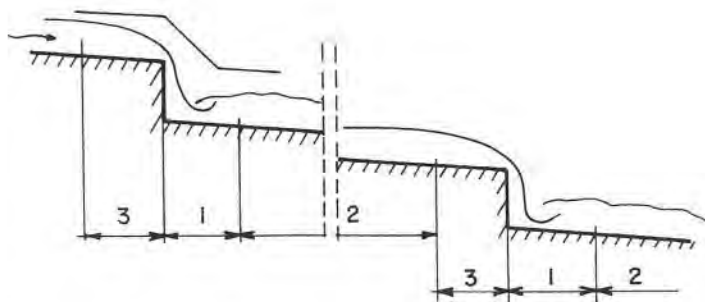


Fig. 10.15. Series of drops – hydraulic division (schematic – not to scale).

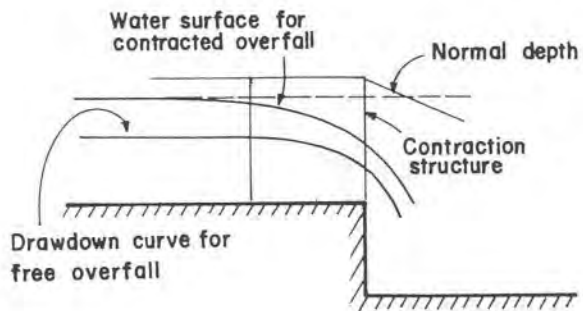


Fig. 10.16. Contracted overfall (schematic – not to scale).

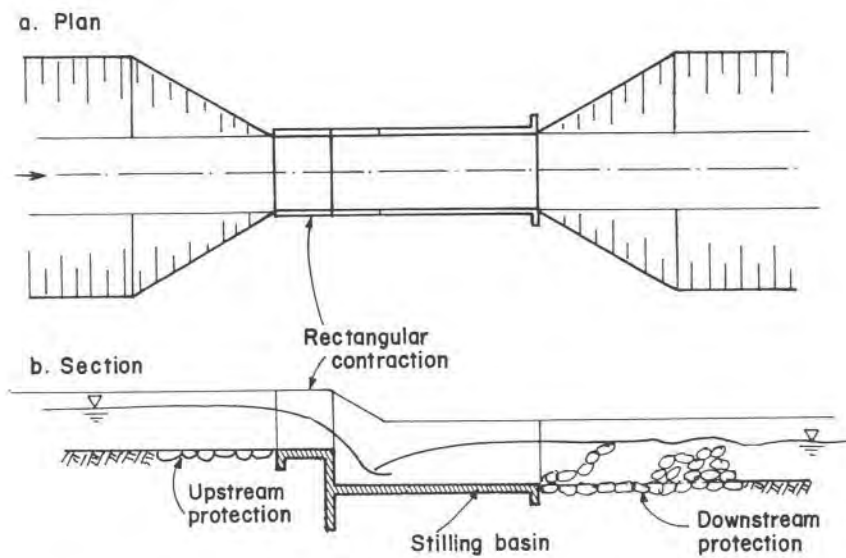


Fig. 10.17. Typical drop structure.

10.3.6 Fixation of the Stream Bed

It is sometimes preferred to let the bed-slope reduction be done essentially by the stream itself. Two such methods are briefly reviewed here.

10.3.6.1 Small Check-Dams

Low check-dams are built across the stream bed, at relatively short distances between them, Fig. 10.18.

With time, sediment will be deposited between the low dams, and consequently a milder longitudinal slope established. Water level is raised because of the backwater curve upstream of each check-dam, and hence hydraulic gradient is reduced. Bank line is supposed to be high enough to contain the backed-up water, since otherwise lateral diking would be required.

Hydraulic efficiency of such a solution should be carefully checked for every given case, because under certain circumstances, hydraulic gradient may remain practically unaffected by the system (see discussion in the previous paragraph, and Fig. 10.14).

When designing any system of sills or check dams, one should be aware of the fact that local scour, both upstream and downstream of these structures, is a common and practically unavoidable feature of such stream-training solutions. It is, therefore, essential to make the foundations deep enough to prevent the destruction of structures due to local scour. It is curious to note that apparently low flows, and not peak discharges, may be the governing factor, at least as far as scour adjacent to the downstream face of sills is concerned [37]. If banks have protective revetment, check-dams or sills should be extended by about 1.0 meter beyond the meeting line between bed and bank.

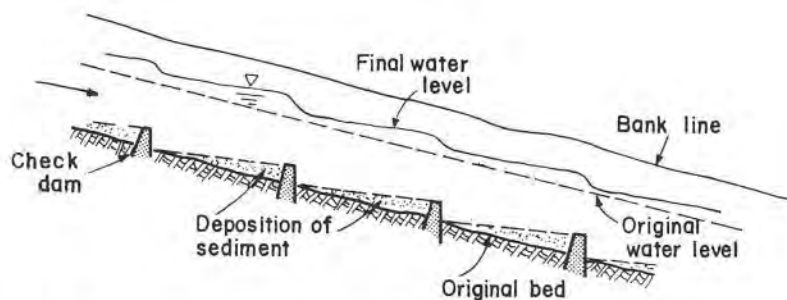


Fig. 10.18. Bed fixation by means of check-dams (not to scale).

10.3.6.2 Bottom Sills

When the previous solution of small check-dams constructed above the bottom of the natural channel is not acceptable, a series of sills built *below* the channel bed and perpendicular to the direction of flow, may be a more convenient approach, Fig. 10.19.

Before the erosion of the original stream bed between the sills takes effect, there is no influence of the sills on the flow. Eventually such erosion will go on until a new equilibrium slope is established, milder than the original one. At that stage, the system will form a cascade of small drops.

Besides the final hydraulic efficiency of any similar engineering solution, which should be examined, the effect downstream of enhanced deposition of the eroded material should also be taken into account.

Bottom sills should always be built strong enough to act as low retaining walls after the erosion has taken place. Distance between the sills, and their depth below the channel bed, have to be determined by thorough study of each particular case, and by economic considerations.

10.3.7 Coarse Sediment Exclusion

At higher flood discharges, large volumes of coarse sediment are likely to be eroded in the upper reaches of the stream, where the longitudinal bed slope is steep and flow velocities are of considerable magnitude, and deposited in the middle course, where velocities are much lower. If stream-training works are planned for such middle reaches, as they generally are, it is often expedient to prevent the coarse sediment, at least to a certain degree, from settling and eventually clogging the regulated channel.

In some special cases it is possible to divert a part of the flow by means of

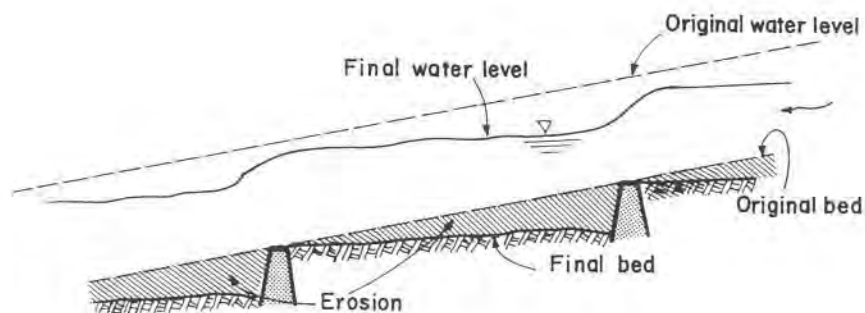


Fig. 10.19. Bottom sills.

a diversion channel to some low-lying part of the flood plain, where sediment deposition may be desirable because of high groundwater levels, and then clearer water returned to the main channel downstream. This alternative will be discussed further later on, in the paragraph dealing with diversions.

A second alternative, used much more frequently, is to build a small coarse-sediment retention basin at the head of the regulation works. Such a basin usually is obtained by widening and often also deepening the existing stream channel. Its capacity is generally determined by a rough estimate of the bed load carried by the stream during a reasonable time period (say, one season or more), but often also by local conditions and constraints. Every now and then, therefore, the basin has to be dredged.

Although such a basin is primarily intended to serve as a coarse-sediment trap, and not as a settling tank, it is nevertheless recommended to shape all the transitions by smooth and gradual passages, in order to avoid stream separation and uneven deposition of sediment. Possible backwater effects because of failure to dredge the basin before the rain season, should be duly taken into account, whenever local conditions warrant it.

In order to increase the efficiency of the basin, sometimes a low sill is placed across its width at the downstream end, thus further preventing coarse sediment from being entrained by the water and entering the new regulated channel.

Schematic drawing of a sediment basin is given in Fig. 10.20. A typical calculation to estimate the size of the coarse-sediment basin is given in Example 10.5.

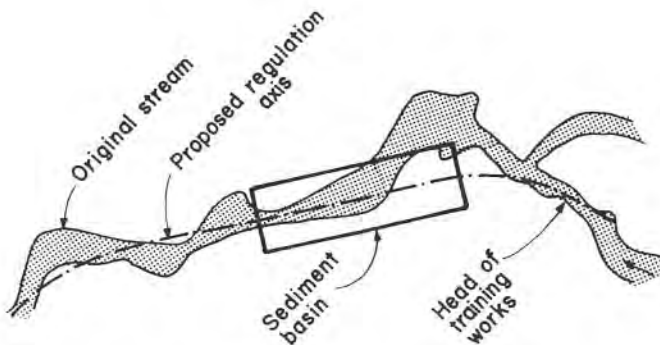


Fig. 10.20. Sediment basin at the head of training works.

Coarse-sediment exclusion, especially in cases of water diversions, is often achieved by construction of groynes upstream of the head works (see par. 10.3.9.8, further on). Sediment is deposited between the groynes before reaching the diversion outlet, and if necessary it can from time to time be dredged from there to make room for more deposition.

Example 10.5

Required: To make an estimate of the necessary volume for a coarse-sediment basin to be placed at the entrance to the stream-training works, on the basis of one-year sediment yield.

Given: Ephemeral stream in the temperate semi-arid region. I – mean longitudinal slope – 0.7‰; $S = \rho_s/\rho$ – specific mass – 2.6; d_{s50} – mean grain size – 1.2 mm; B – mean width of the stream channel – 30 m.

Average hydrogram of a typical 20-year flood wave is given in Fig. 10.21. Q – d curve and Q – \bar{V} curve (\bar{V} – mean velocity) are given in Fig. 10.22.

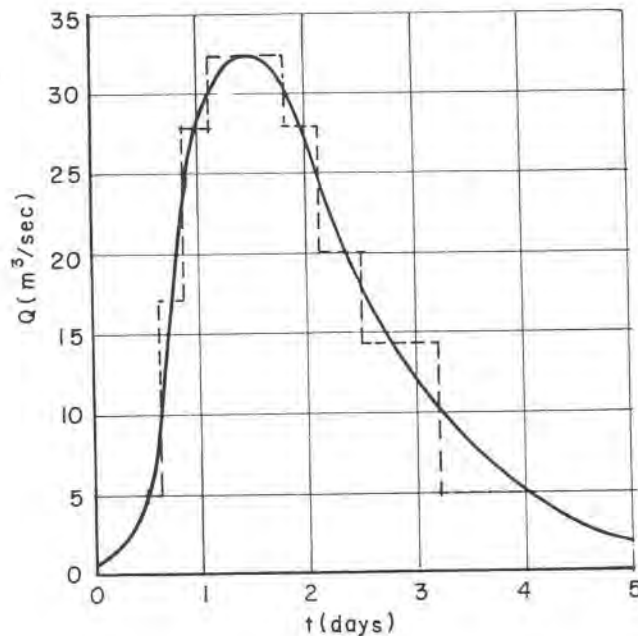


Fig. 10.21. Typical flood-wave hydrogram.

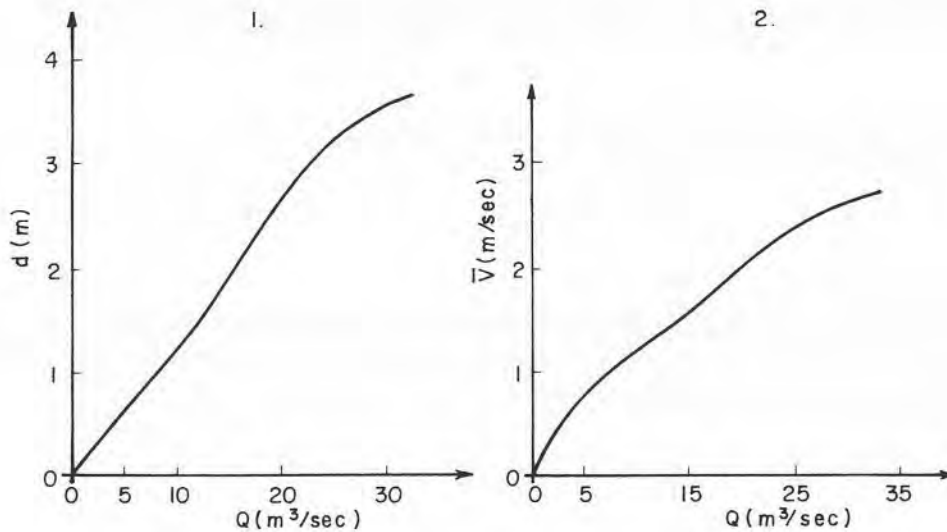


Fig. 10.22. 1) $Q-d$ curve, 2) $Q-\bar{V}$ curve (Ex. 10.5).

Step 1 – For simplicity, the given flood hydrogram (Fig. 10.21) has been substituted by a simpler polygon of approximately equal area.

Step 2 – It was estimated from the Shield's diagram that flow velocities below ~ 0.8 m/sec would cause only negligible movement of the coarse sediment. Hence, all discharges of less than $5 \text{ m}^3/\text{sec}$ have been assumed as non-contributing to the coarse sediment yield.

Step 3 – Data and computation results of partial water volumes during the flood wave given in Fig. 10.21 are summarized in Table 10.5a. All the volumes have been computed above the $5 \text{ m}^3/\text{sec}$ -line.

Step 4 – Let us assume that the sediment load in the given stream can be estimated from the exponential relationship,

$$C_{(\text{mg/lit})} = 335 \times Q_{(\text{m}^3/\text{sec})}^{0.85}$$

Such an expression can be derived from statistical analysis of sediment measurements during a long-term period offering some degree of confidence.

TABLE 10.5a. COMPUTATIONS OF THE WATER VOLUMES (Ex. 10.5)

1	2	3	4	5
Partial area no.	Q m^3/s	Duration (hr)	Duration $\times 10^3$ (s)	Partial volume $\times 10^3$ $2 \times 4 (m^3)$
1	12.0	6.0	21.6	259.2
2	23.0	6.0	21.6	496.8
3	27.5	16.8	60.5	1,663.2
4	23.0	7.2	25.9	596.2
5	15.0	9.0	32.4	486.0
6	9.5	16.8	60.5	574.6
Total water volume — Σ				$4,076 \times 10^3 m^3$

Step 5 — For the computation of the sediment yield for every partial area of the given hydrogram, sediment concentration C (mg/lit) was computed for the discharge at the centroid of the area. Since the empirical relationship linking sediment concentration to discharge is of the exponential type, this procedure is in fact not warranted, and each partial area should be subdivided into a number of smaller unit areas, with concentrations computed for every unit separately. However, owing to the fact that in the present specific case the difference in the computed sediment yield is relatively small (about +0.7%), for clarity the simpler method has been adopted. Table 10.5b gives the summary of the computations.

In this table: Column 2 — partial water volumes (from column 5 of Table 10.5a); Column 3 — average discharge at the centroid of the partial areas; Column 4 — computed sediment concentrations for discharges of the column 3; Column 6 — partial sediment yields.

The cumulative sediment yield for one typical flood wave is the sum of all partial yields — $SY = \sim 14,036 \times 10^3$ kg.

Step 6 — Specific mass of the sediment being $S = 2.6$, sediment volume for one wave is $V_{total} = 14,036/2.6 = \sim 5400 m^3$.

It is estimated that during a flood wave coarse fractions make up about 20% of the measured sediment yield. Hence, the coarse-sediment volume is

TABLE 10.5b. COMPUTATIONS OF THE SEDIMENT YIELD (Ex. 10.5)

1	2	3	4	5	6
Area no.	$V \times 10^3$ (m^3)	Q_{av} m^3/s	C (mg/lit)	C (kg/m^3)	$SY \times 10^3$ kg 2×5
1	259.2	11.0	2,572	2.572	666.66
2	496.8	16.3	3,596	3.596	1,786.49
3	1,663.2	18.7	4,037	4.037	6,714.34
4	596.2	16.3	3,602	3.602	2,147.51
5	486.0	12.5	2,867	2.867	1,393.36
6	574.6	9.7	2,311	2.311	1,327.90
Cumulative sediment yield – Σ					$14,036.26 \times 10^3$ kg

given by $V_{coarse} = \sim 1100 m^3$.

Step 7 – Statistical analysis of the hydrological data during the period of observations shows that on the average there are 5 flood waves during a typical rain season. Accordingly, the average annual coarse sediment yield, which also is the required minimum volume of the coarse-sediment trap, can now be obtained, $\Sigma V_{coarse} \cong 1100 \times 5 = 5500 m^3$.

Step 8 – The mean approximate sediment concentration during the flood wave can now be computed,

$$\bar{C}_{(mg/lit)} = \frac{\text{Total sediment yield (kg)}}{\text{Total water yield (m}^3\text{)}}$$

$$\bar{C} \cong \frac{14.04 \times 10^6}{4.08 \times 10^6} = 3.44 \text{ kg/m}^3 = 3440 \text{ mg/lit}$$

Step 9 – If no empirical expression is available for the estimate of the sediment yield, a suitable sediment-transport formula should be chosen and

applied. Let us suppose that the Engelund-Hansen method was finally chosen (see Appendix 1 to Chapter 9), but obviously any other suitable method could be used.

A typical calculation for the partial discharge of $Q = 16.3 \text{ m}^3/\text{sec}$ is shown in the following. For the given discharge, from the diagrams in Fig. 10.22 the corresponding values of the water depth and velocity can be obtained,

$$d = 2.0 \text{ m}, \quad V = 1.65 \text{ m/sec}$$

$$\theta = \frac{d \cdot I}{(S-1) d_{s50}} = \frac{2.0 \times 0.0007}{(2.6-1) \times 1.2 \times 10^{-3}} = 0.729$$

$$f = \frac{2gdI}{V^2} = \frac{2 \times 9.8 \times 2.0 \times 0.0007}{1.65^2} = \sim 0.01$$

$$\phi = \frac{0.1}{f} \theta^{5/2} = \frac{0.1}{0.01} (0.729)^{5/2} = 4.54$$

$$q_T = \phi [(S-1) g d_{s50}^3]^{1/2} = 4.54 [1.6 \times 9.8 \times (0.0012)^3]^{1/2}$$

From here the partial sediment discharge for unit width of the stream,

$$q_T = 7.47 \times 10^{-4} \text{ m}^3/\text{sec/m}$$

Results of all the calculations are summarized in Table 10.5c. Hence the estimated total sediment transport per unit width of the stream is about $135 \text{ m}^3/\text{m}$. For the whole width of the stream,

$$Q_T = \Sigma q_T b \cong 135 \times 30 = 4050 \text{ m}^3$$

Coarse sediment constitutes about 20% of the total load,

$$V_{\text{coarse}} = 4050 \times 0.2 = \sim 810 \text{ m}^3$$

For 5 flood waves on the average, the total volume is, of course, equal to Q_T , i.e. 4050 m^3 .

The relation between the measured sediment load and the coarse-sediment fraction is certainly not constant during the passage of the flood wave. At

TABLE 10.5c. SEDIMENT TRANSPORT CALCULATIONS (Ex. 10.5)

1	2	3	4	5	6	7
Area no.	Q_{av} (m/s)	d (m)	V (m/s)	$q_T \times 10^{-4}$ (m ³ /s/m)	Duration $\times 10^3$ (s)	5×6 (m ³ /m)
1	11.0	1.20	1.20	1.82	21.6	3.93
2	16.3	2.00	1.65	7.47	21.6	16.13
3	18.7	2.45	1.87	13.00	60.5	78.65
4	16.3	2.00	1.65	7.47	25.9	19.35
5	12.5	1.45	1.30	2.83	32.4	9.17
6	9.7	1.05	1.10	1.26	60.5	7.62
Σ						134.85

lower discharges, coarse sediment is probably not more than 3–5% of the measured load, and maybe as high as 30% or more at peak rates. For simplicity, in the present computations, a flat average rate of 20% has been assumed, but any more elaborate method can be used.

10.3.8 Stream Bank Protection

Stream banks, even in a regulated channel, are constantly attacked by waves and scoured by the erosive action of the shifting water level. Strong local scour is particularly active along the concave bank of bends, and in cases where the soil is non-cohesive and only loosely bound together, bank protection is often indicated. Such protection may be either direct – in which case it is done by a suitable kind of protective rivetment – or indirect, when the protection against scour is achieved by constructions not directly attached to the banks themselves (such as groynes and similar). In the present paragraph, only some direct methods are briefly discussed, while groynes are dealt with in paragraph 10.3.9.8.

10.3.8.1 Protection by Plants

On very small streams, the simplest and cheapest protection may well be the planting of two to three rows of some sturdy growth, such as willow in

temperate climates, or eucalyptus in Mediterranean or similar latitudes. Small seedlings soon develop strong and ramified roots inside the loose soil of the banks, thus conferring to it additional bonding; outside branches and foliage provide a shield against the scour. The growth of the plants, however, should be controlled, because otherwise with time they may obstruct the flow and cause flooding if not trimmed at appropriate intervals.

In all other direct methods of protective rivetments, it is essential that the banks first be graded to a convenient slope, and all irregularities and projections removed. Inadequate or sloppy preparation of the subsoil may cause failure of the revetment.

10.3.8.2 Rip-Rap Revetment

It is often the preferred solution when there is a plentiful and cheap supply of stone in the vicinity of the stream. Quarry chips are most frequently used, but in some cases, where the rock had been found unsuitable, even small concrete blocks have been employed instead. Weight of single stones, or rather their equivalent diameter, obviously depends on the velocity of water impinging upon them, but although there are a few theoretical expressions for the determination of the required stone weight, empirical data are generally more reliable. Stone sizes as recommended by the U.S. Corps of Engineers [10] are given on the graph of Fig. 10.23.

When used as protection to banks of cohesive soils, rip-rap stones generally are placed directly upon the previously straightened and graded soil surface. In the case of non-cohesive soils, however, it is recommended to lay first a graded gravel filter, and to put the stones on top of it, Fig. 10.24. This is particularly indicated in channels of ephemeral streams, where after the rainy season ground-water table outside of the stream is higher than the water level in the channel, and hence the seepage is from the banks into the stream. Graded filter in such a case prevents washing-out of fine grains between the coarse stones, and eventual collapse of the bedding that supports them. Graded filters should be properly designed according to the accepted practice of the soil mechanics.

When scour is anticipated at the connection line between the banks and bed, a *toe-trench*, into which the stone revetment is extended to some depth below the bed line, may be required.

10.3.8.3 Stone Mattresses

Bank protection by stone mattresses (Fig. 10.25) is generally efficient, and due to its flexibility, is not affected by minor local settlements or scour of the subsoil. After careful levelling and grading of the banks, the following

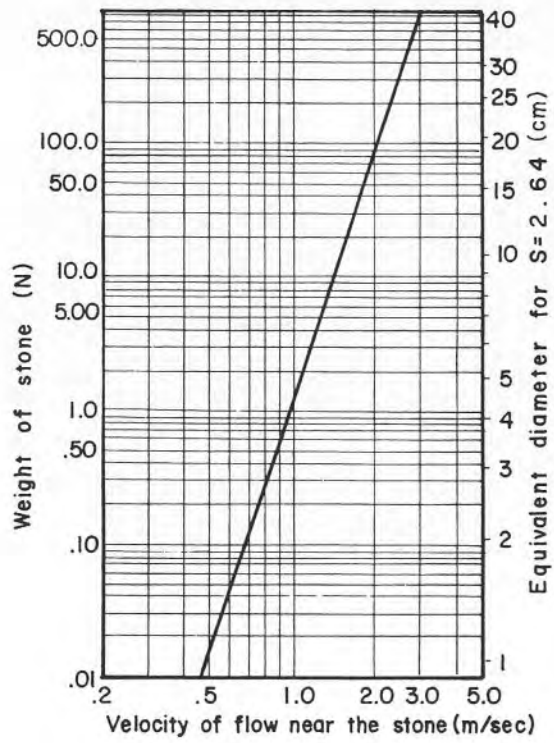


Fig. 10.23. Recommended stone sizes for rip-rap revetment, after [10].

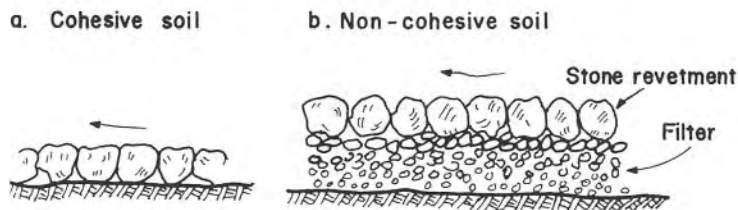


Fig. 10.24. Rip-rap revetment.



Fig. 10.25. Bank protection by stone mattresses (by courtesy of Maccaferri Gabions).

steps should be carried out:

1) Double-galvanized steel-wire mesh is spread out on top of the subsoil. Thickness of the wire should be 3–5 mm, and mesh openings about 8–10 cm. In order to prevent unravelling, wires are double twisted around each other at every node.

2) To this bottom mesh, steel-wire stirrups are attached every 80–100 cm, letting them stick out about 25–30 cm.

3) Stone filling is then spread out upon the mesh, with stones larger than the mesh openings. Stones should be well scattered, and voids between them filled with smaller pieces.

4) On top of the stone fill, a second wire mesh is laid down, identical to the first one. Wire stirrups are used to bind this upper mesh to the lower mesh.

5) At both ends of the mattress, hooked steel pins are driven about 80 cm into the subsoil, to better anchor it to the bank.

6) If the channel is fairly deep (say, 2.5 m or more), it is recommended to divide the mattress by wire partitions into smaller compartments, in order to prevent sliding of the stone fill toward the bottom.

7) It is a good practice to bend the mattress at both ends, and to bury it into the subsoil (see detail b in Fig. 10.26). This prevents possible rolling up of the wire mesh at the loose ends. An alternative solution for the lower end is to extend the mattress covering as an apron onto the channel bed (see Example 10.6). In the case of local scour, the mattress will fold down

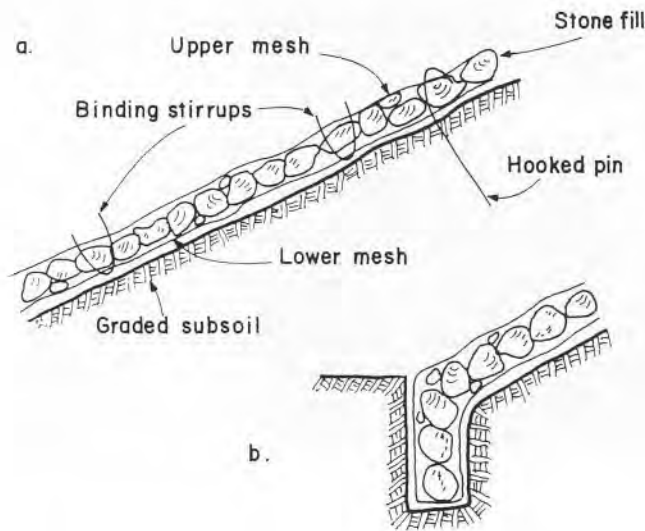


Fig. 10.26. Stone mattress.

into the hole and eventually cover it. The width of the apron depends on the expected scour, but it is usually at least three compartments, i.e. about 2.0 m. Typical details of a stone mattress are shown in Fig. 10.27.

Corrosion of the wire generally does not occur under normal conditions, and well-built mattresses are known to last as long as about twenty years. However, in the vicinity of sea, where the danger of corrosion is much higher, wires should be plastic coated.

The recommended minimum mattress thickness depending on the flow velocity and nature of base soil material is indicated in Table 10.6 [11].

Ready-made wire-mesh, divided into compartments and supplied in sections convenient to handle, is available today on the market. Its main advantages are speedy construction, possibility of laying the mattress in running water (no dewatering necessary), good resistance to wear and tear, and finally the cost which compares well with other materials. A typical design for stream and canal bank protection, as well as schematic methods for underwater placing of mattresses, is given in Figs. 10.27 and 10.28.

On sandy and silty subsoils it is essential to lay an appropriate filter beneath the gabion revetment, in order to prevent washing-out of tiny soil particles through the stone cover. The filter may be either a conventional graded gravel layer (see Example 10.6), or a plastic filter cloth, woven or

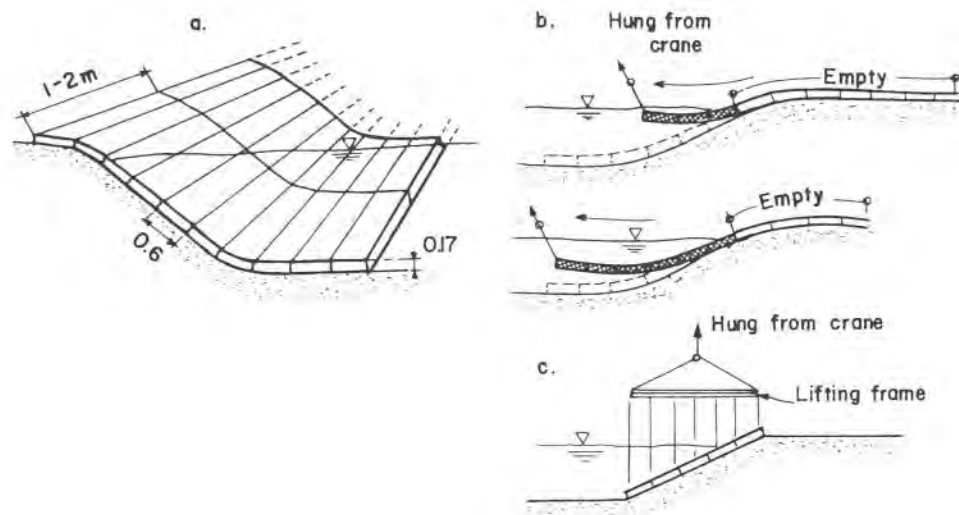


Fig. 10.27. Ready-made stone mattresses – typical design (a), and methods of placing underwater (b, c).



Fig. 10.28. Placing of mattresses over plastic fiber cloth (by courtesy of Maccaferri Gabions).

TABLE 10.6. RECOMMENDED MATTRESS THICKNESS

Base soil	Flow velocity (m/sec)	Mattress thickness (mm)				
		2	3	4.5	5	6
Clays, heavy cohesive soils		170	230	300	—	—
Silts, fine sands		230	300	—	—	—
Shingle with gravel		170	170	200	230	300

nonwoven, as available on the market. There is for the time being no extensive information about the engineering selection of the appropriate filter cloth and the expected performance, and this is no doubt a drawback. However, some pertinent recommendations have been given by Calhoun et al. [31], and these are briefly summarized in the following:

1) Woven or nonwoven filter cloths with less than about 4% open area should not be used where silt is present in sandy soils.

2) When stone or rubble must be dropped directly on the cloth, the minimum tensile strength in the strongest and weakest directions should not be less than about 1500 N and 1000 N respectively. Elongation at failure should not exceed 35%. The minimum burst strength should be about 3.5 MPa. However, when appropriate care is taken in placing revetment stone, the above requirements may be relaxed.

3) Cloths made of polypropylene, PVC (polyvinyl chloride), and polyethylene fibers do not appear to deteriorate under most usually met conditions. On the other hand, all the cloths are affected to some degree by sunlight, and consequently should be protected from exposure to sunrays (this is particularly important in arid and semi-arid regions with high solar radiation intensities).

4) Cloths should preferably be made of monofilament yarns, and the absorption rate of the cloth should not exceed about 1%. These two requirements act to reduce the possibility of the fibers swelling and thus changing the equivalent opening size (in standard sieve gradation) and percentage of open area.

There is generally no need to place any special base layer beneath the cloth, and it is sufficient to shape the slopes to grade. Cloths are best layed with overlapping of 20–25 cm, and fastened at about 1.0 m spacing with 50–70 cm long steel pins. However, the fastening method should always be carefully adapted to local conditions if sliding and other problems are to be avoided. Whenever feasible, cloth-laying should be carried out during the dry season or low water in the channel. As mentioned already, all possible precaution should be taken to avoid dropping stone cover directly on the cloth.

Finally, the great variety of bituminous coatings should certainly be mentioned in this place. A comprehensive review of various products and methods has been given already in Volume I of the Manual, Part 2, Chapter 6. Concrete lining has also been extensively treated in Chapter 5, while a review of other channel coating methods can be found in Chapters 2, 3, 4 and 7 of Part 2.

10.3.9 Protection by Dikes

10.3.9.1 General

Building dikes along a stream as a shield against high water, no doubt has been one of the most ancient means of flood protection. In modern times it is still widely used, either as the only engineering work of protection, or in conjunction with other stream-training works and channel regulation.

Like all earth structures, dikes are highly vulnerable to overtopping by the flowing water. Freeboard above the design stage provides for additional security against flood waves exceeding the design discharge, but if even this is not enough to contain the rising water, dike failure becomes a real threat. The damage to the flood plain in such a case may well be even worse than without protection at all. This only underlines the importance of a thorough hydrological investigation and stream routing in order to obtain reliable stage prediction for extreme flood events. The return period on which to base the statistical analysis should be governed by the principles laid down in the introductory words to the present chapter. Important flood-protection schemes require a comprehensive analysis from different points of view — engineering, economic and social, which should include also the human suffering considerations. If the return period (or the equivalent probability of the occurrence) obtained from engineering considerations is larger than those from economic or social analysis, it should prevail. On the other hand, whenever economic, social or communal safety considerations yield larger

estimates of the return period, these should take precedence over the engineering analysis. Overestimating the amount of protection needed should be avoided from the engineering point of view, but any community willing to pay for it has the right to do so.

10.3.9.2 Height of the Dikes

In order to route the design flood wave along the stream channel and obtain the water stage relationship, channel section must be known. When dikes are built along the main channel, a compound cross-section is obtained, the form of which depends on the distance of the dikes from the stream bank. It is obvious that the same discharge could be carried between higher dikes built close to the stream bank, and low dikes placed away from the stream, see Fig. 10.29.

With the exception of cases in which the distance of the dikes from the stream is limited by circumstances that fall mainly in the legal province (such as property rights, expropriation restraints, etc.), the distance, and hence also their height, is generally based on the considerations as listed below.

1. *Economics.* As far as the cost of the dikes is concerned, low dikes are cheaper to build, not only because of the minor volume of earth work, but also because higher heads require embankments more costly to construct (see par. 10.3.9.4 on construction of dikes). Since dikes usually are built along extended stretches of the stream, the cost of a diking scheme is very sensitive to additional height of dikes. Such a cost increase, however, may be more than offset by the lost revenue from the impounded agricultural land between the low dikes, which cannot be efficiently tilled, if at all. Although some seasonal crops may be grown during low-water periods, and hence the loss of revenue diminished to a certain extent, a thorough economic analysis is indicated in all such cases.

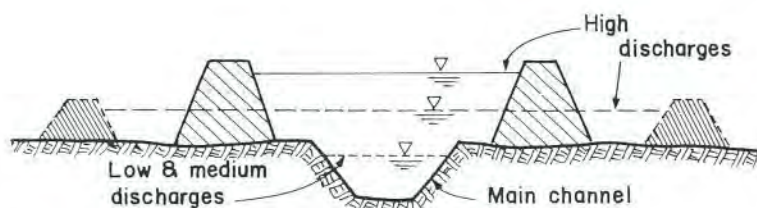


Fig. 10.29. Compound channel cross-section.

2. *Safety.* Dike failure is a possibility which should always be borne in mind. This may happen not only because of overtopping due to an extraordinary flood event (floods corresponding to exceptional return periods, coincidence of simultaneous flood peaks in several tributaries), but also due to some unforeseeable technical accident (piping due to burrowing animals, irregular subsoil settlement, faulty workmanship, etc.). There is little that can be done against overtopping by exceptional flood events, except for an emergency heightening of dikes by means of sacs filled with soil. Regular inspection of embankments and maintenance service are essential for any successful diking system. Any telltale signs of toe erosion due to high flow velocities should be promptly dealt with; signs of dike failure due to water pressure, particularly after prolonged rain storms, can be remedied by strengthening the embankment on the flood-plain side.

Failure with low dikes will cause only minor damages and probably only negligible distress to the streamside people; with high dikes, however, both the material damage and human suffering are likely to be much more severe, causing even loss of life. Safety interests, on the other hand, do not always go hand in hand with the economic considerations, and therefore a careful balance sheet should be drawn before the final decision is made.

3. *Hydraulics.* In many instances, particularly when an overall channel regulation is carried out as part of a stream training scheme, dike protection may be required only along relatively short reaches. Channel enlargement in such cases may sometimes be hydraulically short, and hence act as a local expansion. Water level along the diked reach of the channel will then be higher than the normal depth for the same discharge in the rest of the channel, causing backwater upstream of the reach. Hydraulic conditions should, therefore, be properly understood and examined, corresponding water depth computed and taken into account when determining the height of the dikes. Due consideration, of course, should also be given to the backwater curve upstream. If hydraulic analysis shows that the reach is long enough for normal depth to be established in it, then it will be lower than in the rest of the channel.

It is clear that a similar situation will develop if the dikes happen to form a local constriction, only water configuration will be the reverse of the previously mentioned. Rules for the hydraulic analysis may be found in any good textbook on open-channel hydraulics, such as [12, 13].

4. *Freeboard.* Top of dike is obtained by adding the freeboard to the maximum design stage obtained after taking into account all the pertinent factors as discussed before. The main purpose of the freeboard is to provide for additional safety against exceptional flood events, but it should also give allowance for a few other factors:

a) Wind set-up; b) wave uprush; c) expected settlement of dikes after construction; d) superelevation along bends, e) possible deterioration of the dike top.

On larger streams, the first two factors should be either taken from field observations during storms, or computed with the aid of empirical formulae when the wind fetch (length of the wave-generation path) can be determined with reasonable reliability. A review of such formulae can be found in any textbook on dams, such as [14], but various empirical formulae for the height of wind-induced waves give results that differ as much as 100%. On smaller streams, wind-induced waves are generally not large, and other factors also are of limited extent, so that they may be included in a token freeboard of 30–40 cm.

Consolidation of sandy and similar cohesionless fills, compacted in thin layers (about 15 cm) and at optimum moisture, usually takes place during the construction itself, so that no additional settlement with time is to be expected. Cohesive fills, on the other hand, require much longer periods of time to reach the final consolidation, and hence about 1–5% should be added to the height of the dike to allow for the slow settlement.

Superelevation along the concave banks of bends has been discussed in Part 1, par. 3.8 of the present volume.

10.3.9.3 *Dike Cross-Section*

The design of the dike should be such as to ensure its mechanical stability and safety against failure from seepage or piping. Although dikes usually are not frequently exposed to very high water stages, and even then for relatively short periods of time, they often have to be built in poor foundation conditions, and the choice of fill material is often very limited because of cost restrictions. It is, therefore, a sound policy to give proper thought to the design of the dike.

Mechanical stability is largely dependent on the side slopes of the dike, and for high dikes a soil-mechanics stability analysis is called for. For dikes that do not exceed the height of 4–5 m, and have no particular foundation problems, the recommended water-side slope is 1:3–1:3.5, and dry slope 1:2–1:2.5 [15]. Sand and heavy clay are generally considered unsuitable soil materials, although dikes from well-compacted sand have often been

used in arid zones, where no other material is available. Side slopes in such a case are much flatter, 1:5–1:6, and often protective revetment is used on the water-side slope. On high dikes, berms (horizontal ledges which break the slope) are sometimes used; they increase the stability of the slopes [16], and prevent soil erosion from the surface runoff due to direct precipitations, Fig. 10.30. Berms should have a reverse slope of 1–2% and a drainage ditch running all along that carry the runoff water towards collector ditches distributed at appropriate spacings throughout the length of the berm.

The width of the dike top is mainly dependent on the kind of traffic it is supposed to accommodate. In general, it is in the range of 2.5–5.0 m, with about 3.0 m probably the most frequent choice, because it is large enough for light pedestrian traffic, and also for occasional small motor vehicles.

Seepage and Piping. Most low- and medium-size dikes (say, up to 5–6 m height) are made as homogeneous embankments built from locally found soils. Zoned embankments, consisting of an impervious core and two pervious outside support-shells, which is much more expensive, are generally used for high dikes. Theoretical and practical guidelines for zoned structures are found in textbooks dealing with the design of small dams, such as [15] or [17].

The seepage through a homogeneous embankment involves almost the whole breadth of the dike (Fig. 10.31), and is determined by the phreatic line (seepage line), which is practically the line of saturation, or the uppermost flow line.

In zoned embankments, in which the outer shells are several orders of magnitude more pervious than the central core, practically all of the head is dissipated within it. Consequently, the phreatic line may be assumed to be confined within the impervious zone only, see Fig. 10.31b. Detailed discussion can be found in textbooks dealing with seepage and earth dams, such as [14] and [17]. In cases where foundation problems are anticipated,

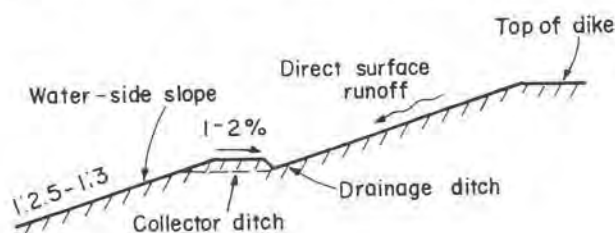


Fig. 10.30. Berm on high dikes.

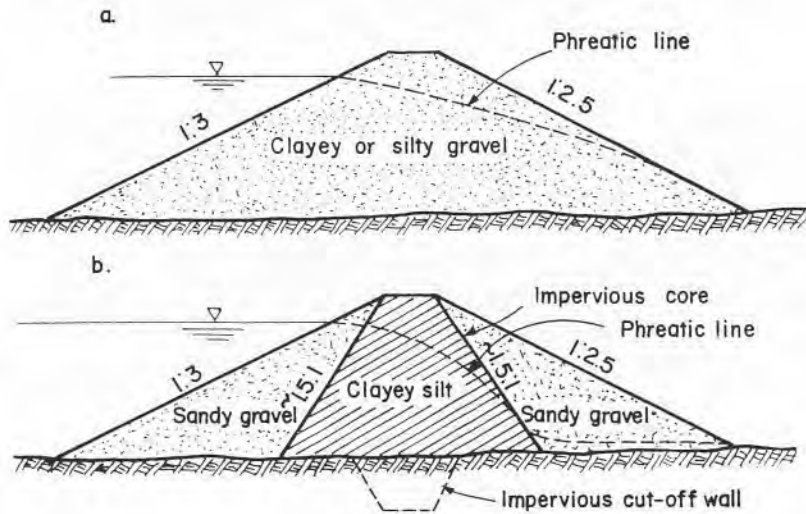


Fig. 10.31. Typical dike cross-sections, a) homogeneous embankment, b) zoned embankment.

especially when seepage below the embankment is feared, an impervious cut-off, extending downwards underneath the central core, may be constructed.

When phreatic line for homogeneous embankments is analyzed, the theoretically parabolic curve may be substituted by a straight line with a slope of about 1:6. If the point at which the line cuts the downstream face is found to be high above the toe of the embankment, and the fill is of relatively high permeability, so that large seepage flow through the dike is anticipated, there may be danger of local scouring that should be avoided. This may be achieved either by adding a filter at the toe, which will shift the phreatic line towards the dike body; or the slope of the downstream face is decreased, and hence the intersection point moved lower. This increased slope may be applied to the lower part of the face only, Fig. 10.32.

It should be borne in mind, however, that seepage is a very slow process, even in well-compacted sandy embankments, and that the establishment of the phreatic line requires long periods of time. As mentioned before, dikes generally are infrequently exposed to high waters, and for relatively short periods only, hence the danger from seepage is much more limited than for dams. For this reason, low and medium dikes under ordinary conditions do not require special investigations of the seepage conditions.

If dikes are built on pervious subsoil, there may be danger from piping.

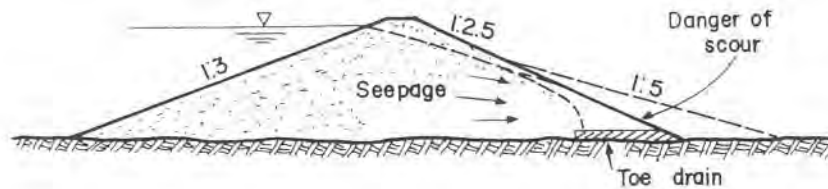


Fig. 10.32. High dike with relatively pervious fill – schematic.

Hydraulic gradient at the exit of the flow lines close to the toe of the downstream face may become excessively high, or soil particles may be entrained and washed away by high velocities through cracked strata or loose gravel layers. In both cases, channels and voids are formed under the embankment along the flow paths, ultimately causing failure of the dike. There are many means to eliminate the danger from piping, and the finally adopted engineering solution should be adjusted to the specific local conditions. These means range from the simple removal of the defective top layers, placing of impermeable blankets, cut-off walls, drainage and relief wells, to a combination of several measures together. Removal of the top layer and replacing it by the embankment fill is recommended in all cases, since thus surface cracks, rootholes, wormholes, etc., which generally abound in this layer and may be instrumental in piping formation, are sufficiently eliminated.

10.3.9.4 Some Construction Criteria

Although in the context of the present manual, construction methods and rules are generally not discussed, in the following a few special aspects concerning the construction of dikes will be briefly reviewed or recapitulated.

- As all other earth structures, dikes should be built on good foundation soil. This is not always possible, and hence appropriate measures should be undertaken to protect the embankment from piping.

- It is a good engineering practice to strip the top layer from the foundation area, and to clean it from vegetation, roots, boulders or organic matter. Depth of the layer should be determined following an inspection on the site.

- Embankment fill should be spread in layers 25–30 cm thick, and compacted at optimum moisture by means of a sheep-foot roller. Simpler means of compaction should be avoided, because results are generally not satisfactory.

- Cohesive fills require long periods to reach final consolidation, hence this must be taken into account when specifying the initial freeboard.

- Alluvial material excavated from the stream bed is in most cases well suited to be used as fill for dike embankments.
- If borrow pits are necessary, they should not be located in the immediate vicinity of the dike, whether they are on the streamside of the flood plain, or on the landside. In both cases, borrow pits close by are likely to favor the piping underneath the dike. Best distance should be about 5–10 times the maximum head on the dike, but in any case not less than about equal to the height of the dike.

10.3.9.5 Drainage of the Flood Plain

After the construction of dikes along a stream, drainage system of the plain is cut off from its natural outlet. Whenever flood protection by dikes is envisaged, an adequate solution to the drainage problems of the flood plain must be incorporated in the overall design of the system.

In many instances drainage canals and ditches have outlets into small tributaries of the main stream. After the erection of dikes, these secondary streams should not be obstructed from draining into the main stream. To avoid flooding of the plain at such junctions, dikes should be extended upstream of the tributary to an adequate distance, Fig. 10.33.

If the number of tributaries or canals which drain directly into the main stream along the diked reach is large, a similar solution for each one of them is often too expensive, or the required area may not be available. In such cases, the alternative should be examined to divert several tributaries (canals) into one of them (collector) and to erect dikes along this one only, Fig. 10.34.

When, because of topographic or any other conditions, the construction of auxiliary dikes along the tributaries becomes excessively expensive or unsuitable, then the alternative should be examined to carry the main dikes uninterrupted across the junction, and to design a controlled outlet structure through the embankment for the secondary channel. Such structures, in the form of culverts with sluice gates or valves, Fig. 10.35, are kept closed during high stages in the main stream, and opened only after subsidence of the flood water. Control gates of any kind have two main drawbacks:

- 1) They are generally expensive to build and require costly appurtenances,
 - 2) Skilled manpower is essential for the proper operation of the gates.
- Automatic control devices are available, but they entail even higher capital investment.

As long as there is high water in the main stream, the possibility to drain the surface run-off from the flood plain into the main stream is severely restricted, and in the case of control gates completely non-existent. In order to

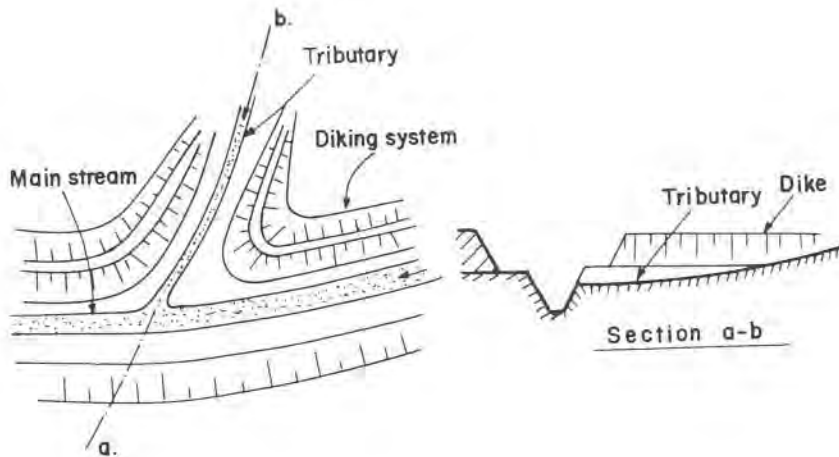


Fig. 10.33. Diking system at the entrance of a tributary.

avoid swamping of lower lands by the run-off from higher grounds, it is often necessary to temporarily store the water within the flood plain itself, and release it later, after the passage of the flood wave. Smooth and efficient operation of such water-removal scheme depends largely on the proper design of the drainage network for the plain, including collector ditches and channels laid out according to the given topography, and even pumping works for low-lying areas which cannot be drained by gravitation. Temporary-storage ponds themselves often require diking to variable extent.

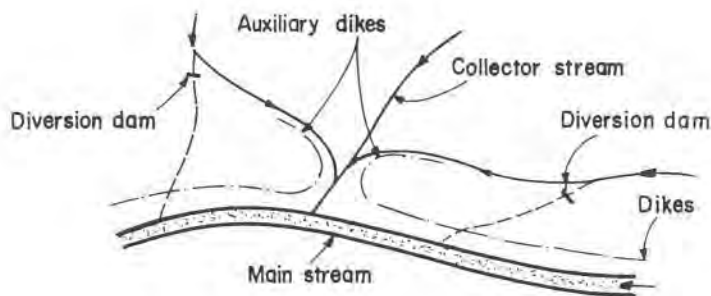


Fig. 10.34. Diversion into collector stream (schematic).

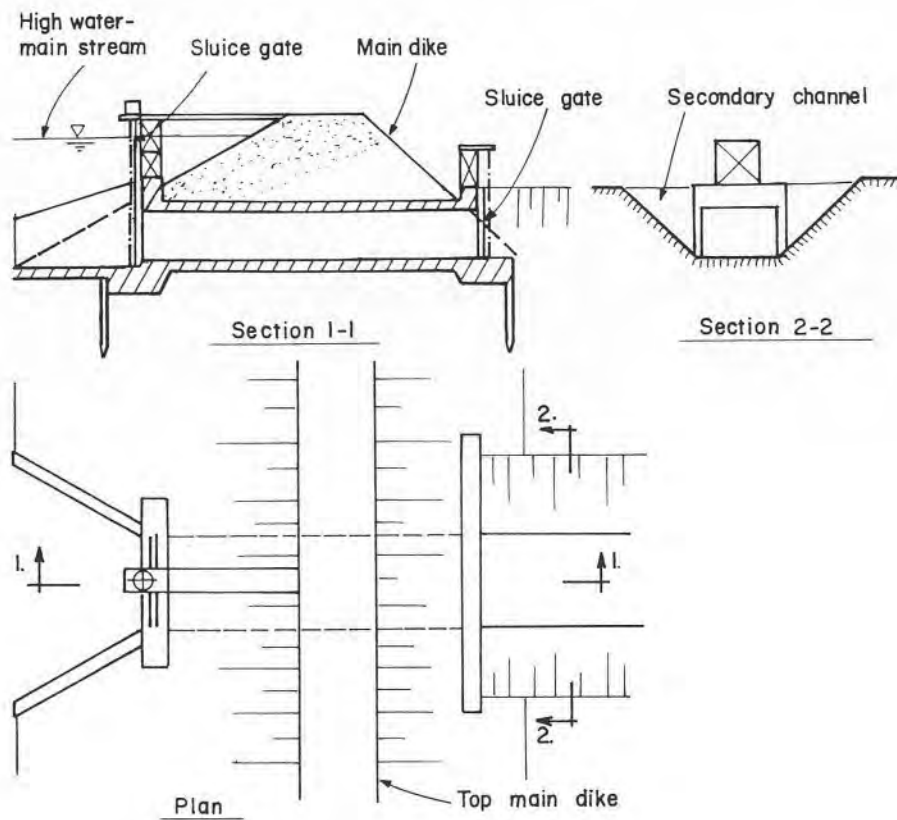


Fig. 10.35. Culvert outlet through dike with sluice gates (schematic drawing).

A schematic and partial drawing of an integrated coastal flood-plain drainage scheme situated in the northern part of Israel is shown in Fig. 10.36. The main stream, draining a large mountainous area, has been regulated and diked almost throughout its course across the plain to the sea. The adjacent flood plain, mainly consisting of impervious clayey soil, prior to the integrated training works had been subjected to heavy and prolonged swamping, which lasted not only during the winter months, but extended well into the spring and summer months as well. The area was practically unusable for agricultural development. It is presently a thriving agricultural reclamation area. No temporary storage ponds have been included in the scheme, for two main reasons: 1) all natural streams, including the main stream, are

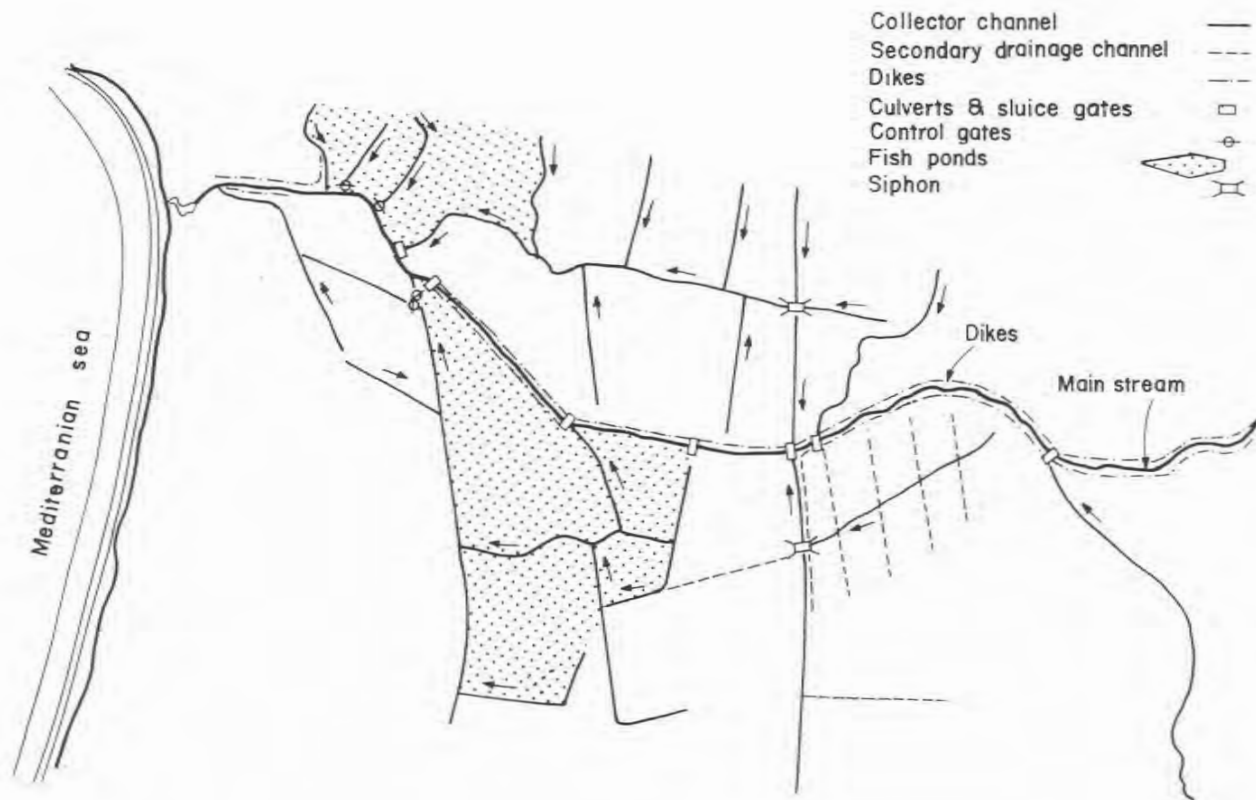


Fig. 10.36. Drainage scheme in the coastal plain of northern Israel (schematic drawing).

ephemeral ones, with flood waves of high peaks, but short duration; and 2) there are many fish ponds in the area, which may be used for temporary storage when needed. For the sake of clarity, all roads, railway, bridges, and many other features have been completely omitted.

Any structure that passes through the dike constitutes a weak point as far as the stability of the dike is concerned; it may also cause seepage problems along the contact area of the fill and the concrete. Although both can generally be easily solved with appropriate measures (for instance, collars to lengthen the seepage path, or berms to strengthen the embankment), for small channels it is often much cheaper to use siphons instead of culverts. To pump the water from the plain-side (higher level) to the stream-side (lower level), siphon is put into action by opening the upstream valve, pumping air out of the duct, and letting the water fill it while the downstream valve is kept closed. After the priming is completed, downstream valve is opened, and the flow started.

10.3.9.6 Alignment of Dikes

When dikes are used as the only engineering measure for the flood protection of a meandering alluvial stream, and not as part of a comprehensive scheme including channel regulation, realignment, etc., they must not follow the stream with all its bends, but may rather form a *dike belt*, Fig. 10.37. Distance of the dike from the stream banks should at no place be less than the minimum as previously discussed, while at other places it is more than that. The overall width of the belt should remain more or less constant throughout the reach. On the land between the dike and the stream, seasonal crops may be grown, so that it should not be considered as a total loss from the agricultural point of view. Dike belt, moreover, does not interfere with the slow migration of meanders downstream (see pars. 3.8 and 3.9).

On the other hand, often dikes are part of a flood-protection scheme which also includes channel regulation and alignment. It has been already mentioned that minimum radius at channel bends depends to a great degree on the width of the stream (see par. 10.3.3.2), and hence radius of bends for the channel width between dikes should be considerably larger than for the main channel, Fig. 10.38. As a result, the axes of the main stream channel and dikes are not parallel, and hence accordingly the distance between the dike stream-side toe and channel bank is variable. The distance is smaller on the concave bank of the channel, and larger on its convex bank. Now, this is contrary to the observed flow pattern in bends (see pars. 3.8 and 3.9), which shows that on the concave bank erosion is to be expected. The problem can be satisfactorily solved either by the appropriate shifting of the inflexion

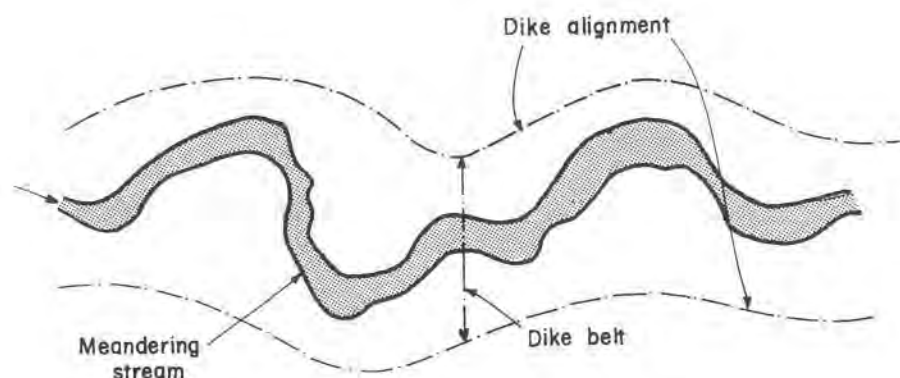


Fig. 10.37. Dike alignment of a meandering stream.

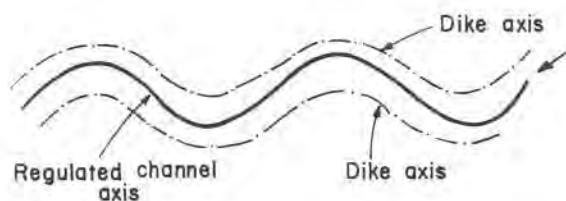


Fig. 10.38. Dikes along a regulated stream channel.

points, or by adopting different and suitable curves, one for the channel, and one for the dikes. In some cases of strong bank erosion, protective revetment will have to be resorted to.

On smaller streams, distinction between different radii is generally neglected, and the main-channel axis is simply made parallel to the dike axis.

10.3.9.7 Summary

Flood protection by dikes has a series of advantages in comparison with other methods of protection, but on the other hand, it has also several drawbacks. All of these have been already discussed in the previous paragraphs, and in the following only a brief recapitulation is given. Main advantages of the method are:

- 1) Building of dikes is relatively inexpensive.
- 2) In most cases, the fill for the embankments can be found on the site, or in close vicinity of it.
- 3) Great part of the building job is done by the aid of heavy soil-moving equipment, and hence no particularly skilled labor force is required.
- 4) Dike systems can be easily carried out in stages, if convenient from the financial point of view; the system can first be started along the most vulnerable reaches, or economically in the most important areas, and only in later stages gradually extended.

As main disadvantages, the following points may be mentioned.

- 1) All dikes, but especially higher ones, are exposed to seepage and piping, and hence are very sensitive to strict observation of the rules of soil mechanics in the execution stages.
- 2) Restriction of the flood-way by dikes may sometimes appreciably change the prevailing stream flood-routing conditions, eliminating the necessary time-lag to avoid the possible coincidence of flood waves in the main stream and tributaries farther downstream.
- 3) Erosion in the diked channel is likely to be stronger because of much higher velocities of flow.
- 4) In certain cases there may be a backwater effect in the upstream reaches of the stream due to the diking of the channel.
- 5) Failure of dikes in many instances causes extensive damage to the flood plain and practical break-down of all economic activities.
- 6) Because of relatively large areas required for a dike system, public expropriation expenses are often very high, and legal proceedings lengthy.
- 7) Proper drainage of the flood plain beyond the dikes is an integral part of any dike system, and this obviously increases the overall cost.
- 8) If the stream is aggrading because of large volume of sediment carried from the upper reaches, the effectiveness of the dikes for flood-protection with time is likely to diminish, and eventually a perched-stream condition may develop that is difficult to confine during major flood events. Further aggradation may cause failure of bridges due to the lack of adequate waterway.

Example 10.6

A small stream that descends from the coastal mountains to the sea causes extensive flooding of agricultural areas. The stream is of the Mediterranean type — it is ephemeral and the flow is practically restricted to winter months and early spring. During the rest of the year it carries only a small

discharge from a few perennial springs in the mountains.

Hydrological service has been measuring peak flows during the last 20 years or so, and the results have been summarized on the probability paper and the statistical extrapolation line drawn, Fig. 10.39.

The natural channel, except in the reaches where it is clogged or entangled, has the mean capacity of about $70 \text{ m}^3/\text{sec}$, which according to the probability curve corresponds to a return period of about 4 years.

It has been decided to design a flood protection scheme along a reach of about 15 kms, consisting of 1) channel regulation, 2) dikes, and 3) slope reduction.

After the investigation of all the pertinent aspects connected with the proposed scheme (such as economic, engineering, social, etc.), the following guidelines have been set down:

- The regulated main channel will be designed to carry the maximum discharge of $70 \text{ m}^3/\text{sec}$, corresponding to the return period of about 4 years.
- The freeboard to the channel will be such that it will be able to clear a bankful discharge of $95 \text{ m}^3/\text{sec}$, having a return period of about 5 years.

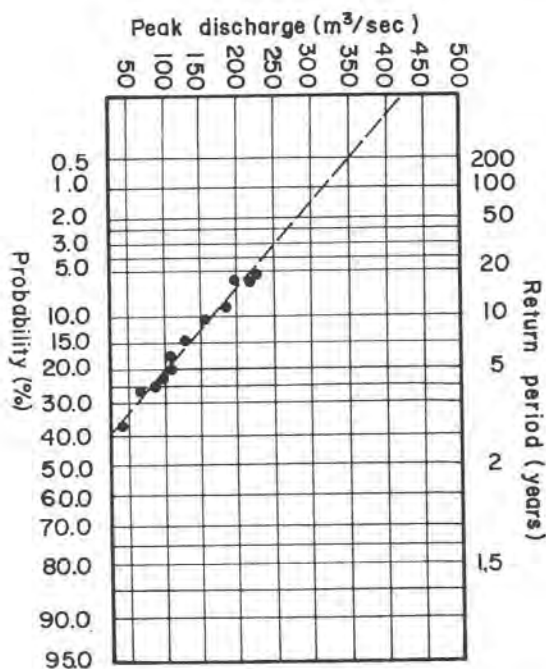


Fig. 10.39. Probability of peak discharges in the stream (Ex. 10.6).

– Distance between the dikes is to be designed so that the compound section has a capacity of $270 \text{ m}^3/\text{sec}$, corresponding to a return period of about 50 years.

– Top elevation of the dikes should be 1.0 m above the water level for the discharge of $350 \text{ m}^3/\text{sec}$, corresponding to a return period of about 200 years.

Mechanical analysis of the bed soil has shown that it is mainly light sandy clay. After considering the possibility to have two different side slopes for the channel – flatter in the lower part, and steeper in the upper part – the final choice, based mainly on economic considerations, has been to have a uniform side slope of 1:3 throughout the whole height of the channel.

Values adopted for the Manning roughness coefficient:

1. Main channel – $n_1 = 0.030$
2. Side channels – $n_2 = 0.035$.

Longitudinal slope of the natural channel along the reach, situated in the upper part of the lower course of the stream, varies in the range of 0.3%–0.5%. Upon the examination of several alternatives, conclusion has been reached to reduce the longitudinal slope of the regulated channel to $I = 0.17\%$. The chosen slope is still relatively high for an earth channel, but any further reduction of slope would require an excessive number of drop structures and dangerously short distances between them. The adopted slope calls for 30 drop structures, more or less evenly distributed along the regulated channel, ranging in height between 1.0 m and 1.3 m, and generally located in the vicinity of the inflexion points between the bends (crossings).

After the necessary hydraulic computations (see Vol. I of the Manual, Part I, Chap. 2; or [1, 12]), the adopted channel cross-section and water levels are given in Fig. 10.40. Wetted area of the main channel is 37 m^2 , and the total area 46.2 m^2 ; freeboard, computed according to the requirements as given before, is 0.4 m. Wetted area for the high flow (HW) between the dikes is 100.4 m^2 , and the area enclosed up to the water level for discharge of $350 \text{ m}^3/\text{sec} = 120.2 \text{ m}^2$.

Average shear stress for the NW (see par. 3.2, of Vol. 1, Part 1, Chap. 3) is about 27.5 N/m^2 , and the mean velocity 1.9 m/sec . These values are relatively high for a sandy clay channel, but owing to the fact that high discharges are infrequent and of short duration, and that the water depth is more than 2 m, they have been considered as acceptable. Mean velocity for HW is about 2.7 m/sec , which again is considered acceptable under the given circumstances. Graphs on Fig. 10.41 show the variation of discharge and mean velocity in the regulated channel.

The stream in question flows through an area of intense agriculture and citrus groves, and hence land appropriation for the protection works posed

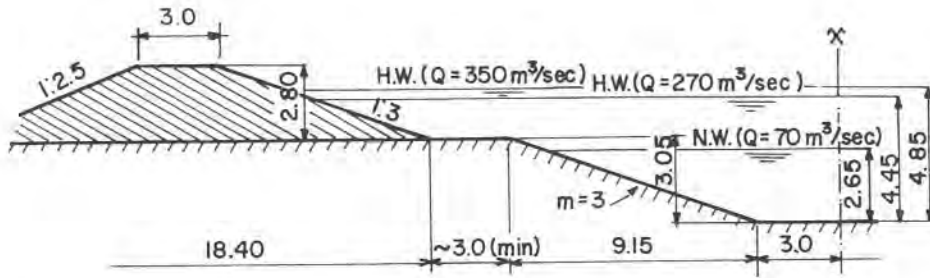


Fig. 10.40. Typical regulated channel cross-section (Ex. 10.6).

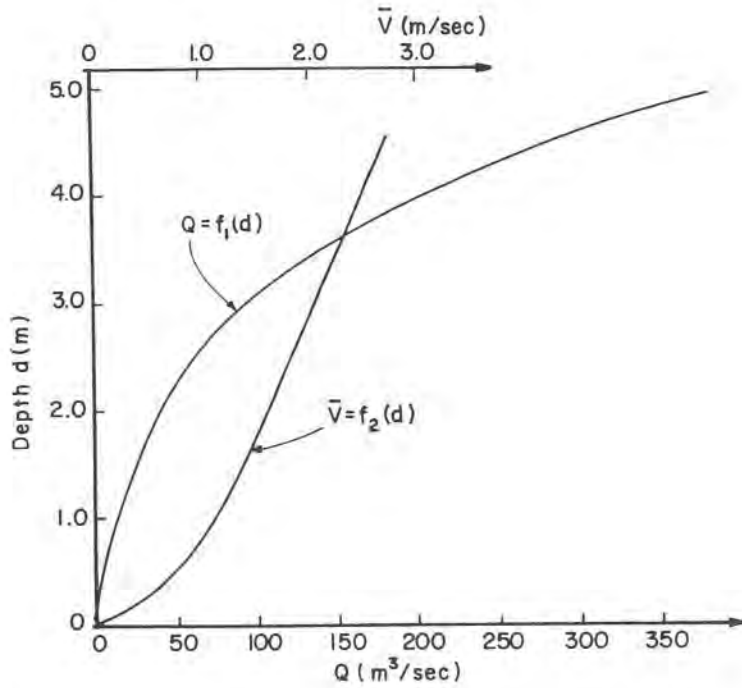


Fig. 10.41. $Q = f_1(d)$ and $\bar{V} = f_2(d)$ for the regulated channel (Ex. 10.6).

serious problems, and has affected both the compound channel cross-section and its alignment. For this reason the distance between the dike toe and the channel has been set at 3.0 m, i.e. about the height of the embankment, and the width of the dike top — 3.0 m.

Channel Alignment. For the same reason of land appropriation difficulties, the layout of the regulated channel has been kept as close as possible to the natural stream. Number of bends in the regulated channel is on the whole identical to that of the natural stream, with the omission of small curves caused by local obstructions. Ideal alignment, however, has been substituted by flatter curves, in order to reduce as far as possible the area required for the scheme. In practical terms, it means that the actual meandering index, which was established to be on the average $M = 1.18$, has been replaced by a lower one.

As mentioned above, the natural mean meandering index for the stream was found to be about $M = 1.18$. In the present case, curve-fitting for bends has been carried out using lemniscates (see par. 10.3.3.2), for both the main channel and dikes. A typical segment of the proposed stream regulation is given in Fig. 10.42.

At the upstream end of the stream-training scheme there will be a sediment-entrapment basin with a capacity of about 10,000 m³ (see par. 10.3.7, and Example 10.5). This basin will have to be periodically dredged in order to keep it operative, and to avoid backwater upstream of the protection works.

10.3.9.8 Channel Stabilization

Bank stabilization by revetment, which is one of the most common means for channel fixation, has already been briefly discussed in par. 10.3.8. Moreover, this is the main technique used within the scope of stream training for flood protection proper.

Two additional channel-fixation techniques, used mainly in river navigation engineering and much less in flood-protection works, will be briefly reviewed here (1) Groynes or spur-dikes and (2) Longitudinal dikes.

Groynes in fact are low dikes constructed more or less perpendicular to the channel banks, with a view to stabilizing the intended channel alignment. When the distance between the intended new alignment of the channel and the existing stream bank is large, longitudinal dikes may be added to the groynes, as shown in Fig. 10.43.

Groynes are generally closed structures, with no passage of water through

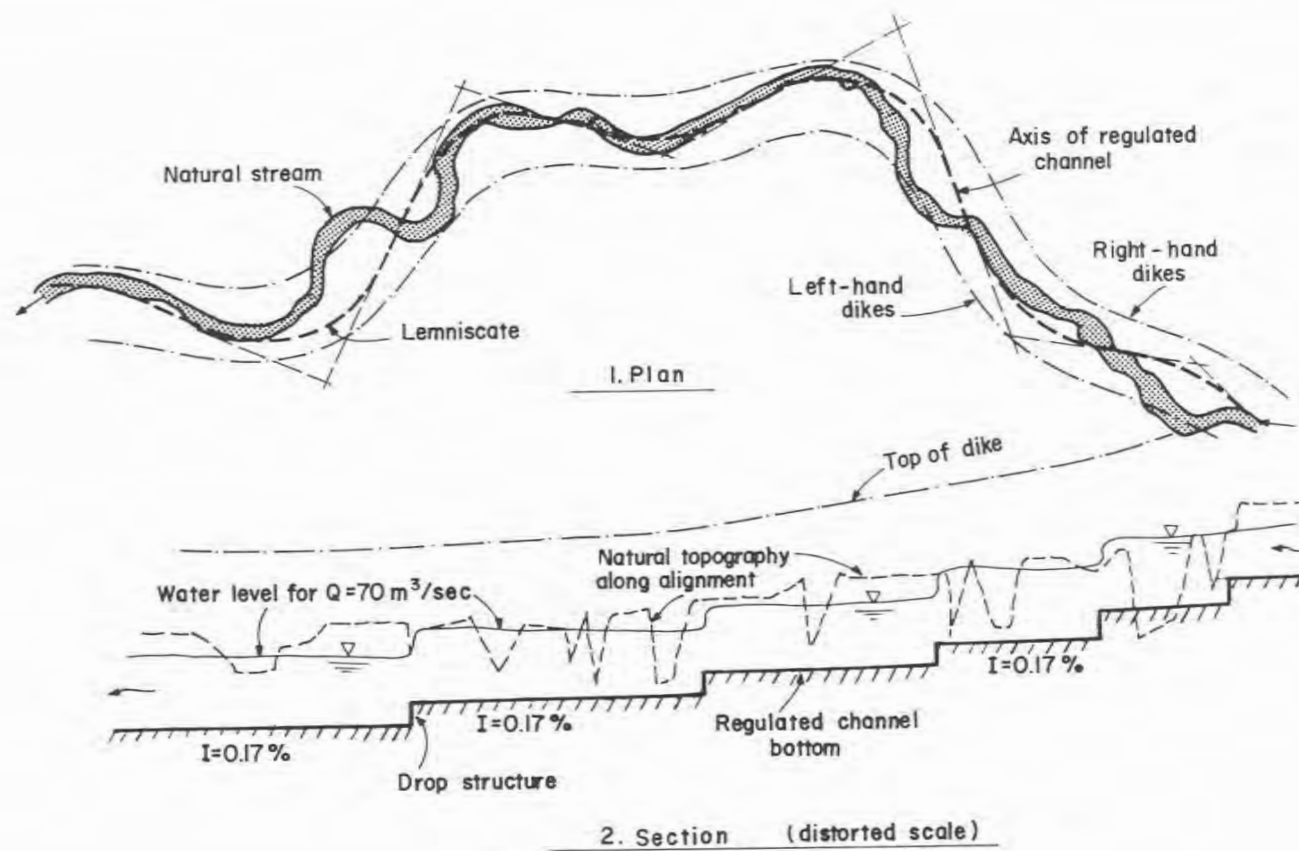


Fig. 10.42. Segment of the proposed stream-training scheme (Ex. 10.6).

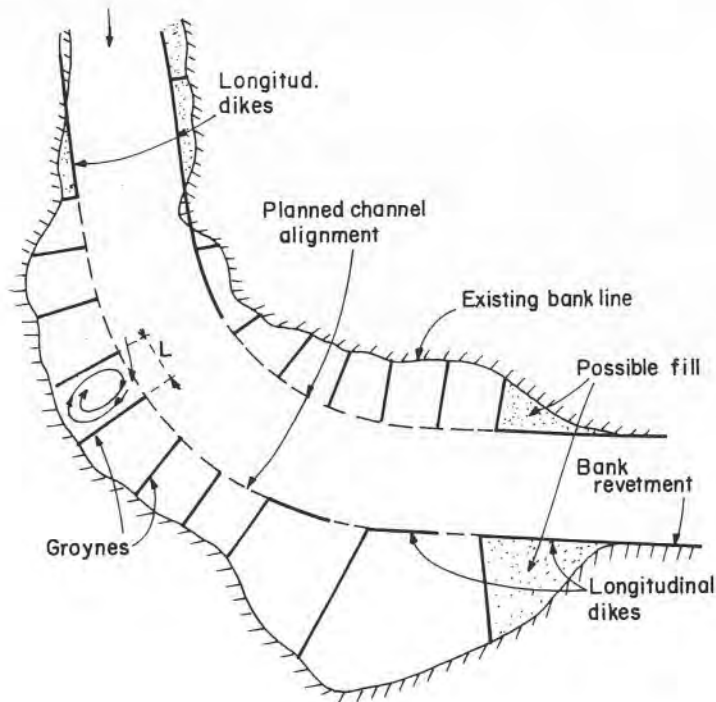


Fig. 10.43. Channel stabilization structures.

them, but there are a few instances of groynes built of concrete or wooden piles driven into the stream bed. A typical groyne structure is shown in Fig. 10.44.

There is for the time being no theoretical way to calculate the distance between the groynes. On the other hand, in many cases the choice between groynes and longitudinal dikes depends largely upon this distance, mainly from the economic point of view. Empirical rules of thumb speak of one to two times the channel width, or 1–5 times the groyne length. According to laboratory tests carried out in the Delft Hydraulic Laboratory [19], there appears to exist a semi-empirical dependency between the distance L between the groynes and a theoretically derived parameter. Test results seem to indicate that the best flow guiding by groynes is obtained when only one strong eddy is formed between each pair. The reasoning follows that the energy required to sustain the backward flow between the groynes (see Fig. 10.43) can only be available if the energy loss in the stream channel JL (J – energy gradient) is smaller than the average velocity head $V^2/2g$.

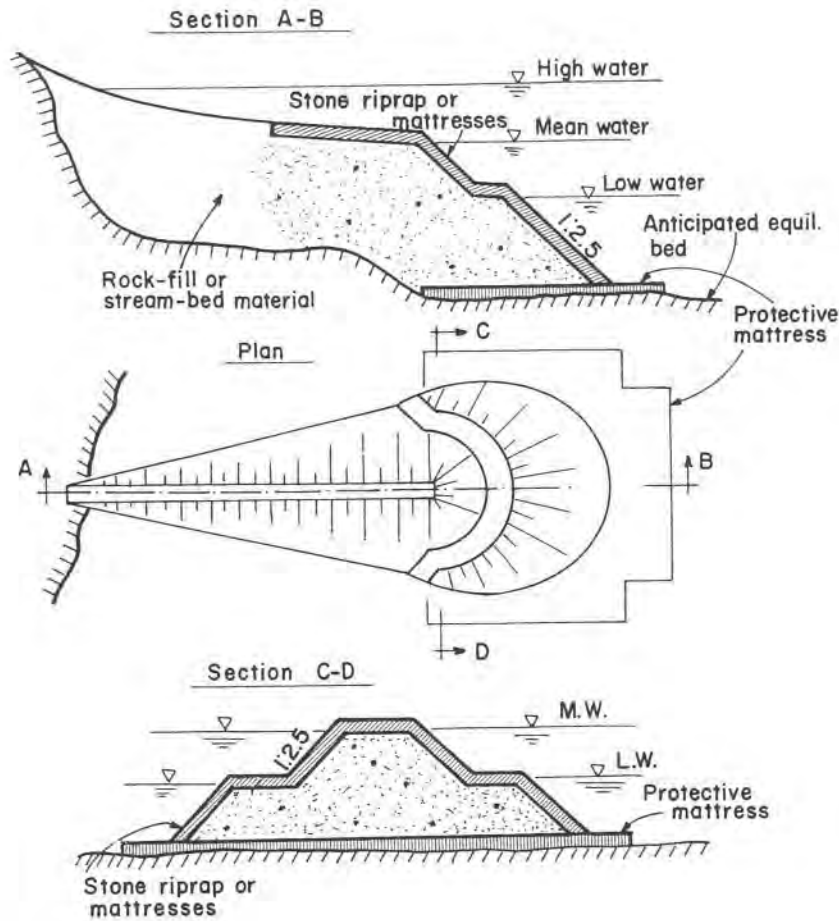


Fig. 10.44. A typical groyne structure.

Writing energy equation between the head points of two adjacent groynes and substituting Manning's equation to express the mean velocity, it can easily be shown that $L = K \cdot d^{4/3} / 2gn^2$, in which $K < 1$ denotes an empirical coefficient, d – mean water depth and n – Manning's roughness coefficient. For a strong eddy, coefficient K has been found to be about 0.6. Thus for instance, assuming a mean depth of 4.0 m and $n = 0.035$, the distance between groynes should be about $L = 160$ m. In practice, however, the distance would be taken somewhat less in order to be on the safe side. On short-radius alluvial bends and relatively narrow stream channels, the spacing

of groynes should be more dense than on wide channels (see Example 10.7).

Currents between the adjacent groynes will slowly deposit sediment and partially fill up the area. On the other hand, there may be strong local scouring around the heads of groynes, and therefore often protective mattresses are used to prevent it, see Fig. 10.44.

There is no definite recommendation as to the angle between the groynes and the channel bank. In fact, the experimental evidence as reported seems to be rather conflicting. Whereas some researchers [32] have found that groynes pointing upstream give minimum scour, others [33] believe that an angle of 90° is the best from this point of view. On the other hand, Gill in the discussion on a paper from Franco gives a graph based on experiments carried out in India which would indicate that groynes directed downstream produce the minimum of local scour, see Fig. 10.45. Hence again, practicing engineers cannot escape using their own judgement for every specific case, since in addition it is claimed that groynes pointing downstream cause less current contraction, while those pointing upstream are more effective in protecting the banks from erosion at higher water stages.

If erosion in front and around the groyne head is expected because of channel contraction, the best policy to adopt would be to dredge the channel down to this level and to extend the foundations of the groyne head and its protective revetment down to and below the dredged bed. Unfortunately, no reliable theoretical estimate of the equilibrium bed configuration is as yet available, hence only previous observations of the stream behavior or engineering intuition can be of any real help. In absence of any

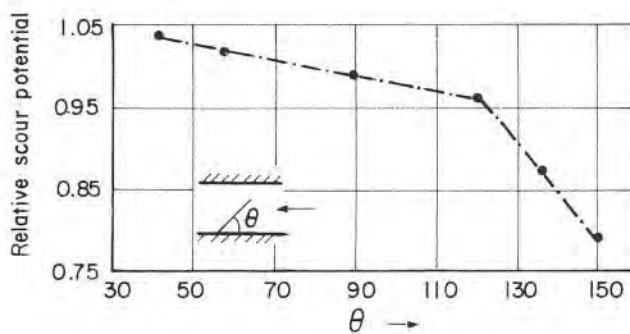


Fig. 10.45. Relative scour potential for groynes in dependence of angle θ , after Gill and Sastri.

reliable data, groyne toe can be laid on the existing channel bed and the erosion left to its natural course. This is not a bad solution, provided that the groyne toe is periodically extended down to the eroded bed and sliding prevented, or at least promptly repaired.

There is a large number of studies concerning the quantitative estimates of the maximum (or equilibrium) *local scour* around bridge piers, but unfortunately scarce information is available in respect of the local scour around groyne heads. The main cause of such local scour seems to be a vortex system which develops at the foot of the embankment as a result of the existing secondary currents and vorticity in the flow, and which involves three-dimensional separation of the viscous sublayer (so-called "horseshoe vortex" [34], see par. 10.3.9.9. This vortex system impinges upon the alluvial bed sediment in front of the groyne head causing local erosion, and the eroded material is eventually carried away downstream by the flow. As with bridge piers, the deepest point of scour is generally located right at the tip of the groyne head.

More extensive studies of local scour around groynes have been carried out by Gill [35]. The results of his laboratory investigations appear to indicate the following:

– Scour depth depends on the depth of flow, and it grows with the increase in depth.

– Scour depth depends on the bed-material size. For the same value of the ratio τ_c/τ_0 , in which τ_c – critical shear stress (par. 9.2) and $\tau_0 = \gamma RI$, coarse sand will be scoured deeper than fine sand; on the other hand, for the same *absolute value* of the shear stress, fine sand will be eroded deeper than the coarse sand (because τ_c for coarse sand is higher than for fine sand).

– Bed load movement does not appreciably affect the scour depth. Indeed, it appears that once the movement of alluvial bed is started, maximum depth of scour tends to remain constant for a given depth of flow.

For design purposes Gill has proposed an empirical formula (the coefficient has been rounded up):

$$\left[\frac{D}{d}\right]_{\max} = 8.4 \left[\frac{d_{s50}}{d}\right]^{0.25} \left[\frac{B}{b}\right]^{6/7} \quad (10.34)$$

in which D – maximum depth of scour below the water surface, d_{s50} – median grain size, B – width of the channel before contraction by groynes, b – width of the channel after contraction.

Garde et al. [33], on the basis of laboratory tests at the University of

Roorkee, has also proposed a semi-empirical formula for the maximum scour at groyne heads:

$$\left[\frac{D}{d}\right]_{\max} = 4.0 \frac{1}{\alpha} \cdot \eta_1 \cdot \eta_2 \cdot \eta_3 \cdot \eta_4 (F_R)^n \quad (10.35)$$

Here α – contraction ratio – b/B , η_1 – coefficient for the effect of sediment size, η_2 – coefficient for the width to length ratio of piers, η_3 – coefficient for the effect of angle of inclination on scour, η_4 – coefficient for the effect of the groyne-head geometry, F_R – Froude number of the undisturbed flow, n – empirical exponent dependent on sediment size.

Variation of coefficient η_1 and exponent n in dependence of the median grain size is shown in Fig. 10.46.

Coefficient η_3 , expressing the influence of groyne inclination to the channel bank upon the maximum scour depth, can be taken from the diagram in Fig. 10.45 (denoted there as “relative scour potential”). The effect of groyne-head geometry on scour depth, η_4 , can be taken as varying between 0.8–0.9 for circular or semicircular shape (usually given to groyne heads).

Finally, two simple formulae, both developed for local scour estimates around embankments, are thought to be adequate for groynes also. For ratios of $0 < L/d < 25$ (where L – length of groyne, and d – undisturbed water depth), formula proposed by Liu [37] is used:

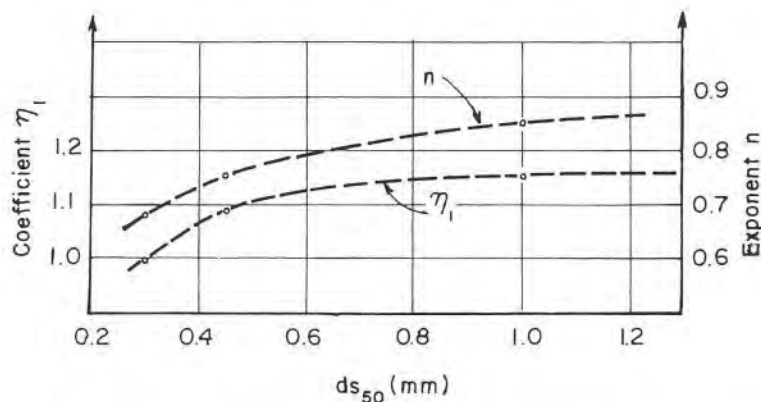


Fig. 10.46. Coefficient η_1 and exponent n vs. median grain size d_{s50} , after [33].

$$\left[\frac{S}{d} \right]_{\max} = 1.1 \left[\frac{L}{d} \right]^{0.4} F_R^{1/3} \quad (10.36)$$

Here S denotes the scour-hole depth *measured below the mean bed level*, and F_R is the Froude number of undisturbed flow.

For ratios $L/d > 25$, empirical formula obtained from field observations on rock dikes is applied:

$$\left[\frac{S}{d} \right]_{\max} = 4 F_R^{1/3} \quad (10.37)$$

The two semi-empirical formulae for the estimate of local scour around groyne heads have been selected not because of any particular merit, but because they belong to the few which specifically refer to groynes, and not bridge piers. Although the basic scouring mechanism is on the whole probably identical, there are nevertheless significant differences concerning various parameters and their relative effect. Both expressions, as well as the others that have not been mentioned, are based on laboratory experiments and not on prototype behavior, and the question whether they can be at all meaningfully applied to alluvial stream flows has in fact still not been answered. Eq. (10.34), when applied to relatively deep flows with fine sediment, will certainly fail to yield acceptable results, and its estimates in general tend to be too low. On the other hand, Eq. (10.35) will generally give too high scour estimates. Applying the two formulae to the same set of data will rather indicate a range within which the practicing engineer will have to take his bearings, until the question of local scour at groynes is better understood and laboratory research fully correlated to prototype flows.

Formulae given by Eqs. (10.36) and (10.37) have been added to this short review mainly because of the simplicity, a quality highly appreciated by practicing engineers.

Crest level of groynes is generally somewhat below or above the mean water level, or the level corresponding to the design discharge. In particular cases of alluvial bend stabilization, the groyne crest is usually above the water level corresponding to the design discharge, with due account taken of the superelevation (see Chapter 3) and any significant morphological features (dunes, bars, etc.).

Crest line is either horizontal or inclined upward to meet the natural bank,

and thus prevent scour at higher flow stages. Franco [32] has also found that with bankward sloping crest line there is less likelihood for flanking or scouring near the bank-ends of groyne dikes. According to the conclusions drawn from his laboratory investigations, sloping-crest groynes should be designed normal to the bank line or angled upstream (contrary to level-crest groynes which should best be placed normal or pointing downstream).

The question whether the crest level of a groyne system should have all crests at the same level or at different levels has so far not been definitely answered, although according to laboratory investigations [32] it has been found that a system stepped-down in the direction of flow gave better performance than any other arrangement.

Embankment fill for the construction of groynes is best taken from the stream-bed material. Should this solution prove to be unsatisfactory, rock-fill may be used, or some sort of gabion-like mesh containers filled with stones and gravel. Revetment, preferably of a pervious type to avoid building up of high pressures with the receding water, should be flexible enough in order not to break following unavoidable settling and erosion of the channel bed. In all cases where washing-out of small grain particles in the fill is feared, a graded filter is recommended, which should effectively prevent it. Dumped or hand-placed stone revetment is used to protect the underlying embankment from currents, waves or impacts by floating debris. Stone size can be approximately estimated using empirical rules developed for dam riprap revetment.

Longitudinal dikes are often attached to groynes in places where the existing bank is distant from the new channel. The distance L between the groynes can then be increased, and if openings are left connecting the channel to the enclosed area, silting is greatly speeded up. It is often advantageous to build longitudinal dikes in stages, with the progress of the silting process, Fig. 10.47.

In the first stage, a small dike is built to approximately the height of the low water. After the process of silt deposition behind the dike has been more or less completed, the dike is raised up to the mean water level. Finally, upon further progress of the silting process and settlement, the dike can be raised even higher if required.

Finally, it should be mentioned that upstream pointing groynes (also called "repelling groynes") have reportedly been successfully used in India to divert the current toward the center of streams and away from flood plains, as a means of flood protection. In many other places groynes have been used with a view to excluding the coarser sediment from the flow, particularly upstream of water diversion projects (see par. 10.3.7).

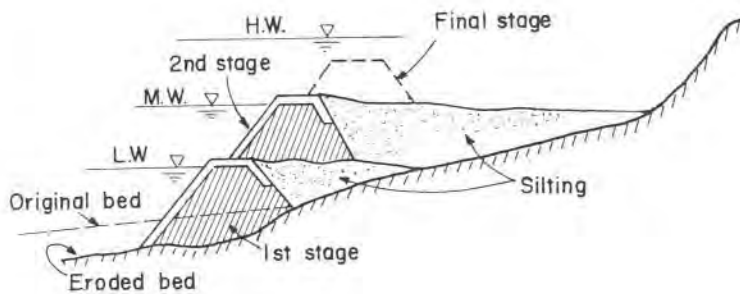


Fig. 10.47. Longitudinal dike in stages.

Example 10.7

A small meandering alluvial stream is encroaching on the industrial property situated near to its southern bank, Fig. 10.48. During the last fifteen years, the migration of the meanders and the erosion of the concave bank (see pars. 3.8 and 3.9) have moved the stream bend about a hundred meters southward, thus endangering the built-up area nearby. It has been decided, therefore, to carry out regulation of the stream channel between the limits as indicated. A general outline of the submitted design alternatives is presented in the following.

Step 1 – The available hydrological measurements of the perennial stream flowing at the foothills of mountains in the temperate semi-arid zone cover a period of 21 years. The graph in Fig. 10.49 shows the measured plotting points on probability paper, with the best-fit line for extrapolation. Two return periods were considered for design purposes – 50 and 100 years. The two maximum discharges to be expected for the respective return periods, as obtained from the graph, are $Q_{50} = 650 \text{ m}^3/\text{sec}$ and $Q_{100} = 740 \text{ m}^3/\text{sec}$.

Step 2 – No reliable water-depth measurements had been available hence it was decided to build a synthetic $Q-d$ curve for the stream channel. For this purpose, three representative cross-sections were measured and then averaged to obtain a single representative cross-section. The final rating curve is given in Fig. 10.50. It has been obtained using Manning equation for uniform flow. The longitudinal slopes of the channel along the reach and beyond it were measured and subsequently averaged. The mean slope thus obtained – $I = 0.001$, and the energy gradient have been assumed to be practically equal.

For the evaluation of the roughness coefficient, it has been estimated that the coefficient due to the grain roughness was about $n' \cong 0.027$; the effect

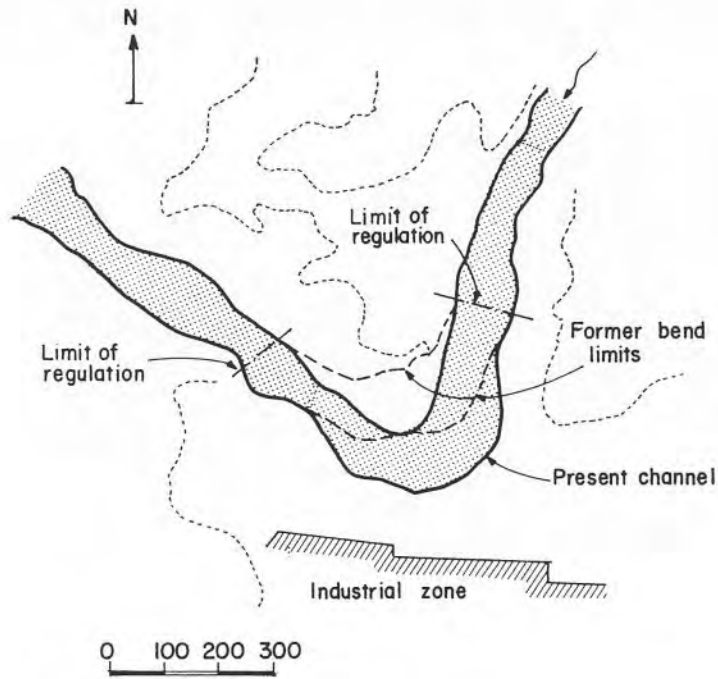


Fig. 10.48. Alluvial stream bend to be regulated (Ex. 10.7)

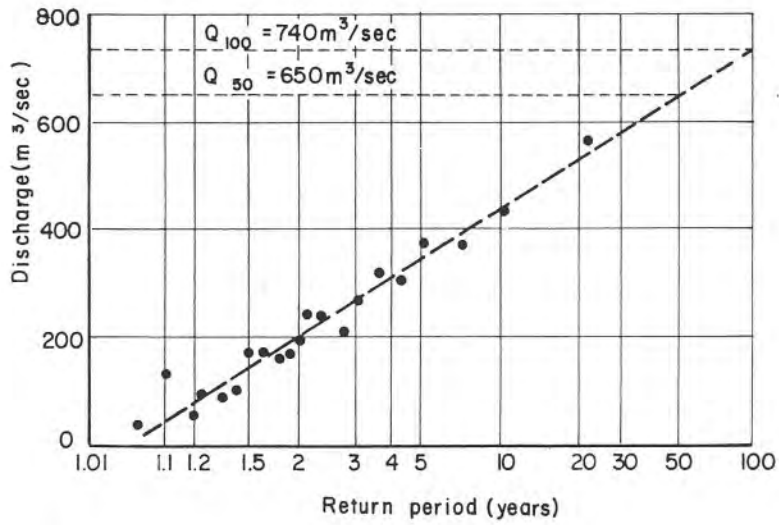


Fig. 10.49. Graph of maximum annual discharges (Ex. 10.7).

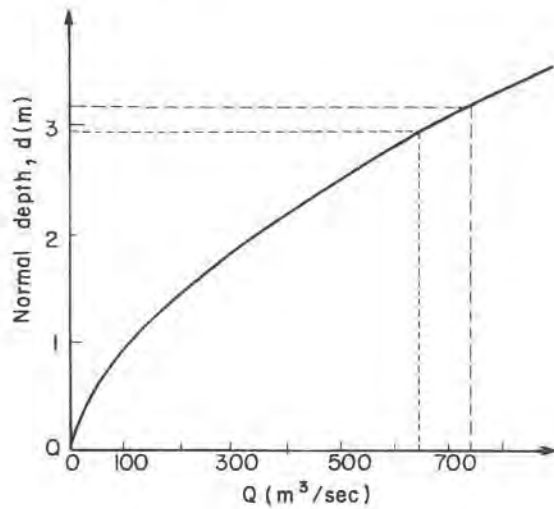


Fig. 10.50. Rating curve for the stream channel (Ex. 10.7).

of bed forms was next estimated using the graph on Fig. 7.6 and the data obtained from the bed-material gradation curve (see Step 3). The value of $d_{s_{35}}$ from the graph in Fig. 10.51 is 0.55 mm. It was further assumed (see par. 7.3) that $R' \cong R = 2.75$ m for the discharge of $650 \text{ m}^3/\text{sec}$ (see Step 4 and Table 10.7).

$$1/\psi' = R'J/1.68 d_{s_{35}} = \frac{2.75 \times 0.001 \times 10^3}{1.68 \times 0.55} \cong 3,$$

and from Fig. 7.6 $n'' = \sim 0.003$

whence

$$n = n' + n'' = 0.027 + 0.003 = \sim 0.03$$

Step 3 – Grain size gradation of the bed material was obtained from sediment sampling at several locations and taking mean values. The average gradation curve is given in Fig. 10.51. Bank material was found to be essentially similar to the bed material and prone to erosion.

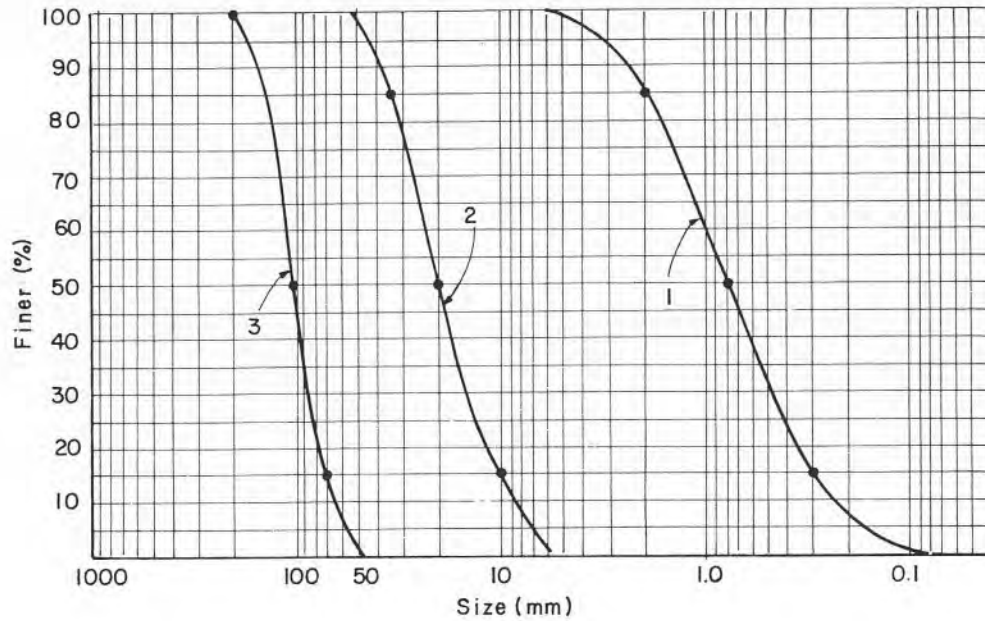


Fig. 10.51. Gradation curves for bed material (1), riprap stone (3) and riprap filter (2), (Ex. 10.7).

Step 4 – Hydraulic computations relative to Q_{50} and Q_{100} are summarized in Table 10.7.

Step 5 – In order to evaluate the bed forms to be expected under the given flow conditions, use of Fig. 7.12 is made. Stream power, $\tau \cdot v$:

$$Q_{50} - \tau \cdot v = 27.5 \times 2.05 = \sim 56 \text{ N/m.sec}$$

$$Q_{100} - \tau \cdot v = 28.6 \times 2.17 = \sim 62 \text{ N/m.sec}$$

Median fall diameter from Fig. 10.51. $1 - d_{s_{50}} = 0.8 \text{ mm}$. Hence, from Fig. 7.12 it can be deduced that the expected bed forms are antidunes or alternatively flat bed.

Step 6 – The approximate height of antidunes can be estimated using the expression given in par. 7.2.3:

TABLE 10.7. HYDRAULIC COMPUTATIONS, EXAMPLE 10.6

1	2	3	4	5	6	7	8	9
50	650	2.95	317	2.75	115	2.05	0.38	27.5
100	740	3.20	334	2.86	116	2.17	0.40	28.6

- 1 – return period (years)
 2 – discharge, Q (m^3/sec)
 3 – normal depth, d_n (m)
 4 – wetted area, A (m^2)
 5 – hydraulic radius, R (m)
 6 – width of channel, B (m)
 7 – mean velocity, V (m/sec)
 8 – Froude number, F_R
 9 – average bed shear stress, $\tau = \gamma R I$ (N/m^2)

$$h = \sim 0.14 \frac{2\pi V^2}{g},$$

hence, for Q_{50}

$$h = 0.14 \frac{2\pi \cdot 2.05^2}{9.8} = \sim 0.37 \text{ m}$$

Step 7 – At this stage, it was decided to proceed with the design for $Q_{50} = 650 \text{ m}^3/\text{sec}$. Three alternative designs have been taken into consideration.

- 1) Leave the bend essentially in its present shape, but provide riprap protection of the concave bank ($r_c = 150 \text{ m}$),
- 2) Regulate the bend to a flatter curvature ($r_c = 250 \text{ m}$), and provide gabion-mattress protection of the concave bank,
- 3) Use groyne along the regulation reach with the aim of guiding the flow away from the concave bank and obtaining with time a new and more stable channel.

In the following, the three design alternatives will be briefly discussed and sketched.

Step 8 – In order to determine the height of the required bank protection, superelevation due to the flow in a curve (see par. 3.8) has first to be evaluated. Using Eq. 3.10a,

For $r_c = 150$ m:

$$\Delta z = \frac{V^2 B}{gr_c} = \frac{2.05^2 \times 115}{9.8 \times 150} = 0.33 \text{ m}$$

For $r_c = 250$ m:

$$\Delta z = \frac{2.05^2 \times 115}{9.8 \times 250} = 0.20 \text{ m}$$

Step 9 – Alternative 1 – The extension of the riprap protection roughly covers the regulation limits as set at the beginning (see Fig. 10.48). Hence the overall length can be taken from the sketch given in Fig. 10.52 – $L = \sim 600$ m.

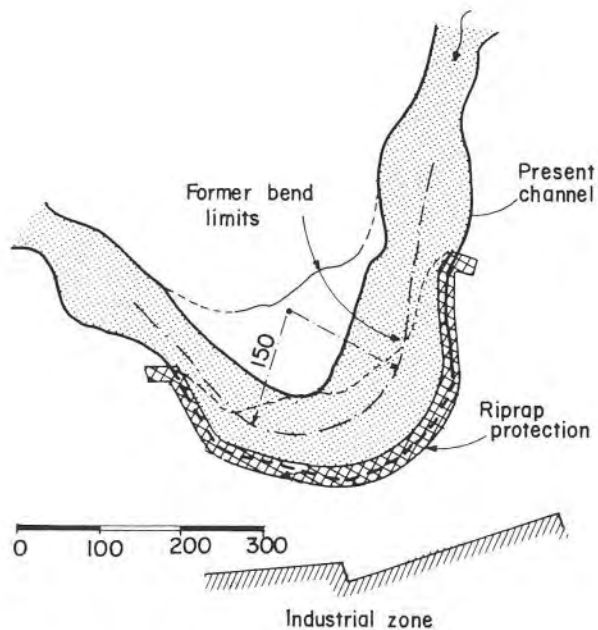


Fig. 10.52. Sketch of alternative 1 (Ex. 10.7).

It was decided that it is best suited to use a well-graded riprap revetment. In order to determine the required maximum stone size, the graph developed by USBR [28], and reproduced in Fig. 10.53, has been applied. For the velocity of 2.05 m/sec, the maximum stone size from the graph is $D_{100} = \sim 0.19$ m.

Accordingly, D_{50} can also be determined conforming to the usual practice,

$$D_{50} = \sim 0.5 D_{100} \cong 0.10 \text{ m}$$

The thickness of the revetment is generally taken as $1.5 D_{100}$, which in the present case gives ~ 0.3 m.

In order to check the values obtained for the riprap size following the recommendations of the USBR, the method proposed by Mayer-Peter [29] has been used. Accordingly, at the condition of incipient motion of riprap particles, Shields factor (see par. 9.2) should be set 0.047 instead of the original value of 0.06:

$$\frac{\tau_c}{(S_s - 1) \gamma D_{50}} = 0.047,$$

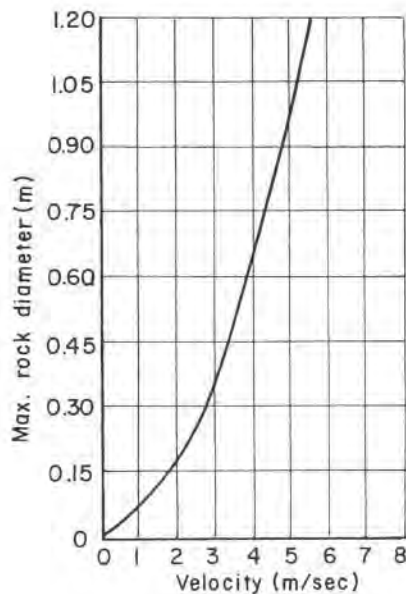


Fig. 10.53. Maximum stone size for riprap revetment, according to USBR [28].

and τ_c should be replaced by the mean shear stress acting on the bank soil, which is generally assumed to be about $0.75 \tau_0$, where τ_0 denotes the maximum average shear stress on the bottom of the channel. Hence, from Table 10.7, $\tau_0 = 27.5 \text{ N/m}^2$, from which $0.75 \tau_0 = \sim 21 \text{ N/m}^2$. If the specific gravity S_s is taken as 2.65, finally D_{50} can be obtained:

$$D_{50} = \frac{0.75 \tau_0}{0.047 (S_s - 1) \gamma} = \frac{21}{0.047 \times 1.65 \times 10^4} = 0.027 \text{ m}$$

The value of the parameter $(u_* D_{50})/\nu$ should be not less than 200 for the flow to be fully turbulent:

$$\frac{u_* D_{50}}{\nu} = \frac{(gRI)^{1/2} \cdot D_{50}}{\nu} = \frac{(9.8 \times 2.75 \times 0.001)^{1/2} \cdot 0.027}{10^{-6}} = 4430 > 200$$

Hence, the flow is fully turbulent, and the method may be applied.

The above value for D_{50} , however, has been deemed as too low, since it would give a maximum stone size of about $1.5 D_{50} = \sim 0.04 \text{ m}$, and this was considered inadequate for the present purpose. Accordingly, the maximum stone size as obtained by the USBR method was retained. The gradation curve for the riprap revetment is given in Fig. 10.51/3. Hence, from the curve:

$$\begin{aligned} D_{50} &= 100 \text{ mm} \\ D_{15} &= 70 \text{ mm} \\ D_{85} &= 150 \text{ mm} \end{aligned}$$

Step 10 – Alternative 1 (continuation)

Slope of the riprap revetment. It is generally accepted that the slope of riprap revetments should be made about 5° less than the *angle of internal friction* determined from ultimate strength measurement (angle of repose). As previously mentioned, the bank material is essentially similar to the bed alluvium, and can be described as a well-graded sand with some clay pockets. According to Hough [30], angle of internal friction for such soils is in the range of 30° – 34° . If the lowest value of 30° is taken, then the revetment slope of 1:2 would not be sufficient ($\sim 27^\circ$); hence, the slope of 1:2.5 ($\sim 22^\circ$) has finally been adopted.

Step 11 – Alternative 1 (continuation)

Filter design. Because of large differences between the gradation curves for the bank material and graded riprap revetment (curves 1 and 3 respectively in Fig. 10.51), there should be a properly designed filter layer between them, in order to prevent the washing-out of fine particles from the base material. For the design of the filter, the method as proposed by the USBR [31] has been followed (see Vol. 1 of the Manual, par. 4.2.2).

a) *Stability criterion*

$$\frac{D_{15} \text{ filter}}{d_{s85} \text{ base mat.}} \leq 5$$

b) *Shape criterion*

$$\frac{D_{50} \text{ filter}}{d_{s50} \text{ base mat.}} \leq 25$$

c) *Permeability criterion*

$$\frac{D_{15} \text{ filter}}{d_{s15} \text{ base mat.}} = 5 - 40$$

Data for the base material (from Fig. 10.51/1):

$$\begin{aligned} d_{s50} &= 0.8 \text{ mm} \\ d_{s15} &= 0.3 \text{ mm} \\ d_{s85} &= 2.0 \text{ mm} \end{aligned}$$

Hence, for the filter:

$$\text{from a) } - D'_{15} = 5 \times d_{s85} = 5 \times 2.0 = 10 \text{ mm}$$

$$\text{from b) } - D'_{50} = 25 \times 0.8 = 20 \text{ mm}$$

$$\text{check of c) } - \frac{D'_{15}}{d_{s15}} = \frac{10}{0.3} = 33 < 40 \quad - \text{O.K.}$$

Check the relationship between the filter and riprap stone revetment. For the riprap graded stone (Fig. 10.51/3):

$$D_{50} = 100 \text{ mm}$$

$$D_{15} = 70 \text{ mm}$$

$$D_{85} = 150 \text{ mm}$$

$$\text{a) } \frac{D_{15}}{D'_{85}} = \frac{70}{35} = 2 < 5 \quad - \text{O.K.}$$

$$\text{b) } \frac{D_{50}}{D'_{50}} = \frac{100}{20} = 5 < 25 \quad - \text{O.K.}$$

$$\text{c) } \frac{D_{15}}{D'_{15}} = \frac{70}{10} = 7 \quad - \text{O.K.}$$

Hence, for the filter layer, curve 2 in Fig. 10.51:

$$D'_{15} = 10 \text{ mm}$$

$$D'_{50} = 20 \text{ mm}$$

$$D'_{85} = 35 \text{ mm}$$

Thickness of the filter – 0.15 m.

Step 12 – Alternative 1 (continuation)

Height of the riprap revetment. The height above the channel bed is obtained by adding:

$$H = \text{flow depth} + \text{superelevation} + \text{bed-form height} + \text{freeboard}$$

$$H = 2.95 + 0.33 + 0.37 + 0.30 = 3.95 \sim 4.0 \text{ m}$$

In order to provide sufficient protection against local scour, the revetment apron should be extended by 1.0–1.5 m below the channel bed. A sketch of the proposed alternative 1 is shown in Fig. 10.54.

At both ends of the protected reach, the riprap revetment should be terminated anchored well into the bank, joint-section between the longitudinal revetment and the bank having the same slope of 1:2.5. Since at these end points flow turbulence is often higher than usual, and hence local scour is likely to be stronger, it is a good practice to extend the protective apron

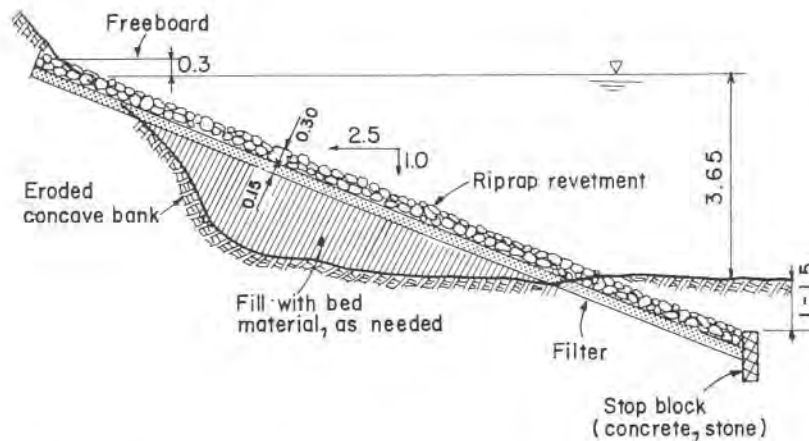


Fig. 10.54. Alternative 1 – sketch of the proposed riprap revetment.

along the end sections even deeper below the channel bed than at regular sections.

Step 13 – Alternative 2. As mentioned in Step 7, in this alternative the regulation curvature should be flatter, $r_c = 250$ m, and the protective revetment made of gabion stone mattresses (see par. 10.3.8.3). A sketch of the proposed regulation is given in Fig. 10.55.

Since the mean flow velocity in the stream channel for the design discharge is about 2 m/sec (see Table 10.7), and the base soil is sand with silt and clay pockets, gabion mattress thickness has been specified as 230 mm (see Table 10.6). Mattress compartments are to be of standard size 0.6×2.0 m, the shorter partition wall running down the slope of the embankment, and the longer one along it. The nominal mesh size of double-twisted galvanized steel wire is 60×80 mm. The stone fill is graded stone, with maximum size of about 150 mm graded down to about 75 mm. The regulated stream channel bank along the gabion protection revetment consists for the most part of alluvial fill (see Fig. 10.55), with a side slope of 1:2.5.

The filter layer between the gabion-mattress revetment and the subsoil could be either of graded gravel or of flexible plastic cloth (see par. 10.3.8.3). In the former case, the filter designed for Alternative 1 could also be used here, with minor changes if considered necessary. If plastic-cloth filter is to be used, a survey should be made of available materials

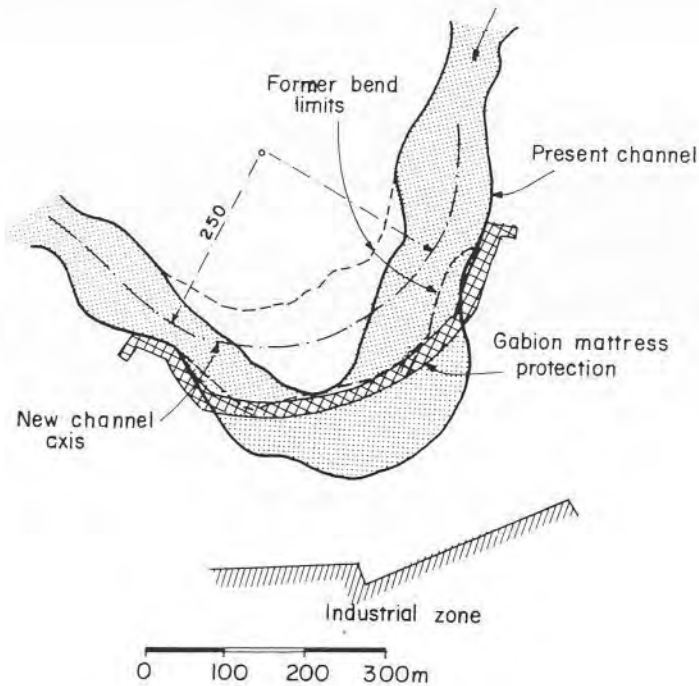


Fig. 10.55. Sketch of alternative 2, (Ex. 10.7).

on the local market, with a thorough study of their mechanical and chemical properties. As already mentioned in par. 10.3.8.3, there are for the time being no firm guidelines as to the choice of plastic filters, and hence previous experience and engineering intuition will have also to be relied upon.

The height of gabion-mattresses revetment above the stream-channel bed should be about 20 cm less than established for the riprap revetment of Alternative 1 – $H \cong 3.80$ m, inclusive of the freeboard (see Steps 8 and 12). The sketch of a typical regulated section with plastic-cloth filter is shown in Fig. 10.56.

As to the actual size of mattress units to be ordered, this is best established in consultation with the manufacturer and taking due account of local conditions.

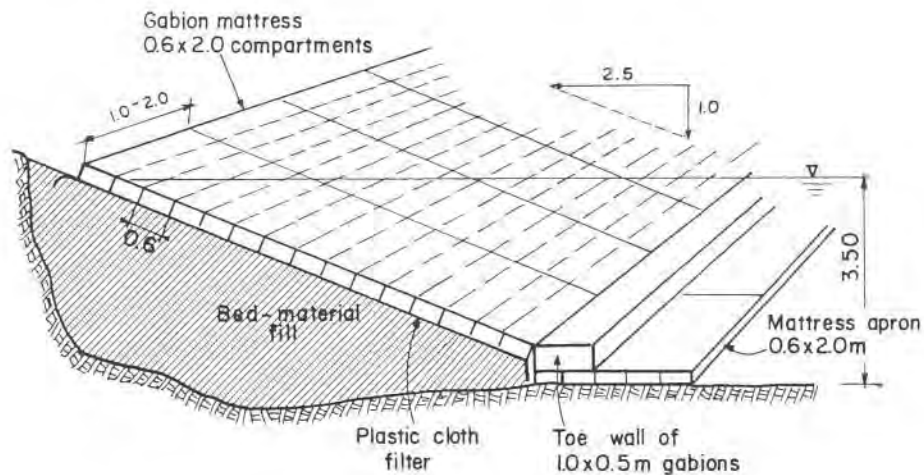


Fig. 10.56. Alternative 2 – sketch of the proposed gabion-mattress revetment.

Step 14 – Alternative 3. In this design alternative the solution is based on the principle of building a new stream channel along the meander bend by means of a series of groynes (see par. 10.3.9.8) and longitudinal dikes. The new channel should with time return the flow roughly to its former bed (see Fig. 10.57a). The stream is known to carry large quantities of sediment, particularly during winter flood-waves, hence a regulation by means of groynes, and sediment deposition between them, should have a good chance to be efficient.

After considering the actual shape of the stream bend to be regulated and the ultimate alignment to be eventually given to the new channel, it has been decided to use a system of round-head groynes with longitudinal dikes at both ends of the reach (see par. 10.3.9.8), Fig. 10.57a, with the radius of curvature as in Alternative 2 – $r = 250$ m. In view of the fact that the question of the angle between the groynes and bank is still controversial, and taking into account the relatively short radius of curvature, all the groynes have been designed perpendicular to the stream bank, which actually gives them a slight inclination downstream.

Length of groynes (the distance from the attachment to the bank to the end of the round head) in the present case is mainly determined by the shape

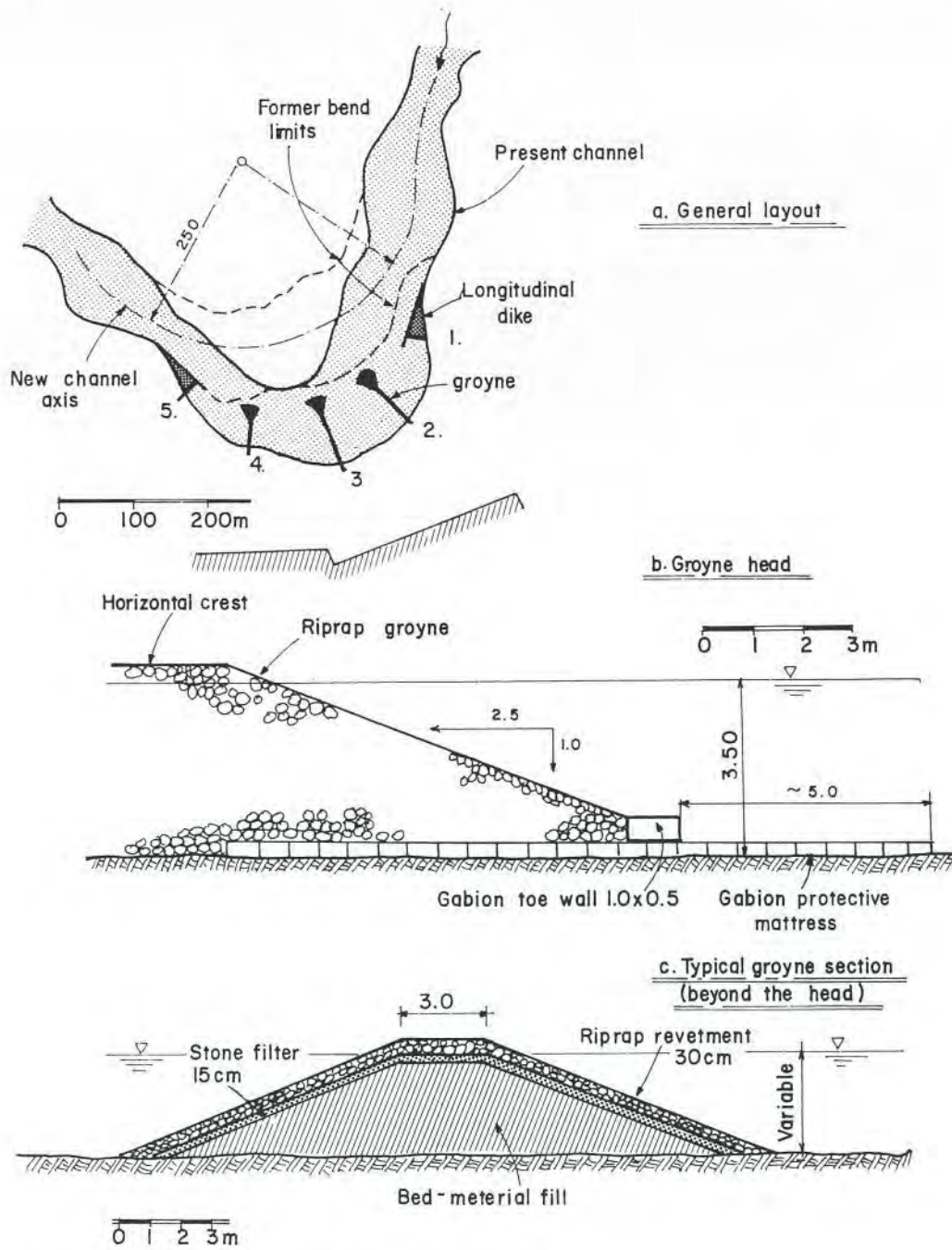


Fig. 10.57. Sketch of the groyne design – alternative 3.

of the new alignment of the stream channel which should be closely followed. Accordingly, the length of groynes 2 and 3 is 100 m, and of groyne 4 – 75 m.

Spacing of groynes is known to vary within a wide range, generally between one to five times the length of the groynes, according to local conditions and the intended results. In the present case of a sharp bend and a relatively short regulation reach, it has been decided to keep the distance between groynes at the lower end, although this entails higher cost. Hence the distance has been set at 100 m, with possible local variations of $\pm 10\%$ to better adjust to the existing conditions on the site.

The height of the groynes above the stream bed should be above the high water for the design discharge of $650 \text{ m}^3/\text{sec}$, inclusive of the super-elevation and dune height. This height has already been estimated to be 3.50 m – see Alternative 2. To this height another 30 cm are to be added for the freeboard. The possibility of a stepped-down solution (see par. 10.3.9.8) in the downstream direction, aiming at an improved performance, had been considered, but finally abandoned because judged as of questionable efficiency for the given case. For the same reason the alternative solution of bankward sloping groyne crests was discarded in favor of horizontal crests.

The core of the groynes is to be built of the alluvial bed material, on top of which riprap revetment of the same type as designed for Alternative 1 is to be placed. Between the riprap and the core material, a filter should be laid, similar to the one previously specified. Underneath the round heads of the groynes, gabion-mattresses should be placed (see Fig. 10.57b) for the protection against local scour, as well as a gabion toe wall. Since the local scouring is likely to be rather extensive in the vicinity of the groyne head, the mattress apron is designed to stretch as far as 5.0 m beyond the head and bankward under all of the round head. On the side slopes of the groynes beyond the head, the riprap revetment may be made of smaller stones, since flow velocities within the enclosed bays between the groynes are much lower.

Considerations regarding construction facilities were the main factor in specifying the crest width of the groynes – 3.0 m.

Since the core material for the groynes is the alluvial bed sediment of the previously discussed properties, the side slope of the groyne flanks has been specified identical to the slopes established for alternatives 1 and 2 – 1:2.5, Fig. 10.57c.

As far as local scour is concerned, particularly around groyne heads, there is to date no reliable way to estimate it with any measure of certainty. Applying Eq. (10.34) – Eq. (10.37) to the present case, the following approximate results are obtained:

1. Eq. (10.34)

$$\left[\frac{D}{d}\right]_{\max} = 8.4 \left[\frac{d_{s50}}{d}\right]^{0.25} \left[\frac{B}{b}\right]^{6/7}$$

$$\left[\frac{D}{d}\right]_{\max} = 8.4 \left[\frac{0.0008}{3.0}\right]^{0.25} \left[\frac{230}{150}\right]^{6/7}$$

$$\left[\frac{D}{d}\right]_{\max} \cong 8.4 \times 0.128 \times 1.44 \cong 1.55$$

2. Eq. (10.35)

$$\begin{aligned} \eta_1 &= 1.13 & \alpha &= \frac{150}{230} = 0.65 \\ \eta_2 &= 1.0 \\ \eta_3 &= 0.85 & n &= 0.83 \end{aligned}$$

$$\left[\frac{D}{d}\right]_{\max} = 4.0 \cdot \frac{1}{\alpha} \cdot \eta_1 \cdot \eta_2 \cdot \eta_3 \cdot (F_R)^n$$

$$\left[\frac{D}{d}\right]_{\max} = 4.0 \frac{1}{0.65} \times 1.13 \times 0.85 \times \left[\frac{2.05}{(9.8 \cdot 3.0)^{1/2}}\right]^{0.83}$$

$$\left[\frac{D}{d}\right]_{\max} \cong 2.65$$

3. Eq. (10.37)

Since $L/d = \sim 100/3 = 33$, Eq. (10.37) should be applied:

$$\left[\frac{S}{d}\right]_{\max} = 4 F_R^{1/3}$$

$$\left[\frac{S}{3.0}\right] = \sim 4 \left[\frac{2.05}{(9.8 \times 3.0)^{1/2}}\right]^{1/3} = \sim 2.9$$

Hence, for the sake of comparison, the ratio $D/d \cong 3.9$. This is much higher than the previously computed values of the ratio, and is no doubt exaggerated.

It should once more be emphasized that the scour depth D in Eqs. (10.34) and (10.35) is measured from the water surface. The engineer will have to decide between the two results, and the design being generally based on the worst conditions, the final choice in the present case would be with the higher value. Gabion protection mattress extending under groyne heads and beyond them should take care of the incipient local scour and prevent it from endangering the structure itself. However, periodic examinations of the scour hole, say once a year after each winter season, will have to be regularly made and necessary repairs carried out whenever deemed necessary. Protective mattress can also be further extended at a later stage to provide additional protection to the scoured channel bed.

Longitudinal dikes at the extremities of the regulation reach have essentially the same shape as the groynes, Fig. 10.57c. Since the space between the dikes and the existing channel bank is to be filled up, no particular revetment is needed on the bankward side.

For all discharges higher than the design discharge, the groynes and the dikes will be overtopped by the flowing water.

An additional alternative of extending the longitudinal dikes all along the regulation reach has also been worked out, but it is not shown here, since it offers no new elements. However, in the present case of a relatively short reach, it may be cheaper and more advantageous than the solution with groynes.

10.3.9.9 Local Scour at Bridge Piers

The question of local scour around groyne heads has been discussed in the previous paragraph in connection with Example 10.7, but the similar problem concerning bridge piers is often also of interest to drainage engineers. Whenever questions of pier foundations or protective measures are considered, hydraulic engineers are called upon to furnish at least a rough estimate of the expected maximum scour at the leading upstream edge of piers or downstream of it.

The general physical mechanism of scour formation, at least as far as blunt-nose piers are concerned, has been described by Shen et al. [34], and it is today widely accepted as correct in principle. According to this model, a strong pressure field in front of the pier, together with the existing secondary currents and vorticity, cause a so-called horse-shoe vortex system around the pier nose, with accompanying separation of boundary layer and

strong shear stresses which are responsible for the scour. It is generally thought that such a vortex system cannot be formed in sufficient strength around sharp-nosed piers, yet large scour holes are likely to develop downstream of the leading edge due to wake-vortex systems along the side walls of the piers.

Unfortunately, the theory so far has not yielded a generally accepted relationship for the quantitative determination of the expected scour depth. There is in fact no agreement between different researchers as to the parameters on which an expression for the quantitative evaluation of scour should be based. It is maybe for this reason that the proposed formulae range from extremely simple empirical rules to elaborate equations which try to include all the parameters thought to have bearing upon the formation and extent of the physical process. In the framework of the present text, necessarily only a few of the many formulae proposed can be reviewed, showing nevertheless the wide range of their complexity. At the present state of the art, not one of the proposed expressions can be unequivocally endorsed or rejected. However, in view of the generally accepted physical model of the local scour generation as mentioned previously, it seems plausible that any general expression for the quantitative evaluation of scour depth should include some sort of Froude number to account for the level of turbulence, contraction ratio of the obstructed channel, coefficient of pier geometry, and probably also a term representing the effect of the grain-size distribution on the depth of scour. The grain-size parameter, interestingly, is disputed by many researchers, but the experimental evidence so far is not conclusive. As soon as the equilibrium condition is reached, the argument goes, at which the rate of particle entrainment from the scour hole roughly equals the rate of deposition into the hole, maximum scour is reached. Since the same bed material is involved in both processes, scour depth should be independent of the grain size. This condition does not exist, of course, in the case of clear water flow. It may, therefore, be a safe policy to evaluate the expected scour depth by more than one single formula, and then either to take an average value, or the largest one (if differences are not extreme).

Larras [41] suggested a simple empirical formula for the terminal scour depth:

$$S = 1.42 K b^{3/4} \quad (10.38)$$

in which S denotes the scour depth in meters measured *below the bed level* before the scouring action, b is the width of the pier in meters perpendicular to the flow, and K is a coefficient dependent on the form of the pier. For cylindrically-shaped blunt piers $K = 1$.

Some time later, Breusers [42] proposed an even simpler formula:

$$S = 1.4 b \quad (10.39)$$

with the same meaning of symbols as before and the same units.

Although such simple formulae are very handy for engineering use, the assumption that the actual scouring action depends only on the width and shape of the pier seems rather simplistic.

A more elaborate expression is suggested by Simons and Senturk [38] for circular cylinders which may also be applied to round-nose piers:

$$\frac{S}{d} = 2.0 \left[\frac{b}{d} \right]^{0.65} F_R^{0.43} \quad (10.40)$$

Here S stands for scour depth as before, d is upstream water depth, b width of the pier, and $F_R = V/(gd)^{1/2}$ is the Froude number of the upstream flow. It is claimed that good agreement has been obtained with experimental results of laboratory investigations and also of field observations.

Finally, a general expression for the quantitative evaluation of local scour depth has been suggested following systematic laboratory investigations at the University of Roorkee, India [43]. This formula has in fact already been given in the previous paragraph in connection with the local scour at groyne heads as Eq. (10.35):

$$\frac{D}{d} = 4.0 \frac{1}{\alpha} \eta_1 \cdot \eta_2 \cdot \eta_3 \cdot \eta_4 F_R^n$$

In the present case, D denotes the maximum scour depth below the water surface, d is the upstream water depth, $\alpha = (B - \Sigma b)/B$ is the contraction ratio, with B as unobstructed channel width and b as pier width normal to flow; coefficient η_1 and the exponent n depend on the median grain size, and can be taken from the graph on Fig. 10.46 for sand fractions, η_2 is a coefficient that represents the influence of the length to width ratio of piers on the scour (found to be unity for ratios up to 5). Coefficient η_3 stands for the effect that angle of inclination has on the scour, and it should be taken as unity for piers placed normal to flow, which is the usual case. Coefficient η_4 takes into account the pier-nose geometry, and it varies between 0.8–0.9 for circular or semicircular shapes, and for triangular shapes from as low as 0.52 for the sharp apex angle of 30° to 0.80 for obtuse angle of 120° . Letters F_R stand for the Froude number of the upstream flow.

As mentioned before, there are wide differences of opinion in respect to the influence of some parameters on the scouring action. While some investigators have given support to the view that only the temporal rate of scour is dependent on the grain size, but not its maximum depth, others believe that depth definitely depends on the grain size. The relative importance of the flow depth still remains an unsettled question. There is also some controversy as to the question whether the Froude number or Reynolds number of the flow should be taken as parameters in regard of the scouring action. Even in respect of the contraction ratio there is little agreement; according to some researchers, its effect is negligible as long as the relative contraction caused by the piers is not very pronounced.

There appears to be enough evidence that local scour by clear water is deeper than scour caused by water carrying sediment, which should be expected in light of the notions reviewed in Chapter 3 and elsewhere.

Whatever formula finally is adopted for any given case, it is obvious that the computed scour depth at best can only be a very rough estimate. On important works, model investigations may well be called for.

During flash floods in arid and semi-arid regions (see par. 10.6 further on), scour depth predicted by any of the proposed formulae, generally derived from experiments with steady discharges of long duration, will probably be too large if based on the peak discharge of the flood wave.

Scour hole formed during the passage of peak flows in a flood wave may be partially filled back during low flows in the tail of flood. This frequently occurs during flash floods in ephemeral streams of arid and semi-arid regions, but has been also observed in larger temperate-climate rivers. Foundation depth of bridge piers, however, should always be set so as to amply cover the maximum scour depth as expected.

Local scour does not account for the general erosion or deposition processes going on in any given stream, nor does it reflect in any way morphological bed forms (dunes, bars, etc.) which might be simultaneously developing. Hence, bed changes due to these sources, if any, should be added to the computed local scour depth.

Finally, it should be recalled that all the reviewed formulae, and many others not mentioned, relate only to non-cohesive bed material. There is little information about local scour in cohesive soils.

Example 10.8

Local scour depth at bridge piers is to be evaluated for the following conditions:

Width of piers normal to the direction of flow – 0.7 m

Form of pier nose – circular

Average water depth upstream of piers, $d = 2.5$ m

Mean velocity of flow upstream of piers, $V = 2.0$ m/sec

Contraction ratio, $\alpha = (B - \Sigma b)/B = 0.98$

Mean grain size – $d_{s50} = 0.8$ mm

1. Larras formula

Using Eq. (10.38), and for $K = 1$ (cylindrical nose):

$$S = 1.42 \cdot 0.7^{3/4} = \sim 1.1 \text{ m}$$

2. Breusers formula

Applying Eq. (10.39), the expected scour depth below the bed level is evaluated as:

$$S = 1.4 \cdot 0.7 = \sim 0.98 \text{ m}$$

3. Equation (10.40)

Using the expression suggested by Simons and Senturk, evaluation of scour depth gives the following result – Froude number of the upstream flow:

$$F_R = V/(gd)^{1/2} = 2.0/(9.8 \cdot 2.5)^{1/2} = \sim 0.4$$

$$\frac{S}{2.5} = 2.0 \left[\frac{0.7}{2.5} \right]^{0.65} \cdot 0.4^{0.43} = 0.59$$

Whence the scour depth below the bed level:

$$S = 2.5 \cdot 0.59 = \sim 1.47 \text{ m}$$

4. University of Roorkee formula

If Eq. (10.35) is chosen for the evaluation of scour, the result is obtained as follows:

First, coefficients for the given case have to be evaluated.

Coefficient η_1 for the mean grain size of $d_{s50} = 0.8$ mm from the graph on Fig. 10.46: $\eta_1 = \sim 1.13$.

Coefficient η_2 can be taken as 1.0.

Coefficient η_3 for piers built normal to flow direction is taken as 1.0.

Coefficient η_4 for circular nose is 0.85.

From Fig. 10.46 again, exponent n is found to be about 0.83. Applying now Eq. (10.35),

$$\frac{D}{d} = 4 \frac{1}{0.98} \cdot 1.13 \cdot 1.0 \cdot 1.0 \cdot 0.85 \cdot (0.4)^{0.83} = 1.83$$

$$D = 1.83 \cdot 2.5 = 4.57 \text{ m}$$

This is scour depth below the water level. Hence, scour depth below the bed level:

$$S = 4.57 - 2.5 = \sim 2.07 \text{ m}$$

10.4 Protection by Means of Flood-Control Reservoirs

The purpose of building a dam across the stream and thus forming a reservoir is to provide for temporary storage of flood water during peak flows, and to release the stored volume to the downstream channel at an acceptable rate during the flood wave, and after its subsidence.

The simplest form of a flood-protection reservoir is the *detention basin*, in which the dam is equipped with a generally uncontrolled bottom-outlet conduit, and a spillway. If economically justified, the best solution for such a basin is to set the elevation of the spillway crest so as to ensure sufficient storage capacity for the maximum *design flood*, without the need for overflowing the crest and causing spillway discharge. General relationships for a typical detention basin are shown in Fig. 10.58.

Design flood wave is obtained from the hydrological analysis of the drainage basin and peak discharges, according to the guidelines discussed in par. 10.2. Variation with time of the water level in the reservoir is schematically shown in Fig. 10.58a; it is assumed that the reservoir is practically empty at the beginning of the flood wave as given in diagram 10.58c, and

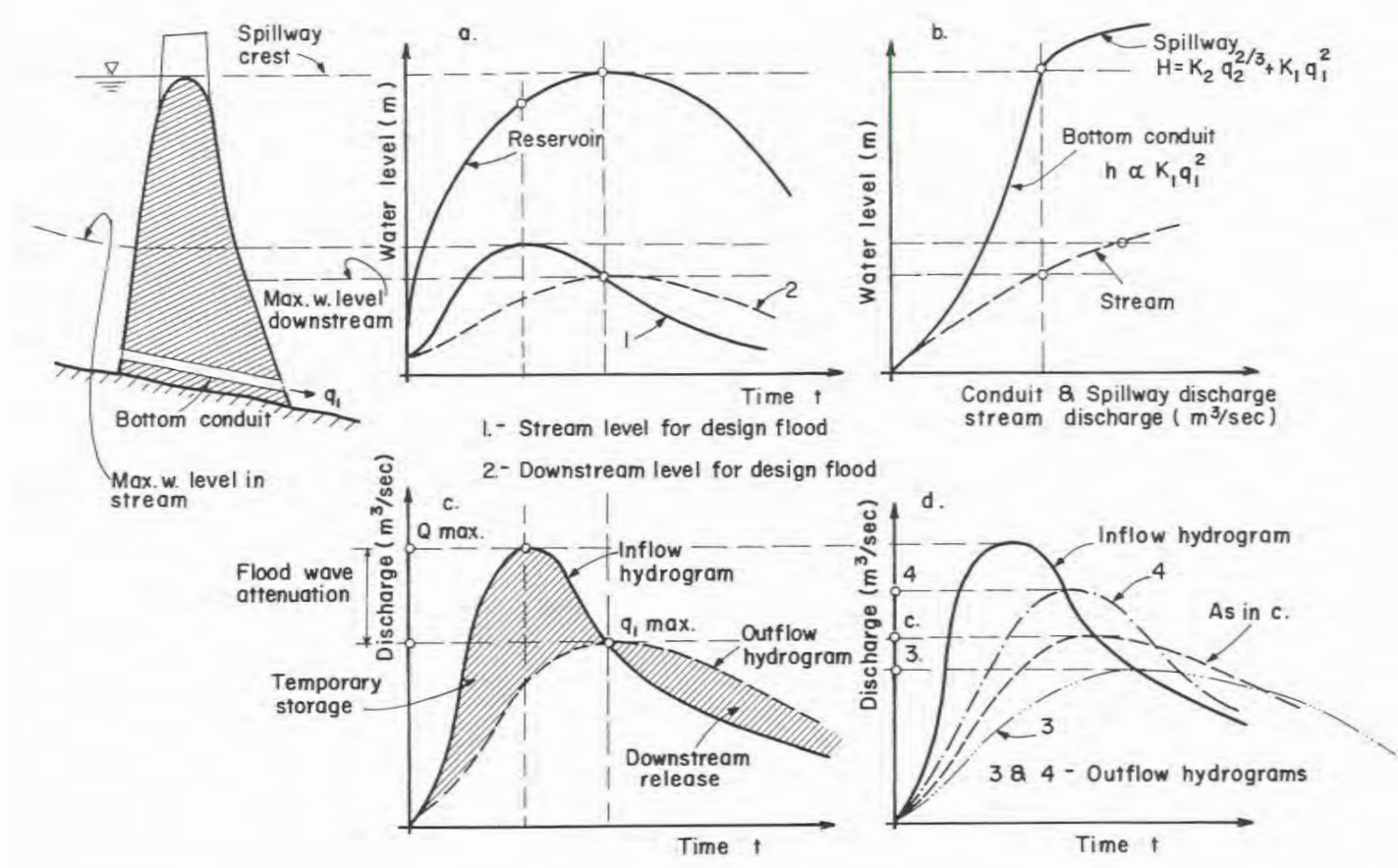


Fig. 10.58. Storage, water level, outflow and flood-routing relationship for a typical detention basin.

that the available storage capacity is just sufficient to temporarily contain the required volume of water up to the crest of the spillway, without any spilling of the impounded water.

As soon as the level of the stored water reaches the outlet conduit at the bottom of the dam, variable discharge q_1 starts leaving the reservoir to the downstream channel. It is evident from the diagram 10.58c that the inflow, given by the design hydrogram, is larger than the outflow, and hence the water level during this stage is continuously rising. Maximum water level in the reservoir will occur sometime during the subsiding branch of the inflow hydrogram, well beyond the peak of the wave, when the inflow discharge Q equals the outflow discharge q_1 , Fig. 10.58a and c.

Outflow discharge q_1 through the bottom conduit is determined by its diameter and the head above its axis, according to the general relation $q_1 \propto K_1 h^{3/2}$, where h denotes the head. This relationship is shown in graph 10.58b. Should there be any flow over the spillway (for instance, when at the beginning of the flood wave the reservoir is already partially filled), the combined outflow discharge will be $(q_1 + q_2)$, in which q_1 is determined as before, and the spillway discharge is given by $q_2 \propto K_2 H^{3/2}$, where H denotes the head over the wear crest.

Due to the temporary storage in the reservoir and the retarded release to the downstream channel, there will be an *attenuation of the peak discharge*, Fig. 10.58c. This reduced maximum discharge should not exceed the carrying capacity of the downstream channel. Given the same inflow hydrogram, peak discharge attenuation largely depends on the storage capacity of the reservoir. Fig. 10.58d schematically shows the influence of the storage capacity on the maximum outflow discharge, in comparison with the case when the capacity of the reservoir is just sufficient to accommodate the design flood without overflowing of the spillway crest, as shown in diagram 10.58c. Outflow hydrogram for the situation where the available storage capacity is *larger* than in the previous case is given by curve 3 on diagram 10.58d. Curve 4, on the other hand, represents the outflow diagram when the available storage capacity is *smaller* than what is required to contain the flood volume up to the crest of the weir, and hence the spillway is also put into action. The attenuation of the peak discharge released to the downstream channel in the case of curve 3 is larger than that shown in diagram 10.58d (point 3 vs. point c), whereas curve 4 yields a smaller reduction (point 4 vs. point c). It should be borne in mind that curves 3 and c represent hydrograms formed by the outflow through the bottom conduit only, while the upper part of curve 4 includes the combined outflow through the conduit and simultaneously over the spillway. The head above the weir crest, though in most cases relatively small as compared to the height of the dam,

furnishes an additional temporary storage, which also serves for the attenuation of the peak discharge, although to a lesser degree.

Due to the reduction of the peak discharge, the water depth in the downstream channel will generally be less than in the stream channel upstream of the reservoir. Variation of the water level with time is given by curves 1 and 2 in diagram 10.58a, whereas the variation in dependence of discharge is shown on the diagram 10.58b.

Diameter of the bottom outlet is generally determined in such a way as to be able to pass the maximum permissible downstream discharge when the water level in the reservoir reaches the crest of the weir. If the water level rises above the spillway crest, the combined discharge of the conduit and spillway released to the downstream channel will be higher than the design maximum. This is likely to cause limited flooding downstream if the excess water is not retained by freeboard or other safety measures connected with the regulated channel downstream (see Example 10.6).

In some cases of flood-control reservoirs, bottom outlet is equipped with a control valve by means of which discharge q_1 can be regulated. If the conduit is large enough, during the initial stages of the flood wave almost all of the flood water is directly discharged through the bottom conduit to the downstream channel, and hence reservoir storage remains very small, leaving a larger volume of the total capacity available for the later stages. In streams that carry large quantities of sediment, and hence induce rapid loss of live storage in the reservoir, the additional advantage of a controlled bottom outlet of adequate size, especially in multiple-purpose flood-control projects, is that it will reduce the amount of sediment deposited within the reservoir itself, thus prolonging its useful lifetime.

As soon as the discharge through the conduit reaches the maximum permissible rate, control valve is put into action and the discharge kept steady. Under these conditions, attenuation of the peak flood discharge can be kept lower without increasing the capacity of the reservoir, Fig. 10.59. The inflow hydrogram is the same as on Fig. 10.58, and the temporary storage is essentially equal to that shown on diagram c of the same figure. Flood-wave attenuation here is comparable to, or even more than, that given by point 3 on Fig. 10.58d, but the reservoir capacity is not larger than the basic one on diagram c. Here again, maximum water level in the reservoir is reached when the flood discharge on the descending branch of the inflow diagram equals the outflow discharge q_1 at point 1 on Fig. 10.59.

The size of the outlet conduit with control valve is generally calculated in such a way as to be able to pass the downstream discharge q_1 with reservoir filled to about 30% of its total capacity. Final diameter depends, of course, on the assumed discharge q_1 , and this is established by a comparative

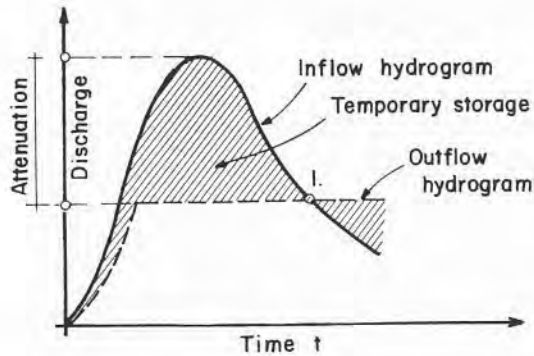


Fig. 10.59. Detention basin with controlled outlet.

economic analysis.

The main disadvantage of a controlled outlet is that it makes necessary a relatively complicated regulation mechanism prone to frequent breakdowns, and hence requiring regular inspection and maintenance service. These are not always available, especially in remote and inaccessible locations.

So far the spillway has been mentioned only as an additional overflow outlet used in conjunction with the bottom conduit to clear the peak of the design flood wave when the capacity of the reservoir, for economic or other reasons, is insufficient to provide for the required temporary storage. The main function of the spillway, however, is to protect the dam itself, and not the downstream flood plain, from exceptional flood events. Failure of the dam because of overtopping is practically always likely to cause a major disaster, while extensive flooding downstream, though economically ruinous and often fraught with human suffering, is of no comparable gravity.

Provided that the elevation of the spillway crest is given (from previous considerations of temporary storage requirements) or assumed for the analysis, there are three additional variables connected with the spillway design which have to be determined: a) Width of the crest, b) Maximum head over the crest, H_{\max} , c) Maximum overflow discharge, q_2 . This is schematically shown in Fig. 10.60 (and also on Fig. 10.58).

The three above values are mutually interconnected, and are computed by means of the *spillway design hydrogram* and the process known as the flood routing through reservoir.

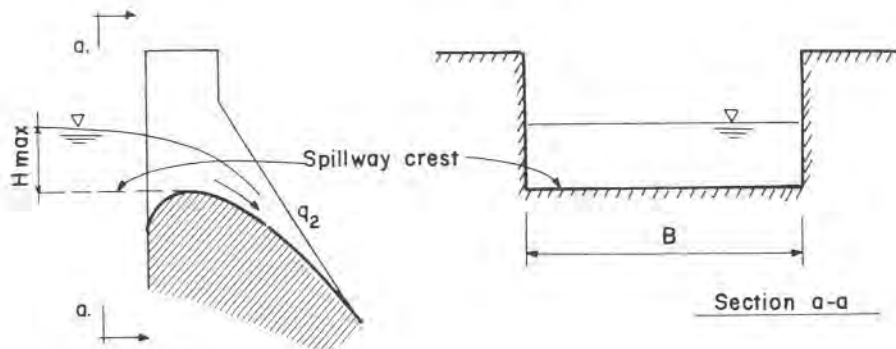


Fig. 10.60. Detention basin-spillway.

Design hydrogram for the spillway is not to be confused with the reservoir design hydrogram, dealt with previously. Return period for the former is generally much larger than for the latter, being in the order of magnitude of between 300–1000 years, and sometimes even much more. Probable peak discharge for such long return periods is obtained by means of various methods of the statistical hydrology and extrapolation, as discussed in par. 10.2 and several other instances.

The obtained flood-wave hydrogram is next routed through the reservoir, assuming the worst possible situation of the water level standing at the crest elevation when the flood wave hits the site. The flood-routing equation has the form,

$$dV/dt = Q - q_2 \quad (10.41)$$

in which V – temporary storage (m^3), $V = f_1(H)$; Q – inflow discharge (m^3/sec), $Q = f_2(t)$; q_2 – outflow discharge (m^3/sec), $q_2 = f_3(H)$.

It says simply that the variation with time of the temporary storage is equal to the difference, in the same period of time, between the inflow and outflow discharges. This differential equation cannot be explicitly integrated, because the functions $Q = f_2(t)$ and $V = f_1(H)$ are not amenable to direct mathematical definition. A numerical solution can easily be arrived at if Eq. (10.41) is written in the form,

$$\bar{Q} \cdot \Delta t = \bar{q}_2 \cdot \Delta t + \Delta V \quad (10.42)$$

where \bar{Q} and \bar{q}_2 denote mean values of the discharges during the period of time Δt , in which the variation of the storage volume was ΔV . Since both q_2 and V are functions of H , assuming a water-level variation during the period Δt , the right-hand side of Eq. (10.42) can be evaluated. If the assumed H was proper, the two sides of the equation must be equal; if not, a new value for H has to be tried, until the equality is obtained. Today, the calculation is generally performed using high-speed computers and iteration methods. Final product of this flood-routing calculation are the variation of the overflow discharge with time, $q_2 = f_1(t)$, and of the weir head (reservoir elevation) with time, $H = f_2(t)$. Similarly to the previously discussed attenuation of the peak discharge released to the downstream channel as related to the reservoir design hydrogram, here also $q_{2\max}$ will be lower than the maximum flood discharge given by the spillway inflow hydrogram, owing to the temporary retention in the reservoir (flood routing). A tabular calculation of the flood routing through a given reservoir ($q_2 = f_1(t)$ and $H = f_2(t)$) is shown in Example 10.9.

It has already been mentioned that the parameters which determine the functioning of the spillway are reciprocally linked, and hence the search for the optimum engineering solution concerning any specific case involves usually several trial calculations with various combinations. A handy method for such analysis, refined and developed in [18], is briefly summarized in the appendix to the present chapter.

Most of flood-control reservoirs today are of the multiple-purpose type, in which stored water is used for irrigation and water supply, or for hydroelectric power generation. In both cases the bottom outlet is of the controlled type, and in some cases of hydroelectric projects, spillway may also be controlled by a radial (Tainter) gate. With such arrangements, the reservoir must be operated according to a pre-established "rule-curve", continually adjusted to the actual hydrological conditions of the drainage basin. An essential prerequisite for such an elaborate and complicated system is a well-organized weather-forecasting and drainage-basin monitoring service in order to provide ample warning time for impending flood-wave movements. Discussion of such systems, however, is not strictly in the province of flood-control detention basins, and more detailed information may be found in textbooks on hydroelectric power stations.

Multiple-purpose reservoirs are generally the result of economic limitations, because it is usually considered too expensive to build a dam for the purpose of flood protection only. On the other hand, however, it is obvious that adding more functions to the reservoir entails accommodating conflicting interests, which cannot be done without striking some compromise between them. Optimum flood protection demands an empty reservoir at

the start of a flood wave, while power generation and irrigation require a full reservoir. Any compromise on these conflicting aspects inevitably leads to much less than maximum benefit for any one use, and inadequacy of flood forecasting may greatly impair the efficiency of flood protection.

In many cases the question may arise whether it is better to protect a given area, lying in the plain beyond the main watershed, by a single higher dam and large reservoir situated on the principal stream, or by a series of smaller dams built on the tributaries. In order to illustrate the situation in general lines, let a watershed area be given as the one shown in Fig. 10.61. A large agricultural town and the flood plain around it, denoted as point A, have to be protected from recurrent floods. One alternative is to build a large dam at location B on the main stream upstream of the point A, and the other to dam instead the tributaries at points C, D, E and F.

Assuming for the sake of simplicity that the watershed is small enough to be covered by a continuous storm, all the tributaries will be contributing to the surface runoff, and their supposed hydrograms are shown according to the approximate sequence of their arrival at point A. The combined hydrogram of the main stream at point A is traced and denoted as "without dams". Now, if dams are built on the tributaries, there will be some attenuation of peaks at every site, as shown by the dashed line on hydrograms C–F. The resulting combined hydrogram for the main stream at point A will be similar to the dashed curve denoted "with dams". It is evident that there will be some attenuation of the peak discharge, say from Q_0 to Q_1 . But on the other hand, with a single dam at point B and a controlled bottom outlet, peak discharge could be even more reduced, say to Q_2 , as schematically shown on the diagram. Hence, the simple conclusion that a single large dam at point B would be more efficient than a series of smaller dams on the tributaries at points C, D, E and F.

That indeed may be the case in some instances, but certainly not as a general rule. The very simplified conditions on which the analysis was based generally exist on small watersheds only; in all other cases hydrological conditions are more complicated, and should be thoroughly analyzed before reaching any conclusions. Furthermore, local interests in the valleys upstream of point B probably would prefer the alternative with dams in the tributaries than the other with a single dam at the downstream end of the watershed, leaving them without any protection, and possibly causing future siltation problems. Economic aspects have so far been left out of the picture, but they certainly would have great influence on the final decision, and again there is no way of telling offhand which one of the two alternatives would be more favorable for any specific case, without a comprehensive investigation.

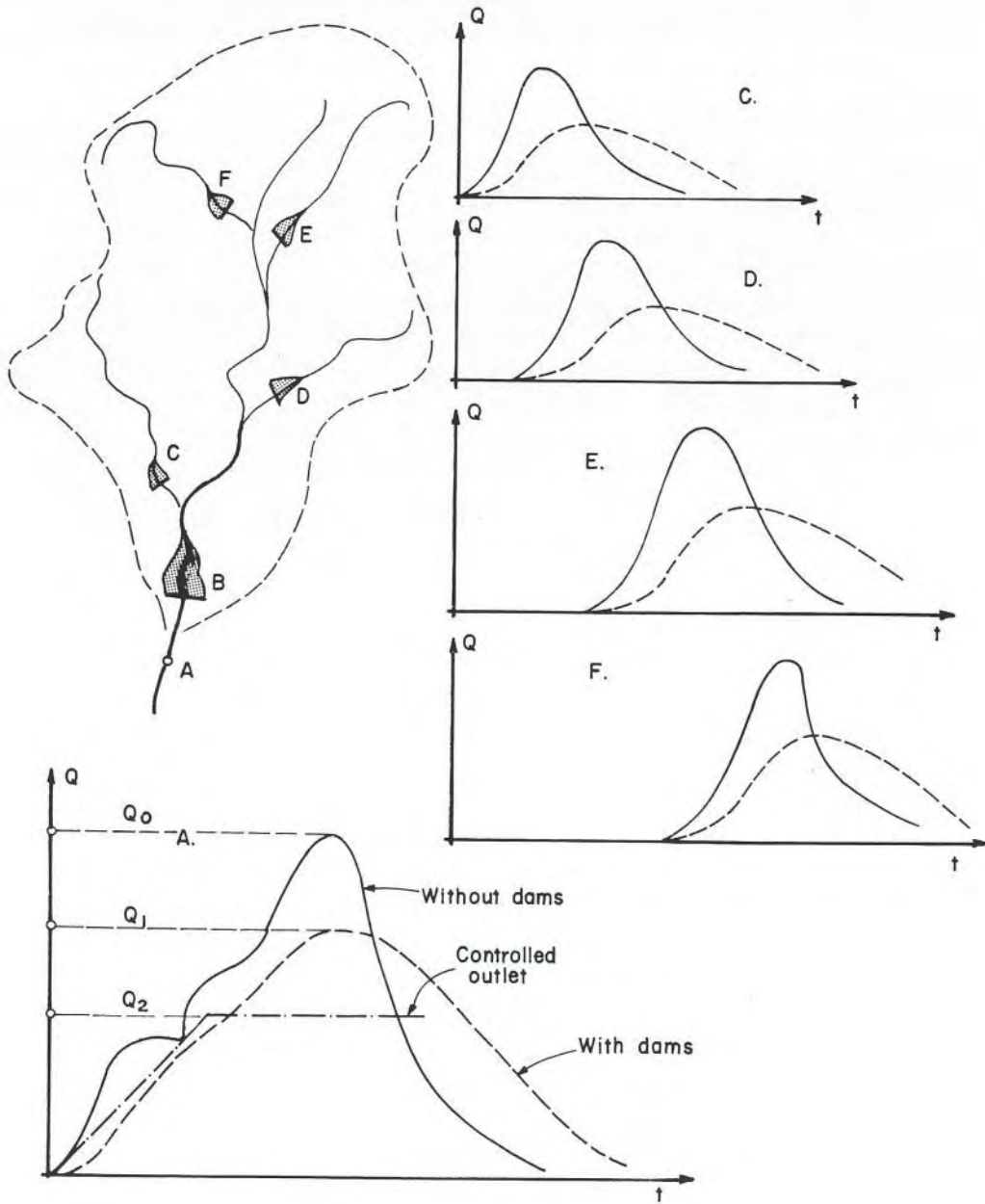


Fig. 10.61. Alternatives for flood protection.

Before closing the present discussion on temporary impounding of flood water for protection purposes, a few remarks should be made about the situation likely to develop in the channel downstream of the dam site, particularly on multiple-purpose projects where the water detention is generally much longer and hence the sediment-settling process more advanced. Since the input sediment load below the dam will be low or practically non-existent, sediment transport capacity of the water will be high and degradation is bound to start. This in turn will reduce the longitudinal slope of the channel and thus also the bed shear stress. As a consequence of this process, the potential of the stream to transport sediment will gradually diminish, until practically all flows will be below the critical discharge at which significant bed-material movement is initiated. The sediment removed during this process is deposited farther downstream, but the progressive reduction of sediment load will eventually again trigger the erosive activity of the stream, and thus the cycle is repeated. If there are unregulated tributaries downstream of the dam site, sediment load brought in will probably form localized deposits, which are best removed from time to time by dredging.

Construction of a flood-protection dam in the main watercourse, and the subsequent great reduction of the sediment content in the water downstream of the dam, may cause severe changes in any diversion channel for irrigation purposes below the dam site. Degradation and bank erosion are likely to occur in the channel, which in due time may expose more permeable materials in the bed and banks. This in turn may increase seepage losses from the channel. Although the consequent reduction of discharge may be tolerable, the possibility of a rise in the water table is very likely to be objectionable. In addition, clear water in the distribution network may also require radical changes of its alignment, either because of the proliferation of aquatic plants, or by reason of the increased seepage.

In the immediate vicinity downstream of the bottom outlet or emergency spillway, extensive *local scour* is most likely to occur, unless rock bed is available. This local scour, due mainly to the development of local currents and turbulence (see discussion of the subject in par. 10.3.9.8), is to be added to the erosion caused by the general degradation process in the downstream channel. Hence, it is advisable always to provide adequate riprap or gabion-mattress protection in the immediate continuation of these structures. For the estimation of local scour, any of the great number of semi-empirical formulae developed for the quantitative evaluation of the scour at bridge piers or embankments (see pars. 10.3.9.8 and 10.3.9.9) will do.

Quantitative evaluation of general degradation or aggradation processes is much more complicated, and can in fact be carried out only with the aid of computers. In a straight alluvial stream, there are three degrees of freedom for

the adjustment of channel geometry in search of the dynamic equilibrium (see Chap. 3) – width, depth and bed slope. If the stream is meandering, three additional degrees of freedom come into play – meander length (wave length), meander height (wave amplitude), and radius of curvature. Bed armouring as consequence of the washing-through process of the fine fractions in the bed-material sediment should also be taken into account, as this may significantly reduce the degradation process. In order to save in computer time, which may become prohibitively long, it is essential to use a relatively simple method for the computation of bed-material transport, and to assume that during any one time period, water discharge remains constant, except of course where any lateral inflow or outflow is found. Finally, it should be emphasized that any such mathematical sedimentation model should best be calibrated by prototype observations, or verified by a suitable physical model. For a detailed discussion of all the pertinent topics and techniques, any competent text on physical and mathematical modelling in hydraulic engineering should be consulted, such as [39] or [40], among many others.

Summary

From the short discussion in the present paragraph, it follows quite clearly that no simple prescription could be given concerning the best flood-protection scheme for a given exposed area. Simplified analyses may often lead up to erroneous conclusions, and it is essential for any specific case to draw up a balance sheet of all the engineering, economic, social and often political pros and cons before taking any final decision. This is particularly true for multiple-purpose flood-control projects of any kind. As a matter of fact, all such projects should be regarded as *stream systems*, which include the whole complex of reservoir deposition, aggradation in the upstream reaches of the system due to backwater, as well as scouring and degradation downstream of the reservoir, to mention only the most important aspects. Economic analysis, on the other hand, will comprise reservoir useful life-time and economics of water supply for irrigation, municipal uses, or any other purpose. Finally, ecological impact of the proposed project on the environment will have to be thoroughly assessed and any negative aspects eliminated or at least attenuated.

From a general point of view, it should be stressed that the previous relative attractiveness of flood protection by reservoirs, even in cases of

multiple-purpose types, has greatly faded in recent years because of ever increasing cost of such works. The inherent engineering drawbacks of any similar scheme add to the negative balance sheet. Silting-up of reservoirs, although taken into account when determining the net storage capacity, has often proved to be much higher than what had been anticipated; their protective effectiveness diminishes downstream, whence the need to locate them close to the protected area; greatly reduced suspended load in the downstream channel may cause severe erosion; often valuable land or other property are flooded by the reservoir, while the ratio of such lost area to protected area is seldom very high; and finally, in developed countries it is becoming increasingly hard to find suitable sites for such projects.

Example 10.9

A detention basin of $20 \cdot 10^6 \text{ m}^3$ design capacity (up to the crest of spillway, V_s) is planned for protection of the downstream plain from flooding. The regulated channel downstream will be designed to safely carry the discharge of $115 \text{ m}^3/\text{sec}$ released by the bottom outlet (q_1). Spillway crest elevation is set at +330.0 and, for geological reasons, maximum head on the spillway weir should not be more than about $H \cong 2.0 \text{ m}$.

1. Design of the bottom outlet

Sketch of the outlet layout is given in Fig. 10.62. Since the outlet is set about 4 m above the stream bed, it was found that the tailwater due to the conduit discharge would not submerge the outlet at the downstream end at any elevation of the water in the reservoir. This is expected also to be the situation even with the overflow through the spillway added to the bottom-outlet discharge, because of the geodetic drop between the channel elevation at the toe of the dam and the point farther downstream, where the spillway chute rejoins the stream channel.

Assumed length of the conduit: $L \cong 200 \text{ m}$

Net head: $h_{\max} = 330.0 - 304.0 = 26.0 \text{ m}$

Inlet head – loss coefficient: $K_i = 0.2$

Outlet head – loss coefficient: $K_o = 0.1$

Manning roughness coefficient for the concrete pipe: $n = 0.015$.

Assumed: 2 pipes $\phi 2.4 \text{ m}$ each

Hydraulic radius: $R = (D/4) = (2.4/4) = 0.6 \text{ m}$

Area of one pipe: $A = 4.52 \text{ m}^2$

Energy equation between points 1 and 2:

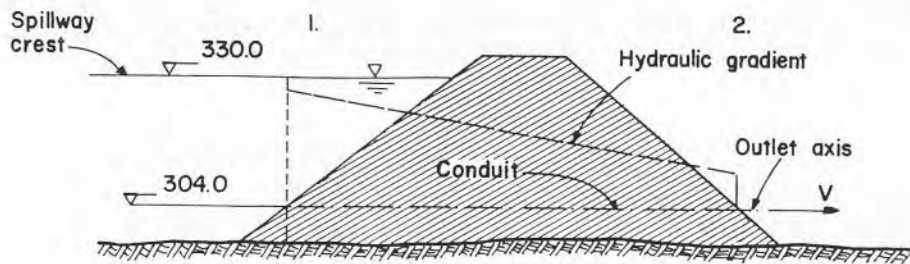


Fig. 10.62. Sketch of outlet layout.

$$h = \frac{V^2}{2g} \left[K_i + K_0 + 1 + \frac{2g \cdot n^2 L}{R^{4/3}} \right]$$

Introducing the given values:

$$26 = \frac{V^2}{2g} \left[0.2 + 0.1 + 1.0 + \frac{2g \cdot 0.015^2 \cdot 200}{0.6^{4/3}} \right]$$

$$26 = \frac{V^2}{2g} (1.3 + 1.74) = 3.04 \frac{V^2}{2g}$$

Whence,

$$V = (2g \cdot 26/3.04)^{1/2} = 12.9 \text{ m/sec}$$

Discharge through one conduit,

$$q_1 = V \cdot A = 12.9 \times 4.52 = 58.3 \text{ m}^3/\text{sec}$$

Total discharge from two conduits,

$$\Sigma q_1 = 2 \cdot 58.3 = 116.6 \sim 115 \text{ m}^3/\text{sec}$$

Assumption accepted: 2 pipes ϕ 2.4 m each

2. Design of the Spillway

Because of the constraint that the required head on the spillway weir should not exceed 2.0 m, it was decided to first determine $q_{2\text{max}}$ and B

using the method outlined in the appendix. As for all spillway design, it is assumed that the reservoir is full up to the spillway crest when the flood wave reaches the dam site. This is, of course, the worst possible situation.

Data given:

1. Spillway design hydrogram, Fig. 10.63.

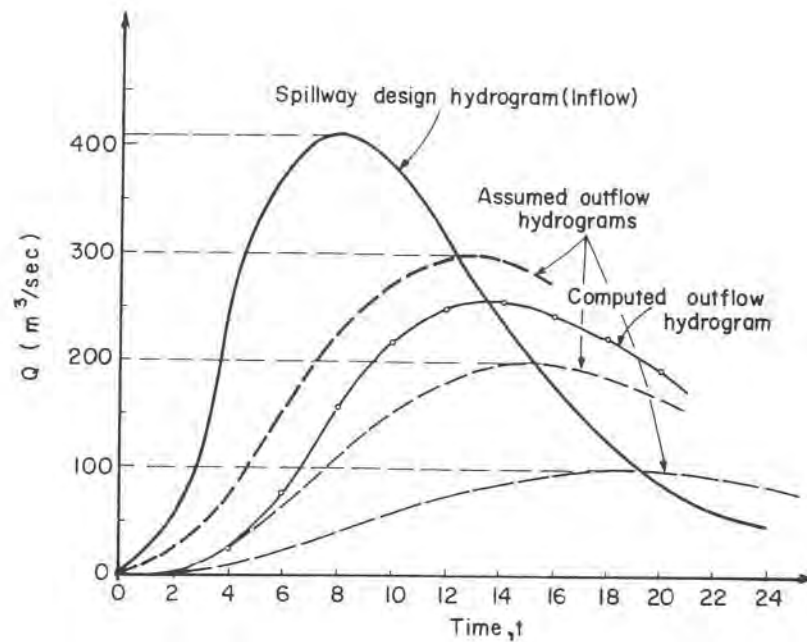


Fig. 10.63. Spillway design hydrogram.

2. Reservoir volume-elevation curve (RVE-curve) along the spillway crest. This curve is, naturally, drawn for the whole of the reservoir, but here it is only partially reproduced for reasons of limited space, Fig. 10.64.

Step 1 – Three different outflow hydrograms have been freely hand-drawn on the graph of the given spillway design flood hydrogram, Fig. 10.63, each one with different $q_{2\max}$.

Step 2 – Temporary storage V_t for each outflow hydrogram is measured next, and then $V_0 = V_s + V_t$. Results are summarized in Table 10.8.

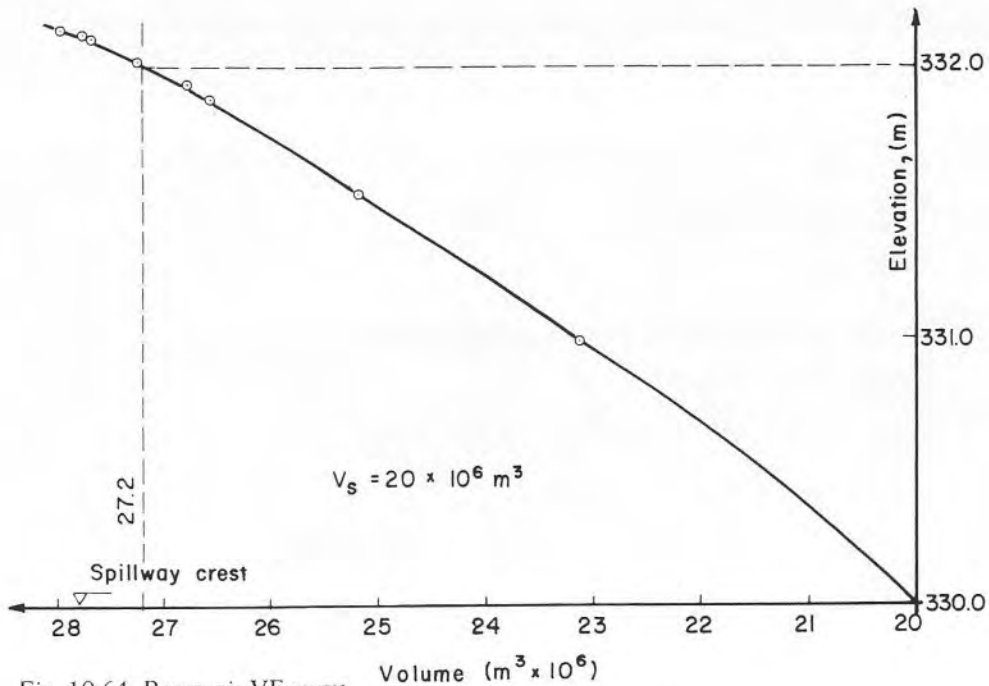


Fig. 10.64. Reservoir VE-curve.

Step 3 – Graph $V_0 = f(q_2)$ can now be drawn, Fig. 10.65.

Step 4 – For the given elevation of the spillway crest (330.0 m) and $H_{max} = 2.0$ m, reservoir elevation is 332.0 m. From RVE-curve, Fig. 10.64, the corresponding volume of water is found to be $V_0 = 27.2 \times 10^6 m^3$. Going back to $V_0 = f(q_{2max})$ -curve, Fig. 10.65, it can be seen that to this volume the matching $q_{2max} = 240 m^3/sec$.

TABLE 10.8. COMPUTATIONAL RESULTS (Ex. 10.9)

q_{2max} (m^3/sec)	V_t ($m^3 \cdot 10^6$)	V_s ($m^3 \cdot 10^6$)	V_0 ($m^3 \cdot 10^6$)
300	5.12	20.0	25.12
200	8.65	20.0	28.65
100	12.33	20.0	32.33

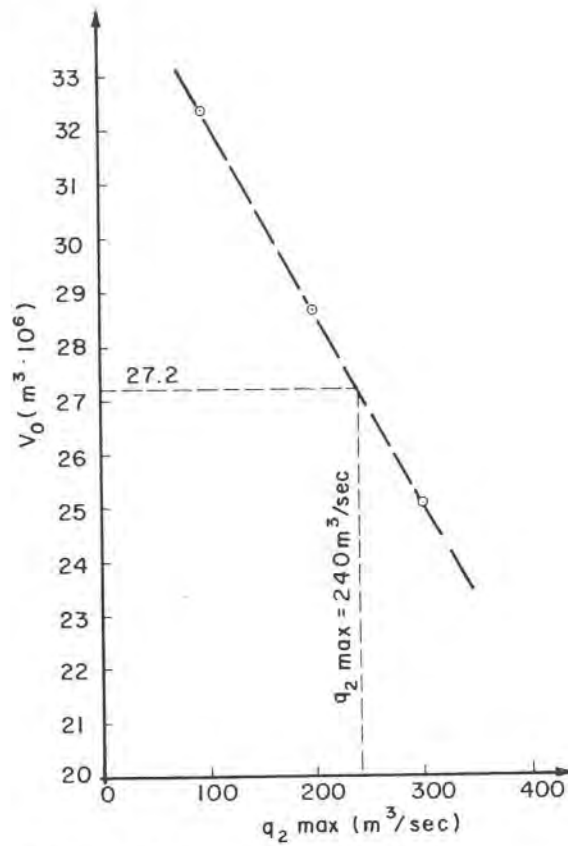


Fig. 10.65. $V_0 = f(q_{2 \max})$ -curve.

Step 5 – Now the required width of the spillway weir can be obtained from:

$$B = \frac{q_{2 \max}}{CH^{3/2}} = \frac{240}{2 \cdot 2^{3/2}} = 42.4 \text{ m}$$

Here, $C = C_q(2g)^{1/2} = 2$

Hence, the required solution:

$$q_{2 \max} = 240 \text{ m}^3/\text{sec} \quad B = 42.4 \text{ m}$$

In order to check now the values obtained by the approximate method, finite difference flood routing through the given reservoir has been carried out in Table 10.9.

TABLE 10.9. NUMERICAL FLOOD ROUTING (Ex. 10.9)

1	2	3	4	5	6	7	8	9	10	11	12	13	14	15
0		0		0	330.00					20,000	333.00	OK	116.6	116.6
2	2	60	30.0	216	330.09	2.3	1.15	8.3	207.7	20,208	330.09	OK	117.2	119.5
4	2	250	155.0	1,116	330.44	24.8	13.5	97.6	1018.4	21,229	330.44	OK	118.0	142.8
6	2	373	311.5	2,243	330.94	77.5	51.5	368.1	1874.9	23,104	330.94	OK	119.1	196.6
8	2	410	391.5	2,819	331.49	154.6	116.0	835.5	1983.5	25,087	331.49	OK	120.3	274.9
10	2	380	395.0	2,844	331.87	217.4	186.0	1339.0	1505.0	26,592	331.87	OK	121.2	338.6
12	2	310	345.0	2,484	332.05	249.5	233.4	1680.8	803.2	27,395	332.05	OK	121.6	371.1
14	2	235	272.5	1,962	332.08	255.0	252.2	1816.1	145.9	27,541	332.08	OK	121.6	376.6
16	2	178	206.5	1,487	332.02	244.0	249.5	1796.5	-309.5	27,232	332.02	OK	121.5	365.5
18	2	130	154.0	1,109	331.90	222.6	233.3	1679.8	-570.8	26,661	331.90	OK	121.2	343.8
20	2	90	110.0	792	331.73	193.4	208.0	1497.6	-705.6	25,955	331.73	OK	120.9	314.3

Column 1 – time from the beginning of the flood wave, hr.

Column 2 – time finite difference Δt , hr.

Column 3 – inflow discharge Q , taken from the spillway design hydrogram, m^3/sec .

Column 4 – average inflow discharge during Δt , \bar{Q} (m^3/sec).

Column 5 – volume of water that entered the reservoir during interval Δt ($\bar{Q} \cdot 7200$), $m^3 \times 10^3$.

Column 6 – assumed reservoir trial elevation (only the final trial value is shown) for the given spillway crest elevation, m.

Column 7 – rate of outflow q_2 over the spillway, computed from equation $q_2 = CBH^{3/2} = 85.0 H^{3/2}$, in m^3/sec .

Column 8 – average rate of outflow \bar{q}_2 during Δt in m^3/sec .

Column 9 – volume of water that left the reservoir during Δt , in $m^3 \cdot 10^6$.

Column 10 – inflow volume minus outflow volume, col. 5–col. 9, in $m^3 \cdot 10^6$.

Column 11 – Total storage at the end of Δt , in $m^3 \cdot 10^3$.

Column 12 – Reservoir elevation from the RVE-curve, Fig. 10.64, in m; if the elevation assumed in column 6 is correct, values in columns 6 and 12 must be equal.

Column 13 – remarks.

Column 14 – bottom outlet discharge q_1 , in m^3/sec .

Column 15 – combined outflow discharge (col. 7 and col. 14), in m^3/sec .

More accurate results could have been obtained by using shorter time intervals for the numerical solution (say, 1-hour intervals instead of 2 hours). It can be seen that the maximum spillway discharge as obtained by the approximate method was about 6% off from the computed maximum discharge ($240 \text{ m}^3/\text{sec}$ instead of $255 \text{ m}^3/\text{sec}$). Maximum water elevation of the reservoir, assumed to be 332.0 in the approximate method, has been computed as 332.08 by numerical solution, which is about 4% difference.

Spillway design alternative considered in the example is only one of many that have to be tried before the optimum solution is found. In order to facilitate the work, an additional graph, as developed by [18], may be useful. The graph is built for a given spillway-crest elevation, and the necessary data are best tabulated as shown in Table 10.10.

TABLE 10.10. AUXILIARY COMPUTATIONS

1	2	3	4
$q_{2\max}$ (m^3/sec)	V_0 ($\text{m}^3 \cdot 10^3$)	H (m)	B (m)

Column 1 – assumed maximum spillway discharge within the desired range.

Column 2 – for every q_2 assumed, corresponding V_0 is found from the graph 10.65.

Column 3 – for V_0 found, maximum reservoir water elevation can be obtained from the RVE-curve, Fig. 10.64.

Column 4 – width of the spillway crest is computed from $B = q_2/CH^{3/2}$.

The graph is shown in Fig. 10.66. If several spillway crest elevations are considered, a separate graph for each elevation has to be made. Should later site investigations show, for instance, that a temporary storage of about $7.5 \times 10^6 \text{ m}^3$ above the assumed spillway crest elevation is not recommended, a lower crest elevation could be tried.

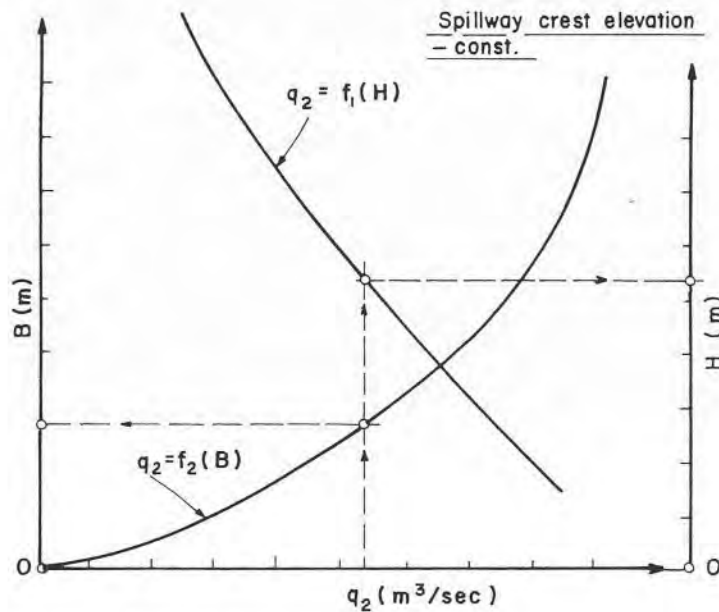


Fig. 10.66. Spillway-design graph.

10.5 Diversion of Flood Waters

It is probably one of the most ancient methods of flood protection, known to have been used by Chinese and Roman engineers. Since it directly gives relief to a channel threatened by high flood waters, its effectiveness can be very high, and when feasible, it is often preferred to any other flood-protection method. Particular techniques, however, to achieve such relief have undergone many changes of emphasis with time, mainly due to altered demographic aspects of flood plains.

Densely populated flood plains of today generally offer little possibility to build large "floodways", wide channels above ground level obtained by diking, which served to convey flood waters away from the threatened stream and to provide temporary storage for them. When temporary storage within the flood plain is available, the simplest way of flood-water diversion even today is to make a controlled opening through the dike embankment (say, a sluice gate), and to excavate a channel leading from the opening to the storage site. If the stored water can subsequently be disposed of without returning it to the stream, the solution is simple and highly efficient; in all

other cases, drainage of the temporarily flooded portion of the plain back to the stream has to be adequately taken care of. On small streams of the Mediterranean region, fixed uncontrolled spillways are often left in the dikes, with a view to diverting a portion of flood waters toward the less valuable part of the plain in order to protect more valuable land downstream.

When the existing channel of a stream is capable of handling all ordinary flows, but causes flooding of the adjacent plain at high water, a *temporary diversion* away from the stream channel may be sufficient. During most of the time, the normal stream channel stays in operation, while the relief (or bypass) channel is brought in to divert a part of the water only when a certain critical level is reached. In the case of a *permanent diversion*, the existing waterway is in fact replaced by another channel, which takes over from it. A sketch of a stream diversion scheme is shown on Fig. 10.67.

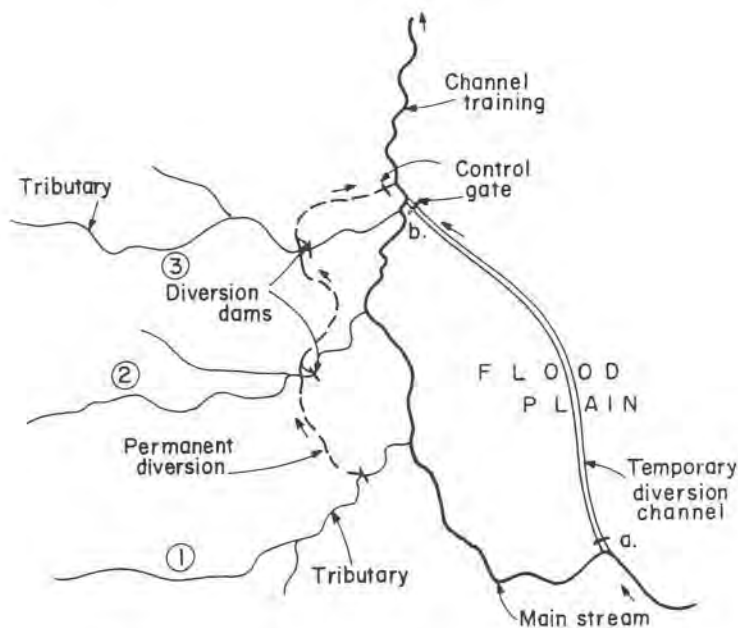


Fig. 10.67. Diversion scheme for flood protection.

The main stream, which traverses the low-lying flood plain, receives tributaries descending from nearby mountains. It can safely convey low and medium rates of flow, but causes extensive flooding at higher discharges. The situation is complicated by two additional factors: 1) when there is coincidence between flood waves in the main stream and one or more tributaries,

flood damages are apt to be very severe; 2) along many reaches of the main stream channel bed often lies above the flood-plain level (“perched channel”), due to many years of silt-deposition.

After weighing several alternatives, the adopted solution for the given hypothetical case is actually based on two diversion schemes:

- The one envisages a temporary relief channel that will be put into operation only at the onset of a dangerous flood wave by opening the gates at a and b. During the rest of the time, the channel will serve as the main collector for the flood-plain drainage scheme (not shown).

- The second scheme contemplates a permanent diversion of the three tributaries. They will be dammed not far from the confluence, and their water diverted by a bypass channel to join the main stream at the downstream end of the flood plain.

The length of the bypassed main channel is long enough to be only marginally affected by the backwater starting at the point where the diverted water is returned to it. However, if necessary, some diking may be provided, or the confluence point be moved farther downstream.

Diversion of flood waters from one stream to another situated not far away is a solution often used for flood-protection purposes, provided that hydrological analysis clearly indicates very low probability of flood-wave coincidence. Otherwise, it may only aggravate flooding problems of the recipient stream. Relief channels which divert flood waters to some nearby lake are excellent solutions, especially when the lake is large enough to act as a flood-routing reservoir without much rise in the water level. Fig. 10.68 schematically shows the two types of diversions.

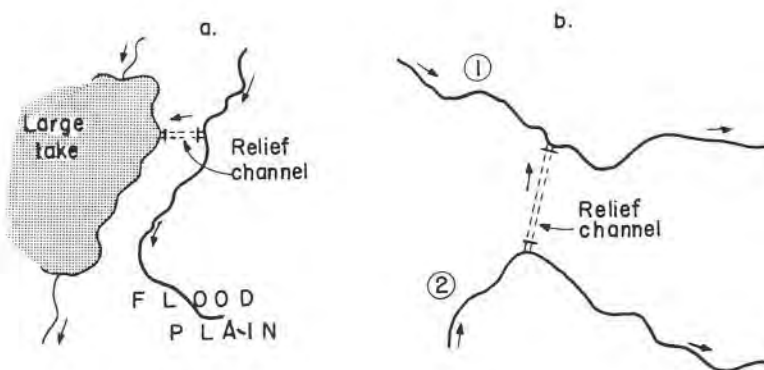


Fig. 10.68. Diversion types, a) diversion to a lake, b) diversion to another stream.

With the exception of permanent diversion works, at the head of the relief channel there is usually an entrance weir, which controls the inflow of flood waters into the diversion. Crest elevation and the width of the weir are fixed in such a way as to pass the maximum diversion discharge when the design flood wave upstream reaches the peak. Up to the weir crest, the stream water will be flowing normally in the main channel; if the water level continues to rise above the crest of the diversion weir, a part of the total discharge Q_0 will start spilling into the relief channel, forming Q_1 . The discharge that will be carried on downstream of the diversion will obviously be $(Q_0 - Q_1)$, reaching its maximum value simultaneously with Q_{0max} . A generalized sketch of such an arrangement is shown in Fig. 10.69. Due to the drawdown effect, partial attenuation of flood stages is obtained also upstream of the diversion.

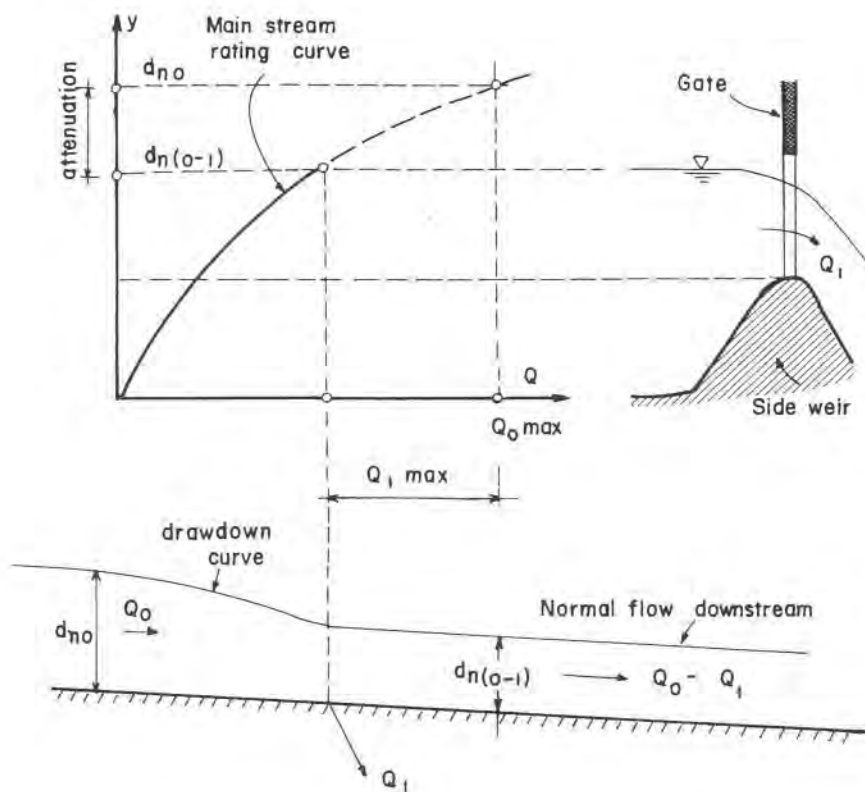


Fig. 10.69. Diversion with side weir.

An alternative solution, applied mainly when the diversion channel is used for some definite water supply scheme in addition to flood control, consists in building a gate-controlled dam across the main stream, immediately downstream of the diversion channel. From the point of view of flood protection, such a solution generally has no outstanding advantages, except for the case that the diversion channel close to the main stream has to be excavated through relatively high terrain, and by raising the head water as much as compatible with upstream interests may considerably reduce the excavation cost. In general terms, the overall control of flood-wave is more flexible and adaptable to the situation at hand.

Morphological changes in the main stream and relief channel, following the construction of a diversion, may with the passage of time, considerably reduce the efficiency of the diversion. This is probably a tolerable effect in the case of a side weir, as previously described, since it only cuts off the upper layer of the flood wave, thus leaving the sediment-water ratio in the main stream essentially unchanged. However, in the case of a relief channel without entrance weir, practically a bifurcation (see par. 3.7), in which a part of the water is diverted for the whole depth of flow, the said ratio may be adversely affected, causing deposition downstream. In any case, if the stream is known to carry high concentrations of sediment, it is always recommended to precede the diversion works by a comprehensive stream training scheme in the upstream course with a view to reducing the solid transport as much as possible, or at least to provide for some sort of sediment-exclusion means at the head-works.

Penetration of silt and clay particles, generally known as the wash load, into the diversion channel can at best be only partially prevented. If the concentration happens to be high, berming in the channel may follow, with berms built of material that holds water well and supports rapid growth of vegetation at the water line. Roots and branches that stick out into the water will increase the rate of trapping and deposition. As a consequence, the channel may eventually narrow considerably, or even become choked, while simultaneously the resistance to flow is increased — the net result being a significant fall in the water-conveying capacity of the channel. Sediment exclusion at the head-work will bring little improvement of the situation, and the only efficient engineering measure is the restoration of the channel to its original dimensions.

Diversion channels, which do not follow the meanders of the main stream, are often much shorter, while the topographic drop between the head point and the re-entry remains the same. Consequently, the longitudinal slope of the diversion channel may become excessively steep (see discussion on stream cut-offs, par. 3.3.3). To overcome this difficulty, the slope has to be flat-

tened by means of one or more drop structures along the course of the channel.

It has been mentioned already that the re-entry of flood waters into the main stream at some point downstream inevitably causes a backwater effect, which may be detrimental if this point is too close to the protected reach. Shifting the re-entry point farther downstream is a simple solution, whenever the prolongation of the diversion channel presents no particular difficulties. In contrary cases, the alternative solution of partial dike construction along the main channel should be considered.

A frequent occurrence in recent years is that of existing stream-training works which become insufficient due to flow changes in the stream caused by intensive urbanization and industrialization of previously rural areas. Such developments are likely to cause increased imperviousness of the watershed area and consequent change of the typical flood hydrogram of the stream, Fig. 10.70. The previously adopted maximum design discharge has been largely exceeded, and there has been a shift of the hydrogram toward the origin.

The remedial measure often undertaken in such or similar cases is to temporarily divert a part of the flood water into a retarding basin, and to restore it back to the stream after the subsidence of the flood wave, Fig. 10.71.

Overflow water can be controlled either by an appropriate gate at the entrance to the diversion channel, or by a side weir in the main stream.

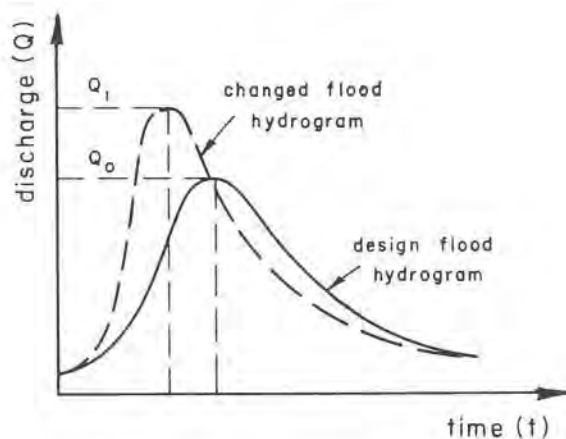


Fig. 10.70. Change in hydrogram due to increased imperviousness of the watershed.

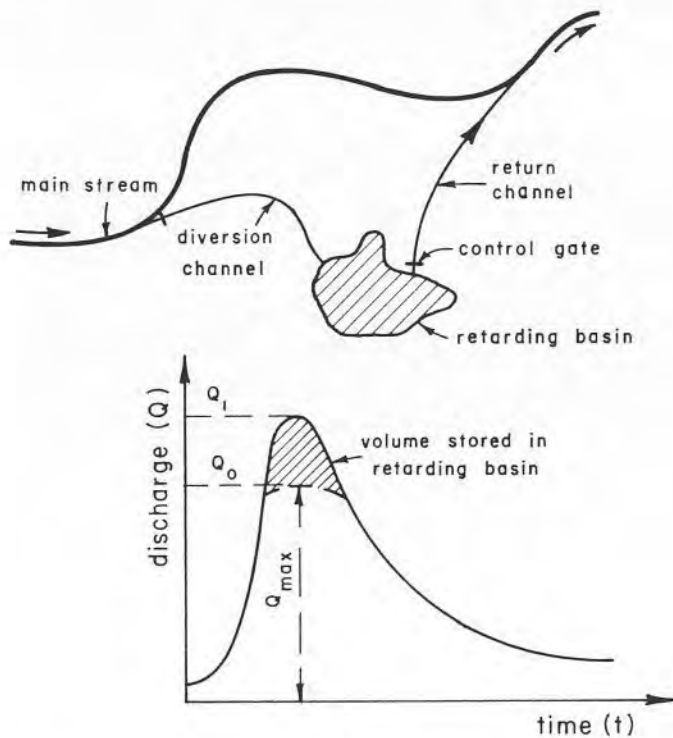


Fig. 10.71. Diversion of overflow flood water to a retarding basin.

10.6 Floods in Arid and Semi-Arid Zones

10.6.1 Introduction

Ephemeral stream characteristic of the more or less temperate zones of the Mediterranean type have already been mentioned on several occasions in the present text. During the summer months they carry negligible base flows from sparse springs, or are completely dry, whereas throughout the winter season they are exposed to flash floods of short duration, but high peak flows. The main reason for flow regimes of this type is the sharp division between the rainy period during the months with precipitation, and very little or no precipitation during the rest of the year. In a very broad sense, such and similar generally coastal regions all over the world are considered as semi-arid, although the degree of their relative aridity may vary within wide limits.

Neglected by the engineering sciences until recently, there has been since the last world war an ever-increasing interest in the methodical study of arid and semi-arid regions in respect of a wide range of disciplines, with a view to laying foundations for their technological development. In fact, the territory of almost half the nations in the world is located partly or wholly within the arid and semi-arid zones [20]. Moreover, a great part of the developing countries of the world belong to this type of region, and the effort to speed up their development has in fact pushed many international institutions to direct much of their funds to this purpose. The global shift in the wealth distribution, brought about by the soaring energy prices, has lately given a further impetus in the same direction, since many of the oil-rich countries are situated in arid or semi-arid zones.

The authors of the present text have for many years been active in a country which, though very small, presents all the gradations from arid desert in the south to semi-arid temperate climate in the north. Because of the finite nature of water resources, from the very beginning the highest possible degree of their engineering utilization has been set as the essential national goal, as the basis for intensive rural and urban development, industrial growth and the protection of densely populated areas. All this has rendered indispensable a thorough study of the varied aspects of the country's climatological, hydrological and flood-flow patterns.

Many mistakes have been made in the process of the hurried engineering activity, but also much has been learnt. Limitations of the present knowledge and our frequent failures when applying in this field the accepted rules of engineering prediction and extrapolation had again and again to be painfully registered.

This is the additional reason for which, besides giving in general so far a prominent place to various engineering aspects of semi-arid zones, the authors have decided to include a paragraph giving a brief survey of the most salient features related to these regions, particularly as far as flood protection is concerned.

10.6.2 Outline of Arid and Semi-Arid Zones

One of the well-known researchers of arid zones once said [21] that they defy specific definition, so varied are the factors that characterize them; but they all have one thing in common: they are all short of water.

In spite of this discouraging opening statement, many attempts have been made to bring forth a specific definition of arid and semi-arid zones, and even make a few tentative trials at quantitatively setting their limits in relation to other climatic zones. Thus again, according to UNESCO [20],

scarcity of rainfall, as well as its temporal and spatial irregularity, characterize these lands. In general, regions which receive less than 600 mm annual precipitation, but more than 250 mm, are considered to be of semi-arid type, while the transition between semi-arid and arid zones can be tentatively located at the 250 mm isohyet.

The main objection to such a convenient, but somewhat simplistic classification is that climatic averages have little practical meaning. It seems, therefore, more to the point to refer to the probability of recurrence with respect to some hydrological phenomena, rather than their absolute values. In accordance with this view it is suggested [20], for instance, that the dividing line which in a broad sense sets apart arid climates from moderate climates is the occurrence of three consecutive rainy seasons with precipitation inferior to the long-term mean.

Pronounced, and often extreme variability of rainfall in time and space is in fact an essential characteristic of these regions. The long-term average precipitation, for example, measured at Lakhish Stream station in the coastal belt of southern Israel, is about 450 mm. At the Zin Creek station, some 30 km more inland and 75 km to the south, the long-term average is about 90 mm, with extreme irregularity [22]. Similarly, in Mauretania, between two stations about 150 km apart, a difference of 160 mm was recorded in 1970 [20].

Variations in time are generally even more extreme, and they tend to increase with aridity. If the so-called relative variability of precipitation is taken as an indicator (the ratio of the standard deviation to the annual mean, in percent) differences in the range of 30% to 130% have been recorded [23]. In 30 years of observations on the Zin Stream in the Negev desert of Israel, maximum discharge of 300 m³/sec was recorded during a 30-year period. During the same period, no flow at all was registered for 5 years [22]. Similarly, in the Namibian coastal belt, at Swakopmund, one year 148 mm precipitation was recorded, while the next year only 1 mm [20].

Another interesting feature, characteristic of all arid and semi-arid zones, is the number of rainy days during a hydrological year. It varies spatially — even on a long-term basis — with the distance from the sea [24]. In the semi-arid coastal belt of Israel, number of rainy days can be as much as 50 and sometimes even more, while on the Negev Highland, some 50–100 km inland, it does not exceed 1–12 days, and on the Red Sea coast, at the southern tip of the country, it seldom is more than 3–4 days [25]. According to the same source, in the Negev Highland of Israel, watersheds larger than a few square kilometers require a threshold rainfall of 8 to 12 mm before any surface runoff appears. It means that the accumulative effect of small daily precipitations may be significant. On Fig. 10.72 a typical

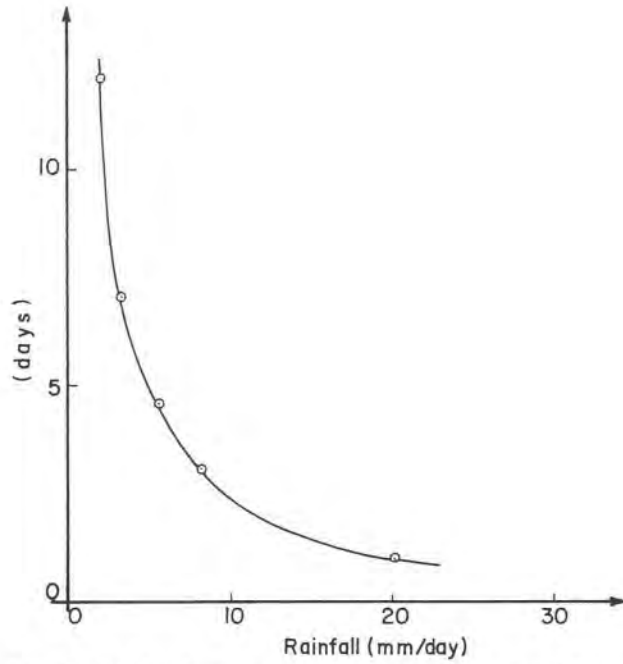


Fig. 10.72. Number of rainy days V to a given rainfall in the Negev Highland [25].

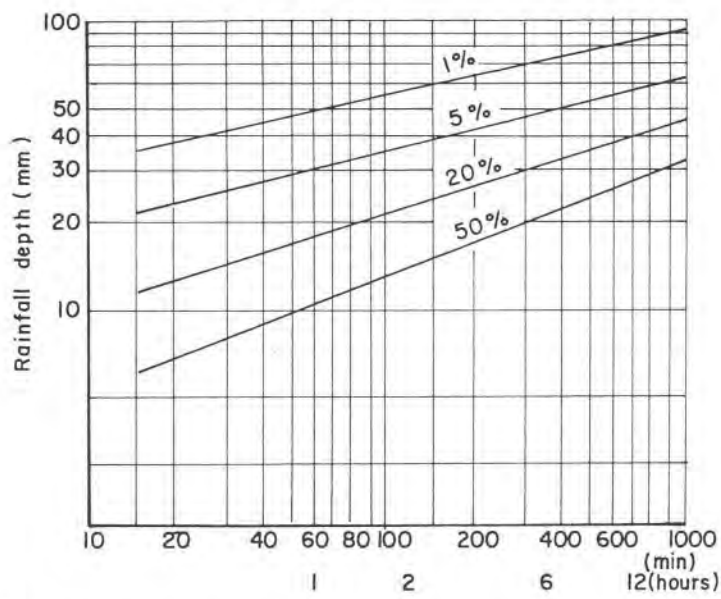


Fig. 10.73. Typical rainfall depth-duration – probability curves for Beersheba region [25].

relationship is shown between the number of rainy days per year in the Negev Highland and daily rainfall [25]. Typical rainfall probability curves for Beersheba Negev region of Israel are given in Fig. 10.73 [25].

In the Nile Delta region, average number of rainy days is about 8 near Alexandria, 3 at a distance of about 80 km southward and about 1 day at a distance of 250 km [24]. Orographic configuration may have a decisive

TABLE 10.11. TEMPERATURE AND PRECIPITATION DATA FOR ARID AND SEMI-ARID COUNTRIES [23]

Location	January		July		Yearly rain- fall (mm)
	Mean temp. °C	Rain- fall (mm)	Mean temp. °C	Rain- fall (mm)	
1. Sacramento, N. America	+ 7.5	96	+23.3	< 3	472
2. Phoenix, N. America	+11.1	20	+32.5	25	191
3. Zaragoza, Europe	+ 5.7	14	+23.5	20	377
4. Marrakesh, Africa	+11.5	28	+28.2	2	242
5. Biskra, Africa	+11.4	18	+34.2	3	158
6. Kashgar, Asia	- 5.3	15	+26.7	10	81
7. Palmyra, Asia	+ 7.9	24	+29.8	0	153
8. Baghdad, Asia	+10.6	25	+34.6	0	151
9. Teheran, Asia	+ 4.0	37	+28.6	0	213
10. Jodhpur, Asia	+16.7	3	+31.4	102	356
11. Cairo, Africa	+13.3	5	+28.4	0	28
12. Le Paz, S. America	+18.0	5	+19.4	10	145
13. Monterey, N. America	+14.4	15	+26.9	58	579
14. Bilma, Africa	17.2	0	+33.0	3	23
15. Khartoum, Africa	+23.6	<3	+31.7	53	157
16. Antofagasta, S. America	+20.8	0	+13.8	6	13
17. Windhoek, Africa	+23.3	76	+13.0	<3	363
18. Alice Springs, Australia	+28.6	43	+11.7	8	251
19. Merredin, Australia	+26.0	18	+10.3	49	300
20. Mendoza, S. America	†23.9	23	+ 8.4	5	191
21. Tel-Aviv*, Asia	+13.9		+26.7		600
22. Beersheba*, Asia	+13		+27		200

* As given by D. Ashbel.

effect in this respect – a mountain range running parallel to the coastline will intercept the rain clouds, and the number of rainy days on the leeward side may fall dramatically.

Temperatures in the arid and semi-arid regions are generally high, with the exception of coastal belts influenced by cool ocean currents (Chile, Namibia), or cold deserts (Patagonia, Central Asia). Some data on mean temperatures and precipitations for a number of arid and semi-arid countries, as given by UNESCO [23], are listed in Table 10.11. All temperatures are in °C, and rainfall in mm (rainfall data have been rounded to the nearest full number). Several attempts have been made to establish a quantitative relationship between the mean yearly temperature and precipitation, but so far no such formula has proved to be adequate.

10.6.3 Soil and Watershed Characteristics of Arid and Semi-Arid Zones

Quality of soils found in arid and semi-arid zones covers a very wide spectrum: from volcanic and sedimentary rocks to small flint pebbles, from coarse gravel-like stones to fine sands, from loams and clays to wind-transported loess. Geomorphology of arid-zone soils has by now acquired a vast amount of knowledge and information, but in the following only those aspects will be briefly discussed that have direct or indirect bearing on hydrology and flow conditions in general, and possible flood hazards in particular.

In spite of this wide variety of soil formations, there are nevertheless some common features that refer to a variable degree to all arid-zone soils. These are: scarce, but high-intensity rains, extreme diurnal temperature changes, abrasion caused by wind-blown particles, and lack of vegetation. All of these natural agents effectively prevent the formation of a protective weathered surface layer of appreciable thickness. During the dry season – most of the year in arid regions, and to a great part of it in semi-arid regions – surface layers dry up and crack to a depth of a few centimeters, Fig. 10.74.

When slightly wetted, most of arid-zone soils are highly erodible. High-intensity rains – although of short duration – quickly wash out finer soil grains, and these then are carried to the base of mountains, where eventually large alluvial fans are formed, Fig. 10.75. When slopes are relatively mild, these fine particles reach the waterways and mountain gorges (wadis), where they to no small measure contribute to the high sediment content of flood flows. Studies in the Negev region of Israel have shown [21] that the almost total lack of organic matter in soil materials on the surface or near to it



Fig. 10.74. Cracked soil surface in arid zones [23].

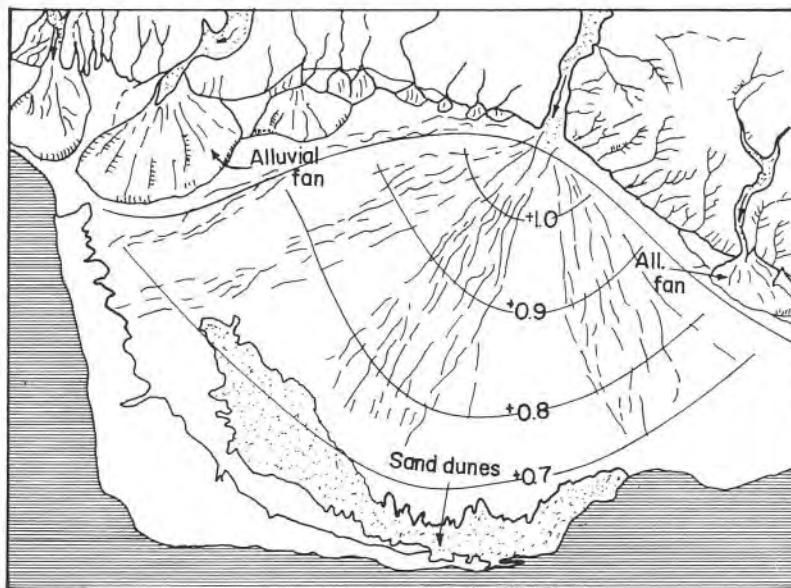


Fig. 10.75. Alluvial fan at the base of arid zone mountains [after J. Kolton, 1980].

causes them to be tight and impervious. Intake of raindrops by the soil is thus greatly reduced.

During heavy and sudden storms, raindrops often reach a diameter of 4–6 mm, falling at a velocity of about 10 m/sec when they near the battered soil surface like small missiles. The splash following the impact further tends to seal the surface pores and cracks. Soil fragments are broken apart and put into suspension by the unabsorbed storm waters with the aid of the splashing action. Measurements have shown sediment contents as high as 20% by weight. As the runoff water moves down the slope, it takes with it this charge of sediment, leaving behind sheet erosion. At the same time, however, a part of this muddy suspension sinks into the surface soil. A thin layer of fine-particle material is gradually formed on the surface from small particles that are filtered out. After drying, a thin impermeable crust is formed all over the surface, and it is this thin surface layer that actually determines the rate of water intake, regardless of how permeable the soil beneath it may be. On Fig. 10.76 are schematically shown the three phases of this process, namely 1) rain impact and splashing, with ensuing pore-sealing and sheet erosion, 2) thick suspension flow over partially sealed surface, and 3) impermeable crust formation upon drying.

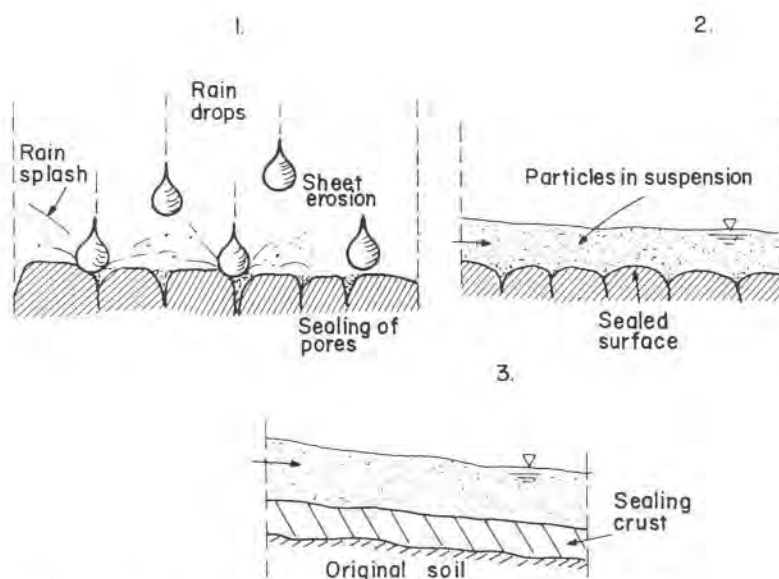


Fig. 10.76. Process of the sealing crust formation on arid soils.

A similar, but even more extreme impermeable crust formation is characteristic of wind-blown very fine loess soils. After only slight addition of moisture, do they develop an almost impermeable thin crust on the surface, which prevents water penetration into the soil and greatly increases the amount of surface runoff.

10.6.4 *Flow Patterns in Arid and Semi-Arid Zones*

Watercourses in arid and semi-arid zones may be classified in three main groups [21]:

1) Streams that cross arid lands, but which have their origin in distant humid mountains or high plateaus. They usually are of the perennial type, with seasonal floods that are unrelated to the arid climate of lands they flow through. These streams practically derive little or no water from the arid region itself, and about the only contribution given by the parched and barren countryside is a heavy sediment load. The best-known desert rivers of this type are the Nile and Colorado River.

2) Streams that bring water to arid lands, but they originate in some mountain ranges that stand like humid islands in an otherwise barren surrounding. They usually have small base flows from perennial springs situated along the mountain slopes, but farther downstream, deep in the arid countryside, they may be reduced during the hot season to a mere trickle, or even completely dry up. During the rainy season, however, or after the snow melt in the high mountains, intermittent flood waves of medium-size volume travel downstream through the arid lands and bring a blessing of water with them, though sometimes also destructive floods along their course.

Typical streams of this class are the Jordan River in Israel (Fig. 10.77), Litani River in Lebanon, as well as many streams that descend from the Atlas range in the north-west coastal region of Africa.

3) The third and the largest group of arid-zone watercourses receive their waters from rains that fall within the zone proper. Their average annual volume is relatively small, while their flow pattern is entirely in the form of short-duration flood waves that at any time involve only comparatively small areas.

Sudden and violent storms, which occur erratically and without any definite time sequence, release large volumes of water in short outbursts. In spite of the brief time-span of the rain, runoff reaches the maximum intensity, because the time of concentration (the time needed for the



Fig. 10.77. Jordan River.

farthest runoff particle to reach the water-collection point at the outlet from the watershed area) is for the most part roughly of the same order of magnitude as the duration of precipitation. There is no way of scientific forecasting, the wave builds up suddenly and rises to a high peak within a very short time (from a few hours to as little as some tens of minutes). The wave front moves down the narrow gorges in form of an almost vertical wall a few meters in height, accompanied by a deafening roar. Such a flood wave would probably be due to some local rain storm on the high plateau above, while the sky a few kilometers farther downstream may be cloudless.

The subsidence of the wave is usually as abrupt as its rise. Typical hydrograms of such arid-zone flash floods resemble an arrow on the time scale, and greatly differ from those of streams of semi-arid zones and still more from hydrograms of humid-region streams, see Fig. 1.12. Flood wave is made up entirely of storm runoff from a restricted area, and there is no tree-like ramification of tributaries with water contribution from a larger watershed area. This is probably a fortunate circumstance, because otherwise such violent floods would be much more destructive. For the lack of tributaries along the way and high rate of evaporation and infiltration on sand-covered stretches, arid-zone floods often do not carry far down the valley, but they certainly are violent although of restricted course. As one

moves toward more humid coastal belts, typical flood hydrograms tend to become more gradual, they extend over longer time periods (hours, and farther away, days), and total volume of water carried by the wave increases.

Sediment content of the sudden flash floods is generally very high, and owing to their extreme violence, they also carry with them down the valley rock fragments and drift debris. Along the bed of the stream, large boulders are rolled down the slope. Local accumulations due to some rock outcrop or an abrupt turn of the stream bed, occur frequently. Because of often long intervals between major floods, these accumulated rock and sediment deposits are not removed, and hence they may block the way for lesser floods. When eventually broken through owing to the hydrostatic pressure of the backed-up water on the upstream side, this may lead to distinctive outbursts, not directly attributable to a specific flood wave.

Sand and fine gravel deposits are often encountered in local depressions along the valley, and they may retain high degree of moisture below the surface, long after the flood event. However, there is in general little sorting out of the total sediment load during flash floods. Only when the greatly attenuated flood wave finally spreads over the alluvial fan, does the swinging and broken-up stream leave behind finer fractions in channels.

According to some researchers of arid zones [21], flood waters often are so laden with sediment and debris that they confer to the flow rheological properties and may be considered as mud flows. No scientific evidence, however, of such flows in nature seems to be available so far, although allegedly telltale signs have been found in many places.

10.6.5. Flood Protection Works

It has been said that one common feature of all arid zones is the lack of water. And yet, paradoxically enough, short but violent flood waves during the rainy season may endanger human lives and cause damage to valuable property as soon as the barren area becomes populated.

Control of floods in arid zones is even today not often called for, since these vast areas even to this time are only sparsely populated, although the situation is rapidly changing due to industrialization efforts of hitherto pre-vaiently nomadic nations and the resulting urbanization where previously only shifting population existed. Whenever such a control is necessary, it is invariably a difficult engineering task, for several reasons.

1) Erratic nature of major flood events in arid zones.

In semi-arid regions an observation period of about 30 years is usually thought to be sufficient to reveal the main characteristics of a stream-flow

pattern or rainfall regime on which more or less reliable extrapolation can be based. Such an observation period is far too short for arid zones, where a 300-year period may be required, and in some cases even longer. This point is further stressed on the graphs of Figs. 10.78 and 10.79 on which hydro-

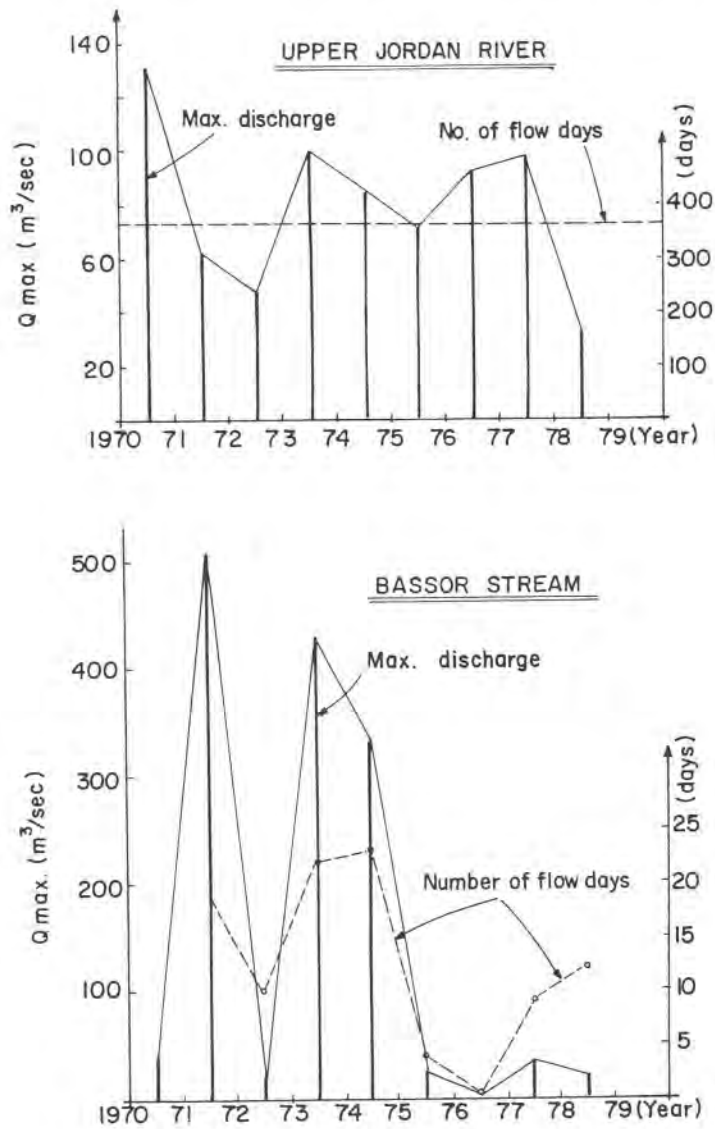


Fig. 10.78. Typical hydrological data for two semi-arid streams in Israel (Hydrological Service, Israel).

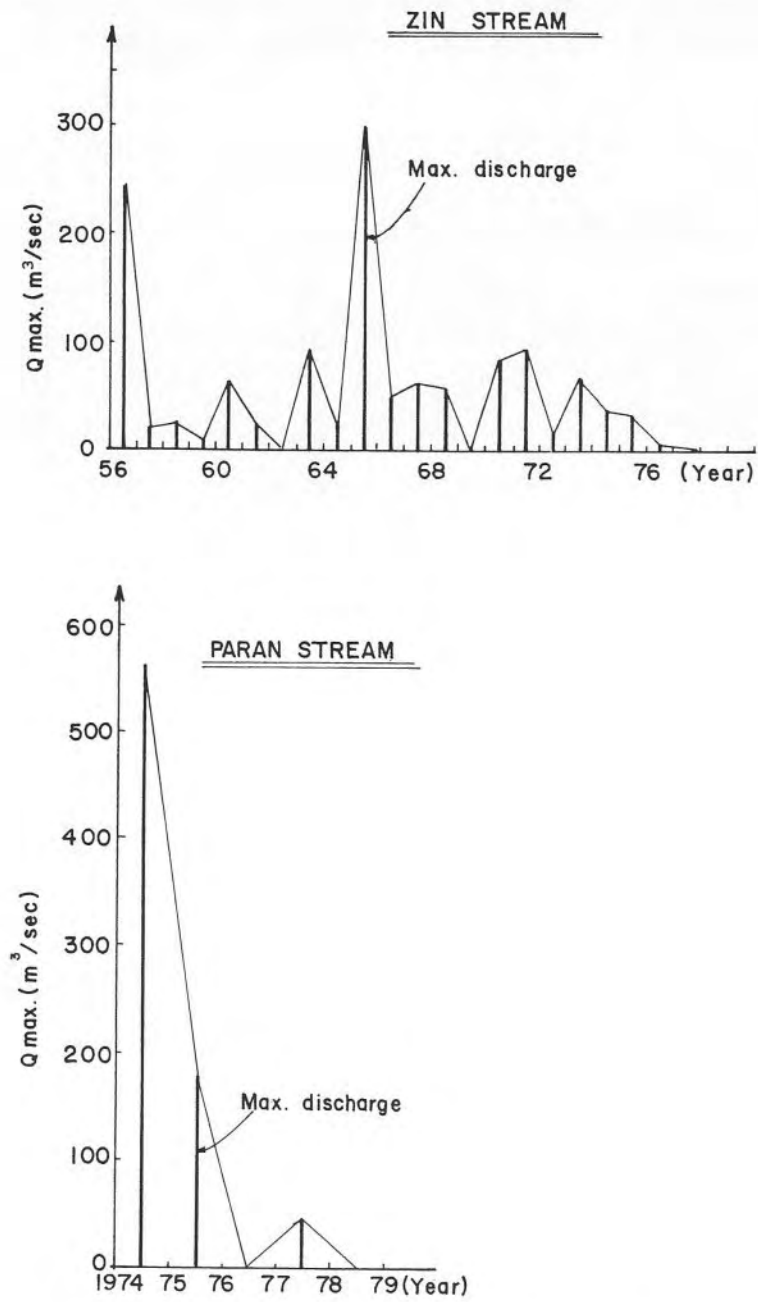


Fig. 10.79. Distribution of maximum yearly discharges for two arid-zone streams in Israel (Hydrological Service, Israel).

logical data for four streams in Israel are shown. One is of the type 2 (Jordan River), after the classification as given in par. 10.6.4; the second one is a typical semi-arid stream (Bassor Stream) of the coastal belt in southern Israel, and the last two are typical of arid-zone streams (Zin Stream and Paran Stream). For the first two streams, besides the maximum yearly discharges, number of days with flow are also indicated. It is noteworthy that the Jordan River is a perennial stream, though flowing through a semi-arid and farther downstream through an arid country-side. On the other hand, Bassor Stream, which draws its waters from the surface runoff throughout its watershed area, is a typical ephemeral Mediterranean stream.

Flow records of semi-arid streams, which mostly cross populated coastal belts, are generally available for a more or less reasonable period of time. On a short-time basis, such records may appear erratic and hardly presenting a well-defined pattern, but when the observation period is longer, they usually sort out to give a clearer picture. Standard statistical analysis and extrapolation for the determination of design discharge for different return periods, are routine engineering procedures in respect of such streams, with variable degree of reliability.

Similar records for any appreciable time sequence concerning arid-zone streams are seldom at hand. This is due not only to the fact that systematic flow measurements are only a quite recent initiative, but also because the calibration of measuring sites is difficult and troublesome. Violent and sudden flood waves easily carry away the instruments or damage the installation, and hence published records are frequently incomplete and with many gaps. All this does not mean, of course, that even on meagre and short-term information as this, statistical analyses, such as distribution matching, extrapolation, synthetic data procurement and correlations, are not carried out in an effort to arrive at least at some tangible quantitative results. The stress is rather on poor reliability of all such efforts, with often misleading conclusions.

It is, therefore, not surprising that the task of deciding on design discharge for hydraulic works on arid-zone streams is often more of an intelligent guess-work than any actual engineering calculation. In many instances the highest discharge on record is taken as the basis for design. Since the useful life-span of any hydraulic work in arid zones is usually no more than 25–30 years, such a simplistic approach might just prove adequate for a number of cases.

2) High content of sediment and debris in flood waters.

Coupled with erratic and violent flood waves, unusually high sediment content poses additional problems. Silting-up of reservoirs often proves to be

much more rapid than the most cautious of provisions; sediment and boulder clogging of channels, diversions and flood-ways can be accelerated far beyond the design estimate. Piling-up of rock chunks, boulders and other debris behind structures may cause stability problems.

3) Economic considerations.

In the introductory notes to the present chapter, it has been emphasized that for a flood-protection work to be acceptable to the community, its overall cost must be commensurable with the estimated reduction of flood damages, inclusive of human suffering and possible loss of life. High cost of such works often makes it necessary to opt for multiple-purpose systems, in which part of the expenditures can be debited on account of a function other than flood protection. From this point of view, there is virtually no difference between similar works in semi-arid zones and temperate or humid regions.

For reasons already mentioned, the need for flood protection in arid zones does not occur frequently. Whenever possible, new industrial population centres are located outside flood plains.

Nevertheless, from time to time flood protection in arid areas becomes a necessity, generally in connection with some industrial development project and population concentration that follows. Water supply clearly remains the major engineering problem, but protection from flood hazards must also be taken care of. It is obvious that in such cases ordinary economic analysis will not do, but community interest in developing the area and promoting its permanent settlement will often outweigh purely economic considerations. As long as this is not the case, and there is no possibility to diminish the cost of flood protection through a multiple-purpose scheme, the desert venture will probably have to live with flood hazards.

In regard to the engineering methods of flood protection, there is essentially no basic difference of approach between semi-arid and temperate or humid zones. All the methods discussed so far, or any combination of them, are used and applied with the same engineering criteria. Specific hydrological aspects, however, may have considerable effect on the engineering solution adopted: often very large ratio of Q_{\max}/Q_{\min} , concentration of flow within a short period of the year, relatively brief duration of the flood wave, with high peaks; less reliability in statistical extrapolation and correlation, etc. Since many of the countries that lie in the semi-arid belt or in the transition areas are still underdeveloped, hydrological data may be scarce or non-existent, and hence the engineer will have to rely mainly on synthetic series obtained by analogy with similar regions, and ultimately on his own intuition and skill.

Flood protection by means of surface reservoirs is far less attractive in arid zones than in semi-arid or temperate regions. Due to needle-like hydrograms, reduction of peak discharge by flood routing through reservoirs is hard to obtain without large storage capacities and high dams. Relatively small Beersheba Stream, which passes close to the Negev capital of Israel, has an estimated 50-year flood peak discharge of about $1000 \text{ m}^3/\text{sec}$, with an average flood duration of about 5 hours. Consequently, the total volume of such a flood wave is about 9 million m^3 . The safe carrying capacity of the regulated channel is about $300 \text{ m}^3/\text{sec}$, and hence a reservoir of about 6–7 million m^3 capacity and a dam of some 20 m height would be necessary in order to achieve the required reduction of the peak discharge by means of flood routing. Such a solution would be costly and economically prohibitive. The big reservoir, moreover, would be handling maybe for all of its useful life flood waves far smaller than the design flood.

High sediment content of flood waters should be no less embarrassing. The efficiency of the reservoir would be greatly reduced within a few years, and unless cleared of alluvium from time to time, its flood-protective capability considerably impaired.

With the possible exception of short storage periods, large multiple-purpose surface reservoirs in arid zones are generally not recommended because of large evaporation losses. In the Negev region of Israel these losses are estimated at about 2000–2500 mm per year, or about 5.5–7 mm per day. At a few locations, where nearby suitable ground-water recharge areas can be found to serve as underground water reservoirs for population centres or industry, such a multi-purpose solution might be feasible and should be studied.

In some transition belts between arid and semi-arid zones, reduction of the surface runoff by terracing and planting of drought-resistant and sturdy desert shrubs has given satisfactory results, provided that uncontrolled grazing is prevented. Attenuation of peak discharges, achieved mainly by prolongation of the time of concentration, depends on the extension of the covered watershed area and the density of the vegetative growths or terracing.

Flood protection by dikes is generally a well-suited solution for the arid zones. The uncertainty of the maximum flood forecasting, however, makes rather difficult the task of deciding on the height of the dikes. Applying a high coefficient of safety may well render the cost of the project out of reach for many clients. On the whole, it appears preferable to keep the dikes as low as possible by increasing the distance between them. This has an additional advantage in the fact that low dikes are less vulnerable to cracking due to long dry periods and extreme temperature differences. One should

never forget that the probability of a dike failure during violent desert storms is much higher than in more temperate regions, and low dikes certainly reduce the potential consequences of a failure.

In the case that higher dikes cannot be avoided, it is recommended to line the embankment, built from local material, by a 30–40 cm layer of imported soil with higher organic content, in order to prevent cracking. On more important locations, a suitable vegetable cover of sod plants should also be provided, with proper maintenance and some watering (see Vol. 1, Appendix 2).

Diversion of flood waters away from the area to be protected is probably the method used in arid zones more than any other. In many cases, it is possible to divert the flood waters to some uninhabited side-plain without much more engineering works. The damming of the main stream and the diversion head-works themselves should always be carefully designed and executed, since they will have to withstand particularly high dynamic forces. However, when a flood channel has to be designed, high sediment content of flood waters must duly be taken into account. In order to determine the slopes and overall dimensions of several diversion channels of desert streams in the Negev region of southern Israel, one of the authors of the present text used with fairly satisfactory results the regime-theory formulae for high sediment content.

Particular situations may arise along narrow coastal belts of arid zones, with steep mountain sides only a short distance from the shoreline. At relatively little distance from each other, narrow gorges pour their flood waters and form alluvial fans (see Fig. 10.75). Such coastal strips are often used for industrial plants, recreation areas or similar. Diversion of flood waters upstream would render channels with deep cuts prohibitively expensive. Two typical cases from the practice of one of the authors will be briefly described.

The first case concerns the narrow coastal strip south of the town of Elath on the Red Sea. The strip is on the average about 200 m large, and on the land side is hemmed in by steep and barren rock mountains with many desert gorges. At some stage of the development, it was decided to build along the strip a power station and a large desalination plant, which had to be protected from flash floods descending from the mountains of the Sinai Peninsula during the rainy season. A schematic sketch of the engineering solution adopted is shown in Fig. 10.80. The diversion floodway is wide and tapering upstream, of a roughly parabolic cross-section. Dike embankment is built from locally available material, and lined with stone mattresses made of folding gabion nettings (see par. 10.3.8.3). The channel has to be cleared from accumulated alluvial debris every now and then.

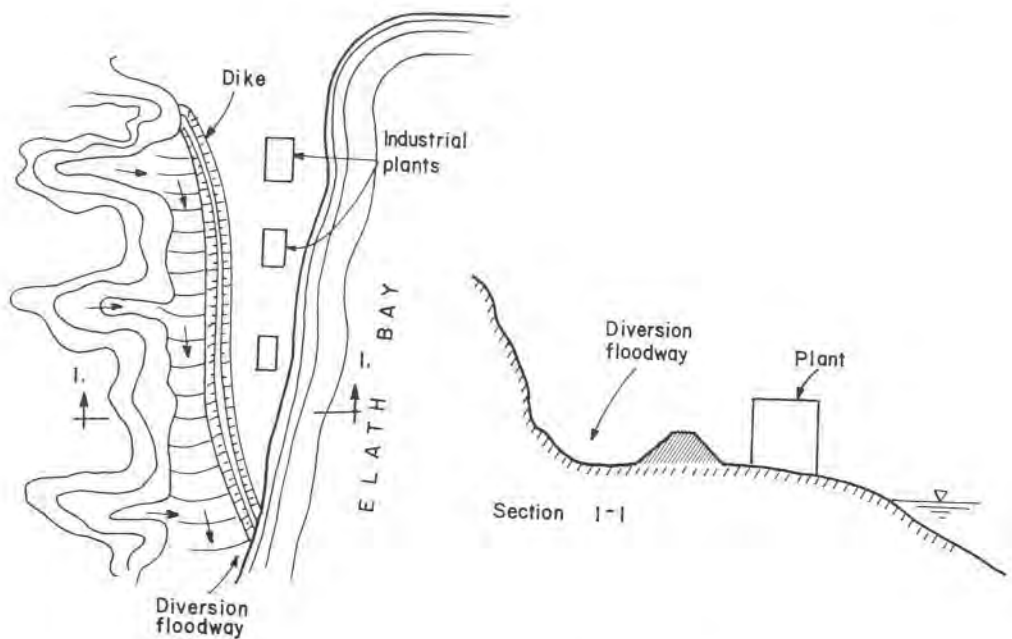


Fig. 10.80. Diversion channel in arid-zone coastal belt (not to scale).

A similar solution was also adopted in the second case, in which a pumping station had to be built opposite the mouth of a desert stream near the southern tip of the Dead Sea. Short but violent flash floods have been known to come roaring down the barren mountain side during the rainy months, and hence the station had to be protected. A dike was built across the flood path, and the water diverted to a wide flat plain descending to the sea, Fig. 10.81.

Channel regulation and other stream-training works for flood protection are used in arid zones only on a limited scale, or within the boundaries of towns. The regulated channel will usually have a wide cross section to be able to convey high-peak flows without flooding, but at the same time formation of meanders by smaller flows should be prevented as far as possible. This can be achieved by making the bottom of the channel in transverse direction not flat, but either slightly triangular or parabolic, to induce concentration of flow at low discharges. Good maintenance routine of such channels is essential if they are to function properly.

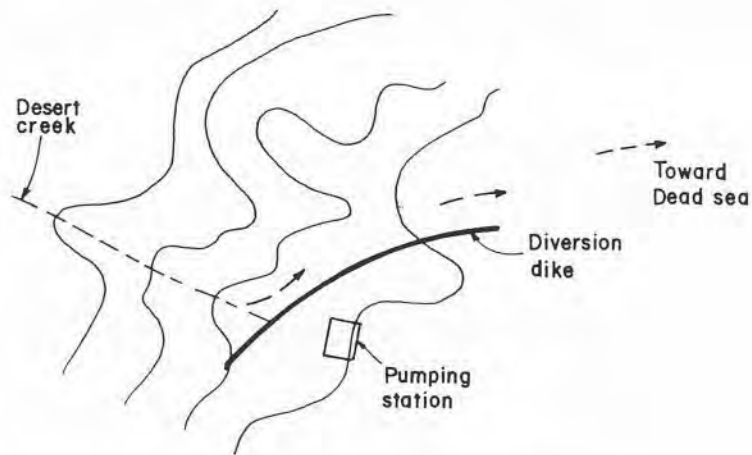


Fig. 10.81. Protection of industrial plant in arid zone.

10.6.6 Summary

1) Flood-protection methods used in temperate or humid regions are generally suitable for semi-arid zones also. Retention reservoirs built for flood protection only, often prohibitively expensive even in temperate regions, are seldom economically warranted.

2) Streams that cross arid regions, but originate in humid mountains outside or separate of them, are mainly governed by these sources, and are only to a lesser degree influenced by climatic conditions of their host country. Flood-protection methods, therefore, should on the whole be adapted to the hydrological and morphological conditions of the stream.

3) Flood-protection methods of streams that draw their waters from the surface runoff of arid-zone watersheds have several limitations and peculiar features. Retention reservoirs are not recommended, and even when of multiple-purpose type, their utility is usually severely restricted. Diking is generally a solution adopted for sensitive areas of rather limited extension.

Diversion of flood waters, whenever feasible, appears to be the best and safest of methods. Stream-training works, such as channel regulation, cross-section enlargement etc., are usually carried out for limited stretches only and when estimated peak discharge is not excessively high.

Design of hydraulic projects in arid zones is in many ways like working under conditions of insufficient hydrological data, or none at all. Even at locations for which some data do exist, these often are, for reasons previously explained, inaccurate and unreliable, while their extent is always

dismally short. Information collected from unscientific sources, such as water marks, size of stones, recollections of local inhabitants etc., may often be very helpful, but should be as a rule taken with a grain of salt. The authors, once trying to come by a rough estimate of discharge in a desert stream, asked a beduin about the highest water level during floods. After some thinking, he said that he still remembered his grandfather once telling him that when he himself had been a child, the water reached the top of an acacia tree some 300 m distant. By observing the stones on the stream bed and other telltale signs, the authors deduced that the average velocity might have been about 3 m/sec, and thus arrived at a rough estimate of the discharge. Two years later, during an exceptionally rainy season in the desert, fresh water marks indicated that the flood-water level at the very same location exceeded by far the top of the acacia tree.

10.7 Rudiments of Engineering Economy for Flood Protection Works

10.7.1 Introduction

Engineering practice at all stages is closely connected with economic considerations, and hence familiarity with the basic aspects of economic evaluation and cost-benefit estimates is indispensable. In the context of the present Manual, only some fundamental concepts and lines of approach can be reviewed, but no engineering text directed to the practicing engineer can dispense with it without leaving a gap.

As far as the capital cost of a flood-protection work is concerned, i.e. the sum of all expenditures required to bring the project to completion, there is practically little or no difference in comparison with other hydraulic projects. The cost-benefit analysis, however, is usually more complicated than with fixed-purpose projects of hydraulic engineering, since for every alternative not only the cost estimate changes, but also the expected benefit.

In the following, first the fundamentals of capital cost estimates, with annual operation and maintenance expenditures, are briefly reviewed, and in continuation an outline of flood-control benefit analysis is given.

10.7.2 Capital Cost Estimate

Advance cost estimates for different alternatives of an engineering project as a rule are made on the basis of preliminary design and average unit prices.

Consequently, they cannot be expected to be very accurate, and round figures are preferable to any unrealistic display of minor denominations. Order of magnitude of the final capital cost estimate, however, should always be realistic, and the analysis procedure for all the alternatives kept equal.

The overall cost consists of a series of direct expenditures, obtained from quantity surveying and adopted unit prices, and some indirect items associated with all engineering projects. These latter include sundry engineering expenses, such as field surveys, design, working drawings, consulting services, works supervision, etc.; interest payments during the construction period, before the project yields any benefits; land appropriation connected with the project; contingencies, which stand for unforeseen expenditures, generally at a flat rate of the direct items; or any other similar item.

TABLE 10.12. COST ESTIMATE

a) <i>Direct expenditures</i>	
1. Earth works	2,400,000
2. Construction of dikes	1,800,000
3. Drop structures	500,000
4. Controlled inlets	400,000
5. Controlled outlets	200,000
6. Protective lining	300,000
7. Culverts through dikes	600,000
8. Access roads	200,000
9. Bridges	700,000
10. Shifting of existing pumping installations	200,000
Total direct cost	<u>7,300,000</u>
b) <i>Indirect expenditures</i>	
11. Land appropriation	200,000
12. Engineering expenses	700,000
13. Interest during construction	1,000,000
14. Contingencies	<u>1,100,000</u>
Total indirect cost	<u>3,000,000</u>

In order to better visualize the procedure, in Table 10.12 is shown the cost estimate for a stream-training project. All cost items are quoted in *unspecified* currency.

In Table 10.12, item 12 of indirect expenditures, engineering expenditures, have been calculated on the basis of about 10% of the total direct cost. For the computation of item 13, interest during construction, it was assumed that the construction period would be three years, and that each year one-third of the total direct cost would have to be borrowed, i.e. about 2,700,000, with a 6% yearly interest rate; that would give 490,000 for the first third, 320,000 for the second third, and 160,000 for the last third. All together round about 1,000,000. Finally, contingencies have been computed on the basis of 15% of the total direct cost.

10.7.2.1 Annual Expenditures

Annual charges of an engineering project are mainly composed of three items: 1) depreciation fund allowance, 2) interest payments and 3) annual operation and maintenance cost.

Basic mathematics of engineering economy, and tables with computed values for different methods of computation, are given in Appendix 2 to the present chapter.

Every engineering project has a finite useful life, generally between 30 and 50 years, and it is assumed that after this period the works are either worn out or obsolete. Hence, a depreciation allowance has to be made every year in order to cover the annual loss of capital value, and to build up a fund from which a new project of the same capital cost could be financed at the end of the useful life span.

When computing depreciation charges, however, due allowance should be made for the interest that will accrue from the depreciation fund. This can be done either 1) by charging each year a varying annual amount, or 2) on the basis of a constant annual cost. For the sake of illustration, let us consider again the stream-training project of Table 10.12. The total capacity cost, for simplicity, is assumed to be 10,000,000, useful life span 35 years, and the interest rate on the capital 6%.

In method 1, the annual depreciation charge is $10,000,000/35 = 286,000$, and it remains constant for the whole period. Interest charge, however, will vary from year to year, because it is only taken over the depreciated value of the project. Hence, it will be as follows (in round figures):

1st year	600,000
After 15 years	228,000
After 20 years	172,000
After 30 years	56,000
In the last year	11,400

At the end of the 35-year period, the whole of the advanced capital is written off, and the interest charge, of course, drops to zero.

The above method is often used in hydraulic-engineering projects, when there is no particular advantage in having a constant annual charge.

In method 2, the depreciation charge is considered to be a sinking-fund payment. Invested at compound interest for 35 years, it will yield at the end of the period the original 10,000,000 capital investment. Let us suppose that the interest rate at which the annual depreciation deposits will grow is 8%, whereas the interest rate on the capital outlay remains 6%.

The required annuity can easily be computed by the aid of Eq. (10.50) or Table 10.15, column 5, for $i = 8\%$ and 35 years.

$$R = 100,000 \times 0.58 = 58,000$$

Interest payment on the advanced capital at 6% will be a constant annual charge of 400,000. Hence, the total annual payment will amount to 458,000 for the whole of the 35-year period.

It was assumed so far that the useful-life span is equal for the project as a whole, hence for all of its component parts. This is not necessarily always the case, and consequently not all the components must have the same depreciation charge. In such a case, depreciation charges for different items have to be computed separately, each one according to the pertinent useful-life estimate, and then summed up to obtain the total charge.

Annual operation and maintenance cost is generally expressed, at least for preliminary estimates and comparison of alternatives, as a flat percentage of the capital cost of the project. In the final cost estimate, more detailed and accurate analysis is carried out according to different items, such as labor, services, materials, etc. Sometimes operation and maintenance costs are not evenly distributed during the useful-life span of the project. If alternatives have to be compared in which different charges are applicable, the best method of comparison is by means of the "present value" calculation (see Appendix 2). In order to illustrate the point, let us again go back to the cost estimate of Table 10.12. Let it be assumed that in one alternative the operation and maintenance annual charge is constant at 400,000, hence the total annual cost is equal to $458,000 + 400,000 = 858,000$. In the second

alternative, operation and maintenance charges are distributed as follows:

	3 years at 900,000 per annum
	3 years at 600,000 per annum
	4 years at 400,000 per annum
	10 years at 300,000 per annum
	10 years at 100,000 per annum
	5 years at 50,000 per annum
Total	35 years

In the first alternative, the present value of the constant sinking-fund annuity is obtained by using Eq. 10.49 or Table 10.14 for $i = 6\%$ (interest on the capital outlay), column 4,

$$P = 858,000 \times 14.50 = 12,439,000$$

Present value of the second alternative has to be computed for each year separately applying Eq. (10.47) for $i = 6\%$,

$$P = 1,358,000 (0.94 + 0.89 + 0.84) + 1,058,000 (0.79 + 0.74 + 0.7) + \\ + 858,000 \times \dots + 508,000 (\dots + 0.14 + 0.13) = 12,866,000$$

Hence in the present hypothetical example, alternative 1, with a constant charge, would be 427,000 cheaper than alternative 2 with variable charge, and this in spite of the fact that the payments for operation and maintenance expense in alternative 1 (constant charge) are actually about 4,000,000 more than in alternative 2 (variable charge).

Taxes and insurance charges are generally not included in the cost estimates of flood-protection projects, since as a rule they are government-sponsored and financed by public funds or state bond issues. Even privately sponsored flood-protection works are usually tax-exempt, but insurance charges should be included in the cost estimate.

10.7.3 Estimate of Benefits

The objective merit of a flood-protection project is measured on a basis of the ratio between the estimated annual benefit and annual cost. A project may be rejected by the community because of excessively high initial capital outlay required, but its intrinsic worthiness is not affected by such a decision

as long as the above ratio is positive. Although preliminary capital cost estimates may require a great deal of assumptions and intelligent guesswork, benefits assessment is often much harder and calls for expertise beyond the hydraulic engineer's competence.

Distinction should be made between tangible and intangible benefits. The former are those that can be expressed and computed in money equivalent, whereas the latter are generally not amenable to such form of a common denominator, as for instance the alleviation of human suffering, loss of life, etc., which belong to social benefits, and should be assessed with a different yardstick.

Tangible benefits, on the other hand, may be either direct or indirect. Direct benefits are derived in straight line from the project – reduction of flood frequency and of potential damages from flood waves. Such benefits may also include reclamation of areas hitherto unused because of flood hazards. Indirect benefits result from the second-line causes – reduction of evacuation expenses, of losses caused by traffic and business-activity interruptions, etc. In common engineering practice it is customary to base the economic analysis of flood-protection projects on tangible and direct benefits only.

It is commonly assumed that the flood damage (hence also the potential benefit) is a function only of the peak discharge above a certain maximum safe value, or its equivalent of water depth above some characteristic datum level. Although this convenient approach may be justified when dealing with prevalently urban or industrial flood plains, it proves often to be inadequate for agricultural lands. In such cases, a few additional parameters should be taken into consideration:

- a) Duration of the flood wave. While some crops may be completely lost if covered with flood waters for more than a few days, others may be only partially or marginally damaged. Depth of water in this respect may be of little or no effect.
- b) Velocity of flow over the flood plain, both during the forward movement and recession of water. These velocities determine the surface erosion and silting pattern.
- c) Damage to agricultural yield depends to a large degree on the time of the flood – whether it is before or after the seeding, sprouting, etc.
- d) Moisture content of the soil just before the flood wave is also important when estimating agricultural damages. This implies a study of average intervals between sequent flood waves.
- e) Sediment concentration in flood water and grain-size distribution. This factor is of particular importance in semi-arid regions.

The generally held view that the higher the stream stage, the larger the flooded area, is not necessarily always correct either. For flood waves of high peak discharge, but short duration, the time needed for the water to reach the outlying parts of the flood plain may be longer than the duration of the wave. Hence, the recession of water may start before it arrives at the distant parts. In other words, flooded area depends not only on the stage (stream discharge), but on the associated wave duration as well, and every peak discharge with variable duration also has variable frequency of occurrence.

In a generalized way, following relations may be written,

$$\begin{aligned} A &\propto (S, D) \\ t &\propto (S, D, A) \\ d &\propto (S, D, t) \end{aligned} \tag{10.43}$$

In the above relations and the following graph, A – flooded area (equivalent to flood damage), Q – stream discharge above some specific safety threshold, S – stream stage equivalent to Q , above the safety threshold, D – duration of the flood wave in the stream, T – total time of direct observations or statistical extrapolation, t – duration of the flooding (forward movement + stagnation + recession), d – depth of water on the flood plain (percentage of S , according to local topography, etc.).

A graphical flood analysis for a given prevalently agricultural area is schematically shown in Fig. 10.82. On the first part of the graph (a), a family of discharge (stage) – duration-frequency curves is given. Durations of the respective flood waves, D_1, D_2, \dots, D_n , can be expressed in any convenient units (hours, days or weeks). In part (b), discharge (stage) – duration-flooded area curves are traced. These curves usually are partly based on direct observations, and partly on synthetic data obtained by a careful analysis of the flood plain. Flooded area, A , can be measured in any convenient units (m^2, km^2). Since the extent of the flooded area directly measures the damage caused by the flooding, it is often substituted by money equivalent. It is worthwhile noticing that the curves indicate that a short-duration flood wave with a higher discharge causes less flooding than a longer-duration wave with lower discharge, a characteristic feature of many flood plains.

Part (c) of the graph, finally, is directly derived from the curves of parts (a) and (b), and it shows frequency – duration-flooded area curves. Area enclosed between the envelope curve and coordinate axes gives the average flooded area. When computing the area, proper attention should be given to

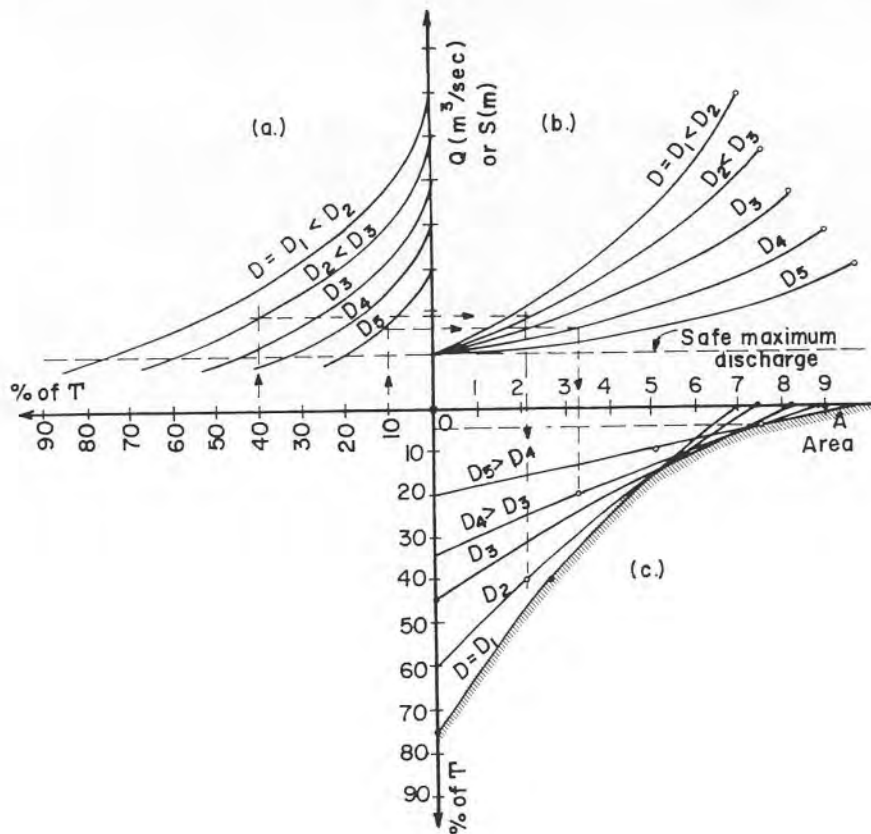


Fig. 10.82. Graphical flood analysis for a prevalently agricultural area.

the units of the graph. Thus, for instance, the partial area of the graph for the interval 0–10% of the time would be:

$$A_1 \cong 0.1 \times 7.5 = 0.75 \text{ units}$$

By summing up all partial areas, total average annual flooded area is obtained:

$$\Sigma A = A_1 + A_2 + \dots + A_n.$$

In the case of a prevalently urban or industrial flood-plain area, a simpler analysis may be sufficient, as schematically shown in Fig. 10.83.

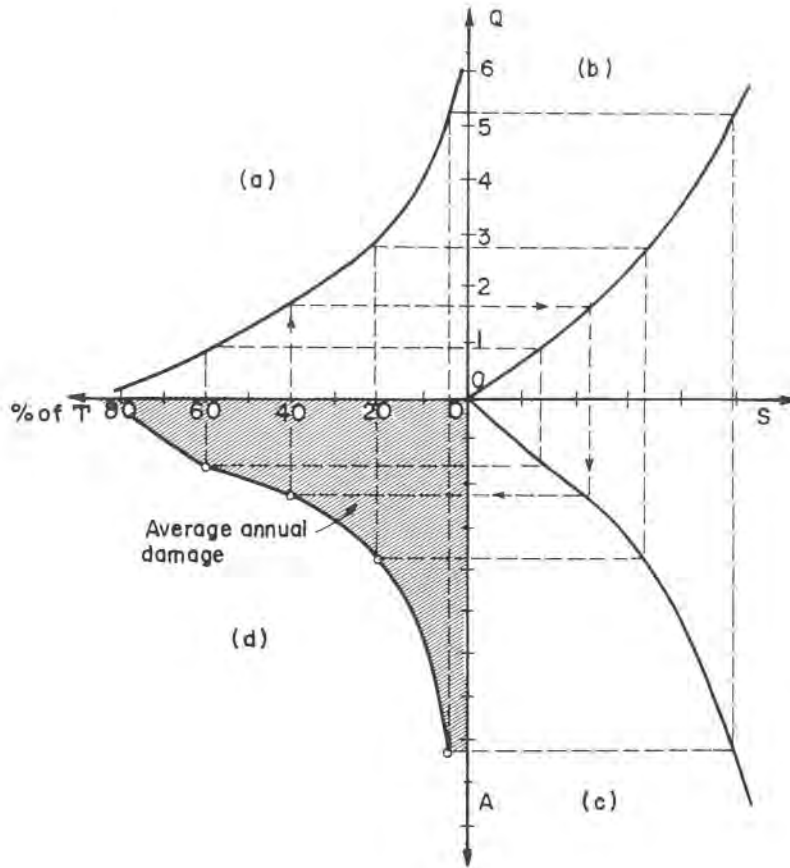


Fig. 10.83. Graphical flood analysis for a prevalently urban or industrial area.

The graph is self-explanatory. While parts (a), (b) and (c) are measured on synthetic data, graph (d) is derived from the given curves. The shaded area represents the average annual damage in the area subject to flooding.

In order to obtain the benefit of a proposed flood-protection project, the effect of the protection works has to be superposed on the previously derived annual flooded area, equivalent to the annual damage.

In the first instance, let us assume that a diking system is proposed along the stretch of the stream where flooding occurs. Maximum design discharge for the dikes is 3 units of Q (see Fig. 10.83), corresponding to a frequency of about 20%. For all discharges less than 3 units, there is full protection of the flood plain. When the discharge exceeds 3 units, the dikes are overtopped and are likely to eventually fail, hence the damage is supposed as large as

without protection at all, and sometimes even more (see par. 10.3.9). This is shown in Fig. 10.84 (a), on which part (d) of Fig. 10.83 is reproduced.

If a diversion is designed to take on the same discharge of 3 units, there will again be no flooding for all flows less than the design discharge. However, for flows higher than 3 units, there will still be a partial relief, the extent of which depends on the characteristics of a given diversion structure. This is shown on part (b) of Fig. 10.84.

Effect of stream-training works, such as channel improvement, is similar to diversions, i.e. partial relief may be expected for flows larger than the design discharge. A retention reservoir, designed for the same peak flow as the previously discussed protection works, also provides full protection up to the design discharge (reservoir design flood, par. 10.4), and partial attenuation for higher flows.

10.7.4 Summary

In the previous paragraphs some basic notions concerning the evaluation of flood-protection works have been given. For further information on these subjects, specialized texts should be consulted, such as [26, 27] and others.

Evaluation of the merit to be assigned to a flood control project is based on the ratio between the expected benefits and the estimated annual capital cost. The latter part of the evaluation, the capital cost, is a more or less

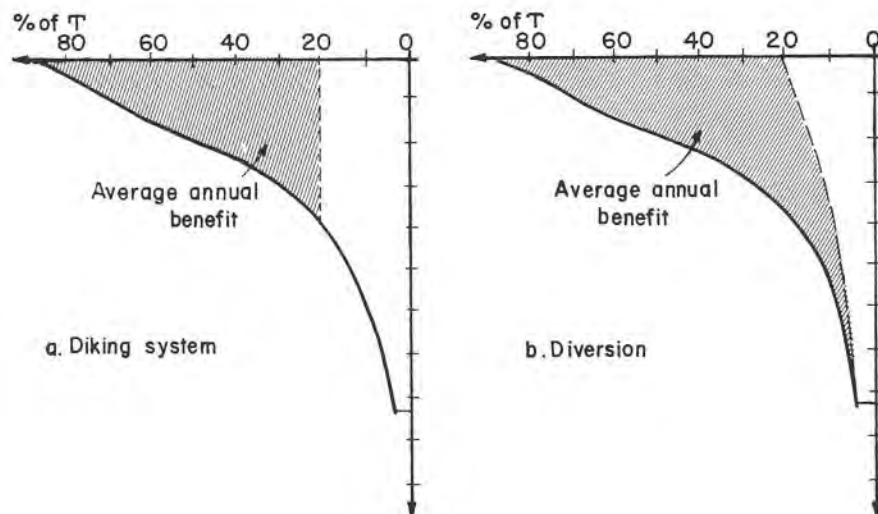


Fig. 10.84. Benefits of flood-protection works, (a) dikes, (b) diversion.

straightforward procedure, but for the fact that in the early stages no detailed drawings and quantity surveying are available, hence a great deal of experienced and intelligent guessing is inevitable.

Estimate of benefits, on the other hand, is generally much more demanding, particularly so of agricultural areas. Although only tangible and direct benefits are economically evaluated, cooperation of economists, social planners and agronomists is usually required. An additional complicating factor of agricultural land protection is the fact that in most cases it is coupled with flood-plain drainage schemes and ground-water control. Reclamation benefits may also be part of the overall improvement, and hence should be evaluated as some sort of "increase in the value of land". Since not all the benefits are likely to be reaped simultaneously, but will probably be spread over several years in pace with the progress of the project, all the benefits are best evaluated in terms of their "present value", as explained in the text.

Coefficients of "uncertainty" are a common practice with the engineers in this field, as in many others. To offset anticipated errors in capital-cost estimates, a reduced useful life of the project is assumed, say 20 years instead of the usual 25–30 years.

It is advantageous to have at the outset of a flood-protection design an estimate of the average annual damage under natural conditions. This represents the ideal maximum benefit if the project could prevent all future flooding. Since this would be unrealistic, a somewhat lower figure may be taken as the upper limit of the cost for the proposed project.

A final word should also be said about environmental and ecological aspects of flood-protection works. Although they generally belong to the intangibles, and hence do not figure in economic evaluations, they should always be thoroughly studied before embarking on any major flood-protection work.

The impact of changed conditions will be felt in both the stream and the flood plain. The morphological equilibrium of the stream may be significantly affected, with erosion, deposition and local scouring appearing at new, and sometimes unexpected locations. Changes on the flood plain are often even more pronounced. Irrigation networks will have to be provided, and the use of artificial fertilizers increased because of the disappearance of natural sources. Generally dryer conditions and lowering of the ground-water table may have far-reaching effects on the fauna and flora of the region, for which appropriate adaptation measures should be taken in time, in order to provide conditions for a smooth transition.

Increased wind erosion is likely to become a problem, necessitating hitherto largely ignored soil-conservation methods. Climatic conditions – both on

micro and macro scales – may also be subjected to changes because of altered humidity content of the air and soil.

Appendix 1: Engineering Analysis for the Spillway Design [18] – a brief summary

1. Basic Data

The following data underlie any spillway design:

- a) Reservoir volume vs. Elevation curve (RVE-curve, Fig. 10.85).
- b) Spillway-design inflow hydrogram (Fig. 10.86).

2. Definition of the Notation

- q_2 – spillway discharge, m^3/sec
 B – width of the spillway weir, m
 H – head on the weir, m
 V_t – temporary storage above the spillway crest, m^3

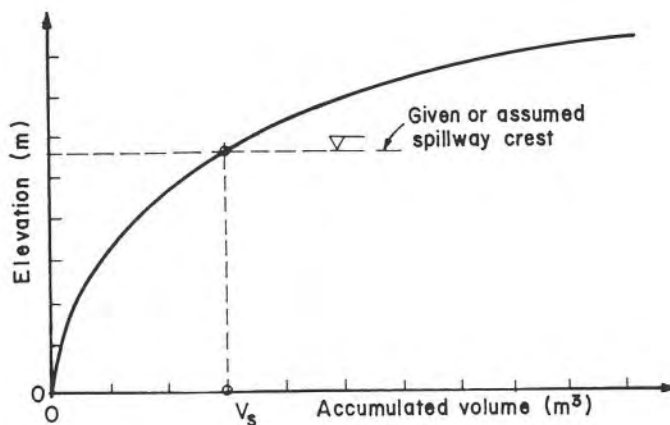


Fig. 10.85. Reservoir volume vs. elevation curve (RVE-curve).

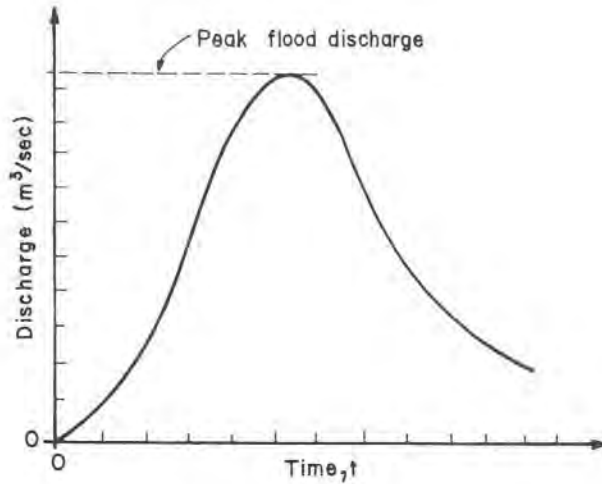


Fig. 10.86. Spillway-design inflow hydrogram.

V_s – reservoir capacity up to the spillway crest, m^3

$V_0 = (V_s + V_t)$, total storage, m^3

C – discharge coefficient of the spillway weir.

The relationship between q_2 , B and H for the weir is given by:

$$q_2 = CBH^{3/2} \quad (10.44)$$

3. Analysis Procedure

It is assumed in all the cases considered that the elevation of the spillway crest is given and fixed.

3 (a) – Case I

Given: $q_{2\max}$ – maximum permissible net discharge of the spillway (without bottom outlet).

To be found: H_{\max} – maximum head on the spillway weir (water elevation in the reservoir), B – width of the weir.

Procedure

1) Draw *by free hand* the outflow hydrogram corresponding to the given $q_{2\max}$ and find the temporary storage V_t with the aid of a planimeter, or some other means, Fig. 10.87.

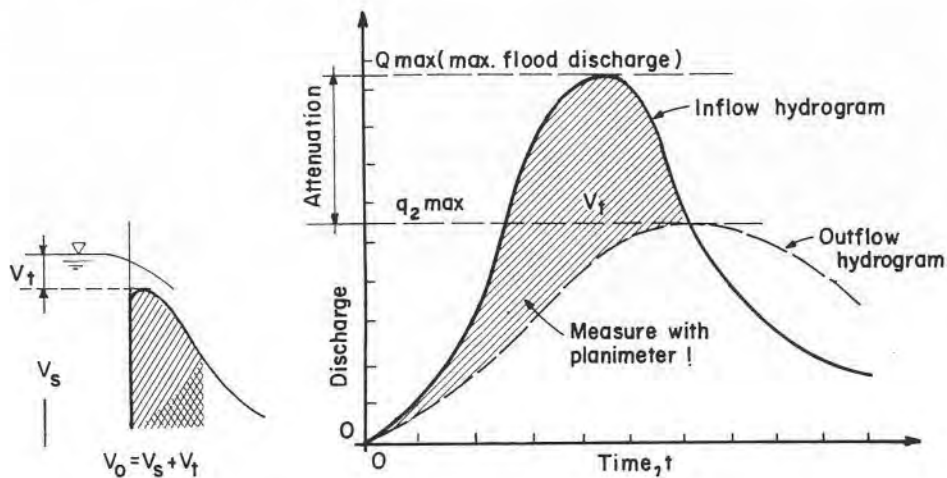


Fig. 10.87. Discharge vs. time curves.

2) From reservoir volume vs. elevation (RVE) curve, Fig. 10.85, find V_s for the assumed crest elevation. Subsequently, compute $V_0 = V_s + V_t$.

3) Again using RVE-curve, find the reservoir elevation corresponding to the obtained V_0 , whence also H_{\max} over the spillway crest.

4) Width of the spillway weir can now be computed from Eq. (10.44),
 $B = q_{2\max} / CH_{\max}^{3/2}$.

3 (b) – Case 2

Given: H_{\max} – maximum permissible head on the spillway crest (maximum reservoir elevation).

To be found: q_{\max} and B .

Procedure

1) Draw by free hand several outflow hydrograms, corresponding to different assumed values of $q_{2\max}$, Fig. 10.88.

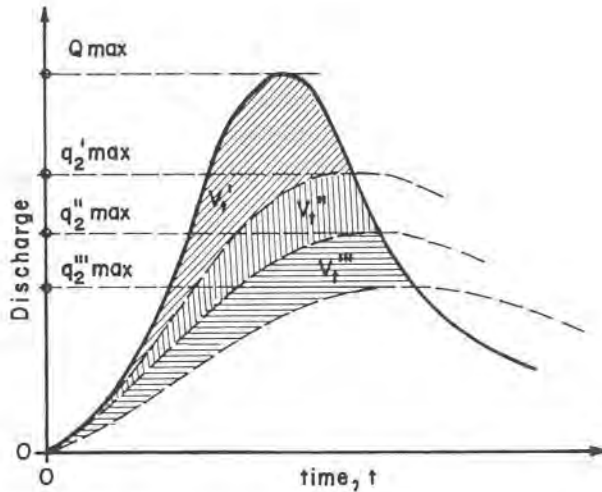


Fig. 10.88. Discharge vs. time curves.

2) For every assumed $q_{2\max}$ measure the corresponding temporary storage V_t (for $q_{2\max} - V_t'$; for $q_{2\max}'' - (V_t' + V_t'')$; for $q_{2\max}''' - (V_t' + V_t'' + V_t''')$, etc.). As before, read from Fig. 10.85 V_s corresponding to the assumed crest elevation, and compute the three matching V_0 values.

3) Now draw the diagram $V_0 = f(q_{2\max})$, Fig. 10.89.

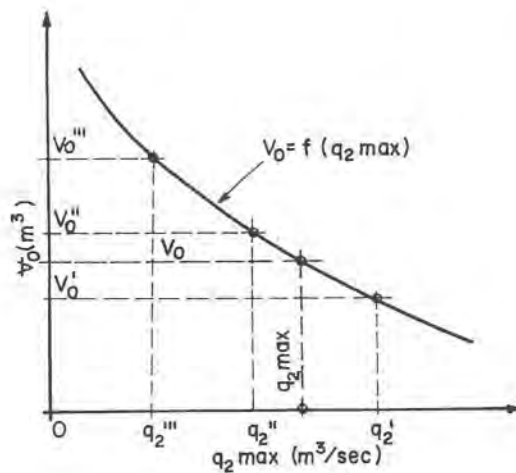


Fig. 10.89. q_2 vs. V_0 curve.

4) From the given H_{\max} and assumed crest elevation, obtain reservoir water elevation; next, from RVE-curve, Fig. 10.85, find the corresponding V_0 and trace it on the graph of Fig. 10.89. Crossing point with curve $V_0 = f(q_{2\max})$ yields the required $q_{2\max}$.

5) Width of the spillway weir is now computed from $B = q_{\max} / CH_{\max}^{3/2}$.

3 (c) – Case 3

Given: B – width of the spillway weir.

To be found: $q_{2\max}$ and H_{\max} , for the assumed crest elevation.

Procedure

Steps 1), 2) and 3) as in Case 2 previously described. The final product of the three steps is $V_0 = f(q_2)$ -curve, as shown on Fig. 10.90.

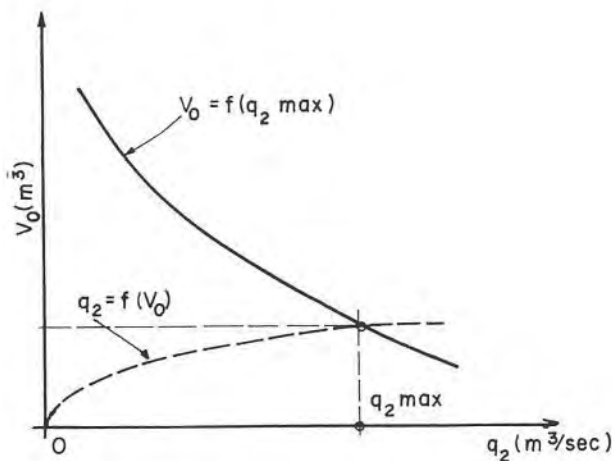


Fig. 10.90. q_2 vs. V_0 curve.

4) On the same diagram trace curve $q_2 = f(V_0)$. This curve can easily be obtained by the aid of some tabulated values, as shown below:

1	2	3
H (m)	V_0 (m ³)	q_2 (m ³ /sec)

In the above table:

Column 1 – values of H are freely assumed within the appropriate range.

Column 2 – corresponding values of V_0 , obtained from RVE-curve, are listed here.

Column 3 – using equation $q_2 = CBH^{3/2}$, values of spillway discharge corresponding to the assumed H -values are listed in this column.

Crossing point between the curve $V_0 = f(q_2)$ and curve $q_2 = f(V_0)$, Fig. 10.90, determines q_{\max} and the corresponding V_0 . In order to obtain H_{\max} , reservoir elevation corresponding to the above determined V_0 is sought on the RVE-curve.

Appendix 2: Basic Mathematical Concepts of Engineering Economy

1. Compound Interest

According to this method of computation, the interest is calculated on the basis of the amount accumulated during the previous period. Be the invested sum P at compound interest of i per year, then after one year the original P will have increased to $P + iP$, and after n years to

$$S = P(1 + i)^n \quad (10.45)$$

If the accumulation is not on a yearly basis as above, but m times a year, then the accumulated sum after n years is given by,

$$S = P \left[1 + \frac{i}{m} \right]^{m \cdot n} \quad (10.46)$$

The question may now be turned around and the present value P be sought that would yield the sum S at the compound interest i after n years. It is given by

$$P = S \frac{1}{(1 + i)^n} \quad (10.47)$$

In Table 10.13–10.18 some numerical values of Eq. (10.45) (column 1) are given for $P = 1$. In column 2 some values of Eq. (10.47) are listed for $S = 1$.

Example 10.10

Find the accumulated value of 1000 invested at compound interest at 5% for 20 years. From Table 10.13, column 1:

$$S = 1000 \times 2.65 = 2,650$$

Example 10.11

An additional stretch of stream-training to be carried out after 5 years is estimated at 1,000,000. Find the present value of the needed investment, if the interest is 10%. Using Table 10.16, column 2:

$$P = 1,000,000 \times 0.621 = 621,000$$

If the cost of the training scheme at the present time is less than the above sum, it may be advantageous to carry out the works today, instead of waiting another 5 years.

2. Annuity

So far only the investment of a single sum P has been considered. The situation changes when instead of a single sum, we consider a series of sums R invested at the end of each year, on a compound interest basis, Fig. 10.91. Required: the sum to which the series of annuities will have grown after n years at the compound interest of i . By the reasoning similar to that adopted before, the sum is obtained as:

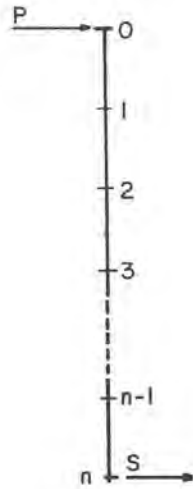
$$S = R [(1 + i)^n - 1/i] \quad (10.48)$$

Some numerical values of Eq. (10.48) for $R = 1$ are given in Tables 10.13–10.18, column 3.

Example 10.12

To cover some future needs, a sum of 10,000 is invested at compound interest of 8% during 30 years. Find the sum to which the fund will have grown. Use Table 10.15, column 3,

1. Eq. 10.45



2. Eq. 10.48

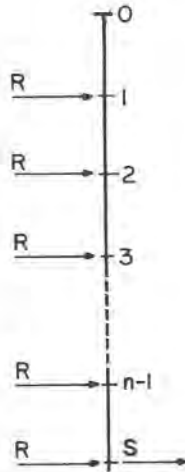


Fig. 10.91. Compound interest, 1) single investment, 2) annuities.

$$S = 10,000 \times 113.3 = 1,133,000$$

The present value of an annuity can easily be found by substituting Eq. (10.47) into Eq. (10.48). At the beginning of the n -year period, the present value is given by:

$$P = R \left[\frac{(1+i)^n - 1}{i(1+i)^n} \right] \tag{10.49}$$

Numerical values of Eq. (10.49) are listed in Tables 10.13–10.18, column 4, for $R = 1$.

Example 10.13

Find the present value of an annuity $R = 5,000$ during 10 years at 12% compound interest (in fact, what sum should be invested at 12% compound interest in order to draw 5,000 each year during the period of 10 years, before the fund is depleted). Using Table 10.17, column 4, it is found

$$P = 5,000 \times 5.65 = 28,250$$

3. Sinking Fund Payment

This is the reverse of Eq. (10.48). Here the annuity R is sought which at a compound interest i will give after n years a sum S . From Eq. (10.48):

$$R = S [i/(1 + i)^n - 1] \quad (10.50)$$

Some numerical values of Eq. (10.50) are to be found in Table 10.13–10.18, column 5, for $S = 100$.

Example 10.14

It is estimated that in 10 years a fund of 1,000,000 has to be provided. Find what should be the annuity into the sinking fund that will yield the above sum at 10% compound interest. Using Table 10.16, column 5,

$$R = 10,000 \times 6.27 = 62,700$$

4. Capital Recovery Factor

This is the reverse of Eq. (10.49), giving the factor that turns the present investment P into a series of equivalent annuities, during n years and at compound interest i ,

$$R = P [i(1 + i)^n / (1 + i)^n - 1] \quad (10.51)$$

Some numerical values of Eq. (10.51) are given in Tables 10.13–10.18, column 6, for $P = 100$.

Example 10.15

Find the annuity that should be invested at the end of each year during 15 years, at a compound interest of $i = 8\%$, in order to recover a present capital investment of $P = 1,000,000$. Using Table 10.15, column 6,

$$R = 10,000 \times 11.68 = 116,800$$

TABLE 10.13

 $i = 5\%$

n	1	2	3	4	5	6
5	1.28	0.783	5.5	4.33	18.10	23.10
10	1.63	0.614	12.6	7.72	7.95	12.95
15	2.08	0.481	21.6	10.38	4.63	9.63
20	2.65	0.377	33.1	12.46	3.02	8.02
25	3.39	0.295	47.7	14.09	2.09	7.09
30	4.32	0.231	66.4	15.37	1.50	6.50
35	5.52	0.181	90.3	16.37	1.11	6.11
40	7.04	0.142	120.8	17.16	0.83	5.83
45	8.98	0.111	159.7	17.77	0.63	5.63
50	11.47	0.087	209.3	18.26	0.48	5.48
60	18.68	0.053	353.6	18.93	0.28	5.28
70	30.43	0.033	588.5	19.34	0.17	5.17
80	49.56	0.020	971.2	19.60	0.10	5.10
90	80.73	0.012	1594.6	19.75	0.06	5.06
100	131.50	0.008	2610.0	19.85	0.04	5.04

TABLE 10.14

 $i = 6\%$

n	1	2	3	4	5	6
5	1.34	0.75	5.6	4.21	17.74	23.74
10	1.79	0.56	13.2	7.36	7.59	13.59
15	2.40	0.42	23.3	9.71	4.30	10.30
20	3.21	0.31	36.8	11.47	2.72	8.72
25	4.29	0.23	54.9	12.78	1.82	7.82
30	5.74	0.17	79.1	13.76	1.26	7.26
35	7.69	0.13	111.4	14.50	0.90	6.90
40	10.28	0.10	154.8	15.05	0.65	6.65
45	13.76	0.07	212.7	15.46	0.47	6.47
50	18.42	0.05	290.3	15.76	0.34	6.34
60	32.99	0.03	533.1	16.16	0.19	6.19
70	59.08	0.02	967.9	16.38	0.10	6.10
80	105.80	0.009	1746.6	16.51	0.06	6.06
90	189.46	0.005	3141.1	16.58	0.03	6.03
100	339.30	0.003	5638.4	16.62	0.02	6.02

 n – period of investment yearsColumn 1 – Eq. (10.45), for $P = 1$ Column 2 – Eq. (10.47), for $S = 1$ Column 3 – Eq. (10.48), for $R = 1$ Column 4 – Eq. (10.49), for $R = 1$ Column 5 – Eq. (10.50), for $S = 100$ Column 6 – Eq. (10.51), for $P = 100$

TABLE 10.15

 $i = 8\%$

n	1	2	3	4	5	6
5	1.47	0.681	5.9	3.99	17.05	25.05
10	2.16	0.463	14.5	6.71	6.90	14.90
15	3.17	0.315	27.2	8.56	3.68	11.68
20	4.66	0.214	45.8	9.82	2.18	10.18
25	6.85	0.146	73.1	10.67	1.37	9.37
30	10.06	0.099	113.3	11.26	0.88	8.88
35	14.78	0.068	172.3	11.65	0.58	8.58
40	21.72	0.046	259.1	11.92	0.39	8.39
45	31.92	0.031	386.5	12.11	0.26	8.26
50	46.90	0.021	573.8	12.23	0.17	8.17
60	101.26	0.010	1253.2	12.38	0.08	8.08
70	218.61	0.005	2720.1	12.44	0.04	8.04
80	471.95	0.002	5886.9	12.47	0.02	8.02

TABLE 10.16

 $i = 10\%$

n	1	2	3	4	5	6
5	1.61	0.621	6.1	3.79	16.38	26.38
10	2.59	0.385	15.9	6.14	6.27	16.27
15	4.18	0.239	31.8	7.61	3.15	13.15
20	6.73	0.149	57.3	8.51	1.75	11.75
25	10.83	0.092	98.3	9.08	1.02	11.02
30	17.45	0.057	164.5	9.43	0.61	10.61
35	28.10	0.036	271.0	9.64	0.37	10.37
40	45.26	0.022	442.6	9.78	0.23	10.23
45	72.89	0.014	718.9	9.86	0.14	10.14
50	117.39	0.008	1163.9	9.91	0.09	10.09
55	189.06	0.005	1880.6	9.95	0.05	10.05
60	304.48	0.003	3034.8	9.97	0.03	10.03
65	490.37	0.002	4893.7	9.98	0.02	10.02
70	789.75	0.001	7887.5	9.99	0.01	10.01

 n – period of investment yearsColumn 1 – Eq. (10.45), for $P = 1$ Column 2 – Eq. (10.47), for $S = 1$ Column 3 – Eq. (10.48), for $R = 1$ Column 4 – Eq. (10.49), for $R = 1$ Column 5 – Eq. (10.50), for $S = 100$ Column 6 – Eq. (10.51), for $P = 100$

TABLE 10.17

 $i = 12\%$

n	1	2	3	4	5	6
5	1.76	0.567	6.3	3.60	15.74	27.74
10	3.10	0.322	17.5	5.65	5.70	17.70
15	5.47	0.183	37.3	6.81	2.68	14.68
20	9.65	0.104	72.0	7.47	1.38	13.39
25	17.00	0.059	133.3	7.84	0.75	12.75
30	29.96	0.033	241.3	8.05	0.41	12.41
35	52.80	0.019	431.7	8.18	0.23	12.23
40	93.05	0.011	767.1	8.24	0.13	12.13
45	163.99	0.006	1358.2	8.28	0.07	12.07
50	289.00	0.003	2400.0	8.30	0.04	12.04

TABLE 10.18

 $i = 15\%$

n	1	2	3	4	5	6
5	2.01	0.497	6.7	3.35	14.832	29.83
10	4.05	0.247	20.3	5.02	4.925	19.92
15	8.14	0.123	47.6	5.85	2.102	17.10
20	16.37	0.061	102.4	6.26	0.976	15.98
25	32.92	0.030	212.8	6.46	0.470	15.47
30	66.21	0.015	434.7	6.57	0.230	15.23
35	133.17	0.007	881.2	6.62	0.113	15.11
40	267.86	0.004	1779.1	6.64	0.056	15.06
45	538.77	0.002	3585.1	6.65	0.028	15.03
50	1083.66	0.001	7217.7	6.66	0.014	15.01

 n — period of investment yearsColumn 1 — Eq. (10.45), for $P = 1$ Column 2 — Eq. (10.47), for $S = 1$ Column 3 — Eq. (10.48), for $R = 1$ Column 4 — Eq. (10.49), for $R = 1$ Column 5 — Eq. (10.50), for $S = 100$ Column 6 — Eq. (10.51), for $P = 100$

References

1. F.M. Henderson, Open Channel Flow, Macmillan, New York, N.Y., 1966.
2. J.F. Friedkin, A laboratory study of the meandering of alluvial rivers, U.S. Waterways Exp. Stat., Vicksburg, 1945.
3. S. Leliavski, An Introduction to Fluvial Hydraulics, Constable & Company, London, 1954.

4. L.B. Leopold and M.G. Wolman, River meanders, *Bul. Geol. Soc. of America*, 71 (1960).
5. M.C. Quick, Mechanism for stream flow meandering, proceedings, ASCE, 100 (HY6) (1974).
6. E. Garev, Lemniscate curves for river training, *Water Planning for Israel*, publication no. 61010, 1968 (in Hebrew with summary in English).
7. G.W. Pickles, *Drainage and Flood Control Engineering*, McGraw-Hill, New York, N.Y., 1961.
8. G.H. Matthes, Mississippi river cutoffs, *Trans. ASCE*, 113 (1948).
9. M.D. Tchertausov, *Gidravlika*, G.E.J., Moscow, 1962.
10. U.S. Corps of Engineers, *Manual of Hydraulic Design Criteria*, Vicksburg, 1961.
11. Maccaferri Reno Mattress, *River and Gabions*, London.
12. V.T. Chow, *Open-Channel Hydraulics*, McGraw-Hill, New York, N.Y., 1959.
13. F.M. Henderson, *Open-Channel Flow*, Macmillan, New York, N.Y., 1966.
14. W.P. Creager and J. Hinds, *Engineering For Dams*, vol. II–III, John Wiley, London, 1950.
15. U.S.B.R., *Design of small dams*, U.S. Dept. of Interior, Water Res. Tech. Pub., Washington, 1977.
16. E. Kuiper, *Water Resources Development*, Butterworths, London, 1965.
17. H.R. Cedergren, *Seepage, Drainage and Flow Nets*, Wiley, New York, N.Y., 1968.
18. N. Cohen, *Spillways and outlet works*, *Water Planning for Israel Ltd.*, EI/70/031, Tel Aviv, 1970.
19. P.Ph. Jansen et al., *Principles of River Engineering*, Pitman, London, 1979.
20. UNESCO, *Development of arid and semi-arid lands*, MAB Techn. notes 6, Paris, 1977.
21. Research Council of Israel, *Desert research, proceedings*, Special publication no. 2, Jerusalem, 1953.
22. Hydrological Service, Water commission, *Hydrological Yearbook of Israel*, yearly edition, Ministry of Agriculture, Jerusalem.
23. UNESCO, *Arid Lands*, E.S. Hills (ed.), Paris, 1966.
24. UNESCO, *Geography of Coastal Deserts*, P. Meigo (ed.), Paris, 1966.
25. L. Shanan and N.H. Tadmor, *Microcatchment Systems for Arid Zone Development*, Hebrew University, Jerusalem, 1976.
26. E.L. Grant, *Principles of Engineering Economy*, Ronald Press, New York, N.Y., 1950.
27. O. Eckstein, *Water Resources Development – The Economics of Project Evaluation*, Harvard University Press, 1958.
28. USBR, *Hydraulic design of stilling basins and energy dissipators*, Eng. Monograph no. 25, Tech. Inf. Branch, Denver, 1958.
29. E. Mayer-Peter and R. Muller, *Formulas for bed-load transport*, proceedings, 3rd Congress, IAHR, Stockholm, 1948.
31. C.C. Calhoun et al., *Performance of plastic filter cloths as a replacement for granular filter materials*, *Highway Res. Record*, no. 373, Washington D.C., 1971.
32. J.J. Franco, *Research for river regulation dike design*, *Jour. Waterways & Harbors Div.*, ASCE, 93 (WW3) (1967).

33. R.J. Garde et al., Scour around spur dikes, Jour. Hydr. Div., ASCE, 91 (HY6) (1961).
34. H.W. Shen et al., Mechanisms of local scour, Colorado State University, Fort Collins, Eng. Res. Center, report no. CER66 HWS22, 1966.
35. A.M. Gill, Erosion of sand beds around spur dikes, ASCE, Jour. Hydr. Div., 98 (HY9) (1972).
36. R.P. Apmann and P.H. Blinco, Experiences with bed sills in stream stabilization, ASCE, Journal (WW3) (1969).
37. H.K. Lin et al., Effect of bridge construction on scour and backwater, Dept. Civil Eng., Colorado State University, Res. no. CER604, KL22, 1961.
38. D.B. Simons and F. Sentürk, Sediment transport technology, Water Resources Publ., Fort Collins, Colorado, 1977.
39. P. Novak and J. Cabelka, Models in Hydraulic Engineering, Pitman, London, 1981.
40. H.W. Shen, editor, Modelling of Rivers, Wiley, New York, N.Y., 1979.
41. J. Larras, Profondeurs maximales d'érosion des fonds mobiles autour des piles en rivières, Annale des Ponts et Chaussées, 33 (4) (1963).
42. H.N.C. Breusers, Scour around drilling platforms, Bulletin Hydr. Res. 1964 & 1965, IAHR, 19 (1956).
43. R.J. Garde and K.G. Ranga Raju, Mechanics of Sediment Transportation and Alluvial Stream Problems, Wiley Eastern, New Delhi, 1978.

CHAPTER 11

STREAM OUTLETS

11.1 Introduction

In order to keep the present manual within a reasonable size, it has been necessary to refrain as far as possible from discussion of hydraulic structures in all but the most general of their aspects. Any attempt to include such topics in the text would probably require a separate volume by itself, much more on the side of a general textbook on hydraulic structures than surface drainage proper. It is felt, furthermore, that on the subject of hydraulic structures there is currently available a vast amount of technical literature and specific monographs, covering practically all of its many engineering aspects.

The question of outlets into stream channels has in fact already been discussed in at least two of the previous paragraphs: in par. 3.7, dealing with stream confluences, and par. 10.3.9.5, in which the drainage of the flood plain has been examined. In both cases, a generally smaller water conduit, either a natural stream, an artificial channel or a pipe, deliver their waters at some point into a larger watercourse, often designated as a *recipient*. It is further assumed that the water discharge of the tributary channel and its sediment load are of some significant magnitude in relation to the main stream. Since confluence of natural streams has already been extensively discussed, in the present chapter only some additional features bearing on artificial-channel outlets and closed conduits will be further reviewed. The terminology here adopted is in respect to the tributary conduit, since in respect to the recipient the same structure operates as an inlet.

Outlets into stream channels may produce various engineering problems, such as local scour, deposition, clogging, backwater effect, etc. In most of the cases these phenomena can be kept under control, if not completely

eliminated, by careful design and location of the outlet structures. The essential requisite for an appropriate engineering solution is a good knowledge and understanding, among many other factors, of the prevailing sediment, hydraulic and bank-stability conditions in the recipient and secondary conduit.

In addition to the basic design principles already mentioned in the previous chapters, in the following a few more aspects will be briefly discussed.

11.2 Open-Channel Outlets

Engineering problems that may arise as a result of open-channel outlets into streams are of similar kind for both natural-channel outlets (actually stream confluences) or man-made open conduits.

The water discharged into the main stream through the outlet as a rule carries its own sediment load, which is added to the existing load of the main stream. Point of entrance, therefore, should be chosen in such a way that probable negative effects be kept as restricted as possible. As shown in Chapter 3, along the concave bank of a meandering stream the transverse current steeply dips downward until it reaches the eroded bed, and then is deflected again toward the convex bank, where it deposits the sediment picked up or eroded on the opposite (concave) bank. Since it is essential for the proper operation of the outlet to keep it unobstructed and to clear away as quickly as possible the incoming sediment load, it should always be located at some point along the concave bank of the stream. The best position is generally considered some point slightly downward from the maximum curvature of the meander, but not shifted too far downstream to enter the more or less straight crossing between two subsequent meanders, and under no circumstance to reach the convex bank of the next meander, Fig. 11.1. If necessary, relocation of the incoming channel to meet these requirements, although increasing the capital cost of the works, will in the long run always prove to be a sound and advantageous decision, Fig. 11.2. Whenever warranted by the circumstances, the concave bank in the vicinity of the outlet structure should be protected against the local scouring action of the transverse current.

Relocation of the channel is not always feasible, either because impracticable for engineering reasons (topographical or geological difficulties, residential or industrial areas, etc.) or economic considerations. In such cases

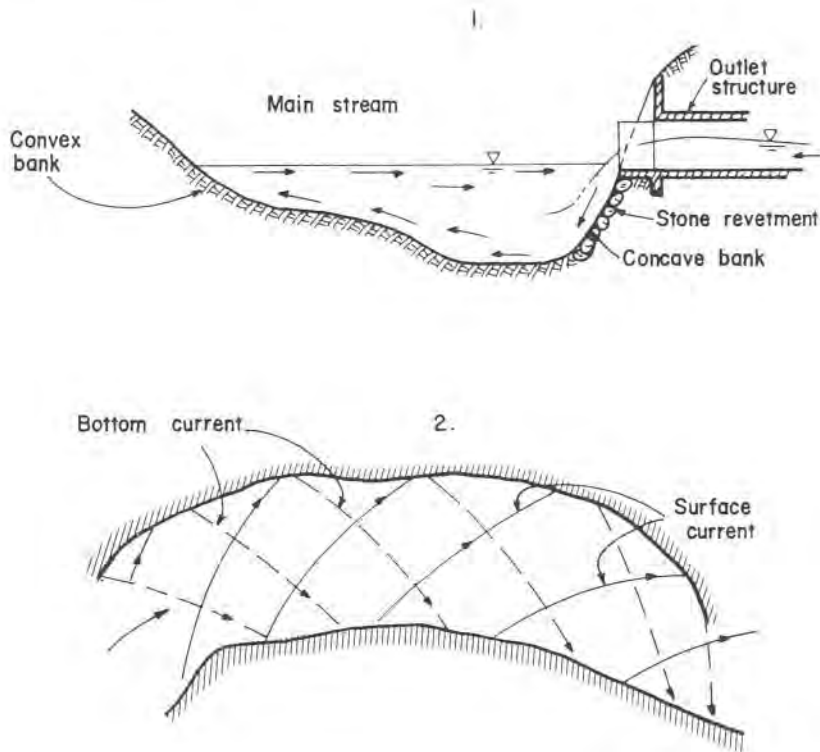


Fig. 11.1. 1) Location of outlet into-stream, 2) Schematic drawing of helical current in a stream bend.

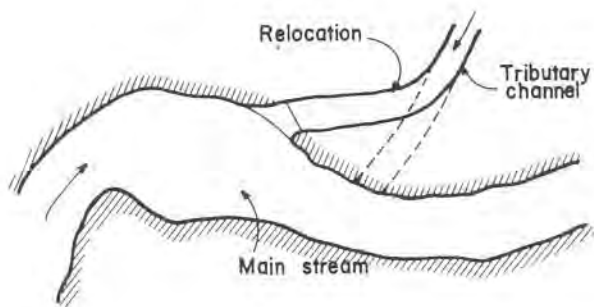


Fig. 11.2. Relocation of the channel.

channel outlet will have to be located at some point where strong sediment deposition and not enough sediment entrainment are to be expected. No engineering device is likely to appreciably improve the situation, and certainly not on a permanent basis. Low submerged deflection groynes immediately upstream of the outlet are sometimes used in order to keep the area in front of the outlet free of clogging, but their efficacy is somewhat questionable, and anyway could be only of a temporary nature because of sediment deposition behind them. Frequent dredging of the accumulated sediment is essential in such cases, and it is probably the most efficient way, though certainly not the most elegant one, to deal with the problem.

The angle between the axis of the tributary channel and the tangent to the axis of the main watercourse (see Fig. 11.3) no doubt can have considerable influence on the hydraulic, and hence also sedimentation performance of a given outlet. The optimum angle from the engineering point of view depends on many parameters, but unfortunately their functional relationship cannot be mathematically expressed, as is generally the case when sedimentation phenomena are concerned. Some of these parameters that influence the deflection of flow lines in the main stream and configuration of its flow, are:

1. Water-surface profile in the tributary channel upstream of the outlet, whether it is a drawdown or backwater curve. This depends on the relative bottom elevations of the two channels in the first place, but clearly also on the respective discharges, which as a rule may vary within a wide range.
2. Alluvial channel geometry of the main stream in the vicinity of the outlet, because it may to a considerable extent affect the velocity distribution, and therefore the resultant flow pattern of the combined flow downstream of the outlet.
3. Total bed roughness of the recipient stream, in which both the grain and form (ripples, dunes, etc.) roughnesses are included, may also affect the vertical velocity distribution, and hence the division and movement of the combined bed-material load.
4. Direction of the entering stream may influence the sediment transporting capacity of the main stream in the neighbourhood of the outlet, especially when the sediment load entering from the tributary channel is high. Changes and deflections in the established flow pattern are possible.

An angle of $\alpha \leq \sim 30^\circ$ is recommended whenever feasible from the engineering point of view.

Local bank scour in the recipient channel opposite to the outlet, especially in relatively narrow main streams, is of frequent occurrence. This is due to the local deflection of flow toward the opposite bank, particularly

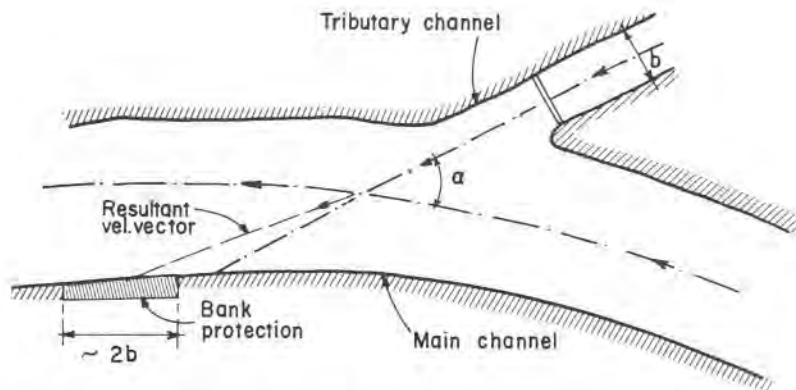


Fig. 11.3. Protection of the opposite bank.

during low stages of flow in the recipient. In severe cases such scour may even disturb the natural meandering pattern of the main stream, ultimately causing unexpected alterations also along the bank where the outlet is situated. When the discharge from the tributary is frequently of the same order of magnitude as in the recipient, partial protection of the opposite bank may be necessary, Fig. 11.3. The centre point of the protective revetment is obtained by taking the resultant of the maximum expected velocity vector of the tributary flow and the low-discharge velocity vector of the recipient. The overall length of the protective revetment may be taken as twice the top width of the tributary channel. The choice of the protective revetment depends on the degree of the expected erosive forces: in mild cases, a simple but sturdy grass cover (see Vol. I, Part 2, Chapter 2) will do; when stronger erosive action is foreseen, more elaborate methods may be called for (see par. 10.3.8 and the following).

In cases where back-erosion (see par. 3.7) in the tributary channel is feared, a drop structure at the inlet into the main stream is often an adequate solution, Fig. 11.4. Hydraulic design of drop structures has been given in Volume I of the present Manual, and some engineering features have been discussed in par. 10.3.5 in connection with stream-training works. The drop structure itself and the adjacent stilling basin should be located inside the tributary channel. When the elevation of the tributary channel in respect to the main stream is such that a single hydraulic drop would be excessively high, a series of smaller drops (a "cascade") within the tributary channel can be made instead (see Fig. 10.15). At very high flows in the tributary,

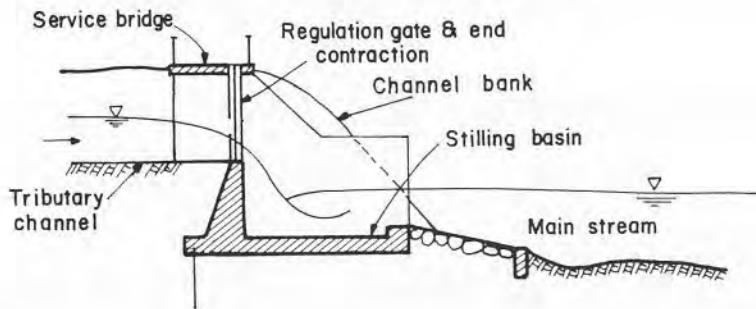


Fig. 11.4. Drop structure at the outlet into the main stream.

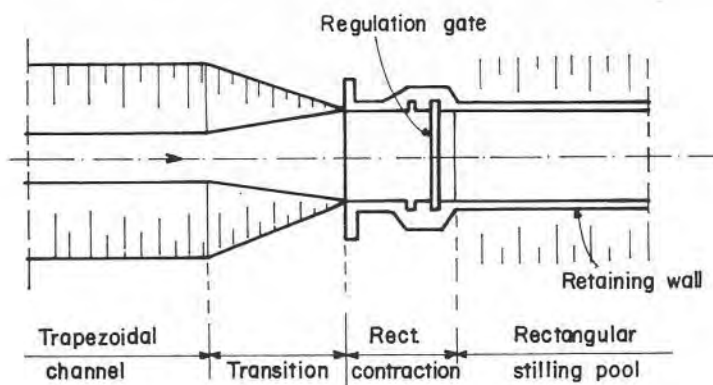


Fig. 11.5. Rectangular concrete contraction.

however, such a system may become ineffective, and an appropriate energy dissipation structure has to be provided in continuation of the end drop.

As already mentioned in par. 10.3.5, drawdown curve which develops upstream of any dydraulic drop structure is liable to cause erosion problems in the tributary channel. The eroded material, furthermore, will end up in the recipient channel, thus possibly causing even more problems. End-contractions at the brink of the drop have given ample evidence of being an effective measure to considerably shorten the drawdown curve, and in this way significantly reduce the upstream erosion problems. The two most frequently used types of end-contractions are:

1. *Rectangular concrete contraction*, Fig. 11.5. It is no doubt hydraulically the better of the two alternatives, yet also the more expensive

one, since it requires a transition section and retaining walls along the rectangular channel of the contraction itself and the stilling pool downstream. If a regulation gate is to be provided, it can easily be located within the rectangular channel, and there are suitable supports for a servicing or field-passage bridge. Rectangular stilling pool is an efficient energy-dissipation device.

2. *End-still in trapezoidal channel, Fig. 11.6.* This is obviously a cheaper solution, since it does not require extensive longitudinal retaining walls. It is usually made in conjunction with a trapezoidal stilling pool, which is often subjected to hydraulically unstable conditions, [1, 2]. The channel immediately upstream of the sill should be protected by stone paving for a length of at least 4–5 times the critical depth. To reduce the silting upstream of the sill, one or more drainage openings should be provided, which also serve for the emptying of the water after the flow has stopped. Regulation-gate arrangement, when required, is more difficult, and hence more costly, and similarly also the servicing bridge.

Hydraulic computation of end-contractions is reviewed in Appendix 1 to the present chapter.

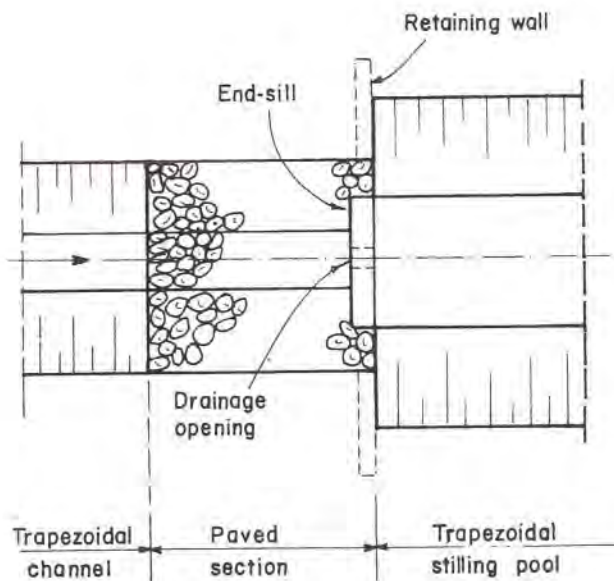


Fig. 11.6. End-sill in trapezoidal channels.

Sedimentation problems in the main stream likely to arise when the tributary channel carries flows of significant magnitude as compared to flows in the recipient stream, with relatively large sediment load, have already been extensively discussed in par. 3.7. In some cases a coarse-sediment trap in the tributary channel, at some suitable location upstream of the outlet, may be necessary if serious sedimentation problems in the main stream are anticipated. Such a sediment trap may be constructed either on the channel itself (see par. 10.3.7, Fig. 10.20, and Example 10.5), or in the close vicinity by means of a diversion channel.

In recent years there has been a constant increase in channel outlets pouring into recipient streams scarcely treated sewage effluents or toxic industrial wastes. Deposition of such materials in the vicinity of outlets or farther downstream, particularly at low water stages, is bound to cause not only engineering problems, but often severe sanitary problems as well and public concern. Sludge deposits will eventually form anaerobic sublayers producing malodorous gases, such as H_2S . Industrial waste products and agricultural runoff, on the other hand, besides toxic materials often contained in them, may substantially increase the quantity of nitrogenous and similar matter in the main stream, such as nitrogen and phosphorous compounds, thus further increasing the BOD (biochemical oxygen demand) required to be supplied by the stream waters. This process, together with the algal growth due to the influx of organic nutrients, may significantly contribute to the eutrophication process of the recipient-stream waters. All the above-mentioned biochemical processes which tend to increase the BOD in the main stream, are likely to be particularly strong in warm-climate regions, where the stream water often reaches the optimum temperature for the biochemical reactions (25° – $28^{\circ}C$) and at the same time conditions unfavourable for the absorption of atmospheric oxygen.

11.3 Closed-Conduit Outlets

Engineering aspects of such outlets depend largely on their position in respect to the water level in the recipient stream. When the position of the conduit is such that at no time but the very low-probability events the water level in the stream is likely to submerge the outlet, the main concern will be local scour caused by the falling water directly on the channel bank, or on relatively shallow water layer in the stream. In order to prevent free outfall of water directly on the channel bank at lower stream stages, the conduit

should often be extended beyond the bank line and into the stream channel proper for a considerable distance. This requires either a special support structure or a cantilevered section capable of withstanding the stresses and forces caused by the overturning moment, Fig. 11.7. In the latter case, the jutting-out portion of the conduit together with the anchored part will have to be made out of steel or light-weight corrugated iron.

When any of these solutions is not feasible, and the water jet from the outlet cannot be prevented from directly falling on the earth bank of the stream channel, stone revetment should be provided, Fig. 11.8.

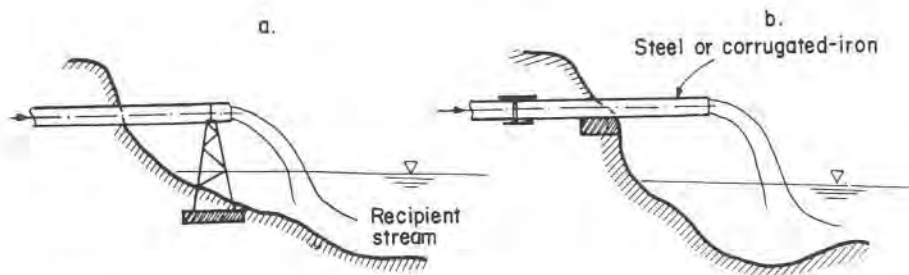


Fig. 11.7. Pipe outlet, a) with a support, b) with a cantilevered section.

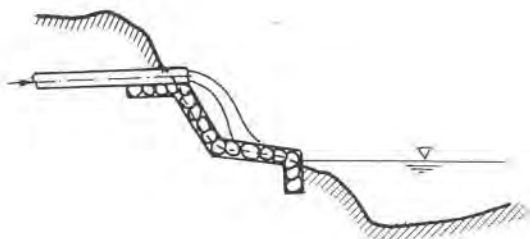


Fig. 11.8. Stone revetment of the main channel bank.

If there is no way to avoid placing the outlet pipe low enough to be periodically submerged at higher water stages in the recipient stream, its carrying capacity may be greatly reduced, and in some cases even a reverse hydraulic gradient may develop, forcing the stream water into the outlet pipe. Low-head agricultural drainage and sewage mains are particularly susceptible to this latter possibility.

On small pipe outlets, a simple solution is attaching a flap gate at the stream-side end of the pipe, Fig. 11.9. At normal and low stages, the effluent flows freely into the stream, while at higher stages the gate is held shut by higher head on the stream-side of the outlet. The main drawback of any flap-gate or similar arrangement is that it is difficult, if not outright impossible, to keep them unhampered by the floating debris. If the gate closure is only partial, its function may be lost to a great extent.

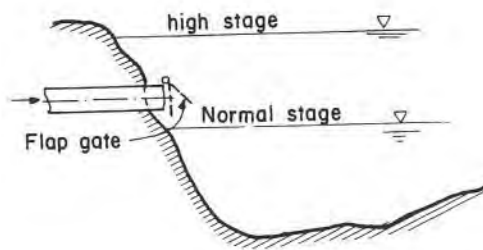


Fig. 11.9. Pipe outlet with flap gate.

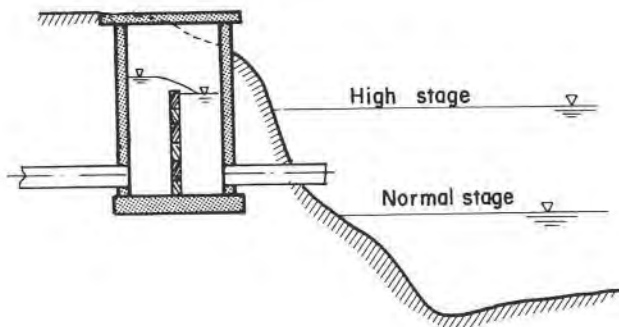


Fig. 11.10. Control structure at the pipe outlet.

When the available hydraulic head in the pipeline is large enough to secure streamward flow even at higher stages, a temporary reduction of the carrying capacity may be tolerable, but the back-flow of the stream water into the pipeline inadmissible. A control structure with an adjustable partition gate will prevent the stream water from penetrating into the pipeline, while allowing the backed up effluent to slowly drain into the stream, Fig. 11.10.

In cases of low-lying sewage lines draining into streams, backing-up of the effluent and stream water may cause highly objectionable consequences bearing on human suffering and sanitary conditions. Complete shut-down of the stream outlet main may then be a mandatory engineering measure, coupled with the pumping of the effluent into the stream, or some temporary storage.

As far as the location along the main stream of large pipe outlets is concerned, the same rules apply as for channel outlets previously discussed. For small pipes and negligible outflows in respect to the recipient stream, the vertical positioning is usually of much more importance.

Appendix 1. Hydraulic Computation of End Contraction in Drop Structures

1. Rectangular Contraction, (Fig. 11.5)

Specific-energy level in the trapezoidal channel is given as E_n . Energy loss along the transition to rectangular section is assumed to be about 10%, but more accurate calculation can be made at the final stage. Hence the energy level at the entrance to the rectangular section is $\sim 0.9 E_n$, and the critical depth:

$$d_{cr} = \frac{2}{3} E \cong \frac{2}{3} (0.9 E_n) \quad (11.1)$$

Further, for a rectangular section,

$$d_{cr} = \left[\frac{Q^2}{b^2 \cdot g} \right]^{1/3} \quad (11.2)$$

and from here

$$b = \left[\frac{Q^2}{d_{cr}^3 \cdot g} \right]^{1/2} \quad (11.3)$$

Example 1

In order to prevent erosion in a tributary channel with a hydraulic drop-structure, a rectangular end-contraction is to be designed for the discharge of $Q = 10 \text{ m}^3/\text{sec}$.

The data for the trapezoidal earth channel are as follows:

Longitudinal slope, $I = 0.3\%$

Bottom width, $b = 2.5 \text{ m}$

Bank slope, $m = 2$

Manning roughness coefficient, $n = 0.025$

Using Manning's equation, normal depth is obtained as $d_n = 2.0 \text{ m}$, and the corresponding wetted area $A = 13.0 \text{ m}^2$. Specific energy is next computed:

$$E_n = 2.0 + 10^2/13.0^2 \cdot 2g \cong 2.03 \text{ m}$$

Energy at the entrance to the rectangular contraction is accordingly assumed to be about $0.9 \times 2.03 \cong 1.83 \text{ m}$.

Hence, the critical depth for the rectangular section (Eq. 11.1):

$$d_{cr} = 2/3 \times 1.83 = 1.22 \text{ m},$$

and finally the required width of the same section (Eq. 11.3):

$$b = \left[\frac{Q^2}{d_{cr}^3 \cdot g} \right]^{1/2} = \left[\frac{100}{1.22^3 \times 9.8} \right]^{1/2} \cong 2.4 \text{ m}$$

Accordingly, the channel bed will be slightly converging along the transition from the trapezoidal to rectangular cross-section, Fig. 11.5. Since the transition is a converging one, it can be made relatively short – say 4 to 5 meters length. The length of the rectangular section is generally made about 2 to 3 times the critical depth, in our case 2.5 to 3.0 m. This allows for a service bridge spanning the rectangular concrete channel.

The design discharge for the end-contraction should be carefully chosen, especially if the tributary channel is a natural stream. It should be the discharge most likely to cause extensive damage to the channel, since for all lower rates of flow the efficiency of the contraction is bound to be much reduced, while for rates higher than the design flow, the contraction will cause some backwater effect. For the given channel, this point is clearly evident from the graph on Fig. 11.11, representing the optimum width of the rectangular contraction as function of discharge.

2. End-Sill in Trapezoidal Channels, (Fig. 11.6)

As previously mentioned, when for economy reasons rectangular end-contraction is not possible, an end-sill in the trapezoidal section will also shorten the drawdown curve caused by the drop.

The hydraulic computation of the required height of the sill is more laborious, and it can be carried out either by a trial-and-error or a graphical method.

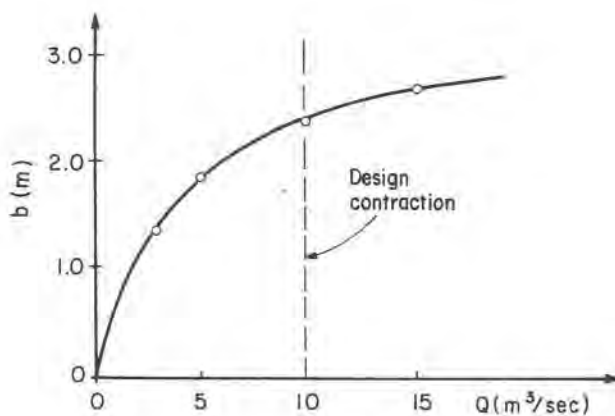


Fig. 11.11. Rectangular contraction width vs. discharge.

2.1 Trial-and-Error Procedure

A sketch of the end section with sill is shown in Fig. 11.12. The trial-and-error procedure of computation is as follows:

Step 1 – A sill height z is arbitrarily assumed.

Step 2 – Using the general equation for critical flow

$$Q^2/g = A^3/B, \quad (11.4)$$

critical depth d_{cr} is computed by trial-and-error.

Step 3 – Compute the kinetic energy $V^2/2g$.

Step 4 – Available net flow energy is obtained from the given energy level in the channel E_n (uniform flow) minus the estimated losses. These can be assumed to be about 5%.

Check point:

Verify whether the energy level obtained is reasonably equal to the available energy $(z + d_{cr} + V^2/2g) \approx 0.95 E_n$. If this is the case, the assumed height of the sill is to be retained and the computation is finished; if not, another value for z is assumed, and steps 1 to 3 are repeated. The procedure is carried on until equality of energy levels is achieved.

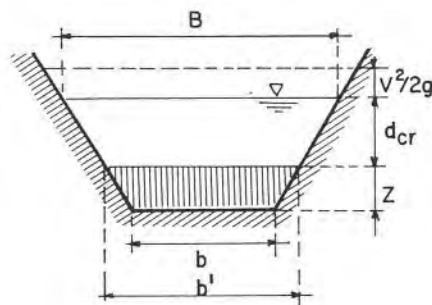


Fig. 11.12. Sketch of end sill in trapezoidal section.

Example 2

Given the same trapezoidal channel as in Example 1. Normal depth $h_n = 2.0$ m, specific energy $E_n = 2.03$ m, net energy at contraction $E = 0.95 E_n = 1.93$ m.

Results of the trial-and-error computations are summarized in Table 11.1. Hence the required height of the end-sill is 1.15 m above the channel bottom.

2.2 Graphical Method

This method is explained with reference to the graphs in Fig. 11.13.

Step 1 – Three arbitrary values for sill height (z_1, z_2 and z_3) are taken, and for each one of these values three arbitrary values for the critical depth d_{cr} are assumed.

Step 2 – For each set of z and d_{cr} values, the expression A^3/B is evaluated, and thus three curves are drawn on the left side of the diagram giving A^3/B vs. $(z + d_{cr})$.

TABLE 11.1. TRIAL-AND-ERROR CALCUATIONS (Ex. 2)

1	2	3	4	5	6	7	8	9
0.5	4.5	0.71	10.1	10.2	0.29	1.50	1.93	Repeat
0.8	5.7	0.63	10.2	10.2	0.27	1.70	1.93	Repeat
1.0	6.5	0.58	10.0	10.2	0.25	1.83	1.93	Repeat
1.15	7.1	0.55	10.0	10.2	0.25	1.95	1.93	O.K

Column 1 – assumed height of the sill, z (m)
 Column 2 – width at the top of the sill, b' (m)
 Column 3 – computed critical depth, d_{cr} (m)
 Column 4 – computed values of A^3/B (m^5)
 Column 5 – value of Q^2/g (m^5)
 Column 6 – kinetic energy, $V^2/2g$ (m)
 Column 7 – $z + d_{cr} + V^2/2g$ (m)
 Column 8 – given specific energy, E (m)
 Column 9 – final state of computation

Step 3 – Compute Q^2/g and draw a perpendicular at the appropriate point on the graph crossing the three curves previously drawn. The three intersection points determine the correct d_{cr} -values for the three assumed z -values.

Step 4 – By means of horizontal lines, the three intersection points 1, 2, and 3 are transferred to the right side of the diagram with coordinates z and $(z + d_{cr})$.

Step 5 – Draw perpendiculars to the z -values according to the assumed ones in Step 1.

Step 6 – Intersection points between the horizontals drawn in Step 4 and perpendiculars of Step 5 determine the $(z + d_{cr})$ -curve.

Step 7 – To this curve at each intersection point the value of $V_c^2/2g = A/2B$ is added.

Step 8 – Draw the total-energy curve passing through the three points obtained in Step 7.

Step 9 – On the ordinate axis the given value of the available energy is marked.

Step 10 – From the intersection point between the horizontal starting from the available-energy point as marked on the ordinate axis in Step 9, and the total-energy curve obtained in Step 8, a perpendicular is drawn to the abscissa. This intersection point renders the required height of the sill, z .

Example 3

All the data as in Example 2. The auxiliary calculations needed for the drawing of different curves are summarized in Table 11.2.

The curves for the given channel are all shown in Fig. 11.13. The intersection point according to Step 10 gives the required height of the sill – $z = 1.15$ m.

As previously mentioned, judicious choice of the design discharge here also is of great importance. For rates of flow lower than the design discharge, there will be some backwater effect, whereas at higher flows, the effectiveness of the sill will be diminished.

TABLE 11.2. AUXILLIARY VALUES (Ex. 3)

z (m)	d_{cr} (m)	A^3/B (m^5)	$z + d_{cr}$ (m)	$V^2/2g$ (m)
0.4	0.6	4.9	1.0	0.29
	0.8	13.0	1.2	
	1.0	28.0	1.4	
0.7	0.6	7.7	1.3	0.27
	0.8	19.8	1.5	
	1.0	41.8	1.7	
1.1	0.6	12.5	1.7	0.25
	0.8	31.1	1.9	
	1.0	64.7	2.1	

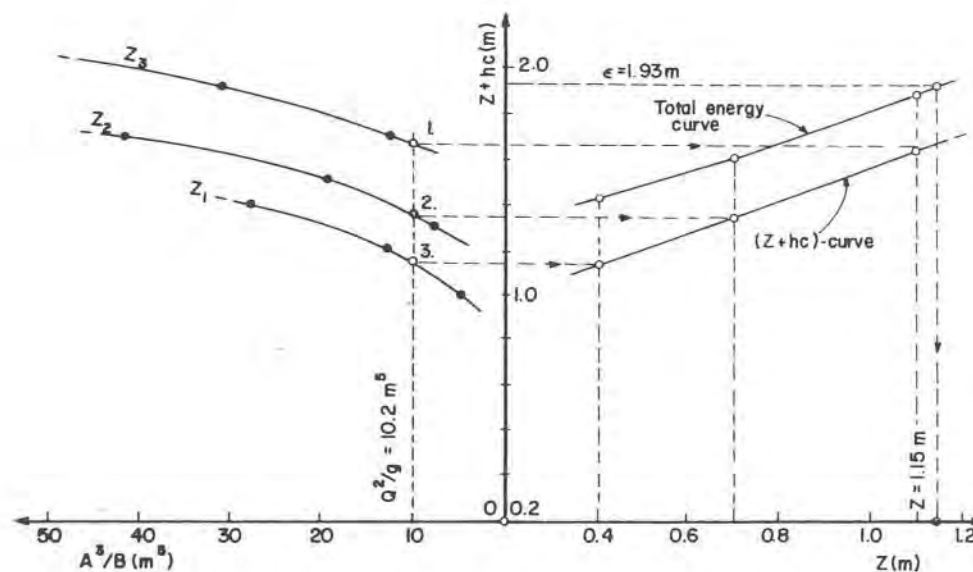


Fig. 11.13. Graphical determination of the end sill.

References

1. E.A. Elevatorski, Hydraulic Energy Dissipators, McGraw-Hill, New York, N.Y., 1959.
2. K.A. Senshina, Gidravlicheski prizhok v ruslakh trapezoidalnevo sechenia, Gidrotehnika i meljorazija, no. 8, 1958.
3. B.A. Witton, River Ecology, Studies in Ecology, vol. 2, Blackwell Science Publications, London, 1975.

Name Index

- Abdel-Aaal, 185, 263
Ackers, P., 86, 127, 129, 151
Albertson, M.L., 155–157, 158, 159, 163
Anderson, A.G., 128, 129
Antsyferov, S.M., 266
A.S.M.A., 40
- Bagnold, R.A., 266, 315
Bajorunas, L., 225
Barbarossa, 223, 231
Bathurst, J.C., 114, 117
Benedict, P.C., 73
Benson, M.A., 59
Benson, R.W., 129
Blench, T., 135, 136, 140, 144, 150, 164
Bogardi, J.L., 235, 281
Bordas, M., 152
Borland, W.M., 272
Bos, M.G., 53
Brahms, A., 276
Breusers, H.N.C., 425, 427
Brooks, N.H., 184, 225, 233, 249, 252, 312
Bull, W.B., 102
- Cabelka, J., 438
Calhoun, C.C., 380
Carlson, E.J., 212
Carter, R.W., 41
Cedergren, H.R., 385
Chang, C.L., 249
Charlton, F.G., 42, 45, 59, 86, 127, 129, 151
Chatou, Centre R., 44
Cheong, H.F., 314
Chien, W., 207
Chow, V.T., 4, 15, 53, 84, 383
CIRIA, 30, 39, 42, 48, 49
- Cohen, N., 434, 445, 482
Coleman, N.L., 186
Creager, W.P., 385
Crickmore, U.J., 74
Culbertson, J.K., 234
- David, H., 56
Davis, R., 105
Debski, K., 72
De Vries, M., 83, 316
Dowdy, D.R., 103, 234
Du Boys, P., 291
Dumas, H., 41
- Eckstein, E.M., 480
Einstein, H.A., 135, 175, 185, 207, 223, 231, 241, 249, 263, 274, 302
Elevatorski, E.A., 503
Engel, P., 219
Engelund, E., 120, 235, 316
- Forchheimer, P., 276
Fortier, S., 276
Franco, J.J., 402, 406
Friedlin, J.F., 151, 343
- Garde, R.J., 276, 284, 402, 404, 425
Garev, E., 359
Gill, A.M., 403
Gils, H., 44
Gladki, H., 236
Goncharov, V.N., 276, 284
Gonzales, D.D., 73
Gottlieb, L., 116
Grant, E.L., 480
Gray, D.M., 23

- Hansen, E., 129, 316
 Hayes, F.C., 40
 Henderson, F.M., 232, 342, 383
 Hinds, J., 385
 Hjulstrom, F., 285
 Hubbel, D.W., 73, 74
 Huges, W.C., 84

 Indri, G., 277
 Inglis, C.C., 129, 135
 I.S.O., 35, 42, 46, 74
 Itakura, T., 248

 Jarocki, W., 313

 Kalinske, A.A., 248, 315
 Karaki, S., 73, 86, 118, 119
 Kennedy, J.F., 219, 220, 235, 236, 315
 Keulegan, G.H., 175, 212
 Kikkawa, H., 116
 Kinosita, T., 45
 Kishi, T., 248
 Kornitz, D., 64
 Kos'yan, R.D., 266
 Krone, R.R., 211
 Kuiper, E., 87

 Lacey, G., 135
 Lane, E.W., 124, 125, 157, 212, 272, 281
 Larras, J., 424, 427
 Laudermilk, W., 453
 Lavelle, J.W., 207
 Leliavski, S., 127, 343
 Leopold, L.B., 129, 136, 153–155, 434
 Levi, J.J., 283
 Lin, H.K., 366, 404
 Lindley, E.S., 135
 Linsley, R.K., 4, 10, 15

 Maddock, T., 153–155
 Mamdouh, A.N., 117
 Manning, R., 79, 93, 119
 Matthes, G.H., 361
 Mercer, A.G., 235
 Meyer-Peter, E., 212, 289, 413
 Mikhailova, N.A., 266
 Miller, T.K., 96
 Morisowa, M., 103
 Mueller, R., 212, 289, 413
 Murphy, P.J., 272

 Nedeco, 23, 35, 37, 40, 65, 68, 263

 Neill, C.R., 276, 284
 Nemeč, J., 10, 23
 Nikuradse, J., 171, 173, 174
 Nixon, M., 136
 Nordin, C.F., 74
 Novak, P., 438

 Onesti, L.J., 96

 Pica, M., 315
 Pickles, G.W., 359
 Poreh, M., 273
 Prandtl, L., 171, 245
 Prins, J.E., 316

 Quick, M.C., 343

 Ranga Raju, K.G., 425
 Rathburn, R.E., 74
 Raudkivi, A.J., 4, 219
 Richards, B.D., 7, 8, 18
 Richardson, E.V., 217, 219, 233, 313
 Rouse, H., 182, 245
 Rozovski, J.L., 116
 Rubey, W.W., 203

 Scheidegger, A.E., 274
 Schlichting, H., 171
 Schoklitsch, A., 277, 287
 Schultz, E.F., 206
 Schumm, S.A., 96, 153
 Scobey, F.C., 276
 Seginer, I., 71, 273
 Semjonov, V.I., 56
 Senshina, K.A., 503
 Sentuerk, F., 234, 425
 Shahjahan, M., 152, 153
 Shanani, L., 454
 Shen, H.W., 236, 314, 318, 403, 423, 438
 Shields, A., 79, 277
 Shulits, S., 20, 286, 294, 295
 Simons, D.B., 79, 155–157, 159, 161,
 163, 217, 219, 221, 233, 313, 425
 Skovgaard, O., 120
 Sony, J.P., 83
 Stokes, G., 199
 Straub, L.G., 291

 Tadmor, N.H., 454
 Tchertausov, M.D., 364
 Thacker, W.C., 207
 Toffaleti, F.B., 318

- Tonini, D., 21
Troskolanski, A.T., 40
- Van den Berg, J., 316
Vanoni, V.A., 184, 225, 233, 241, 247,
251, 274, 312
Veiga de Cunha, 236
Velikanov, M.A., 266
Vid, V.E., 56
- White, C.M., 281
Willis, J.C., 236, 315
Wilson, E.M., 7
Wolman, M.G., 129, 136, 153, 343
- Zagustin, K., 187
Zayc, R., 33
Zeller, J., 129, 153, 272
- Yalin, M.S., 315

Subject Index

- Aggradation, 83
 - main parameters, 340–341
- Alluvium, 78
- Alluvial cones, 100–103
 - formation stages, 101
- Alluvial fans, 100–103
 - see also* arid and semiarid zones
- Alluvial processes,
 - downstream of dams, 437–438
- Antidunes, 220–221
 - see also* bed forms
- Arid and semiarid zones,
 - alluvial fans, 457–458
 - definition, 453–457
 - economic considerations, 466
 - ephemeral streams, 452, 462–465
 - flood protection works, 462–471
 - flow patterns, 460–462
 - sealing crust formation, 459
 - sediment content, 465
- Back erosion, 91, 109
- Backwater effect, 83, 368
 - at bifurcation, 111
 - at channel confluence, 107
 - at channel curves, 117
- Bank protection,
 - see* stream-training works
- Bed configuration prediction, 235
- Bed forms, 216–222
 - in mountain streams, 236
- Bed form roughness,
 - see* roughness
- Bed level measurement,
 - sounding rod, 34
 - lead line, 34
 - echo sounding, 35–36
- Bed load,
 - criteria for quantitative evaluation, 273–274
 - definition, 84, 241
 - transport, *see* sediment transport
- Bed material gradation, 19
- Bed transition regime, 219
- Bends,
 - see* flow in channel curves
- Berms in earth channels, 385
- Bifurcation, 110
- Bottom sills, 367
- Braided channels, 124–125
- Bridge piers,
 - local scour, 423–428
- Catchment area,
 - see* watershed
- Centrifugal and centripetal forces, 111
- Channel,
 - flow, 6, 16
 - rectification, 359–361
- Check dams, 366
- Chezy coefficient, 118
 - influence of sediment, 186–187
- Concentration,
 - point of, 5
 - time of, 10, 13, 25
 - see* sediment transport
- Critical velocity,
 - see* sediment transport
- Crossing, 122
- Culverts, 53, 390
- Current meters, 38–41
 - accuracy, 40
 - turbulence influence, 40–41

- Curves,
 characteristic, 17, 25
 cumulative duration, 21, 23
 hypsometric, 17
- Curve fitting,
 circular arc, 345–351
 lemniscate, 354–359
 sinoidal arc, 351–353
- Cut-off,
see meandering channels
- Degradation,
 main parameters, 340–341
- Delta, 103–106
 formative stages, 105
- Deposition,
 general process, 82–83
- Detention basin, 428–431
 attenuation of peak discharge, 430
 spillway design, 432–434, 439–446, 482–487
- Dikes, 381–398
 advantages and drawbacks, 394
 alignment, 392–393
 construction criteria, 387–388, 394–398
 cross-section, 384–385
 economics, 382
 hydraulics, 383–384
 safety, 383
 seepage and piping, 385–387
- Discharge,
 bankful, 136
 computation of, 10, 12, 14
 dominant, 136, 137, 154, 316
 median and modal, 21, 22
 peak discharge, 15, 23
- Discharge measurement,
 air bubbling method, 56–58
 at culverts, 53
 by boats or gauging rafts, 50
 by wading, 47
 cable station, 48–49
 chemical methods, 54–56
 intermittent injection method, 54
 continuous feeding method, 55
 conveyance-slope method, 58
 methods of computation, 50–53
 arithmetical method, 50–51
 graphical method, 52–53
 Q–H curve method, 61
- Diversions,
 in arid zones, 468–469
 of flood waters, 446–452
 permanent and temporary, 447
 retarding basin, 451–452
 sideweir, 449
- Drag, definition, 199
- Drop structures, 361–365
 drawdown curve, 364
 end contraction, 507–513
 hydraulic jump, 364–365
 main hydraulic parts, 364
 typical structure, 365
see also outlets
- Dunes, 217–219
- Einstein velocity correction factor, 175
- Elevation, mean, 18
- End contraction,
see drop structures
- Engineering economy, 471–481
 annual expenditures, 473–475
 basic mathematical concepts, 487–490
 benefits evaluation, 480–481
 calculation tables, 491–493
 capital cost estimate, 471–473
 estimate of benefits, 475–476
 flood damage, 476–480
 graphical flood analysis, 477–480
- Erosion,
 general process, 82–83
- Exclusion of coarse sediment, 367–374
- Fall velocity,
see settling velocity
- Filter design, 378–381, 415–417
- Fixation of bed,
see stream training works
- Flat bed, 219
- Floats, 36–38
 hydrodynamic pendulum, 37–38
- Flood plain drainage, 388–392
- Flood protection,
 alternatives, 436
 design discharge, 336–338
 engineering methods, 335–336
 flood control reservoirs, 428–446
 location of dams, 435–436
- Flood storage,
 in flood plain, 389
 in reservoirs, *see* detention basin
- Flow,
 channel, 4
 in channel curves, 111–120
 normal high and low, 21

- pattern, 112, 115
 - secondary circulation, 114
 - velocity distribution, 119
- Flow boundary,
 - hydrodynamically smooth and rough, 173–176
- Form roughness,
 - see* roughness
- Friction velocity,
 - see* shear velocity
- Gabions,
 - see* stone mattresses
- Gauges,
 - Archimedes, 33
 - bubble type pneumatic, 33
 - electromagnetic, 33
 - peak stage, 34
 - permanent automatic, 32
 - portable automatic, 31
 - staff, 29
 - suspended weight, 31
- Grain size gradation,
 - see* sediment gradation
- Groynes, 369, 398–406, 419–421
 - crest line, 405–406
 - distance between, 400
 - local scour, 402–405, 422–423
 - longitudinal dikes, 406
 - typical structure, 401
- Hydraulic jump
 - see* drop structures
- Hydraulically smooth and rough,
 - see* flow boundary
- Hydrograph, 8, 10, 12, 16
 - computation of, 10, 12, 14
- Hydrogram,
 - see* hydrograph
- Incipient motion, 275–283
 - Shields diagram, 278
- Index,
 - cross-section, 85, 343
 - density of drainage system, 22
 - density of tributaries, 21
 - meandering, 85, 151–153, 343–344, 398
- Isochronal lines, 23–26
- Karman, von, constant, 172
 - influence of sediment, 183–185
 - calculation of, 252–254
- Kinematic eddy viscosity, 244
- Laminar sublayer, 175, 178, 182–183
- Loess soil, 460
- Longitudinal dikes,
 - see* groynes
- Longitudinal channel slope,
 - variation with STC, 88–90
- Longitudinal stream profile, 18–20
 - analytical expression for, 20
- Loop rating curve, 232
- Loop sediment discharge curve, 263
- Manning equation, 79, 216
- Manning coefficient, 139, 148, 180–181, 205–206, 212–213
 - due to bed forms, 226
- Meanders, 85
- Meandering channels, 120–129, 150–153
 - crossings, 122
 - cut-off, 90–91, 127
 - empirical relationships, 127–129
 - erosion pattern, 124
 - radius of curvature, 121
 - velocity distribution at exit, 119
- Mediterranean zones,
 - see* arid and semiarid zones
- Mixing length theory, 171
- Multipurpose systems,
 - see* flood protection reservoirs
- Nominal diameter,
 - see* sediment
- Outlets,
 - bank protection, 501
 - closed conduit, 504–507
 - drop structures, 501–504
 - flap gate, 506
 - flow lines deflection parameters, 500
 - open channel, 498–504
 - relocation of tributaries, 498–499
- Piping,
 - see* dikes
- Porosity, 196
- Prandtl–von Karman velocity
 - distribution law, 172
- Rainfall,
 - duration, 11
 - intensity, 9, 15
- Rational formula, 10, 12
- Regime theory, 134–165
 - bed factor, 137, 138, 140–150

- side factor, 137, 138, 140–150
- stream meandering, 150–153
- Reservoirs,
 - see flood protection
- Retarding basin,
 - see diversions
- Return period, 24
 - recommended for flood control, 340
- Revetment,
 - see stream training works
- Ripples, 217–219
 - see also bed forms
- Roughness,
 - effect of bed configuration, 223–236
 - height, 173
- Runoff, 4, 15
 - coefficient, 9
- Samplers,
 - see sediment transport measurement
- Scour,
 - downstream of bottom outlets, 437
 - see bridge piers, groynes
- Sealing crust on arid-zone soils, 459
- Sediment,
 - aggregation, 211
 - concentration, 138, 140, 144, 146, 147, 198
 - definition, 84
 - density, 195
 - grain size gradation, 96–100, 207–211
 - along a stream, 99
 - dependence on liquid discharge, 97
 - nominal diameter, 194
 - shape, 195
 - sieve diameter, 194
 - specific weight, 195–196
- Sedimentation diameter, 194
- Sediment transport,
 - critical shear stress, 276–283
 - critical velocity, 275–276, 283–286
 - Einstein bed load method, 302–311
 - Engelund-Hansen method, 316–318
 - formulae based on bed-load movement, 313–315
 - Meyer-Peter and Mueller formulae, 289–291, 298–302
 - Schoklitsch formula, 287–288, 296–297
 - selection of bed-load formula, 292–295
 - suspended load transport,
 - definition, 84, 241
 - diffusion theory, 243
 - discharge, 248–265
 - Einstein I-function, 250, 264–265
 - mechanism, 243–248
- Sediment transport measurement,
 - bed-load measurement, 67–72
 - acoustic method, 72
 - automatic sampler, 72
 - bed forms method, 72
 - box (basket) sampler, 68
 - pit sampler, 70
 - sediment composition sampling, 73
 - tracer method, 73
 - tray sampler, 69
 - suspended load measurement, 63–67
 - depth integrating sampler, 66
 - point integrating sampler, 63
 - sampling across stream, 67
- Settling velocity, 198–207
 - effect of sediment concentration, 207
 - effect of shape, 206–207
 - influence of temperature, 203
 - Re number greater than unity, 202–207
 - Stokes range, 199–202
- Shear stress, 79, 216
 - additional forces causing it, 80
 - permissible, 82
 - variation, 163
- Shear velocity, 79, 172, 176
- Sieve diameter,
 - see sediment
- Slope, mean, 19, 20
 - reduction, see drop structures
- Soil characteristics in arid zones, 457–460
- Specific weight, 195–196
- Spillway,
 - see detention basin
- Spur dikes,
 - see groynes
- Stage-discharge curve,
 - see discharge measurement, Q–H curve
- STC (sediment transport capacity), 86–96
 - definition, 83, 108, 124
- Stilling basin, 365
- Stone mattresses, 375–381
 - filter, see filter design
- Stream,
 - alluvial, 78
 - cross-section self-adjustment, 91–96
 - development process, 86–91
 - lower course, 19
 - middle course, 18
 - upper course, 18
- Stream power, 236

- Stream training works,
 - channel alignment, 343–359
 - channel stabilization, 398–423
 - cross-section improvement, 341–343
 - definition, 338–341
 - fixation of bed, 366–367
 - stream bank protection, 374–381
- Superelevation, 113, 412
- Suspended load,
 - see* sediment transport
 - see also* sediment transport measurement
- Thalweg, 126
- Total load, definition, 242
- Tractive force,
 - see* shear stress
- Transition zone, 174
- Triaxial grain size, 195
- Tributaries, 5, 16
- Velocity,
 - distribution rigid-boundary channels, 171–181
 - distribution logarithmic, 175
 - distribution universal law, 172
 - of bed forms, 313–314
 - permissible mean, 84
- Velocity measurement, 36–45
 - average velocity, 45–47
 - five-point method, 46
 - one-point method, 45
 - three-point method, 46
 - two-point method, 45–46
 - chemical methods, 41
 - color velocity method, 43
 - magnetic induction, 43–44
 - salt velocity method, 41–43
 - ultrasonic method, 44–45
- Wash load,
 - definition, 84, 242
- Watercourses, 17
 - classification, 4
- Water divide, 5
- Watershed, 5–26
 - definition, 5
 - graphical representation, 6
 - influencing factors, 7
 - shape, 7–15
- Weathering process, 193

